

# **Petrological and Geochemical Investigation of the Michelin Uranium Deposit, Central Mineral Belt, Labrador**

by

© Christopher L. Hicks

A thesis submitted to the

School of Graduate Studies

in partial fulfillment of the requirements for the degree of

**Master of Science**

**Department of Earth Sciences**

Memorial University of Newfoundland

September 2015

St. John's

Newfoundland

## **Abstract**

The Michelin deposit of Labrador's Central Mineral Belt is a Na-metasomatic uranium deposit which has an approximate resource of 103 M lbs.  $U_3O_8$ . The deposit is hosted in a broad series of ca. 1857 Ma fine grained porphyritic (FP) and coarse grained porphyritic (CP) felsic volcanic rocks of the Aillik Group, which have been intruded by several generations of mafic and felsic intrusives. Individual felsic volcanic units are tabular and generally maintain their thickness, striking 070 and dipping southeast 40-60°. These rocks were metamorphosed to lower amphibolite facies during the ca. 1800 Ma Makkovikian Orogeny where they were also deformed, imparting a regional penetrative foliation. Individual FP and CP units are nearly identical consisting of a 1:1:1 quartz-potassium feldspar-albite matrix which hosts phenocrysts of potassium feldspar, albite and quartz; the only distinguishable difference being the sizes and abundances of the phenocrysts. Geochemically these rocks are classified as metaluminous, high-K, subalkaline, calc-alkaline rhyolites with an average  $SiO_2$ ,  $Na_2O$  and  $K_2O$  content of 74.0, 3.5 and 5.3 wt. % respectively.

Mineralization occurs in an approximate 300-350 m wide zone that extends from surface continuously to a depth of ~700 m. This zone ranges in thickness from 20-80 m, which reaches a maximum thickness of 60-80 m at 300-500 m depth, narrowing away from this zone, eventually dying out. The mineralized zone is hosted in a tight sequence of alternating CP and FP units termed the Mine Series. These units are geochemically related and texturally identical to unaltered units but have a drastically different mineralogy and geochemistry due to intense alteration and mineralization. These units are



comprised predominantly of albite, which can reach up to 85 %, which forms through the sodic metasomatism of potassium feldspar grains and as secondary albite in spaces created from quartz dissolution. Geochemically these rocks are now metaluminous to peralkaline, low-K, alkaline, calc-alkaline rhyolites with an average SiO<sub>2</sub> concentration of 67.5 wt. %, and Na<sub>2</sub>O and K<sub>2</sub>O averaging 9.5 and 0.10 wt. % respectively.

Uranium mineralization is concentrated within the CP units, and along the contacts with adjacent FP units, adjacent to the contacts with syn-kinematic mafic dikes, and in strongly deformed areas including shear and mylonite zones. Uranium mineralization consists of micron-sized uraninite grains that contain variable amounts of cation substitutions, consisting of radiogenic Pb, Ca, Si, Fe, Zr, Ti, and LREE. Three distinct groupings are recognized 1) uraninite grains that only contain radiogenic Pb, these are often partially-completely surrounded by 2) uraninite grains with Si-Ca-Pb-Zr-Ce, these still contain some radiogenic Pb but interaction with the altering hydrothermal fluid most likely caused the substitution of Ca-Si-Zr-Ce into the uraninite structure, finally group 3) contains large Si concentrations with Ca-Fe-Zr-Ti, these partially surround group 2 and most likely represent continued interaction between uraninite grains and the altering fluid. Uranous ions in the hydrothermal fluid precipitated through the oxidation of hematite and are closely associated with titanite grains.

Two styles of alteration affect the felsic volcanic rocks. The first being a widespread pervasive sodic metasomatism, marked by the ion exchange of K<sup>+</sup> for Na<sup>+</sup> in potassium feldspar, that envelopes the deposit. This completely strips the rocks of K<sub>2</sub>O,

Rb and Tl and increases the Na<sub>2</sub>O content by as much as 3-5 wt. %. The second style of alteration is concentrated within the mineralized zone and consists of several different styles. The first being quartz dissolution, during which quartz is nearly completely removed from the rock. This is marked by a decrease in SiO<sub>2</sub> by ~8 wt. %. The space created from the dissolved quartz in the groundmass and phenocrysts is filled with secondary alteration minerals including albite, sodic amphibole and pyroxene, calcite, and uraninite. Increased sodic alteration, involving the alteration of biotite and hornblende to sodic amphiboles and pyroxenes, and the formation of secondary albite and sodic amphibole and pyroxene occurs concurrently with quartz dissolution, increasing the Na<sub>2</sub>O content of the rock to 9-11 wt. %. The rocks also undergo variable hematitization, due to the oxidation of magnetite. Hematite alteration and uranium mineralization are closely related and higher mineralized zones within the mineralized zone show a more intense hematite alteration, and greater magnetite destruction. Zr is also mobilized during alteration, forming new secondary growth around pre-existing grains, the Zr content within the mineralized zone doubles, from an average of 450 ppm in unaltered rock to 950 ppm in mineralized rock. Mass balance calculations indicate that there are slight enrichments of Al<sub>2</sub>O<sub>3</sub>, CaO, FeO, Sr, V, Y, LREE, As, and Be associated with alteration, and minor depletions in Ba and Sb. Finally, calcite forms during the later stages of alteration filling remaining available pore space within the rock.

## **Acknowledgements**

I would like to thank my supervisor Dr. Derek Wilton for his much appreciated time, support and guidance during the course of this study. The enthusiasm Derek expressed for this study was continuous throughout and contagious providing me with much needed motivation when my own was lacking. His encouragement to “just get it done” gave me the final push to finish, and for that I am thankful.

I would also like to acknowledge and thank the staff and faculty of the Earth Science Department at Memorial University. Michael Shaffer and Glenn Piercey for providing technical assistance and support during SEM-MLA analysis and Mike Tubrett for providing technical assistance and support during LA-ICP-MS U-Pb age dating, and professors Steve Piercey, Graham Layne, and Paul Sylvester for providing me with much appreciated advice and guidance.

This study was made possible through financial and technical support from Aurora Energy Resources. There are numerous people from Aurora that I would like to thank who provided much needed guidance, technical support, and assistance during the early portion of this thesis. In particular Dave Barbour, who taught me everything he knew about the Michelin deposit. A special thanks to the tech crew at Michelin for helping me dig through boxes of core and hand splitting my samples.

Lastly I would like to thank my family for providing much needed support and encouragement throughout this study, in particular my father, Larry Hicks whose help and support were invaluable through the duration of this study and my geological career.

## Table of Contents

<b>Abstract.....</b>	<b>ii</b>
<b>Acknowledgements .....</b>	<b>v</b>
<b>List of Tables .....</b>	<b>xi</b>
<b>List of Figures.....</b>	<b>xii</b>
<b>List of Plates .....</b>	<b>xix</b>
<b>Chapter 1: Introduction</b>	
1.1 Preamble .....	1-1
1.2 Location and Access .....	1-2
1.3 Physiography.....	1-4
1.4 Work History .....	1-5
1.4.1 Industry .....	1-5
1.4.2 Government and Academic.....	1-6
1.5 Purpose of Study .....	1-9
1.6 Methods of Study.....	1-12
<b>Chapter 2: Overview of Uranium Deposits</b>	
2.1 Introduction.....	2-1
2.2 Important Uranium Properties .....	2-1
2.3 Major Uranium Deposit Types .....	2-4
2.3.1 Uranium Deposit.....	2-4
2.3.2 Metasomatic Uranium Deposits.....	2-5
2.3.3 Intrusive Uranium Deposits .....	2-6
2.3.4 Volcanic Associated Uranium Deposits .....	2-7
2.3.5 Vein Type Uranium Deposits .....	2-7
2.3.6 IOCG Deposits.....	2-9
2.3.7 Metamorphic Associated Uranium Deposits .....	2-9
2.4 Uranium in Labrador.....	2-10
2.4.1 Central Mineral Belt .....	2-11
2.4.2 Classification History.....	2-11
2.4.3 Uranium Showings of the Kitts-Post Hill Belt .....	2-13
2.4.4 Uranium Showings Hosted in Felsic Volcanic Rocks .....	2-15
2.4.5 Uranium Showings Associated with Plutonic Rocks.....	2-16
2.4.6 Uranium Showings of the Moran Lake Belt .....	2-19
2.4.7 Unconformity Related Showings.....	2-21
<b>Chapter 3: Geology of the Michelin Deposit</b>	
3.1 Introduction.....	3-1

3.2	Regional Geology .....	3-3
3.2.1	Aillik Domain .....	3-4
3.3	Michelin Geology .....	3-7
3.4	Fine Grained Porphyritic Metamorphosed Felsic Volcanic Rocks.....	3-9
3.4.1	Petrography of the Finely Porphyritic Felsic Volcanic Rocks.....	3-12
3.4.2	Non-Porphyritic Metamorphosed Felsic Volcanic Rocks .....	3-14
3.4.3	Geochemistry of the Fine Grained Porphyritic Felsic Volcanic Rocks....	3-16
3.4.3.1	Discrimination Diagrams .....	3-16
3.4.3.2	Major Elements .....	3-17
3.4.3.3	Trace Elements.....	3-18
3.4.3.4	Rare Earth Elements .....	3-20
3.4.3.5	Geochemical Comparison of the Fine Grained Porphyritic Felsic Volcanic Rocks.....	3-21
3.5	Coarse Grained Porphyritic Metamorphosed Felsic Volcanic Rocks.....	3-23
3.5.1	Petrography of the Coarse Grained Porphyritic Felsic Volcanic Rocks...	3-25
3.5.2	Mafic-Rich Coarse Grained Porphyritic Metamorphosed Felsic Volcanic Rocks .....	3-28
3.5.3	Petrography of the Mafic-Rich Coarse Grained Porphyritic Volcanic Rocks.....	3-30
3.5.4	Geochemistry of the Coarse Grained and Mafic-Rich Coarse Grained Porphyritic Volcanic Rocks .....	3-32
3.5.4.1	Discrimination Diagrams .....	3-32
3.5.4.2	Major Elements .....	3-34
3.5.4.3	Trace Elements.....	3-35
3.5.4.4	Rare Earth Elements .....	3-37
3.5.4.5	Geochemical Comparison of the Coarse Grained Porphyritic Felsic Volcanic Rocks.....	3-38
3.5.4.6	Geochemical Comparison of the Mafic-Rich Coarse Grained Porphyritic Felsic Volcanic Rocks.....	3-39
3.6	Granitoid Intrusive .....	3-41
3.6.1	Petrography of the Granitoid Intrusive .....	3-42
3.6.2	Geochemistry of the Granitoid Intrusive .....	3-44
3.6.2.1	Discrimination Diagrams .....	3-44
3.6.2.2	Major Elements .....	3-45
3.6.2.3	Trace Elements.....	3-46
3.6.2.4	Rare Earth Elements .....	3-47
3.7	Mafic Intrusives .....	3-47
3.7.1	Biotite-Hornblende Schist (Pre-Kinematic Dikes) .....	3-48
3.7.1.1	Petrography of the Biotite-Hornblende Schist Dikes.....	3-49
3.7.2	Gabbroic (Syn-Kinematic Dikes) .....	3-50
3.7.2.1	Petrography of the Gabbroic Dikes.....	3-51
3.7.3	Strongly Magnetic Gabbroic (Post-Kinematic Dike) .....	3-52
3.7.3.1	Petrography of the Strongly Magnetic Gabbroic Dikes.....	3-52
3.7.4	Andesitic (Post-Kinematic Dikes) .....	3-53

3.7.4.1	Petrography of the Andesitic Dikes .....	3-54
3.7.5	Geochemistry of Mafic Intrusives .....	3-54
3.7.5.1	Discrimination Diagrams .....	3-55
3.7.5.2	Major Elements .....	3-57
3.7.5.3	Trace Elements .....	3-60
3.7.5.4	Rare Earth Elements .....	3-62

## **Chapter 4: Geology of the Ore Zone**

4.1	Introduction .....	4-1
4.2	Michelin Ore Zone .....	4-2
4.3	Ore Zone Geology .....	4-6
4.3.1	Coarse Grained Porphyritic Metamorphosed Felsic Volcanics of the Ore Zone .....	4-7
4.3.2	Fine Grained Porphyritic Metamorphosed Felsic Volcanics of the Ore Zone .....	4-10
4.3.3	Petrography of the Coarse and Fine Grained Porphyritic Felsic Volcanic Rocks of the Ore Zone .....	4-13
4.3.4	Geochemistry of the Coarse Grained Porphyritic Felsic Volcanic Rocks of the Ore Zone .....	4-18
4.3.4.1	Discrimination Diagrams .....	4-19
4.3.4.2	Major Oxides .....	4-23
4.3.4.3	Trace and Rare Earth Elements .....	4-25
4.3.4.4	Geochemical Comparison of the Mineralized Coarse Grained Porphyritic Felsic Volcanic Rocks .....	4-26
4.3.5	Geochemistry of the Fine Grained Porphyritic Felsic Volcanic Rocks of the Ore Zone .....	4-27
4.3.5.1	Discrimination Diagrams .....	4-28
4.3.5.2	Major Oxides .....	4-31
4.3.5.3	Trace and Rare Earth Elements .....	4-32
4.3.5.4	Geochemical Comparison of the Mineralized Fine Grained Porphyritic Felsic Volcanic Rocks .....	4-34
4.3.6	Mafic Intrusives of the Ore Zone .....	4-36

## **Chapter 5: Uranium Mineralization**

5.1	Introduction .....	5-1
5.2	Uranium Mineralization .....	5-2
5.3	Uranium-Bearing Phases .....	5-5
5.4	Location of Uranium-Bearing Phases in the Mineralized Zone .....	5-11
5.5	Accessory Minerals to Mineralization .....	5-13
5.5.1	Sodic Minerals .....	5-14
5.5.2	Opaque Minerals .....	5-14
5.5.3	Silicate Minerals .....	5-16

5.5.4	Phosphate Minerals.....	5-20
5.5.5	Other Mineral Phases.....	5-21

## Chapter 6: Alteration

6.1	Introduction.....	6-1
6.2	Sodic Alteration .....	6-3
6.2.1	Mineralogical Changes .....	6-5
6.2.2	Geochemical Changes.....	6-10
6.3	Hematite Alteration.....	6-13
6.3.1	Mineralogical Changes .....	6-16
6.3.1.1	Magnetite Destruction.....	6-17
6.3.2	Geochemical Changes.....	6-18
6.4	Silica Alteration .....	6-19
6.4.1	Mineralogical Changes .....	6-21
6.4.2	Geochemical Changes.....	6-22
6.5	Mass Balance Calculations .....	6-23
6.5.1	Mass Changes within the Mineralized Zone.....	6-25
6.5.1.1	Major Oxides .....	6-26
6.5.1.2	Trace Elements.....	6-28
6.5.1.3	Rare Earth Elements .....	6-31
6.5.1.4	Volatile Elements.....	6-32
6.5.2	Mass Changes within the Sodic Envelope.....	6-33
6.5.2.1	Major Oxides .....	6-34
6.5.2.2	Trace Elements.....	6-36
6.5.2.3	Rare Earth Elements .....	6-38
6.5.2.4	Volatile Elements.....	6-38
6.6	Other Alteration Styles .....	6-39
6.6.1	Calcite Alteration .....	6-39
6.6.2	Garnet Alteration .....	6-41
6.6.3	Other Possible Alteration Halos.....	6-42
6.7	Alteration of the Mafic Dikes .....	6-43
6.7.1	Alteration of Mafic Dikes within the Sodic Envelope.....	6-45
6.7.2	Alteration of Mafic Dikes within the Mineralized Zone .....	6-47
6.7.3	Interpretation of Mafic Dike Alteration.....	6-49
6.8	Elemental Alteration Halos.....	6-51

## Chapter 7: Age Dating and Relative Timing of Events

7.1	Introduction.....	7-1
7.2	Age Dating of the Felsic Volcanic Units .....	7-2
7.3	Relative Timing of the Felsic Volcanic Units and Deformation .....	7-9
7.4	Relative Timing of the Various Alteration Styles.....	7-16
7.4.1	Widespread Sodic Metasomatism.....	7-16

7.4.2	Hematitization.....	7-18
7.4.3	Quartz Dissolution .....	7-19
7.4.4	Increased Sodic Alteration.....	7-21
7.4.5	Formation of Secondary Zircon and Other Minerals.....	7-23
7.4.6	Calcite Alteration .....	7-25
7.4.7	Uranium Mineralization.....	7-26
7.4.8	Mafic Dikes.....	7-29
7.4.9	Relative Timing of Deformation, Mineralization and Alteration Events ..	7-32

## **Chapter 8: Discussion and Conclusion**

8.1	Introduction.....	8-1
8.2	Genetic Model for Metallogenesis.....	8-2
8.2.1	Source of Uranium.....	8-3
8.2.2	Leaching and Transport of Uranium.....	8-4
8.2.3	Precipitation and Concentration.....	8-8
8.3	Deposit Classification .....	8-10
8.4	Conclusion .....	8-12
8.5	Recommended Work .....	8-16

<b>References.....</b>	<b>R-1</b>
------------------------	------------

## **Appendices**

<b>Appendix 1: Sample Information .....</b>	<b>9 Pages</b>
<b>Appendix 2: Geochemical Data .....</b>	<b>66 Pages</b>
<b>Appendix 3: Mass Balance Calculations.....</b>	<b>45 Pages</b>
<b>Appendix 4: Aurora Energy Drill Logs .....</b>	<b>25 Pages</b>
<b>Appendix 5: Industry Work History.....</b>	<b>12 Pages</b>



## List of Tables

<b>Table 2.1:</b> Common characteristics of the six different depositional settings that are similar, or potentially similar to uranium occurrences in Labrador .....	<b>2-22</b>
<b>Table 3.1:</b> Average (avg), low and high values for the fine grained (FP), coarse grained (CP), mafic-rich coarse grained porphyritic felsic volcanics, and granitoid intrusive of the major oxides (oxide wt.%), transition metals (ppm), low field strength elements (ppm), high field strength elements (ppm), rare earth elements (ppm), volatile elements (ppm), and the normative mineral percentages after Irvine and Baragar (1971). ....	<b>3-65</b>
<b>Table 3.2:</b> Average (avg), low and high values for the biotite-hornblende schist dikes, gabbroic dikes, strongly magnetic gabbroic dikes, and andesitic dikes of the major oxides (oxide wt.%), transition metals (ppm), low field strength elements (ppm), high field strength elements (ppm), rare earth elements (ppm), volatile elements (ppm), and the normative mineral percentages after Irvine and Baragar (1971). ....	<b>3-69</b>
<b>Table 4.1:</b> Average (avg), low and high values for the coarse grained (CP) and fine grained (FP) felsic volcanic rocks of the mineralized zone, and the fine grained (FP) felsic volcanic rocks within the sodic envelop of the major oxides (wt.%), transition metals (ppm), low field strength elements (ppm), high field strength elements (ppm), rare earth elements (ppm), volatile elements (ppm), and the normative mineral percentages after Irvine and Baragar (1971). ....	<b>4-39</b>
<b>Table 6.1:</b> Average mass changes for the major oxides, trace elements, rare earth elements and volatile elements during mass balance calculations for CP and FP felsic volcanic rocks within the mineralized zone and the FP felsic volcanic rocks within the sodic alteration envelope. ....	<b>6-54</b>

## List of Figures

<b>Figure 1.1:</b> Location of the Michelin deposit with reference to the major community's within Labrador. ....	<b>1-17</b>
<b>Figure 1.2:</b> Longitudinal section through the Michelin deposit showing Grade x Thickness contours. Grade and thickness are based on the % $U_3O_8$ and true thickness of the mineralized intercept for each drill hole. Blue areas represent lower grade x thickness and red colors represent a greater grade x thickness (Hertel <i>et al.</i> , 2009). ....	<b>1-18</b>
<b>Figure 1.3:</b> Longitudinal section of the Michelin deposit showing the location of the 10 drill holes used for this study. These 10 drill holes create a three-dimensional cross-section through the largest part of the Michelin deposit (modified from Cunningham-Dunlop and Giroux, 2007). ....	<b>1-19</b>
<b>Figure 2.1:</b> Reported uranium occurrences within Labrador. Figure 2.3 provides a more detailed view of the Central Mineral Belt (modified from Wardle <i>et al.</i> , 1997; Newfoundland and Labrador Geological Survey, 2015). ....	<b>2-25</b>
<b>Figure 2.2:</b> General map of the CMB highlighting the six Proterozoic sequences consisting of the Post Hill, Moran Lake, Aillik, Bruce River, Letitia Lake, and Seal Lake groups and the Archean Florence Lake Group with associated basement rocks (modified from Wilton, 1996; Wardle <i>et al.</i> , 1997). ....	<b>2-26</b>
<b>Figure 2.3:</b> Geology map of the Central Mineral Belt, with known uranium occurrences (modified from Wardle <i>et al.</i> , 1997; Newfoundland and Labrador Geological Survey, 2015). ....	<b>2-27</b>
<b>Figure 2.4:</b> Geology of the Kitts – Post Hill belt, highlighting the trend of the belt with known mineral occurrences including the Kitts deposit, and Gear, Inda and Nash showings (modified from Gandhi, 1978; Wardle <i>et al.</i> , 1997; Newfoundland and Labrador Geological Survey, 2015). ....	<b>2-28</b>
<b>Figure 2.5:</b> Geology of the Michelin – White Bear Mountain belt and area, highlighting the general trend of the belt with known mineral occurrences including the Michelin and Jacques Lake deposit, and Rainbow and White Bear showings. The Melody Hill showing is also included (modified from Wardle <i>et al.</i> , 1997; Sparkes and Kerr, 2008; Newfoundland and Labrador Geological Survey, 2015). ....	<b>2-29</b>
<b>Figure 2.6:</b> Geology of the Aillik – Makkovik belt, highlighting the general trend of the belt with known mineral occurrences including the Sunil, Pitch Lake, and John Michelin showings (modified from MacDougall, 1988; Wardle <i>et al.</i> , 1997; Newfoundland and Labrador Geological Survey, 2015). ....	<b>2-30</b>
<b>Figure 2.7:</b> Geology of the Moran Lake belt and area, highlighting the trend of the belt with known mineral occurrences including the C-Zone deposit and B-Zone and A-Zone showings. The Two Time and Stormy Lake showings are also included (modified from Wardle <i>et al.</i> , 1997; Newfoundland and Labrador Geological Survey, 2015). ....	<b>2-31</b>
<b>Figure 3.1:</b> 1:1 Million geology map of Labrador indicating the five distinct structural provinces (modified from Wardle <i>et al.</i> , 1997). ..	<b>3-73</b>
<b>Figure 3.2:</b> Geology map of the Makkovik Province, divided into its three lithotectonic domains; Kaipokok, Aillik, and Cape Harrison (modified from Wardle <i>et al.</i> , 1997; Hinchey, 2007). .	<b>3-75</b>

**Figure 3.3:** Geology map of the Michelin area, centered on Ranjan Lake (modified after Wilton *et al.*, 2007). FP – Fine Grained Porphyritic; CP – Coarse Grained Porphyritic; GT – Granitoid. The orange cross-hatch represents the surface expression of the mineralized zone .....3-76

**Figure 3.4:** Cross section through the Michelin deposit (Hertel *et al.*, 2009). Shows the relative stratiform nature of the FP and CP units, and how the CP units pinch and swell down dip. ....3-76

**Figure 3.5:** Discrimination diagrams of the FP felsic volcanic rocks (open red circles), (a) classification diagram based on Total Alkalies ( $\text{Na}_2\text{O} + \text{K}_2\text{O}$ ) vs. Silica ( $\text{SiO}_2$ ) (in terms of oxide wt.%) (TAS) (LeBas *et al.*, 1986), (b) classification diagram based on ratios of Nb/Y (ppm) vs. Zr/TiO<sub>2</sub> (ppm/oxide wt.%) (Winchester and Floyd, 1977), (c) TAS with alkaline-subalkaline fields (Irvine and Baragar, 1971), (d) Ternary plot of Total Alkalies-MgO-FeO\* (in terms of oxide wt.%) with calc-alkaline and tholeiitic fields (Irvine and Baragar, 1971), (e) K<sub>2</sub>O vs. SiO<sub>2</sub> (in terms of oxide wt.%) with high-K calc-alkaline, med-K calc-alkaline and low-K tholeiitic fields (Peccerillo and Taylor, 1976), (f) Shands index with Al/(Na+K) vs. Al/(Ca+Na+K) (in terms of mol.%) (Maniar and Piccoli, 1989).....3-77

**Figure 3.6:** Harker variation diagrams for the major oxides plotted against SiO<sub>2</sub> (in terms of oxide wt.%) of the FP felsic volcanic rocks.....3-78

**Figure 3.7:** Harker variation diagrams for the low field strength elements (in terms of ppm) plotted against SiO<sub>2</sub> (in terms of oxide wt.%) of the FP felsic volcanic rocks. ....3-79

**Figure 3.8:** Harker variation diagrams for the high field strength elements (in terms of ppm) plotted against SiO<sub>2</sub> (in terms of ppm and oxide wt.%) of the FP felsic volcanic rocks. ....3-80

**Figure 3.9:** Log-standardized rare earth element plot normalized to upper continental crust after Taylor and McLennan (1986) for the FP felsic volcanic rocks. ....3-81

**Figure 3.10:** Log-standardized extended trace element plot normalized to upper continental crust after Taylor and McLennan (1986) for the FP felsic volcanic rocks. ....3-81

**Figure 3.11:** Discrimination diagrams of the CP felsic volcanic rocks (open blue circles) and the mafic-rich CP unit (solid blue squares), (a) classification diagram based on Total Alkalies ( $\text{Na}_2\text{O} + \text{K}_2\text{O}$ ) vs. Silica ( $\text{SiO}_2$ ) (in terms of oxide wt.%) (TAS) (LeBas *et al.*, 1986), (b) classification diagram based on ratios of Nb/Y (ppm) vs. Zr/TiO<sub>2</sub> (ppm/oxide wt.%) (Winchester and Floyd, 1977), (c) TAS with alkaline-subalkaline fields (Irvine and Baragar, 1971), (d) Ternary plot of Total Alkalies-MgO-FeO\* (in terms of oxide wt.%) with calc-alkaline and tholeiitic fields (Irvine and Baragar, 1971), (e) K<sub>2</sub>O vs. SiO<sub>2</sub> (in terms of oxide wt.%) with high-K calc-alkaline, med-K calc-alkaline and low-K tholeiitic fields (Peccerillo and Taylor, 1976), (f) Shands index with Al/(Na+K) vs. Al/(Ca+Na+K) (in terms of mol.%) (Maniar and Piccoli, 1989). ....3-82

**Figure 3.12:** Harker variation diagrams for the major oxides plotted against SiO<sub>2</sub> (in terms of oxide wt.%) of the CP (open blue circles) and mafic-rich CP (solid blue squares) felsic volcanic rocks. ....3-83

**Figure 3.13:** Harker variation diagrams for the low field strength elements (in terms of ppm) plotted against SiO<sub>2</sub> (in terms of oxide wt.%) of the CP (open blue circles) and mafic-rich CP (solid blue squares) felsic volcanic rocks. ....3-84

**Figure 3.14:** Harker variation diagrams for the high field strength elements (in terms of ppm) plotted against SiO<sub>2</sub> (in terms of ppm and oxide wt.%) of the CP (open blue circles) and mafic-rich CP (solid blue squares) felsic volcanic rocks. ....3-85

**Figure 3.15:** Log-standardized rare earth element plot normalized to upper continental crust after Taylor and McLennan (1986) for the CP felsic volcanic rocks. ....3-86

**Figure 3.16:** Log-standardized extended trace element plot normalized to upper continental crust after Taylor and McLennan (1986) for the CP felsic volcanic rocks. ....3-86

**Figure 3.17:** Log-standardized rare earth element plot normalized to upper continental crust after Taylor and McLennan (1986) for the mafic-rich CP felsic volcanic unit. ....3-87

**Figure 3.18:** Log-standardized extended trace element plot normalized to upper continental crust after Taylor and McLennan (1986) for the mafic-rich CP felsic volcanic unit. ....3-87

**Figure 3.19:** Discrimination diagrams of the granitoid rocks (solid pink diamonds), (a) Ternary classification diagram based An vs. Or vs. Ab (Barker, 1979), (b) Shands index with Al/(Na+K) vs. Al/(Ca+Na+K) (in terms of mol.%) (Maniar and Piccoli, 1989), (c) Magma classification based on Zr (ppm) vs. ratio of 10<sup>4</sup>Ga/Al (ppm/oxide wt.%) (Whalen *et al.*, 1987), (d) TAS with alkaline-subalkaline fields (Irvine and Baragar, 1971), (e) Ternary plot of Total Alkalies-MgO-FeO\* (in terms of oxide wt.%) with calc-alkaline and tholeiitic fields (Irvine and Baragar, 1971), (e) K<sub>2</sub>O vs. SiO<sub>2</sub> (in terms of oxide wt.%) with high-K calc-alkaline, med-K calc-alkaline and low-K tholeiitic fields (Peccerillo and Taylor, 1976). ....3-88

**Figure 3.20:** Harker variation diagrams for the major oxides plotted against SiO<sub>2</sub> (in terms of oxide wt.%) of the granitoid rocks. ....3-89

**Figure 3.21:** Harker variation diagrams for the low field strength elements (in terms of ppm) plotted against SiO<sub>2</sub> (in terms of oxide wt.%) of the granitoid rocks. ....3-90

**Figure 3.22:** Harker variation diagrams for the high field strength elements (in terms of ppm) plotted against SiO<sub>2</sub> (in terms of ppm and oxide wt.%) of the granitoid rocks. ....3-91

**Figure 3.23:** Log-standardized rare earth element plot normalized to upper continental crust after Taylor and McLennan (1986) for the granitoid rocks. ....3-92

**Figure 3.24:** Log-standardized extended trace element plot normalized to upper continental crust after Taylor and McLennan (1986) for the granitoid rocks. ....3-92

**Figure 3.25:** Discrimination diagrams of the pre-kinematic, biotite-hornblende schist, dikes (solid blue x's), syn-kinematic gabbroic dikes (solid green triangles), post-kinematic magnetic gabbroic dikes (solid black plus-sign), and post-kinematic andesitic dikes (solid yellow pentagram), (a) classification diagram based on Total Alkalies (Na<sub>2</sub>O + K<sub>2</sub>O) vs. Silica (SiO<sub>2</sub>) (in terms of oxide wt.%) (TAS) (LeBas *et al.*, 1986), (b) classification diagram based on ratios of Nb/Y (ppm) vs. Zr/TiO<sub>2</sub> (ppm/oxide wt.%) (Winchester and Floyd, 1977), (c) TAS with alkaline-subalkaline fields (Irvine and Baragar, 1971), (d) Ternary plot of Total Alkalies-MgO-FeO\* (in terms of oxide wt.%) with calc-alkaline and tholeiitic fields (Irvine and Baragar, 1971). ....3-93

**Figure 3.26:** Harker variation diagrams for the major oxides plotted against SiO<sub>2</sub> (in terms of oxide wt.%) of the pre-kinematic (solid blue x's), syn-kinematic (solid green triangles), and post-kinematic (solid black plus-sign and solid yellow pentagram). .....3-94

**Figure 3.27:** Harker variation diagrams for the low field strength elements (in terms of ppm) plotted against SiO<sub>2</sub> (in terms of oxide wt.%) of the pre-kinematic (solid blue x's), syn-kinematic (solid green triangles), and post-kinematic (solid black plus-sign and solid yellow pentagram). .....3-95

**Figure 3.28:** Harker variation diagrams for the high field strength elements (in terms of ppm) plotted against SiO<sub>2</sub> (in terms of ppm and oxide wt.%) of the pre-kinematic (solid blue x's), syn-kinematic (solid green triangles), and post-kinematic (solid black plus-sign and solid yellow pentagram). .....3-96

**Figure 3.29:** Log-standardized rare earth element plot normalized to chondrite after McDonough and Sun (1995) for the (a) pre-kinematic, biotite-hornblende schist dikes (solid blue x's), (b) syn-kinematic gabbroic dikes (solid green triangles), (c) post-kinematic magnetic gabbroic dikes (solid black plus's), and (d) post-kinematic andesitic dikes (solid yellow pentagrams). .....3-97

**Figure 3.30:** Log-standardized extended trace element plot normalized to primitive mantle after Sun and McDonough (1989) for the (a) pre-kinematic, biotite-hornblende schist dikes (blue x's), (b) syn-kinematic gabbroic dikes (green triangles), (c) post-kinematic magnetic gabbroic dikes (black plus's), and (d) post-kinematic andesitic dikes (yellow pentagrams). .....3-98

**Figure 4.1:** Approximate dimensions of the mineralized zone. The mineralized zone extends from surface to a continuous depth of ~700 m down dip in a ~100-150 m wide zone, this zone narrow along strike in both directions and at depth. In the center there is a ~200x250 m section at ~400 m depth that is 60-80m thick (modified after Hertel *et al.*, 2009). .....4-43

**Figure 4.2:** Mine series of the Michelin deposit (Evans, 1980). .....4-43

**Figure 4.3:** Discrimination diagrams of the CP felsic volcanic rocks from the mineralized zone (solid blue circles), (a) classification diagram based on Total Alkalies (Na<sub>2</sub>O + K<sub>2</sub>O) vs. Silica (SiO<sub>2</sub>) (in terms of oxide wt.%) (TAS) (LeBas *et al.*, 1986), (b) classification diagram based on ratios of Nb/Y (ppm) vs. Zr/TiO<sub>2</sub> (ppm/oxide wt.%) (Winchester and Floyd, 1977), (c) TAS with alkaline-subalkaline fields (Irvine and Baragar, 1971), (d) Ternary plot of Total Alkalies-MgO-FeO\* (in terms of oxide wt.%) with calc-alkaline and tholeiitic fields (Irvine and Baragar, 1971), (e) K<sub>2</sub>O vs. SiO<sub>2</sub> (in terms of oxide wt.%) with high-K calc-alkaline, med-K calc-alkaline and low-K tholeiitic fields (Peccerillo and Taylor, 1976), (f) Shands index with Al/(Na+K) vs. Al/(Ca+Na+K) (in terms of mol.%) (Maniar and Piccoli, 1989). .....4-44

**Figure 4.4:** Log-standardized rare earth element plot normalized to upper continental crust after Taylor and McLennan (1986) for the CP felsic volcanic rocks of the mineralized zone. ....4-45

**Figure 4.5:** Log-standardized extended trace element plot normalized to upper continental crust after Taylor and McLennan (1986) for the CP felsic volcanic rocks of the mineralized zone, uranium peak has been cut-off. ....4-45

**Figure 4.6:** Discrimination diagrams of the FP felsic volcanic rocks from the mineralized zone (solid red circles), (a) classification diagram based on Total Alkalies ( $\text{Na}_2\text{O} + \text{K}_2\text{O}$ ) vs. Silica ( $\text{SiO}_2$ ) (in terms of oxide wt.%) (TAS) (LeBas *et al.*, 1986), (b) classification diagram based on ratios of Nb/Y (ppm) vs. Zr/TiO<sub>2</sub> (ppm/oxide wt.%) (Winchester and Floyd, 1977), (c) TAS with alkaline-subalkaline fields (Irvine and Baragar, 1971), (d) Ternary plot of Total Alkalies-MgO-FeO\* (in terms of oxide wt.%) with calc-alkaline and tholeiitic fields (Irvine and Baragar, 1971), (e) K<sub>2</sub>O vs. SiO<sub>2</sub> (in terms of oxide wt.%) with high-K calc-alkaline, med-K calc-alkaline and low-K tholeiitic fields (Peccerillo and Taylor, 1976), (f) Shands index with Al/(Na+K) vs. Al/(Ca+Na+K) (in terms of mol.%) (Maniar and Piccoli, 1989). .....4-46

**Figure 4.7:** Log-standardized rare earth element plot normalized to upper continental crust after Taylor and McLennan (1986) for the FP felsic volcanic rocks of the mineralized zone. ....4-47

**Figure 4.8:** Log-standardized extended trace element plot normalized to upper continental crust after Taylor and McLennan (1986) for the FP felsic volcanic rocks of the mineralized zone, uranium peak has been cut-off. ....4-47

**Figure 4.9:** Log-standardized rare earth element plot normalized to upper continental crust after Taylor and McLennan (1986) for the average REE concentration of unaltered FP (open red circles), sodic altered FP (red triangles), mineralized zone FP (red circles), unaltered CP (open blue circles), mineralized zone CP (blue circles), and mafic-rich CP (blue squares). The average REE concentration for each group displays the same profile, with the only difference being a concentration increase in the REE. ....4-48

**Figure 4.10:** REE ratio-ratio plot of La/Sm vs. Dy/Yb (in terms of ppm) for the unaltered FP (open red circles), sodic altered FP (red triangles), mineralized zone FP (red circles), unaltered CP (open blue circles), mineralized zone CP (blue circles), and mafic-rich CP (blue squares). All samples roughly plot together with a Dy/Yb ratio of ~0.8 and a La/Sm ratio of ~7. The samples show a linear trend with the La/Sm ratio. ....4-49

**Figure 4.11:** Immobile-immobile bivariate element plots of TiO<sub>2</sub> vs. P<sub>2</sub>O<sub>5</sub> (in terms of oxide wt.%) and TiO<sub>2</sub> vs. Zr (in terms of oxide wt.% and ppm respectively) for the unaltered FP (open red circles), sodic altered FP (red triangles), mineralized zone FP (red circles), unaltered CP (open blue circles), mineralized zone CP (blue circles), and mafic-rich CP (blue squares). With the exception of samples from the mineralized zone, all samples plot in a linear trend that projects through the origin. ....4-50

**Figure 5.1:** EDX analysis of uraninite grains showing a large U peak with cationic substitutions of (a) Si, Ca, Pb and Ce, (b) Si, Ca, Pb, and (c) Si, Ca, Pb and Zr. ....5-23

**Figure 5.2:** EDX analysis of uraninite grains showing a large Si peak with smaller U peak and cationic substitutions of (a) Ca, Zr and Fe, (b) C and Zr, and (c) Ca, Zr and Ti. ....5-24

**Figure 5.3:** EDX analysis of uraninite showing a large U peak with a smaller Pb peak. ....5-25

**Figure 5.4:** Back scatter electron (BSE) image of uraninite showing uraninite with Pb (Pb\_U) occurring as shall anhedral grains (lightest grey) surrounded by uraninite with Si-Ca-Pb (Si-Ca-Pb\_U) (slightly darker grey), which are then surrounded by uraninite with Si-Ca (Si-Ca\_U) and uraninite with Si-Ca-Zr-Fe (Si-Ca-Zr-Fe\_U) which are both slightly darker grey still. ....5-26

**Figure 5.5:** BSE of mineral aggregate consisting of titanite (Ti), Hematite (Hm), Zircon (Zr), sodic pyroxene (Px), Calcite (Cal) in an albite (Ab) matrix. Uraninite grains are hosted throughout but are mostly associated with Ti grains, they occur as uraninite with Pb (Pb\_U) which are the lightest grey and uraninite with Si-Ca (Si-Ca\_U) which are slightly darker grey. Individual uraninite grains occur within the matrix. ....5-27

**Figure 5.6:** BSE image of mineral aggregate consisting of zircon (Zr), titanite (Ti), sodic pyroxene (Px), albite (Ab), calcite (Cal) in an albite matrix. Uraninite grains occur throughout but are predominantly associated with titanite grains and occur a euhedral uraninite with Pb (Pb\_U) that is surrounded by uraninite with Si-Ca (Si-Ca\_U). Two distinct varieties of zircon are present, euhedral grains with secondary growth rims, and a rounded grain with a different color core, most likely an inherited grain.....5-28

**Figure 5.7:** BSE of a mineral aggregate of titanite (Ti), calcite (cal), albite (ab), and sodic pyroxene (Px) in an albite matrix. Hosts large grains of uraninite with silica (Si\_U), possibly coffinite. ....5-29

**Figure 5.8:** BSE image of a small aggregate of titanite (Ti) and sodic pyroxene (Px) within an albite (Ab) rich matrix. Uraninite grains are associated with the sodic pyroxenes and consist of uraninite with Pb (Pb\_U) which is surrounded by uraninite with Si-Ca-Pb (Si-Ca-Pb\_U). ....5-30

**Figure 5.9:** BSE image of a mineral aggregate consisting of titanite (Ti), sodic pyroxene (Na\_Px) and calcite (Cal) in an albite (Ab) matrix. The aggregate is strongly mineralized with grains of uraninite with Pb (Pb\_U) being almost completely surrounded by uraninite with Si-Ca (Si-Ca\_U). ....5-31

**Figure 5.10:** BSE image of the albite (Ab) rich matrix hosting individual uraninite grains at the triple-point junctions between grains. Uraninite grains consist of uraninite with Pb (Pb\_U), and uraninite with Si-Ca (Si-Ca\_U). ....5-32

**Figure 6.1:** Bivariate plot of Na<sub>2</sub>O vs. K<sub>2</sub>O (in terms of oxide wt.%) for all felsic volcanic samples within the Michelin deposit. Unaltered FP (open red circles) and CP (open blue circles) plot together at ~5.5 wt.% K<sub>2</sub>O and 3.5 wt.% Na<sub>2</sub>O, samples trend towards samples within the sodic envelope (red triangles) which show an increase in Na<sub>2</sub>O and decrease in K<sub>2</sub>O, mineralized FP (red circles) and CP (blue circles) show a further increase in Na<sub>2</sub>O. ....6-57

**Figure 6.2:** Bivariate plot of SiO<sub>2</sub> (oxide wt.%) vs. U (ppm), the plot shows that nearly all of the mineralized samples have a decrease in SiO<sub>2</sub>. ....6-57

**Figure 6.3:** SEM-MLA mineral map from within the sodic envelope (top) and mineralized zone (bottom), (top) the light green color is albite which occurs as phenocrysts and constitutes most of the matrix, the pink color is quartz which occurs as phenocrysts and about 30 % of the matrix, the remaining colors are various amounts of magnetite, biotite, hornblende and calcite, and (bottom) the light green color is albite which constitutes most of the rock, equating to about 80 %, the blue color(s) are sodic amphibole and pyroxene which is located throughout the rock, and forms a large mafic clot with calcite (grey), the red and green are a combination of other alteration minerals including titanite, zircon, and hematite. ....6-58

**Figure 6.4:** Immobile-immobile element bivariate plots of unaltered and altered felsic volcanic rocks from the Michelin deposit. TiO<sub>2</sub> appears to be the most conserved element during alteration and generally forms the more linear trends. ....6-59

**Figure 6.5:** Mass change for the major oxides for the (a) CP and (b) FP felsic volcanic rocks from the mineralized zone. Both rock types display an overall large total mass loss, attributed to a large mass loss in  $\text{SiO}_2$ , there are slight mass gains in  $\text{Al}_2\text{O}_3$ ,  $\text{Fe}_2\text{O}_3$  (total iron) and  $\text{CaO}$ ,  $\text{Na}_2\text{O}$  shows a strong mass gain while  $\text{K}_2\text{O}$  displays a strong mass loss. ....6-60

**Figure 6.6:** Mass change for the trace elements for the (a) CP and (b) FP felsic volcanic rocks from the mineralized zone. The trace elements for each rock type display a similar mass change, with U experiencing a strong mass gain, Zr having a moderate mass gain, and Y and Sr having a weak mass gain, and Ba having a strong mass loss, and Rb having a weak mass loss. ....6-61

**Figure 6.7:** Mass change for the rare earth elements for the (a) CP and (b) FP felsic volcanic rocks from the mineralized zone. The rare earth elements for each rock type display a similar mass change, with the LREE displaying a strong mass gain, and the MREE and HREE displaying slight mass gains. ....6-62

**Figure 6.8:** Mass change for the volatile elements for the (a) CP and (b) FP felsic volcanic rocks from the mineralized zone. The volatile elements display different mass changes between the FP and CP units with the (a) CP units displaying a mass gain in As, Be and Sn, and a mass loss in Bi and Tl, while the (b) FP units display a mass gain in As, Be, Bi and Mo, and a mass loss in Sb and Tl. ....6-63

**Figure 6.9:** Mass change for the major oxides for the FP felsic volcanic rocks from the sodic alteration envelope. These rocks show an overall total mass loss, attributed to a mass loss in  $\text{SiO}_2$  and,  $\text{Al}_2\text{O}_3$  and  $\text{K}_2\text{O}$ ,  $\text{Na}_2\text{O}$  displays a strong mass gain, attributed to sodic metasomatism. ....6-64

**Figure 6.10:** Mass change for the trace elements for the FP felsic volcanic rocks from the sodic alteration envelope. These rocks show a strong mass loss in Rb, and a weak mass loss in Zr. They also display a strong mass gain in U, and weak mass gains in Ba and Sr. ....6-64

**Figure 6.11:** Mass change for the rare earth elements for the FP felsic volcanic rocks from the sodic alteration envelope. These rocks show a strong mass gain in La and Ce, but a mass loss in Pr and Nd of the LREE, the MREE and HREE for the most part show no change, with the exception of very weak mass loss in some elements. ....6-65

**Figure 6.12:** Mass change for the trace elements for the FP felsic volcanic rocks from the sodic alteration envelope. These rocks show a strong mass gain in As and Mo with weak mass gains in Be and Bi, they show a strong mass loss in Sb, Sn and Tl. ....6-65



## List of Plates

**Plate 1.1:** Aerial view of the Michelin area, centered on Ranjan Lake, view towards the southwest. Typical physiography of the area - consisting of small lakes, streams and bogs in lower areas and spruce covered higher areas. The Michelin deposit outcrops in the far right of the picture. ....1-20

**Plate 1.2:** Aerial view of the Michelin Camp, located at the northeastern end of Ranjan Lake, view towards the southeast. The Michelin deposit outcrops in the lower-right of the picture.....1-20

**Plate 3.1:** Drill core segments of unaltered FP felsic volcanic rocks from throughout the Michelin deposit (core diameter is 4.2 cm), (a) typical FP rocks, (b) split-sample of mafic-poor FP, (c) close-up of drill core, (d) mafic wisps in FP rocks, (e) noticeably foliated FP rocks, and (f) close-up of foliated FP with noticeable phenocrysts. ....3-99

**Plate 3.1cont.:** Continuation of drill core segments of unaltered FP felsic volcanic rocks from throughout the Michelin deposit (core diameter is 4.2 cm), (h) mafic-rich section, (i) split-sample of mafic-rich FP, (j) strongly fractured section, fractures opposite foliation, (k) fault zone, strongly chloritized gouge and brecciated, (l) top 4 rows of core in the non-porphyritic unit, and (m) close-up of the non-porphyritic unit. ....3-100

**Plate 3.2:** Petrographic sections of the FP felsic volcanic rocks, (a) feldspar and quartz phenocrysts within a fine-grained matrix (magnification (mag.) = 2.5x, cross polarized light (cpl)), (b) recrystallized quartz phenocrysts composed of several grains sutured together (mag. = 2.5x, cpl), (c) subhedral potassium feldspar phenocryst with microcline twinning (mag. = 2.5x, cpl), (d) potassium feldspar phenocryst with micro-fractures containing sericite alteration (mag. = 2.5x, cpl), (e) subhedral albite phenocryst (mag. = 2.5x, cpl), and (f) strongly sericitized albite phenocryst with Carlsbad twinning (mag. = 2.5x, cpl). ....3-101

**Plate 3.2cont.:** Petrographic sections of the FP felsic volcanic rocks, (g) fine-grained quartz-feldspar matrix, grains are equant and polygonal (mag. = 10x, cpl), (h) fine-grained quartz-feldspar matrix in plain polarized light (ppl) displays the opaque minerals within the matrix (mag. = 10x, ppl), (i) lath-shaped biotite grains within the matrix (mag. = 5x, cpl), (j) biotite-hornblende-opaque-titanite grains (mag. = 5x, ppl), (k) elongated biotite and stretched quartz phenocryst defining the foliation (mag. = 2.5x, ppl), and (l) elongated, recrystallized quartz phenocryst defining the foliation (mag. = 2.5x, cpl). ....3-102

**Plate 3.3:** Drill core segments of unaltered CP felsic volcanic rocks from throughout the Michelin deposit (core diameter is 4.2 cm), (a) typical CP rocks, (b) split-sample of CP rocks showing augened potassium feldspar, (c) two units of CP felsic volcanics, separated by a FP unit in the center, (d) split-section of a CP unit, (e) contact between a CP unit and mafic dike, concordant with foliation, and (f) close-up of foliated CP with wavy foliation augening phenocrysts. ....3-103

**Plate 3.4:** Petrographic sections of the CP felsic volcanic rocks, (a) recrystallized, elongated quartz phenocryst (mag. = 2.5x, cpl), (b) albite phenocryst composed of several grains sutured together, with calcite (mag. = 2.5x, cpl), (c) large potassium feldspar phenocryst comprised of 3-4 individual grains (mag. = 2.5x, cpl), (d) large potassium feldspar phenocryst comprised of a single grain (mag. = 2.5x, cpl), (e) fine-grained quartz-feldspar matrix (mag. = 5x, cpl), and (f) biotite-laths within the fine-grained matrix (mag. = 5x, cpl). ....3-104

**Plate 3.5:** Drill core segments of the mafic-rich CP felsic volcanic unit from throughout the Michelin deposit (core diameter is 4.2 cm), (a) close-up of the mafic-rich unit showing coarse phenocrysts and getting more mafic-rich towards the bottom, (b) split-sample from within the felsic-rich center of the unit, (c) top two rows of core show the unit becoming increasingly more mafic, (d) split-section from a more mafic-rich area showing coarse phenocrysts strongly augened by wisps of mafic material, (e) second row shows the mafic margin of the unit, and (f) split-section on the mafic margin of the unit. ....**3-105**

**Plate 3.6:** Petrographic sections of the mafic-rich CP felsic volcanic unit, (a) mafic-rich matrix characteristic of the mafic-rich CP unit (mag. = 2.5x, cpl), (b) biotite-hornblende-rich matrix with zircon (mag. = 2.5x, ppl), (c) large potassium feldspar phenocryst wrapped by thin mafic wisps of biotite and hornblende (mag. = 2.5x, ppl), (d) large potassium feldspar phenocryst comprised of a single grain with weak sericite alteration (mag. = 2.5x, cpl), (e) sericitized potassium feldspar phenocryst within the predominantly mafic margin, lath-shaped biotite-hornblende grains wrap the phenocryst (mag. = 2.5x, cpl), and (f) same image in ppl (mag. = 2.5x, ppl). ....**3-106**

**Plate 3.7:** Drill core segments of the granitoid intrusive (core diameter is 4.2 cm), (a) coarse-grained granite to granodiorite intrusives, (b) split-sample of a mafic-rich portion of granitoid, mafic minerals define foliation of the rock, (c) close up of granitoid unit showing the coarse-grained texture of the rock, (d) split-section from a mafic-poor area, granitoid no longer appears foliated without mafic minerals to define the foliation, (e) contact between the granitoid and small pre-kinematic dikes, contact is concordant with foliation, and (f) lower box contains granitoid rock that has become hematitized, giving it a reddish-color.....**3-107**

**Plate 3.8:** Petrographic sections of the granitoid intrusive (a-d) and pre-kinematic biotite-hornblende schist, dikes (e-f), (a) granitoid consisting of coarse grain potassium feldspar, medium grained albite, quartz and biotite, and fine grained quartz (mag. = 2.5x, cpl), (b) biotite and titanite (mag. = 2.5x, ppl), (c) mafic-rich clot within the granitoid consisting of biotite-hornblende-magnetite-titanite (mag. = 2.5x, cpl), (d) same image in ppl (mag. = 2.5x, ppl), (e) pre-kinematic dike with large elongated biotite-lath in a fine-grained matrix of albite-biotite-hornblende (mag. = 2.5x, cpl), and (f) same image in ppl (mag. = 2.5x, ppl). ....**3-108**

**Plate 3.9:** Drill core segments of the mafic dikes (core diameter is 4.2 cm), (a) pre-kinematic biotite-hornblende schist, (b) split-sample of strongly foliated biotite-hornblende schist, grain size is large enough to give it a salt and pepper appearance, (c) massive fine-grained syn-kinematic gabbroic dike, (d) split-section of a syn-kinematic gabbroic dike that is weakly foliated and salt and pepper in appearance, (e) massive, very fine-grained post-kinematic, strongly magnetic dike, and (f) split-sample of the strongly magnetic post-kinematic dike, grain size is very small and rock has not been foliated. ....**3-109**

**Plate 3.10:** Petrographic sections of the syn and post-kinematic mafic dikes, (a) syn-kinematic gabbroic dike with plagioclase laths, and hornblende with biotite, clinopyroxene and magnetite (mag. = 2.5x, cpl), (b) same image in ppl (mag. = 2.5x, ppl), (c) strongly magnetic post-kinematic gabbroic dike with large plagioclase laths, medium magnetite grains and finer mafic grains (mag. = 2.5x, cpl), (d) same image in ppl (mag. = 2.5x, ppl), (e) post-kinematic andesite dike with fine-grained plagioclase mixed with hornblende and biotite (mag. = 2.5x, cpl), and (f) same image in ppl (mag. = 2.5x, ppl). ....**3-110**

**Plate 4.1:** Approximate surface expression of the Michelin deposit outlined in red, view is towards the south. Deposit strikes SW-NE at 070 and dips to the SE approximately 40-60° underneath Ranjan Lake. **4-51**

**Plate 4.2:** Complete drill section (core diameter 4.2 cm) through the Ore Zone in drill hole M06-027, zone is approximately 31 m thick. Ore zone starts with the start of the upper most CP unit (A Group) which is ~12.5 m thick, within the middle of the zone is the second CP unit ~5 m thick (one of either A or B or C Groups), the ore zone ends with two small (~1 m and 0.5 m) thick CP units (either C and F Group) (groupings are difficult to extrapolate to this depth, ~500 m below surface). ..... **4-52**

**Plate 4.3:** Drill core segments of CP felsic volcanic rocks from throughout the mineralized ore zone (core diameter is 4.2 cm), (a) typical hematitized CP rocks, (b) split-sample of altered CP with large phenocrysts and abundant mafic material, (c) strongly altered CP, (d) split-sample showing large feldspar phenocrysts augened by the foliation, (e) elongated-joined section of drill core showing a CP unit, alteration and mineralization vary down hole. .... **4-53**

**Plate 4.4:** Drill core segments of FP felsic volcanic rocks from throughout the mineralized ore zone (core diameter is 4.2 cm), (a) typical hematitized FP rocks, (b) split-sample of altered FP, with foliation defined by mm-thin mafic streaks, (c) elongated section showing a FP unit and the variation change in color, alteration, mineralization (cps) down hole, and concordant contacts with pre-kinematic strongly foliated dikes, (d) split-sample of strongly altered FP rock, (e) split-section showing individual fine-grained phenocrysts. .... **4-54**

**Plate 4.5:** Petrographic sections of the CP and FP felsic volcanic rocks from throughout the mineralized ore zone, (a) sodic-altered potassium feldspar (kf) phenocrysts consisting of a single grain showing chessboard-style twinning (mag. = 2.5x, cpl), (b) potassium feldspar phenocryst consisting of 2-3 grains, part of grain has been replaced by mafic minerals (mag. = 2.5x, cpl), (c) large, recrystallized primary albite phenocryst with abundant mafic material (mag. = 2.5x, cpl), (d) secondary albite phenocryst with chessboard twinning, with a pressure shadow filled with multiple calcite grains (mag. = 2.5x, cpl), (e) possible dissolved quartz phenol with cavity space filled with secondary alteration minerals (mag. = 2.5x, cpl), and (f) same as (e) (mag. = 5x, cpl). .... **4-55**

**Plate 4.5:** Continuation of Plate 4.5, (g) fine-grained quartz-feldspar matrix, individual grains are equant, polygonal and slightly elongated parallel to foliation (mag. = 5x, cpl), (h) same view but in ppl showing the increased mafic content of the matrix within the mineralized zone (mag. = 5x, ppl), (i) elongated sodic amphibole with 120/60 cleavage, defining the foliation, possibly pseudomorph of original biotite (mag. = 2.5x, ppl), (j) mafic mineral clot consisting of sodic amphibole and pyroxene, opaque grains (mag. = 2.5x, ppl), (k) abundant, euhedral calcite grains in pressure shadow of larger phenocryst (mag. = 5x, cpl), and (l) mafic minerals (mag. = 5x, cpl). .... **4-56**

**Plate 5.1:** Location of uranium mineralization throughout the Michelin deposit (core diameter 4.2 cm), (a-b) spots of anomalous mineralization associated with small concordant, patches of weak hematite alteration, cps values between 250-650cps, (c) sporadic hematite patches become more frequent approaching the start of the main ore zone, with is marked by the start of the first CP unit within the Mine Series (lowest row of core), (d) CP unit (second row of core) within FP units, mineralization is concentrated within this unit and the adjacent contacts of the FP units, gradually decreasing to the centers of the FP units, (e) small, intensely foliated, non-porphyritic mylonite zone with strong hematite alteration and mineralization, (f-h) zones adjacent to the syn-kinematic mafic dikes display a strong increase in both hematite alteration and mineralization, which gradually returns to background away from the dike contact, (h) zone of intense shearing and abundant calcite, marked by increase hematite alteration and mineralization (within the 5<sup>th</sup> row of core), (i) Showing the CP unit (bottom 2 rows of core) being strongly mineralized and altered, the FP units above it are not as strongly mineralized or altered, (j) small zone of strong mineralization associated with strong hematite and calcite alteration, pre-kinematic dike above this zone has no mineralizing-upgrade effect on the adjacent core. ....5-33

**Plate 5.2:** BSE images of zircon grains from the unaltered felsic volcanics (a-b) and mineralized zone (c-f), (a and b) euhedral, prismatic, zoned zircon grains from FP felsic volcanic units , (c) un-zoned equant zircon grain showing secondary growth along the outside rim that includes several small uraninite grains, zircon grain is a part of a mineral aggregate that contains abundant uranium mineralization, (d) equant, un-zoned zircon grain with secondary grown along its outside rim which contains a couple f tiny uraninite grains, (e) zoned, euhedral grain with uraninite grains developing along fractures within the grain, and (f) anhedral zircon grain with strongly mottle appearance. ....5-36

**Plate 6.1:** Drill core sections from the unaltered and sodic altered hanging wall of the Michelin deposit (core diameter 4.2 cm), (a) pinkish-grey color of unaltered FP felsic volcanics, (b) whitish-grey color of sodic altered FP felsic volcanic, and (c) drill section covering the onset of sodic alteration from unaltered, pinkish-grey rock into sodic altered whitish-grey rock. The change gradually occurs over ~20 m, note the small CP unit 5-6 rows from the bottom does not display a color change despite being in sodic altered FP rock. ....6-66

**Plate 6.2:** Petrographic sections of FP felsic volcanic rocks from throughout the sodic alteration envelope, (a) potassium feldspar phenocryst in the process of being altered to albite showing early stages of chessboard-style twinning (mag. = 2.5x, cpl), (b) recrystallized phenocryst with individual grains showing chessboard-style twinning suggesting they are altered potassium feldspar grains (mag. = 5x, cpl), (c) large, recrystallized potassium feldspar phenocryst altered to albite, showing chessboard-style twinning (mag. = 2.5x, cpl), (d) chessboard-style twinning in altered albite grain (mag. = 2.5x, cpl), (e) primary albite phenocryst that has an inner core strongly altered to sericite (mag. = 2.5x, cpl), and (f) large recrystallized phenocryst showing chessboard-style twinning indicating it has been altered to albite (mag. = 2.5x, cpl). ....6-67

**Plate 6.3:** Petrographic sections of FP felsic volcanic rocks from throughout the sodic alteration envelope and mineralized zone, (a) primary brown biotite within unaltered FP rock (mag. = 5x, ppl), (b) blue sodic amphibole as a pseudomorph of primary biotite within the sodic envelope (mag. = 5x, ppl), (c) large, grass-green sodic amphibole grain with distinct cleavage as a pseudomorph of original elongated mafic grain (mag. = 5x, ppl), (d) secondary, fine-grained grass-green sodic amphibole grains (mag. = 5x, ppl), (e) secondary, equant, fine-grained sodic amphibole grains (mag. = 5x, cpl), and (f) opaque grains surrounded by fine-grained aggregates of sodic pyroxene, individual grains are not elongated but the mineral agglomerate is elongated suggesting that these grains altered from a primary mafic mineral (mag. = 5x, cpl). .....6-68

**Plate 6.4:** Petrographic sections of FP felsic volcanic rocks, (a) very fine-grained magnetite within the quartz-feldspar matrix of an unaltered FP unit (mag. = 10x, ppl), (b) larger grain of magnetite in unaltered FP associated with biotite and hornblende (mag. = 5x, ppl), (c) magnetite (darker grey) grain oxidizing to hematite (lighter grain) within the mineralized zone (mag. = 10x, rfl), (d) mineral aggregate within the mineralized zone containing abundant hematite (light grey) (mag. = 5x, rfl), (e) multiple sodic amphibole grains within the matrix in the mineralized zone, dissolution of individual quartz grains within the matrix left the rock like a sponge creating open space for alteration minerals to form (mag. = 5x, ppl), and (f) agglomerate of secondary alteration minerals taking the shape of a quartz phenocryst, space most likely created from the dissolution the quartz phenocrysts and then filled with alteration minerals (mag. = 5x, cpl). .....6-69

## **Chapter 1     Introduction**

### **1.1     Preamble**

The dramatic rise in the price for uranium during the mid-2000's breathed new life into a commodity that was for a long time considered an unfavorable target for exploration. This price increase, brought on by a new found global demand for cheaper and cleaner electricity sparked a global uranium exploration renaissance, bringing uranium exploration to the forefront for the first time since the late 1970's. Uranium became a major exploration target; nowhere was this more evident than in the Central Mineral Belt (CMB) of Labrador, Canada, where from 2004 to 2009 (peaking in 2007), uranium exploration occurred at a torrid pace.

Uranium in the CMB was initially discovered in the early 1950's and the 2004-2009 exploration efforts in the CMB focused mainly on these earlier discoveries, of which the Michelin deposit, discovered in 1968, was the largest. Originally worked by BRINEX in the late 1960's and 1970's, the Michelin deposit had an estimated resource of 7,458,800 tons grading 2.6 lbs./ton of  $U_3O_8$  (BRINEX, 1979a) and was at a mine planning stage until uranium prices dropped in the early 1980's. During the uranium boom of the mid 2000's, Aurora Energy Resources conducted extensive work on the Michelin deposit which resulted in new discoveries and more than tripling the total reserves to the present-day measured, indicated and inferred resource of 103.22 million pounds of  $U_3O_8$  (Hertel *et al.*, 2009). The Michelin deposit is once more being evaluated for potential mine start-up.

Despite the extensive research and development over the past five decades, there are many unanswered geological questions concerning the deposit. Answers to these questions will be of great importance in optimizing mineral development and further exploration on both the deposit itself and similar regions in the uranium-rich CMB. Uranium mineralization at Michelin most likely developed as a result of widespread uranium stripping from Aillik Group felsic volcanic host rocks, but this connection has yet to be definitely proven and the reasons for uranium concentration at specific sites such as Michelin remain unknown. Other aspects that are of particular importance include definition of the geological setting, the style and extent of alteration and the timing of deformation and mineralization.

This M.Sc. thesis was initiated by Aurora Energy Resources and Memorial University of Newfoundland to document the basic geological context of the Michelin deposit in an attempt to explain some of the above unanswered questions. In this regard, the study will focus on four main aspects with respect to the deposit; host rock lithology, mineralization, alteration and geochronology.

## **1.2 Location and Access**

The Michelin uranium deposit is located in the Kaipokok Bay region of eastern Labrador approximately 140 km northeast of the town of Happy Valley – Goose Bay and 30 km southwest of the coastal community of Postville, the nearest community to the deposit (Figure 1.1). The approximate center of the deposit is at UTM coordinates

307036 E, 6052470 N in UTM Zone 21, North American Datum 83 projection for Canada.

The project is in an isolated area with no road infrastructure. Access to the project area is best gained via the town of Postville which hosts sufficient amenities necessary to support field personnel, including a permanent fixed-wing gravel airstrip. Passenger service flights by both Air Labrador and Innu Mikun airlines, based out of Happy Valley – Goose Bay, operate on a daily, year round schedule. A coastal supply ferry service also operates a bi-weekly northern route to Postville during ice-free periods (June to October). The preferred mode of transport for personnel and supplies from Postville to the field area, however, is by helicopter. Float planes can be utilized during the summer and fall. Witch Doctor Lake located 5 km from the deposit provides a suitable landing location. During the winter months an ice airstrip at Ranjan Lake makes landing at the deposit possible.

Access throughout the project area is best suited to foot traversing as there are no ATV trails and the terrain is too rough to permit ATV access, however, during winter months it is possible to travel by snowmobile throughout the project area. A forty plus person exploration camp located on the northern edge of Ranjan Lake provides year round accommodations and facilities suitable for office space, core logging, core sampling and core storage (Plate 1.2).



### **1.3 Physiography**

The area surrounding the Michelin deposit is defined by mostly low topography averaging 334 m above sea level. The terrain consists of low lying parallel ridges trending towards the northeast. These ridges flank lower lying valleys comprised of bogs and marshes with many small streams and lakes, including Ranjan Lake which is situated over the deposit, just to the southeast of the surface exposure of the deposit (Plate 1.1). Elevation towards the northeast rises gradually to approximately 400 m above sea level; then quickly drops off to about 300 m. Till overburden which varies in thickness from 5 to 20 m is quite extensive, particularly within the valleys surrounding the low lying ridges. It consists mostly of sub-rounded to sub-angular boulders, ranging in diameter from 20 cm to 4 m in a loose soil and gravel matrix. Outcrop exposure in the area is generally poor with the majority of outcrops exposed along the low lying ridges. Along the ridges, outcrop can be accessed by removing small layers of moss and gravel, whereas in the valleys, outcrop is almost impossible to expose.

The area was heavily affected by glaciation during the last ice age, drastically changing and transforming the landscape. . According to Batterson and Liverman (2000), ice flow direction in the area was towards the northeast. Evidence for this direction is provided by radiometric surveys which indicate that mineralized uranium boulders are distributed away from the deposit in a clearly defined boulder train towards the northeast. Glaciation over the area left a thick layer of glacial till which includes an excessive amount of rounded boulders.

Vegetation in the area is typical of a sub-arctic climate of the north-eastern Canadian Shield and consists of sparse strands of black spruce with minor balsam fir, birch and tamarack. Trees are predominantly located along the small ridges and along the edges of bogs and marshes. In the valleys and bogs, vegetation consists of alders and small shrubs as well as grass and moss.

## **1.4 Work History**

### **1.4.1 Industry**

The Michelin uranium deposit was discovered by the British Newfoundland Exploration Limited (BRINEX) in 1968 when prospector Leslie Michelin identified the bedrock source for airborne radiometric anomalies identified the previous year (Booth *et al.*, 1979). Throughout the next 13 years BRINEX conducted several exploration campaigns on the deposit focusing on surface sampling and drilling, underground sampling and drilling, and several metallurgical, engineering, environmental and feasibility studies. By 1980 BRINEX had defined an indicated and inferred reserve of 7,458,800 tons grading 2.6 lbs./ton of  $U_3O_8$ , equivalent to almost 20 million lbs.  $U_3O_8$  (BRINEX, 1979a).

Minimal work was conducted on the deposit until the mid-2000's when Aurora Energy Resources (Aurora) began drilling the deposit to test the historic results and to extend the known zones of mineralization (Wilton and Cunningham-Dunlop, 2006). Aurora was successful in discovering new areas of mineralization at depth and by 2009 had over quadrupled the historic resource. As of 2009 the Michelin deposit has a

measured resource of 34,080,000 lbs.  $U_3O_8$  and an indicated and inferred resource of 72,910,000 lbs.  $U_3O_8$  (Hertel *et al.*, 2009). A more comprehensive review of the historic work conducted by BRINEX and Aurora on the Michelin deposit can be found in Appendix 5.

#### **1.4.2 Government and Academic**

The Michelin deposit and surrounding area have been included in a limited number of government and academic studies since its discovery. These studies when added to the wealth of information collected by exploration companies provide a fairly detailed knowledge base in all aspects of the deposit and its surrounding area. In the mid-1970's the provincial Department of Natural Resources conducted a mapping campaign throughout the CMB. During this mapping program, rocks surrounding the deposit were described as feldspar and quartz-feldspar porphyritic, rhyolitic ash-flow tuff, welded and non-welded; minor non-porphyritic rhyolitic ash-flow tuff and tuffaceous sandstone and siltstone; as well as minor basic flows and tuffs (Bailey, 1978; Bailey, 1979).

During the 1980's, the Michelin area was included in a regional mapping program of the entire CMB, undertaken by the Department of Mines and Energy at a scale of 1:100,000. They identified rocks within the Michelin area as ash-flow and ash-fall tuffs displaying crystal and lithic components, plus a range of quartz/feldspar phenocryst ratios and grain sizes as well as some indication of variation on the degree of welding or porosity (Gower *et al.*, 1982).

In 2005, a detailed lake sediment and water survey sampling program was conducted by the Newfoundland and Labrador Department of Natural Resources. They collected 809 lake sediment samples which were analyzed for 50 elements and 747 water samples which were tested for pH, conductivity and 25 elements, including uranium, copper, nickel and zinc (McConnell and Ricketts, 2008). The results of this survey clearly indicated that some of the higher uranium anomalies were concentrated near the Michelin deposit.

Minatidis (1976) completed a comparative study of trace element geochemistry and mineralogy of eight separate uranium showings in the region, including the Michelin deposit. Rock samples were analyzed for Zr, Sr, Rb, Zn, Cu, Ba, Ni, Cr, U and Th and thin sections were examined under petrographic microscope and auto-radiographed. For the Michelin deposit samples, Minatidis (1976) concluded that mineralized rocks are characterized by higher contents of hornblende, sodic amphibole, zircon, aegirine-augite, biotite, hematite, stilpnomelane and minor calcite. He also noted that the main radioactive mineral appeared to be davidite rimmed by sphene which occurred within feldspar porphyroblasts and associated with the amphiboles. Furthermore, based on the mineralogical assemblage of the Michelin deposit (sodic, amphiboles and pyroxenes and albite) and the presence of carbonatites in the vicinity of Makkovik he suggested that fenitization may have taken place. He also correlated elevated uranium values with higher contents of sodic amphibole and K-feldspar, and interpreted the quartzo-feldspathic host rocks associated with mineralization to be clastic sedimentary rocks.

Gandhi (1978) described the geological setting and genetic aspects of the Kitts and Michelin deposits as well as associated showings previously worked on by BRINEX. He postulated that uranium mineralization was contemporaneous with the syn-volcanic alkali metasomatism of the host rocks and that uranium precipitated as a titanium-bearing mineral (pitchblende) intergrown with sphene.

Evans (1980) completed a detailed study on the geology and petrochemistry of the Kitts and Michelin uranium deposits. He described the Michelin deposit as a series of tabular zones containing disseminated pitchblende mineralization within porphyritic rhyolite ash-flow tuffs. The rhyolites were potassic ( $K_2O \sim 5.39$  wt. % &  $Na_2O \sim 4.29$  wt. %) but become sodium-enriched ( $Na_2O > 7.28$  wt. %) and potassium-depleted ( $K_2O < 0.20$  wt. %) in the ore zone, as well as oxidized, due to alteration by the ore-forming fluid. In addition, altered rhyolites exhibited anomalous Zr contents. He noted two alteration facies of soda-enriched rhyolite distinguishable by their mineralogies, major element ( $Na_2O$ ,  $K_2O$ ,  $SiO_2$ ,  $Al_2O_3$ ) and trace element (U, Zr) concentrations, along with diagnostic ratios such as  $Fe^{3+} / (Fe^{2+} + Fe^{3+})$  and  $Na_2O / (Na_2O + K_2O)$ . Evans (1980) suggested that the deposits formed via a diagenetic - hydrothermal mechanism involving the leaching of uranium from uranium-enriched rhyolite source rocks by neutral to weakly alkaline, oxidizing groundwaters (meteoric and/or connate marine) under low temperature conditions. Uranium was transported as uranyl carbonate and/or hydroxyl complexes at ppb level concentrations along permeable unwelded felsic tuff layers within the Michelin belt and uranium precipitation was controlled by chemical reduction onto Fe-Ti-Mn oxides.

In 2006, Aurora Energy Resources Inc. sent 156 drill core samples from the deposit to Panterra Geoservices Inc. for petrographic study. The samples were collected from ten different drill holes along four cross-sections through the deposit. The polished sections were viewed on a standard petrographic microscope in transmitted and reflected light. Twelve samples were also examined on a Philips XL30 scanning electron microscope (SEM) to confirm mineral compositions (Ross, 2006). Although the sample suite was primarily from around the mineralized zone, the study confirmed that uranium mineralization occurs within intense sodic alteration that consists dominantly of the albitization of fine to coarse grain felsic porphyritic rocks (Ross, 2006). The study also indicated that there is nothing texturally or mineralogically distinctive between the mineralized and unmineralized sodic assemblages.

## **1.5 Purpose of Study**

Over the past several years Aurora Energy Resources has carried out extensive exploration work on the Michelin deposit and in doing so, has increased their reserves by almost triple over the 1980's resource estimates of BRINEX. The deposit has been extended a further 500 m at depth, exposing a central area which zones out in all directions and contains the thickest sequence of mineralization and alteration (Figure 1.2). An excellent three dimensional perspective of the geology, alteration assemblage and mineralizing style is now obtainable due to the large number of drill holes piercing the deposit. Despite this, there are still numerous, geological questions which must be addressed before successful mine development is achieved and ongoing exploration for

new reserves can become more focused and cost effective. In general, more information is required to accurately characterize deposit lithologies, styles and extent of alteration, and deposit mineralogy. A detailed examination addressing the above aspects would permit a better understanding of the nature and form of uranium mineralization at the Michelin deposit and more importantly, potentially identify advanced exploration techniques for use within the deposit and throughout the Central Mineral Belt.

It is with this premise that the author undertook this study as an investigation into the Michelin deposit. This research is an attempt to answer some of the unanswered geological questions posed above and as a means to derive and build a mineralogical and geochemical database for the deposit. In order to achieve these objectives, the focus will center on four main objectives: geology, mineralization, alteration, and geochronology. Insights into each will help provide answers to some of the geological questions which need to be addressed in order to achieve successful mine development, operation and continued exploration into the future.

The first objective will be to accurately characterize and define the primary unaltered and unmineralized lithological units comprising the Michelin deposit. Once this baseline data has been assembled, it should become possible to distinguish the type and degree of alteration and mineralization associated with the deposit. Drill core and field samples will be evaluated and described in detail, thereby providing insight into contact relationships, textures, deformation history and mineralogy. Petrographic thin sections are also be used to identify mineralogy and mineral relationships. In addition, major, trace and rare earth element geochemical data will be used to characterize each rock type.

The second objective is to characterize the ore zone and uranium mineralization. This will involve: a) characterizing the lithological units which comprise the ore zone, focusing on those which are host to uranium mineralization, b) defining the areas and mineral assemblages associated with the uranium mineralization and finally, c) identifying the uranium-bearing mineral species and their relationships with the host rock. Determining each of the above would provide insight into understanding the timing of mineralization, source of the mineralization and the relationship of mineralization to alteration. To achieve this, drill core and hand samples will be examined with the aim to identify contact relationships, textures, mineralization, deformation histories and mineralogy. Petrographic thin sections are also utilized to identify mineralogy and mineral relationships. Major, trace and rare earth element geochemistry will be used to characterize and classify rock types and mineralization. Finally, the Scanning Electron Microprobe (SEM) and Mineral Liberation Analyzer (MLA) is used to scan and map out thin sections at the micron level to identify mineral locations and relationships, as well as elemental compositions within individual microscopic grains, in particular the uranium bearing minerals.

The third objective is to document and characterize the several styles of alteration and extent of this alteration throughout the deposit. Doing so should provide a framework for future exploration at the Michelin deposit and be an excellent exploration tool within the Aillik Group. This will be achieved through examination of drill core and hand samples, noting both the physical and textural changes in the rock due to alteration, and examining the mineralogy of the altered rocks. Petrographic thin sections are used to



determine alteration mineralogy and which mineral grains being altered. Major, trace and rare earth element geochemistry is used to define geochemical changes that result due to each type of alteration. Finally, thin section samples are analyzed with the SEM-MLA to define and characterize the alteration minerals and their relationships with one another.

Finally, a select number of samples from different lithological units will be analyzed to determine their geochronology. This is done to obtain ages for the various lithologies which can then be possibly used to determine timing of emplacement and overall age of mineralization. If a mineralization age is known, it can be related to a specific deformational event throughout the CMB and could possibly be used as a tool for mineral exploration. Selected samples will be scanned with the SEM to locate zircons. Images and coordinates for these zircons will then be collected to use for Laser Ablation Inductively Coupled Plasma Mass Spectrometry (LA-ICP-MS). The LA-ICP-MS process will determine isotopic concentrations of the uranium-lead decay series and should provide an accurate age date for the zircons.

## **1.6 Methods of Study**

In order to achieve the objectives outlined for this study a total of 10 drill holes were selected. When plotted on a longitudinal section these holes create a three-dimensional cross-section through the center of the ore deposit (Figure 1.3). The longitudinal section portrays the ore zone as a single composite zone and is contoured based on ore zone grade multiplied by overall ore zone thickness. This cross-section allows for an accurate view of the geology throughout the deposit, mineralization within

the ore zone and alteration trends both within the ore zone and extending outward from the ore zone.

The ten drill holes: M06-010, M06-016, M06-019, M06-020A, M06-021, M06-024, M06-025, M06-026, M06-027 and M06-039 were examined by the author during the 2007 field season and then systematically sampled from top to bottom, the Aurora drill logs for each of these 10 holes can be found in Appendix 4. Samples were selected to best represent a) the different lithologies present throughout the hanging wall, foot wall, and ore zone; b) the mineralized and unmineralized zones from within the ore zone; and c) alteration, to track alteration changes throughout the deposit. Sample spacing was approximately every 50 m down-hole, except M06-019, which was sampled in more detail at a 15-25 m interval. A tighter spacing was necessary in order to better define and track alteration trends throughout the deposit. Basic information for these samples can be found in Appendix 1.

In total, 208 samples were collected from the ten drill holes. These samples were split onsite with a manual core splitter and sent to Activation Laboratories (Actlabs) in Ancaster, Ontario. The samples were analyzed using Actlabs 4lithores Fusion ICP and ICP-MS analysis. Along with these samples, a further 57 samples that were collected from these ten drill holes by Dr. Derek Wilton during a field visit to the Michelin site in summer 2006 were also included. These samples were subjected to the same Actlabs geochemical package as that utilized for this study. See Appendix 2 for information regarding the 4lithores Fusion ICP and ICP-MS analysis; the accuracy and precision of

certified reference material conducted by Actlabs, and the raw geochemical data for the 209 samples collected during the study.

Before the geochemical data could be used for this study it had to be properly organized and recalculated to volatile free. The geochemical analysis provided by Actlabs gave a value for loss on ignition (LOI) for each sample. LOI is a measure of the weight of the sample that is lost when it is heated up to 1,000 degrees C. This loss is due to a number of factors, including volatiles such as H<sub>2</sub>O, CO<sub>2</sub>, hydroxyl ions, or organic material being burned off (Best and Christiansen, 2001). Since the LOI makes up a percentage of the total, then the major oxides are not presented as their actual percentage, but as a percentage with the total, taking into account the LOI amount. In order to find the LOI free value for the oxides they need to be re-calculated to an anhydrous state. To perform this calculation, the major oxide percent is multiplied by 100 and divided by the total percentage of the sample minus the LOI amount for that sample.

Elements that analyzed below their respective detection limits were given a value equal to half of the lower limit of detection for that element. Elements were then arranged into groups based on similar characteristics. These groups included the major oxides - SiO<sub>2</sub>, Al<sub>2</sub>O<sub>3</sub>, Fe<sub>2</sub>O<sub>3</sub>, MgO, MnO, CaO, Na<sub>2</sub>O, K<sub>2</sub>O, TiO<sub>2</sub> and P<sub>2</sub>O<sub>5</sub>; the transition elements - Co, Cr, Cu, Ni, Sc, V and Zn; the low field strength elements - Ba, Cs, Ga, Rb, Sr, Pb, Th and U; the high field strength elements Hf, Nb, Ta, Y and Zr; the rare earth elements - La, Ce, Pr, Nd, Sm, Eu, Gd, Tb, Dy, Ho, Er, Tm, Yb and Lu; and finally the volatile elements - Ag, As, Be, Bi, Ge, In, Mo, Sb, Sn, Tl, and W.

Along with the geochemical samples collected from the ten drill holes, a small representative 10.0 – 15.0 cm sample of core was also collected, from which a piece was sent to Vancouver Petrographics and turned into a polished thin section. The remaining piece of core was saved for reference. A total of 238 polished thin sections were prepared for this study, along with an additional 57 provided by Dr. Wilton from the 2006 study. Basic information for the polished thin sections can be found in Appendix 1.

In order to achieve some of the objectives outlined in section 1.5, a select number of samples were analyzed with the scanning electron microprobe (SEM) – mineral liberation analyzer (MLA), thereby ensuring an automated, accurate and qualitative analysis of the samples. Samples representative of mineralization and alteration were analyzed as well as samples set aside for age dating analysis. The samples were then analyzed at the INCO Innovation Center, St. John's, Newfoundland on a FEI Quanta 400 environmental SEM equipped with a Bruker XFlash Energy Dispersive X-Ray (EDX) Detector. The SEM and EDX can correctly identify the mineral phases and determine their absolute abundances, while the MLA software allows for quantitative evaluation of the abundance, association, size and shape of minerals within the thin section (Wilton and Winter, 2012). When the SEM is in back-scatter electron (BSE) mode, the image portrays minerals in grey-scale where a mineral that contains denser elements portrays a brighter image and vice versa. The MLA detects mineral particles in a thin section based on variations in BSE grey scale and then analyses each particle with the EDX. The MLA then compares the elemental spectra for a particle with a library of mineral spectra to identify the mineral phase (Wilton and Winter, 2012). The EDX component of the SEM

provides an elemental spectrum for each phase that the MLA software identifies. The spectra indicate what elements are present in the mineral and their relative concentration. Real time EDX analysis of a mineral grain is possible

Most of the thin sections used for this study were only mapped for denser minerals such as zircons and uranium bearing phases. A threshold was set with the BSE imagery so that less dense phases such as quartz and feldspar would not be scanned. This allowed for a quick and accurate scan of a thin section to identify zircon grains, which would later be used for age dating analysis; uranium bearing minerals; and denser minerals related to alteration and associated with mineralization. A select number of thin sections were scanned in their entirety, with no BSE threshold set for both the lighter and denser minerals. This was done to identify alteration changes, to see what minerals are being altered and the different intensities of alteration.

A total of six petrographic thin sections, representing various lithological units throughout the deposit, including units from within the ore zone were selected for in situ uranium-lead zircon geochronology using Laser Ablation Inductively Coupled Plasma Mass Spectrometry (LA-ICP-MS). The samples were analyzed at the INCO Innovation Centre, St. John's, Newfoundland using a Finnigan Neptune multicollector and ELEMENT-XR single collector magnetic sector ICP-MS instrument coupled to a GeoLas deep-UV (193 nm) argon-fluorine excimer laser ablation system to provide high-resolution isotope analysis for in situ minerals. Uranium isotopes  $^{235}\text{U}$  and  $^{238}\text{U}$  and lead isotopes  $^{204}\text{Pb}$ ,  $^{206}\text{Pb}$ , and  $^{207}\text{Pb}$  are measured and used for uranium-lead geochronology (Bouman *et al.*, 2014).

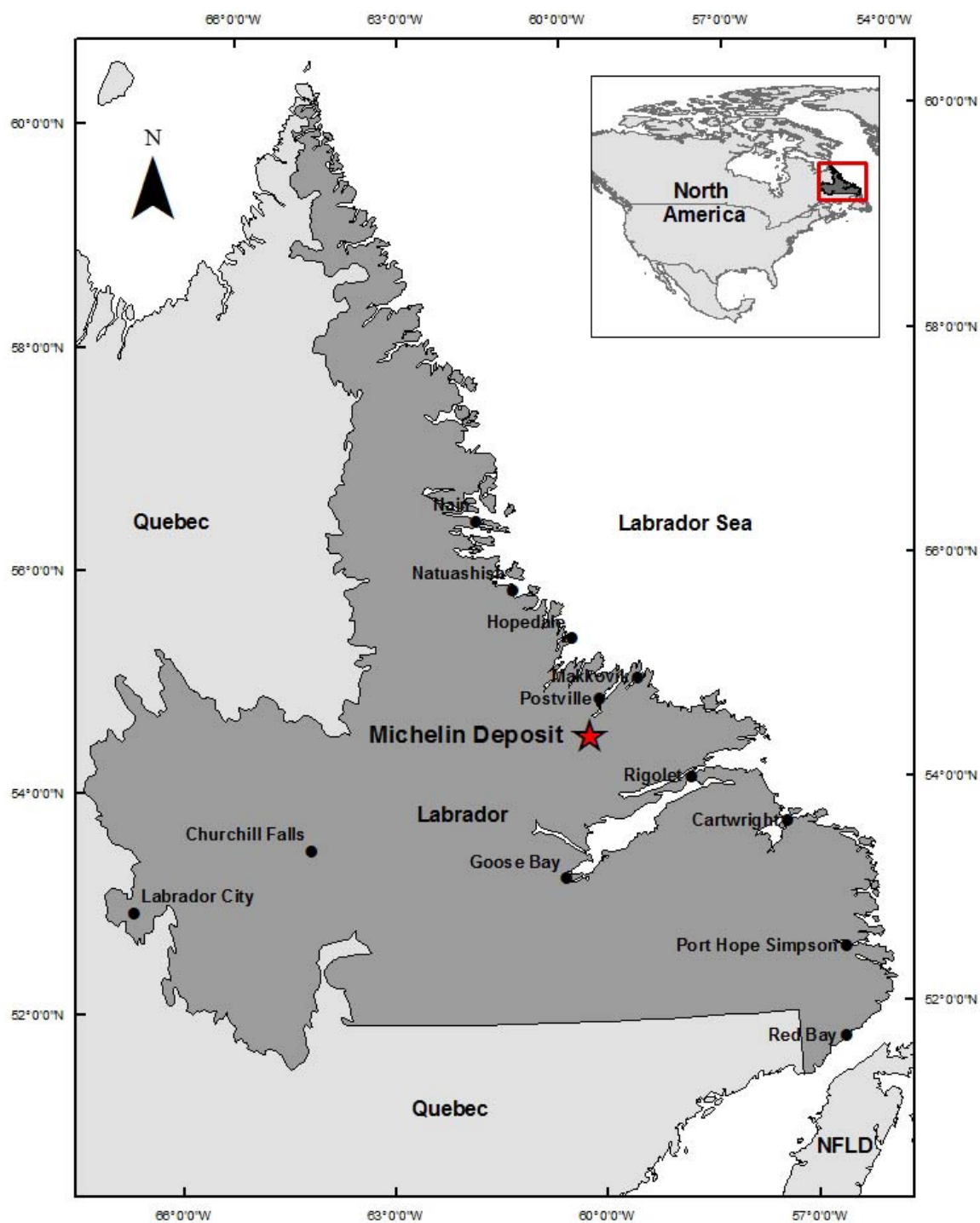


**Figure 1.1:** Location of the Michelin deposit with reference to the major communities within Labrador.

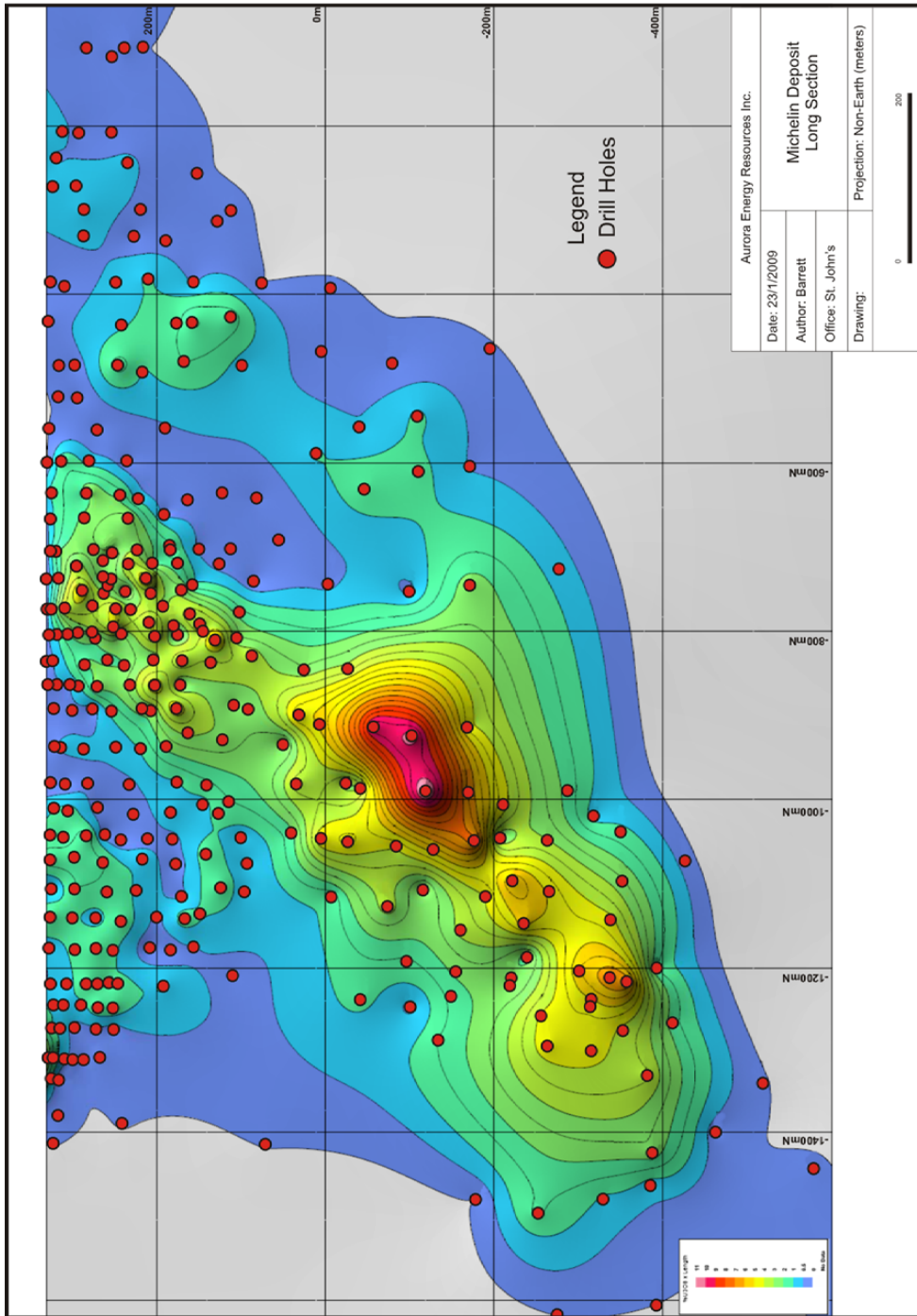


**Figure 1.2:** Longitudinal section through the Michelin deposit showing Grade x Thickness contours. Grade and thickness are based on the %  $U_3O_8$  and true thickness of the mineralized intercept for each drill hole. Blue areas represent lower grade x thickness and red colors represent a greater grade x thickness (Hertel *et al.*, 2009).

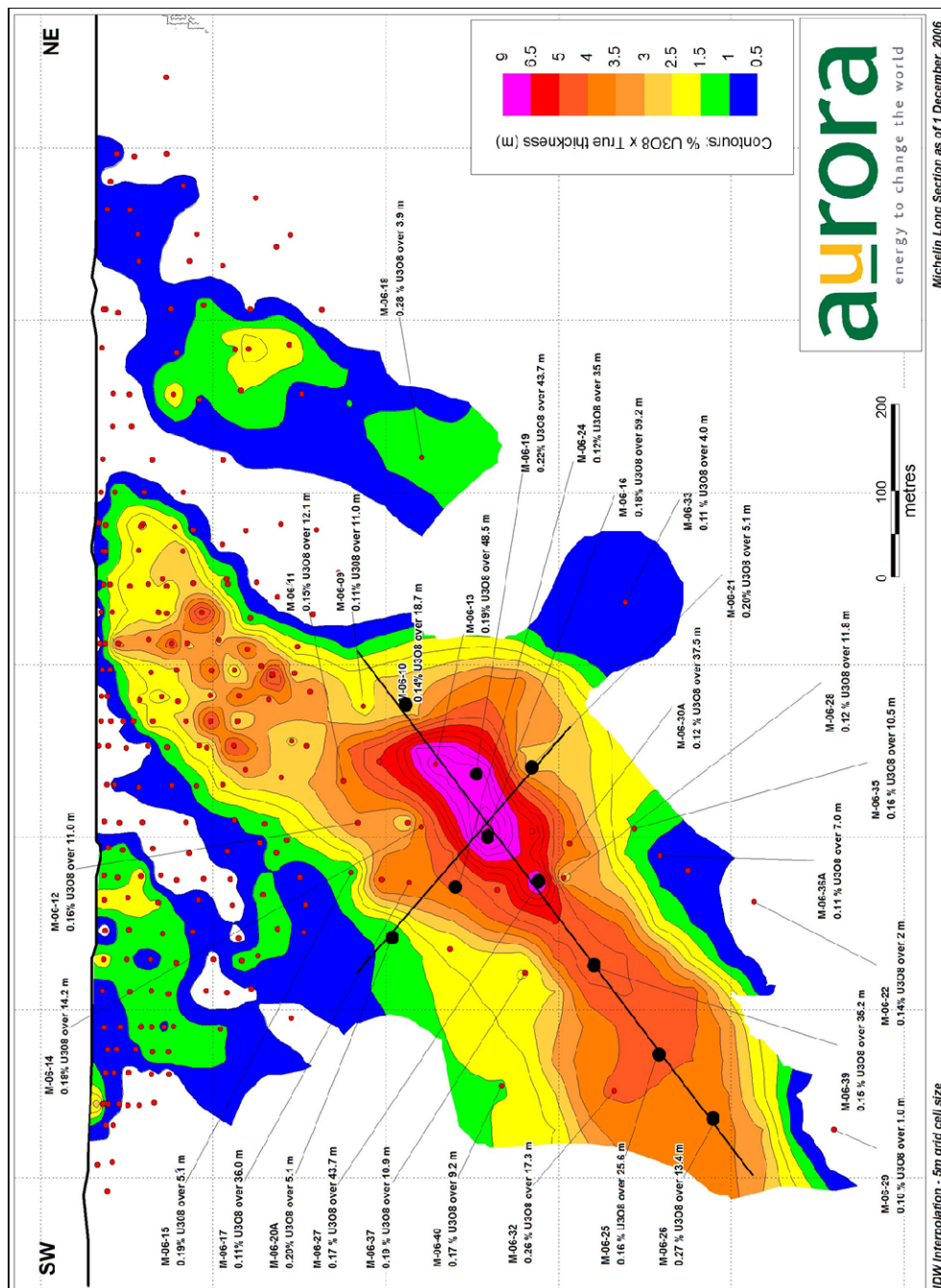


**Figure 1.3:** Longitudinal section of the Michelin deposit showing the location of the 10 drill holes used for this study. These 10 drill holes create a three-dimensional cross-section through the largest part of the Michelin deposit (modified from Cunningham-Dunlop and Giroux, 2007).





**Plate 1.1:** Aerial view of the Michelin area, centered on Ranjan Lake, view towards the southwest. Typical physiography of the area - consisting of small lakes, streams and bogs in lower areas and spruce covered higher areas. The Michelin deposit outcrops in the far right of the picture.



**Plate 1.2:** Aerial view of the Michelin Camp, located at the northeastern end of Ranjan Lake, view towards the southeast. The Michelin deposit outcrops in the lower-right of the picture.

## **Chapter 2    Overview of Uranium Deposits**

### **2.1    Introduction**

Through the 20<sup>th</sup> century uranium progressed from being an element of relative obscurity, with unique radioactive properties, to a major sought-after commodity. Presently utilized as a nuclear fuel and in nuclear medicine, the element was mainly viewed as the source for nuclear weapons.

This chapter will briefly examine the element and its properties. Those properties which are unique to uranium enable it to be concentrated in a wide variety of geological settings forming several different deposit types. In this regard world deposit types will also be examined. Finally, uranium mineralization as it relates to Labrador will be discussed. This will include a focus on the regional setting of Labrador's Central Mineral Belt (CMB), the styles of mineralization and possible deposit types.

### **2.2    Important Uranium Properties**

Uranium (atomic number 92) is an extremely dense, silvery-grey metal of the Actinide series (Ewing, 1999). It is a radioactive element that has three main naturally occurring isotopes ( $^{234}\text{U}$ ,  $^{235}\text{U}$ , and  $^{238}\text{U}$ ), of which  $^{238}\text{U}$  is the most abundant at 99.3 %, and most stable with a half-life of  $4.46 \times 10^9$  years (Cuney and Kyser, 2008). It is a lithophile element with an average crustal abundance of 2-4 ppm (Marmont, 1987). Although present in nearly all rock types, due to its strongly incompatible nature uranium concentrations differ widely from one rock type to another. Mafic rocks have an average

uranium abundance of 0.1-0.6 ppm, intermediate rocks average around 0.8 ppm, whereas felsic rocks typically contain 5 ppm and alkaline magmas contain 10 ppm (Robb, 2005). Due to its large ionic radius and high electrostatic charge, uranium is not easily accommodated in lattices of common rock forming minerals. Therefore, within any fractionating magma, uranium will concentrate in the residual melt until very late in the crystallization process. Eventually uranium minerals do crystallize or the uranium becomes incorporated within the crystal structure of accessory minerals, such as thorite, zircon, monazite, apatite and sphene. For this reason, higher concentrations of uranium, up to 15 ppm are associated with late magmatic differentiates such as granitic pegmatitic rocks (Misra, 2000).

Uranium has several valence states but only two are naturally dominant; the quadrivalent uranous ion  $U^{4+}$  and the hexavalent uranyl ion  $U^{6+}$  (Robb, 2005). The uranous ion, the reduced species, is characterized by very low solubilities in aqueous solutions, hence most fluid related transport takes place as the oxidized species  $U^{6+}$  (Robb, 2005; Burns, 1999). In aqueous solutions,  $U^{4+}$  is readily oxidized to  $(U^{6+}O_2)^{2+}$  which commonly forms stable complexes with hydroxyl, carbonate, fluoride, chloride, sulphate and phosphate ions (Misra, 2000). In other words, uranium exhibits extreme mobility in oxidizing fluids.

In most deposits of uranium, primary uranium minerals such as uraninite and coffinite occur in the uranous state. According to Minatidis (1976), the stability of  $U^{4+}O_2$  accounts for the preponderance of uraninite as the primary ore mineral. As uranous complexes are less soluble than uranyl complexes, accumulation of uranous minerals is

attributed either to transport as detrital particles in reducing atmospheres of the early Archean or to the reduction of uranyl complexes at the site of deposition (Misra, 2000).

There are well over 200 minerals that contain uranium and according to Misra (2000), around 135 of these mineral species contain uranium as the essential constituent and another 25 contain the element as a major though non-essential constituent. Uranium minerals are divided into two categories: primary and secondary minerals. Primary uranium minerals generally occur in the unoxidized state and make up only a handful of minerals; however these comprise the bulk of the uranium ore in uranium deposits. They consist of uraninite  $[\text{UO}_2]$ , brannerite  $[(\text{U,Ca,Ce})(\text{Ti,Fe})_2\text{O}_6]$ , coffinite  $[\text{U}(\text{SiO}_4)_{1-x}(\text{OH})_{4x}]$ , and uranothorite  $[(\text{Th,U})\text{SiO}_4]$ . The most abundant mineral is the poorly crystalline variety of uraninite, termed pitchblende. This mineral does not contain thorium (Th) or Rare Earth Elements (REE) and typically exhibits a botryoidal or colloform texture intergrown with gangue minerals, giving it a somewhat pitchy luster. Secondary minerals generally occur in the oxidized state, forming from the weathering of primary uranium minerals. There are numerous secondary minerals with the most common being uranophane  $[\text{Ca}(\text{UO}_2)_2\text{Si}_2\text{O}_7 \cdot 6\text{H}_2\text{O}]$ , autunite  $[\text{Ca}(\text{UO}_2)_4(\text{PO}_4)_2 \cdot 10-12\text{H}_2\text{O}]$ , carnotite  $[\text{K}_2(\text{UO}_2)_2(\text{VO}_4)_2 \cdot 3\text{H}_2\text{O}]$  and tyuyamunite  $[\text{Ca}(\text{UO}_2)_2(\text{VO}_4)_2 \cdot 5-8\text{H}_2\text{O}]$ . They manifest themselves as brightly colored stains and although being of limited economic significance they often serve as field indicators for primary uranium mineralization (Misra, 2000).

Aside from industrial uses, uranium is commonly used for isotopic age dating. Since uranium is a radioactive element all three of its isotopes,  $^{238}\text{U}$ ,  $^{235}\text{U}$  and  $^{234}\text{U}$  decay

at a constant rate. Through a series of decay chains,  $^{238}\text{U}$  and  $^{235}\text{U}$  eventually decay into daughter isotopes  $^{206}\text{Pb}$  and  $^{207}\text{Pb}$ , respectively (McSween *et al.*, 2003). By measuring the chemical composition of each isotope and using the respective parental half-life, an age of the crystal can be determined.

## **2.3 Major Uranium Deposit Types**

### **2.3.1 Uranium Deposits**

Uranium deposits are quite diverse in terms of their host rocks, geologic setting, controls on mineralization, and genesis. The reasons for this have to do with the strong incompatibility of uranium in magmas, allowing it to easily accumulate in a residual melt; the high valence charge of  $\text{U}^{4+}$  allows it to substitute for  $\text{Th}^{4+}$ ,  $\text{Zr}^{4+}$ , REE, and in rare cases  $\text{Ca}^{2+}$ ; and the ability to easily oxidize to  $\text{U}^{6+}$ , form stable complexes which makes it extremely mobile, and the ease of being reduced back to the more stable  $\text{U}^{4+}$  ion to form concentrations of uranium bearing minerals.

As it is difficult to accurately define and characterize uranium mineral deposits, the deposits are generally grouped together into broad categories based on one or two similar identifying criteria. The most common global depositional settings include: Unconformity Related, Sandstone Hosted, Conglomerate, Vein Type, IOCG, Intrusive, Metamorphic Associated, Metasomatic, Volcanic Associated, Calcrete, Phosphate, and Black Shale. A selection of these deposit types which contain individual criteria or their depositional settings are similar, or potentially similar to uranium occurrences observed in Labrador, including the Michelin deposit, will be described in sections 2.3.2 to 2.3.7,

with further detail provided in Table 2.1. The remaining depositional settings will not be discussed as they are not closely associated with known Labrador occurrences.

### **2.3.2 Metasomatic Uranium Deposits**

Metasomatic uranium deposits or albitite-hosted deposits consist primarily of uranium mineralization associated with alkali metasomatism (Cuney and Kyser, 2008). Sodic (Na) -metasomatism is the predominant alteration mechanism in these deposits, where host rocks are altered to albite with the end result being the formation of albitite. Calcic and potassic metasomatism also occur, but these alteration types are rare or are late-stage to Na-metasomatism. These deposits are thought to form through high temperature (300 to 550 °C) hydrothermal processes, where Na-metasomatism selectively alters rock within structurally disturbed areas, resulting in discontinuous altered zones meters in width and potentially extending several hundred meters to several kilometers in length (Cuney and Kyser, 2008). Uranium is leached from the host rock by an alkaline-rich, oxidizing solution and transported through the deformed zone until conditions warrant precipitation of the uranium. Uranium precipitation is sporadic in the Na-metasomatized rock and therefore most of the altered rock remains totally barren. Areas that are concentrated in uranium mineralization require a mechanism to reduce the oxidized  $U^{6+}$  ions from solution and enough space to allow for the precipitation of uranium in concentrations large enough to be economically viable (Cuney and Kyser 2008; Cuney, 2010).

### **2.3.3 Intrusive Uranium Deposits**

Intrusive or granitic uranium deposits are economically viable concentrations of uranium associated with felsic plutonic to epizonal igneous bodies (Guilbert and Park, 1986). Concentration of uranium in these rocks is due to the fact that  $U^{4+}$  and  $U^{6+}$  ions are too large and too highly charged to participate in main-line silicate fractional crystallization, therefore they concentrate increasingly in late siliceous melts. Uranium concentrations in the melt steadily increase until they reach concentrations at which uranium minerals are able to crystallize by themselves or where uranium can partition into accessory minerals (Guilbert and Park, 1986). Mineralization typically occurs as disseminations within the differentiated granite but also occurs as small veins and veinlets in specific zones related to late crystallization (Guilbert and Park, 1986). S-type granites are the most uranium enriched granitoids and form by the anatectic melting of sedimentary rocks or continental crust, which tend to be rich sources of uranium, and tend to form a continuum with metamorphic complexes, migmatites and other evidences of partial melting of crustal rocks where mineralization is associated with high silica alaskites and pegmatites (Guilbert and Park, 1986). I-type granites are derived from an igneous source and are more oxidized than S-type granites. This would enhance enrichment of uranium mineralization in late stage pegmatites and veins (Ferguson, 1988). A-type granitic rocks are more anorogenic and are formed by the melting of a felsic granulite source which is the material remaining after the extraction of I-type melts. These are high temperature, vapour absent melts rich in high field strength elements as

well as potassium, thorium and uranium relative to I and S-type granites (Ferguson, 1988).

#### **2.3.4 Volcanic Associated Uranium Deposits**

Volcanic associated uranium deposits are a broad range of deposits which consist of disseminations or veins of uranium in volcanic rocks. This category excludes IOCG and vein deposits in which mineralization age is much younger than the age of the host rock (Gandhi and Bell, 1996). These deposits occur in felsic volcanic complexes occurring as calderas, lava and ash-flow fields, taphrogenic volcanic-sedimentary basins, domes and breccias that develop in late and post-orogenic settings, and extensional tectonic environments (Gandhi and Bell, 1996). Mineralization is thought to result from concentration of uranium metal by magmatic – hydrothermal fluids and/or meteoric waters circulating through uranium rich felsic volcanic host rocks. Ore precipitation occurs in areas of structural discordance related to the volcanic activity, for instance, in areas subjected to weak to moderately intense folding, brecciation or shearing. Resultant mineralization would manifest as stratabound disseminated deposits or as discordant veins and fracture fillings (Gandhi and Bell, 1996).

#### **2.3.5 Vein Type Uranium Deposits**

Uranium vein deposits are reported as concentrations of uranium mineralization in fractures, shear zones and stockworks (Ruzicka, 1996). Vein deposits are hosted in a wide variety of lithological units, however in terms of their geological setting can be



divided into three fundamental categories: intragranitic veins hosted by granitic or syenitic rocks, perigranitic veins hosted typically by metasedimentary and metavolcanic rocks surrounding granitic plutons, and structurally controlled veins in shear and fault zones unrelated to granitic plutons (Misra, 2000). Intragranitic veins typically develop in highly differentiated granitic rocks, for instance, two mica leucocratic granites that have been subjected to pre-mineralization sodic, potassic or carbonate alteration along with desilicification. The alteration fluids introduce uranium mineralization into fractures, faults, lineaments or other open spaces developed through dissolution of rock-forming minerals (Ruzicka, 1996). Perigranitic veins develop in similar fashion to intragranitic veins as fracture, fault and open space infills, however they form in country rocks peripheral to the granitic intrusions. Uranium may be sourced from the intrusion itself or from surrounding host rocks. Organic-rich black shales with elevated uranium contents constitute ideal depositional sites (Ruzicka, 1996). The final variety of uranium bearing veins occurs in mylonite or shear zones and fault zones where mineralization is present as narrow veinlets or irregularly distributed lenses of differing thickness. The uranium is sourced from the surrounding sedimentary and volcanic host rocks and mobilized during metamorphic, tectonic and igneous events. It is then redistributed by hydrothermal processes to form lenses, fracture fillings, stockworks and disseminations in the host rock (Ruzicka, 1996).

### **2.3.6 IOCG Deposits**

IOCG or Iron-Oxide Copper Gold systems are a class of shallow level hydrothermal deposits characterized by iron oxides, hematite and magnetite as the principal ore forming minerals along with copper and gold; uranium mineralization, typically as a by-product, may or may not be present (Misra, 2000). Deposits are found in a number of different tectonic settings such as rifts, subduction zones and areas undergoing basin collapse, and generally show a spatial relationship to major, crustal-scale fault zones. These deposits can occur in numerous lithologies but overall they are spatially and temporally associated with batholithic complexes of intermediate to felsic composition. It is unknown whether the deposits are directly related to these magmas or whether these intrusive bodies simply provide the thermal energy to drive the large-scale hydrothermal systems responsible for metal scavenging from surrounding host rocks (Hitzman and Valenta, 2005). The extent of uranium mineralization in these deposits varies and most of the deposits exhibit very low grades, however large tonnages ensure a high percentage of metal. The Olympic Dam deposit in southern Australia, currently the world's largest producer of uranium, contains an estimated resource of 1.2 million tons of ore with only an average grade of 0.06 %  $U_3O_8$  (Roberts, 1998).

### **2.3.7 Metamorphic Associated Uranium Deposits**

Metamorphic uranium deposits (aka ultra-metamorphic) form during high temperature, high level metamorphism, where high rank metamorphic rocks are in continuum with S-type felsic igneous material derived through the partial melting of the

host metamorphic rocks. These host rocks are thought to represent metamorphic volumes taken near the melting point, with local partial melting and auto-injection. During high temperature metamorphism of the proto-lithologies which are commonly sedimentary and/or volcanic rocks slightly enriched in uranium, the uranium becomes mobilized from sediments and volcanic rocks, forming oxides which concentrate to form irregular pods in the tectonic foliation and in bands roughly paralleling to original bedding (Guilbert and Park, 1986).

## **2.4 Uranium in Labrador**

According to the Newfoundland and Labrador Mineral Occurrence Database System (MODS), there are approximately 180 known uranium occurrences throughout Labrador (Newfoundland and Labrador Geological Survey, 2015), ranging from almost fully developed deposits to small indications (Figure 2.1). Although these occurrences are scattered throughout Labrador the vast majority of them are located within the Central Mineral Belt (CMB), particularly concentrated in the eastern portion of the belt (Figure 2.3). Outside of the CMB there are several minor indications, most important being in the Double Mer - Backway Area, north of Lake Melville, where uranium mineralization is contained within the melt fraction of highly migmatitic, metasedimentary gneisses; grades up to 0.02 %  $U_3O_8$  over a 1.6 m core interval have been noted (Wardle, 2005). Other notable occurrences include minor indications in pegmatitic bodies located throughout the Grenville Province; associated with granitoid rocks of the Nain Plutonic Suite and adjacent granitoid gneisses of the Churchill Province (Winter *et al.*, 2009);

associated with sandstone and black shale in the Mugford Group of the Nain Province (Wilton, 1994); and possible unconformity related mineralization within the Sims Formation in western Labrador (Wardle, 2005).

#### **2.4.1 Central Mineral Belt**

Labrador's Central Mineral Belt (Figure 2.2) is an approximately 260 by 75 km area stretching from the central interior to the east coast (Wilton, 1996). The region is defined by a combination of its geology, consisting of Proterozoic supracrustal sequences and associated basement and by its extensive and broad selection of mineralization. It contains abundant Cu, Mo and rare metals (Zr, Be, Nb & REE) mineralization along with almost all of the uranium mineralization known within Labrador, leading Beavan (1958) to declare the area an uranium metallogenic province. The CMB includes portions of the Archean Nain Province, the Paleoproterozoic Makkovik and Churchill Provinces and the Mesoproterozoic Grenville Province. The geology consists of the Archean aged Maggo gneiss, Weeks amphibolite, Florence Lake Group and the Kanairiktok intrusive suite which are overlain by six successive Proterozoic supracrustal sequences. These sequences are the Post Hill, Moran Lake, Aillik, Bruce River, Letitia Lake and Seal Lake groups which respectively range in age from ca. 2100 to 1225 Ma (Wilton, 1996).

#### **2.4.2 Classification History**

Due to the fact that uranium is extremely mobile coupled with the complex geology and deformational history of the CMB, uranium occurrences within the CMB

encompass a broad range of geological settings and rock types, occurring in all of the Proterozoic supracrustal sequences and basement rocks with the exception of the western Letitia Lake Group. Uranium occurrences form in a wide variety of deposit types, most being specific to the supracrustal group in which they occur. Often similar occurrences will form mineralized belts or zones where the style and geological setting of the occurrence is the same. The vast majority of uranium occurrences in the Central Mineral Belt occur in the eastern sequences of the Post Hill, Moran Lake, Aillik and Bruce River Groups as well as being associated with numerous felsic plutonic intrusions.

There have been many attempts to classify these deposits by numerous authors each one taking a different approach to classify the region. Gandhi (1978), Evans (1980), MacDougall (1988), and Wardle (2005) focused on the mineral occurrences within the Post Hill and Aillik Groups, formally the Lower and Upper Aillik Groups, respectively. Mineralization was classified into different districts or belts of similar geological setting and mineralizing styles. These included the Kitts-Post Hill belt, the Michelin-White Bear Mountain belt, the Aillik-Makkovik belt and the Round Pond zone. Wardle (2005) further classifies the Moran Lake belt, Melody Hill zone and Stormy Lake zone. Wilton (1996) breaks the CMB down into each one of its Proterozoic sequences and describes the uranium occurrences that occur within each sequence.

Beavan (1958), Ruzicka (1971), and Sparkes and Kerr (2008) classify the uranium occurrences into their respective deposit types. Beavan (1958) divided the uranium showings into four deposit styles 1) mineralization occurring in fracture and shear zones in volcanic rocks, 2) mineralization in sedimentary rocks, 3) mineralization

in fault zones, and 4) mineralization in granitic rocks. Ruzicka (1971) added a fifth type to include the Michelin deposit and other related occurrences 5) sedimentary-metamorphic type which is represented by disseminations.

Sparkes and Kerr (2008) do an excellent job reviewing all of the historic uranium occurrences and taking the newly discovered occurrences in the mid 2000's and classifying them into distinct deposit types. Here they recognize nine different mineralizing styles that fit into several different deposit styles throughout the CMB with the potential for a tenth being unconformity related. These include 1) mineralization without associated alteration in plutonic rocks, 2) mineralization associated with shearing and/or alteration in plutonic rocks, 3) disseminated or fracture-hosted mineralization in felsic volcanic rocks without associated deformation or metasomatism, 4) disseminations in felsic metavolcanic rocks associated with shear zones and wide spread metasomatism, 5) mineralization hosted in pelitic metasedimentary rocks 6) mineralization hosted in sandstones and conglomerates, 7) mineralization hosted by breccia zones in mafic volcanic rocks, 8) mineralization hosted in breccia zones in granitoid plutonic rocks, and 9) mineralization associated with hydrothermal veins. Below is a brief discussion of the main uranium occurrences and mineralizing styles within the CMB.

#### **2.4.3 Uranium Showings of the Kitts-Post Hill Belt**

The Kitts-Post Hill belt hosts significant uranium occurrences within pelitic metasedimentary rocks of the Post Hill Group (Sparkes and Kerr, 2008). Uranium occurrences can be traced along the length of the belt, which strikes for over 20 km, and

occurs almost parallel to the eastern shore of Kaipokok Bay. It contains the Kitts deposit in the north and other major showings, namely Kiwi, Inda, Nash and Gear towards the south (Figure 2.4). According to Wilton (1996) the Kitts deposit contains 1.36 million kg of  $U_3O_8$  with an average grade of 0.73 %  $U_3O_8$ . This style of mineralization is only found within the Kitts-Post Hill belt and not found anywhere else in the CMB.

Mineralization is hosted within pelitic metasedimentary rocks comprised of argillites and tuffs, associated with mafic pillow lava flows. Within the northern portion of the belt, which includes the Kitts deposit, mineralization is hosted within the argillites while in the central and southern portions of the belt mineralization is hosted within the tuffaceous sediments (Gandhi, 1978; Evans, 1980; Wilton, 1996). Most of the mineralization is structurally controlled and is concentrated along certain thin beds and laminae within argillite where it occurs in thin, discordant to concordant veinlets and shears, as well as fracture coatings and as disseminations (Gandhi, 1978; Evans, 1980). According to Gandhi (1978) mineralization is within a complexly folded area and the ore zone and host argillite is thickened due to folding; individual beds of argillite are difficult to follow as discontinuities are frequent.

Within these deposits graphite in the range of 1-2.5 % is typically present, and pyrrhotite is also relatively abundant; silver and copper enrichment have also been noted. Overall, visible wall rock alteration is poorly developed but calcite, mainly as veinlets is present in the range of 2-7 %. The calcite seems to be associated with hematite alteration, and geochemical evidence does suggest the presence of a sodic metasomatic halo (MacDougall, 1988). The presence of graphite and pyrrhotite would indicate a reducing

environment which could lead to the precipitation of uranium during deposition (Wilton, 1996). Uranium mineralization is thought to be syngenetic, to late-syngenetic, and that subsequent deformational events remobilized uranium into veins and shear zones.

It is interesting to note that analogous argillaceous and sulphide-bearing rocks of the Moran Lake Group are not mineralized. There are, however, trace radioactive enrichments in dolostones within these sedimentary rocks (Sparkes and Kerr, 2008).

#### **2.4.4 Uranium Showings Hosted in Felsic Volcanic Rocks**

The felsic volcanic rocks of the Aillik Group hold most of the significant uranium occurrences within the CMB. Many of these occurrences occur in a regional mineralized trend, almost 30 km in length. This trend, known as the Michelin-White Bear Mountain belt (Figure 2.5) includes both the Michelin and Jacques Lake deposits (Gandhi, 1978; Evans, 1980; Wilton, 1996; Wardle, 2005; Sparkes and Kerr, 2008). Evidence suggests that this trend may be related to a regional shear-zone structure, responsible for concentrating fluid flow and subsequently leaching uranium from the surrounding host rocks, followed by precipitation along permeable horizons (Wardle, 2005; Sparkes and Kerr, 2008). Mineralized zones generally occur as tabular or lenticular, stratabound bodies, conformable with or transverse to the structure of the host rocks (Evans, 1980).

Most lithologies within the Aillik Group contain uranium occurrences, the main host rock lithologies include coarsely, finely and non-porphyritic rhyolites and rhyolitic ash-flow tuffs, intermediate ash-flow tuffs, and mafic tuffaceous rocks (Gandhi, 1978; Evans, 1980; Sparkes and Dunning, 2009). Mineralization consists of finely disseminated



uraninite, and to a lesser extent, as massive to disseminated uraninite in veins, shears and fractures (Gandhi, 1978). Mineralization appears to be related to host rock lithology and is associated with pyroxene, amphibole, sphene, andradite, carbonate and Fe-Ti oxides in more felsic rocks like at Michelin (MacDougall, 1988), and carbonate, actinolite, magnetite and calc-silicates in more intermediate to mafic rocks like at the Jacques Lake and Rainbow deposits (Gandhi, 1978; Sparkes and Dunning, 2009). Alteration is intense and distinctive, consisting of a wider pronounced zone of sodic metasomatism around the deposit, extending well out into the wall rock and more localized hematization within the ore-zone (Wilton, 1996).

There are also some examples of uranium deposits hosted within metavolcanic rocks of the Aillik Group that are not associated with widespread metasomatism or strong deformation. Here, mineralization still consists of disseminated or fracture-hosted uraninite in stratigraphically controlled sequences with relatively weak deformation (Sparkes and Kerr, 2008).

#### **2.4.5 Uranium Showings Associated with Plutonic Rocks**

Uranium mineralization associated with felsic plutonic rocks is widespread throughout the CMB within both Archean basement rocks and overlying supracrustal Proterozoic sequences. There are four distinct styles of mineralization related to granitoid plutons: 1) syngenetic mineralization within the plutons due to enrichment during crystallization, 2) mineralization within plutons concentrated due to deformation, alteration and epigenetic enrichment, 3) hydrothermal activity related to the emplacement

of granitic stocks which remobilized uranium from the surrounding host rocks and deposited it in favourable environments, and 4) mineralization hosted in breccia zones.

Many granitoid and particularly pegmatitic bodies throughout the CMB are slightly enriched in uranium and thorium indicating an epigenetic style of mineralization. Mineralization is usually weakly disseminated or concentrated in small veinlets and associated with allanite, magnetite, amazonite and fluorite (Gandhi, 1978; Sparkes and Kerr, 2008). None of the showings observed so far are economic. The best showings appear to be associated with pegmatites within the Kanairiktok Intrusive Suite hosted in Archean gneiss; these pegmatites also contain epigenetic mineralized veins (Wilton, 1996).

Most of the uranium mineralization hosted within granitic rocks is associated with shearing and/or alteration, indicating that mineralization was epigenetic in origin; either stripped from the pluton itself or the surrounding host rocks. Overall, uranium grades tend to be much higher than those found in other mineralizing styles with many showings having assays of over 1.0 %  $U_3O_8$ . Uranium mineralization tends to be concentrated within shear zones. The best example of this would be the Melody Hill zone (Figure 2.5) where strongly deformed, well mineralized granitic boulders contain uranium grades up to 28.2 %  $U_3O_8$  (Wardle, 2005; Sparkes and Kerr, 2008). The Melody Hill showing consists of a train of high grade granitic boulders on the eastern side of Melody Lake. These boulders belong to the Melody Lake granite but are strongly deformed and display intense hematite alteration. The source of these boulders has not been identified to date.

Drilling programs have only been able to identify weak mineralized zones within the granite.

The intrusion of granitic bodies within the host Aillik Group felsic volcanics is related to many uranium occurrences throughout the Aillik Group, most notably those located within the Aillik-Makkovik belt (Figure 2.6) and the Round Pond zone (MacDougall, 1988; Wardle, 2005). It is thought that the intrusion of these small cupolas remobilized uranium from the volcanic host rocks and deposited it in hydrothermal veins, which generally occur in the vicinity where granitoid rocks have intruded felsic volcanics. Uranium is often associated with molybdenum and base-metal mineralization (Sparkes and Kerr, 2008).

The Round Pond zone is a small area within the western portion of the Aillik Group and is strongly associated with molybdenum and base-metal mineralization in quartz and pegmatite veins that are adjacent to high-level granitic stocks (MacDougall, 1988; Wilton, 1996).

The Aillik-Makkovik belt is located in the northern Aillik Group and contains a number of occurrences with either uranium mineralization or uranium and molybdenum mineralization. Uranium generally occurs intergrown with amphibole or as uraninite and sphene fracture fillings associated with possible albite metasomatism (MacDougall, 1988). Wilton (1996) suggests that the skarnoid nature of the mineralization could suggest a link to concealed granitic plutons.

Brecciated zones within granitic rocks also contain uranium mineralization throughout the CMB. The best example of this is the Two Time Zone showing (Figure

2.7) which is hosted in granitoid plutonic rocks of the late Archean Kanairiktok Intrusive Suite (Sparkes and Kerr, 2008). Mineralization is hosted within an in-situ breccia with a dark fine grained matrix composed of chlorite, hematite and iron-carbonate. The breccia zones have random orientations and show no signs of pervasive deformation or shearing (Sparkes and Kerr, 2008).

#### **2.4.6 Uranium Showings of the Moran Lake Belt**

The Moran Lake belt (Figure 2.7) is situated at the northern unconformable contact between the Bruce River Group and the Moran Lake Group (Wardle, 2005). This area is structurally and stratigraphically complex with a small sliver of Moran Lake Group positioned in the Bruce River Group through thrusting and reverse faulting, leading to the repetition of stratigraphy (Wilton, 1996). This area of thrusting is known as the Moran C-zone and contains both mineralization in the Bruce River and Moran Lake groups, respectively known as the lower C-zone and upper C-zone. The Bruce River Group also includes the B-zone and the A-zone which are hosted within different stratigraphic levels of the Heggart Lake Formation, the basal formation of the Bruce River Group.

The Lower C-zone is hosted in sandstones and interbedded conglomerates of the Heggart Lake Formation. Uranium mineralization is strongly associated with vanadium enrichment, with near-economic values of ~0.33 %  $V_2O_5$  and minor enrichment in copper and silver (Sparkes and Kerr, 2008).

The Upper C-zone is hosted within mafic pillow lavas, and to a lesser extent argillic sedimentary rocks of the Moran Lake Group (Sparkes and Kerr, 2008). Mineralization is hosted in discrete hydrothermal breccia zones within the mafic rocks where protolith textures have been completely obliterated. The matrix contains intense orange iron-rich carbonate and strong hematite alteration. Mineralization also extends to the non-brecciated wall rock and strongly correlates with vanadium, copper and silver; much like in the lower C-zone. Grades of over one percent  $U_3O_8$  have been reported (Wilton, 1996; Wardle, 2005; Sparkes and Kerr, 2008).

The A-zone located stratigraphically high in the Heggart Lake Formation is hosted in polymictic conglomerates interbedded with sandstones. Uranium is accompanied by weak to moderate sericite and pyrite alteration and carbonate veins. Mineralization is very low and is strongly associated with copper (Wilton, 1996; Sparkes and Kerr, 2008).

The B-zone is stratigraphically between the C and A zones and is hosted in red arkosic sandstones and siltstones that are adjacent to minor intrusive rocks of leucogabbroic composition. Uranium grades are relatively higher than those found elsewhere throughout the CMB and correlate strongly with vanadium, copper, silver and carbonate (Wilton, 1996; Sparkes and Kerr, 2008).

Elsewhere along the contact between the Moran Lake and Bruce River groups small epigenetic shear hosted uranium occurrences occur. Veinlets containing chalcopyrite cut through the basal conglomerates of the Heggart Lake Formation. Several small radioactive zones have been reported (Wilton, 1996).

#### **2.4.7 Unconformity Related Showings**

The Stormy Lake showing (Figure 2.7) exists at the base of the Seal Lake Group at the unconformity surface with the underlying Bruce River Group (Wilton, 1996; Wardle, 2005). The showing is hosted within the basal conglomerate and stratigraphically higher quartzites of the Seal Lake Group, directly above the unconformity. Mineralization consists of Uraninite in fracture fillings and quartz veins and is associated with fluorite, chalcopyrite, galena, chalcocite and native silver (Wilton, 1996). The Stormy Lake showing may represent an example of unconformity related mineralization within the CMB.

**Table 2.1:** Common characteristics of the six different depositional settings that are similar, or potentially similar to uranium occurrences in Labrador.

	<b>Metasomatic</b>	<b>Intrusive</b>	<b>Volcanic Associated</b>	<b>Vein Type</b>	<b>IOCG</b>	<b>Metamorphic Associated</b>
<b>Global Localities</b>	Central Ukraine, Sweden, China, CMB Labrador, Brazil, Australia & Cameroon <sup>1,2</sup>	Alaska, Arizona, Washington US, Namibia, South Africa, Nigeria, Australia & Greenland <sup>5,6</sup>	Sereltsov Region, eastern Russia; China, Sweden, southeast US, Mexico, British Columbia & CMB Labrador <sup>7</sup>	Massif Central in France, Spain and Portugal; Xiazhuang district, southern China; Pribram and Jachymov districts , Czech Republic; Great Bear Lake and Beaverlodge districts , Canada <sup>1,8</sup>	Southern Australia, Chile, Brazil, India, China <sup>10</sup>	Namibia, Zaire, Australia, Quebec & Northwest Territories <sup>5,12</sup>
<b>Global Reserves</b>	9% <sup>1</sup>	5% <sup>1</sup>	3-5% <sup>1</sup>	7% <sup>1</sup>	15% <sup>1</sup>	?
<b>Age Range</b>	1.9 – 1.7 Ga; 1.5 – 1.4 Ga; ca. 500 Ma <sup>1,2</sup>	Varies	Early Proterozoic - Cenozoic <sup>7</sup>	Late Archean - late Tertiary <sup>8</sup>	Late Archean – Pliocene <sup>10</sup>	Proterozoic - Tertiary <sup>5,12</sup>
<b>Host Rock</b>	Granitic, Metavolcanic & Metasediment Rocks <sup>1,2</sup>	Granitic Rocks (I, S, & A-type), Pegmatites and Alaskites <sup>5</sup>	Felsic Volcanic Rocks <sup>7</sup>	Granitic, Syenitic, Metasediment or Metavolcanic rocks <sup>8</sup>	Batholithic complexes of intermediate to felsic composition <sup>10</sup>	Amphibolites, Granulites, Migmatites <sup>5</sup>

**Table 2.1: Continued.**

<b>Uranium Minerals</b>	Uraninite & Brannerite, minor titanium-bearing uraniferous minerals and Coffinite <sup>1,3</sup>	Uraninite, minor Brannerite, Coffinite, Uranothorite <sup>7</sup>	Uraninite & Pitchblende, minor Brannerite, Coffinite, Thucholite, Liebigite, Becquerelite <sup>9</sup>	Uraninite, minor Brannerite & Coffinite <sup>10</sup>	Uraninite, Brannerite & Uraniferous Magnetite, minor Uranophane, Torbernite, Carnotite, Gummite <sup>13</sup>
<b>Associated Minerals</b>	Zircon, REE, Yttrium & Vanadium <sup>1</sup>	Thorium, Fluorine, Molybdenum, Lead, Zinc, REE <sup>7</sup>	Silver, Arsenic, Nickel, Cobalt, Vanadium, Selenium, Copper & Bismuth <sup>8,9</sup>	Copper, Gold, Silver, REE, Molybdenum, Zinc, Lead, Cobalt, Tungsten, Bismuth, Fluorine, Boron, Chlorine <sup>10</sup>	None
<b>Average Ore Grade (U<sub>3</sub>O<sub>8</sub>)</b>	0.15%, ranging from 0.03% - 0.6% <sup>1,3</sup>	0.1%, as high as several % <sup>7</sup>	Ranging from 0.1 - 1% <sup>8</sup>	< 0.05%, ranging from 0 - 0.2% <sup>11</sup>	0.1%, ranging from 0.03 - 1-2% <sup>13</sup>
<b>Tonnage</b>	Varies	Very little to several tens of thousands <sup>7</sup>	Up to tens of thousands <sup>8</sup>	High to very high <sup>11</sup>	Varies



**Table 2.1: Continued.**

Associated Alteration	1 <sup>st</sup> stage: Sodic metasomatism (albitization); 2 <sup>nd</sup> stage: Desilicification, Hematitization, Increased Sodic metasomatism (albite, sodic amphiboles & pyroxenes), Carbonatization (calcite); 3 <sup>rd</sup> stage: Calcium-Magnesium metasomatism (diopside, andradite, epidote & calcite); 4 <sup>th</sup> stage: Potassic metasomatism (biotite, phlogopite & orthoclase) <sup>1,3,4</sup>	Very Little	Hematitization, Carbonatization, Albitization <sup>7</sup>	Sodic Metasomatism, Hematitization, Feldspatization & Carbonatization, Chloritization <sup>9</sup>	1 <sup>st</sup> stage: Magnetite bearing sodic-calcic alteration (albite, actinolite, diopside); 2 <sup>nd</sup> stage: Potassic alteration (orthoclase, magnetite/hematite, biotite); 3 <sup>rd</sup> stage: Hydrolytic alteration (hematite, sericite, carbonate & quartz) <sup>10</sup>	None
-----------------------	--	-------------	--	--	--	------

**Sources:** 1 - Cuneo and Kyser, 2008; 2- Cuneo, 2010; 3 - Polito *et al.*, 2009; 4 - Cuneo *et al.*, 2012; 5 - Guilbert and Park, 1986; 6 - Ferguson, 1988; 7 - Gandhi and Bell, 1996; 8 - Misra, 2000; 9 - Ruzicka, 1996; 10 - Hitzman and Valenta, 2005; 11 - Roberts, 1988; 12 - Cornelius, 1976; 13 - Gregory *et al.*, 2005

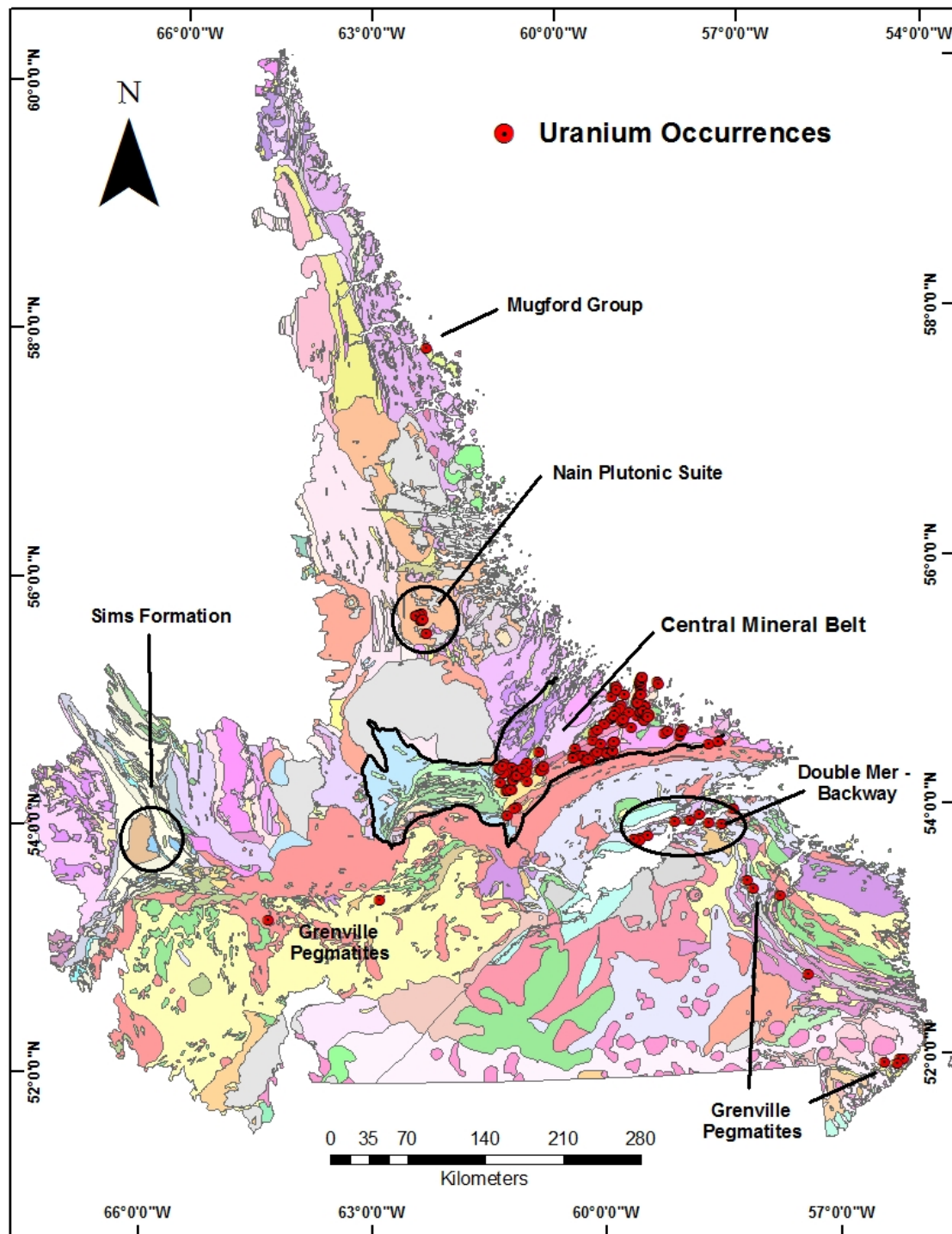


**Figure 2.1:** Reported uranium occurrences within Labrador. Figure 2.3 provides a more detailed view of the Central Mineral Belt. Geology legend can be found with Figure 3.1 (modified from Wardle *et al.*, 1997; Newfoundland and Labrador Geological Survey, 2015).

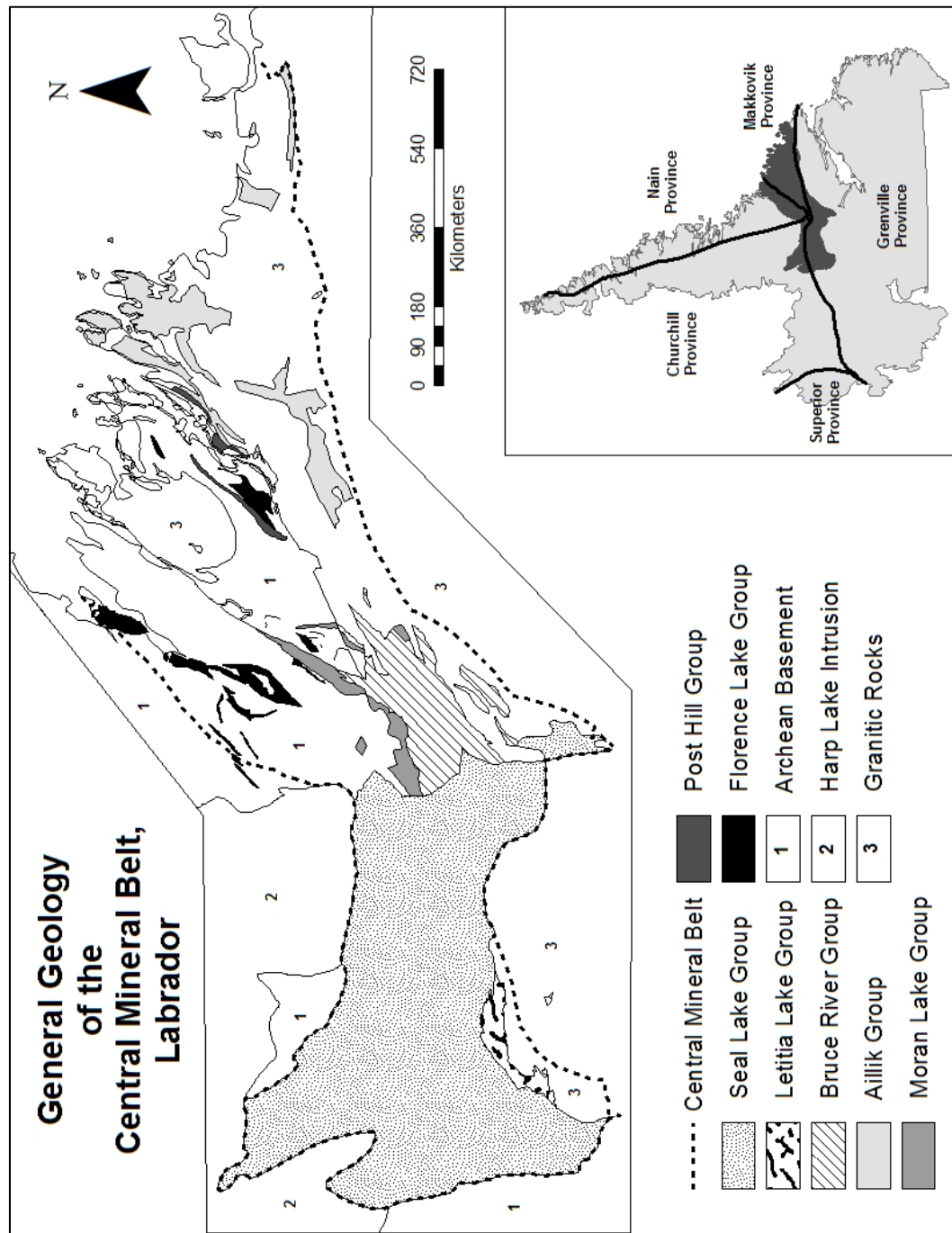


**Figure 2.2:** General map of the Central Mineral Belt highlighting the six Proterozoic sequences consisting of the Post Hill, Moran Lake, Aillik, Bruce River, Letitia Lake, and Seal Lake groups and the Archean Florence Lake Group with associated basement rocks (modified from Wilton, 1996; Wardle *et al.*, 1997).

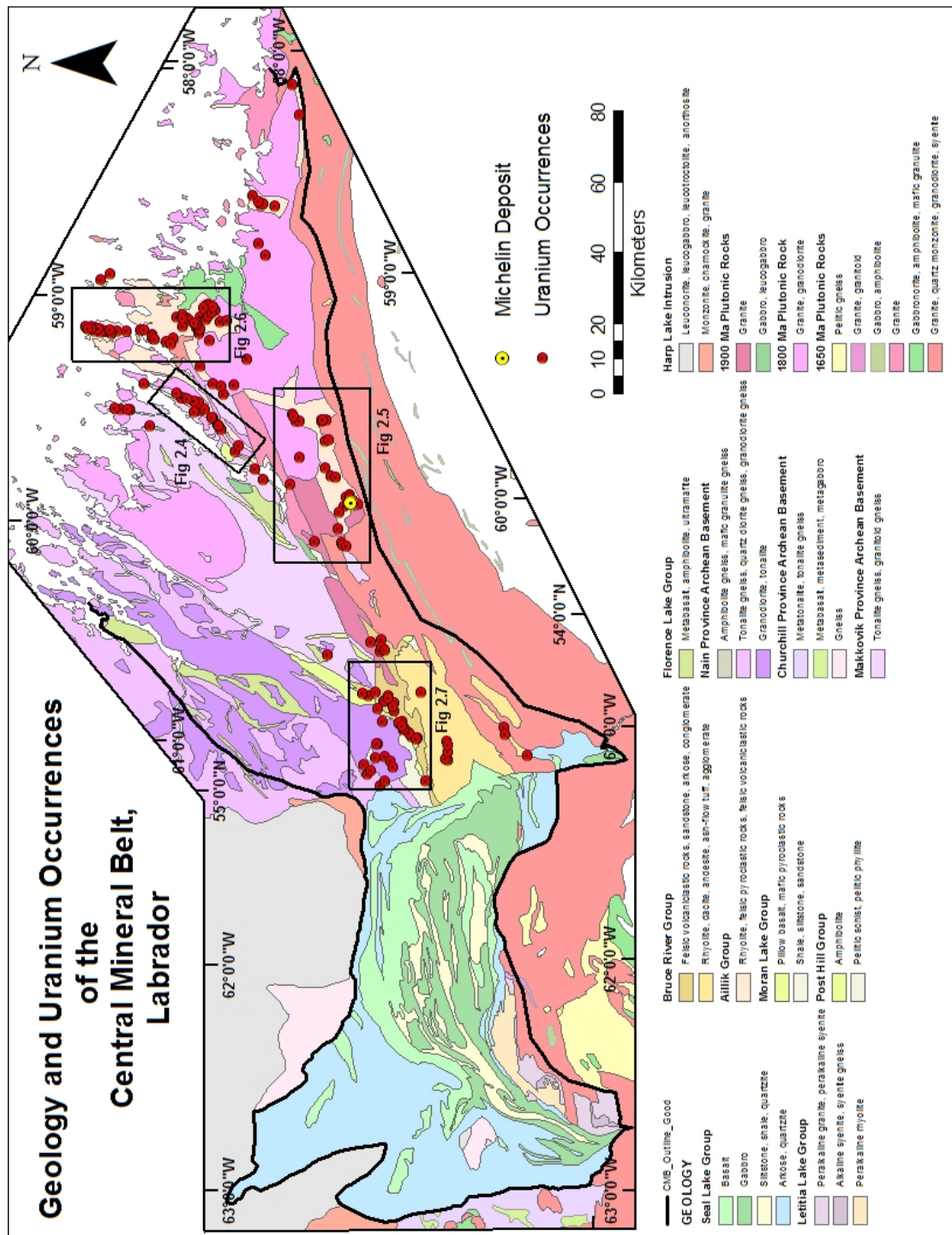


**Figure 2.3:** Geology map of the Central Mineral Belt, with known uranium occurrences (modified from Wardle *et al.*, 1997; Newfoundland and Labrador Geological Survey, 2015).

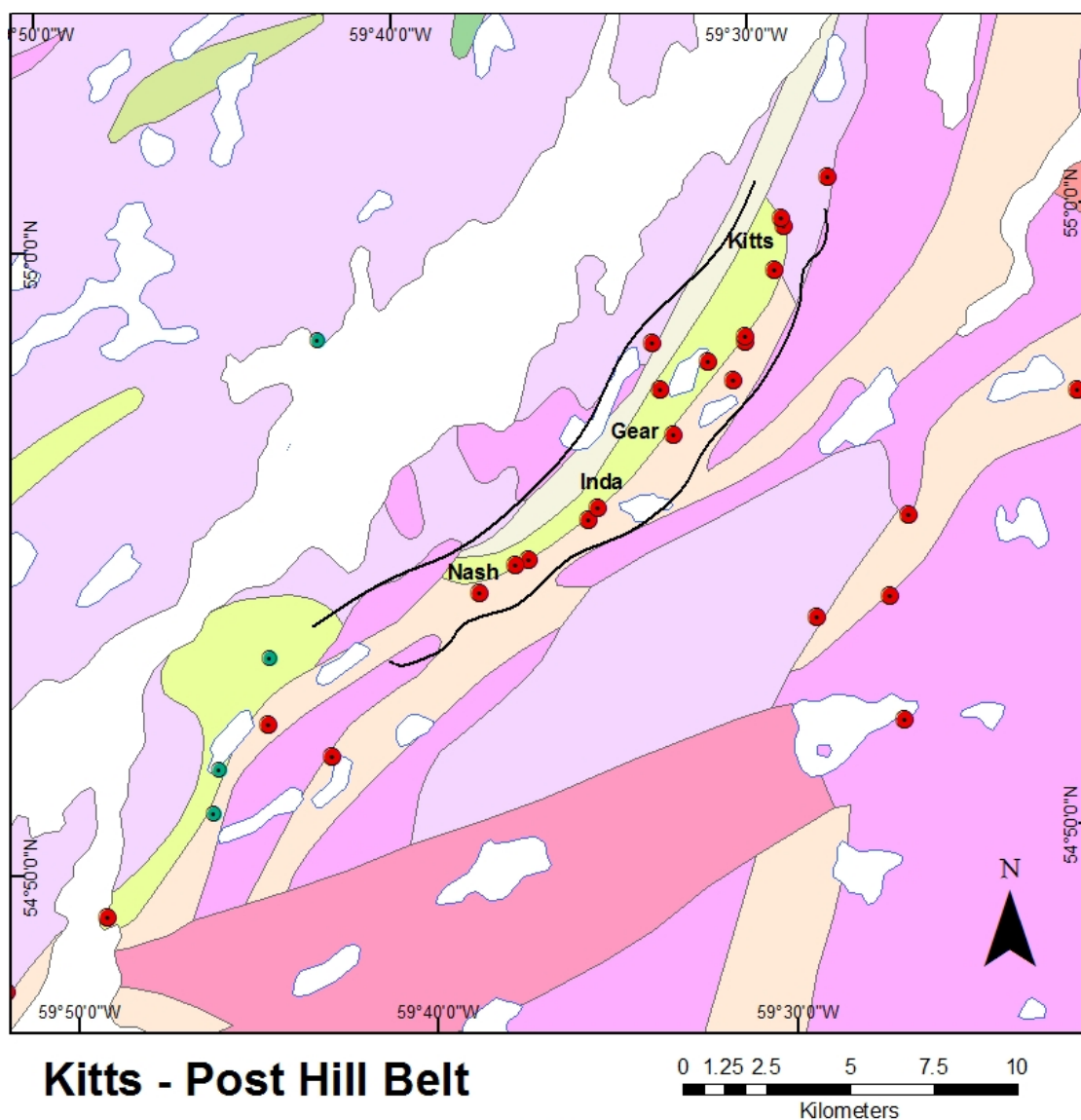


**Figure 2.4:** Geology of the Kitts – Post Hill belt, highlighting the trend of the belt with known mineral occurrences including the Kitts deposit, and Gear, Inda and Nash showings (modified from Gandhi, 1978; Wardle *et al.*, 1997; Newfoundland and Labrador Geological Survey, 2015).



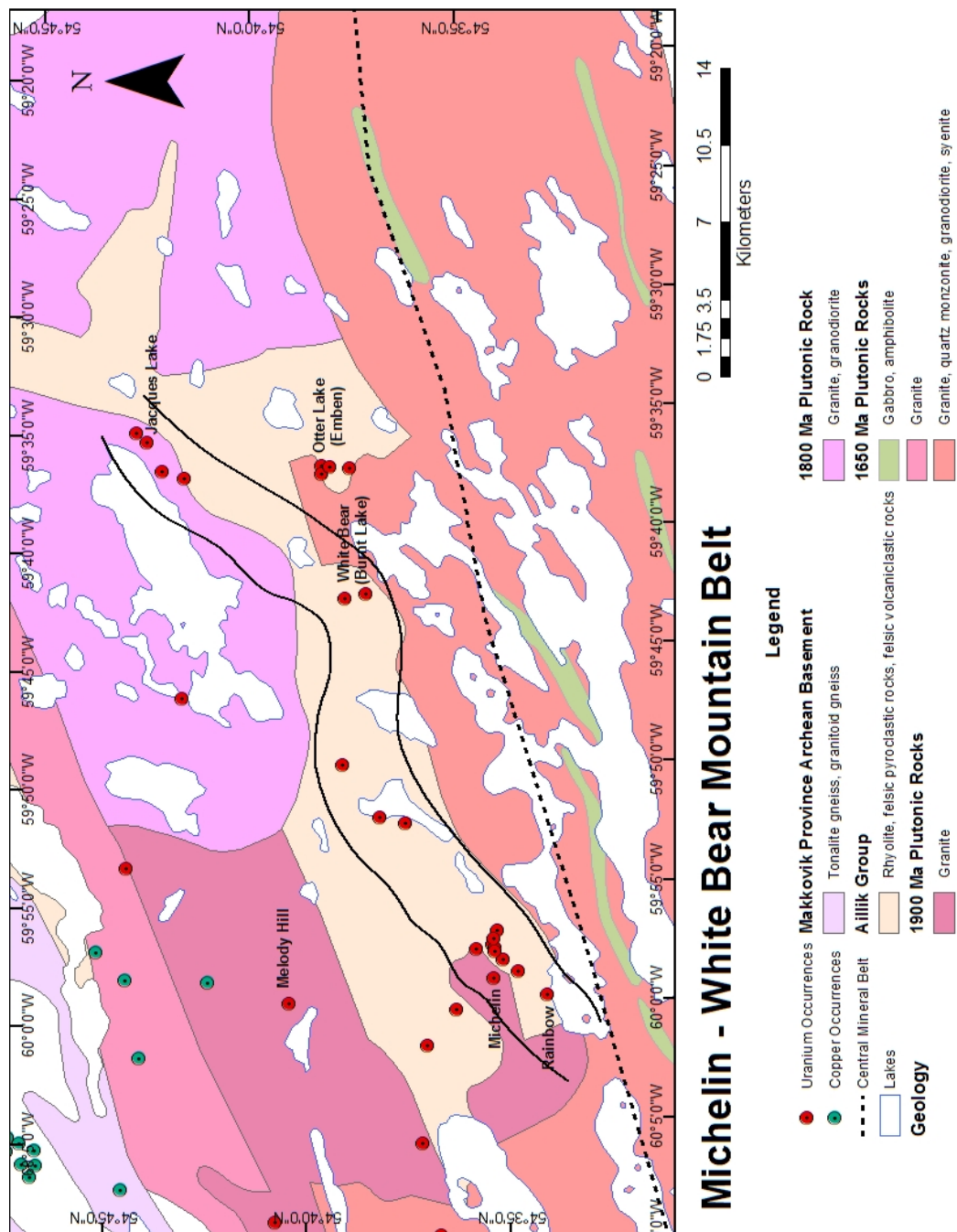


**Figure 2.5:** Geology of the Michelin – White Bear Mountain belt and area, highlighting the general trend of the belt with known mineral occurrences including the Michelin and Jacques Lake deposit, and Rainbow and White Bear showings. The Melody Hill showing is also included (modified from Wardle *et al.*, 1997; Sparkes and Kerr, 2008; Newfoundland and Labrador Geological Survey, 2015).

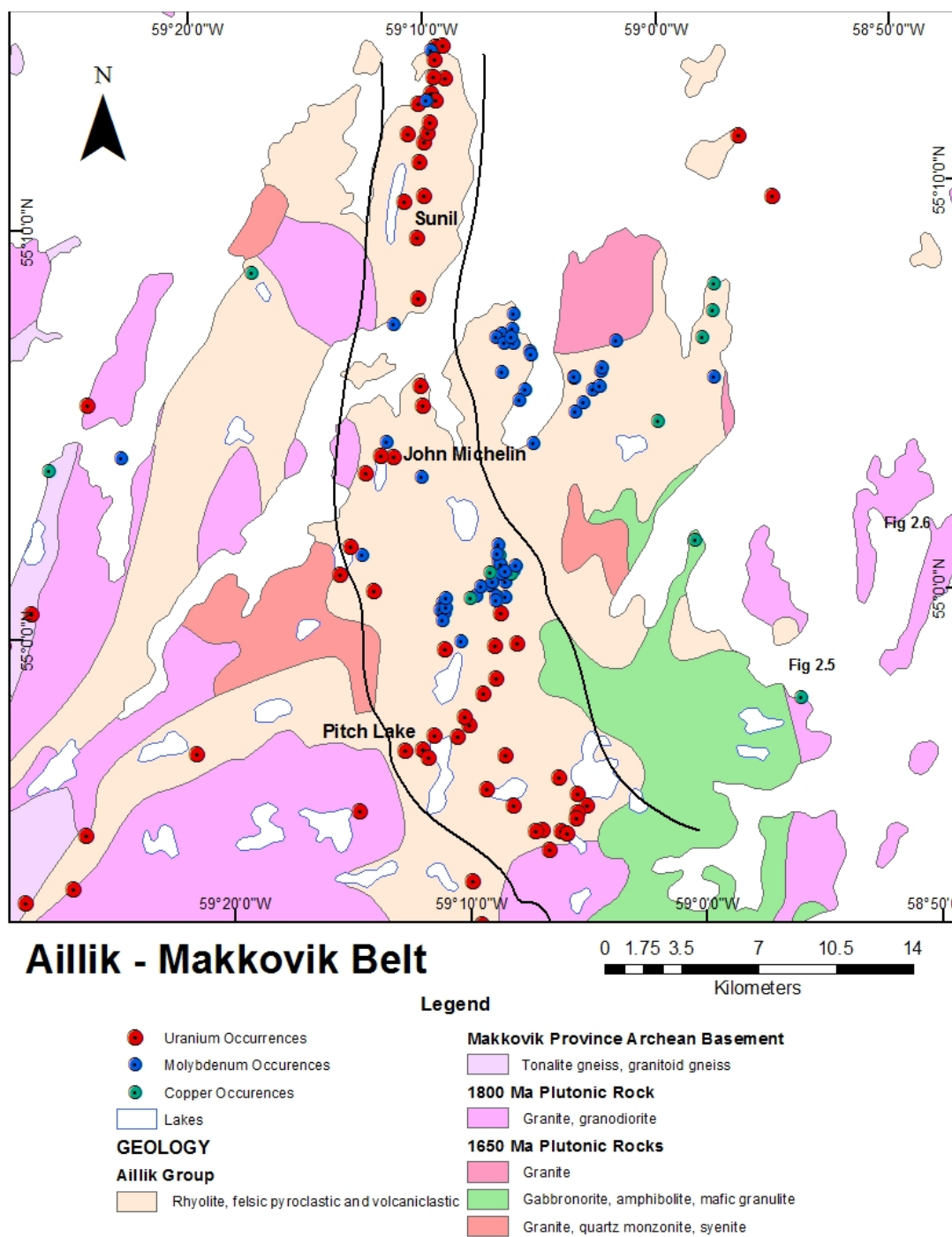


**Figure 2.6:** Geology of the Aillik – Makkovik belt, highlighting the general trend of the belt with known mineral occurrences including the Sunil, Pitch Lake, and John Michelin showings (modified from MacDougall, 1988; Wardle *et al.*, 1997; Newfoundland and Labrador Geological Survey, 2015).

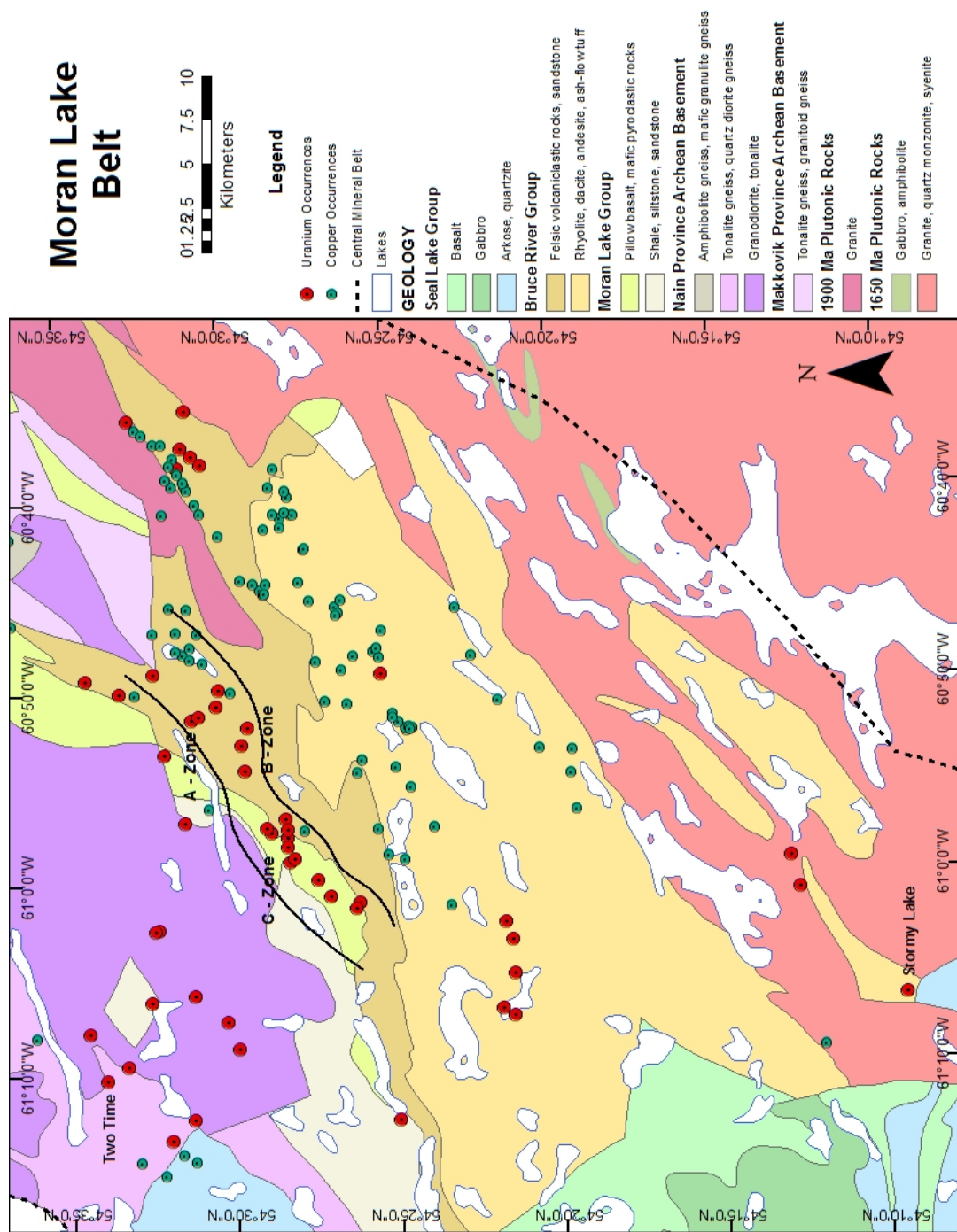


**Figure 2.7:** Geology of the Moran Lake belt and area, highlighting the trend of the belt with known mineral occurrences including the C-Zone deposit and B-Zone and A-Zone showings. The Two Time and Stormy Lake showings are also included (modified from Wardle *et al.*, 1997; Newfoundland and Labrador Geological Survey, 2015).



## **Chapter 3     Geology of the Michelin Deposit**

### **3.1     Introduction**

The geology of the Michelin deposit has been studied and reviewed several times (e.g., Gandhi, 1978; Evans, 1980; Ross, 2006; Wilton and Cunningham-Dunlop, 2006), however, the strongly deformed nature of the rocks coupled with the intense overprinting alteration has made definition of the protolithologies very difficult leading to a variety of interpretations. Early BRINEX geologists interpreted the rocks as quartzitic meta-sediments, while subsequent investigations have resulted in reclassification of the rocks as a variety of Aillik Group porphyritic felsic volcanic rocks that have been intruded by several granitoid bodies and mafic dikes. All of these studies tend to treat the unaltered and altered rocks together, often focusing more on mineralized samples. There has never been an attempt to just characterize the unaltered lithologies at Michelin. However, in order to understand, define, and characterize the alteration and mineralization processes associated with the deposit it is important to first define the unaltered and unmineralized lithological units which make-up the deposit.

This chapter will characterize and define the primary unaltered and unmineralized geology of the Michelin deposit. It is important to note that the rocks at Michelin have been affected by metamorphism during the ca. 1810 to 1790 Makkovikian Orogeny (Wilton, 1996). Most of the rocks have been metamorphosed to lower amphibolite facies. Therefore, observed mineral assemblages, textures and geochemistry are representative of these peak metamorphic conditions. Thus making an accurate determination of the

original protoliths is difficult. Once the unaltered lithological units of the deposit are defined then an accurate measure of the type(s) and degree of alteration and mineralization can be determined.

As this chapter attempts to define what constituted unaltered, unmineralized rocks, criteria need to be defined that distinguish altered from unaltered. The best criteria proved to be Na<sub>2</sub>O content, as variation in this component represents the most widespread alteration event in the Michelin camp. Examination of geochemical data from the Michelin region indicates that the unaltered average for Na<sub>2</sub>O was approximately 4.5 wt. %. Thus a comparative cut-off was established at 5.0 wt. % Na<sub>2</sub>O, wherein any sample containing > 5.0 wt. % Na<sub>2</sub>O is deemed to have undergone alteration to some degree and no longer classified as unaltered. This is verified petrographically, as samples with > 5.0 wt. % Na<sub>2</sub>O generally contained visible signs of sodic alteration, while those < 5.0 wt. % did not. It is important to note that even though these rocks are considered to be unaltered and unmineralized, samples containing < 5.0 wt. % Na<sub>2</sub>O could potentially have some weak alteration and mineralization associated with them, and it is possible that classifications based on geochemistry could be erroneous. Therefore, geochemical plots will be predominantly used to show where the samples plot and trends that the samples create in order to form a baseline for which altered and mineralized samples can be compared.

This chapter will first focus on the regional geology, with a brief overview of the geology of Labrador, including a more focused examination of the geology of the Aillik Group so as to overview the regional setting in which the Michelin deposit is situated.

The geology of the deposit will then be discussed and each lithological unit will be broken out individually and examined. This work is based on observations of drill core and hand samples, vitally important for contact relationships and textures. Thin sections of each unit are examined to identify textures, minerals and mineral percentages. Finally the geochemistry of each unit, both the major, trace and rare earth elements are examined in order to characterize and classify each rock type.

### **3.2 Regional Geology**

Labrador forms the easternmost edge of the Canadian Shield and comprises a wide variety of igneous and metamorphic rocks overlain by less deformed volcanic and sedimentary sequences (Ryan, 1989). It has been affected by at least five different orogenic events and multiple non-orogenic, plutonic intrusive episodes. These five, Precambrian tectonic events have been used to subdivide Labrador into five distinct structural provinces; Superior, Nain, Churchill, Grenville and Makkovik (Figure 3.1).

Sandwiched between the Nain and Grenville provinces on the central-east coast is a small, wedge-shaped accretionary orogen known as the Makkovik Province. It is bounded to the north by 3200-2800 Ma amphibolite facies tonalitic gneisses of the Hopedale Block of the southern Nain Province. The Hopedale gneisses contain two linear greenstone belts and were intruded by voluminous tonalite plutons (Wardle *et al.*, 1995). To the south, The Makkovik Province is bounded by metamorphosed tonalites of the Mesoproterozoic Trans Labrador Batholith (Scharer *et al.*, 1988; Ketchum *et al.*, 1997; Hinchey, 2007). The Makkovik province itself consists of Archean gneissic basement

that was overlain by, and infolded with, supracrustal metavolcanic and metasedimentary rocks, and intruded by numerous synkinematic to postkinematic granitoid plutons along with a variety of kinematic mafic dikes (Scharer *et al.*, 1988; Kerr *et al.*, 1994; Hinchey, 2007). According to Ketchum *et al.* (1997) the Makkovik province can be subdivided into three separate lithotectonic domains; the Kaipokok, Aillik and Cape Harrison (Figure 3.2).

### **3.2.1 Aillik Domain**

The Aillik Domain, in which the Michelin deposit is situated, consists of a variety of metavolcanic and metasedimentary rocks (the Aillik Group) which were intruded by foliated and non-foliated mafic to felsic intrusive suites and mafic dikes along with small slices of reworked Archean Gneiss. Hinchey, (2007) described the small slices of quartzo-feldspathic to granodioritic orthogneiss in the Aillik Domain as reworked Archean gneiss similar to those in the Kaipokok Domain. The Aillik Group structurally overlies the Post Hill Group and their contact is characterized by a zone of intense deformation. The nature of the contact between the two groups is uncertain and has been suggested to be a transitional contact, an unconformity, a disconformity, and a ductile shear zone (MacDougall, 1988; Kerr *et al.*, 1994).

The Proterozoic Aillik Group, formally termed the Upper Aillik Group, is a ca. 1883-1807 Ma supracrustal sequence of felsic volcanic, volcanoclastic and associated sedimentary rocks which have been metamorphosed at upper-greenschist to lower-amphibolite facies during the ca. 1810 to 1790 Ma Makkovikian Orogeny (MacDougall,

1988; Wilton, 1996; Hinchey, 2007). According to Wilton (1996) the Aillik Group is exposed in two zones: a coastal area termed the Makkovik Zone that extends from Cape Aillik to Cape Makkovik and inland for 35 km, and a 40 x 10 km inland area, termed the Michelin Zone, located to the southwest of the Makkovik Zone. These two zones are separated from each other by the Adlavik Brook Fault (ABF), along with synkinematic to postkinematic granitoid rocks.

The Aillik Group rocks of the Makkovik and Michelin zones, although very similar, do exhibit differences. The Makkovik Zone lithologies have undergone amphibolite facies recrystallization resulting in the development of coarse-grained sucrosic textures, whereas the Michelin Zone rocks were subjected to greenschist facies metamorphism and locally retain their primary textures (Wilton, 1996). Other differences between the two zones include contrasting metallogenic styles of mineralization and different styles of granitoid intrusions. The Makkovik zone is cut by numerous high-level, post tectonic granitoid cupolas, but in the Michelin Zone, granitoid bodies are more massive and homogeneous suggesting a deeper level of intrusion (MacDougall, 1988; Wilton, 1996).

The Aillik Group consists of felsic tuff; flow-banded to non-banded rhyolite, which may or may not contain phenocrysts of quartz and/or alkali feldspar; quartz-feldspar-porphyritic granite; volcanoclastic breccia and conglomerate; tuffaceous sandstone; thin-bedded to laminated sandstone and siltstone; and lesser components of basalt and mafic tuff (Hinchey, 2007). Historically, the Aillik Group was divided into a lower sequence of dominantly arkosic sandstone, siltstone, conglomerate, shale,

tuffaceous sandstone with minor dacitic to rhyolitic flows and an upper (later) sequence of dominantly ash flow tuff, flow banded rhyolite, volcanic breccia, lapilli tuff, syn-volcanic porphyritic granite, with minor volcanoclastic sedimentary rocks (Gandhi, 1978). The two sequences are separated from each other by a predominately mafic tuffaceous unit with minor pillow lava, basaltic breccia and possible subaerial basaltic flows (Gower and Ryan, 1987; Hinchey, 2007). Numerous other stratigraphic sequences have been proposed for the Aillik Group, both in the Makkovik Zone and Michelin Zone. However, these sequences lack any continuity throughout the group due in part to the complexity of the felsic volcanism and sedimentation, lack of recognizable marker units, structural complexities, and lack of observable outcrop, particularly in the more interior regions (MacKenzie, 1991; Wilton, 1996).

Minimal age dating has been completed on the Aillik Group but Scharer *et al.* (1988) defined U-Pb zircon ages of 1856 Ma for a rhyolite at Michelin Ridge to the northwest of the Michelin deposit, 1861 Ma for a felsic volcanic rock near the town of Makkovik, and 1807 Ma for a subvolcanic quartz-feldspar porphyry at White Bear Mountain in the northeast Michelin Zone. Hinchey and Rayner (2008) reported ages of 1861, 1883 and 1876 Ma from a felsic tuff and two rhyolites located in the Makkovik Zone.

The Aillik Domain was intruded by numerous granitoid plutons with at least four distinct ages. The first group consists of ca. 1858 Ma pre-synkinematic, foliated quartz-feldspar porphyritic granite in the Makkovik Bay area (Wilton, 1996; Hinchey and LaFlamme, 2009). A second group of ca. 1800 Ma monzogranite to monzonite plutons

also intrudes near the Makkovik Bay area and primarily includes the Kennedy Mountain Intrusive Suite. LaFlamme *et al.*, (2009) suggest that this suite intruded during the final transpressive phase of the Makkovikian orogeny. The third group comprises the small, post-tectonic, ca. 1720 Ma, Strawberry Intrusive Suite monzogranite to alkali-feldspar granite (Hinchey, 2007). The final plutonic phases in the region intruded at ca. 1650 Ma as products of the Labradorian orogeny. These Trans Labrador batholith suites include the Adlavik Intrusive Suite layered gabbroic and dioritic rocks, the Monkey Hill Intrusive Suite monzonite to monzogranite, and the Burnt Lake Granite leucogranite to quartz monzonite (MacKenzie, 1991; Wilton, 1996; LaFlamme *et al.*, 2009). In total these 1650 Ma suites are the most extensive in the region, particularly in the south where they almost completely surround the southern Michelin Zone.

Numerous pre-, syn- and post-deformational mafic and granitoid dikes intrude most of the other rock units throughout the Aillik Domain. These include at least two swarms of amphibolite mafic dikes, diabase dikes, gabbroic dikes, lamprophyric dikes, aplitic granitic dikes, pegmatitic granitoid dikes, and diatreme dikes (LaFlamme *et al.*, 2009).

### **3.3 Michelin Geology**

The Michelin deposit is located in the southwestern portion of the Michelin Zone within the Aillik Group. The area is underlain by a variety of metamorphosed felsic volcanics intruded by minor foliated intrusive rocks. These in turn have been cut by various granitoid intrusives as well as by several phases of mafic dikes (Figure 3.3).

Rocks in the area were affected by the ca. 1810 to 1790 Ma Makkovikian Orogeny and have been metamorphosed to lower amphibolite facies (Wilton, 1996).

The individual lithological units that comprise the Michelin deposit are interpreted to be crystal rich, quartz-feldspar porphyritic, rhyolitic, subaerial ash-flow tuffs based on their regional extent and uniformity, texture, composition, lack of bedding, and primary textures that is still preserved in less-deformed and weakly metamorphosed equivalent rocks in certain localities throughout the Aillik Group. These most likely represent pyroclastic eruptions where there was density separation of units upon emplacement. Therefore, individual units are distinguished on variations in the size, abundance, color, and quartz to feldspar ratio of the phenocryst assemblage (Gandhi, 1978; Evans, 1980; White and Martin, 1980).

Host rocks to the deposit are dominated by two main lithologies; fine grained porphyritic, metamorphosed felsic volcanic rocks intercalated with several coarse grained porphyritic, metamorphosed felsic volcanic rocks. Other subordinate metamorphosed felsic volcanic rocks include a distinctly mafic-rich, coarse grained porphyritic, felsic volcanic unit as well as non-porphyritic felsic volcanics. The groundmass to all lithologies has been completely recrystallized, obscuring primary structural and paragenetic textures. In general, mineral assemblages are representative of peak metamorphic conditions. Likewise, pre-existing primary igneous textures such as fiamme or welding, if originally present, have now been obliterated by metamorphism.

Lithological units appear to be rather stratiform and individual units can be traced from drill hole to drill hole (Figure 3.4), but the felsic volcanic rocks actually exhibit a



consistently strong foliation throughout the deposit. These units strike approximately  $070^{\circ}$  and dip around  $50^{\circ}$  to the southwest. The hanging wall panel of the deposit was intruded by a granitoid body and the deposit in general has been subjected at various times to four distinct phases of mafic dyke injection, all exhibiting several phases of deformation. According to Otto *et al.* (2013), it is assumed that the footwall sequence outcrops to the north of the deposit with a stratigraphic younging direction towards the south. Although way-up indicators have yet to be established, these sequences are interpreted to be right side up on the basis of facings in cross-bedded rhyolitic tuffs and flow tops in metabasalt flows along strike to the northeast of the deposit (Evans, 1980).

### **3.4 Fine Grained Porphyritic Metamorphosed Felsic Volcanic Rocks**

The predominant rock type hosting the Michelin deposit are fine grained porphyritic (FP), metamorphosed felsic volcanic units of the Aillik Group (Plate 3.1a-f). This lithology constitutes approximately 70 % of the deposit, and comprises most of the hanging wall, almost all of the foot wall, and accounts for roughly 40 % of the mineralized ore zone. These units are somewhat tabular in shape, and along with other interspersed felsic lithologies, define a crude stratigraphic layering throughout the sequence. Individual layers, some tens of meters to  $100^{+}$  m thick, can be traced without difficulty from drill hole to drill hole across section, as seen in Figure 3.4.

Throughout the deposit, textures and mineral assemblages within the FP, felsic volcanic rocks are uniform and consistent. Unaltered varieties exhibit an overall grey to pinkish-grey color, which transitions into whitish-grey regions of sodic metasomatism.

The rocks have an overall porphyritic texture, containing phenocrysts of both quartz and feldspar set in a fine grained, aphanitic matrix. There is no evidence to suggest that the phenocrysts are metamorphic in origin. Visual examination of drill core and thin sections suggest that the phenocrysts were part of the original protolith, therefore for simplicity they will be referred throughout this study as phenocrysts, reflecting the original protolith.

Quartz phenocrysts are small, 1-3 mm in size and constitute 2-3 % of the rock. They are translucent to milky white, elongated, and aligned parallel with foliation. Feldspar phenocrysts are slightly larger, averaging 2-5 mm in size, ranging up to 1 cm in diameter. Unlike the quartz, feldspar phenocrysts are not elongated and two distinct varieties, potassium and plagioclase are recognized. Both varieties are similar in size and shape, and in combination, constitute approximately 5-10 % of the rock. Potassium feldspar phenocrysts are translucent to pale grey with no visible twinning. In contrast, plagioclase phenocrysts are pale-yellow, appear to be saussuritized, and locally display Carlsbad-style twinning.

The phenocrysts are hosted in a fine-grained, feldspar and quartz-rich matrix containing anywhere from 5-15 % mafic minerals (Plate 3.1g-h). Mafic minerals are generally elongated and mostly define a wispy foliation, in many cases as augens around feldspar phenocrysts. The mafic minerals are fine-grained aggregates of predominantly biotite, with decreasing amounts of chlorite, magnetite and hornblende. These mm-thin wispy mafic streaks typically define a network of millimeter to five centimeter thick, strongly foliated concordant mafic patches or dikes, which increase in concentration near

mafic dike contacts and appear to be akin to the pre-kinematic mafic dikes described in section 3.7.1. Magnetite content of these mafic aggregates is approximately 0.5-1 %, making the rocks moderately magnetic with magnetic susceptibility readings averaging between 15 and 20, and up to 25.

This lithology is commonly cut by mm-wide, concordant calcite veinlets; calcite is also disseminated throughout the groundmass. Less common are thin 1.0-5.0 mm wide concordant gypsum veins and 2.0-10.0 mm wide purple fluorite veins. Epidote-rimmed 0.5 cm wide garnet patches are also interspersed through the lithology. The epidote, which may have been developed during retrograde metamorphism, imparts a soft, greenish hue to the rock. In general, there is very little sulfide mineralization present in these felsic volcanic rocks, however, minor veins of galena, chalcopyrite and pyrite cut the rocks, and disseminated pyrite is observed primarily within mafic aggregates.

Overall, the rocks display a consistent foliation and exhibit other signs of ductile deformation. Throughout the deposit there are several small, localized, 5-15 cm wide mylonitic zones. These are relatively mafic-poor, finely laminated, and play host to an admixture of stretched quartz and feldspar phenocrysts. Brittle deformation in the form of small faults cut the volcanics in a number of areas. The faults, where traced, exhibit minor movement or offset and contain mm to cm-sized fault gouge seams (Plate 3.1j). Fracture zones are prevalent in the upper portion of the hanging wall. A section of the hanging wall in particular displays a 50 m wide zone of strongly fractured, crushed rock. Minor amounts of reddish hematite infill the fractures (Plate 3.1i).

### **3.4.1 Petrography of the Fine Grained Porphyritic Felsic Volcanic Rocks**

Petrographic examination of the FP felsic volcanic rocks (Plate 3.2a-l) indicates a 3:1 ratio of potassium feldspar to plagioclase feldspar phenocrysts. Quartz phenocrysts are also present. The matrix which hosts the phenocrysts is a fine-grained crystalline matrix of quartz and feldspar (Plate 3.2a).

Quartz phenocrysts are small (1-3 mm across) and euhedral. All grains have been recrystallized and consist of multiple quartz crystals with sutured crystal boundaries (Plate 3.2b). These individual grains commonly exhibit undulose extinction due to the deformed nature of the phenocrysts. The phenocrysts are elongated and generally stretched with their long-axes aligned parallel with foliation (Plate 3.2l). The stretching of these grains becomes over-exaggerated in mylonitic zones. According to Ross (2006), where a rock has been highly deformed, like in mylonitic zones, quartz phenocrysts are stretched to such an extent that they often grade into discontinuous lenses aligned with foliation.

Potassium feldspar phenocrysts are subhedral in shape, and range from 2-5 mm in diameter (Plate 3.2c); phenocrysts up to 1 cm in diameter have been rarely observed. There are two distinct textural varieties of phenocryst present. Smaller phenocrysts appear to be fresh and consist of an aggregate of two to three smaller feldspar crystals, with very fine grained subgrain development along inner crystal boundaries. This is most likely a metamorphic effect related to recrystallization of the smaller phenocrysts. Larger phenocrysts are single grained and display a slight to moderate sericitic alteration (Plate 3.2d). These phenocrysts are commonly augened, with distinct pressure shadows

developed along their outer rims. Grains in both subsets of phenocrysts display distinct tartan twinning.

Plagioclase phenocrysts are very similar to their potassic counterparts, being subhedral in shape and ranging from 3-8 mm in diameter (Plate 3.2e); occasional rare phenocrysts are up to 1.2 cm in diameter. The plagioclase phenocrysts tend to be slightly larger than the potassic variety and are less recrystallized. Smaller phenocrysts are composed of aggregates of two to four smaller size plagioclase grains, while the larger plagioclase phenocrysts are comprised of single crystals that have undergone stronger sericite alteration (Plate 3.2f). These plagioclase phenocrysts show distinct Carlsbad twinning and typically have pressure shadows, yielding an augen shape. For the most part, both types of feldspar phenocrysts maintain their blocky or tabular outlines except within mylonitic zones, where they become stretched, in similar fashion to the quartz phenocrysts described above.

The matrix or groundmass has an overall completely recrystallized mosaic texture in which all primary textures have been destroyed. In detail, the matrices consist of interlocking, subhedral, generally equant, grains of quartz and feldspar (Plate 3.2g). Feldspar grains seem to outnumber quartz by a ratio of 2:1, and there are two distinct feldspar varieties. Similar to phenocrysts there is both potassium and plagioclase feldspar present in the matrix. Based on staining experiments by Ross (2006) there is almost a 1:1 ratio of plagioclase to potassium feldspar. Therefore, there is an equal percentage of quartz, plagioclase feldspar and potassium feldspar in the rock, each constituting about 25-35 % of the total.

Intermixed mafic minerals are present throughout the groundmass and account for 5-20 % of the total bulk volume. The predominant mafic mineral is biotite which occurs as elongated laths (Plate 3.2i). There is also minor chlorite and hornblende which are generally subhedral and equant in shape (Plate 3.2j). These mineral phases typically form mineral aggregates that are aligned with foliation. In fact, it is these wispy-textured aggregates along with the elongated quartz phenocrysts that define the foliation in the rock (Plate 3.2k). In the more highly deformed, mylonites, the groundmass becomes foliated and consists of fine-grained, banded quartz–feldspar.

The matrix also contains minor amounts of magnetite (Plate 3.2h), which is disseminated throughout matrix but is predominantly associated with mafic mineral aggregates. Trace, euhedral pyrite is locally disseminated throughout the groundmass and is also commonly associated with the mafic aggregates. Calcite as either anhedral grains disseminated throughout the groundmass or associated with the feldspar phenocrysts is common. Trace amounts of euhedral zircon, apatite and titanite are present in the matrices, typically aligned with the foliation.

### **3.4.2 Non-Porphyritic Metamorphosed Felsic Volcanic Rocks**

The non-porphyritic variety of the meta-felsic volcanic rocks occurs within the hanging wall of the deposit, appearing to be a non-porphyritic equivalent of the FP units that dominate the geology of the deposit area (Plate 3.1k). The unit is well exposed in deeper drill hole intersections southeast of Ranjan Lake, where there is a thick hanging

wall section. Drilling has not delineated the southern extent of this unit, but drill intercepts indicate a gradual thickening towards the south.

At current drill hole depths, the non-porphyrific variety sits stratigraphically above the ore zone and outside the ore zone alteration halo. Stratigraphically it is situated between two FP felsic volcanic horizons; the contacts are generally gradational over approximately 0.5 m. Plagioclase and potassium feldspar phenocrysts disappear over the narrow contact zone, but quartz phenocrysts remain, though are less common. The quartz phenocrysts are small, averaging 1-2 mm in size and collectively, represent approximately 2 % of the rock. Overall the unit is relatively mafic poor, with less than 5 % mafic material; predominantly biotite with minor amounts of hornblende and chlorite.

The unit is moderately foliated; with the fabric being concordant to that observed in the deposit area. Due to a low percentage of mafic minerals, the foliation is only weakly defined by elongated quartz phenocrysts and by scarce, small veinlets of biotite, fluorite, calcite, and greenish colored mica. In places, the unit appears to be flow-banded which is generally discordant to the overall foliation (Plate 3.11).

In thin section the unit is dominated by quartz, as the matrix consists of recrystallized, interlocking, equant, euhedral grains of quartz with minor amounts of potassium and plagioclase feldspar, intermixed with biotite and hornblende. Similar to the FP units, the quartz phenocrysts have been recrystallized, consisting of interlocking quartz grains mosaics. In the ten diamond drill holes examined for this study, the non-porphyrific unit was observed in only one drill hole. One sample was collected for a petrographic thin section and geochemical analysis.

### **3.4.3 Geochemistry of the Fine Grained Porphyritic Felsic Volcanic Rocks**

#### **3.4.3.1 Discrimination Diagrams**

Unaltered samples, based on a Na<sub>2</sub>O content of 5 wt. % or less of the FP and non-porphyritic metamorphosed felsic volcanics are plotted on several discrimination diagrams (Figure 3.5a-f) in order to see where they plot and how they trend. Since there was only one sample of the non-porphyritic variety collected, it is grouped with the FP volcanics for simplicity as they are geochemically closely related.

On a LeBas *et al.* (1986) Total Alkalis versus Silica (TAS) diagram (Figure 3.5a), all samples plot in the rhyolite field. Even though these samples seem to be unaltered, there may be some slight alteration occurring with the sodium and/or potassium values as these alkali metals are often very mobile. To determine if the samples are in fact rhyolites and not alkali metal-altered, the samples were also plotted on the Winchester and Floyd (1977) Nb/Y vs. Zr/Ti immobile element ratio-ratio diagram (Figure 3.5b); the felsic volcanic rocks plot still within the rhyolite field.

To further discriminate these samples they were plotted on an Irvine and Baragar (1971) diagram (Figure 3.5c) to determine if they are alkaline or subalkaline. According to Winter (2001) alkaline rocks are richer in alkalis, and are commonly silica-undersaturated, whereas subalkaline rocks are silica-saturated to oversaturated. All samples cluster well inside the subalkaline field suggesting that they are subalkaline volcanic rocks, containing free quartz. Subalkaline rocks can be further divided into the tholeiitic and calc-alkaline series. Tholeiitic rocks show stronger enrichment in iron relative to magnesium and have less variation in silica, whereas calc-alkaline rocks show



enrichments in silica and alkalis (Best and Christiansen, 2001). On an Irvine and Baragar's (1971) AFM diagram (Figure 3.5d), the samples plot along a trend in the Calc-Alkaline field towards the Alkaline apex of the triangle.

These rocks can be further subdivided on the basis of their  $K_2O$  concentrations using a Peccerillo and Taylor (1976) diagram (Figure 3.5e) which is divided into high potassium (High-K), medium potassium (Med-K) and low potassium (Low-K) fields. The Michelin samples all plot within the high potassium Calc-Alkaline Series with a slight downward trend towards the medium potassium Calc-Alkaline Series. According to Best and Christiansen (2001) medium to high potassium calc-alkaline rocks develop on thicker continental crust. Finally, in order to determine whether the samples are peralkaline, peraluminous, or metaluminous, they were compared using Maniar and Piccoli (1989) Shands Index (Figure 3.5f). All the samples plot in the metaluminous field, suggesting that  $Al_2O_3$  contents are less than  $(CaO + K_2O) + Na_2O$  but also, that the  $Al_2O_3$  contents are greater than  $(Na_2O + K_2O)$ . The samples cluster near the peralkaline field boundary indicating that in some samples the  $Al_2O_3$  content may equal the  $Na_2O + K_2O$  content.

Based on the information from the discrimination diagrams, the FP and non-porphyritic metamorphosed felsic volcanic rocks can be classified as being metaluminous, high-K, subalkaline, calc-alkaline rhyolites.

### **3.4.3.2 Major Elements**

The FP and non-porphyritic rhyolites (Table 3.1) contain an average 74.3 wt. %  $SiO_2$ , which ranges between 71.4 wt. % to 77.6 wt. %. These rocks also average 12.3 wt.

%  $\text{Al}_2\text{O}_3$ , 2.9 wt. % FeO (total iron), 0.3 wt. % MgO, 1.1 wt. % CaO, 3.7 wt. %  $\text{Na}_2\text{O}$ , and 5.0 wt. %  $\text{K}_2\text{O}$ . According to Best and Christiansen (2001) this is on par with the average chemical composition for rhyolites, with the exception of  $\text{Al}_2\text{O}_3$  which is approximately 1 % lower, and  $\text{K}_2\text{O}$  which is over a half percent higher.

As silica shows the maximum variability of all of the Major Elements, and these are felsic volcanic rocks, Harker variation diagrams can be used to examine variations between samples and to identify elemental trends. Figure 3.6 displays Harker diagrams for all of the Major Oxides.  $\text{Al}_2\text{O}_3$ , FeO, MgO, CaO, MnO,  $\text{TiO}_2$ , and  $\text{P}_2\text{O}_5$  define a linear trend of decreasing abundances with increasing  $\text{SiO}_2$  contents. These straight linear trends suggest that all samples are part of the same chemical series with each other. Both  $\text{Na}_2\text{O}$  and  $\text{K}_2\text{O}$  contents define more scattered plots with increasing  $\text{SiO}_2$ . This is most likely due to weak sodic metasomatism leading to slight alteration of the host.

#### **3.4.3.3 Trace Elements**

Harker variation diagrams for the Low Field Strength Elements (LFSE) show three distinct trends with increasing silica, as well as some scatter (Figure 3.7). Both Ba and Sr have negative linear trends with a somewhat steep slope as  $\text{SiO}_2$  increases. These tend to mimic the Major Oxides and suggest that these elements were crystallizing out of the melt, possibly as substitutions for CaO. Th defines a linear trend that has a positive slope with increasing silica. This is only element that shows this correlation. Increasing Th with silica increases indicates that Th was not crystallizing out of the magma during fractional crystallization, but was still behaving as an incompatible element (Winter,

2001). Both U and Pb have straight linear trends with increasing silica that have no slopes; as silica concentrations increase their elemental concentrations remain relatively the same. Cs, Ga, and Rb are scattered and show no real trends with  $\text{SiO}_2$ . These elements mimic  $\text{K}_2\text{O}$  and  $\text{Na}_2\text{O}$ , and like these major elements are most likely affected by slight alteration.

Uranium values in the unaltered, unmineralized felsic volcanics average about 9.3 ppm, ranging from 5.1-79.3 ppm. The majority of the samples average between 5-12 ppm U. The few samples with greater than 12 ppm may be weakly mineralized. Pb has a ratio of almost 3:1 compared to U, and Th has a ratio of about 2:1 when compared to U.

The Harker variation diagrams for the High Field Strength Elements (HFSE) (Figure 3.8) show two distinct, negative trends with increasing silica as well as scatter. Both Hf and Zr exhibit strong linear trends with steep negative slopes with the increasing silica. Y also has a negative slope but not as steep, and also forms a linear trend, with the exception of a few samples that are highly elevated in Y. These elements crystallize out of the magma with increasing differentiation, and the steep slopes for Zr and Hf would suggest that these have become very compatible elements, most likely in crystallizing zircons, which are visible in thin section. Both Nb and Ta are generally scattered as silica increases, similar to  $\text{K}_2\text{O}$  and  $\text{Na}_2\text{O}$ ; again this is most likely due to slight alteration or an effect of metamorphism.

#### **3.4.3.4 Rare Earth Elements**

Taylor and McLennan's (1985) upper continental crust-normalized rare earth elements (REE) plot, indicate that all of the unaltered samples define a very distinct pattern (Figure 3.9). The light rare earth elements (LREE) and medium rare earth elements (MREE) define almost horizontal lines with only a very slight negative slope towards the heavy rare earth elements (HREE). There is a noticeable negative Eu (-Eu) anomaly. The strong negative Eu anomalies suggest that calcium-rich plagioclase feldspar had already crystallized, depleting the remaining magma in Eu compared with the other REE (Winter, 2001).

There are a few samples with anomalous HREE enrichments that also show Y enrichments. This is interpreted to have been caused by garnet crystallization within those samples. Both Y and the HREE strongly partition into garnets when they crystallize (Rollinson, 1993; Winter, 2001). Garnets, although not a major mineral constituent have been identified in drill core and in the petrographic study performed by Ross (2006). It is interesting to note that these samples also have the strongest negative Eu anomalies, strong negative Ba anomalies, as well as having the highest concentrations of silica. The increase in silica would indicate that these samples are more quartz-rich, and therefore possibly have less plagioclase feldspar, for which Ba and Eu would substitute for Ca (Winter, 2001).

On Taylor and McLennan's (1985) upper continental crust-normalized extended trace element plot (Figure 3.10), the samples define distinct negative Ti and Sr anomalies. A majority of samples have a slight positive anomaly in Ba, whereas a few samples have

strong negative anomalies. Some samples show a slight uranium anomaly but this may be due to trace uranium mineralization.

#### **3.4.3.5 Geochemical Comparison of the Fine Grained Porphyritic Felsic Volcanic Rocks**

A total of 101, unaltered, FP samples, representing rocks from throughout the hanging wall and foot wall of the deposit have a major element geochemistry suggesting that they are all geochemically equivalent. The following section will utilize log-standardized REE profiles, ratio-ratio plots of LREE vs HREE, and immobile-incompatible bivariate element plots to determine, 1) if the individual, unaltered samples are geochemically related to each other, 2) if they are derived from the same magma source, and 3) if these units are geochemically related to unaltered CP, and altered FP and CP felsic volcanic rocks.

When the average REE concentration of unaltered FP felsic volcanic rocks are plotted on an upper continental crust-normalized REE plot, after Taylor and McLennan (1985), the resulting diagram has an almost horizontal to slightly negative profile across the LREE, a moderate negative Eu (-Eu) anomaly, and an almost horizontal profile across the MREE and HREE (Figure 4.9). This profile matches the REE profile of every sample in Figure 3.9 with the exception of three. These display a slightly more pronounced negative slope across the LREE, a stronger -Eu anomaly, and a slightly higher total REE concentration.

When these samples are plotted on immobile-incompatible bivariate element plots of  $\text{TiO}_2$  vs Zr and  $\text{TiO}_2$  vs  $\text{P}_2\text{O}_5$  (Figure 4.11) they align in positive, sloping linear trends that project through the origin. Plotting the samples on a REE ratio-ratio plot of La/Sm vs Dy/Yb (LREE vs HREE respectively) shows that all of the samples lie within a single group along a slight linear trend (Figure 4.10). The HREE ratio of Dy/Yb averages approximately 1.8, with very little variation between samples, while the LREE ratio of La/Sm ranges from 6.5 to 9, averaging about 8.5. The large range in La/Sm suggests that the concentration of light to medium REE is not consistent between samples and that some samples are relatively LREE depleted as their ratios lie below the average of 8.5. A ratio-ratio plot minimizes the effects of fractionation and will also eliminate the apparent concentration differences caused by mass and/or volume change due to alteration and closure during geochemical analysis, thus allowing an examination of the character of the magma source, because different sources will plot on different correlation lines.

The geochemical data suggest that the unaltered FP rocks throughout the deposit are geochemically equivalent to each other. Nearly all of the samples share an almost identical REE profile, they form tight linear trends on immobile-incompatible element plots, and they group together along a slight correlation trend on REE ratio-ratio plot. The data also suggest that these samples were derived from the same magma source. The linear trends on the bivariate diagrams projects through the origin and the trend along the La/Sm ratio most likely indicates a correlation line reflecting the evolution of the magma source, suggesting all samples along this line are derived from the same source. It is possible that there are several sub-units within these unaltered FP felsic volcanic rocks

and the three samples which contain a slightly different REE profile could represent one such sub-unit. Geochemically however, the samples are too similar to identify separate sub-groupings, suggesting that all samples are geochemically equivalent and derived from the same magma source.

### **3.5 Coarse Grained Porphyritic Metamorphosed Felsic Volcanic Rocks**

Coarse grained porphyritic (CP), metamorphosed felsic volcanic rocks are mapped as small 2.0-15.0 m thick units, and appear to be coarse-grained equivalents of the FP units. They are the dominant rock type within the ore zone, comprising over half of the lithologies present, and they also occur locally throughout the hanging wall and foot wall (Plate 3.3a, c, and e). These units are near stratiform and are intercalated throughout the deposit interspersed within the FP felsic volcanics. They are readily traced between drill holes in section plots. These units tend to pinch and swell throughout their strike length. Thickness variations between units vary throughout the deposit, throughout the hanging wall and foot wall these units are generally tens of meters apart, however in the ore zone individual CP units are within meters of each other.

Contacts between the units of the CP and FP felsic volcanics vary throughout. Typically the contacts are concordant and sharp, marked by an abrupt change in the size and percentage of phenocrysts. Contacts are rarely gradational over long distances, however, and at times the increase phenocryst size occurs over a distance of 20-30 cm. In some intersections, the contacts are marked by gradational areas of higher strain, possibly representing small mylonitic zones which are generally 5-25 cm in length where

deformation is intense. The mylonite contacts are sometimes bleached in appearance or hematite altered.

Individual CP beds are very similar to each other both texturally and mineralogically. There is very little variation between unaltered units, but alteration does change the mineralogy and texture of the units, particularly within the ore zone. This rock type is porphyritic containing quartz and very large feldspar phenocrysts/porphyroclasts in a fine grained, aphanitic matrix (Plate 3.3b). Quartz phenocrysts are euhedral, 1-3 mm in diameter and comprise approximately 2-4 % of the rock. They are clear to grey-white and are elongated, with the elongated axis aligned parallel to the foliation and about 3x longer than the short axis.

Feldspar phenocrysts comprise approximately 10-20 % of the rock. They are coarse grained, ranging in size from 0.5 mm to 1.5 cm. The grains are usually equant and not elongated. Two distinct feldspar varieties are present: potassium and plagioclase. Potassium feldspars are the dominant species and range in color from grey to pink. They are translucent and larger grains typically exhibit visible microcline twinning. Plagioclase phenocrysts are generally pale yellow and less abundant than the potassium feldspar variety. The host volcanic rocks exhibit an augen texture as a result of the regional foliation wrapping around the feldspar phenocrysts (Plate 3.3d). Pressure shadows adjacent to the phenocrysts are usually filled with mafic minerals or calcite.

This rock type contains approximately 5-15 % mafic material consisting of biotite, chlorite and hornblende (Plate 3.3f). These mafic minerals typically form dark colored, mm wide streaks or wisps which help define the foliation and usually these



streaks are curved or wrapped around the coarser feldspar phenocrysts. The matrix is fine-grained, almost aphanitic in texture, yielding the porphyry-like appearance. These rocks are slightly more magnetic than their FP counterparts, with magnetic susceptibility readings averaging 25, and as high as 35. Magnetite is disseminated throughout, and is strongly associated with the mafic material. Units are strongly foliated throughout, with a foliation consistent with that found in the FP felsic volcanics. Foliation is defined by thin streaks of mafic minerals as well as elongated quartz phenocrysts.

### **3.5.1 Petrography of the Coarse Grained Porphyritic Volcanic Rocks**

The CP metamorphosed felsic volcanics have a matrix, or groundmass, that is very similar to that of the FP counterparts. The matrices consist predominantly of very fine grained, interlocking polygonal crystals of quartz and feldspar. These grains, which have been recrystallized, give the matrix a mosaic texture (Plate 3.4e). The grains are mostly euhedral and equant in shape, however some are elongated parallel to the plane of foliation; this mostly occurs in samples with greater deformation.

The exact content of the groundmass is difficult to determine because of the fine grain size and texture. Feldspar, however, does appear to predominate over quartz in about a 2:1 ratio. There is little twinning in the feldspar grains making it difficult to distinguish between plagioclase and potassium varieties. Ross (2006) acid etched a sample with sodium cobalt nitrate and found that potassium feldspar is the main constituent, followed by quartz and then by albite, with all of these mineral species ranging in the 25-35 % range.

Mafic minerals in the matrices are typically amalgamated together forming thin wisps and streaks that help define the foliation. The primary mafic mineral is biotite, which occurs as small laths aligned with foliation (Plate 3.4f). Anhedral grains of hornblende, chlorite and minor pyroxene are intergrown with the biotite. Magnetite is disseminated throughout the matrix, as micron-sized grains at the triple-point junctions of quartz and feldspar grains, but is also strongly associated with the mafic mineral aggregates. Trace amounts of pyrite are disseminated throughout the matrices closely associated with the mafic material. Zircon, apatite and titanite are all present in trace amounts, mainly associated with mafic grains, or interlocked within the quartz and feldspar grains. The same is true with calcite, which is disseminated throughout but has an affinity for plagioclase grains.

Quartz phenocrysts are small, approximately 2-4 mm in diameter; however they are slightly larger than those in the FP volcanics. The phenocrysts are euhedral, but elongated in an approximate 3:1 ratio with the phenocrysts long axis aligned parallel with foliation. The grains have been recrystallized and are comprised of several quartz crystals sutured together (Plate 3.4a).

Potassium feldspar is the dominant phenocryst species and ranges in size from 0.5 mm up to 1.5-2 cm in diameter. They are subhedral in shape with most of their edges cut, or eaten away by the matrix. There are two distinct varieties present, both displaying distinct tartan twinning. Smaller phenocrysts, which average around 0.5 mm in size, are fresh and appear recrystallized, resulting in an aggregate of three to four different potassium feldspar grains (Plate 3.4c). Unlike the quartz phenocrysts where the

individual grains are sutured together, in places the potassium feldspar grains display a very fine-grain subgrain development along inner crystal boundaries. Larger phenocrysts, which range in size from 1-2 cm, have not been recrystallized and consist of a single grain that is slightly to moderately altered (Plate 3.4d). These larger phenocrysts are commonly augened by wispy streaks of mafic minerals and typically have pressure shadows developed adjacent to the phenocrysts. The pressure shadows are commonly filled with calcite or mafic material.

Plagioclase phenocrysts occur in lesser abundance but are very similar to the potassic equivalents. They have an approximately similar size, shape and texture and in addition display Carlsbad twinning. Again there are two subsets, one subset is a fine-grained variety composed of recrystallized plagioclase grains (Plate 3.4b). This is the dominant plagioclase phenocryst type. The other subset consists of large, non-recrystallized plagioclase phenocrysts which are strongly altered to sericite, particularly towards their centers, with alteration intensity decreasing towards the outer rims of the grains. This may be due to the fact that phenocryst centers formed under slightly different chemical conditions than their outer rims, causing the grain centers to be out of equilibrium with current magma conditions and as a result breaking down or altering to sericite.

### **3.5.2 Mafic-Rich Coarse Grained Porphyritic Metamorphosed Felsic Volcanic Rocks**

Within the hanging wall there is a distinctive single unit of mafic-rich CP metamorphosed felsic volcanics. Although very similar to the other CP units throughout the deposit, this unit is distinctly mafic-rich and contact zones with adjoining units appear to be comprised of highly deformed mafic dikes. The unit, which ranges in thickness from 3-10 m, is situated approximately 180-200 m above the main ore zone, outside the limit of sodic metasomatism, defined in Chapter 6, section 6.2. Unit thickness values are based on drill hole intersections and do not reflect the true vertical thickness of the unit.

This unique mafic-rich unit, which outcrops near the northeast end of Ranjan Lake, is consistent throughout the deposit in overall appearance and texture. Its upper contact is sharp and concordant with foliation. At the contact, the unit is comprised of fine-grained, chloritized and strongly foliated mafic material (Plate 3.5e-f). Inwards from the contact zone mafic material gradually becomes intermixed with the CP felsic volcanics (Plate 3.5c-d). The percentage of mafic material eventually decreases to background levels and the unit then resembles the CP, metamorphosed felsic volcanic unit described above (Plate 3.5a-b). The lower half of this unit is reverse of the sequence described above. Towards and at the lower contact, the unit is again mafic-rich, fine grained and strongly foliated. The lower contact with the host felsic volcanics is sharp and concordant. Most of the mafic rich content is confined to within two meters of the upper and lower contacts. Between the mafic-rich contact zones, the remainder of the

rock contains on average a slightly higher percentage of mafic material than the typical coarsely porphyritic units. The percentage of mafic material is about 15-20 %.

The coarsely porphyritic material contains feldspar phenocrysts ranging in size from 0.5 mm upwards to 1.5-2 cm and make up about 10-20 % of the rock. Two varieties of feldspar are present: potassium and plagioclase. Potassium feldspar phenocrysts are the dominant variety and especially so for the large size phenocrysts. Some of the larger phenocrysts have been tilted and rotated in the plane of foliation and locally appear to be wrapped by mafic streaks, thus creating an augen appearance. Quartz phenocrysts are generally small, averaging about 2-4 mm in diameter, and comprise approximately 2-5 % of the rock. The quartz grains have been stretched or elongated at a ratio of about 3:1, with the long axis parallel to the plane of foliation.

The 15-25 % mafic material within the felsic volcanic rich center is comprised of biotite with moderate amounts of hornblende, chlorite, and minor magnetite. These mafic grains are typically amalgamated together forming thin laminations, streaks and wisps which predominantly define the foliation. The mafic material near the contacts is strongly foliated, fine-grained and dark green, very similar in appearance to the pre-kinematic mafic dikes described below in section 3.7.1. It consists of predominantly biotite with moderate amounts of hornblende and chlorite and contains moderate amounts of calcite and minor magnetite. Overall, this unit is only weakly magnetic when compared to the felsic volcanic center.

### **3.5.3 Petrography of the Mafic-Rich Coarse Grained Porphyritic Volcanic Rocks**

Petrographically the central mafic-rich CP felsic volcanic unit is very similar to the CP metamorphosed felsic volcanics described in section 3.5.1, and the mafic-rich boundaries are similar to the syn-kinematic mafic dikes described in section 3.7.2.1.

The groundmass within this unit consists of recrystallized, interlocking potassium feldspar, quartz and plagioclase feldspar, all within the 25-35 % range. These grains are generally equant and euhedral, however, they are slightly elongated, stretched parallel with foliation. Intermixed within these felsic grains is approximately 15 % mafic material consisting predominantly of hornblende, with biotite and minor chlorite, pyroxene, and magnetite (Plate 3.6a-b). These grains are all elongated, subhedral and generally define the foliation as small, elongated aggregates which appear as mm-thin wisps throughout the unit. Pyroxene occurs as very small clusters of multiple fine grains surrounding magnetite grains, within these aggregates. Pyroxene has been altered to hornblende. The matrix also contains disseminated, fine-grained, euhedral zircons as well as minor apatite, minor calcite, pyrite and titanite.

Situated within the matrix are large potassium feldspar megacrysts that range in size up to 2.5 cm (Plate 3.6d), display distinct microcline twinning and have been slightly altered to sericite. These crystals were euhedral but some crystal edges have been damaged from the recrystallizing groundmass. The large phenocrysts are not elongated but are strongly augened by thin wisps of the mafic minerals (Plate 3.6c). Calcite typically appears within the created pressure shadows. Some of the smaller potassium feldspar phenocrysts have been recrystallized, and were not altered to sericite.

There are also rare phenocrysts of albite which tend to be slightly smaller than their microcline counterparts. They are euhedral, weakly sericitized and display distinct Carlsbad twinning. They have also been augened by thin wisps of mafic material, very similar to, but not as pronounced as, the potassium feldspar phenocrysts. Quartz phenocrysts have all been recrystallized and are comprised of aggregates of four to five small, interlocking quartz grains. These phenocrysts have been elongated, with their long axis aligned parallel with foliation, helping to define it. Since these grains are much smaller than the feldspar phenocrysts and are aligned with foliation, they have not been augened by thin wisps of mafic material.

The mafic-rich intervals at the boundaries of the unit are comprised predominantly of hornblende with lesser amounts of biotite and plagioclase feldspar as well as minor amounts of pyroxene, chlorite and quartz (Plate 3.6e-f). All minerals are fine-grained, with hornblende and biotite predominantly defining the foliation. Pyroxene grains are altered to hornblende, whereas plagioclase grains have been partially converted to sericite. In general, the mafic section displays an almost gabbroic texture and compositionally it appears to be very similar to the syn-kinematic dikes described in section 3.7.2.1 with the exception that the mafic unit is much finer grained. Trace amounts of magnetite, pyrite and calcite are disseminated throughout the host. With respect to magnetite, it appears to be more abundant in the felsic-rich center.

### **3.5.4 Geochemistry of the Coarse Grained and Mafic-Rich Coarse Grained Porphyritic Volcanic Rocks**

#### **3.5.4.1 Discrimination Diagrams**

Unaltered samples from several units of the coarsely porphyritic metamorphosed felsic volcanics and samples from the mafic-rich coarsely porphyritic metamorphosed felsic volcanics were plotted together on several discrimination diagrams (Figure 3.11a-f). These two lithological units are plotted together because the mafic-rich unit appears to be a subset of the CP variety.

On LeBas *et al.* (1986) TAS diagram (Figure 3.11a), all samples (except one), plot within the rhyolite field. The exception is from the mafic-rich, CP unit and it plots within the trachy dacite field; the reason for this discrepancy can be explained in terms of sample location as the sample was collected closer to the mafic-rich contact of the unit and it contained more mafic material than the samples taken towards the felsic center of the unit. All of the CP samples plot well within the rhyolite field and group closely together and almost all of the samples from the mafic-rich unit samples plot together, close to the boundary with the trachy dacite field. Since they are more mafic, they therefore contain less silica. On a Winchester and Floyd (1977) diagram (Figure 3.11b), all of the samples plot together in the rhyolite field, with the exception of one outlier in the rhyodacite/dacite field (same outlier sample as on the TAS diagram).

All samples of both rock types plot within the subalkaline field on an Irvine and Baragar (1971) SiO<sub>2</sub> vs. Alkalis diagram (Figure 3.11c), suggesting that they are silica-saturated to oversaturated. Subalkaline rocks can be further divided into tholeiitic or calc-



alkaline with Irvine and Baragar's (1971) AFM diagram (Figure 3.11d). According to this diagram the CP samples are similar to the FP units and plot along a trend in the calc-alkaline field towards the alkaline apex of the triangle. In contrast the mafic-rich CP samples cluster together within the tholeiitic field. According to Best and Christiansen (2001) tholeiitic rocks have less variation in silica when compared to calc-alkaline rocks and show iron enrichment relative to magnesium. The mafic-rich unit contains less silica than its CP counterpart, and is enriched in iron in comparison to magnesium. This is evident on the Harker diagrams presented in Figure 3.12.

All samples of both units plot within the High-K calc-alkaline series on a Peccerillo and Taylor (1976) diagram (Figure 3.11e) but with a gradual trend towards the Med-K calc-alkaline series. On the Maniar and Piccoli (1989) Shands Index diagram (Figure 3.11f) all samples, except one CP sample, plot within the metaluminous field. The single CP outlier plots within the peralkaline field but straddles the border with the metaluminous field. All samples plot close to the peralkaline border, indicating that the one outlying sample within the peralkaline field is slightly more alkaline-rich and aluminum poor than the others.

Overall the geochemical data indicate that the CP metamorphosed felsic volcanics are very similar to the FP varieties and can be classified as metaluminous, High-K, subalkaline, calc-alkaline rhyolites. The mafic-rich unit is slightly different and can be classified as metaluminous, High-K, subalkaline, tholeiitic rhyolites.

### 3.5.4.2 Major Elements

Major element data for the CP volcanics (Table 3.1) show a range from 71.4 wt. % to 75.8 wt. % in  $\text{SiO}_2$  contents, with an average of 73.7 wt. %. These rocks also average 12.3 wt. %  $\text{Al}_2\text{O}_3$ , 3.1 wt. % FeO (total iron), 0.3 wt. % MgO, 1.0 wt. % CaO, 3.5 wt. %  $\text{Na}_2\text{O}$  and 5.6 wt. %  $\text{K}_2\text{O}$  which are remarkably similar to the FP varieties; with only  $\text{SiO}_2$  and  $\text{K}_2\text{O}$  being different. The CP units contain less silica, generally by  $< 1$  % and are higher in potassium by about 0.5 %.

The mafic-rich subset of the CP volcanics (Table 3.1) contains a range of 66.1 wt. % to 73.5 wt. %  $\text{SiO}_2$ , with an average of 69.985 wt. %. This rock unit also averages 13.3 wt. %  $\text{Al}_2\text{O}_3$ , 5.0 wt. % FeO (total iron), 0.5 wt. % MgO, 2.0 wt. % CaO, 3.9 wt. %  $\text{Na}_2\text{O}$  and 4.7 wt. %  $\text{K}_2\text{O}$ . These values differ than those of the CP volcanics but are considered normal range for a subset of this unit that is more mafic-rich. This would explain the decrease in silica and potassium and the increase in iron, magnesium, calcium and sodium, as these elements are more abundant in mafic minerals, i.e. hornblende and plagioclase.

Harker variation diagrams presented in Figure 3.12 indicate that  $\text{Al}_2\text{O}_3$ , FeO, MnO, CaO,  $\text{TiO}_2$  and  $\text{P}_2\text{O}_5$  exhibit near linear trends of decreasing abundance with increasing silica. These diagrams also indicate that the mafic-rich unit lies within the same linear trend as the CP units suggesting that they could be derived from the same source material and within the same chemical series as each other. The increasing negative trend indicates that all of these oxides were crystallizing out of the magma as it evolved. MgO displays a near horizontal linear trend with increasing silica, indicating

that as the magma evolved, magnesium was removed at a rate equal to that of silica. Both  $\text{Na}_2\text{O}$  and  $\text{K}_2\text{O}$  show more scattered profiles with increasing  $\text{SiO}_2$ . These possibly reflect sodic metasomatism effects or effects from metamorphism. It is interesting to note that the CP samples have on average a higher percentage of potassium and lower percentage of sodium than the mafic-rich subset.

#### **3.5.4.3 Trace Elements**

Harker variation diagrams of the LFSE for the CP volcanics (Figure 3.13) do not define strong linear trends, with only strontium and uranium displaying discernible trends. Sr has a moderate sloping, negative trend with increasing silica. Whereas U has a shallow sloping positive trend with increasing silica indicating that it is accumulating within the melt as the magma evolves. The remaining elements, Ba, Cs, Pb and Th exhibit a more scattered profile which vaguely resembles a linear trend as silica content increases. Ba displays a moderate sloping, negative profile, while Th displays a steeply sloping positive profile. In contrast, Cs and Pb display near horizontal profiles with increasing silica. Due to the highly scattered spread of Ga and Rb samples, both elements display no discernible patterns with increasing silica. Uranium values for the unaltered, unmineralized coarsely porphyritic felsic volcanics average 8.4 ppm, and range from 5.0-21.8 ppm. Pb has a ratio of almost 5:1 compared to U and Th has a ratio of a little over 2:1 when compared to U.

The mafic-rich coarsely porphyritic volcanic samples all tend to cluster more closely together rather than displaying variation between the LFSE. Ba, Ga, Cs, Rb, Pb

and Th all exhibit scattered profiles with increasing silica and show no discernible trends. Sr displays a negative trend with increasing silica, comparable to the slope seen in the CP samples. U has an almost horizontal trend with increasing silica. Uranium values for the mafic-rich unit average 4.4 ppm with a tight range from 3.9-5.1 ppm, which is similar to the more silica-poor samples of the CP volcanics. Pb has a ratio of just under 6:1 in comparison to U, and Th:U is 4:1.

Harker variation diagrams of the CP felsic volcanics for the HFSE (Figure 3.14) display several distinguishable trends as silica content increases. Both Ta and Y display positive trends with increasing silica. Ta has a moderate slope and a great deal of scatter between samples, whereas Y has a steep slope with very little scatter. Hf displays a shallow sloping, negative trend with increasing silica, but with a great deal of scatter between samples. Zr plots along an almost linear, horizontal trend with minor scatter between samples. Nb displays no distinguishable trend as all samples show a high degree of scatter with increasing silica

For the mafic-rich subunit, all of the samples plot closely together with three elements displaying linear trends. Both Hf and Ta display near horizontal linear trends with increasing silica. Y displays a shallow sloping, negative trend with increasing silica. Both Nb and Zr have no real trends with increasing silica and samples for both elements have a scattered profile. HFSE concentrations differ between the mafic-rich and regular CP volcanics as the former have higher Hf, Nb and especially Zr concentrations. Zr has an almost 2:1 ratio between the two rock types, as evidenced by the increase in visible zircon observed in thin sections of the mafic-rich unit.

#### 3.5.4.4 Rare Earth Elements

Taylor and McLennan's (1985) upper continental crust-normalized REE plot, indicate that all of the unaltered CP samples define a distinct pattern (Figure 3.15) with an almost straight horizontal line across the LREE, MREE and HREE with only very slight, negative slopes in the LREE. Eu has a negative anomaly, which is stronger in some samples than others. Trending towards the HREE one of the outlying samples increases in concentration until it equals that of the average concentration for the CP volcanics. The remaining two samples become more of an outlier, decreasing in concentration towards the HREE.

The mafic-rich CP felsic volcanics (Figure 3.17) show patterns similar to those in the mafic-poor counterparts. They plot as an almost straight horizontal line across the LREE, MREE and HREE with only a slight negative slope within the LREE. Eu has a moderate negative anomaly, due to its substitution for Ca in hornblende and plagioclase.

On a Taylor and McLennan (1985) extended trace element plot the CP volcanic samples (Figure 3.16), all display strong negative anomalies for Cs, Sr and Ti. Certain samples display slight positive anomalies in Ba and U and one sample has a slight negative anomaly for Zr. These partial anomalies could be caused by a number of reasons, including metamorphism or weak alteration. The heavier, more incompatible elements towards the right of the diagram show a more distinct linear trend in comparison to the lighter elements towards the left.

The mafic-rich CP volcanics display similar patterns to those that in the CP units (Figure 3.18), with strong negative Cs, Sr and Ti anomalies and positive anomalies for

Ba. The only difference is that this unit does not exhibit a positive U anomaly most likely due to the fact that the unit is more mafic in character and it is located well outside the ore zone so there would be no chance for uranium mineralization to occur.

#### **3.5.4.5 Geochemical Comparison of the Coarse Grained Porphyritic Felsic Volcanic Rocks**

Unaltered units of CP felsic volcanic rocks occur as small, sporadic units intercalated throughout the FP volcanic rocks outside of the mineralized zone. Major element data for these samples suggest that all units are geochemically equivalent. When samples are plotted on a normalized REE plot (Figure 3.15), they display very similar REE profiles. There does appear to be distinctive sub-groups in the samples, most likely reflecting individual CP units throughout the deposit. The samples from some sub-groups can be traced between individual drill holes, thus corresponding to an individual unit, and samples from the same unit within the same drill hole plot within the same sub-group. This suggests that the slight sub-groups in the REE data are attributable to the fact that each CP unit is a separate unit. However, several sub-groups contain samples from different CP units from within the same drill hole that are located stratigraphically above or below. This suggests that some of the CP units are the same, or that thrusting has moved equivalent units on top of each other in the stratigraphic sequence.

When the average REE value for all of the CP units (Figure 4.9) is plotted on the same normalized diagram it displays an almost horizontal profile across the LREE, a -Eu anomaly, and a horizontal profile across the MREE and HREE. When compared to the

average REE value for the unaltered FP felsic volcanics, the profiles are nearly identical with the exception that the REE concentrations within the CP rocks are greater. The CP rocks also display slight depletions in LREE relative to HREE in comparison to the FP rocks.

On a La/Sm vs Dy/Yb diagram (Figure 4.10) the samples plot as a group with an average Dy/Yb of 1.8 and an average La/Sm of 7. When compared to the FP volcanic rocks, the CP units overlap, but have lower La/Sm ratios, suggesting that these units are depleted in LREE compared to most of the FP samples. On the same immobile-incompatible bivariate element plots (Figure 4.11) as the FP volcanic rocks, the CP samples lie in the exact same linear trend. The geochemical evidence suggests that the CP units are geochemically similar to the FP felsic volcanics and that the two rock types are most likely related to each other and derived from the same magma source.

#### **3.5.4.6 Geochemical Comparison of the Mafic-Rich Coarse Grained Porphyritic Felsic Volcanic Rocks**

The distinct mafic-rich marker unit of CP felsic volcanic rocks has been interpreted to be a conformable composite dike, or sill, with mafic amphibolite margins, that grades into a more felsic-rich, CP center (Evans, 1980; Otto *et al.*, 2013). The depositional setting for this unit is complicated and appears to be different than that of the other CP units. The mafic-rich margins and felsic-rich center appear to have a gradational contact, which could be the result of differentiation of the unit with a later, more felsic crystal-rich center. The position of mafic-rich section at both margins would suggest that

it did not form as a separate ash-flow layer, but more than likely intruded into the FP felsic volcanic host as a syn-volcanic sill.

Examining the average REE concentration of the mafic-rich CP unit (Figure 4.9) shows a horizontal profile across the LREE, a -Eu anomaly, a horizontal profile across the MREE and a slightly negative sloping profile across the remaining HREE. This is very similar to that of the average REE concentration of the other CP units, with the exception that the overall REE concentration in the mafic rich unit is slightly higher, with the exception of the HREE which seem to be depleted relative to the LREE.

Plotting the samples on a La/Sm vs Dy/Yb diagram shows that the mafic rich unit groups together in the same vicinity as the other CP units with the exception that they plot higher on the y-axis (Figure 4.10). The two groups have a similar LREE ratio of approximately 7, but the HREE ratio of Dy/Yb of the mafic rich unit is slightly elevated, averaging 1.9 compared to 1.8 in the other CP units. This indicates depletion in the HREE in comparison to the MREE, which is also displayed on the log standardized REE profile.

When the samples are plotted on the immobile-incompatible bivariate plot (Figure 4.11) of  $\text{TiO}_2$  vs  $\text{P}_2\text{O}_5$ , the mafic rich unit clusters together, but are situated within the same linear trend as all other felsic volcanic units in the Michelin area. When plotted on a  $\text{TiO}_2$  vs Zr diagram, the samples still clump together, but it is obvious that they have a higher  $\text{TiO}_2$  percentage than the other felsic volcanic units. They still appear to be on the same linear trend, but there is a lot of separation on the trend between these samples and the other felsic volcanics. The distinctly mafic rich unit of CP felsic volcanic appears to



be geochemically similar to the other CP units. There are some geochemical differences, but these could be attributed to the increased mafic content of this unit. It is also possible that this unit is derived from a different source and is not related to the other CP units throughout the Michelin deposit.

### **3.6 Granitoid Intrusive**

On the southeast side of Ranjan Lake there are limited outcrops of a granitoid intrusion (Figure 3.3). This intrusion is also intersected in drill core throughout the hanging wall of the deposit to a depth of approximately 200 m (Plate 3.9a). The exact dimensions of the granitoid cupola are unknown but judging from surface mapping (Barrett *et al.*, 2008) and diamond drilling, it is at least one km<sup>2</sup>. In drill core this unit occurs near the top of the hanging wall, situated approximately 400 m above the ore zone. The emplacement of this unit does not appear to have had any effect on the FP and CP units of the ore zone, and this unit does not appear to be affected by sodic metasomatism described in Chapter 6, section 6.2.

The unit is foliated, with foliation intensity increasing towards the contacts. The foliation is concordant to that in the FP metamorphosed felsic volcanic rocks and is defined by mafic minerals and feldspar grains (Plate 3.7b). Contacts between the two rock types are generally sharp and concordant, but are sometimes marked by small 1-2 m strongly foliated mafic dikes (Plate 3.7e). Near contacts, the felsic volcanic host rocks typically exhibit a local thermal alteration effect of intense hematization and minor potassic alteration. This thermal effect can extend into the host rocks for several meters

but is not associated with uranium mineralization. Hematite alteration also occurs within the granitoid unit adjacent to small fractures which cross-cut the foliation (Plate 3.7f). Typically, the granitoid contains xenoliths of the FP volcanics and is intruded by several mafic dikes.

The granitoid has an almost megacrystic texture, defined by large 1-2 cm grains of both potassium and plagioclase feldspar set in a phaneritic matrix of quartz, biotite and hornblende (Plate 3.7c). Overall, the granitoid is weakly magnetic, pink and medium to coarse-grained (Plate 3.7d). In areas where the rock has been subjected to pervasive potassic alteration, the color transitions from pink to a strong orange.

In the hanging wall, the granitoid is present as small, 1-5 m wide dikes which display similar megacrystic textures, grain size, foliation and contact relationships as the larger intrusive body. Thus they most likely represent off-shoot dikes emanating from the main intrusive body.

There is a second set of felsic intrusive dikes that are rarely intersected in drill core. These dikes average 1-2 m wide and thus far have only been observed within the foot wall; deeper than the lower levels of widespread sodic metasomatism. The dikes are compositionally similar to the granitoid, but have a more equigranular texture compared to the granitoid in the hanging wall.

### **3.6.1 Petrography of the Granitoid Intrusive**

Petrographically, this unit consists primarily of potassium feldspar, plagioclase feldspar, and quartz, with variable amounts of biotite and hornblende (Plate 3.8a-b).

Titanite, magnetite, apatite and zircon are present in minor amounts. Microcline feldspar is the main constituent of the granitoid, comprising approximately 30-35 % of the rock, occurring as grains that average three to four times larger than all other grains. Microcline grains are generally equant and subhedral, ranging in size from 0.5-2 cm. Larger grains are zoned with the interiors weakly altered to sericite.

Albite plagioclase feldspar crystals are generally smaller (0.5-1 cm), comprising 20-25 % of the intrusive as elongated and subhedral, grains that exhibit megacrystic textures similar to those of the microcline. Most plagioclase grains have visible zoning; grain interiors have undergone variable degrees of sericite alteration.

Quartz comprises approximately 30 % of the rock, as small, sub to anhedral grains. Typically multiple small quartz grains are grown together defining larger aggregates that range in size from 1-1.5cm. These aggregates may have originally been larger grains that recrystallized during metamorphism, similar to the quartz phenocrysts in the FP and CP units

Biotite, as sub to euhedral, needle-shaped grains, is generally aligned parallel to the plane of foliation. But the presence of biotite is localized and proportions can range from 5 % upwards to 20 % (Plate 3.8c). The small, euhedral, hornblende grains comprise approximately 5 % of the rock, displaying a distinct 60/120 cleavage and an alignment parallel to foliation. Titanite, a minor constituent, comprising 2 % upwards to 10 % of the rock, occurs as small euhedral grains, loosely associated with the mafic minerals (Plate 3.8d). Small euhedral to anhedral magnetite grains are present in close association with

biotite. Trace, euhedral zircon and apatite are disseminated throughout the megacrystic feldspar, subordinate quartz, biotite and hornblende matrix.

### **3.6.2 Geochemistry of the Granitoid Intrusive**

#### **3.6.2.1 Discrimination Diagrams**

In total there were eight granitoid samples examined (Figure 3.19a-f), seven from the granitoid intrusion in the hanging wall on the southeast side of Ranjan Lake and one of the scarce granitoid dikes intruding the foot wall of the deposit. On a Barker (1979) plutonic classification diagram (Figure 3.19a) six of the eight samples plot within the granite field and the other two samples within the granodiorite field. This plot defines an almost linear trend towards the granite field

The granitic intrusives were discriminated with a Maniar and Piccoli (1989) Shands Index plot (Figure 3.19b) on which all of the samples plot within the meta-aluminous field. With the exception of one outlier, the samples form an almost linear trend towards the peraluminous field. On Whalen *et al.*'s (1987) discrimination diagram (Figure 3.19c), samples all plot along the boundary between A-type granites and I and S-type granites.

The samples are subalkaline (Figure 3.19d) after Irvine and Baragar (1971) with a calc-alkaline affinity (Figure 3.19e) after Irvine and Baragar, (1971), trending towards the Alkaline apex. Based on a Peccerillo & Taylor (1976) diagram (Figure 3.19f) the samples all plot as High-K Calc-Alkaline; the samples form a linear trend with increasing potassium as silica increases.

Based on these discrimination diagrams, the granitoid intrusives can be classified as meta-aluminous, high-K, subalkaline, calc-alkaline, A and S-I type granites to quartz monzonites.

### **3.6.2.2 Major Elements**

The granitoid intrusives (Table 3.1) contain an average 69.0 wt. %  $\text{SiO}_2$ , ranging from 64.3-74.0 wt. % and averages 15.3 wt. %  $\text{Al}_2\text{O}_3$ , 3.0 wt. % FeO (total iron), 0.9 wt. % MgO, 2.3 wt. % CaO, 4.2 wt. %  $\text{Na}_2\text{O}$ , and 4.8 wt. %  $\text{K}_2\text{O}$ . These concentrations are slightly off the average chemical compositions for granites (Best and Christiansen, 2001) in that the Michelin granites contain about 3 % less silica which is compensated by slightly higher abundances of aluminum, magnesium, calcium and alkalis.

Figure 3.20 consists of Harker variation plots for the major elements. In general, FeO (total Iron), MnO, CaO,  $\text{TiO}_2$ , and  $\text{P}_2\text{O}_5$  all display moderate decreasing linear trends with increasing silica.  $\text{Al}_2\text{O}_3$  and MgO both define more curved trends as silica increases;  $\text{Al}_2\text{O}_3$  is almost flat to shallow negative for the samples with silica values ranging from 64-68.5 wt. %  $\text{SiO}_2$ . MgO is similar in that it has a curved, negative trend with the apex being at approximately 68.5%  $\text{SiO}_2$ . The main difference is that samples below 68.5 wt. %  $\text{SiO}_2$  display a moderate to strong slope as compared to samples above 68.5 wt. %  $\text{SiO}_2$  which display an almost flat to shallow slope. The  $\text{K}_2\text{O}$  plot displays some scatter but has a moderate sloped, positive trend with increasing silica,  $\text{Na}_2\text{O}$  defines no discernible trend. The granitic dike within the foot wall, which is the most siliceous, is generally an outlier on each plot.

### 3.6.2.3 Trace Elements

The LFSE (Figure 3.21) define several distinct trends, with Ba, Cs and Sr all displaying moderately sloping negative linear trends with increasing silica. Ga displays a negative trend for samples with silica concentrations above 68.5 wt. %; samples below this concentration have a more horizontal trend. Pb has an almost horizontal linear trend, with a slight positive slope as silica increases. Th displays an interesting pattern; samples with a low concentration of silica (64-68.5 wt. %) have a shallow, negative trend with increasing silica, whereas samples with silica concentrations above 68.5 wt. % have a shallow to moderate positive trend with increasing silica. Finally, Rb has no distinguishable pattern and samples are extremely scattered with increasing silica. Uranium concentrations for the granite averages about 4.0 ppm, ranging from 1.8-9.4 ppm. U displays a similar negative trend with increasing silica. Except, its slope is very shallow and there is far more scatter between samples. The foot wall sample is an outlier with a much greater uranium concentration than the granite in the hanging wall. The U content is within the average range for typical granites (Robb, 2005) and do not show any indication of enrichment or depletion related to the mineralizing event.

HFSE (Figure 3.22) show several interesting trends with both Hf and Zr displaying a profile with samples having < 68.5 wt. % SiO<sub>2</sub> being very scattered and samples having > 68.5 wt. % SiO<sub>2</sub> a moderate to steep negative linear trend. Y displays a similar pattern to this having a moderate negative linear trend with increasing silica after 68.5 wt. % SiO<sub>2</sub>, samples less than 68.5 wt. % have a positive trend. Ta has a shallow,

positive linear trend with increasing silica. Nb has no distinguishable trend with increasing silica.

#### **3.6.2.4 Rare Earth Elements**

Taylor and McLennan's (1985) upper continental crust-normalized REE plot (Figure 3.23) shows a shallow, negative slope for the LREE leveling off to a near horizontal profile for the MREE and HREE. Some samples show a negative Eu anomaly that is associated with Eu substituting for Ca in the chemical structures of albite and hornblende which has a greater concentration in these samples.

On Taylor and McLennan's (1985) upper continental crust-normalized extended trace element plot (Figure 3.24), the samples define distinct negative anomalies for both Ta and Nb. Some samples display a negative Sr and Ti anomaly while some samples display a positive Ba anomaly. The granitic dike located in the foot wall has a positive U anomaly and a negative Cs anomaly in comparison to the granites in the hanging wall. The dike also has the strongest negative Sr and Ti anomaly.

### **3.7 Mafic Intrusives**

Mafic dikes are a common component in the Michelin deposit geology and are extensive throughout the area. The deposit hosts several phases of mafic dikes within the hanging wall, foot wall and ore zone. Detailed logging has led to the identification of four distinct mafic dike types, differentiated by their deformation histories, textures, mineralogies, physical properties, petrography and geochemistry. There is some variation

within these four dike types, making it possible to consider any dike with a variation to be a separate dike species from the four main types but these will not be considered in this study.

Based on the differing deformation intensities exhibited by each dike type, it is concluded that each type was emplaced at different times in the kinematic history of the deposit. The earliest phase, now a biotite-hornblende schist, was very strongly deformed and metamorphosed having been intruded prior to, or very early in the onset of deformation; as such they are classified as “pre-kinematic dikes”. The second dike phase, a gabbroic variety which has been moderately deformed and metamorphosed, is interpreted to have been emplaced during the main kinematic event affecting the area, most likely during the later stages; these are termed “syn-kinematic or late syn-kinematic mafic dikes”. The final two phases intruded the deposit following the main kinematic event and are weakly to non-deformed and unmetamorphosed. They consist of strongly magnetic gabbroic dikes and andesitic dikes; these are grouped together as “post-kinematic dikes”.

### **3.7.1 Biotite-Hornblende Schist (Pre-Kinematic Dikes)**

The biotite-hornblende schists, or pre-kinematic mafic dikes, are the most common dike variety within the property. Intruded throughout the hanging wall, foot wall and ore zone, they cut the FP and CP felsic volcanic host rocks as well as the granitoid intrusion (Plate 3.9a). These dikes range in size from a couple of centimeters up to about



ten meters in thickness, but for the most part are generally no thicker than one to two meters. They commonly occur as clusters of multiple, thin dikes, roughly 10-50 cm wide.

The dikes display a schistose texture with a very strong foliation concordant with the main foliation displayed by the felsic volcanic host rocks (Plate 3.9b). Locally, the dikes have centimeter scale folds in the form of crenulations and kink bands. Contacts between the dikes and all other units are sharp and predominantly concordant to foliation; although these contacts can be irregular. FP felsic volcanic and granitic xenoliths occur in close proximity or adjacent to dike contacts. Locally, strongly chloritized, millimeter to centimeter-thick, fault gouge zones define the contacts with the FP felsic volcanics.

Overall, the biotite-hornblende dikes are fine-grained, greenish-black and generally soft with variable degrees of biotitization and chloritization. Generally the dikes are non-magnetic, with magnetic susceptibility readings between 1 and 3, but locally they can be moderately magnetic. Minor calcite is present, predominantly occurring as disseminations and minor, concordant 1-2 mm veinlets. In very rare locations, these dikes contain trace euhedral phenocrysts of white plagioclase, which range in size from 1-10 mm. Trace amounts of millimeter size, disseminated pyrite are also present throughout.

#### **3.7.1.1 Petrography of the Biotite-Hornblende Schist Dikes**

Petrographically, the pre-kinematic dikes are very fine to fine-grained in appearance. They are very strongly foliated, with the foliation being defined by elongated grains of biotite, chlorite and lesser hornblende (Plate 3.8e-f). Euhedral, elongated lath-shaped biotite grains comprise 20-35 % of the dike. Equant, subhedral hornblende grains

comprise another 30-50 % and elongated subhedral chlorite grains comprise 5-10 %, but locally can account for 20 %. The remainder of the unit (40-50 %) consists mainly of equant, non-lath shaped, subhedral to anhedral plagioclase grains. Trace to minor amounts of pyroxene, epidote, calcite, pyrite, magnetite, ilmenite and titanite are present. Hornblende, a common dike constituent, has been locally retrograded to by biotite and chlorite, whereas plagioclase grains appear to be weakly sericitized

### **3.7.2 Gabbroic (Syn-Kinematic Dikes)**

The syn-kinematic, gabbroic dikes (Plate 3.9c) are the second most abundant mafic dike variety throughout the deposit and they intrude the hanging wall and footwall, as well as the ore zone. These dikes range in thickness from < 1 m to as much as 12 m. Contacts between dikes and the surrounding metamorphosed volcanics are generally concordant to the foliation of the volcanic rocks. There are some instances, however, where contacts are discordant and strike at a shallower angle than the foliation. In some instances, a Hornfels effect has developed within the host volcanics adjacent to dike contacts.

These dikes are moderately to well foliated, with the foliation generally more intense at the contacts, weakening towards the dike center, grading inwards to more massive mafic rock. The degree of gradation from foliated to massive is related to dike thickness. Grain sizes also increase towards dike centers as the margins are typically very fine to fine-grained. Towards the center, the dikes become more medium grained, making it possible to distinguish individual mineral grains (Plate 3.9d).

The dikes contain 50-60 % plagioclase, some of which are small euhedral crystals, and minor quartz. This is intermixed with approximately 50 % mafic material consisting of amphibole, biotite and chlorite. Originally, the dike must have had a dioritic (“salt and pepper”) appearance, but is now greenish-black due to chloritization. Overall, these rocks are non-magnetic with magnetic susceptibility readings of 1 to 3. In other drill holes on the property, not utilized for this study, magnetic varieties of these dikes have been noted (Barrett *et al.*, 2008). Trace disseminated pyrite is common throughout the dikes as well as thin, late calcite veinlets that are usually concordant with the foliation.

#### **3.7.2.1 Petrography of the Gabbroic Dikes**

In thin section these dikes have an almost equigranular texture. A foliation defined primarily by biotite grains is visible. The rock is comprised of approximately 60 % subhedral, equant plagioclase grains. Some grains appear more lath-shaped and generally display a more pronounced Carlsbad twinning. Intermixed with the plagioclase grains are subhedral, lath-shaped biotite grains and anhedral, equant hornblende grains, each comprising approximately 15 % of the rock. In places hornblende has been altered to biotite. The rock also contains minor amounts of euhedral clinopyroxene (typically altering to hornblende), pyrite, magnetite, chlorite and quartz (Plate 3.10a-b).

### **3.7.3 Strongly Magnetic Gabbroic (Post-Kinematic Dike)**

The strongly magnetic gabbroic dikes occur within both the hanging wall and foot wall of the deposit but have yet to be observed in the ore zone. In general, the dikes are 0.5-10 m thick, and for the most part are wider than 2 m (Plate 3.9e). In many drill holes, contact zones between the dikes and the surrounding host rock are zones of weakness, thus core retrieval can be very difficult. Where intact, contacts are discordant to the fabric of the host felsic volcanic rocks, and often display an irregular appearance. A distinct hornfelsic effect is developed within the host felsic volcanics along the contact.

These dikes are generally massive and fine grained, appearing almost aphanitic in texture (Plate 3.9f). In some of the wider dikes, the grain size increases slightly towards the center. The dikes are very weakly foliated, particularly towards the contacts, indicating that they were most likely emplaced during the final stages of regional deformation. They are greenish-black and display weak chloritization. This variety of mafic dike is very distinct by virtue of its strong magnetic character, with magnetic susceptibility readings in the range of 45 to 70. The dikes also contain randomly oriented veinlets of calcite and rarer gypsum. Trace amounts of fine grained pyrite is disseminated throughout. Euhedral plagioclase phenocrysts are only observed rarely, and the presence of plagioclase might represent a minor variation of this gabbroic dike category.

#### **3.7.3.1 Petrography of the Strongly Magnetic Gabbroic Dikes**

In thin section, plagioclase, magnetite, and mafic mineral grains all display distinct grain size differences of approximately 4-10 mm, 2-5 mm, and < 1 mm

respectively (Plate 3.10c-d). Plagioclase comprises approximately 60 % of the rock as lath shaped, euhedral crystals which are considerably larger than the other minerals, thus imparting a cumulate-like texture to the rock. These grains are dusted with magnetite, imparting a dark coloration adding to the magnetic properties of the rock. The second largest grains, approximately  $\frac{1}{4}$  to  $\frac{1}{3}$  the size of the plagioclase grains, are anhedral magnetite grains that comprise approximately 10-15 % of the rock. These grains account for the strong magnetic properties of the rock. The remainder of the rock is comprised of very fine-grained mafic minerals that are closely associated with the magnetite grains, typically surrounding them. The mafic minerals are altered clinopyroxene (up to 10-15 % of the rock) and a mix of lath-shaped biotite, anhedral hornblende, chlorite, needle-shaped actinolite, with trace amounts of euhedral, cracked olivine. Alteration with the clinopyroxene grains consists of fine-grained, clay material along grain boundaries. Grain sizes for all the mafic minerals are generally consistent, appearing to be approximately one quarter the size of the magnetite grains.

#### **3.7.4 Andesitic (Post-Kinematic Dike)**

This second subset of post-kinematic mafic dike is far less common than the strongly magnetic gabbro dikes and they occur sporadically throughout the hanging wall and foot wall, ranging from 1-5 m wide. This dike variety has not yet been observed within the ore zone. Dike contacts are discordant to the fabric in the host felsic volcanic rocks. Similar to the magnetic dikes, a distinct hornfelsic effect is developed in the host felsic volcanics at the dike contacts.

These dikes are non-foliated and very fine-grained; although grain size does increase slightly towards the center within some of the wider dikes. They are greenish-black, non-magnetic, weakly chloritic, and contain about 8-10 % dispersed plagioclase phenocrysts. The phenocrysts are roughly 1-4 mm in size, but rarely range up to 2 cm.

#### **3.7.4.1 Petrography of the Andesitic Dikes**

In general these dikes are fine-grained, equigranular displaying no foliation. The dikes contain about 60-65 % small, anhedral plagioclase grains, some of which are lath-shaped, locally with Carlsbad twinning. The plagioclase is intergrown with approximately 10-15 % euhedral, lath-shaped biotite grains and around 10 % anhedral, hornblende grains with trace anhedral pyroxene (Plate 3.10e-f). These mafic grains are randomly oriented. Intermixed with the mafic grains are anhedral, opaque grains of pyrite, with subordinate magnetite which comprise about 5 % of the host dike. Larger size plagioclase phenocrysts are typically euhedral, lath-shaped, and predominantly fresh with little to no sericite alteration.

#### **3.7.5 Geochemistry of the Mafic Intrusives**

Each mafic dike sample examined in this section was from either the hanging wall or foot wall of the deposit. No samples were collected from inside the ore zone and most of the samples were taken outside of the limits of intense alteration. Sampling was completed in this manner to derive the most accurate geochemical profile for the dikes without any influence from strong alteration zones. Some samples, however, were

collected from weakly altered areas due to the local unavailability of suitable dike material; therefore there may be some geochemical effects from weak alteration and metamorphism.

For this section all four varieties of mafic dike are discussed together on each geochemical plot in order to define the geochemical signatures of each type and at the same time highlight potential geochemical differences between the varieties. Type classification of the mafic dikes was based on both hand sample and thin section identification. The latter was particularly important as several of the pre and syn-kinematic mafic dikes look very similar in hand sample and can be mistaken for each other. This mainly results from the syn-kinematic dikes being emplaced at different times during deformation and some are more deformed than others, taking on the appearance of the pre-kinematic dikes. These dikes are only distinguishable from one another in thin section. Major, trace and rare earth element data for each variety of mafic dike are listed in Table 3.2.

#### **3.7.5.1 Discrimination Diagrams**

The majority of the biotite-hornblende schists plot together within the basaltic-andesite and basaltic-trachy-andesite fields on a LeBas *et al.* (1986) TAS diagram (Figure 3.25a). The rest of the samples display a distinct trend towards the trachy-basalt field with decreasing silica. All of the samples display consistent total alkalis of approximately 5 %, but display a variance of 1-2 % for sodium and potassium for each. The totals always equal 5 %, where samples high in sodium are low in potassium and vice versa. On

a Winchester and Floyd (1977) diagram (Figure 3.25b) there is a large grouping of samples within the andesite/basalt field with the remaining samples forming a linear trend, within the same field.

On the TAS diagram (Figure 3.25a), the gabbroic syn-kinematic dikes all plot very tightly together within the basalt field. These dikes have, on average, lower total alkalis contents when compared to the other dike varieties. On Figure 3.25b all of the samples plot in a tight, positive sloping, linear trend along the boundary between subalkaline basalt and andesite/basalt.

The strongly magnetic post-kinematic gabbroic dikes all plot tightly together in the andesite/basalt field on Figure 3.25a. On Figure 3.25b, the samples plot within the trachy-basalt field but display a very steep negative trend with increasing silica. The range in silica concentrations, however, is extremely low for these samples so it may be possible that this is a false trend caused by different subsets within this dike variety.

The intermediate post-kinematic dikes plot within the basaltic-trachy-andesite field on Figure 3.25a; there are outlier samples enriched in both silica and total alkalis. On Figure 3.25b, these dikes plot within the subalkaline basalt field but define a trend similar to that of the pre-kinematic biotite-hornblende schists.

On Figure 3.25c, both the biotite-hornblende schists and syn-kinematic gabbroic dikes plot along the dividing line between alkaline and subalkaline affinities, with approximately half of the samples from each dike, plotting within each field. For these dikes it is apparent that the samples with lower silica concentrations are alkaline whereas those with higher silica concentrations are subalkaline, this is independent of the alkali



content. This suggests that some of these samples are silica-saturated and may contain free quartz; free quartz is identified in thin section in some of the syn-kinematic dikes. Both varieties of the post-kinematic dikes plot within the alkaline field, with some outliers of the intermediate variety.

Almost every mafic dike sample plots very closely together on an AFM diagram (Figure 3.25d), almost in the center of the triangle, with a few outliers trending towards the MgO apex. The pre-kinematic biotite-hornblende schists plot across the boundary between tholeiitic and calc-alkaline fields, with some of the samples within the calc-alkaline field trending towards the magnesium apex. The gabbroic syn-kinematic dikes all plot within the tholeiitic field, with the exception of one outlier that plots in the calc-alkaline field. The post-kinematic dike varieties are mixed. The strongly magnetic dikes plot mostly within the tholeiitic field, with some plotting along the boundary and down into the calc-alkaline field. The more intermediate andesitic dikes plot within the calc-alkaline field.

#### **3.7.5.2 Major Elements**

The pre-kinematic biotite-hornblende schists average 50.8 wt. %  $\text{SiO}_2$ , with a range from 46-53 wt. %. These dikes also average 14.7 wt. %  $\text{Al}_2\text{O}_3$ , 11.7 wt. % FeO (total iron), 6.6 wt. % MgO, 8.6 wt. % CaO, 3.2 wt. %  $\text{Na}_2\text{O}$ , 2.1 wt. %  $\text{K}_2\text{O}$  and 1.3 wt. %  $\text{TiO}_2$ . This variety of dike is particularly elevated in total alkali contents compared to the other dike types, probably because of the significant component of albite and biotite within the rock.

In all the mafic dikes,  $\text{SiO}_2$  has the greatest variability of all the major oxides, including MgO. Therefore Harker variation diagrams (Figure 3.26) are used, instead of Fenner variation diagrams (MgO), to query the geochemical data and identify trends in the major oxide distributions. The pre-kinematic biotite-hornblende schists display the greatest degree of scatter, most likely due to the metamorphic overprint.  $\text{Al}_2\text{O}_3$ , CaO,  $\text{Na}_2\text{O}$  and  $\text{K}_2\text{O}$  have almost horizontal profiles with increasing silica and excepting  $\text{Na}_2\text{O}$ , there is a considerable amount of scatter between samples. FeO, MnO, MgO and  $\text{TiO}_2$  all display shallow to moderately slopping negative profiles with increasing silica. There is considerable degree of scatter between samples for both FeO and  $\text{TiO}_2$ , but MnO and MgO display tighter profiles.  $\text{P}_2\text{O}_5$  is the only oxide that displays a shallow, positive slope as silica increases. The degree of scatter does not indicate the presence of separate subsets of the dikes as there are no distinct groupings between the oxides, and each sample has a different concentration of the oxide elements.

The syn-kinematic gabbroic dikes average 47.7 wt. %  $\text{SiO}_2$ , ranging from 46-49 wt. %, 16.8 wt. %  $\text{Al}_2\text{O}_3$ , 12.3 wt. % FeO (total iron), 7.9 wt. % MgO, 9.7 wt. % CaO, 2.9 wt. %  $\text{Na}_2\text{O}$ , 1.0 wt. %  $\text{K}_2\text{O}$  and 1.3 wt. %  $\text{TiO}_2$ . These dikes have an overall lower percentage of total alkali metals and  $\text{SiO}_2$ , and a higher concentration of  $\text{Al}_2\text{O}_3$ , MgO and CaO in comparison to all of the other mafic dike varieties. They have a chemical composition more closely related to that of a gabbro, despite containing a more intermediate mineral composition.

The syn-kinematic gabbroic dikes display a much more tightly spaced profile between samples, with much less scatter, than the pre-kinematic schists. Both CaO and

P<sub>2</sub>O<sub>5</sub> display an almost horizontal profile with increasing silica. Al<sub>2</sub>O<sub>3</sub> and MgO display a moderate and shallow positive sloping profile, respectively with increasing silica. FeO, MnO, Na<sub>2</sub>O, K<sub>2</sub>O and TiO<sub>2</sub> all display a negative sloping profile with increasing silica.

The strongly magnetic, post-kinematic gabbroic dikes average 48.1 wt. % SiO<sub>2</sub>, ranging from 46-48 wt. %, 15.2 wt. % Al<sub>2</sub>O<sub>3</sub>, 13.9 wt. % FeO (total iron), 5.7 wt. % MgO, 8.8 wt. % CaO, 3.3 wt. % Na<sub>2</sub>O, 1.9 wt. % K<sub>2</sub>O and 1.9 wt. % TiO<sub>2</sub>. Major element values for these dikes also have a very tight range. These dikes are slightly elevated in FeO when compared to the other dike varieties which are probably attributable to the high concentration of magnetite.

The strongly magnetic, post-kinematic gabbroic dikes display very little variability with silica but linear trends within the major oxides are visible. Al<sub>2</sub>O<sub>3</sub>, MgO and CaO all display very steep positive profiles with increasing silica whereas FeO, MnO, K<sub>2</sub>O, TiO<sub>2</sub> and P<sub>2</sub>O<sub>5</sub> display very steep negative trends with increasing silica. Na<sub>2</sub>O is the only major oxide that does not display any trend, and all Na<sub>2</sub>O samples plot in close proximity to each other.

The post-kinematic intermediate dikes average 52.9 wt. % SiO<sub>2</sub>, ranging from 51-56 wt. %, and 15.3 wt. % Al<sub>2</sub>O<sub>3</sub>, 10.7 wt. % FeO (total iron), 4.4 wt. % MgO, 6.9 wt. % CaO, 3.9 wt. % Na<sub>2</sub>O, 2.7 wt. % K<sub>2</sub>O and 1.8 wt. % TiO<sub>2</sub>. These values are normal range for a rock with an intermediate composition (Robb, 2005), containing the mineral constituents; plagioclase, biotite and hornblende.

The major oxide trends in the post-kinematic intermediate dike data match those within the pre-kinematic biotite-hornblende schists. Al<sub>2</sub>O<sub>3</sub> is the only oxide that displays

a relatively horizontal profile with increasing silica. All other elements, with the exception of  $K_2O$  display negative sloping profiles with increasing silica.  $K_2O$  displays a moderately sloping positive trend with increasing silica.

### **3.7.5.3 Trace Elements**

Concentrations of the LFSE between the dike varieties are similar and tend to reflect the major oxide chemistry and mineral composition of the dikes. Ba, Cs, Ga, Rb, Sr, Pb, Th and U (Figure 3.27) display very scattered profiles for each mafic dike variety. Both post-kinematic dikes have higher concentrations of Ba and Sr than what would be equated with Ca substitution. Th and U concentrations for all of the mafic dikes are very low, averaging below 2.0 and 1.0 ppm, respectively; the intermediate suite has slightly higher U concentrations than the others.

The pre-kinematic biotite-hornblende schists display very scattered, but distinctive, moderately sloping positive trends with increasing silica for Rb, Th and U. Ba, Cs, Ga and Sr all display almost horizontal trends with increasing silica, whereas Pb displays no distinguishable trend at all. All of the LFSE for this dike suite present a great deal of scatter probably attributable to metamorphism or weak alteration.

The syn-kinematic gabbroic dikes also display considerable scatter within the LFSE. For several elements, like Ga, Rb and Pb there is such a high degree of scatter between samples that no discernible trends can be identified. Cs, Sr and U display almost horizontal trends with increasing silica, while Ba displays a negative sloping trend and Th displays a positive sloping trend with increasing silica.

The post-kinematic strongly magnetic, gabbroic dikes also display a large degree of scatter between samples, masking any linear trends that may be present. Cs, Ga, Pb and U, in particular, all display considerable scatter. Ba, Rb and Th all display steep, negative trends with increasing silica but again there is such a large degree of scatter between the samples that the trends are almost unrecognizable. Sr is the only LFSE that displays a discernible positive slope with increasing silica.

The intermediate post-kinematic dikes, like all of the other dike varieties display a moderate amount of scatter between samples. Although not as distinct as those displayed by the pre and syn-kinematic dikes, several linear trends can still be identified. Ba, Ga, Rb and Sr all display a negative sloping trend with increasing silica, while Cs, Th and U display a positive sloping trend. As with all other dikes, Pb has no recognizable trend and displays a great deal of scatter between samples associated with each dike.

Plots of the High Field Strength Elements, Hf, Nb, Ta, Y and Zr display very similar trends for each variety of mafic dike (Figure 3.28). Concentrations of the HFSE between each dike variety are fairly consistent with each other. The most noticeable difference is Nb. Besides this, the strongly magnetic gabbroic dikes average slightly higher concentrations of Y and Zr, although these variations are within a reasonable range.

The pre-kinematic biotite-hornblende schists all display the same patterns. Some elements display an almost secondary trend which may indicate a second subset or subgroup of the pre-kinematic dikes. Within this subgroup Hf, Nb, Y and Zr appear to have a moderate sloping negative trend with increasing silica, while Ta shows a positive

trend. Dividing this dike into two separate groups is difficult, due to the great amount of scatter between samples.

The syn-kinematic gabbroic dikes all display a similar negative, shallow to moderate sloping trend with increasing silica. Samples with higher concentrations of silica display a large amount of scatter. It appears that once the samples hit an apex of low concentration for the HFSE, concentrations then begin to increase with increasing silica, thereby giving the plots an almost curved or V shaped appearance.

The strongly magnetic, post-kinematic gabbroic dikes all display what appears to be a very steep, negative trend with increasing silica. This is similar to what was displayed for the major oxides FeO, TiO<sub>2</sub> and P<sub>2</sub>O<sub>5</sub>. However, this trend may just be the result of two separate subgroupings of samples with both low and high concentrations of silica and no actual trend may exist.

The intermediate post-kinematic dikes display a moderate to shallow, negative profile with increasing silica. Again, similar to the major oxides there is a variable amount of scatter for each element between different samples. The second subset identified within the major oxides is still present but these samples are now situated along slope with the rest of the dike samples, indicating that both subsets may in fact be related.

#### **3.7.5.4 Rare Earth Elements**

Each of the mafic dikes exhibits a very similar chondrite-normalized pattern profile (Figure 3.29a-d). An examination of McDonough and Sun's (1995) REE plot shows that the pre-kinematic biotite-hornblende schists display a negative slope towards

the HREE (Figure 3.29a). The degree of slope is moderate for the LREE and gradually shallows, to almost horizontal towards the HREE. The diagram shows that there is some cross over between samples, indicating that there could be separate subsets within these pre-kinematic dikes. There are no Eu negative anomalies, indicating that calcium mineral bearing phases where  $\text{Eu}^{2+}$  often substitutes have not been crystallizing out of the melt.

The syn-kinematic dikes display an almost horizontal trend across the REE (Figure 3.29b). Within the LREE there is a larger disparity in concentrations compared to the MREE and HREE as some samples display a shallow positive slope while others display a shallow to moderate negative slope. In all samples Eu has a slight positive anomaly. The positive anomaly would suggest that there are significant calcium-bearing mineral components in the dikes (e.g., plagioclase and hornblende).

The strongly magnetic and intermediate post-kinematic gabbroic dikes both display similar trends to the pre-kinematic dikes; with a negative sloping trend throughout (Figure 3.29c). The LREE display a moderate sloping trend which shallows out towards the HREE. The distinct subset identified within the intermediate post-kinematic from major oxides chemistry is also identified in the REE with overall lower concentrations of REE when compared to the main subgroup (Figure 3.29d). The profiles of the two subgroups, however, are very similar indicating that they are most likely related, and derived from the same magma source.

When compared on a primitive mantle-normalized (Sun and McDonough, 1989) extended trace element plot (Figure 3.30a-d), the mafic dike suites reveal some very interesting trends. All four suites exhibit almost identical profiles, particularly the biotite-

hornblende schists (Figure 3.30a) and the intermediate post-kinematic dikes (Figure 3.30d). These two dike varieties display an overall negative slope going from left to right, towards the more immobile elements, and display negative anomalies in Rb, Nb, Ta, Zr and Hf (i.e. The majority of the HFSE with the exception of Y, which is similar in concentration to the HREE). The main difference between the two varieties is that the pre-kinematic suite display weak, negative Ti and Th anomalies. Both of these anomalies are also exhibited by the strongly magnetic, post-kinematic gabbroic dikes (Figure 3.30c). The gabbroic, syn-kinematic dikes display similar trends with negative Th, Nb, Ta, Zr, and Hf anomalies (Figure 3.30b). These dikes also have positive Sr and Eu anomalies, which are explained by a higher concentration of CaO-bearing minerals. Positive Pb anomalies are defined for all of the dikes, but, in half of the dikes lead concentrations are below detection levels.



**Table 3.1:** Average (avg), low and high values for the fine grained (FP), coarse grained (CP), mafic-rich coarse grained porphyritic felsic volcanics, and granitoid intrusive of the major oxides (oxide wt.%), transition metals (ppm), low field strength elements (ppm), high field strength elements (ppm), rare earth elements (ppm), volatile elements (ppm), and the normative mineral percentages after Irvine and Baragar (1971).

	FP felsic volcanics			CP felsic volcanic			Mafic-rich CP			Granitoid		
	avg	low	high	avg	low	high	avg	low	high	avg	low	high
Major Oxides (wt.%)												
SiO <sub>2</sub>	74.3	71.4	77.6	73.7	71.4	75.8	69.9	66.1	73.5	69.0	64.3	74.0
Al <sub>2</sub> O <sub>3</sub>	12.2	11.5	12.9	12.3	11.5	12.9	13.3	12.3	13.5	15.3	13.2	16.2
Fe <sub>2</sub> O <sub>3</sub>	2.9	1.5	4.4	3.1	2.5	4.0	5.0	3.4	6.5	3.0	1.6	4.8
MnO	0.04	0.007	0.09	0.04	0.02	0.04	0.07	0.05	0.10	0.07	0.03	0.10
MgO	0.3	0.07	0.7	0.3	0.2	0.3	0.5	0.2	1.8	0.9	0.3	1.8
CaO	1.1	0.4	2.6	1.2	1.0	1.5	2.0	1.3	3.3	2.3	1.0	3.8
Na <sub>2</sub> O	3.7	2.6	5.0	3.5	3.0	4.4	3.9	3.4	5.4	4.2	3.9	4.7
K <sub>2</sub> O	5.0	3.3	6.3	5.6	4.2	6.5	4.7	3.1	5.6	4.8	3.9	5.8
TiO <sub>2</sub>	0.3	0.1	0.5	0.3	0.2	0.4	0.5	0.3	0.6	0.5	0.2	0.7
P <sub>2</sub> O <sub>5</sub>	0.06	.01	0.4	0.06	0.02	0.07	0.1	0.03	0.2	0.1	0.04	0.2
LOI	0.7	0.3	1.2	0.8	0.3	1.1	0.5	0.2	0.8	0.6	0.4	0.7
Transition Elements (ppm)												
Co	2	0.5	4	1	.5	2	4	0.5	13	4	1	9
Cr	21	10	90	16	10	50	17	10	30	18	10	40
Cu	20	5	220	14	5	80	14	5	40	24	5	70
Ni	12	10	50	10	10	10	10	10	10	11	10	20
Sc	5	1	8	4	2	6	8	3	13	7	3	12
V	9	3	24	11	3	21	17	9	65	36	7	75

Zn	72	15	190	86	40	130	120	80	170	57	15	90
----	----	----	-----	----	----	-----	-----	----	-----	----	----	----

Low Field Strength Elements (ppm)

Ba	1286	53	2110	1226	602	1684	1303	757	1741	1097	669	1437
Cs	0.9	0.3	2.7	0.5	0.3	1.6	1.1	0.3	2.3	3.0	0.8	4.4
Ga	20	17	26	23	19	26	25	23	27	19	16	21
Rb	135	81	190	140	105	154	118	78	149	125	113	136
Sr	75	13	135	70	26	129	107	49	141	311	114	493
Pb	30	9	380	40	22	104	26	11	42	18	14	22
Th	18.0	15	26.6	18.7	15.8	21.3	18.2	16.1	20.2	12.7	9.2	19.2
U	9.3	5.1	79.3	8.4	5.0	21.8	4.4	3.9	5.1	4.0	1.8	9.4

High Field Strength Elements (ppm)

Hf	11.2	7.7	14.4	12.5	9.3	15.7	18.0	14.0	20.2	7.5	6.3	8.7
Nb	23	20	32	29	22	36	36	28	42	16	13	18
Ta	1.9	1.7	3.1	2.23	1.9	3.0	2.1	2.0	2.5	1.1	0.7	1.8
Y	46	40	89	82	41	119	89	85	96	29	22	38
Zr	436	217	598	449	235	556	712	499	798	281	221	335

Rare Earth Elements (ppm)

La	81	64	104	110	81	146	140	116	155	58	48	80
Ce	162	133	209	228	163	304	283	243	327	118	98	163
Pr	18.8	16.1	23	26.2	~	33.9	33.	26.9	36.6	13.4	11.3	16.9
Nd	60.8	51.9	78.3	83.4	.1 55.9	111	114	87.3	134	43.0	34.8	50.3
Sm	10.2	8.5	13.6	15.3	9.4	20.0	19.7	16.4	21.8	7.0	5.8	8.5
Eu	1.2	0.2	1.7	1.9	1.1	2.5	2.7	2.1	2.9	1.2	0.7	1.5
Gd	8.3	7.1	11.9	13.4	7.6	17.7	16.9	15.0	19.5	5.4	4.7	6.8

Tb	1.4	1.1	2.2	2.3	1.2	3.0	2.8	2.5	3.1	0.8	0.7	1.1
Dy	7.9	6.8	13.6	13.6	7.0	18.2	16.1	14.6	17.1	4.8	4.0	6.1
Ho	1.6	1.3	2.8	2.8	1.4	3.7	3.2	2.9	3.4	1.0	0.7	1.2
Er	4.6	3.9	8.3	8.3	4.1	11.3	9.2	8.5	9.8	2.8	2.2	3.5
Tm	0.7	0.6	1.3	1.2	0.6	1.7	1.4	1.2	1.5	0.4	0.4	0.5
Yb	4.5	3.8	8.2	7.8	4.2	10.7	8.6	7.9	9.4	2.9	2.4	3.4
Lu	0.7	0.6	1.2	1.2	0.7	1.6	1.3	1.2	1.4	0.5	0.4	0.5
Volatile Elements (ppm)												
Ag	0.5	0.3	1.4	0.3	0.3	0.3	0.6	0.3	1.0	0.5	0.3	1.9
As	4.6	2.5	34	4.7	2.5	27	9.9	2.5	38	5.7	2.5	28
Be	3	2	5	3	2	7	3	1	4	3	2	3
Bi	1.1	0.2	69.4	1.2	0.2	11.2	0.4	0.2	1.4	0.2	0.2	0.2
Ge	1	0.5	2	1	0.5	2	1	1	2	1	0.5	1
In	0.1	0.1	0.1	0.1	0.1	0.1	0.1	0.1	0.1	0.1	0.1	0.1
Mo	3	1	18	4	1	14	4	3	4	1	1	2
Sb	1.6	0.3	13.9	0.8	0.3	3.6	1.2	0.3	3.4	1.2	0.3	3.6
Sn	3	2	14	4	3	7	4	3	7	2	1	3
Tl	0.7	0.3	1.1	0.8	0.6	1.0	0.6	0.4	1	0.6	0.5	0.7
W	1.7	0.5	28	1	0.5	2	0.8	0.5	3	0.6	0.5	1
Normative Mineralogies (%)												
%AN	6.3	0.07	14.9	4.6	0	12.0	12.4	4.5	21.2	19.0	3.5	30.2
Q	31.3	26.6	37.7	29.6	24.3	34.9	23.5	17.6	29.4	20.4	15.0	27.2
or	29.7	19.3	37.0	32.7	24.8	38.2	27.7	18.1	32.9	28.2	23.2	34.0
ab	31.1	21.8	42.0	29.6	25.5	36.9	33.3	28.4	46.0	35.4	33.0	39.6

an	2.1	0.02	5.2	1.5	0	4.0	4.6	1.4	7.6	8.7	1.3	14.3
C	0	0	0	0	0	0	0	0	0	0.02	0	0.1
di	1.9	0.2	6.0	2.6	1.0	4.6	4.0	1.9	7.3	1.1	0	3.3
hy	0.3	0	2.5	0.3	0	1.	2.9	0	6.6	2.5	0	5.4
wo	.3	0	2.6	0.4	0	1.1	0.02	0	.02	0.1	0	0.7
ol	0	0	0	0	0	0	0	0	0	0	0	0
ac	0	0	0	0.1	0	1.3	0	0	0	0	0	0
mt	2.3	0	2.9	2.5	2.0	2.7	2.9	2.6	3.1	1.6	0	3.2
il	0.6	0.02	1.0	0.6	0.4	0.7	0.9	0.5	1.2	0.8	0.1	1.4
hem	0.2	0	1.6	0	0	0	0	0	0	0.8	0	1.9
ap	0.1	0.02	0.9	0.1	0.1	0.2	0.3	0.1	0.4	0.3	0.1	0.5
ru	0	0	0	0	0	0	0	0	0	0.03	0	0.3

**Table 3.2:** Average (avg), low and high values for the biotite-hornblende schist dikes, gabbroic dikes, strongly magnetic gabbroic dikes, and andesitic dikes of the major oxides (oxide wt.%), transition metals (ppm), low field strength elements (ppm), high field strength elements (ppm), rare earth elements (ppm), volatile elements (ppm), and the normative mineral percentages after Irvine and Baragar (1971).

	Bt-Hb Schists			Gabbroic			Magnetic Gab			Andesitic		
	avg	low	high	avg	low	high	avg	low	high	avg	low	high
Major Oxides (wt.%)												
SiO <sub>2</sub>	50.8	46.5	53.4	47.7	46.6	49.0	48.1	46.5	48.7	53.0	51.5	56.0
Al <sub>2</sub> O <sub>3</sub>	14.7	11.1	16.5	16.8	15.1	18.1	15.2	13.3	16.7	15.3	14.3	18.6
Fe <sub>2</sub> O <sub>3</sub>	11.7	8.1	15.1	12.3	10.9	13.8	13.9	12.1	16.5	10.7	8.2	12.0
MnO	0.2	0.1	0.3	0.2	0.2	0.2	0.2	0.2	0.3	0.1	0.1	0.2
MgO	6.6	4.4	15.8	7.9	7.2	9.1	5.7	4.7	6.6	4.4	3.4	4.9
CaO	8.6	6.7	9.9	9.7	9.4	10.2	8.4	7.6	9.2	7.0	5.5	7.7
Na <sub>2</sub> O	3.2	1.1	4.6	2.9	2.5	3.5	3.3	3.0	4.0	3.9	3.3	5.2
K <sub>2</sub> O	2.1	1.2	3.9	1.0	0.5	1.7	1.9	1.4	2.9	2.7	2.2	3.2
TiO <sub>2</sub>	1.3	0.5	2.4	1.3	1.0	1.6	1.8	1.3	2.4	1.8	0.7	2.2
P <sub>2</sub> O <sub>5</sub>	0.7	0.2	2.4	0.2	0.1	0.4	1.4	0.8	2.4	1.2	0.3	2.0
LOI	1.3	0.5	2.4	1.2	0.8	1.6	0.7	0	1.1	1.1	0.4	1.4
Transition Elements (ppm)												
Co	36	21	58	46	29	53	39	31	46	25	21	31
Cr	222	0	1310	95	40	270	61	0	130	77	0	110
Cu	48	0	100	41	20	50	75	20	100	32	20	40
Ni	78	0	510	73	30	100	62	0	110	24	0	60
Sc	28	19	35	30	25	39	27	22	31	16	11	18
V	212	131	259	181	151	217	230	191	332	167	106	204

Zn	120	60	210	105	0	40	152	90	230	129	90	200
Low Field Strength Elements (ppm)												
Ba	946	358	2700	294	97	855	1437	925	2490	1878	1460	2320
Cs	2.5	0.4	15.3	1.4	0.5	2.5	0.7	0.4	1.3	1.7	0.5	4.1
Ga	19	13	22	17	12	19	20	18	23	20	18	22
Rb	64	19	156	43	27	65	29	19	50	60	25	142
Sr	750	227	4200	317	254	417	759	585	898	1275	820	1530
Pb	9	0	17	7	0	19	5	0	12	7.4	0	12
Th	2.1	0.3	4.6	0.4	0.1	0.7	0.7	0.4	1.1	1.5	0.6	4.8
U	1.0	0.2	2.9	0.8	0.2	4.4	0.6	0.4	1.1	1.0	0.4	1.8
High Field Strength Elements (ppm)												
Hf	2.7	1.3	5.3	2.7	1.6	11.2	3.0	2.3	4.0	2.7	1.5	4.9
Nb	4.4	2.2	7.7	1.6	0.9	3.1	3.7	2.9	5.1	5.6	3.2	8.5
Ta	0.3	0.1	0.4	0.1	0	0.2	0.2	0.1	0.3	0.3	0.2	0.4
Y	24.7	13.5	50.4	23.8	19.4	27.2	34.3	23.7	51.4	22.2	9.8	28.5
Zr	109	50	223	105	59	488	118	85	167	107	55	200
Rare Earth Elements (ppm)												
La	28.2	14.6	62.0	6.4	2.9	15.8	34.5	22.5	52.7	45.8	15.8	72.7
Ce	62.3	31.9	130	15.5	8.2	35.2	79.4	60.6	116	102	35.1	159
Pr	7.9	3.7	15.9	2.2	1.3	5.0	10.4	6.7	15.8	13.3	4.4	20.3
Nd	28.8	13.3	62.1	10.6	7.3	19.6	40.5	25.3	61.9	45.5	15.7	67.0
Sm	6.4	2.8	14.4	3.1	2.4	4.5	9.5	6.0	15.3	9.3	3.5	13.2
Eu	1.9	0.8	4.7	1.3	1.0	1.6	3.0	1.9	4.9	2.8	1.2	3.8
Gd	5.5	2.7	12.3	3.6	3.0	4.3	8.4	5.5	13.2	7.0	2.8	9.6

Tb	0.8	0.4	1.7	0.7	0.6	0.8	1.2	0.8	1.9	0.9	0.4	1.3
Dy	4.6	2.3	9.4	4.2	3.4	5.1	6.4	4.4	9.8	4.5	2.0	6.1
Ho	0.9	0.5	1.8	0.8	0.7	1.0	1.2	0.8	1.8	0.8	0.3	1.0
Er	2.5	1.4	4.9	2.5	2.1	3.0	3.3	2.5	4.9	2.1	0.9	2.6
Tm	0.3	0.2	0.7	0.4	0.3	0.4	0.5	0.3	0.7	0.3	0.1	0.4
Yb	2.1	1.2	3.8	2.3	1.9	2.7	2.8	2.0	4.0	1.6	0.8	2.1
Lu	0.3	0.2	4.6	0.3	0.3	0.4	0.4	0.3	0.6	0.2	0.1	0.3

Volatile Elements (ppm)

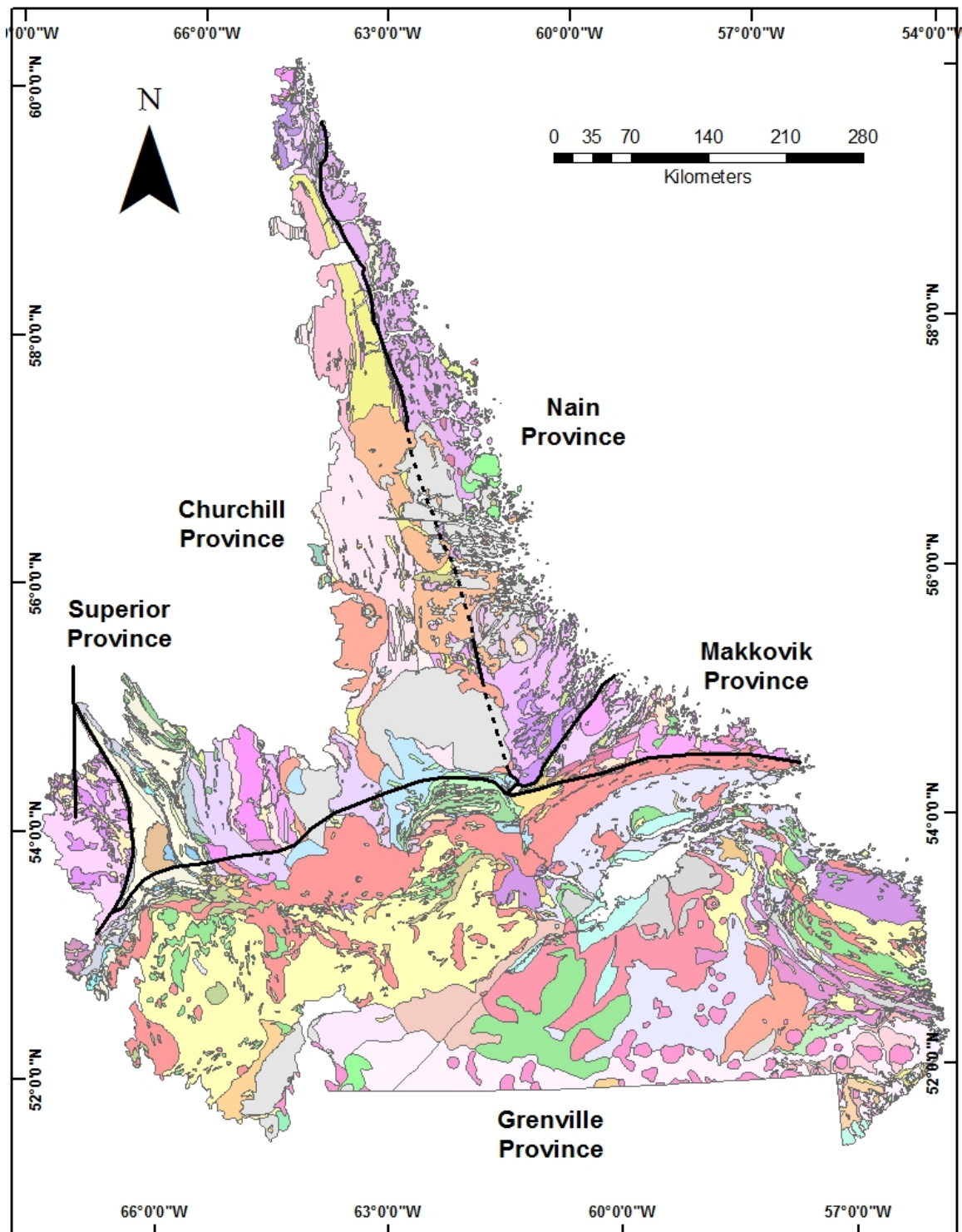
Ag	0	0	0	0	0	0	0	0	0	0	0	0
As	0	0	0	0	0	0	0.5	0	6	0.5	0	5
Be	2	1	3	1	1	2	2	2	3	2.5	2	3
Bi	0	0	0.3	0	0	0	0	0	0	0.1	0	0.3
Ge	19	13	22	1.0	0	1.6	1.2	0.9	1.7	0.9	0.7	1.0
In	0	0	0	0	0	0	0	0	0	0	0	0
Mo	0.2	0	3	0	0	0	0	0	0	0	0	0
Sb	9.2	0	200	1	0	2	0.8	0	4.1	1.3	0	4.5
Sn	0.5	0	2	0.1	0	1	0.3	0	1	0.7	0	2
Tl	0.5	0.1	1.4	0.4	0.1	1.0	0.3	0.1	0.5	0.5	0.1	1.8
W	0.4	0	0.8	0	0	0	0	0	0	0	0	0

Normative Mineralogies (%)





































%AN	43.9	30.1	78.4	57.2	49.5	61.3	42.3	32.0	49.9	34.6	29.6	37.8
Q	0.5	0	3.5	0	0	0	0	0	0	1.6	0	6.2
or	12.6	6.9	23.2	5.7	2.8	10.0	11.3	8.2	17.0	15.7	13.1	19.0
ab	25.5	4.2	34.2	22.2	19.5	25.1	27.4	25.6	29.4	31.5	27.9	38.7

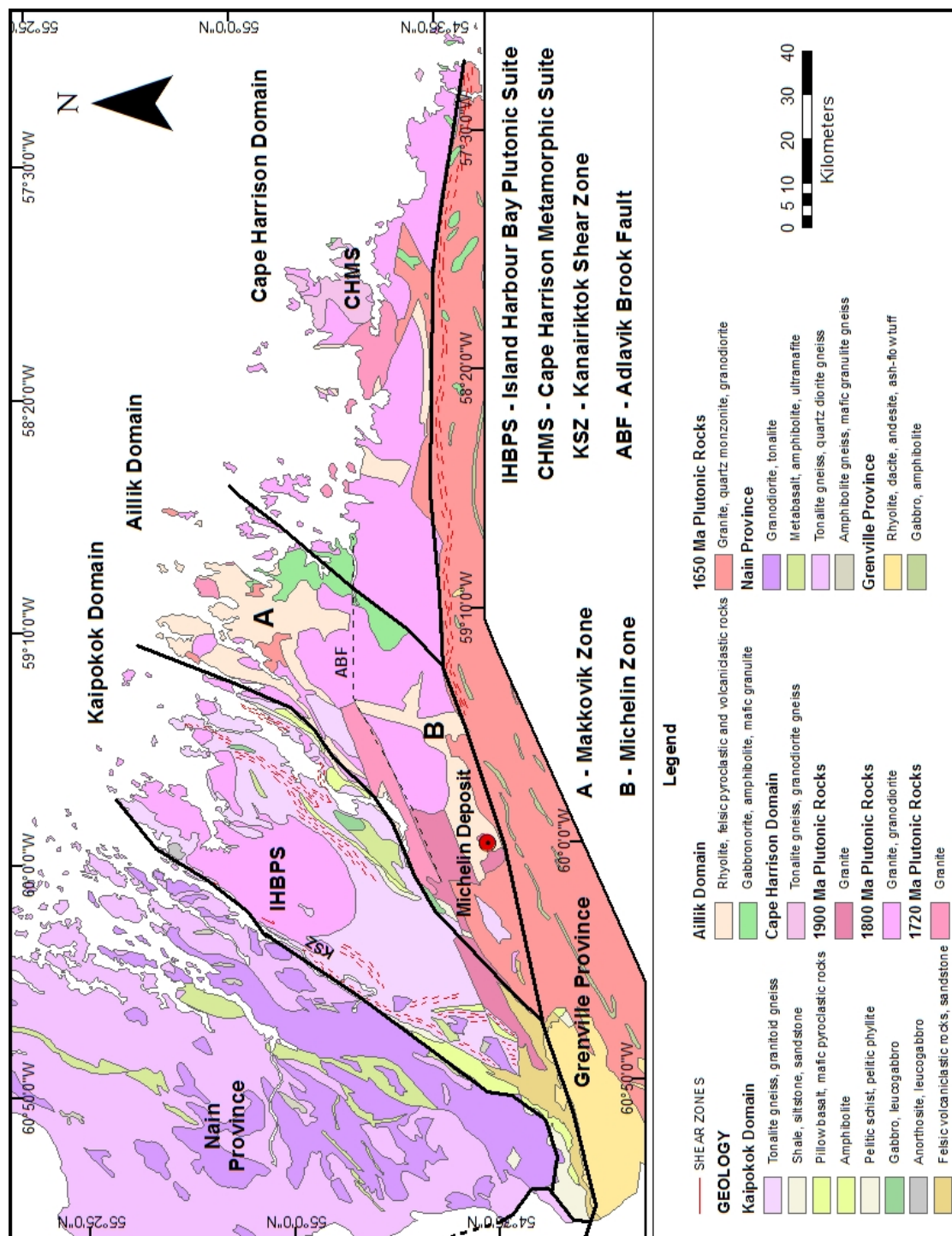
an	19.3	10.1	24.2	29.8	20.5	34.8	20.6	12.9	26.4	16.6	13.7	19.1
ne	1	0	5	1.3	0	4.6	0.4	0	3.3	0.6	0	3.1
C	0	0	0	0	0	0	0	0	0	0	0	0
di	15.2	6.9	22.5	14.1	11.3	19.7	10.1	7.8	11.9	8.1	5.8	9.7
hy	7.3	0	19.7	2.2	0	13.4	4.6	0	13.5	13.0	0	17.5
wo	0	0	0	0	0	0	0	0	0	0	0	0
ol	10.4	0	30.5	17.9	9.4	20.1	14.0	6.5	19.2	2.0	0	10.7
ac	0	0	0	0	0	0	0	0	0	0	0	0
mt	4.1	2.9	5.3	4.0	3.5	4.5	4.8	4.1	5.6	4.7	3.2	5.4
il	2.5	0.9	4.6	2.4	1.8	3.0	3.5	2.5	4.5	3.3	1.3	4.2
hem	0	0	0	0	0	0	0	0	0	0	0	0
ap	1.6	0.4	5.4	0.4	0.2	0.8	3.2	1.8	5.5	2.8	0.8	4.5
ru	0	0	0	0	0	0	0	0	0	0	0	0

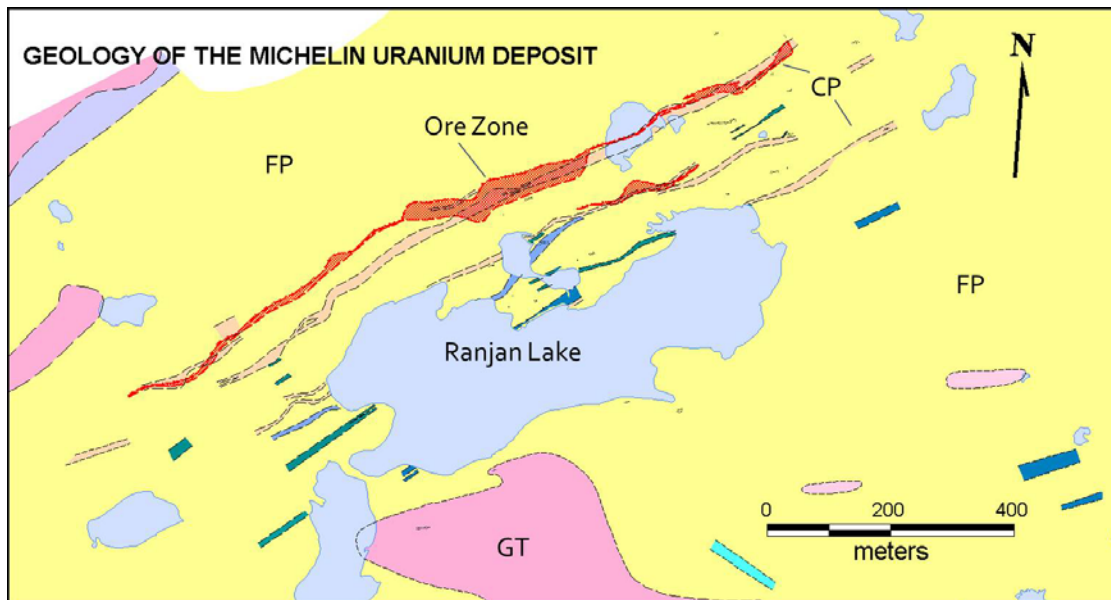




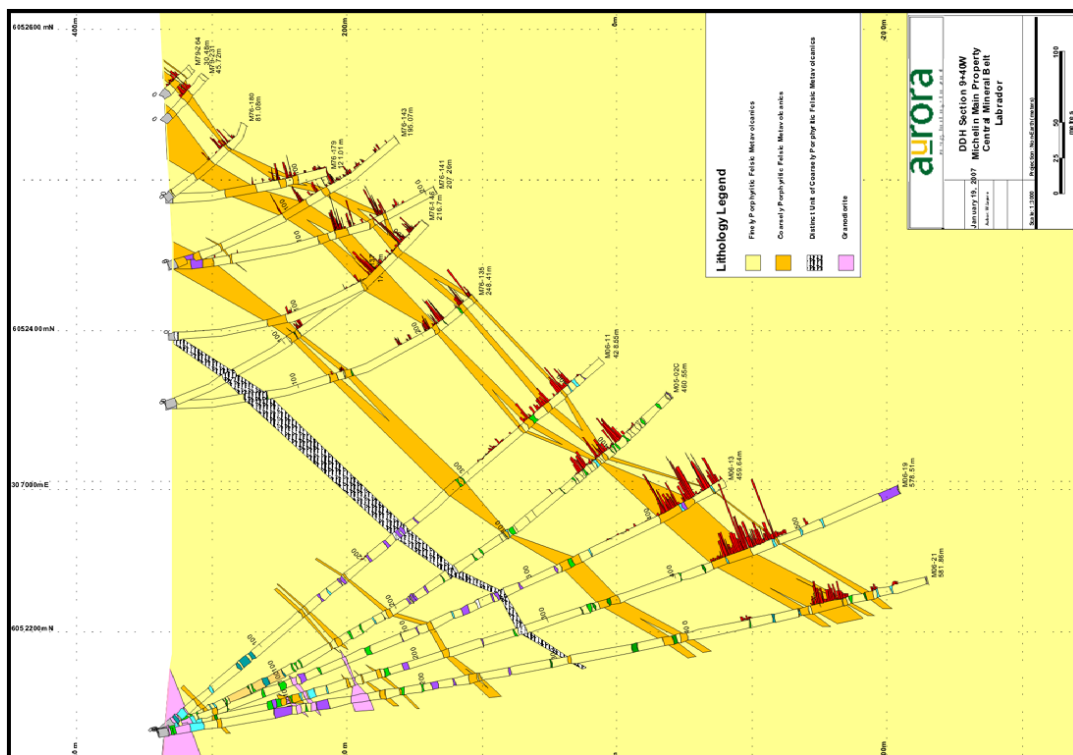
**Figure 3.1:** 1:1 Million geology map of Labrador indicating the five distinct structural provinces. A legend for the geology map is on the next page (modified from Wardle *et al.*, 1997).

GEOLOGY		
<b>Tertiary</b>		
	Breccia, melt rocks	
<b>Neoproterozoic-Cambrian</b>		
	Sandstone, limestone	
<b>Neoproterozoic</b>		
	Arkose, conglomerate	
<b>Late Mesoproterozoic</b>		
	Granite, syenite	
	Granite, monzonite, charnockite	
	Syenite, monzonite, granite	
	Monzonite, granite	
	Leuconorite, leucotroctolite, leucogabbro and anorthosite	
	Gabbro	
<b>Mid Mesoproterozoic</b>		
	Leuconorite, leucogabbro, leucotroctolite, anorthosite	
	Granite	
	Peralkaline rhyolite	
	Peralkaline granite, peralkaline syenite	
	Alkaline syenite, syenite gneiss	
	Troctolite, gabbro, norite, anorthosite	
	Basalt	
	Arkose, quartzite	
	Gabbro	
	Granite, monzonite, charnockite	
	Ferrodiorite	
	Siltstone, shale, quartzite	
<b>Early Mesoproterozoic</b>		
	Gabbro, anorthosite, ultramafite	
	Gabbro, amphibolite	
	Leuconorite, leucogabbro, leucotroctolite, anorthosite	
	Arkose, quartzite	
	Quartz diorite	
	Monzonite, charnockite, granite	
<b>Paleo or mesoproterozoic</b>		
	Gabbro, amphibolite	
	Gneiss	
	Granite, syenite, monzonite, granitoid gneiss, diorite	
	Syenite, monzonite, diorite	
	Granitoid	
<b>Late Paleoproterozoic</b>		
	Felsic volcanoclastic rocks, sandstone, arkose, conglomerate	
	Leuconorite, leucotroctolite, leucogabbro, anorthosite	
	Metasedimentary rocks, felsic volcanic rocks	
	Pelitic gneiss	
	Granitic gneiss	
	Rhyolite, dacite, andesite, ash-flow tuff, agglomerate	
	Amphibolite gneiss, mafic granulite gneiss	
	Granite	
	Gabbro, troctolite and anorthosite	
	Gabbro, amphibolite, mafic granulite	
	Granite, granitoid	
	Granodiorite gneiss	
	Dolomite marble, calc-silicate rock	
	Granite, quartz monzonite, granodiorite, syenite	
	Quartz diorite, tonalite, granodiorite	
	Granite, monzonite, charnockite	
<b>Mid Paleoproterozoic</b>		
	Tonalite, quartz diorite, granodiorite, granite	
	Granite, tonalite, tonalite gneiss	
	Granite	
	Metasedimentary gneiss	
	Pelitic gneiss	
	Tonalite gneiss, granodiorite gneiss, monzogranite gneiss	
	Alkaline basalt, mafic pyroclastic rocks	
	Granitic gneiss	
	Arkose, conglomerate	
	Gabbro, leucogabbro	
	Amphibolite	
	Pillow basalt, mafic pyroclastic rocks	
	Basalt, mafic pyroclastic rocks	
	Basalt	
	Shale, siltstone, sandstone	
	Peridotite	
	Rhyolite, felsic pyroclastic rocks, felsic volcanoclastic rocks	
	Ironstone, quartzite	
	Shale, siltstone, sandstone	
	Pelitic schist, pelitic gneiss	
	Basalt, andesite, dacite, conglomerate	
	Pelitic schist, pelitic phyllite	
	Arkose, siltstone, sandstone	
<b>Early Paleoproterozoic</b>		
	Dolomite marble	
	Amphibolite, mafic granulite	
	Granite, granodiorite	
	Tonalite, granodiorite	
	Dolomite, chert	
	Meta-ironstone, quartzite	
<b>Early Paleoproterozoic</b>		
	Gabbro, amphibolite gneiss	
<b>Archean or Proterozoic</b>		
	Granitic gneiss	
	Pelitic gneiss	
	Tonalite gneiss, granodiorite gneiss, granitoid gneiss	
	Leuconorite, leucogabbro, anorthosite	
	Amphibolite, mafic granulite	
	Gneiss	
<b>Neoaarchean</b>		
	Charnokite, granite	
	Granodiorite gneiss, monzogranite gneiss	
	Granitoid, granitoid gneiss	
	Gabbro	
	Granitic gneiss	
	Metatonalite, tonalite gneiss	
	Tonalite gneiss, granitoid gneiss	
	Tonalite, quartz diorite	
	Metasedimentary gneiss	
	Metatonalite, tonalite gneiss	
<b>Mesoarchean</b>		
	Granodiorite, tonalite	
	Amphibolite gneiss, mafic granulite gneiss	
	Metabasalt, amphibolite, ultramafite	
	Tonalite gneiss, granitoid gneiss	
	Tonalite gneiss, quartz diorite gneiss, granodiorite gneiss, amphibolite	
<b>Eo-Paleoarchean</b>		
	Granite	
	Anorthosite, leucogabbro	
	Amphibolite, mafic granulite	
	Tonalite gneiss, granitoid gneiss	
	Pelitic gneiss	
	Tonalite gneiss, quartz diorite gneiss, granodiorite gneiss, amphibolite	
<b>Undivided Archean</b>		
	Anorthosite, leucogabbro	
	Metabasalt, metasediment, metagabbro	



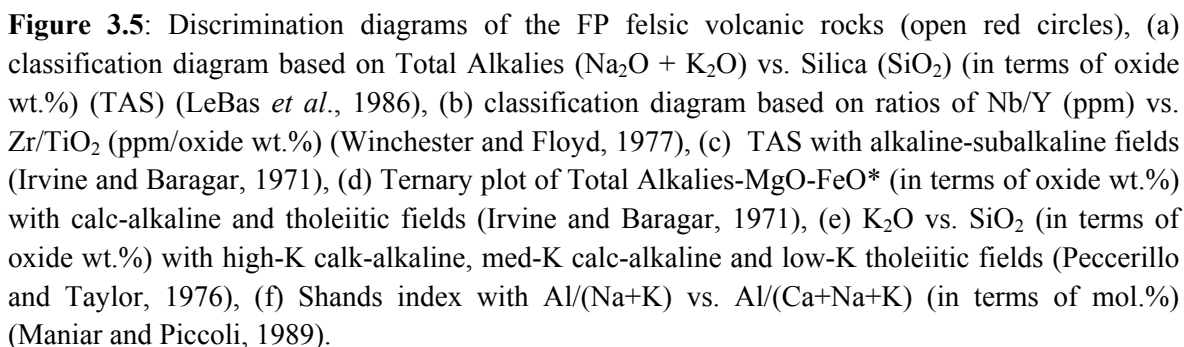


**Figure 3.3:** Geology map of the Michelin area, centered on Ranjan Lake (modified after Wilton *et al.*, 2007). FP – Fine Grained Porphyritic; CP – Coarse Grained Porphyritic; GT – Granitoid. The orange cross-hatch represents the surface expression of the mineralized zone.



**Figure 3.4:** Cross section through the Michelin deposit (Hertel *et al.*, 2009). Shows the relative stratiform nature of the FP and CP units, and how the CP units pinch and swell down dip.





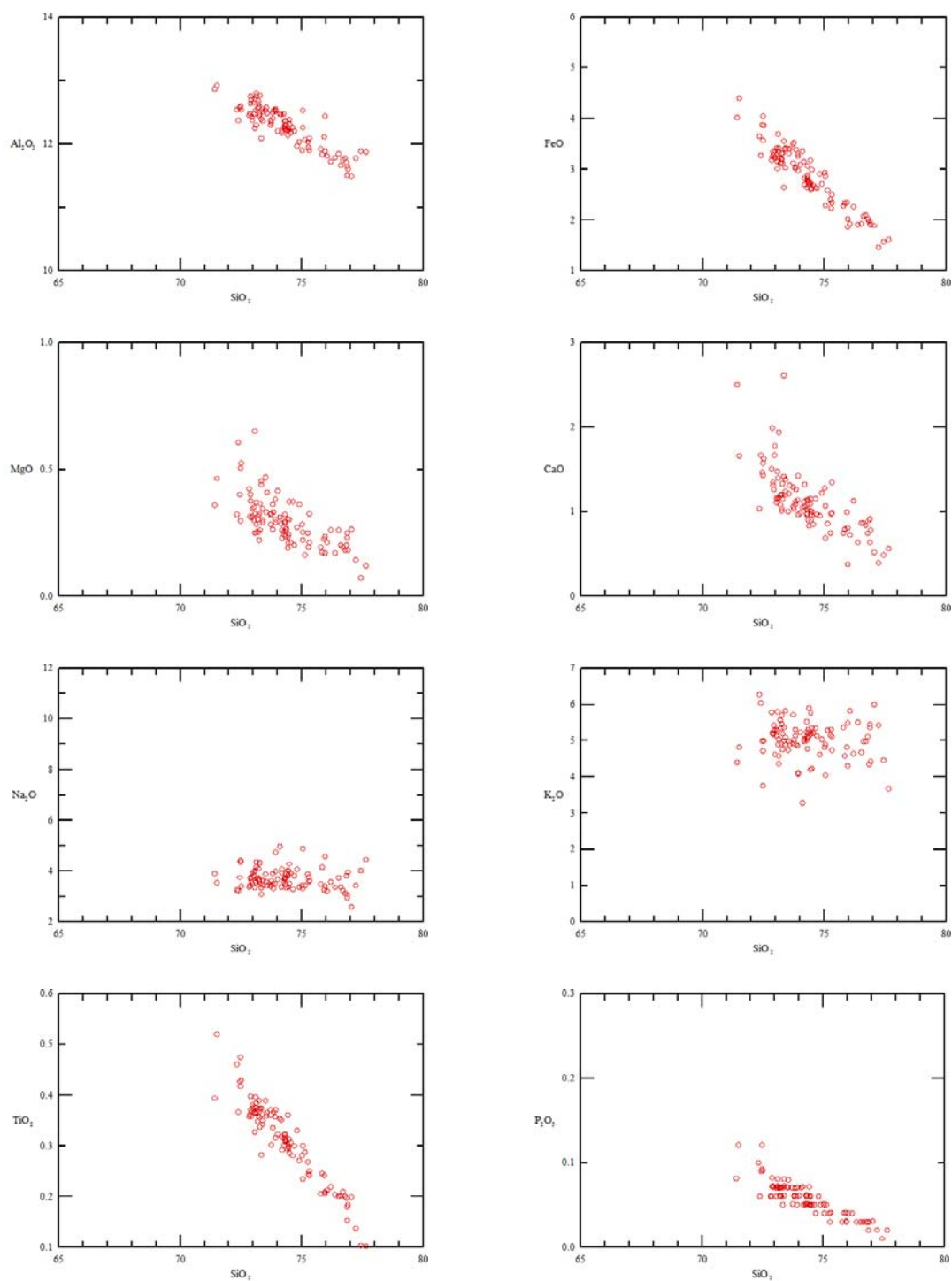


**Figure 3.6:** Harker variation diagrams for the major oxides plotted against  $\text{SiO}_2$  (in terms of oxide wt.%) of the FP felsic volcanic rocks.

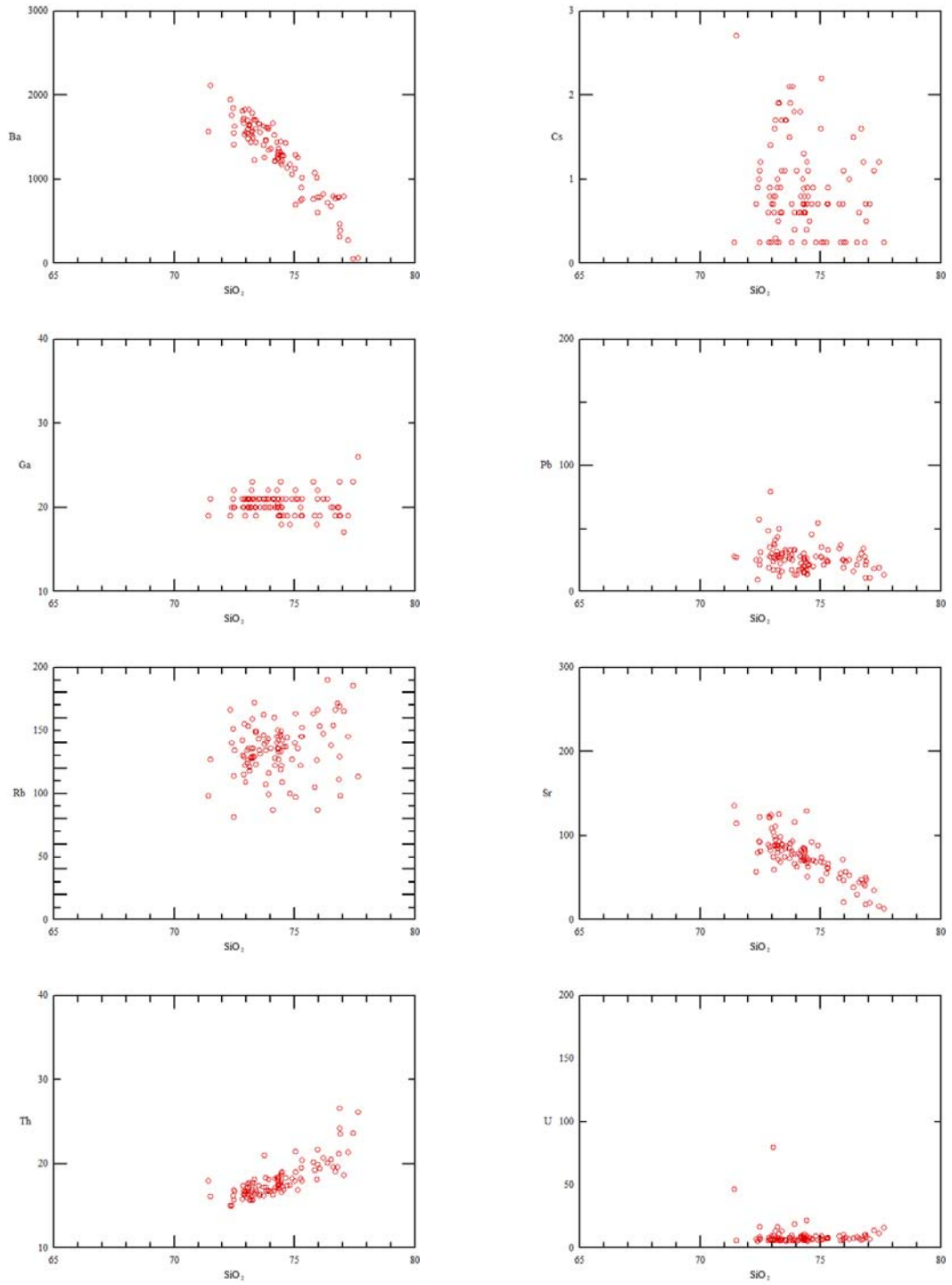


**Figure 3.7:** Harker variation diagrams for the low field strength elements (in terms of ppm) plotted against SiO<sub>2</sub> (in terms of oxide wt.%) of the FP felsic volcanic rocks.

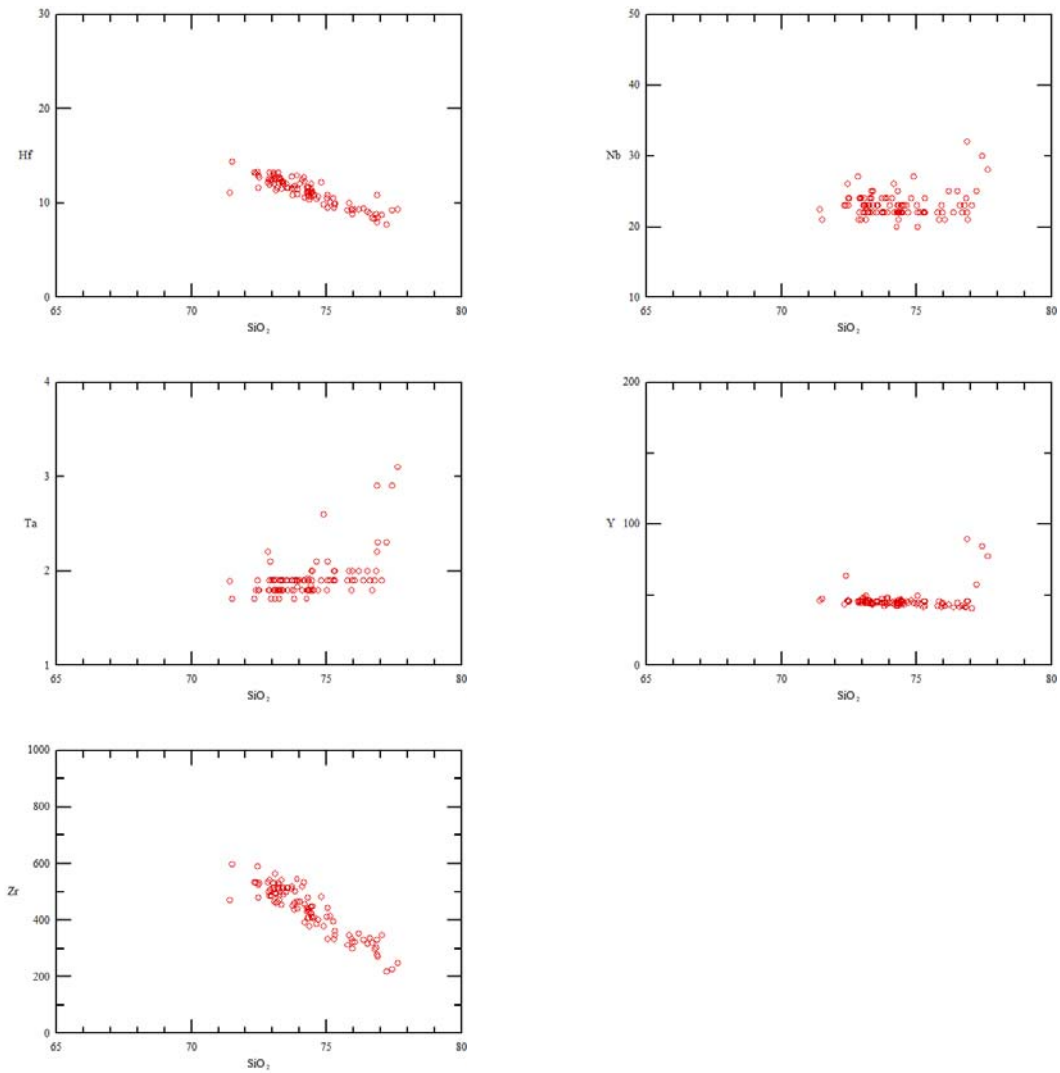


**Figure 3.8:** Harker variation diagrams for the high field strength elements (in terms of ppm) plotted against SiO<sub>2</sub> (in terms of ppm and oxide wt.%) of the FP felsic volcanic rocks.



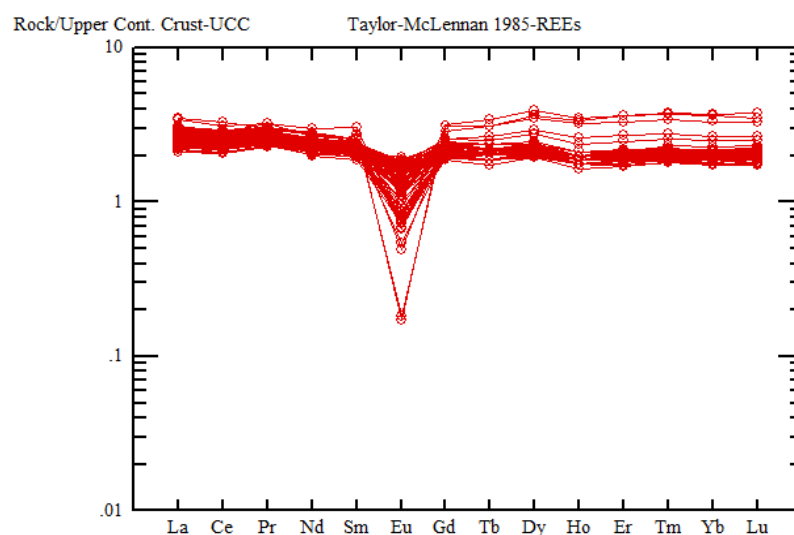


**Figure 3.9:** Log-standardized rare earth element plot normalized to upper continental crust after Taylor and McLennan (1986) for the FP felsic volcanic rocks.

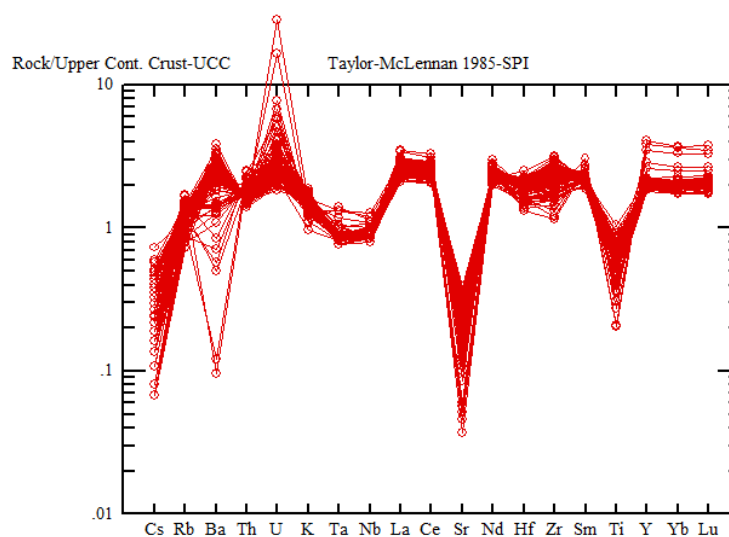


**Figure 3.10:** Log-standardized extended trace element plot normalized to upper continental crust after Taylor and McLennan (1986) for the FP felsic volcanic rocks.

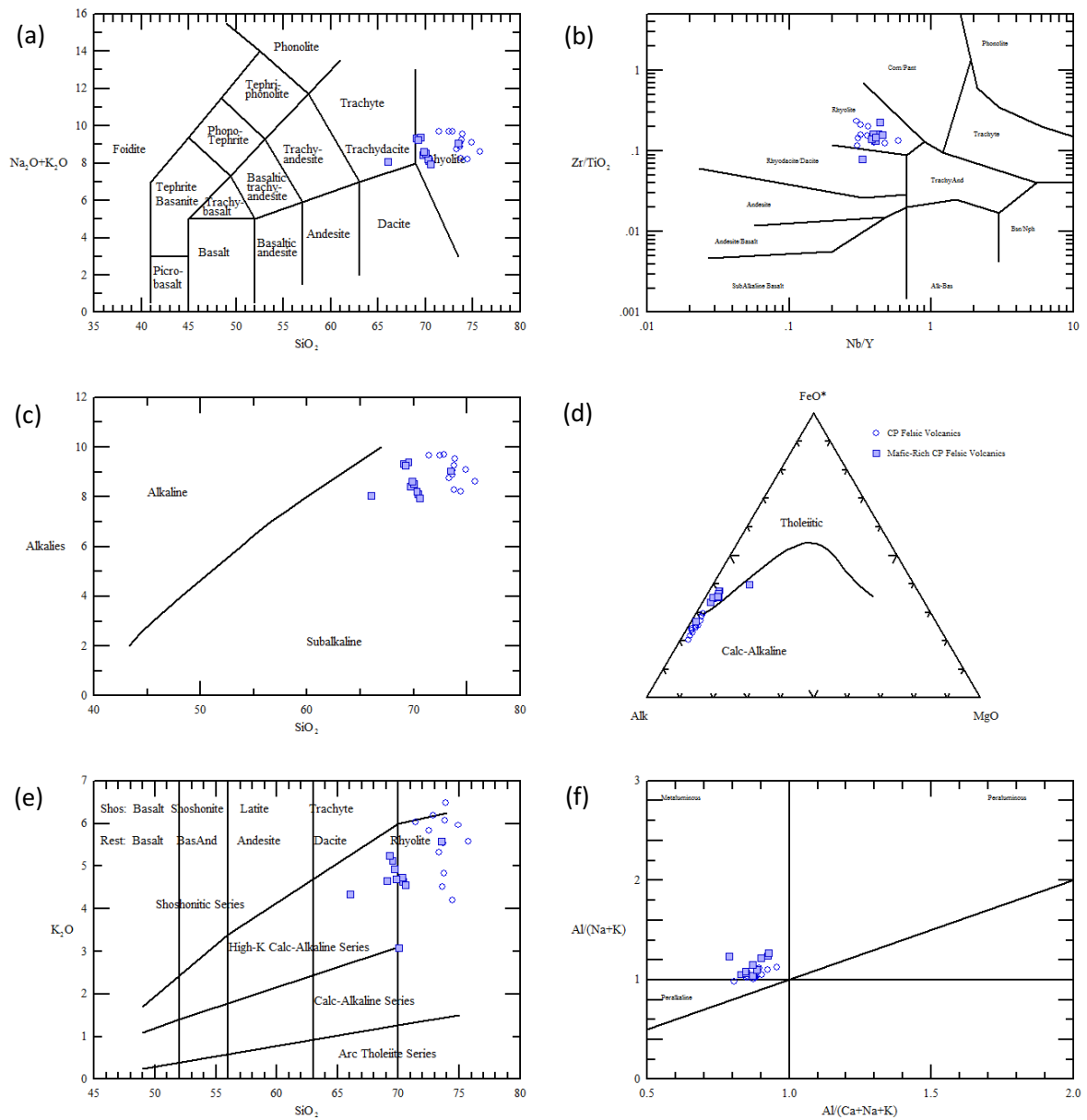


**Figure 3.11:** Discrimination diagrams of the CP felsic volcanic rocks (open blue circles) and the mafic-rich CP unit (solid blue squares), (a) classification diagram based on Total Alkalies ( $\text{Na}_2\text{O} + \text{K}_2\text{O}$ ) vs. Silica ( $\text{SiO}_2$ ) (in terms of oxide wt.%) (TAS) (LeBas *et al.*, 1986), (b) classification diagram based on ratios of Nb/Y (ppm) vs. Zr/TiO<sub>2</sub> (ppm/oxide wt.%) (Winchester and Floyd, 1977), (c) TAS with alkaline-subalkaline fields (Irvine and Baragar, 1971), (d) Ternary plot of Total Alkalies-MgO-FeO\* (in terms of oxide wt.%) with calc-alkaline and tholeiitic fields (Irvine and Baragar, 1971), (e) K<sub>2</sub>O vs.  $\text{SiO}_2$  (in terms of oxide wt.%) with high-K calc-alkaline, med-K calc-alkaline and low-K tholeiitic fields (Peccerillo and Taylor, 1976), (f) Shands index with Al/(Na+K) vs. Al/(Ca+Na+K) (in terms of mol.%) (Maniar and Piccoli, 1989).

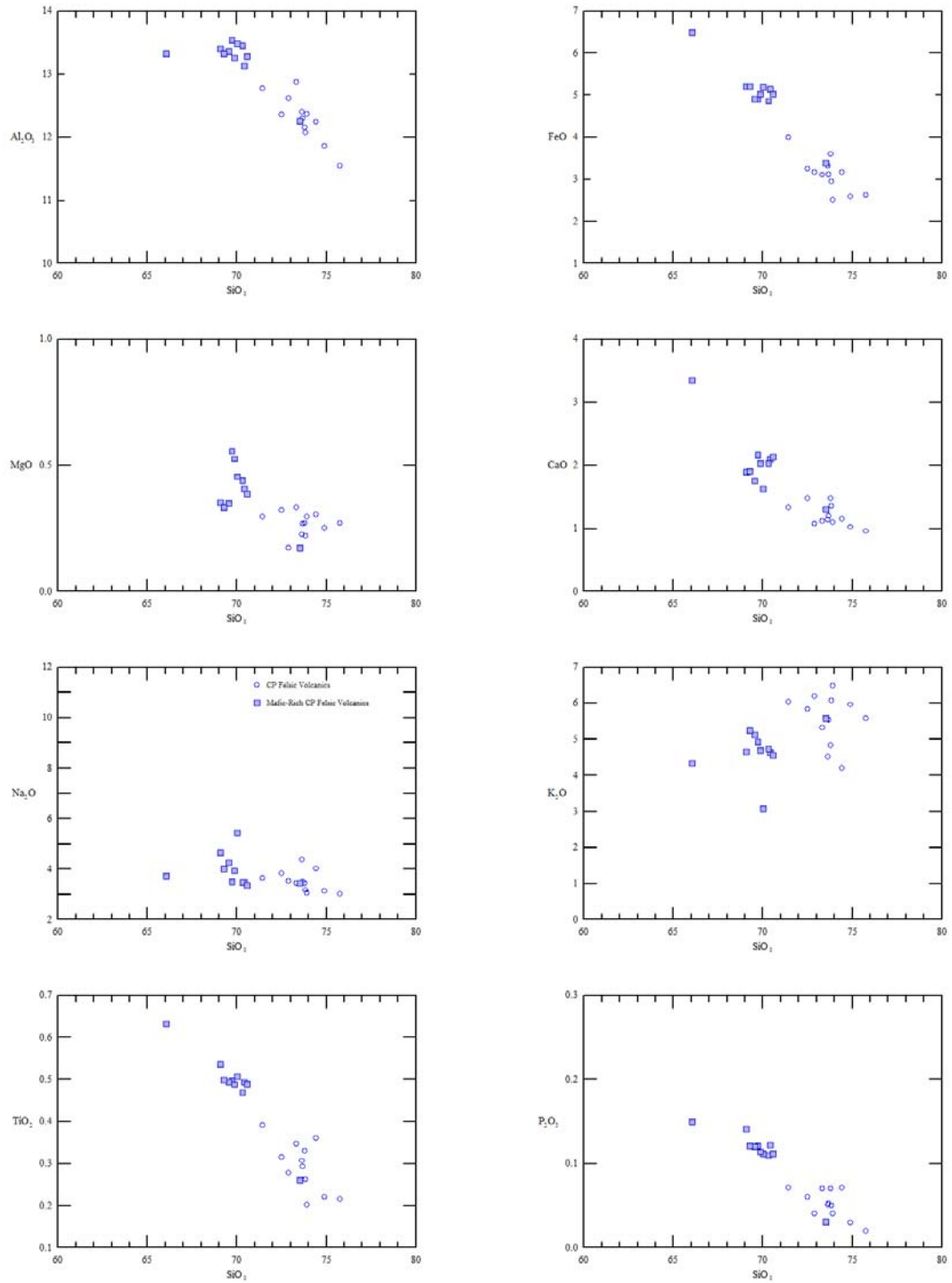


**Figure 3.12:** Harker variation diagrams for the major oxides plotted against  $\text{SiO}_2$  (in terms of oxide wt.%) of the CP (open blue circles) and mafic-rich CP (solid blue squares) felsic volcanic rocks.

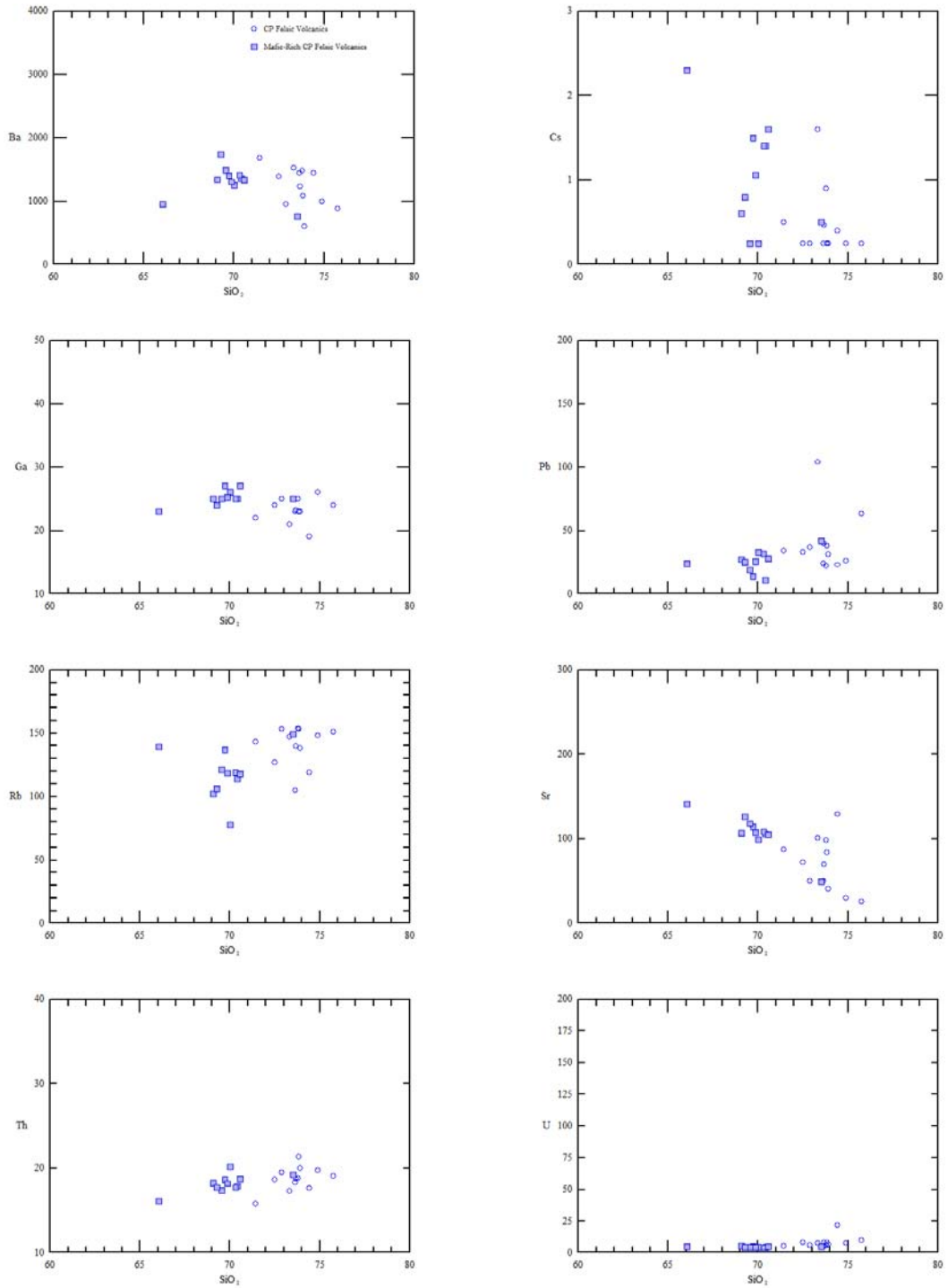


**Figure 3.13:** Harker variation diagrams for the low field strength elements (in terms of ppm) plotted against SiO<sub>2</sub> (in terms of oxide wt.%) of the CP (open blue circles) and mafic-rich CP (solid blue squares) felsic volcanic rocks.

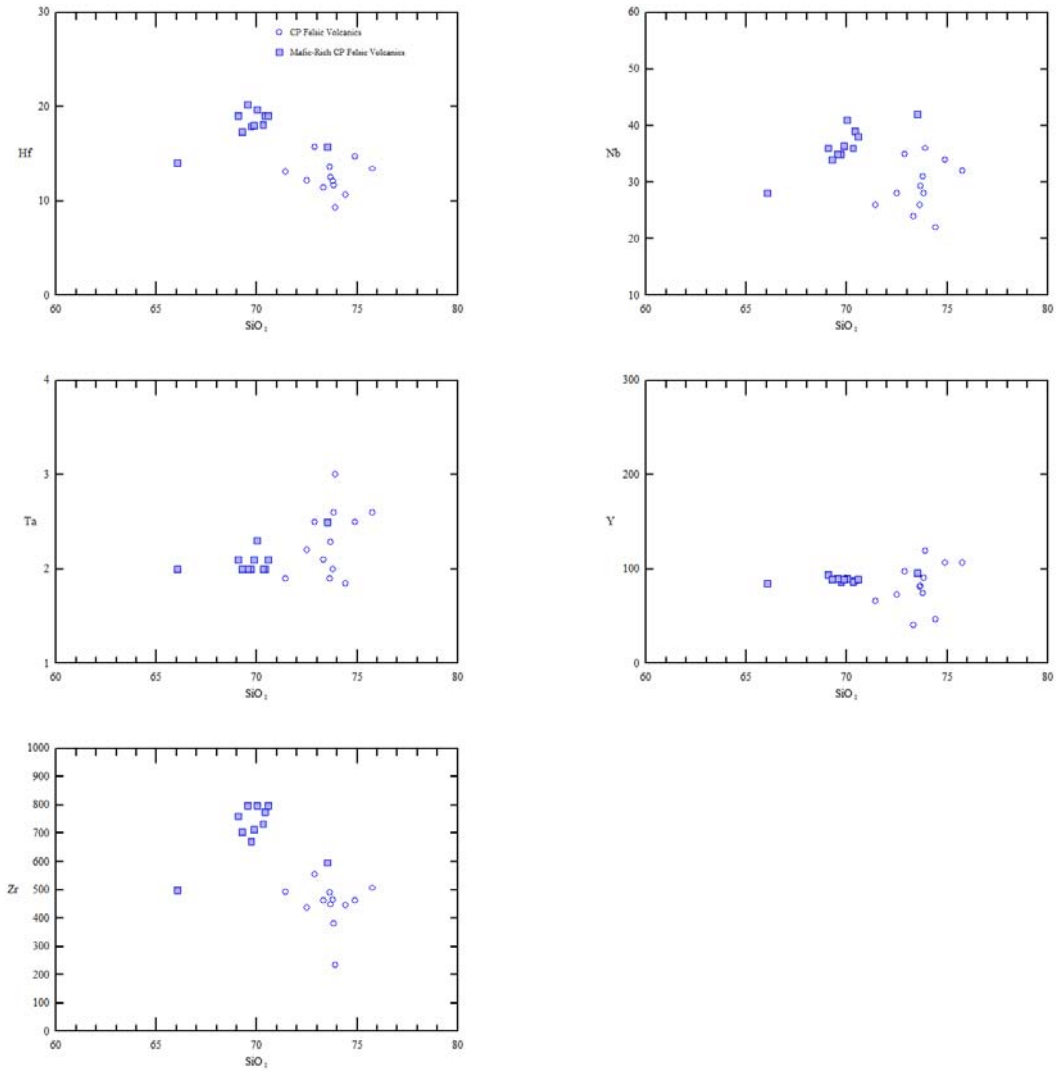


**Figure 3.14:** Harker variation diagrams for the high field strength elements (in terms of ppm) plotted against SiO<sub>2</sub> (in terms of ppm and oxide wt.%) of the CP (open blue circles) and mafic-rich CP (solid blue squares) felsic volcanic rocks.

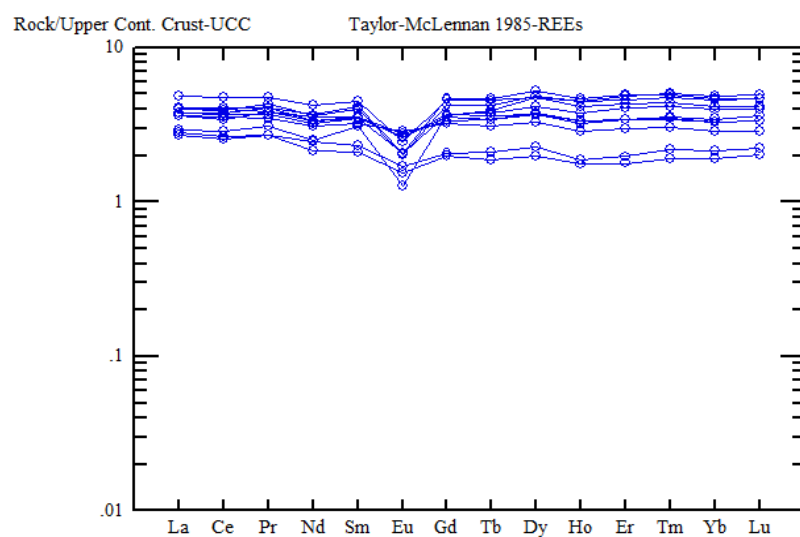


**Figure 3.15:** Log-standardized rare earth element plot normalized to upper continental crust after Taylor and McLennan (1986) for the CP felsic volcanic rocks.

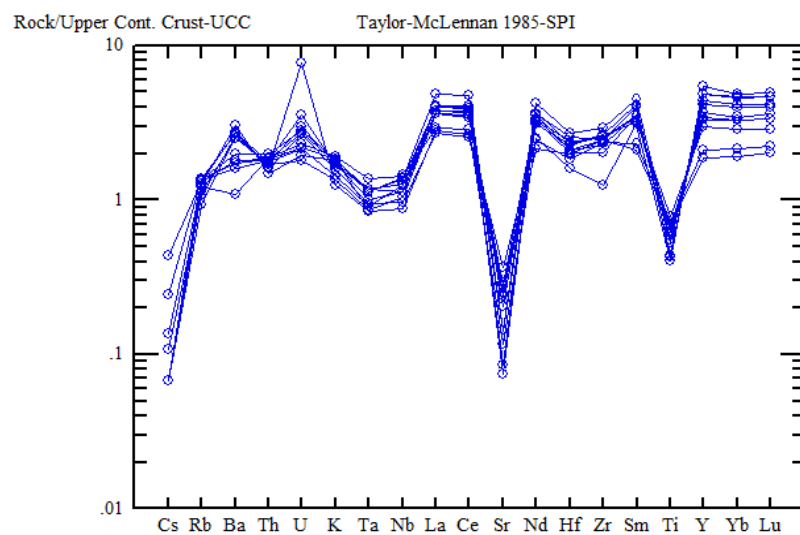


**Figure 3.16:** Log-standardized extended trace element plot normalized to upper continental crust after Taylor and McLennan (1986) for the CP felsic volcanic rocks.

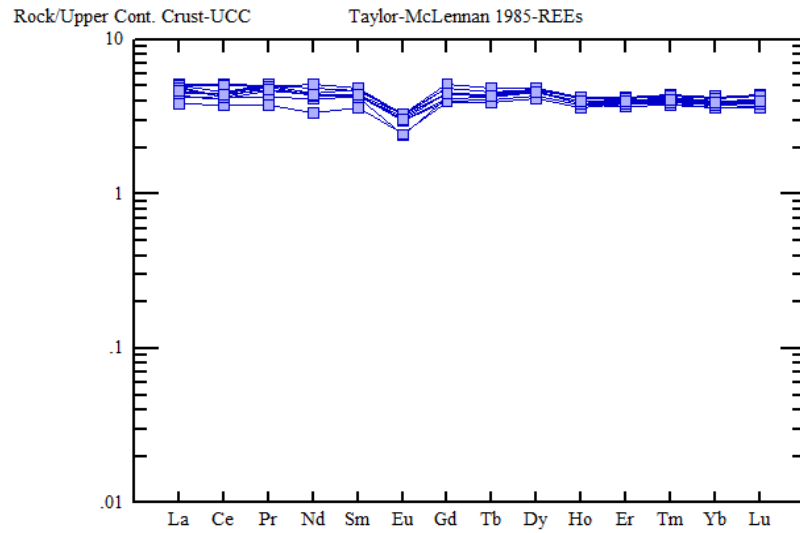


**Figure 3.17:** Log-standardized rare earth element plot normalized to upper continental crust after Taylor and McLennan (1986) for the mafic-rich CP felsic volcanic unit.

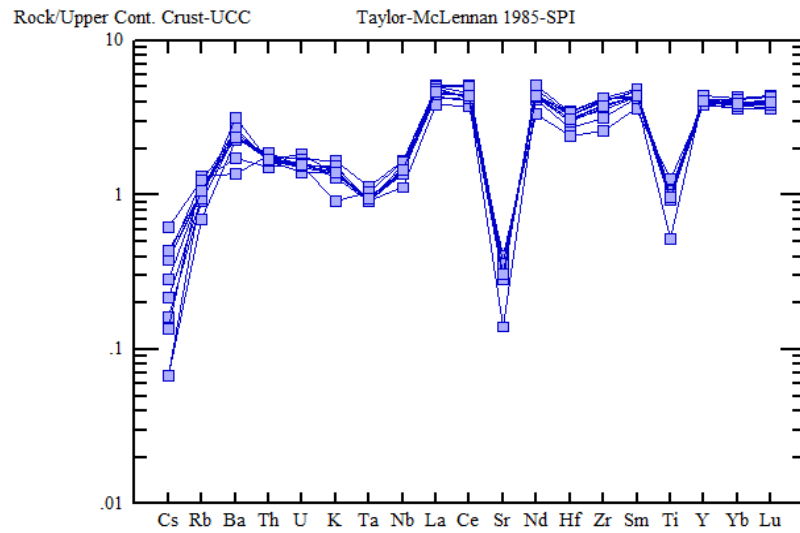


**Figure 3.18:** Log-standardized extended trace element plot normalized to upper continental crust after Taylor and McLennan (1986) for the mafic-rich CP felsic volcanic unit.

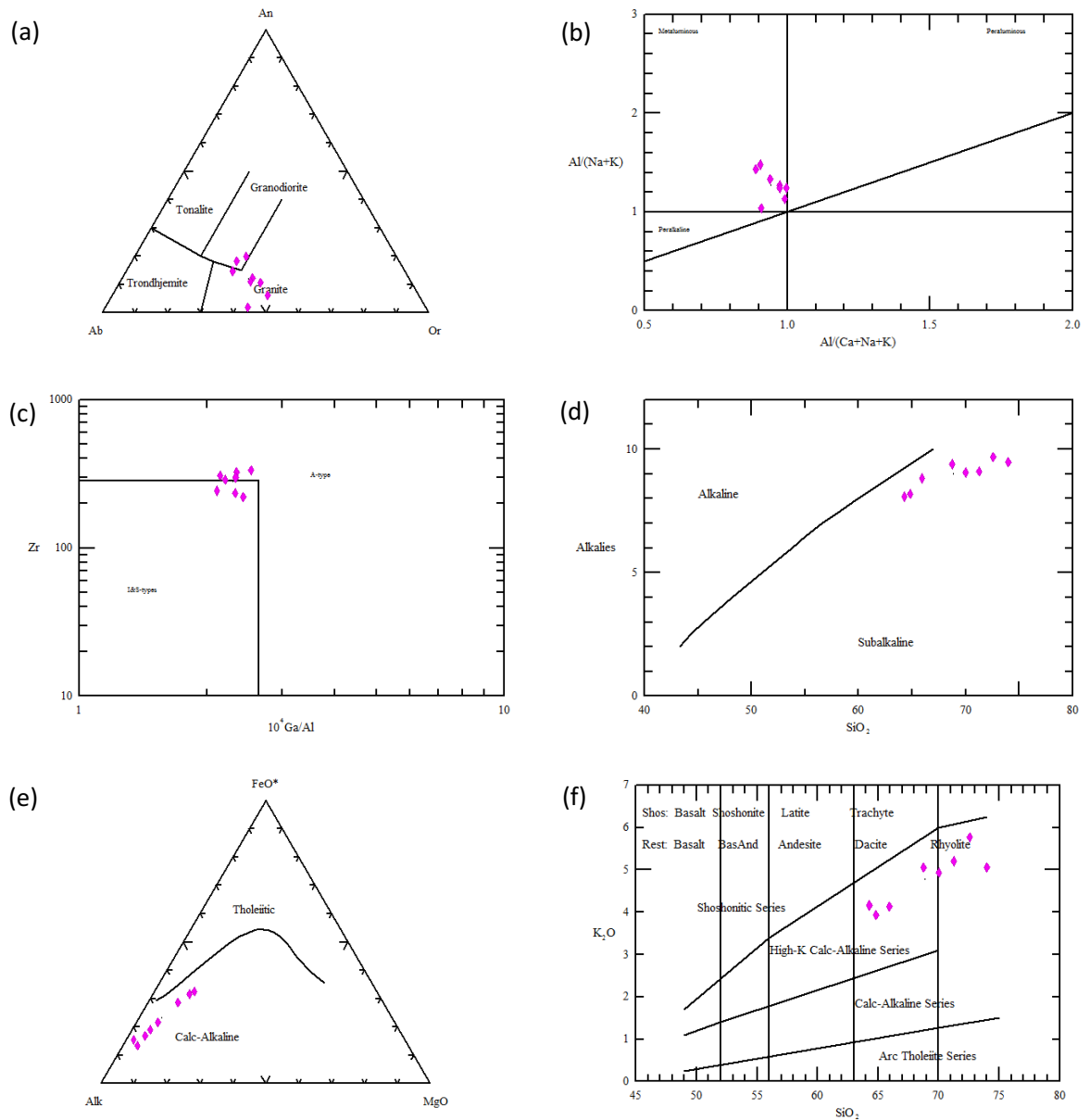


**Figure 3.19:** Discrimination diagrams of the granitoid rocks (solid pink diamonds), (a) Ternary classification diagram based An vs. Or vs. Ab (Barker, 1979), (b) Shands index with  $Al/(Na+K)$  vs.  $Al/(Ca+Na+K)$  (in terms of mol.%) (Maniar and Piccoli, 1989), (c) Magma classification based on Zr (ppm) vs. ratio of  $10^4 Ga/Al$  (ppm/oxide wt.%) (Whalen *et al.*, 1987), (d) TAS with alkaline-subalkaline fields (Irvine and Baragar, 1971), (e) Ternary plot of Total Alkalies-MgO-FeO\* (in terms of oxide wt.%) with calc-alkaline and tholeiitic fields (Irvine and Baragar, 1971), (f)  $K_2O$  vs.  $SiO_2$  (in terms of oxide wt.%) with high-K calc-alkaline, med-K calc-alkaline and low-K tholeiitic fields (Peccerillo and Taylor, 1976).



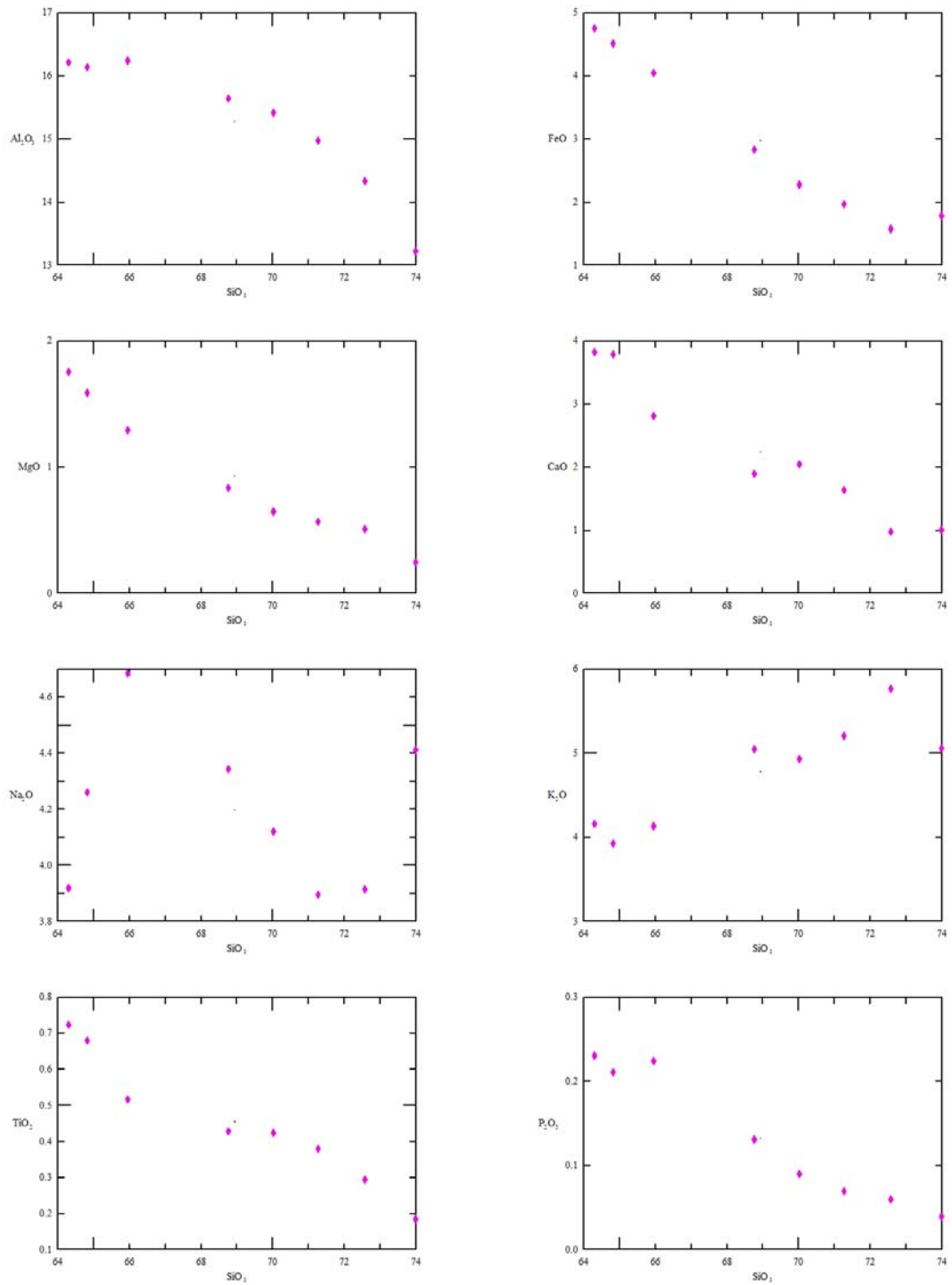


**Figure 3.20:** Harker variation diagrams for the major oxides plotted against SiO<sub>2</sub> (in terms of oxide wt.%) of the granitoid rocks.

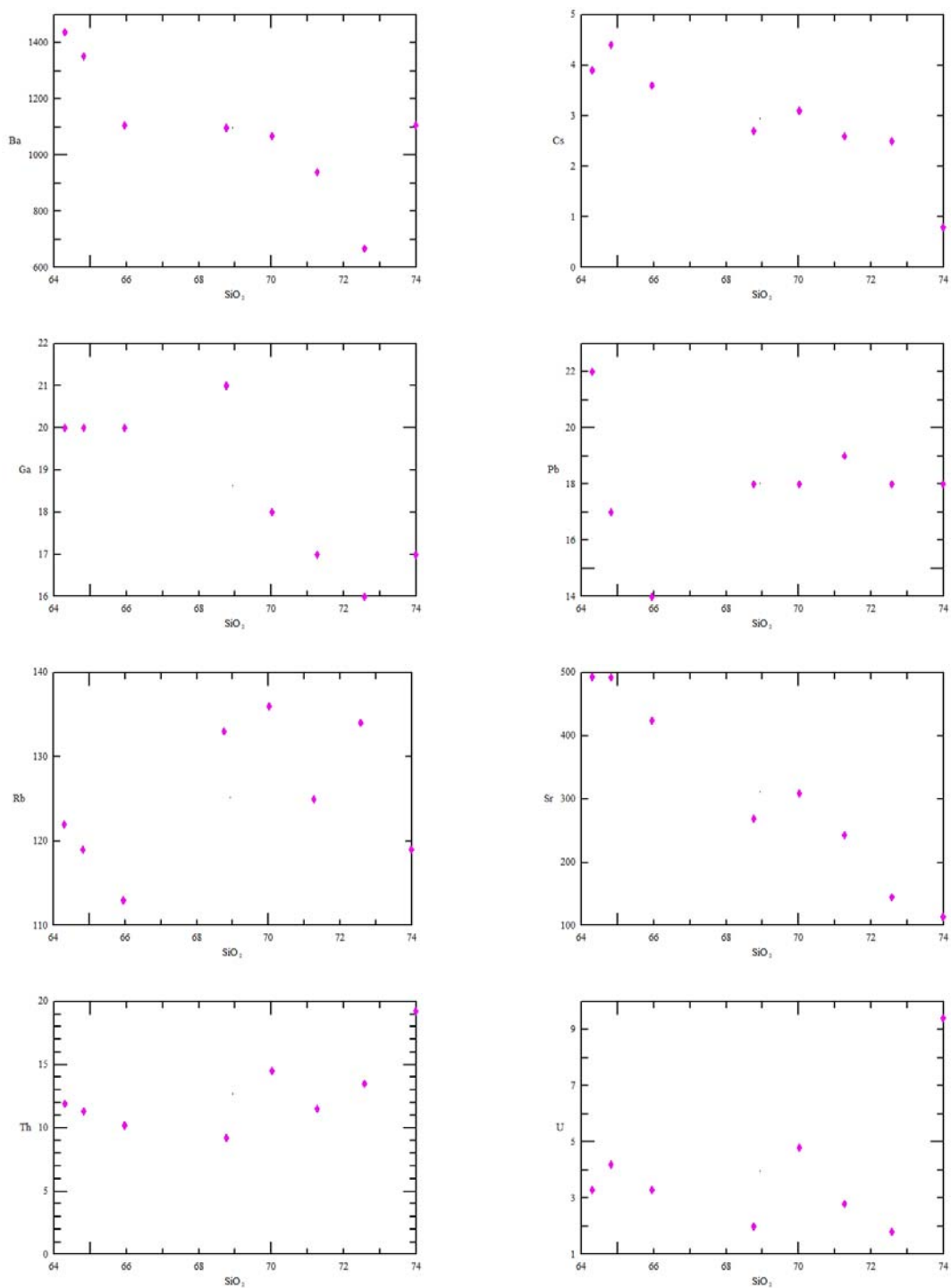


**Figure 3.21:** Harker variation diagrams for the low field strength elements (in terms of ppm) plotted against  $\text{SiO}_2$  (in terms of oxide wt.%) of the granitoid rocks.

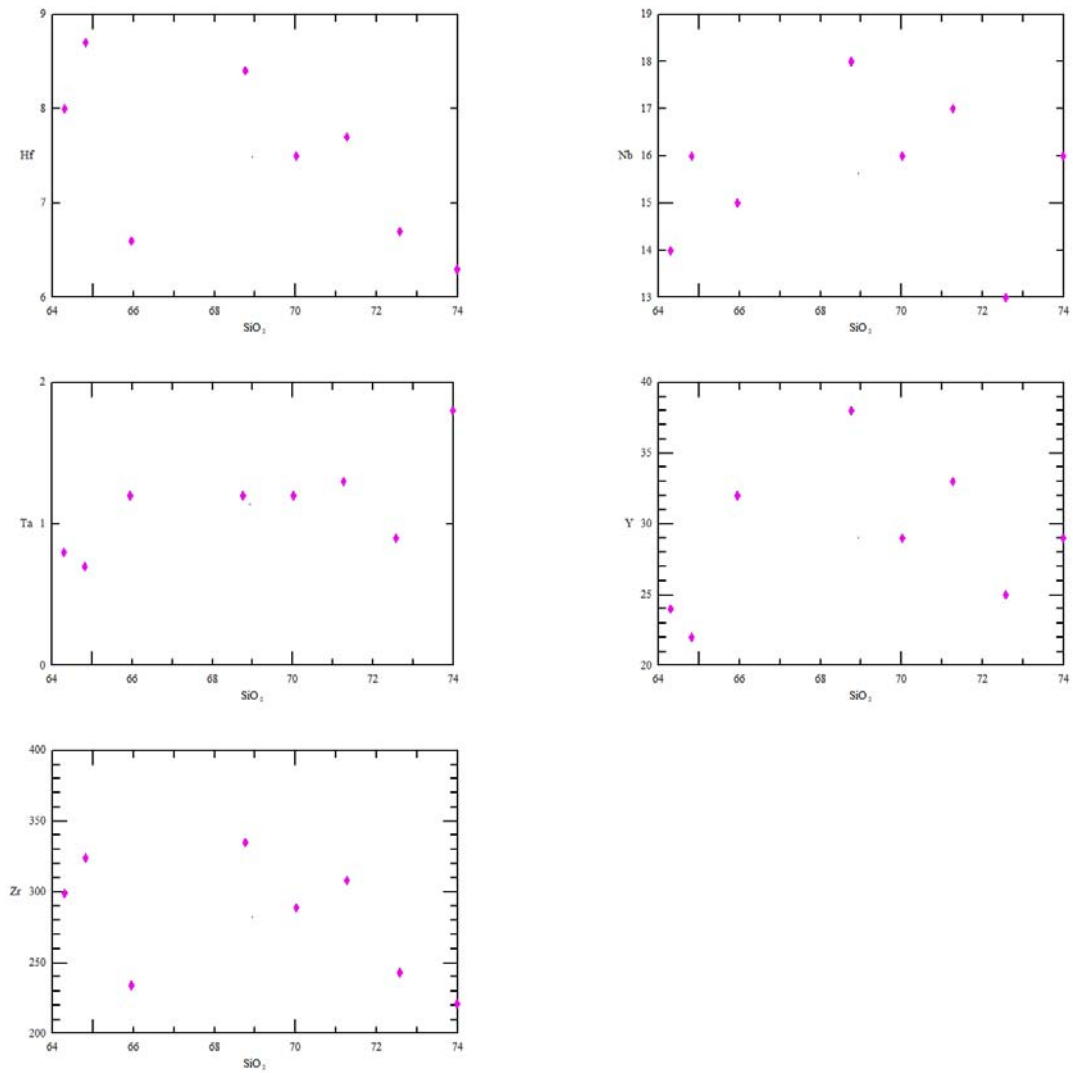


**Figure 3.22:** Harker variation diagrams for the high field strength elements (in terms of ppm) plotted against SiO<sub>2</sub> (in terms of ppm and oxide wt.%) of the granitoid rocks.

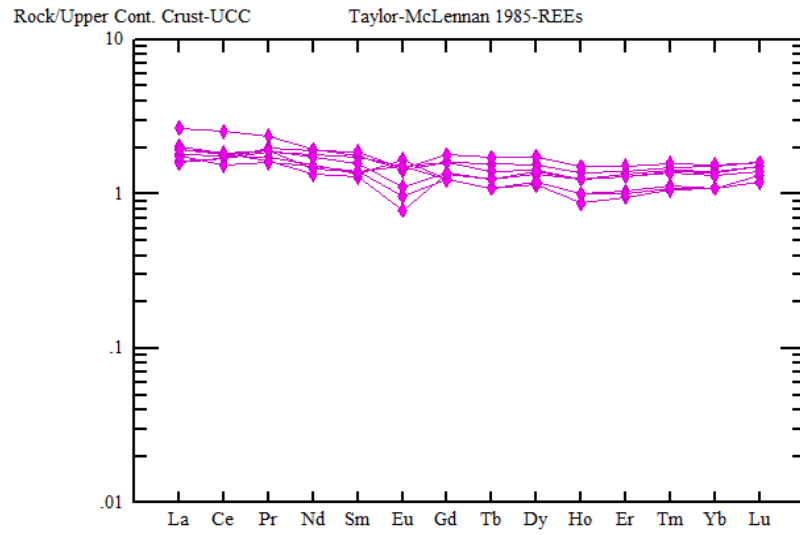


**Figure 3.23:** Log-standardized rare earth element plot normalized to upper continental crust after Taylor and McLennan (1986) for the granitoid rocks.

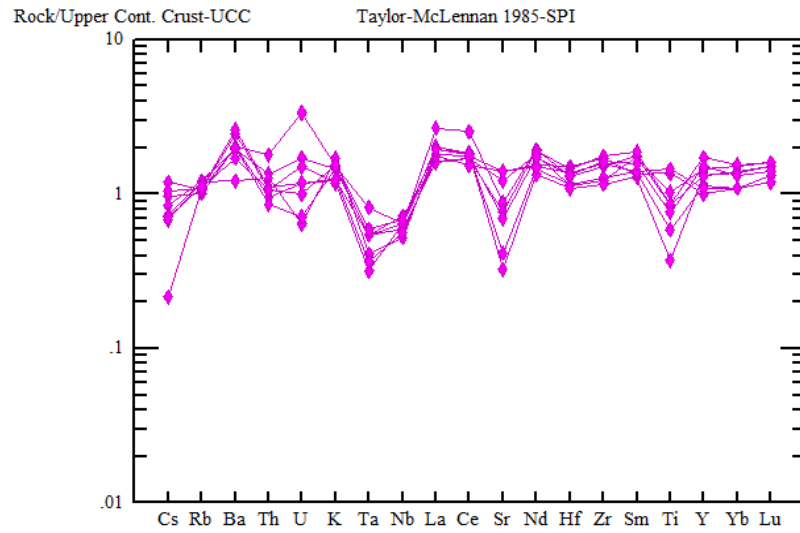


**Figure 3.24:** Log-standardized extended trace element plot normalized to upper continental crust after Taylor and McLennan (1986) for the granitoid rocks.



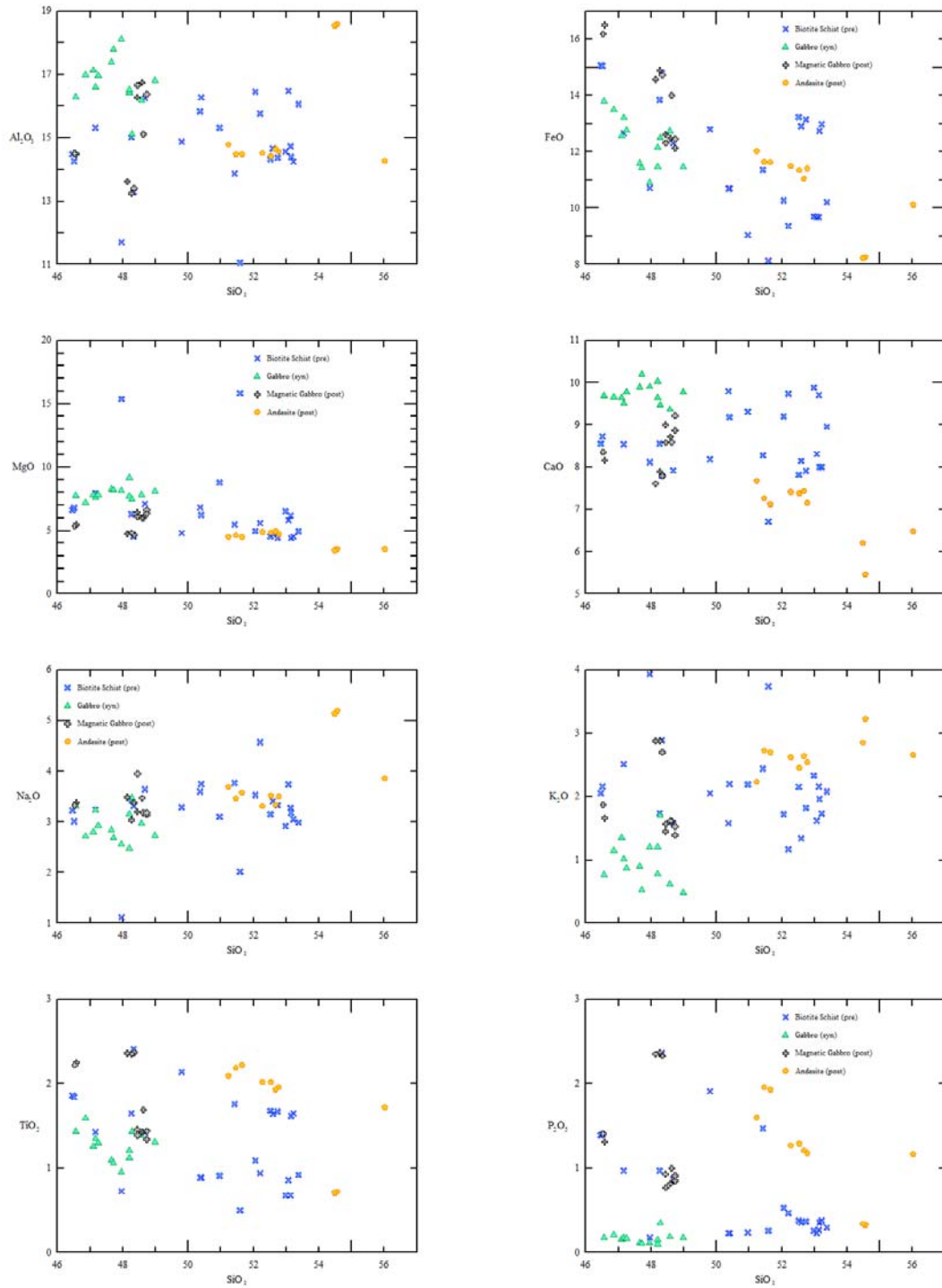


**Figure 3.26:** Harker variation diagrams for the major oxides plotted against  $\text{SiO}_2$  (in terms of oxide wt.%) of the pre-kinematic (solid blue x's), syn-kinematic (solid green triangles), and post-kinematic (solid black plus-sign and solid yellow pentagon).

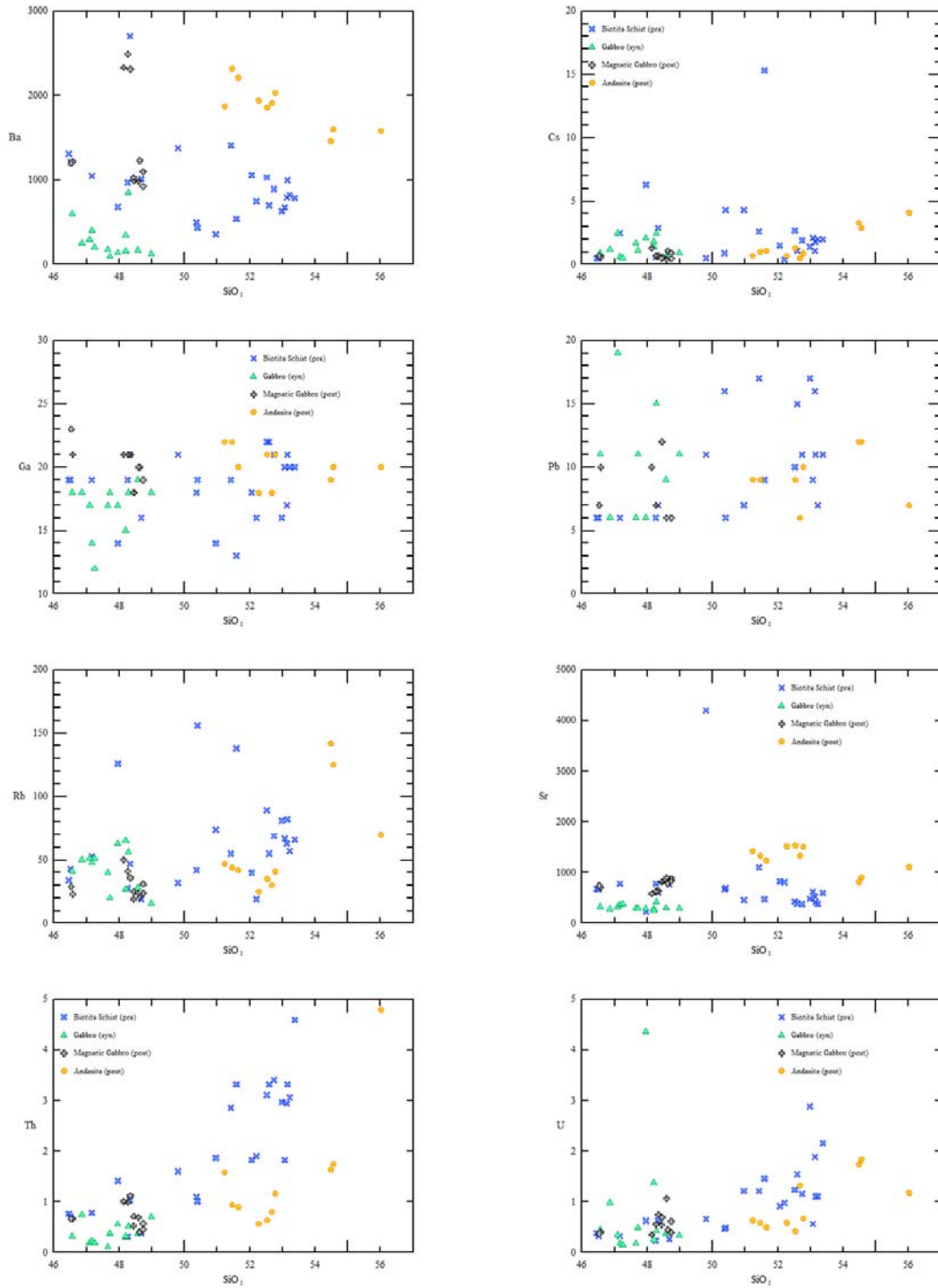


**Figure 3.27:** Harker variation diagrams for the low field strength elements (in terms of ppm) plotted against SiO<sub>2</sub> (in terms of oxide wt.%) of the pre-kinematic (solid blue x's), syn-kinematic (solid green triangles), and post-kinematic (solid black plus-sign and solid yellow pentagram).

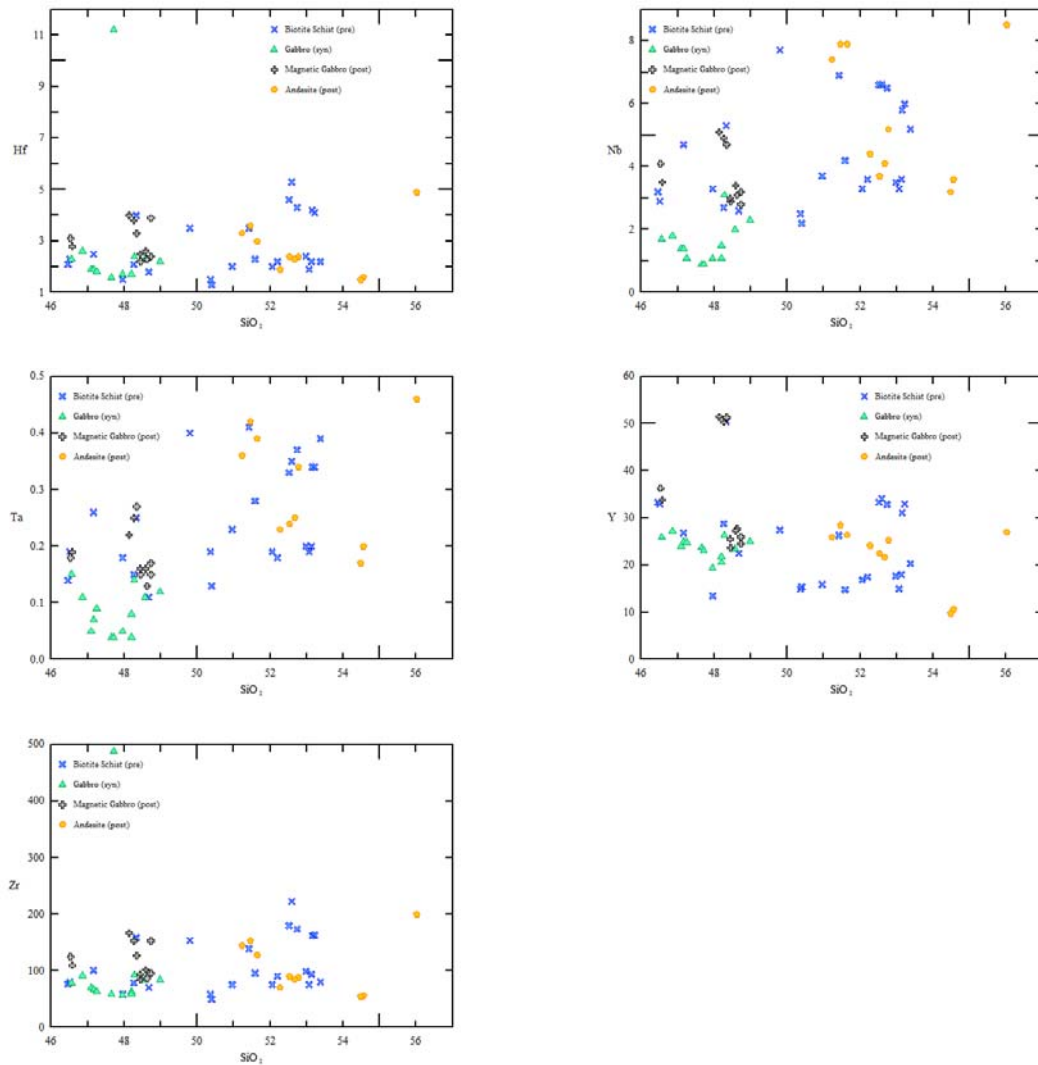


**Figure 3.28:** Harker variation diagrams for the high field strength elements (in terms of ppm) plotted against SiO<sub>2</sub> (in terms of ppm and oxide wt.%) of the pre-kinematic (solid blue x's), syn-kinematic (solid green triangles), and post-kinematic (solid black plus-sign and solid yellow pentagram).



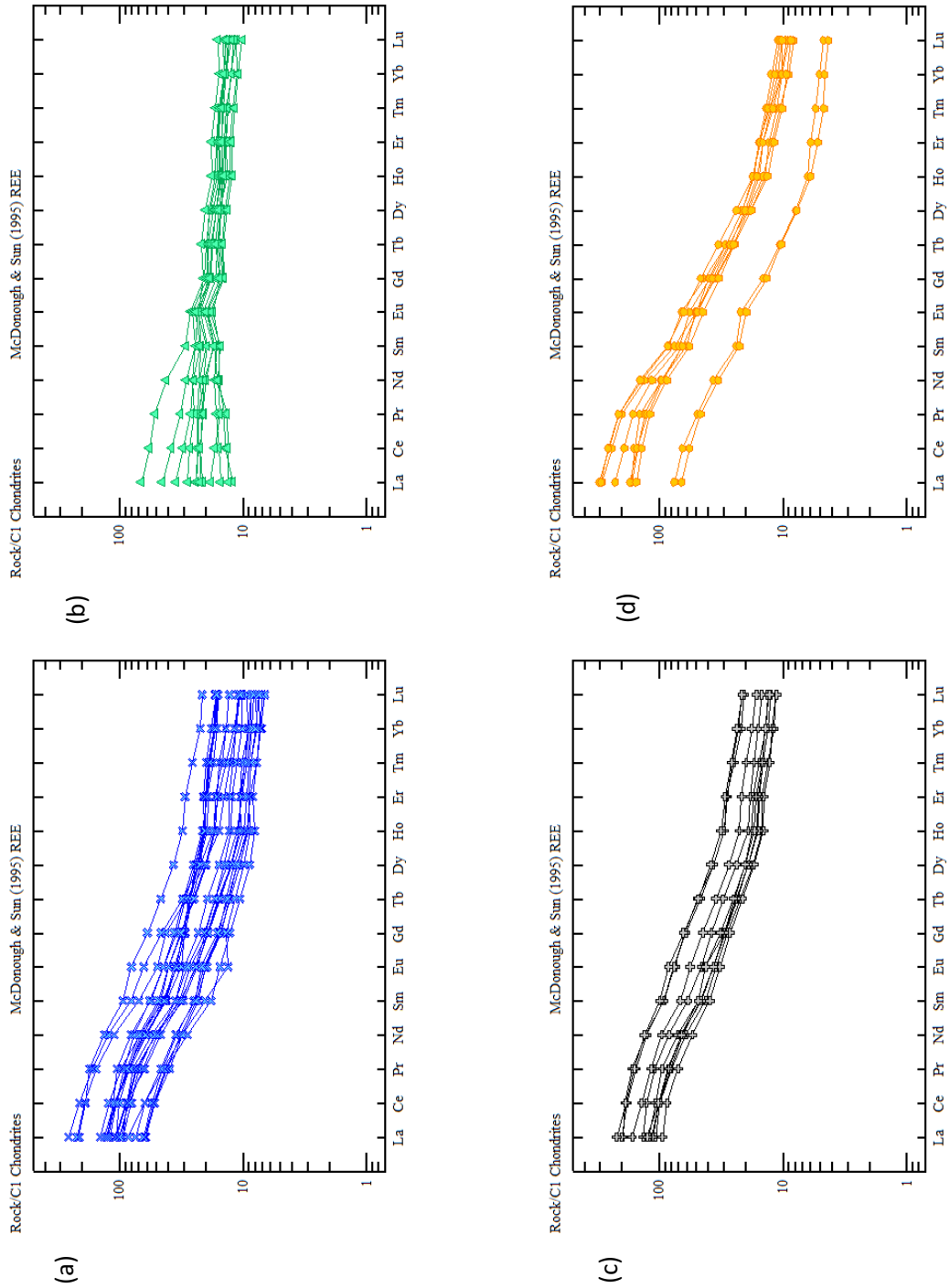


**Figure 3.29:** Log-standardized rare earth element plot normalized to chondrite after McDonough and Sun (1995) for the (a) pre-kinematic, biotite-hornblende schist dikes (solid blue x's), (b) syn-kinematic gabbroic dikes (solid green triangles), (c) post-kinematic magnetic gabbroic dikes (solid black plus's), and (d) post-kinematic andesitic dikes (solid yellow pentagrams).

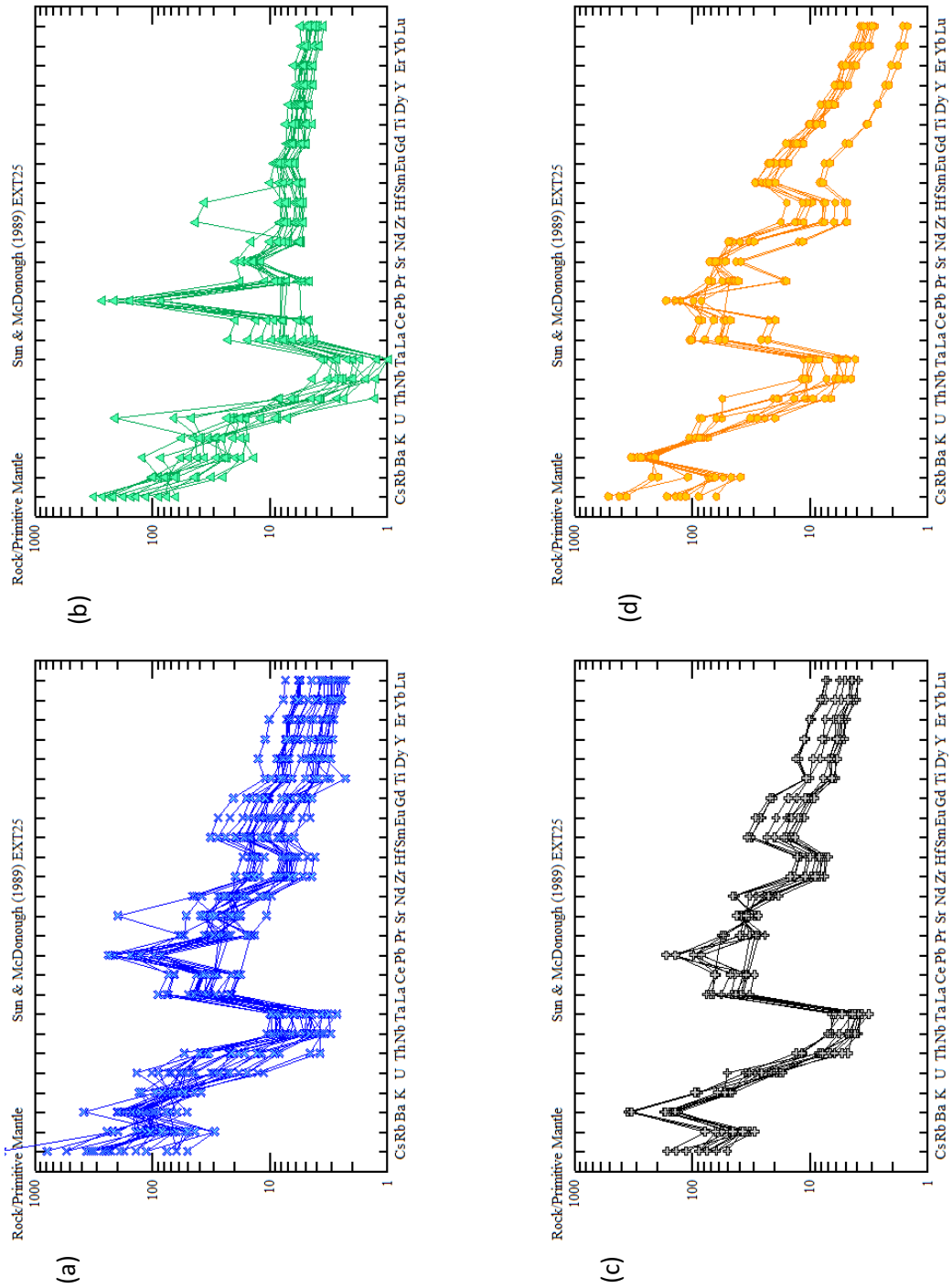


**Figure 3.30:** Log-standardized extended trace element plot normalized to primitive mantle after Sun and McDonough (1989) for the (a) pre-kinematic, biotite-hornblende schist dikes (blue x's), (b) syn-kinematic gabbroic dikes (green triangles), (c) post-kinematic magnetic gabbroic dikes (black plus's), and (d) post-kinematic andesitic dikes (yellow pentagrams).

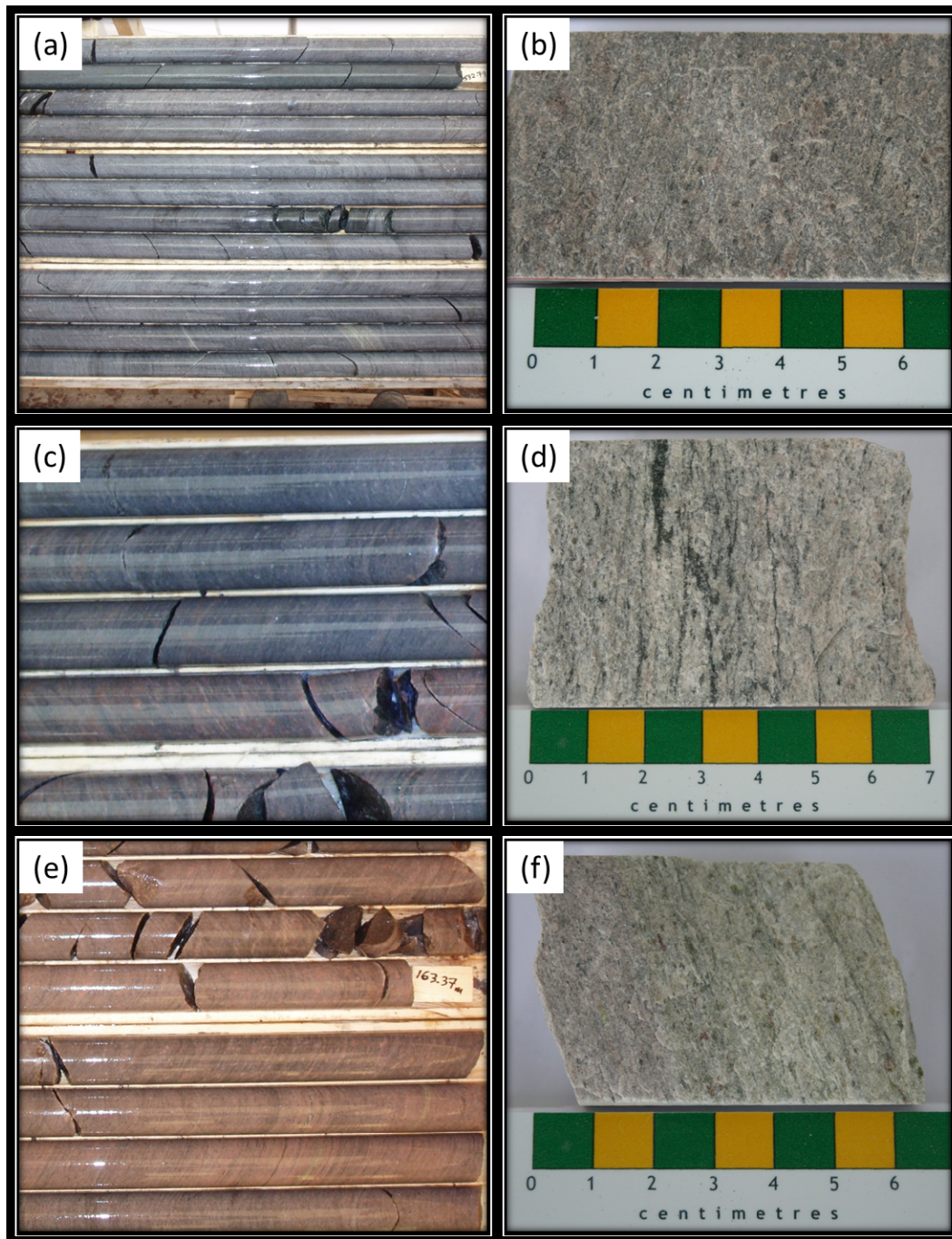


**Plate 3.1:** Drill core segments of unaltered FP felsic volcanic rocks from throughout the Michelin deposit (core diameter is 4.2 cm), (a) typical FP rocks, (b) split-sample of mafic-poor FP, (c) close-up of drill core, (d) mafic wisps in FP rocks, (e) noticeably foliated FP rocks, and (f) close-up of foliated FP with noticeable phenocrysts.



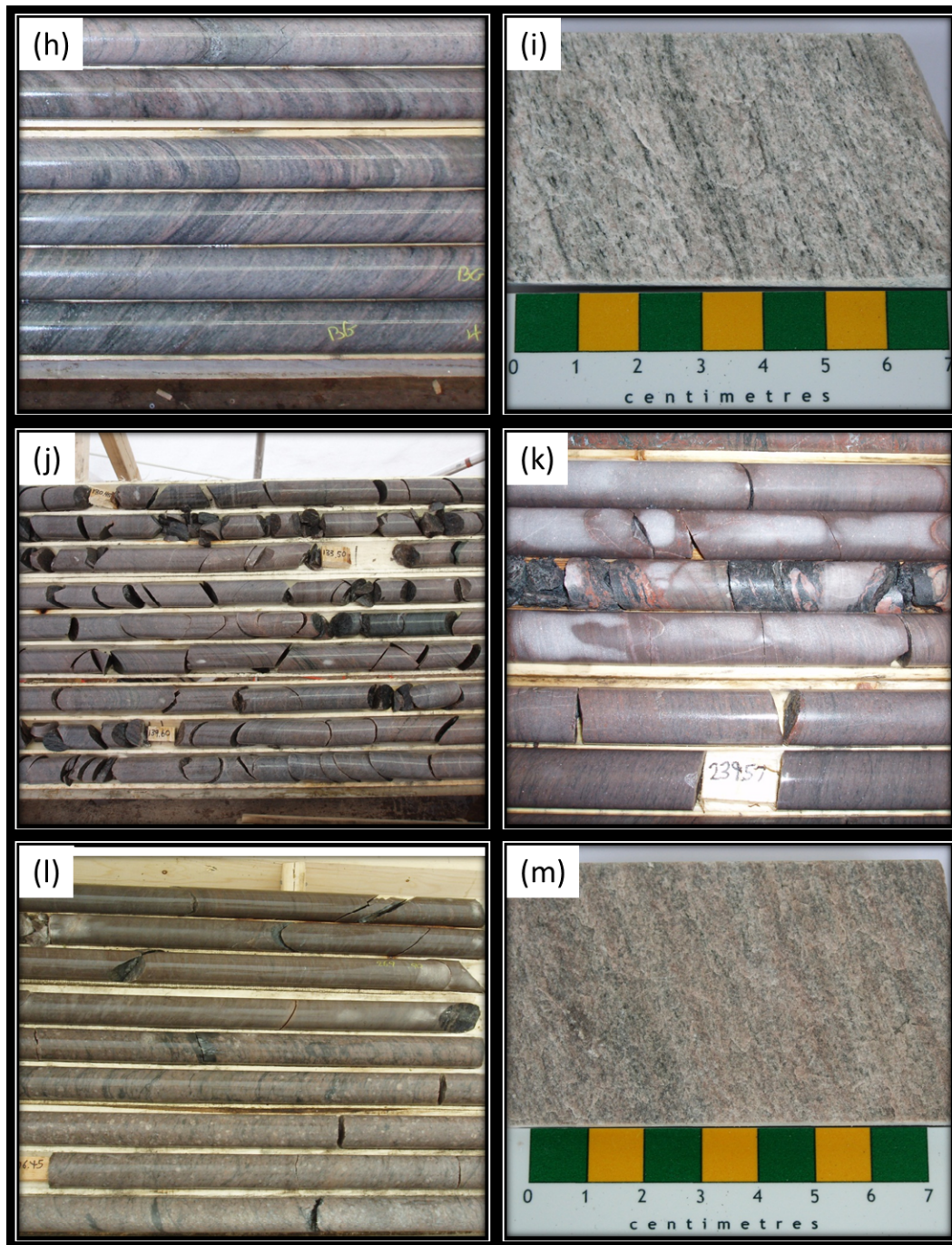


**Plate 3.1:** Continuation of drill core segments of unaltered FP felsic volcanic rocks from throughout the Michelin deposit (core diameter is 4.2 cm), (h) mafic-rich section, (i) split-sample of mafic-rich FP, (j) strongly fractured section, fractures opposite foliation, (k) fault zone, strongly chloritized gouge and brecciated, (l) top 4 rows of core in the non-porphyritic unit, and (m) close-up of the non-porphyritic unit.



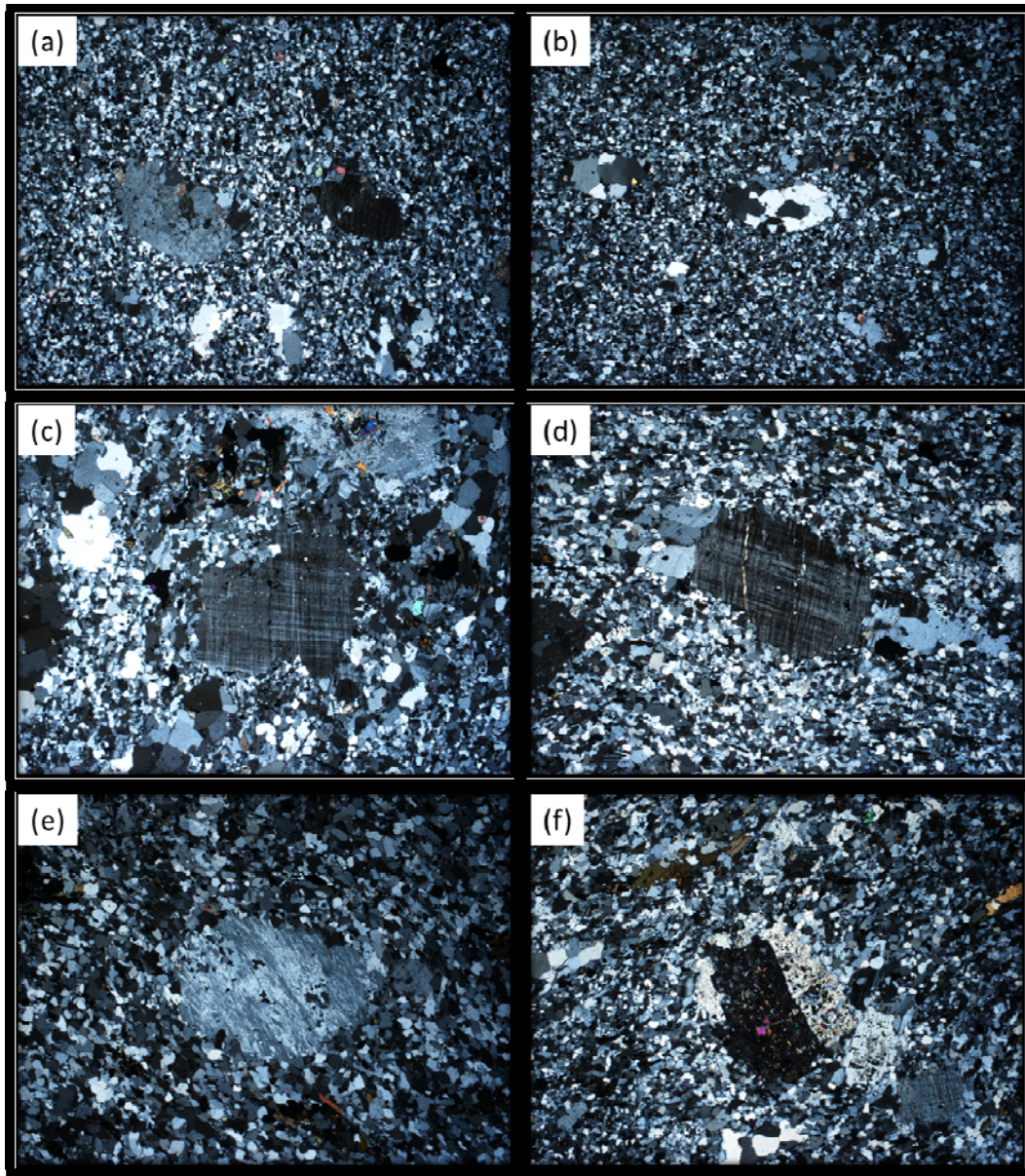


**Plate 3.2:** Petrographic sections of the FP felsic volcanic rocks, (a) feldspar and quartz phenocrysts within a fine-grained matrix (magnification (mag.) = 2.5x, cross polarized light (cpl)), (b) recrystallized quartz phenocrysts composed of several grains sutured together (mag. = 2.5x, cpl), (c) subhedral potassium feldspar phenocryst with microcline twinning (mag. = 2.5x, cpl), (d) potassium feldspar phenocryst with micro-fractures containing sericite alteration (mag. = 2.5x, cpl), (e) subhedral albite phenocryst (mag. = 2.5x, cpl), and (f) strongly sericitized albite phenocryst with Carlsbad twinning (mag. = 2.5x, cpl).



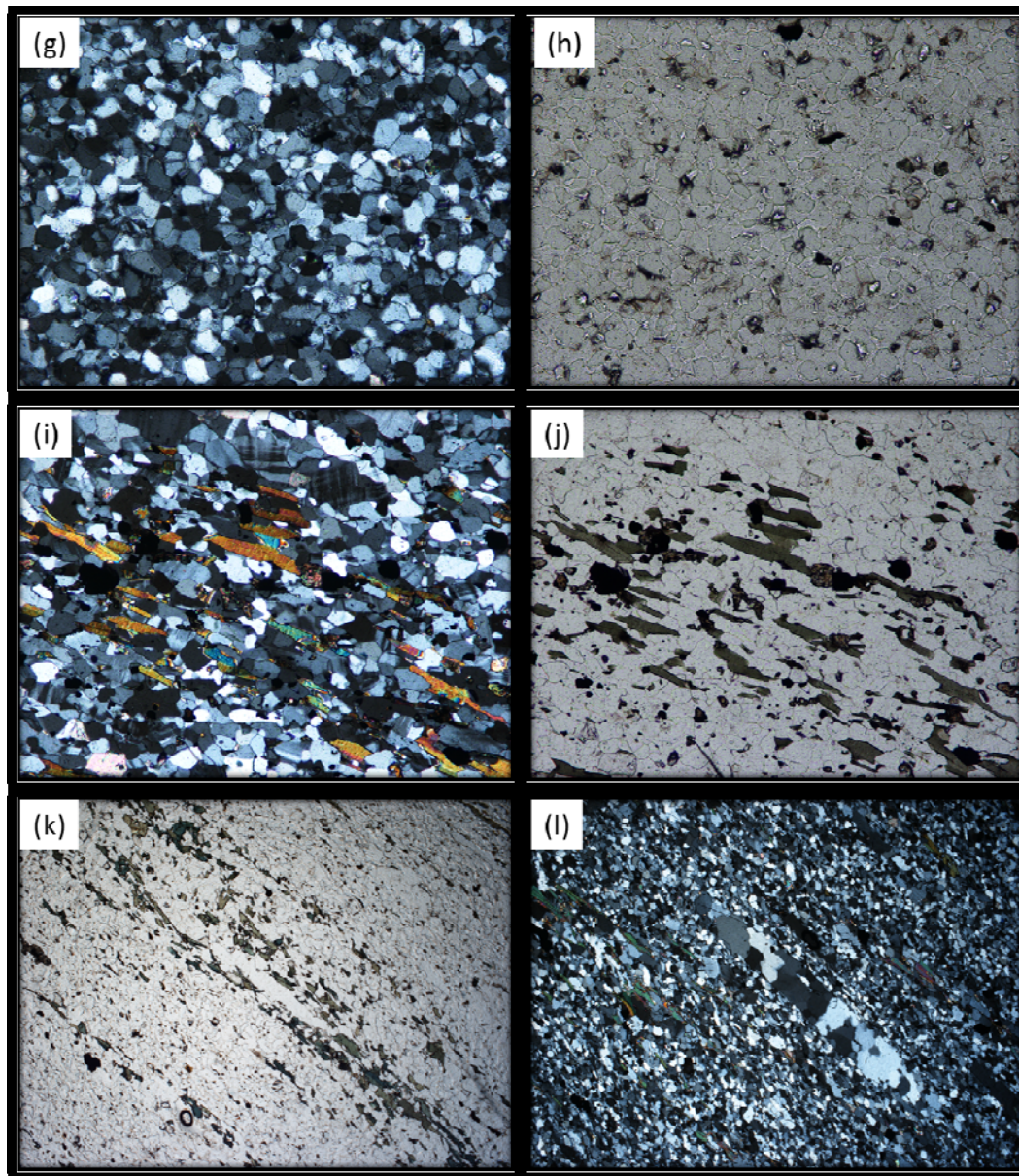


**Plate 3.2:** Petrographic sections of the FP felsic volcanic rocks, (g) fine-grained quartz-feldspar matrix, grains are equant and polygonal (mag. = 10x, cpl), (h) fine-grained quartz-feldspar matrix in plain polarized light (ppl) displays the opaque minerals within the matrix (mag. = 10x, ppl), (i) lath-shaped biotite grains within the matrix (mag. = 5x, cpl), (j) biotite-hornblende-opaque-titanite grains (mag. = 5x, ppl), (k) elongated biotite and stretched quartz phenocryst defining the foliation (mag. = 2.5x, ppl), and (l) elongated, recrystallized quartz phenocryst defining the foliation (mag. = 2.5x, cpl).



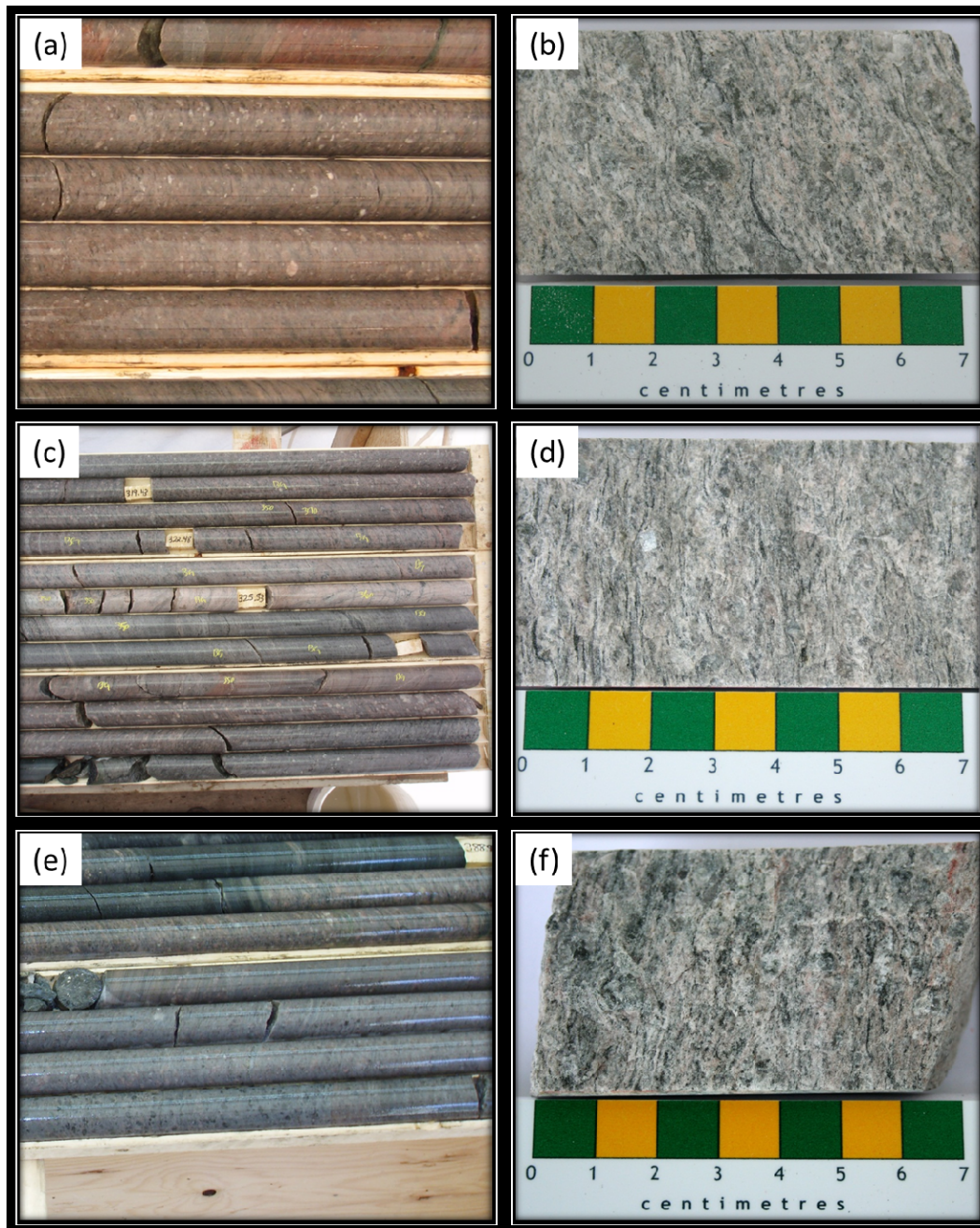


**Plate 3.3:** Drill core segments of unaltered CP felsic volcanic rocks from throughout the Michelin deposit (core diameter is 4.2 cm), (a) typical CP rocks, (b) split-sample of CP rocks showing augened potassium feldspar, (c) two units of CP felsic volcanics, separated by a FP unit in the center, (d) split-section of a CP unit, (e) contact between a CP unit and mafic dike, concordant with foliation, and (f) close-up of foliated CP with wavy foliation augening phenocrysts.



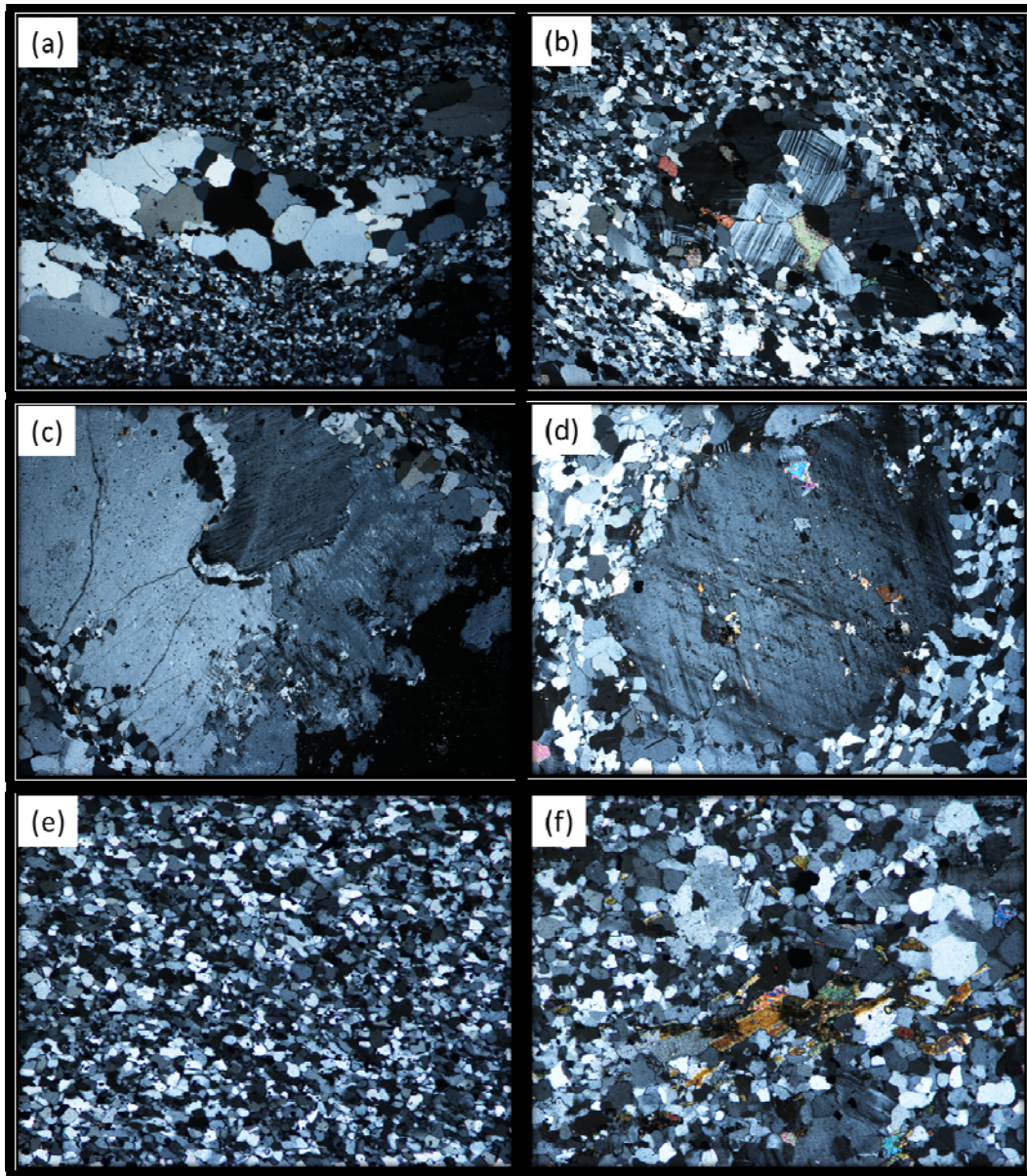


**Plate 3.4:** Petrographic sections of the CP felsic volcanic rocks, (a) recrystallized, elongated quartz phenocryst (mag. = 2.5x, cpl), (b) albite phenocryst composed of several grains sutured together, with calcite (mag. = 2.5x, cpl), (c) large potassium feldspar phenocryst comprised of 3-4 individual grains (mag. = 2.5x, cpl), (d) large potassium feldspar phenocryst comprised of a single grain (mag. = 2.5x, cpl), (e) fine-grained quartz-feldspar matrix (mag. = 5x, cpl), and (f) biotite-laths within the fine-grained matrix (mag. = 5x, cpl).



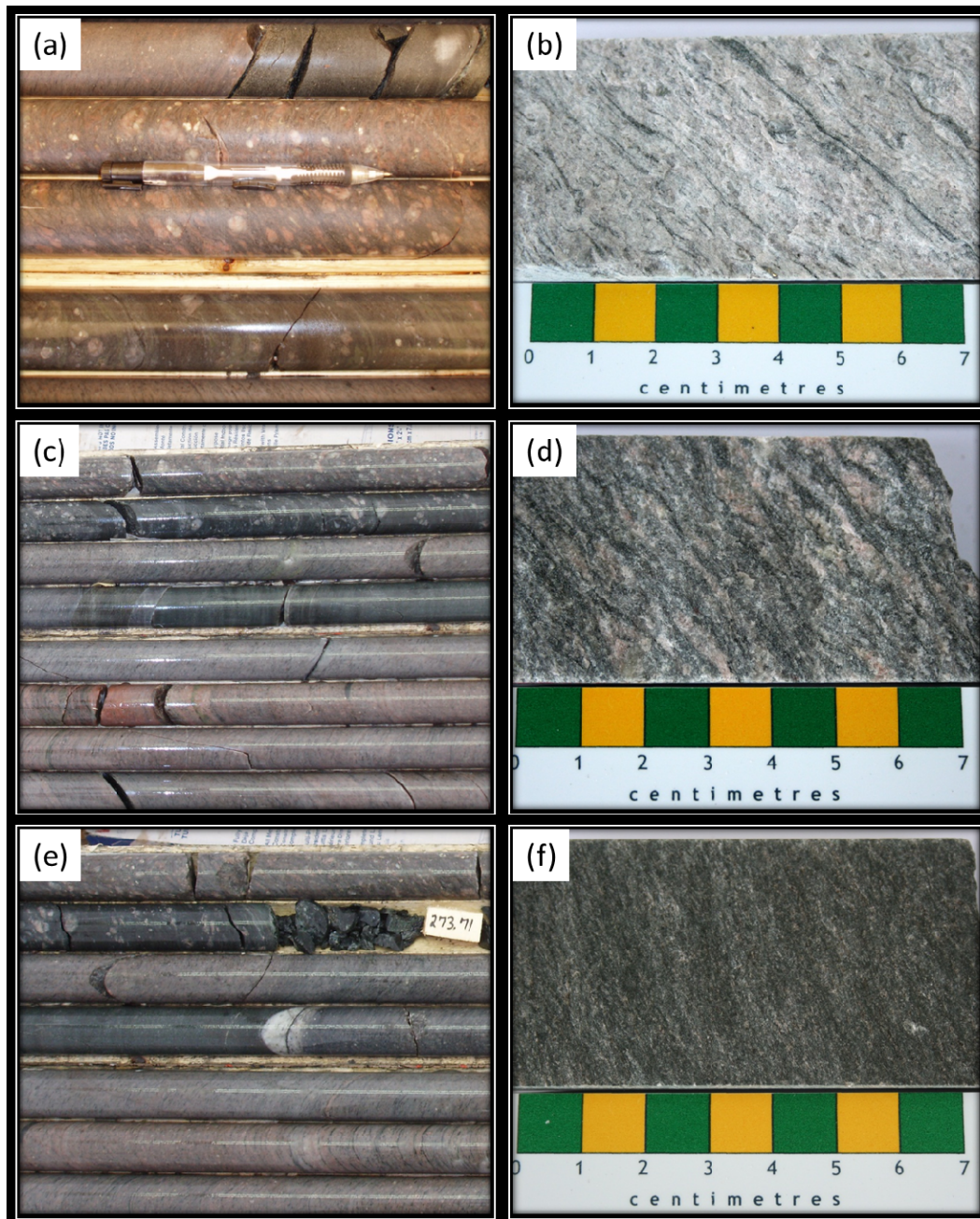


**Plate 3.5:** Drill core segments of the mafic-rich CP felsic volcanic unit from throughout the Michelin deposit (core diameter is 4.2 cm), (a) close-up of the mafic-rich unit showing coarse phenocrysts and getting more mafic-rich towards the bottom, (b) split-sample from within the felsic-rich center of the unit, (c) top two rows of core show the unit becoming increasingly more mafic, (d) split-section from a more mafic-rich area showing coarse phenocrysts strongly augened by wisps of mafic material, (e) second row shows the mafic margin of the unit, and (f) split-section on the mafic margin of the unit.



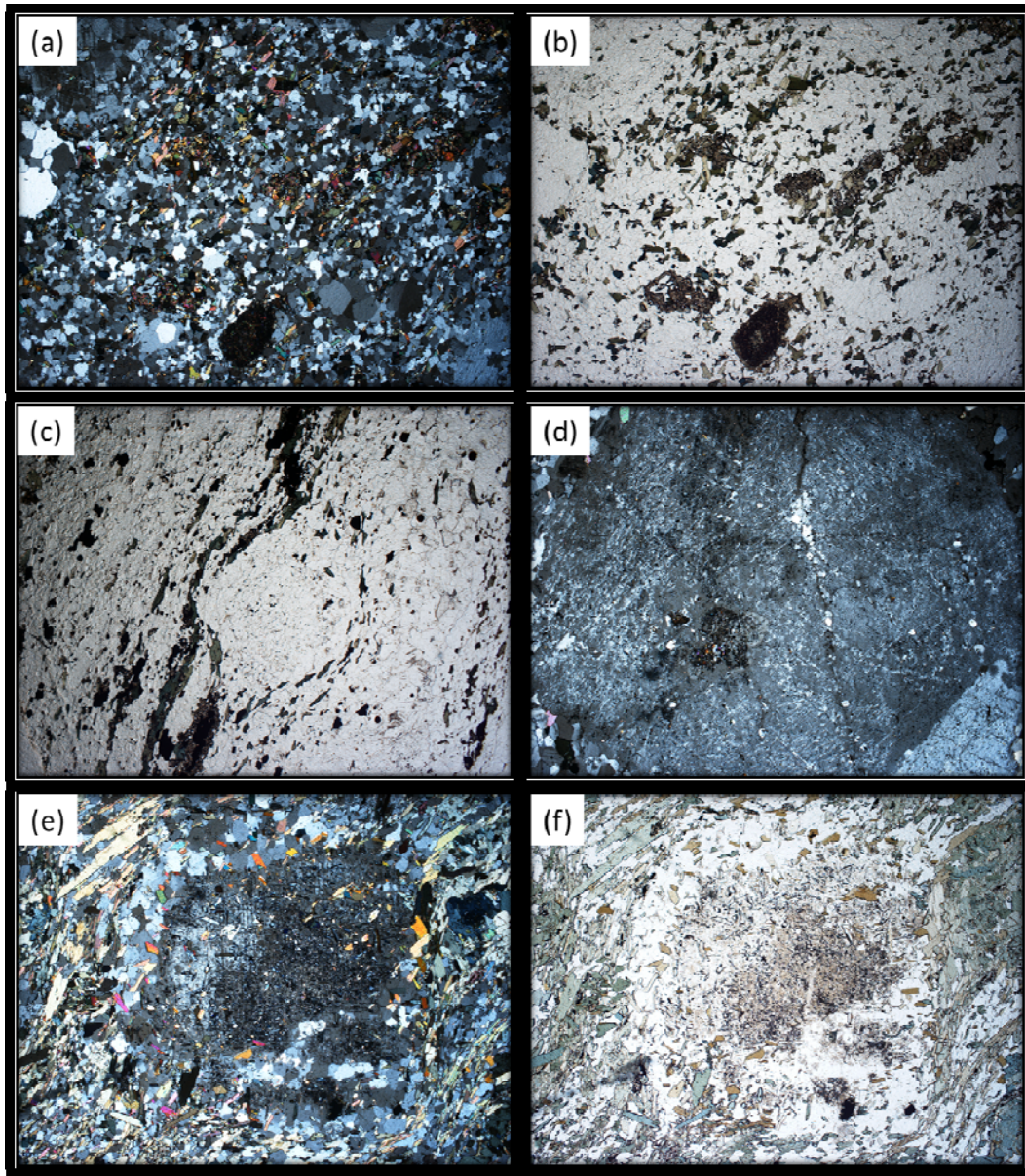


**Plate 3.6:** Petrographic sections of the mafic-rich CP felsic volcanic unit, (a) mafic-rich matrix characteristic of the mafic-rich CP unit (mag. = 2.5x, cpl), (b) biotite-hornblende-rich matrix with zircon (mag. = 2.5x, ppl), (c) large potassium feldspar phenocryst wrapped by thin mafic wisps of biotite and hornblende (mag. = 2.5x, ppl), (d) large potassium feldspar phenocryst comprised of a single grain with weak sericite alteration (mag. = 2.5x, cpl), (e) sericitized potassium feldspar phenocryst within the predominantly mafic margin, lath-shaped biotite-hornblende grains wrap the phenocryst (mag. = 2.5x, cpl), and (f) same image in ppl (mag. = 2.5x, ppl).



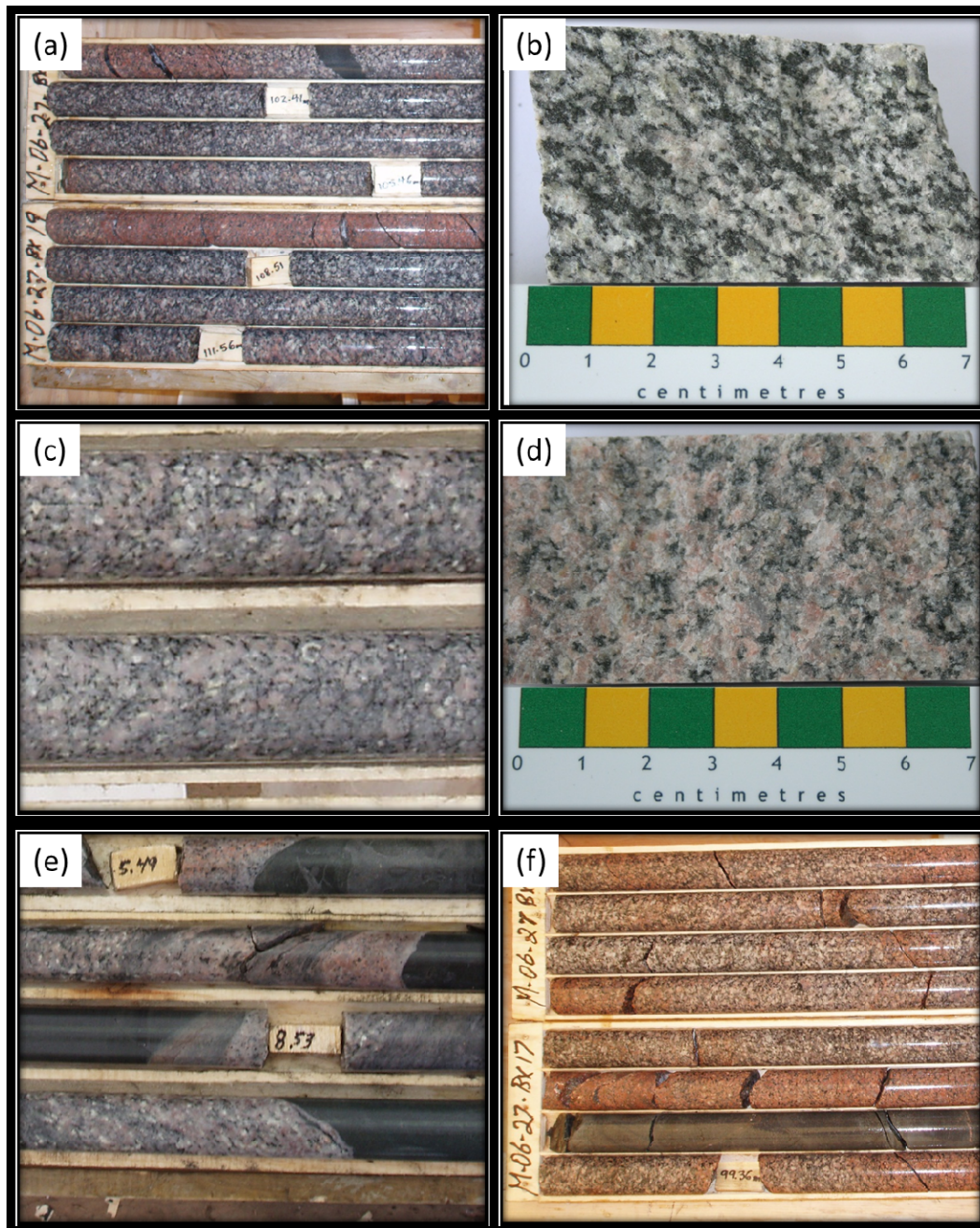


**Plate 3.7:** Drill core segments of the granitoid intrusive (core diameter is 4.2 cm), (a) coarse-grained granite to granodiorite intrusives, (b) split-sample of a mafic-rich portion of granitoid, mafic minerals define foliation of the rock, (c) close up of granitoid unit showing the coarse-grained texture of the rock, (d) split-section from a mafic-poor area, granitoid no longer appears foliated without mafic minerals to define the foliation, (e) contact between the granitoid and small pre-kinematic dikes, contact is concordant with foliation, and (f) lower box contains granitoid rock that has become hematitized, giving it a reddish-color.



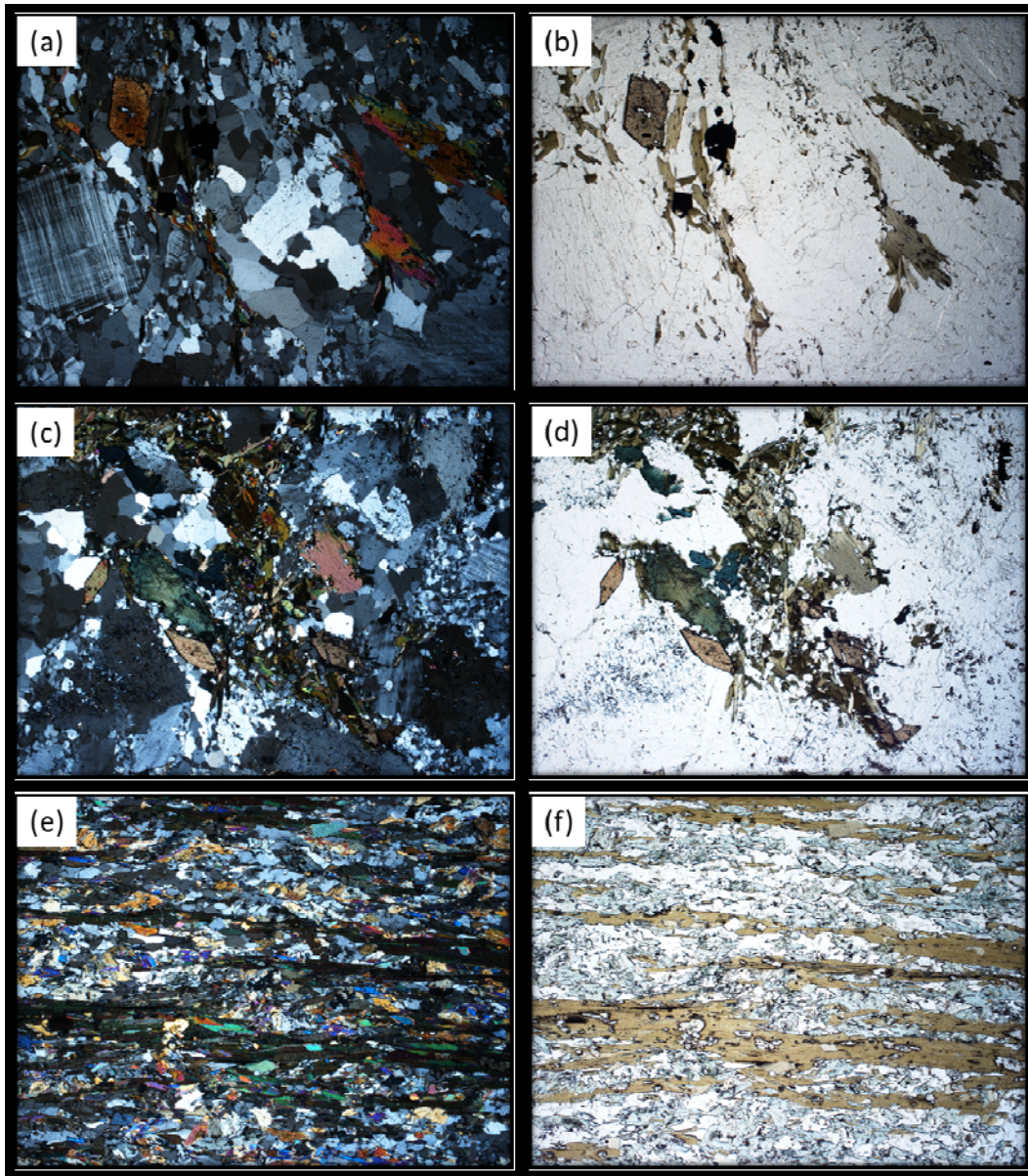


**Plate 3.8:** Petrographic sections of the granitoid intrusive (a-d) and pre-kinematic biotite-hornblende schist, dikes (e-f), (a) granitoid consisting of coarse grain potassium feldspar, medium grained albite, quartz and biotite, and fine grained quartz (mag. = 2.5x, cpl), (b) biotite and titanite (mag. = 2.5x, ppl), (c) mafic-rich clot within the granitoid consisting of biotite-hornblende-magnetite-titanite (mag. = 2.5x, cpl), (d) same image in ppl (mag. = 2.5x, ppl), (e) pre-kinematic dike with large elongated biotite-lath in a fine-grained matrix of albite-biotite-hornblende (mag. = 2.5x, cpl), and (f) same image in ppl (mag. = 2.5x, ppl).



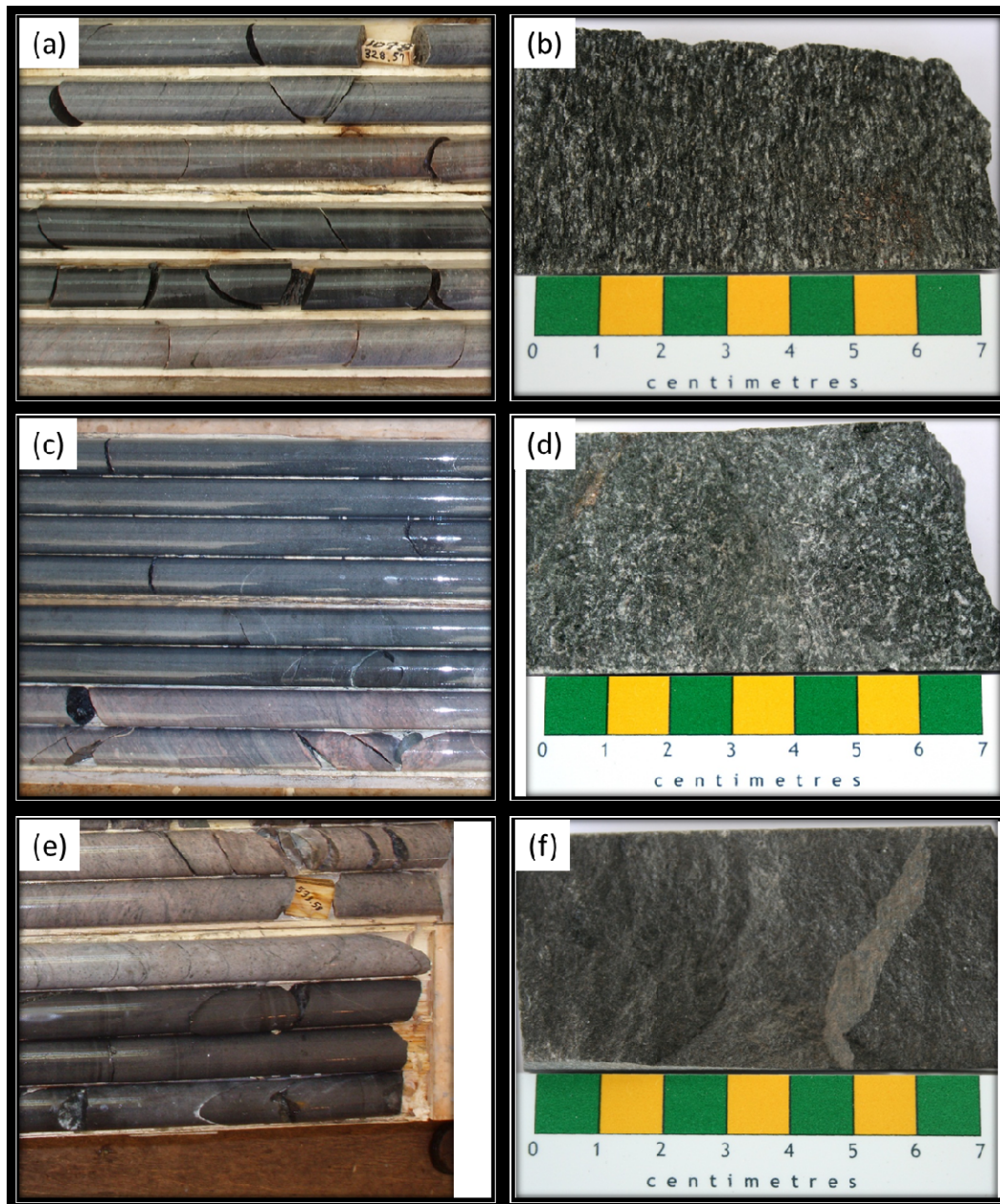


**Plate 3.9:** Drill core segments of the mafic dikes (core diameter is 4.2 cm), (a) pre-kinematic biotite-hornblende schist, (b) split-sample of strongly foliated biotite-hornblende schist, grain size is large enough to give it a salt and pepper appearance, (c) massive fine-grained syn-kinematic gabbroic dike, (d) split-section of a syn-kinematic gabbroic dike that is weakly foliated and salt and pepper in appearance, (e) massive, very fine-grained post-kinematic, strongly magnetic dike, and (f) split-sample of the strongly magnetic post-kinematic dike, grain size is very small and rock has not been foliated.



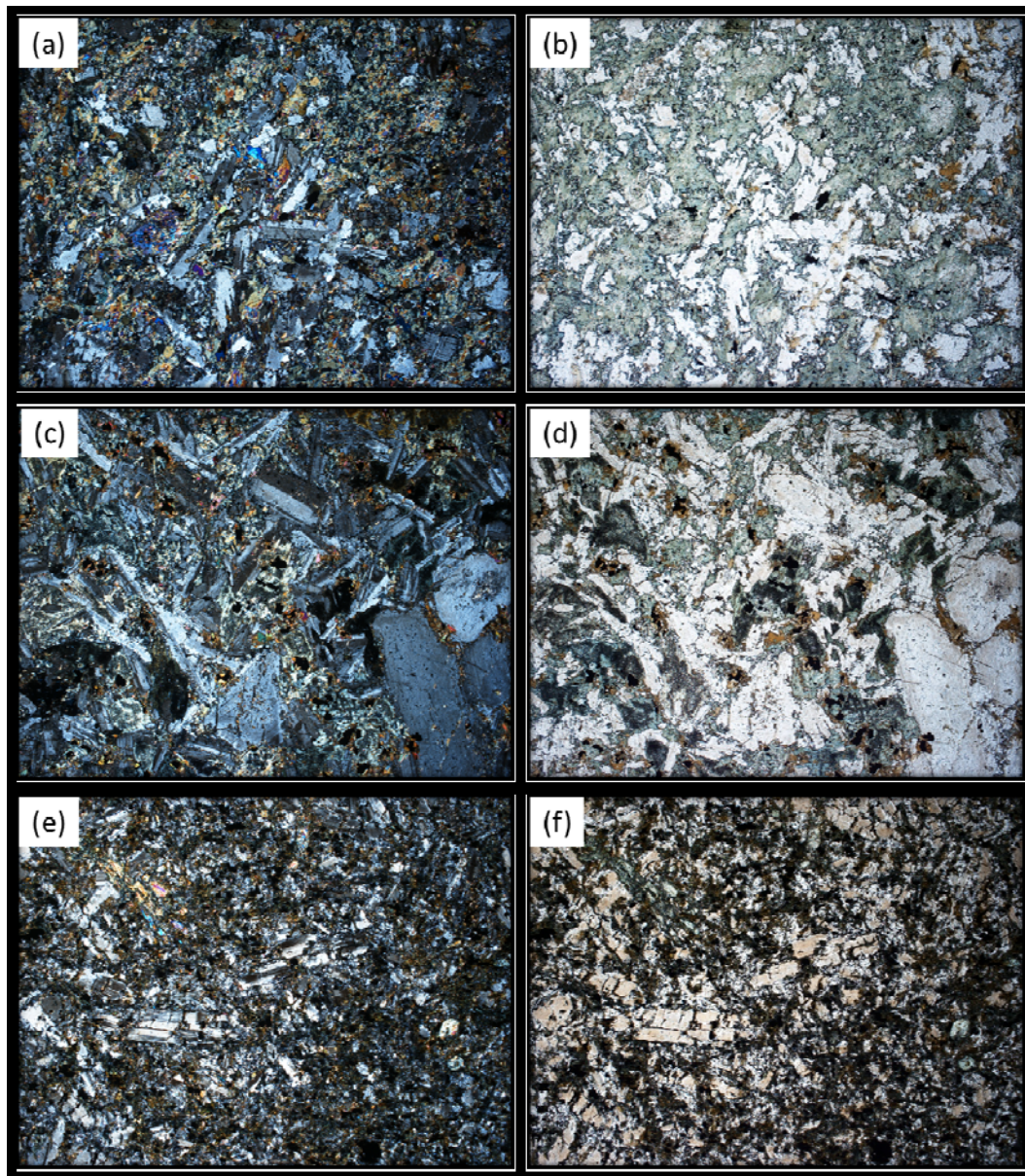


**Plate 3.10:** Petrographic sections of the syn and post-kinematic mafic dikes, (a) syn-kinematic gabbroic dike with plagioclase laths, and hornblende with biotite, clinopyroxene and magnetite (mag. = 2.5x, cpl), (b) same image in ppl (mag. = 2.5x, ppl), (c) strongly magnetic post-kinematic gabbroic dike with large plagioclase laths, medium magnetite grains and finer mafic grains (mag. = 2.5x, cpl), (d) same image in ppl (mag. = 2.5x, ppl), (e) post-kinematic andesite dike with fine-grained plagioclase mixed with hornblende and biotite (mag. = 2.5x, cpl), and (f) same image in ppl (mag. = 2.5x, ppl).

## **Chapter 4     Geology of the Ore Zone**

### **4.1     Introduction**

The mineralized ore zone of the Michelin deposit consists of multiple sequences of CP and FP, metamorphosed felsic volcanic rocks that have been intruded by several pre-kinematic, now biotite-hornblende schists, dikes and syn-kinematic gabbroic dikes. The felsic volcanic units appear to be equivalent to similar units within the hanging wall and foot wall of the deposit, except they have undergone varying styles and intensities of mineralization and alteration.

The aim of this chapter is to define the geometry, or dimensions of the ore deposit and describe and characterize the lithological units which make up the ore zone. It is important to characterize these units using the same methods as those used to characterize similar, unaltered units within the hanging wall and foot wall in order to show the mineralogical and geochemical changes that are caused by alteration and mineralization. This will also provide insight into the relationship between similar, altered and unaltered lithological units to determine if they are related or separate lithological units.

The geometry and geology of the ore zone were examined in detail through drill core analysis; core observations helped in delineating the different units which make up the ore zone, provided insight into ore mineralogy, alteration intensity, size of the alteration envelope and deposit dimensions. Petrographic thin section and SEM-MLA analysis were utilized to identify overall mineralogy and mineral percentages of rocks within the ore zone and to identify textural relationships. Finally, major, trace and rare

earth element geochemical data was used to characterize each rock type. It is important to note that these samples are altered so the classifications provided by most of the geochemical diagrams are not accurate and do not reflect the true rock type. The geochemistry used for this section is not corrected by mass balance calculations to reflect changes in mass due to alteration and apparent changes due to closure. These effects are discussed in Chapter 6, section 6.5.

## **4.2 Michelin Ore Zone**

The Michelin deposit is located in the central portion of the poorly defined White Bear Mountain – Walker Lake Belt (Gandhi, 1978; Booth *et al.*, 1979). This belt, which is roughly 48 km long by 13 km wide, has been identified as a regional fold belt which hosts most of the uranium showings in the Michelin Zone of the Aillik Domain. Of all the uranium showings, the Michelin deposit is by far the biggest with a current estimated resource of 106.99 million pounds  $U_3O_8$  measured, indicated, and inferred (Hertel *et al.*, 2009). In the immediate vicinity of the deposit, there are a number of smaller showings that display similar mineralization and alteration styles to those seen at Michelin. These showings, namely Asha, Chitra, Munna and Mikey, are poorly defined. Although similar to Michelin, they lack some of the alteration and mineralization characteristics of the Michelin deposit and therefore appear to be separate deposits, unrelated to the Michelin ore zone itself.

The mineralized ore zone at Michelin extends to surface, however, due to an extreme lack of outcrop exposure in the area, surface exposure of the ore zone is confined



to a series of hand dug trenches located to the north of Ranjan Lake. As a result, most of the information about the mineralized zone is from extensive diamond drilling and a 400 m long adit that BRINEX tunneled along strike at the 30 m level. Drilling has determined that the ore zone is somewhat tabular in shape, having an approximate surface length of 1,200 m, with a near continuous strike trending 060° towards the northeast (Plate 4.1). The deposit has a consistent dip of 50 to 70 degrees towards the southeast, extending underneath Ranjan Lake. To depth it is almost 1,000 m long in the dip direction and has been intersected by drilling to a vertical depth of roughly 800 m.

The thickness of the mineralized zone is not consistent, ranging from just a few meters near the deposit boundary to as much as 80-90 m thick at the deposit center. The change in thickness from the center outwards is also not consistent, since the zone has a tendency to pinch and swell both across and along strike. The ore zone is thickest in the middle, defining a 100-150 m wide zone that extends from surface, downwards towards the south to a depth of approximately 700 m. This is highlighted by an approximate 200 by 250 m zone located at about 400-500 m depth which has a maximum thickness of 85 m. Laterally along strike from this central area, the mineralized zone narrows in both directions along strike until it eventually dies out. The deposit also begins to narrow at 700 m vertical depth (Figure 4.1). Near surface, the mineralized zone has a greater thickness along strike than at depth, but this could be due to inadequate drill coverage. Currently the ore zone is open in all directions, although, limited drilling results at depth and laterally along strike indicate that the ore zone narrows and then dies out. This could

however be attributed to pinch and swell and therefore, it is possible for the mineralized zone to widen in the strike or dip direction.

The mineralized zone is comprised of a series of stratiform, sub-parallel, CP felsic volcanic rock units separated by units of FP volcanic rocks. These units collectively are referred to as the main Mine Series or Mine Sequence. In general, this series consists of four separate CP units, but due to the fact that these units often pinch and swell in thickness both along and across strike, the total number of CP units could be as low as one. The reasons for this can be related to a thickness increase in the CP units, whereby they often combine with a sub-parallel unit, thus creating a much thicker unit. This is especially apparent in the center of the ore zone. These units will also terminate along strike or alteration becomes so intense that a distinction between the CP and FP units is impossible. Finally, along the periphery of the ore zone where the effects of mineralizing fluids are less intense, only one or two CP units within the Mine Series are altered and mineralized while other units are unaffected.

Through infill drilling in the 1960's and 1970's, BRINEX defined in detail the upper portion of the mineralized zone to a depth of approximately 250 m. They were able to establish that mineralization occurred in zones, largely confined to the CP units and parts of the adjacent FP units. In their evaluation, they designated these zones the "A", "B", "C", "D", "E", "F" and "G" Groups (Booth *et al.*, 1979). Figure 4.2 depicts these mineralized zones extended to surface. From the diagram it is easy to see a correlation between mineralization and the CP units. Of these groups, the "A", "B", "C" and "F" Groups are the most significant and host almost 80 % of the Michelin mineralization,

defining the so-called Mine Series (BRINEX, 1977). Group “A” is the largest mineralized zone and is associated with the top CP unit within the Mine Series. It ranges from 5-35 m thick, averaging 10 m. The zone extends uninterrupted from surface down to the bottom of the deposit. At a depth of 400-500 m, it thickens in the center to 25-35 m. The cause of the increase in thickness can be attributed to the unit merging with the CP unit located below and in addition, alteration is so intense in this area that distinctions between the CP and FP units is almost impossible to determine. Originally a separate mineralized zone, the “B” group is considered by Booth *et al.* (1979) to be a part of the “A” group. The remaining groups, “C” and “F” comprise the remaining mineralized CP units within the main Mine Series. These units are comprised of 2-3 CP units that extend from surface to the bottom of the deposit. These units are thinner, approximately 1-5 m thick; and although they pinch and swell, they usually do not coalesce together (Plate 4.2).

Groups “D” and “E” are in the eastern extension of the Mine Series and account for 20 % of the mineralization (BRINEX, 1977). These groups, which form a separate zone along strike from the main mineralized horizon, are most likely an extension of the “A” and “C” groups (Booth *et al.*, 1979). These groups gradually decrease in thickness and appear to eventually disappear towards the east and they do not appear to extend to the depth observed for the main mineralized zone (Barrett *et al.*, 2008). Finally, Group “G” is a series of thin, CP units situated above the Mine Series within the hanging wall. This group, termed the Southern Group, accounts for only 2 % of the mineralization in the deposit (BRINEX, 1977). It ranges from 5-10 m thick and occurs anywhere from 60-

110 m above the start of the main Mine Series. This unit extends from surface to a depth of approximately 400 m where it eventually disappears. Although all six groups are associated with separate, CP units, or apparent extensions of some CP units, the ore grades of the six groups is fairly consistent, ranging from a low of 0.12 %  $\text{U}_3\text{O}_8$  in Group “E” to a high of 0.19 %  $\text{U}_3\text{O}_8$  in Group “D”, with the main difference being the size or tonnage for each group (BRINEX, 1977).

### **4.3 Ore Zone Geology**

The ore zone is dominated by two main lithologies: CP, metamorphosed felsic volcanic rocks and FP, metamorphosed felsic volcanic rocks. The CP units constitute the Mine Sequence, consisting of two to four different units separated from each other by FP, units. Both lithologies in turn have been injected by multiple mafic intrusives, including pre-kinematic, biotite-hornblende schists, dikes and syn-kinematic gabbroic dikes; no post-kinematic dikes have been identified intruding through the ore zone.

The lithological units that comprise the ore zone appear to be strongly altered equivalents of the units within the hanging wall and foot wall. The reasoning for the above statement centers around the fact that altered rocks within the ore zone still maintain the same textures and some of the same mineralogy as the unaltered, equivalent rocks that were created during peak metamorphism during the Makkovikian Orogeny (ca. 1,810 to 1,790 Ma) (Wilton, 1996). The felsic volcanic rocks within the ore zone exhibit the same consistent foliation present throughout the deposit and individual CP and FP

units are still rather stratiform, striking approximately 060° and dipping roughly 50° to the southeast.

Also, the onset of alteration within the hanging wall and foot wall occurs within the same lithological units and the alteration changes are visible in the rock, indicating that alteration is not constrained to any particular lithological unit. The rocks within the ore zone have been affected by intense, pervasive hydrothermal alteration during the mineralizing process, drastically altering the mineralogy and geochemistry of the rock. It is because of these drastic changes that the units within the ore zone will be described separately to properly identify the alteration changes. The alteration is not as intense outside of the ore zone causing only slight mineralogical and geochemical changes and therefore they do not need to be described in detail (alteration changes will be described in Chapter 6).

#### **4.3.1 Coarse Grained Porphyritic Metamorphosed Felsic Volcanic Rocks of the Ore Zone**

The CP, metamorphosed, felsic volcanic rock is the dominant lithology within the ore zone (i.e., is the rock type associated with most of the uranium mineralization within the Michelin deposit). Individual CP units range in thickness from 2-10 m but these units sometimes pinch and swell they sometimes merge together, reaching a maximum thickness of ~35 m, or individual units can pinch out altogether. These units however are still rather stratiform, and for the most part can be traced between individual drill holes, unless two units merge together or a unit pinches out entirely (Plate 4.3a and e).

In total, these units comprise approximately 50 % of the mineralized zone, varying between 40 to 60 %. Even though the CP units are thickest in areas where the overall mineralized zone is thicker, they comprise a lesser percentage of the overall mineralized zone than the FP units which are thicker, and therefore comprise a greater percentage of the ore zone. Vice versa, in areas where the mineralized zone is thin, the CP units comprise a greater percentage of the mineralized zone, as the FP units which are generally very thin in these sections.

Unit contacts between CP and FP felsic volcanic rocks within the ore zone are highly variable throughout and are identified by different features. Individual textural features such as phenocrysts and overall grain size are difficult to identify due to the intense alteration, which leaves the rock soft, porous, and discolored. This creates difficulty in identifying the exact contact between two units, especially where the contact may be sharp or gradational over a 10-20 cm interval. These contacts are marked by a change in phenocryst size and concentration, and such changes are generally only noticeable away from the contact. Some contacts are more easily defined as they are either marked by small mylonite zones or mafic dikes. Small, approximately 0.5 m mylonitic zones with very intense foliation locally mark contacts between units. These zones are generally phenocryst-poor making the proto-lithology difficult to determine, but based on grain size, they are most likely within the FP units. Mafic dikes, in particular, the pre-kinematic biotite-hornblende schists, commonly occur between the contacts of the two units. These dikes, which range in thickness from 0.5-2 m, mask the original contact but allow the contact to be mapped.

Individual CP units within the mineralized zone are similar to each other and display textures similar to CP units outside of the mineralized zone. However, due to the intensity of alteration and deformation, the units within the mineralized zone exhibit a different mineralogy than unaltered equivalents. These mineralized zone units are medium to deep red and soft and porous, yielding a more granular appearance and feel. In general, these units are porphyritic, containing large feldspar phenocrysts/porphyroclasts set in fine-grained, aphanitic matrices (Plate 4.3b).

Feldspar phenocrysts comprise approximately 10-20 % of the rock and are predominantly equant in shape and coarse grained, ranging in size from 0.5 mm up to 2 cm. Individual phenocrysts are not elongated but are locally rotated and typically augened by thin wisps of mafic minerals that wrap around the phenocrysts (Plate 4.3d). Pressure shadows created during rotation are filled with calcite or mafic mineral phases. All of the phenocrysts are grey, most likely due to alteration and there is no distinction between individual phenocrysts, indicating that they are all of the same phase, namely plagioclase feldspar. These rocks are predominantly devoid of quartz phenocrysts, although rare quartz phenocrysts are present in weakly altered sections.

These units contain approximately 15-25 % mafic material, consisting of predominantly amphibole and pyroxene. These grains are generally light green and occur as thin, millimeter wide streaks or wisps or may be found as larger, 0.5-2 cm, equant shaped blebs. The matrix is primarily aphanitic in texture and individual mineral grains are almost impossible to detect without the aid of a microscope. The matrix is very strongly hematitized, giving the rock its deep red color. These units are almost non-

magnetic with magnetic susceptibility readings between 1 and 5, averaging approximately 2.5. Calcite is also abundant in these units, averaging approximately 2-4 %, as small blebs associated with the mafic minerals, within pressure shadows of the augened phenocryst, or disseminated throughout the matrix.

Each one of the CP units within the mineralized zone is strongly foliated and this foliation is consistent with the rest of the deposit (Plate 4.3c). The foliation is defined by thin streaks and wisps of mafic minerals, other alteration minerals and to a minor extent, calcite. Some units display a more intense foliation, wherein thin wisps of mafic minerals strongly wrap around feldspar phenocrysts, often causing them to rotate. This creates an augen effect with the feldspar phenocrysts. There are also several small mylonitic zones located within these units. These zones are generally 0.2-0.5 m wide and appear strongly foliated and finely laminated. They are generally phenocryst poor and phenocrysts that are present have been greatly stretched, parallel to the foliation.

#### **4.3.2 Fine Grained Porphyritic Metamorphosed Felsic Volcanic Rocks of the Ore Zone**

The FP, metamorphosed felsic volcanic rocks comprise the second most common lithology within the ore zone and appear to be associated with weak to moderate, locally intense uranium mineralization (Plate 4.4a). These units occur between the CP units of the main Mine Sequence and they constitute an integral part of the ore zone. FP units also flank the outer CP units of the main Mine Sequence. As a result, they are often strongly altered and well mineralized, to a level consistent with equivalent rocks within the ore



zone. Areas that display consistent alteration and mineralization equivalent to that within the ore zone are included as part of the ore zone and will be referred to as the mineralized zone.

These units are relatively stratiform, ranging in thickness from 2-20 m, and can be traced between individual drill holes. However, similar to the CP units, the FP units also pinch and swell both across and along strike. Individual units will locally merge together when a CP unit pinches out, or will pinch out when two CP units merge together. The FP units comprise approximately 45 % of the mineralized zone, varying between 40-60 %. In areas where the ore zone is thickest, most of the FP units are 15-20 m thick and comprise approximately 60 % of the mineralized zone. This includes areas that flank the outer CP units of the Mine Sequence. In areas where the ore zone is thinner, FP units are about 2-5 m thick with only one unit reaching a thickness of about 20 m. Thinner units comprise approximately 40 % of the mineralized zone.

The FP units are altered and mineralized, with individual units throughout the mineralized zone displaying variable degrees of alteration and mineralization (Plate 4.4c). Hematite alteration, which changes the color of the rock to various shades of red, depending on intensity, is variable throughout individual FP units within the mineralized zone (Plate 4.4d). As a result, rock color varies from light pinkish-grey, generally towards the center of thicker intervals to deep red near the edges. Sodic and silica alteration are also variable throughout the ore zone and where present, leave the rock soft and porous in texture with a more granular feel. These rocks have an overall porphyritic texture and are similar to the FP units within the hanging wall and foot wall. They consist

of small phenocrysts/porphyroclasts in fine-grained variably hematized (imparting a pinkish-grey to red color to the rock) matrices (Plate 4.4e).

There appears to be two different phenocryst varieties in the FP units. The predominant phenocryst type is plagioclase feldspar which comprises approximately 10 % of the rock. These phenocrysts are light grey, exhibit an overall equant shape, and range from 3.0-5.0 mm, but can be as large as 1.0 cm. Individual phenocrysts do not appear to have been rotated during deformation in contrast to those in the CP units. Quartz phenocrysts comprise the second type and are generally milky white to translucent, range in size from 1.0-3.0 mm and are elongated, with their long axis parallel to foliation. The frequency of quartz phenocryst appearance throughout individual units appears to be dependent on alteration intensity. In areas where alteration intensity is moderate to intense, quartz phenocrysts are absent or rare; in areas where alteration is weak, they are present and comprise approximately 2-3 % of overall rock volume. Most quartz phenocrysts occur towards the center of thicker units where alteration is weakest and absent near unit contacts where alteration is stronger.

Similar to the CP units, the FP units contain approximately 15-25 % mafic material, consisting mostly of amphibole and pyroxene. These grains are generally light green and occur as thin, millimeter wide streaks or wisps (Plate 4.4b) or as larger, 0.5-2 cm equant shaped blebs. These units are weakly magnetic having magnetic susceptibility readings between 2 and 15, averaging 10. In select areas these units are very weakly magnetic with magnetic susceptibility readings between 2 and 8, averaging 5. In general, the FP units are more magnetic than the CP rocks within the mineralized zone. These

units contain calcite, but not in similar percentages as the CP units. The calcite occurs as very small blebs associated with mafic minerals, either disseminated throughout the groundmass or more rarely, within rare pressure shadows of augened phenocrysts.

The FP felsic volcanic units within the Michelin deposit are strongly foliated, with a foliation that is consistent with other units throughout the mineralized zone. The foliation is defined by thin streaks or wisps of mafic minerals, secondary alteration minerals, and to a minor extent by elongated quartz phenocrysts. Locally, these mafic wisps wrap around larger feldspar phenocrysts yielding an augened texture. There are also several small mylonitic zones located within these units which are generally 0.2-0.5 m wide, strongly foliated, and finely laminated. They are generally phenocryst-poor. Any phenocrysts that are present have been stretched substantially, exhibiting a ratio of almost 10:1 with long axes parallel to foliation.

#### **4.3.3 Petrography of the Coarse and Fine Grained Porphyritic Volcanic Rocks of the Ore Zone**

Petrographic examination of the CP and FP felsic volcanic rocks from within the ore zone reveals several mineralogical changes from equivalent units within the hanging wall and foot wall. These changes are a direct result of alteration and for the most part are consistent throughout each unit for each respective rock type within the ore zone. Since the CP and FP units share the same mineralogical changes and appear very similar to each other in thin section, their petrographic descriptions are combined in this section. However, due to the variability in alteration intensity some of the mineralogical changes

differ between the two rock types. Where this occurs, these changes will be identified and described below.

The vast majority of phenocrysts within the two rock types consist of plagioclase feldspar; more specifically they are all albite phenocrysts. These phenocrysts consist of primary albite, and secondary albite that formed from the alteration of potassium feldspar during sodic metasomatism. The primary albite phenocrysts are less abundant, are smaller, and have the same appearance as albite phenocrysts within unaltered rocks in the hanging wall and foot wall. These phenocrysts are a primary constituent of the felsic volcanic host rock and have remained relatively unaffected, with the exception of increased sericitization, during alteration. In general, these phenocrysts are subhedral to euhedral, equant in shape, ranging from 0.5-1.5 cm within the CP felsic volcanics and 0.3-1.0 cm within FP units; although very rarely they can reach up to 1.5 cm in diameter. Within both rock types there are two distinct subtypes of these phenocrysts: phenocrysts that seem to have been recrystallized and now consist of three or four smaller, subhedral grains, and phenocrysts solely comprised of one large grain. The first subset seems to have been recrystallized during metamorphism, whereby albite phenocrysts recrystallized into three or four smaller grains, but still maintained the general shape of the original phenocryst (Plate 4.5c). The individual albite grains are subhedral, display weak Carlsbad twinning, and have been weakly sericitized. Typically, micron-sized grains develop along internal grain boundaries and locally host weak uranium mineralization. The second subset consists of a single grain that comprises the entire phenocryst. These grains are

usually larger than the first subset and display weak Carlsbad twinning which is often masked by alteration and late sericitization.

The secondary albite phenocrysts were originally potassium feldspar phenocrysts and they formed during sodic metasomatism. They are the more common phenocryst species, outnumbering the primary albite grains by almost two to one. They are also larger, ranging in size from 0.5-2.0 cm in the CP units and 0.5-1.2 cm in the FP units. These phenocrysts are subhedral to euhedral, equant, and display chessboard style twinning, a common result when potassium feldspar is altered to albite (Kaur *et al.*, 2012). These grains also occur in two distinct subsets, similar to the primary albite phenocrysts. The first subset appears to have been recrystallized during metamorphism and now consists of three to five, subhedral grains that maintain the shape of the original phenocryst (Plate 4.5b and d). Typically there is micron-sized subgrain development along internal grain boundaries, which locally hosts trace uranium mineralization. The second subset consists of large single grain phenocrysts (Plate 4.5a). Both subsets display chessboard twinning in individual albite grains and both have been completely altered, exhibiting for the most part a very weak sericite alteration.

Both primary and secondary albite phenocrysts exhibit irregular external crystal boundaries. A similar effect is observed in equivalent phenocrysts within the hanging wall and foot wall rocks but is generally more pronounced within the mineralized zone. This appears to be the result of metasomatism with enhanced destruction caused by alteration, damaging or eating away at the edges of the grains. These irregular

embayment's are typically filled with secondary alteration minerals and can host trace amounts of uranium.

Quartz phenocrysts are rare within the mineralized zone and occur only where alteration is less intense. Typically towards the centers of the thicker FP units, or within the FP units that flank the Mine Sequence. When quartz phenocrysts are present, they are similar to the quartz phenocrysts within equivalent, unaltered rocks, occurring as small, 2.0-4.0 mm sized grains within the CP rocks and 1.0-3.0 mm sized grains within the FP units. Despite the differences in grain size these phenocrysts are similar in both rock types, occurring as euhedral grains, slightly elongated in the plane of foliation, generally with a ratio of about 3:1. These grains have been recrystallized during metamorphism and now consist of 5-6, individual anhedral quartz grains sutured together, White and Martin (1980) postulate that this eliminated strain from increased deformation. Typically individual grains display undulose extinction in reflected light, indicative of deformation. When alteration is more intense, quartz phenocrysts are absent, having been dissolved during the alteration process. The secondary vug space created by dissolution is filled with secondary alteration minerals. Some of these filled vugs maintain the original shape of the phenocryst, but are filled with multiple, sodic amphibole grains (Plate 4.5e-f).

The mafic minerals, which comprise 15-25 % of the rock within the ore zone result from alteration and consist of sodic amphiboles and pyroxenes (Plate 4.5i, j and l). These minerals are associated with several other minerals that formed, or whose concentrations increased, as a result of alteration and mineralization. These phases include zircon, titanite, hematite, magnetite, albite, calcite, and uranium-bearing phases.

All of these minerals are closely associated with the mafic minerals and are included in the 15-25 % estimation for each rock type. These grains will be discussed in further detail in section 5.5 and Chapter 6.

The phenocrysts and mafic minerals are hosted in fine-grained matrices that consist of interlocking, euhedral grains, thus imparting an overall mosaic texture to the rock (Plate 4.5g). Due to the very small grain size, individual features such as extinction and twinning are difficult to determine for the mineral grains that comprise the matrices. Matrices are composed predominantly of feldspar and quartz with minor amounts calcite, hematite, magnetite, mafic minerals and uranium-bearing mineral phases. Visual estimation combined with SEM-MLA analysis and normative calculations suggest that the groundmass is primarily (65-85%) albite. Albite grains occur as primary albite, (25-30%) and secondary albite (30-35 %) from sodic metasomatism and (0-30 %) newly formed albite in the spaces created from the dissolution of quartz within the matrix.

Depending on alteration intensity, the percentage of quartz within the groundmass ranges from 30 % to as low as 10 %. As the intensity of alteration increases, more quartz is removed from the rock therefore areas with a lower percentage of quartz have undergone a higher intensity of alteration. Generally the FP units contain more quartz within the groundmass than the CP units. The space created from the dissolved quartz allows secondary alteration and mineralization minerals to form, in particular albite, but sodic amphiboles and pyroxenes, calcite, and uranium-bearing phases are common (Plate 4.5k). In total, these grains constitute approximately 5 to 15 percent of the total matrix (Plate 4.5h). These grains can also form through the alteration of already pre-existing

grains within the groundmass, for instance, biotite and hornblende alters to sodic amphibole and pyroxene during alteration.

The matrix also contains a small amount of opaque minerals which commonly occur as micron-sized grains at triple-point junctions between feldspar and quartz grains. In the unaltered rocks, these grains are predominantly magnetite. Due to alteration, the same grains within the mineralized zone are now hematite, or a combination of both. In general, the more intensely altered rocks contain more hematite; whereas in the less intensely altered rocks, these micron-sized grains remain mostly magnetite. This alteration effect is described in Chapter 6, section 6.3 and this effect on the micron-sized grains is what gives the mineralized zone rocks their pervasive pinkish-red to red, locally dark red color. Sulfide grains do occur within the matrix but only in very trace amounts, primarily as either pyrite or galena. There is no real difference in sulfide variety or concentration between the rocks of the mineralized zone and equivalent, unaltered rocks within the hanging wall and foot wall.

#### **4.3.4 Geochemistry of the Coarse Grained Porphyritic Felsic Volcanic Rocks of the Ore Zone**

As a result of alteration and mineralization, the CP rocks in the ore zone are no longer geochemically similar to equivalent, unaltered CP rocks. The samples utilized for this section were collected throughout the mineralized zone and represent the multiple CP units that comprise the Mine Series. These samples also encompass a variety of alteration intensities that affect these rocks. Examination of the geochemical data indicates that



there are numerous geochemical differences between altered and unaltered rocks, as nearly every element analyzed has changed in concentration. It is important to note that some of these changes are accurate and result from an element being mobilized during alteration and either added or removed from the rock. However, some changes are apparent and although the element remained conserved during alteration, geochemical analyses indicate concentration changes for these conserved elements that are not real.

Due to the apparent concentration change for conserved elements, and the strong mobility of several of the major and trace elements it is difficult to geochemically define altered rocks in the same detail that was undertaken in Chapter 3. Therefore most of the rock type classification from discrimination diagrams is inaccurate, and reflect alteration, not the actual rock type. Despite this, discrimination diagrams along with major oxide concentrations and log-standardized plots for trace and rare earth elements will be utilized to characterize the altered rock. It is important to understand the current geochemical signature of these rocks, in order to compare the altered rocks to equivalent unaltered rocks, to investigate the changes that occurred during alteration and to geochemically characterize these rocks as an aid in future exploration. Average, low and high values for the major oxides, trace elements, REE, and normative mineral percentages for the CP felsic volcanic rocks are in Table 4.1.

#### **4.3.4.1 Discrimination Diagrams**

Samples of the CP felsic volcanics from within the mineralized zone are plotted on several discrimination diagrams (Figure 4.3a-f) in order to accurately classify them

geochemically. The discrimination diagrams utilized for this section will be the same used in section 3.5.4.1 to classify the unaltered CP rocks. It should be noted that these rocks are strongly altered as will be evident in each diagram and the classification given in each diagram is not an accurate representation for the actual rock. For example, potassium is completely removed from the rock during alteration, on a Silica versus Potassium diagram, samples plot in the Low-K field which would indicate that they are tholeiitic, when in fact they formed as calc-alkaline rocks and this is just an effect of alteration.

When the samples are plotted on a LeBas *et al.* (1986) TAS diagram (Figure 4.3a) the majority of the samples plot within the trachydacite-trachyte field, with four samples plotting in the rhyolite field. The four samples that plot within the rhyolite field are considered least altered and have lost little to no quartz, having SiO<sub>2</sub> values above 70 wt. % which is equivalent to unaltered rocks as on Figure 3.17. For the majority of samples that plot in the trachydacite-trachyte field, these rocks have undergone alteration strong enough to dissolve quartz and form new sodic amphiboles and pyroxenes and albite. This explains the approximate 7 wt. % decrease in SiO<sub>2</sub> and the 2-3 wt. % increase in total alkali content of these samples compared to unaltered samples. According to Neuendorf *et al.* (2005), samples that contain greater than 20 % normative quartz are classified as trachydacite and samples that contain less than 20 % normative quartz are classified as trachyte.

In an attempt to eliminate the effects of alteration, samples were plotted on a Winchester and Floyd (1977) diagram. This diagram plots immobile element ratios

against each other, by plotting  $\text{Zr/TiO}_2$  on the y-axis versus  $\text{Nb/Y}$  on the x-axis. In principle these immobile elements should remain conserved during alteration and plotting them as a ratio enables the identification of any elements that may have been mobilized during alteration. This would cause samples to move in a horizontal or vertical straight line. As can be seen from Figure 4.3b, all of the samples plot within the rhyolite field, in a nearly identical location as equivalent, unaltered rocks. The only difference being, that the samples from the mineralized zone generally plot higher on the y-axis within the rhyolite field. This is because Zr was not conserved during alteration and experiences a slight to moderate mass gain, as discussed in sections 5.5.3 and 6.5. This causes the  $\text{Zr/TiO}_2$  ratio to increase, therefore causing the altered samples to plot higher within the rhyolite field.

On an Irvine and Baragar (1971) Silica versus Alkalis diagram (Figure 4.3c) most of the altered samples plot as alkaline in nature. Most samples plot within the alkaline field, with some straddling the dividing line between alkaline and subalkaline, and several samples plotting within the subalkaline field. This is in stark contrast to the unaltered rocks which plot entirely within the subalkaline field. It appears that the intense alteration responsible for an increase in  $\text{Na}_2\text{O}$  content combined with a loss in  $\text{SiO}_2$  has caused the samples to plot away from the subalkaline field, which are silica saturated to alkaline rocks which have an excess of alkalis over silica and appear undersaturated with respect to silica (Best and Christiansen, 2001). The samples that plot within the subalkaline field are the least altered and still remain silica-saturated due to the fact that quartz remains in these rocks. Although the majority of mineralized zone samples are

alkaline, when plotted on an Irvine and Baragar (1971) AFM diagram (Figure 4.3d), they still plot in a linear trend within the calc-alkaline field. Some samples straddle the calc-alkaline-tholeiitic dividing line, mostly due to an increase in FeO contents during alteration. This increase in iron over magnesium would explain why some of the samples plot near or within the tholeiitic field, as tholeiitic rocks shows a stronger enrichment in iron relative to magnesium, more so than calc-alkaline rocks (Best and Christiansen, 2001). Similar to unaltered samples, these samples from the mineralized zone plot in a linear trend towards the alkaline apex of the triangle. Samples that plot closer to the alkali apex do not necessarily contain a higher concentration of alkalis than other samples, but instead contain lower concentrations of FeO and MgO and higher concentrations of  $\text{Al}_2\text{O}_3$ . This suggests that samples which plot closer to the alkali apex have a higher percentage of albite, explaining the increase in  $\text{Al}_2\text{O}_3$ . Samples that plot further away from this apex have a higher percentage of sodic amphiboles and pyroxenes. This explains the increase in FeO while maintaining the same  $\text{Na}_2\text{O}$  concentration.

A Peccerillo and Taylor (1976) diagram of  $\text{SiO}_2$  versus  $\text{K}_2\text{O}$  divides samples based on potassium content into Low-K, Medium-K and High-K rocks. In this study, unaltered samples all plotted within the High-K, calc-alkaline field as they contained approximately 4.5 %  $\text{K}_2\text{O}$ . Samples from within the mineralized zone have been completely stripped of potassium through sodic metasomatism and plot near the bottom of the y-axis in the Low-K, arc tholeiite series (Figure 4.3e).

Finally, using the Maniar and Piccoli (1989) Shands Index (Figure 4.3f), which plots the molecular ratio of  $\text{Al}/(\text{Na} + \text{K})$  along the y-axis versus  $\text{Al}/(\text{Ca} + \text{Na} + \text{K})$  along

the x-axis, shows that ore zone samples plot along the dividing line between the metaluminous and peralkaline fields, with about half of the samples plotting within each field. This is in contrast to equivalent unaltered rocks which plot entirely within the metaluminous field, suggesting that alumina content is greater than  $(\text{Na}_2\text{O} + \text{K}_2\text{O})$  but less than  $(\text{CaO} + \text{K}_2\text{O} + \text{Na}_2\text{O})$ . Samples within the peralkaline field have  $\text{Al}_2\text{O}_3$  values less than  $(\text{Na}_2\text{O} + \text{K}_2\text{O})$  and  $(\text{CaO} + \text{K}_2\text{O} + \text{Na}_2\text{O})$ . The mineralized zone samples that plot within the peralkaline field are strongly altered and contain elevated  $\text{Na}_2\text{O}$  contents, mainly due to the presence of secondary sodium bearing minerals, such as sodic amphiboles and pyroxenes. These grains increase the  $\text{Na}_2\text{O}$  contents of the rocks but not the  $\text{Al}_2\text{O}_3$  contents, therefore shifting the alumina saturation into the peralkaline field. Samples that contain a large amount of secondary albite would still plot within the metaluminous field as the ratio of Al to  $(\text{Na} + \text{K})$  would still be similar as in unaltered rocks.

Based on the information provided from the discrimination diagrams, the CP felsic volcanic rocks from the mineralized zone would be classified as metaluminous to peralkaline, Low-K, alkaline, calc-alkaline rhyolites.

#### **4.3.4.2 Major Oxides**

Major element chemistry for the CP felsic volcanics within the mineralized zone contains an average 67.6 wt. %  $\text{SiO}_2$ , ranging from 63.2-77.9wt. %. The wide range in  $\text{SiO}_2$  is directly related to alteration. The absence of quartz phenocrysts and groundmass quartz due to alteration reduces average  $\text{SiO}_2$  contents by nearly 7 wt. % in strongly

altered samples. Most of the samples within the ore zone range between 63-67 wt. %  $\text{SiO}_2$ , with only a handful of samples assaying above 70 wt. %  $\text{SiO}_2$ . These silica-enriched samples are weakly altered and contain quartz contents similar to those of unaltered hanging wall and foot wall rocks.

Rocks of the mineralized zone also average about 15.5 wt. %  $\text{Al}_2\text{O}_3$ , 4.3 wt. % FeO (total iron), 0.4 wt. % MgO, 2.0 wt. % CaO, 9.5 wt. %  $\text{Na}_2\text{O}$ , and 0.1 wt. %  $\text{K}_2\text{O}$ . The elevated  $\text{Na}_2\text{O}$  contents and extremely low  $\text{K}_2\text{O}$  contents are a direct reflection of sodic metasomatism and further sodic alteration. During sodic metasomatism of the rocks,  $\text{K}_2\text{O}$  is nearly completely removed and replaced by  $\text{Na}_2\text{O}$  which is then added to the system as secondary sodium-bearing alteration minerals formed during the most intense alteration.

The remaining major oxides all have wt. %'s greater than in equivalent, unaltered hanging wall and foot wall rocks. This is partially a result of alteration, whereby small quantities of  $\text{Al}_2\text{O}_3$ , FeO (total iron) and CaO have been added during alteration. Section 6.5 explains this in greater detail. Most of the increases displayed by these oxides and increases in MgO, MnO,  $\text{TiO}_2$ , and  $\text{P}_2\text{O}_5$  contents appear to result from apparent gains in concentration due to closure in the system. These oxides remain conserved during alteration. There was such a change in mass due to  $\text{SiO}_2$  and  $\text{K}_2\text{O}$  loss and  $\text{Na}_2\text{O}$  gain during alteration, these elements assay at a higher concentration than unaltered samples. In actuality, these oxides experience little to no change in wt. %, but when assayed they all display a slight to moderate increase.

#### **4.3.4.3 Trace and Rare Earth Elements**

Upper continental crust-normalized (after Taylor and McLennan, 1985) REE plot indicate several distinct patterns for CP samples from the Mine Series. In general, all samples display similar trends, with no real slopes and slight to moderate negative Eu anomalies (Figure 4.4). A more detailed examination reveals distinct groupings of the samples. Each group shares a similar profile across the REE but have discernible variations. It is possible that these groupings relate to specific individual CP units within the Mine Series.

When plotted on a continental crust-normalized (after Taylor and McLennan, 1985) extended trace element plot (Figure 4.5) the mineralized zone samples exhibit strong negative anomalies for Cs, Rb, K, Sr, and Ti, and strong positive anomalies in U for nearly every sample. Zr also displays a positive anomaly but only for a select number of samples.

The LFSE such as Cs, Rb, Ba, and U define wide ranges in concentration between samples. Alteration is responsible for some of these variations, as Rb and K<sub>2</sub>O have been completely removed from the rock during sodic metasomatism, and U has been added to the rock during mineralization. The Cs and Ba concentration are more a result of the original rock composition as some samples contain these elements in high concentrations while others do not. For example, barite occurs throughout the deposit but its occurrence is very sporadic. Th is the only LFSE that does not change during alteration. It maintains the same profile as in unaltered rocks indicating it was a conserved element. Sr and Ti

both show strong negative anomalies which is similar to the negative anomalies for both elements displayed by unaltered rocks (i.e. they remained unchanged during alteration).

The REE and HFSE display rather similar profiles in both the mineralized zone samples and unaltered samples, suggesting that their concentrations that are equal to those of unaltered rocks. The obvious exception is Zr which displays an increase in most mineralized zone samples (i.e. Zr is not conserved during alteration but was added).

#### **4.3.4.4 Geochemical Comparison of the Mineralized Coarse Grained Porphyritic Felsic Volcanic Rocks**

The CP units that constitute the Mine Series from within the mineralized zone display major mineralogical and geochemical differences compared to unaltered, equivalent rocks. Plotting CP samples from the mineralized zone on a normalized REE plot indicates that all samples display a very similar REE profile, the average REE profile for the mineralized CP units (Figure 4.9) displays a horizontal profile across the LREE, a -Eu anomaly, slight positive profile across the MREE followed by a horizontal profile across the HREE. The MREE appear to have higher concentrations relative to the LREE and HREE. Comparing this profile to the average profile for unaltered CP rocks indicates that the two are nearly identical, except the mineralized samples contain a greater REE concentration.

When the mineralized CP samples are plotted on a La/Sm vs Dy/Yb diagram (Figure 4.10), they generally group together, with the majority exhibiting a La/Sm ratio of about 6.5 and a Dy/Yb ratio of about 1.8. When compared to unaltered CP rocks, the



two groups overlap somewhat, evidence that the altered rocks are slightly more LREE depleted or MREE enriched. This mimics the REE plot with MREE enrichment.

The immobile-incompatible element plot of  $\text{TiO}_2$  vs  $\text{P}_2\text{O}_5$  (Figure 4.11) shows that the CP samples from the mineralized zone remain on the same linear trend as the unaltered samples, with the exception of a few outliers. However, on a  $\text{TiO}_2$  vs Zr plot most of the samples lie somewhat off the linear trend, with most of the samples displaying an increase in Zr values, suggesting that zirconium was not conserved during alteration.

The geochemical data of CP samples from the mineralized zone indicate that these units are geochemically similar to each other and to the unaltered equivalent units in the hanging wall and foot wall. Although REE profiles display sub-groupings related to individual CP units, these units all appear to be geochemically related and have been derived from the same source. It appears that the geochemical changes that occur within the mineralized zone are entirely related to alteration as the altered samples that plot Zr somewhat off the linear trend are few and show no definition of another linear trend, which would suggest a different rock type or source.

#### **4.3.5 Geochemistry of the Fine Grained Porphyritic Felsic Volcanic Rocks of the Ore Zone**

Although the FP units are geochemically very similar to the CP within the ore zone, they were affected by different alteration intensities. Therefore, it is important to define the geochemical distributions in these units. The samples utilized for this section

were collected throughout the mineralized zone and represent the multiple FP units within the mineralized zone and the variety of alteration intensities that affect these rocks. The samples come from several units that are situated between the CP units of the Mine Series as well as several samples that immediately flank the outer CP units of the Mine Series. Examination of the sample data indicates there are numerous geochemical differences between altered and unaltered FP rocks. These differences are very similar to those expressed in the CP rocks. The geochemical investigation for these rocks will be completed in the same manner as with the CP rocks. Average, low and high values for the major oxides, trace elements, REE, and normative mineral percentages for the FP felsic volcanic rocks are in Table 4.1.

#### **4.3.5.1 Discrimination Diagrams**

Samples of the FP felsic volcanics from within the mineralized zone are plotted on several discrimination diagrams (Figure 4.6a-f) as in section 3.4.3.1. For the most part, these samples display the same patterns and trends as the CP mineralized rocks. Some of the least altered samples, which generally include samples that have not lost any silica, are similar to the unaltered FP felsic volcanics and plot in the same locations as the unaltered rocks. This is misleading because even though these samples are considered to be least altered, they are still from within the mineralized zone and have undergone sodic metasomatism.

On a LeBas *et al.* (1986) TAS diagram (Figure 4.6a), the majority of the FP samples from the mineralized zone plot within the trachydacite–trachyte field, with a

handful of samples plotting in the rhyolite field. Those samples which plot within the rhyolite field are considered to be least altered and contain approximately 71-75 wt. %  $\text{SiO}_2$  and 7-9 wt. % alkalis. These samples plot in the same location as equivalent, unaltered rocks as seen in Figure 3.5. The samples that cluster within the trachydacite–trachyte field are more strongly altered and contain approximately 64-68 wt. % silica and 9-11 wt. % alkalies. These samples experienced a loss of quartz during alteration and the space created was infilled by secondary sodium-bearing minerals.

To eliminate the effects of alteration, samples are plotted on a Winchester and Floyd (1977) diagram (Figure 4.6b). Nearly all of the samples plot within the rhyolite field, in nearly the identical location as unaltered FP rocks outside of the mineralized zone. Two samples plot to the right of this group, towards the trachyte-trachyandesite field. Both of these samples assay a low value for yttrium, much lower than the average value for the other samples. This causes the Nb/Y ratio to be higher. Several of the samples plot higher on the y-axis and slightly to the left of the main group of samples. This is because Zr is not conserved during alteration and experiences a slight to moderate mass gain. In addition, a couple of the samples exhibit low  $\text{TiO}_2$  concentrations which increased their Zr/ $\text{TiO}_2$  ratios. These samples are shifted to the left due to an increase in yttrium, which also experiences a slight mass gain in altered samples. However, samples that have low  $\text{TiO}_2$  and Nb concentrations shift to the left of the x-axis.

On an Irvine and Baragar (1971) Silica versus Alkalis diagram (Figure 4.6c) about half of the samples plot as alkaline and half as subalkaline. The subalkaline samples are the least altered and plot in near identical locations as equivalent, unaltered

rocks from outside of the mineralized zone. The alteration undergone by the FP rocks within the mineralized zone causes a loss of  $\text{SiO}_2$  and a gain in  $\text{Na}_2\text{O}$ , with the result that samples plot within the alkaline field, indicating they are no longer silica saturated but silica undersaturated and have an excess of alkalis over silica (Best and Christiansen, 2001). On an Irvine and Baragar (1971) AFM diagram (Figure 4.6d), the samples plot along a linear trend, close to the alkaline apex of the triangle diagram within the calc-alkaline field. Some samples plot close to the calc-alkaline–tholeiitic dividing line, indicating that these samples are more iron-rich compared to magnesium. Samples plot in a nearly identical position as equivalent, unaltered samples, which also plot in a linear trend towards the alkali apex.

A Peccerillo and Taylor (1976) diagram indicates that all FP samples within the mineralized zone were nearly completely stripped of potassium (Figure 4.6e). Every sample plots within the Low-K, arc tholeiite series of rocks, which is a big change from equivalent unaltered rocks which plot in the High-K, calc-alkaline series.

A Maniar and Piccoli (1989) Shands Index (Figure 4.6f) diagram indicates that the FP mineralized zone samples plot along the dividing line between metaluminous and peralkaline fields, with about half of the samples plotting within each field. This is a change from equivalent, unaltered rocks which plot very close to the peralkaline dividing line, but within the metaluminous field. This diagram suggests that half of the FP rocks from the mineralized zone are peralkaline and that they have molecular ratios of  $\text{Al}_2\text{O}_3$  less than  $(\text{Na}_2\text{O} + \text{K}_2\text{O})$  and less than  $(\text{CaO} + \text{Na}_2\text{O} + \text{K}_2\text{O})$ , suggesting the formation of alkali mafic minerals (Best and Christiansen, 2001). Secondary sodic amphiboles and

pyroxenes from alteration shift the samples into the peralkaline field. The samples in the peralkaline field would be more enriched in these minerals than secondary albite, as samples rich in sodium from the occurrence of secondary albite still plot within the metaluminous field due to their higher wt. % of  $\text{Al}_2\text{O}_3$ .

Based on information provided from the discrimination diagrams, FP felsic volcanic rocks from the mineralized zone are classified as metaluminous to peralkaline, Low-K, alkaline to subalkaline, calc-alkaline rhyolites.

#### **4.3.5.2 Major Oxides**

FP felsic volcanic rocks from the mineralized zone contain an average 68.9 wt. %  $\text{SiO}_2$ , with individual samples ranging from 63.9-75.1 wt. %  $\text{SiO}_2$ . Quartz was removed from the rock during moderate to strong alteration so samples exhibiting between 64-67 wt. %  $\text{SiO}_2$  have undergone strong alteration. There is a group of samples that plot between 64-67 wt. % silica, only one sample between 67-72 wt. % silica, and finally, the least altered samples which plot above 72 wt. %. These samples are located closer to the center of the thicker, FP units from the mineralized zone where alteration is weakest or on the flanks just outside of the main Mine Series; with respect to  $\text{SiO}_2$  wt. %, these samples appear similar geochemically to unaltered rocks, which average about 74.3 wt. %  $\text{SiO}_2$ .

These rocks also average 15.3 wt. %  $\text{Al}_2\text{O}_3$ , 3.7 wt. % FeO (total iron), 0.3 wt. % MgO, 1.7 wt. % CaO, 9.5 wt. %  $\text{Na}_2\text{O}$  and 0.1 wt. %  $\text{K}_2\text{O}$  which are very similar to those in the CP units in the mineralized zone with the exception of FeO and CaO, which are

nearly 0.5 % higher and  $\text{Al}_2\text{O}_3$  which is about 0.25 % higher within the CP felsic volcanic rocks of the mineralized zone. This discrepancy is not related to alteration, as both the FP and CP rocks display similar alteration styles, intensities, and mineralogies. Instead, this increase may be attributed to FP units within the mineralized zone containing on average approximately 1.25 % more  $\text{SiO}_2$  than the CP rocks. This higher  $\text{SiO}_2$  wt. % and slight increase in quartz causes the other oxides to assay lower, closer to their actual value as the effects of mass gain due to closure and the mass change in the rock from the loss of silica is less within the FP rocks than within the CP rocks.

The high  $\text{Na}_2\text{O}$  contents and extremely low  $\text{K}_2\text{O}$  contents are a direct result of sodic metasomatism. Sodium is then further added to the system through the formation of secondary sodium bearing minerals such as albite and sodic amphiboles and pyroxenes. This is similar to what is seen in the CP rocks, with concentrations of both these major oxides near identical in the two rock types.

#### **4.3.5.3 Trace and Rare Earth Elements**

Most samples have a similar pattern, an almost horizontal straight line across the REE, on a Taylor and McLennan (1985) upper continental crust-normalized REE plot (Figure 4.7), but with distinctive, individual groupings. There is a very slight negative slope within the LREE, a strong negative Eu anomaly, followed by a relatively flat MREE and HREE profile. Some samples display a very slight negative and/or positive slope in both the MREE and HREE. A more detailed examination reveals distinct groupings of the samples. Each group shares a similar profile across the REE but have

discernible variations. It is possible that these groupings relate to specific FP units within the mineralized zone.

On a Taylor and McLennan (1985) upper continental crust-normalized extended trace element plot (Figure 4.8), the samples exhibit strong negative anomalies in Cs, Rb, K, Sr, and Ti, and strong positive anomalies in for U for nearly every sample. The LFSE such as Cs, Ba, and U all display a wide range in concentrations between samples. The wide range in U concentrations is due to mineralization, as some samples are more mineralized than others. In comparison to unaltered rocks, the U concentrations in the mineralized zone are considerably greater. The Cs and Ba concentrations are more a result of the original composition of the rock; some samples contain these elements in high concentrations while others do not. For example, barite occurs sporadically throughout the deposit and there is no difference for Ba for samples within the mineralized zone and unaltered samples. Rb displays a strong negative profile as it substitutes for K in potassium-bearing minerals (thus both Rb and K were removed from the rock during sodic metasomatism). These rocks also display strong negative anomalies in Sr and Ti, which is similar to the negative anomaly for both elements in unaltered rocks as seen in Figure 3.16. It appears for the most part that these elements were unaffected during alteration.

The HFSE display a similar pattern to equivalent, unaltered rocks with some samples having higher HFSE concentrations than others; these same samples also display elevated REE concentrations. It is most likely that these higher concentrations are due to the effects of mass change and closure of the system. Zr does show a slight positive

anomaly for some samples, similar to what was seen in the CP rocks of the mineralized zone.

#### **4.3.5.4 Geochemical Comparison of the Mineralized Fine Grained Porphyritic Felsic Volcanic Rocks**

FP units of the Mine Series from within the mineralized zone display major differences in mineralogy and geochemistry compared to unaltered or even sodic-altered equivalent rocks from the hanging wall and foot wall. Although it is interpreted that these differences are attributed to alteration and mineralization, it is possible that these units may not be geochemically similar to equivalent rocks within the hanging wall and foot wall. On a normalized REE plot, the samples define a similar profile across the REE, however distinct patterns, possibly relating to individual units within the Mine Series, emerge. When the average REE concentrations for these samples are plotted on the same diagram (Figure 4.9), it displays a horizontal profile across the LREE, -Eu anomaly, and a horizontal profile across the MREE and HREE. This profile is almost identical to that of the unaltered and sodic altered equivalent felsic volcanic rocks, with the exception that the overall REE concentration is greater. The change in total concentration is most likely an apparent effect due to the effect of the change in mass and/or volume during alteration and closure during geochemical analysis. These two effects in combination cause the concentrations of the more altered samples to plot higher, which is the effect seen for the more strongly altered samples on the log-standardized plot. The samples that are least



altered (i.e. that did not experience a loss in silica) all plot with lower concentrations, equivalent to the unaltered samples.

To eliminate the effects of mass and/or volume change and closure, the samples were plotted on the REE ratio-ratio plot of La/Sm vs Dy/Yb. Utilizing ratios eliminates the apparent concentration differences as each REE would experience the same concentration gain or loss, unless they were not conserved during alteration. Comparing the ratio of LREE to that of the HREE will allow any changes in LREE and HREE to be evident. Figure 4.10 indicates that the FP samples from the mineralized zone plot in the same position generally as unaltered and sodic altered samples, with the exception of a few outliers. Most of the samples have a HREE ratio of 1.8, which is consistent with unaltered samples. There are a few samples that plot below this ratio indicating they are enriched in HREE, possibly indicating garnet mineralization. There are also a couple above this ratio, indicating they are depleted in HREE or enriched in the MREE which could then indicate MREE are partitioning into the sodic amphiboles and pyroxenes. The LREE ratio follows the same range as the unaltered samples and could be related to allanite, brannerite and/or monazite enrichment in some of these samples.

Plotting samples from the mineralized zone on the same immobile-incompatible element plots as the unaltered and sodic altered samples (Figure 4.11) reveals two things. First, on the  $\text{TiO}_2$  vs  $\text{P}_2\text{O}_5$  plot, all samples, with the exception of a few outliers remain on the same linear trend as the unaltered samples, suggesting that titanium and phosphorus remain conserved during alteration. When plotting on the  $\text{TiO}_2$  vs Zr diagram most of the samples plot along the same linear trend as unaltered samples, but some

samples plot above this trend, as they are elevated in zirconium. This suggests that zirconium has not remained conserved during strong alteration and has been enriched during the alteration and mineralization.

The geochemical data suggests that the FP felsic volcanic rocks from within the mineralized zone are geochemically equivalent to the unaltered and sodic altered FP felsic volcanic rocks within the hanging wall and foot wall, and that these rocks all share a common parent and are derived from the same magma source. The evidence suggests that geochemical differences between the FP units of the mineralized zone and the unaltered hanging wall and foot wall are caused by a more intense alteration than that observed within the sodic envelope, and by mineralization, and not due to different rock types derived from a separate a magma source.

#### **4.3.6 Mafic Intrusives of the Ore Zone**

Mafic dikes occur throughout the ore zone and comprise approximately 5-10 % of the total rock volume. The dikes within the ore zone, which appear similar to dikes outside the ore zone, are not mineralized but do locally increase the uranium grade within the felsic volcanic host rocks, adjacent to the dike contacts. There are two varieties of mafic dike within the ore zone; pre-kinematic, biotite-hornblende schists, dikes and syn-kinematic gabbroic dikes. Post-kinematic dikes have not been observed within drill sections from the ore zone. In general, all dikes are very similar to those described in Chapter 3 observed within the unaltered hanging wall and foot wall of the deposit.

The pre-kinematic, biotite-hornblende schists, dikes are the more common dike within the ore zone. Their thicknesses range from 0.5-4 m, averaging about 1 m. Contacts between these dikes and the host felsic volcanics are generally sharp and concordant with foliation. The pre-kinematic dikes are well foliated, very weakly magnetic and moderately chloritized. In many locations, these dikes mark the contact between the CP and FP units within the ore zone. Although present within the ore zone, these dikes only exhibit minimal changes due to alteration or mineralization. As these dikes are equivalent to similar dikes seen within the hanging wall and foot wall, they will not be described in detail in this section. Their textures and mineralogies are similar to those described in Chapter 3, section 3.7. These dikes show a slight degree of alteration as a slight enrichment in Na<sub>2</sub>O. This is discussed in Chapter 6, section 6.7 and therefore will also not be discussed in this section.

The syn-kinematic gabbroic dikes, which average about 1 m thick, are the least common dike variety having been observed only a couple of times in the 10 drill holes examined for this study. These dikes are foliated, very weakly magnetic, and weakly to moderately chloritized. Contacts between these units and the felsic volcanic host rocks are generally sharp and predominantly concordant, but can be discordant to foliation. These dikes do not exhibit intense alteration but do display a slight Na<sub>2</sub>O enrichment which is discussed in Chapter 6, section 6.7.2. The gabbroic dikes are unmineralized but produce a strong mineralizing effect in the surrounding felsic volcanic host rock immediately adjacent to the dike contact and grading away from the contact. This is explained in further detail in section 5.2. It is possible that these dikes remobilized

uranium mineralization, thus increasing the uranium grade at their contacts. These dikes in general are equivalent to similar dikes located throughout the hanging wall and foot wall described in Chapter 3, section 3.7, and will therefore not be discussed further here.

**Table 4.1:** Average (avg), low and high values for the coarse grained (CP) and fine grained (FP) felsic volcanic rocks of the mineralized zone, and the fine grained (FP) felsic volcanic rocks within the sodic envelop of the major oxides (wt.%), transition metals (ppm), low field strength elements (ppm), high field strength elements (ppm), rare earth elements (ppm), volatile elements (ppm), and the normative mineral percentages after Irvine and Baragar (1971).

	CP Min. Zone			FP Min. Zone			FP Sodic Envelope		
	avg	low	high	avg	low	high	avg	low	high
Major Oxides (wt.%)									
SiO <sub>2</sub>	66.8	63.2	75.9	67.5	64.0	73.3	74.0	67.6	77.1
Al <sub>2</sub> O <sub>3</sub>	15.8	12.3	17.8	15.9	12.7	18.0	12.7	10.9	14.9
Fe <sub>2</sub> O <sub>3</sub>	4.5	2.8	6.3	3.9	2.9	5.9	3.2	1.9	4.0
MnO	0.1	0	0.1	0.1	0	0.1	0.1	0	0.1
MgO	0.5	0.2	0.9	0.4	0.1	1.2	0.3	0.2	0.7
CaO	2.1	0.8	3.3	1.8	1.1	3.4	1.3	0.7	2.3
Na <sub>2</sub> O	9.6	7.5	11.0	9.8	7.9	11.0	7.5	3.9	9.8
K <sub>2</sub> O	0.1	0.1	0.3	0.1	0	0.2	0.5	0	4.6
TiO <sub>2</sub>	0.4	0.2	0.6	0.4	0.2	0.7	0.4	0.2	0.5
P <sub>2</sub> O <sub>5</sub>	0.1	0.1	0.2	0.1	0.1	0.2	0.1	0	0.4
LOI	0.9	0.2	1.9	1.0	0.4	2.8	0.8	0.3	1.2
Transition Elements (ppm)									
Co	2.5	0.5	8	2	0.5	7	2	0	3
Cr	42	0	80	38	20	70	35	0	80
Cu	6	0.5	70	1.6	0.5	10	11	0	210
Ni	11	0	30	10	10	10	7	0	40
Sc	7	3	13	7	2	11	6	4	8

V	106	31	212	107	29	239	41	8	114
Zn	115	40	300	84	40	170	74	40	110

Low Field Strength Elements (ppm)

Ba	871	78	3392	1038	48	2537	1486	378	2527
Cs	0.1	0	1	0.1	0.1	0.6	0.1	0	0.7
Ga	33	21	44	31	20	46	21	18	27
Rb	3	0.5	26	1	0.5	6	12	0	109
Sr	129	65	318	132	51	232	106	77	156
Pb	32	12	98	26	13	60	24	9	60
Th	27.8	16.6	40.0	26.0	18.0	44.5	18.5	16.0	25.2
U	1385	7.6	4420	1278	31.2	4680	177	6.9	4530

High Field Strength Elements (ppm)

Hf	17.2	11.6	24.5	15.1	11.5	20.9	11.4	8.7	14.9
Nb	44.3	28.0	60.7	35.1	22.8	67.8	23.1	19.8	28.0
Ta	3.1	2.0	4.5	2.9	1.8	5.5	1.9	1.6	2.1
Y	113.7	55	232	75.8	30.2	163.0	46.9	39.0	103.0
Zr	988	580	1858	757	477	1210	465	284	598

Rare Earth Elements

La	138	85.3	213	120.7	80.0	186	82.2	65.4	98.1
Ce	283	174	386	242	157	372	164	132	200
Pr	34.2	21.3	45.1	28.4	18.4	43.8	18.8	16.8	21.9
Nd	117.6	74.5	167.0	95.2	62.1	151.0	62.8	57.6	70.9
Sm	21.0	11.9	37.5	15.9	9.8	27.9	10.4	9.2	12.8
Eu	2.6	1.2	5.0	1.7	1.0	3.8	1.4	0.7	2.0

Gd	18.2	10.0	37.5	13.4	6.8	24.6	8.4	7.3	13.5
Tb	3.3	1.6	7.2	2.2	1.0	4.3	1.4	1.2	2.6
Dy	19.8	9.4	44.9	13.2	5.5	27.2	8.1	7.3	15.5
Ho	3.8	1.8	8.3	2.5	1.0	5.3	1.6	1.4	3.0
Er	11.5	5.6	23.3	7.7	3.3	15.7	4.7	4.1	8.8
Tm	1.8	0.8	3.3	1.2	0.5	2.5	0.7	0.6	1.3
Yb	11.2	5.4	19.9	7.8	4.0	16.0	4.6	3.9	7.4
Lu	1.6	0.8	2.7	1.2	0.6	2.3	0.7	0.6	1.0

Volatile Elements (ppm)

Ag	0.8	0.3	7.6	1	0.3	4.3	0.4	0	1.3
As	5	0	10	3	2.5	6	3	0	13
Be	8	3	15	8	3	17	4	3	8
Bi	0.6	0	1.4	0.8	0.2	1.3	0.5	0	6.7
Ge	1.2	0	2.3	1.3	0.6	1.9	0.8	0	1.4
In	0.1	0	1.2	0.1	0.1	0.1	0	0	0.1
Mo	4.6	1	45	2	1	5	5	0	30
Sb	0.9	0.1	5.3	0.2	0.1	0.5	0.8	0	7.6
Sn	6	4	18	5	3	9	3	2	4
Tl	0	0	0.2	0	0	0.1	0.1	0	0.5
W	0.7	0	1.7	1	0.3	7.9	1.3	0	27

Normative Mineralogies (%)

%AN	1.2	0	6.7	0.5	0	3.7	1.0	0	7.2
Q	6.6	0	30.4	7.6	0	24.8	26.5	6.9	36.6
or	0.7	0.4	1.7	0.7	0.1	1.3	3.2	0.1	27.1

ab	78.5	62.7	85.1	79.6	65.1	90.3	61.1	33.1	76.2
an	1.0	0	5.5	0.4	0	3.0	0.5	0	2.6
ne	0.1	0	1.8	0.4	0	4.6	0	0	0
di	6.7	2.3	13.0	5.2	2.6	8.2	3.6	0.9	9.2
hy	0.9	0	2.6	0.4	0	3.1	0.2	0	1.4
wo	0.4	0	2.7	0.7	0	4.9	0.5	0	1.7
ol	0.1	0	1.4	0.1	0	1.7	0	0	0
ac	2.0	0	5.5	1.8	0	5.8	1.7	0	5.7
mt	1.8	0	3.1	1.9	0	3.2	1.8	0	2.9
il	0.8	0.5	1.2	0.8	0.3	1.3	0.7	0.4	0.9
hem	0	0	0	0	0	0	0	0	0
ap	0.2	0.1	0.4	0.2	0.1	0.3	0.2	0.1	0.9
ru	0	0	0	0	0	0	0	0	0



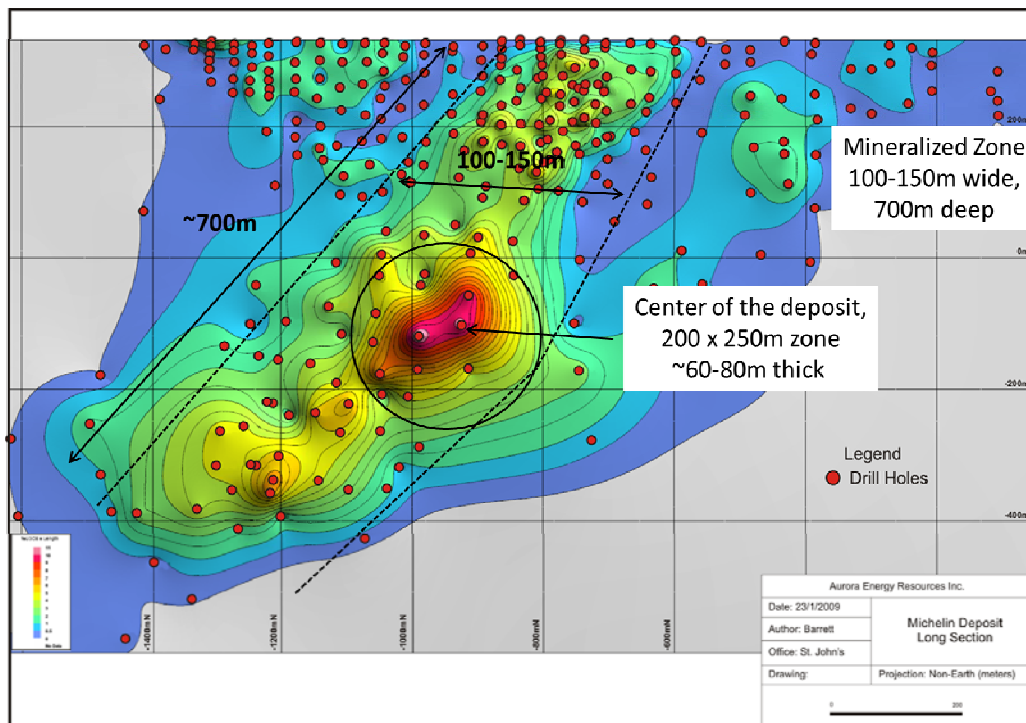


**Figure 4.1:** Approximate dimensions of the mineralized zone. The mineralized zone extends from surface to a continuous depth of ~700 m down dip in a ~300-350 m wide zone, this zone narrow along strike in both directions and at depth. In the center there is a ~200x250 m section at ~400 m depth that is 60-80m thick (modified after Hertel *et al.*, 2009).

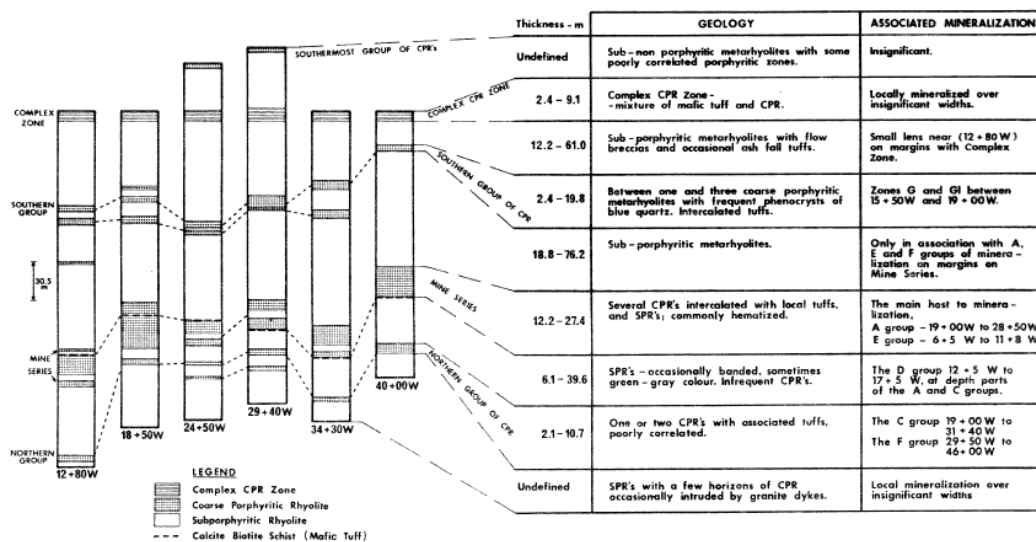


**Figure 4.2:** Mine series of the Michelin deposit (Evans, 1980).

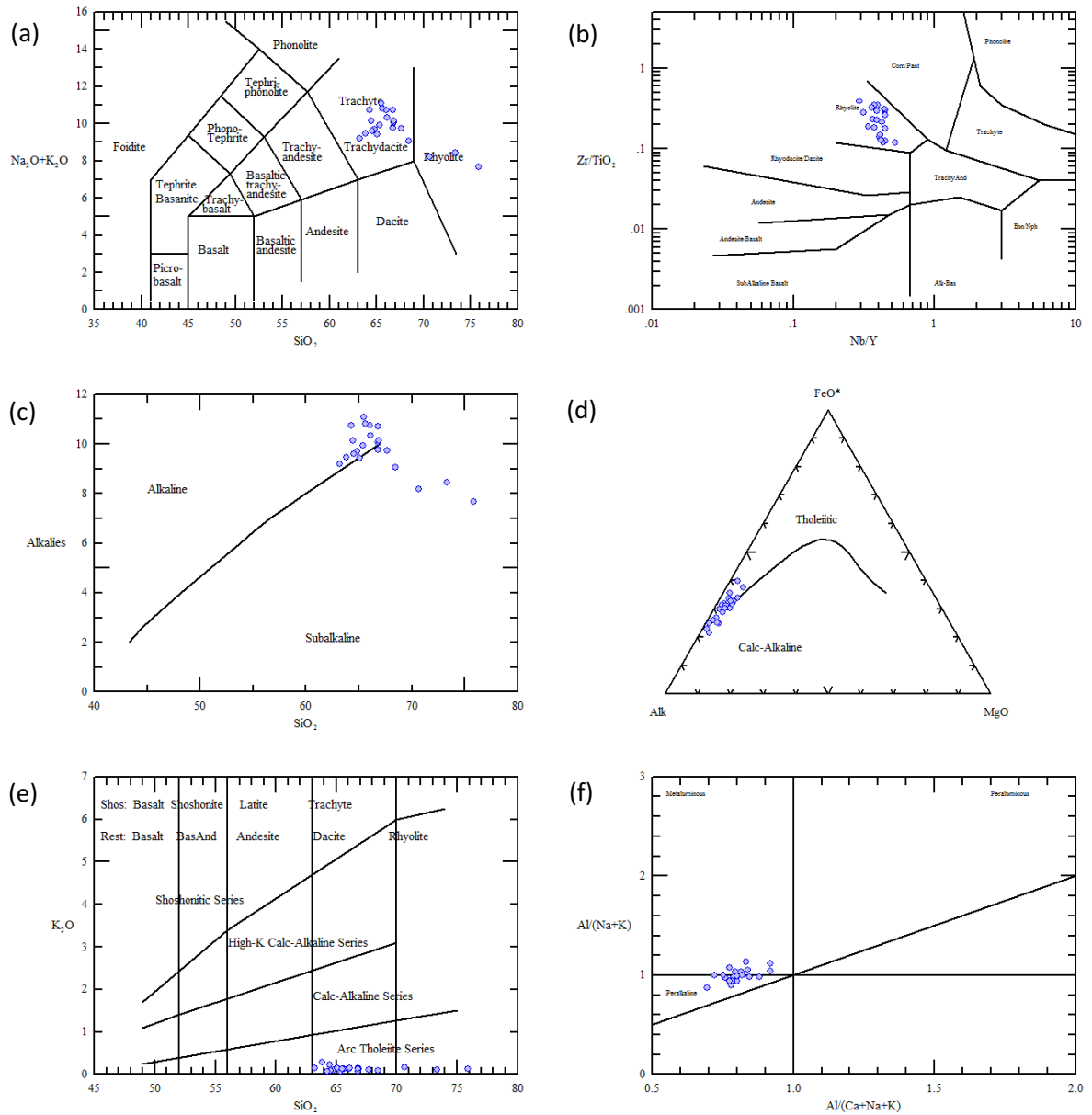


**Figure 4.3:** Discrimination diagrams of the CP felsic volcanic rocks from the mineralized zone (solid blue circles), (a) classification diagram based on Total Alkalies ( $\text{Na}_2\text{O} + \text{K}_2\text{O}$ ) vs. Silica ( $\text{SiO}_2$ ) (in terms of oxide wt.%) (TAS) (LeBas *et al.*, 1986), (b) classification diagram based on ratios of Nb/Y (ppm) vs. Zr/TiO<sub>2</sub> (ppm/oxide wt.%) (Winchester and Floyd, 1977), (c) TAS with alkaline-subalkaline fields (Irvine and Baragar, 1971), (d) Ternary plot of Total Alkalies-MgO-FeO\* (in terms of oxide wt.%) with calc-alkaline and tholeiitic fields (Irvine and Baragar, 1971), (e) K<sub>2</sub>O vs.  $\text{SiO}_2$  (in terms of oxide wt.%) with high-K calc-alkaline, med-K calc-alkaline and low-K tholeiitic fields (Peccerillo and Taylor, 1976), (f) Shands index with Al/(Na+K) vs. Al/(Ca+Na+K) (in terms of mol.%) (Maniar and Piccoli, 1989).

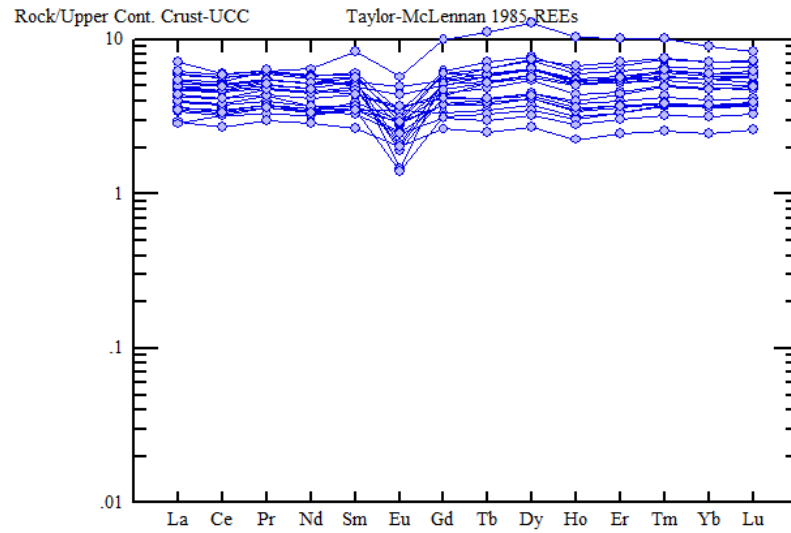


**Figure 4.4:** Log-standardized rare earth element plot normalized to upper continental crust after Taylor and McLennan (1986) for the CP felsic volcanic rocks of the mineralized zone.

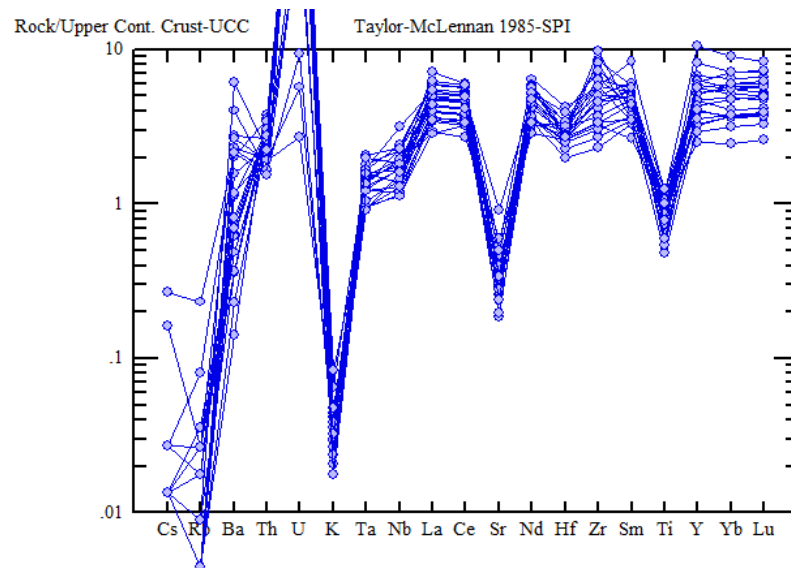


**Figure 4.5:** Log-standardized extended trace element plot normalized to upper continental crust after Taylor and McLennan (1986) for the CP felsic volcanic rocks of the mineralized zone, uranium peak has been cut-off.

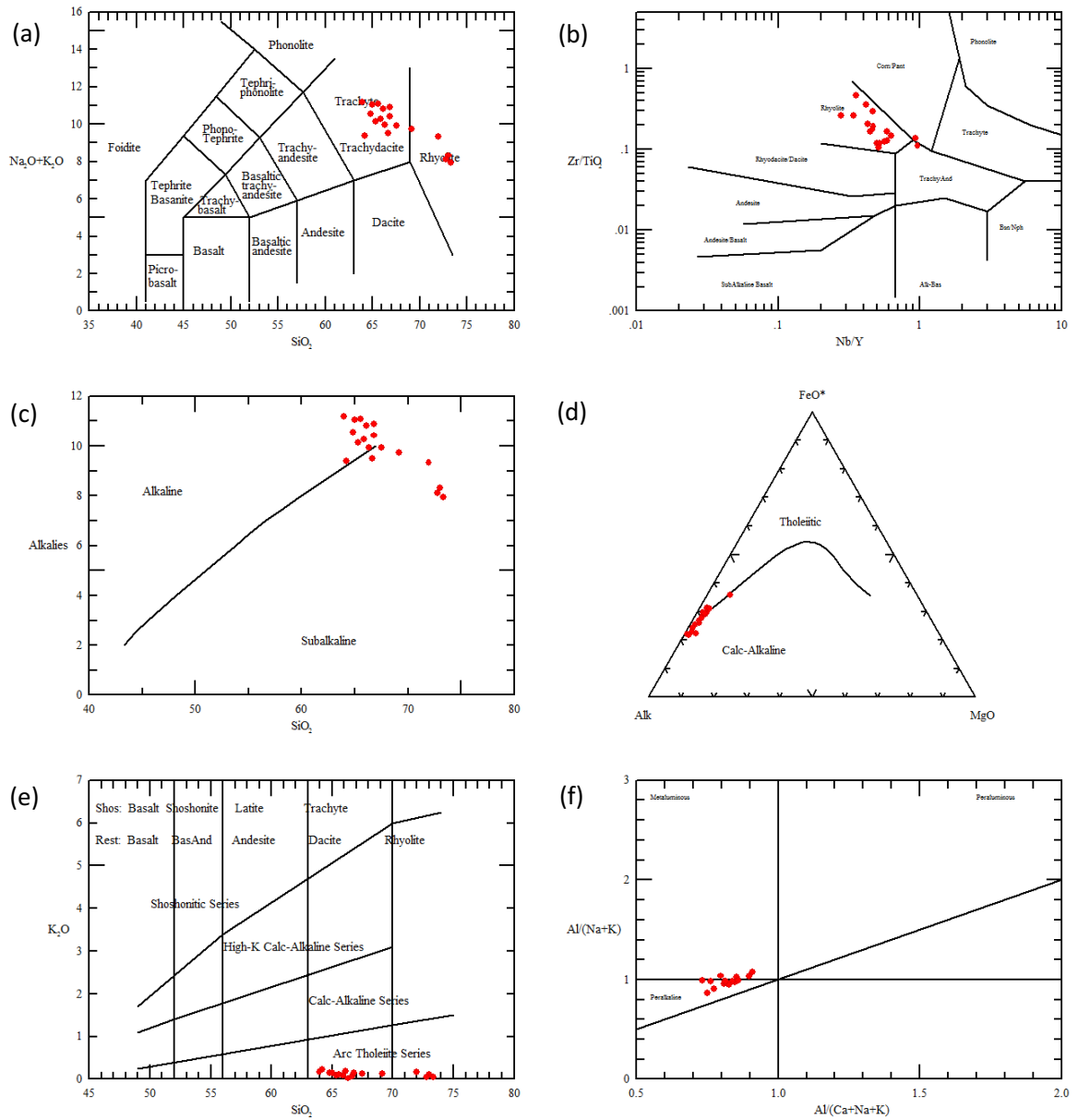


**Figure 4.6:** Discrimination diagrams of the FP felsic volcanic rocks from the mineralized zone (solid red circles), (a) classification diagram based on Total Alkalies ( $\text{Na}_2\text{O} + \text{K}_2\text{O}$ ) vs. Silica ( $\text{SiO}_2$ ) (in terms of oxide wt.%) (TAS) (LeBas *et al.*, 1986), (b) classification diagram based on ratios of Nb/Y (ppm) vs. Zr/TiO<sub>2</sub> (ppm/oxide wt.%) (Winchester and Floyd, 1977), (c) TAS with alkaline-subalkaline fields (Irvine and Baragar, 1971), (d) Ternary plot of Total Alkalies-MgO-FeO\* (in terms of oxide wt.%) with calc-alkaline and tholeiitic fields (Irvine and Baragar, 1971), (e)  $\text{K}_2\text{O}$  vs.  $\text{SiO}_2$  (in terms of oxide wt.%) with high-K calc-alkaline, med-K calc-alkaline and low-K tholeiitic fields (Peccerillo and Taylor, 1976), (f) Shands index with  $\text{Al}/(\text{Na}+\text{K})$  vs.  $\text{Al}/(\text{Ca}+\text{Na}+\text{K})$  (in terms of mol.%) (Maniar and Piccoli, 1989).

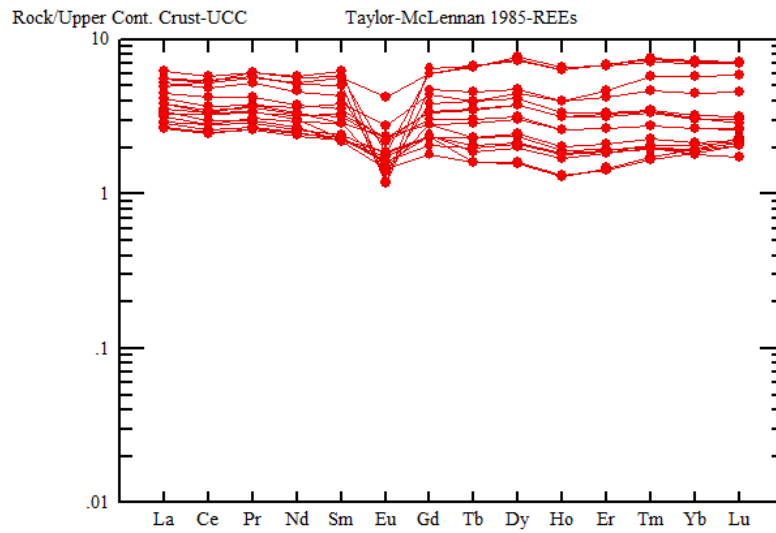


**Figure 4.7:** Log-standardized rare earth element plot normalized to upper continental crust after Taylor and McLennan (1986) for the FP felsic volcanic rocks of the mineralized zone.

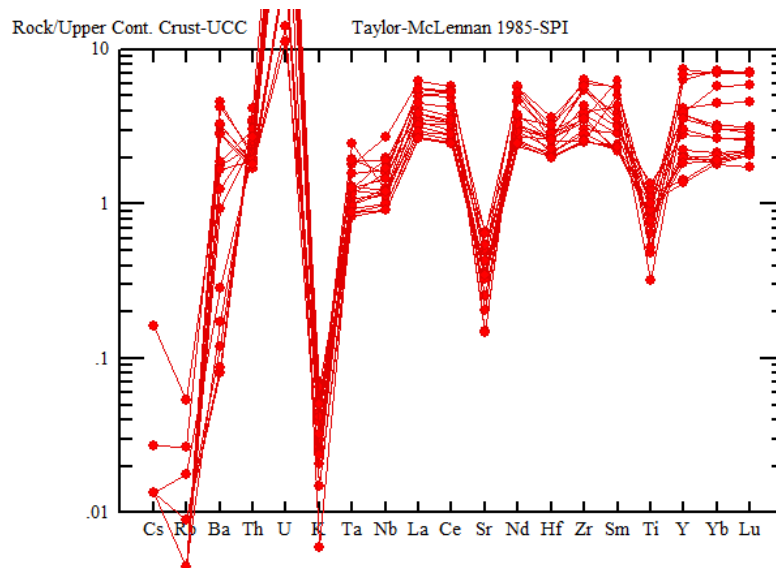


**Figure 4.8:** Log-standardized extended trace element plot normalized to upper continental crust after Taylor and McLennan (1986) for the FP felsic volcanic rocks of the mineralized zone, uranium peak has been cut-off.

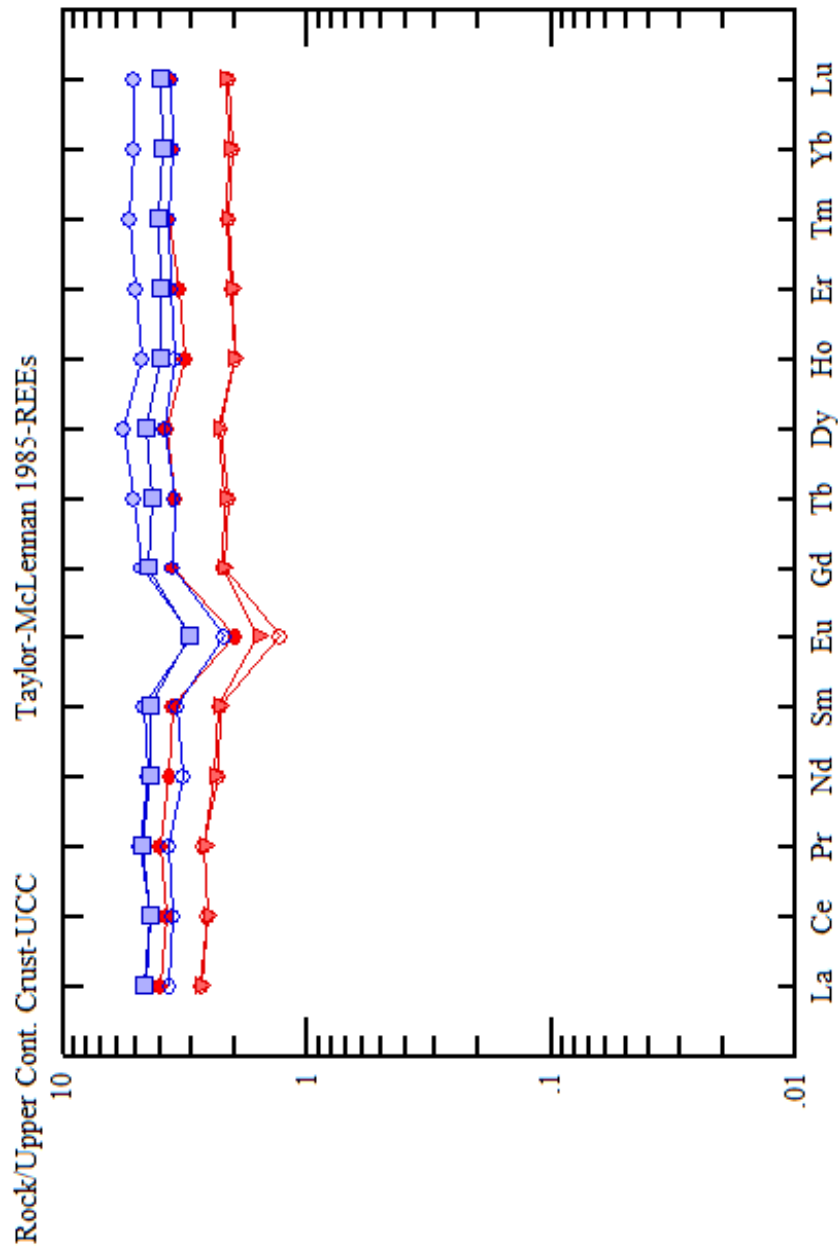


**Figure 4.9:** Log-standardized rare earth element plot normalized to upper continental crust after Taylor and McLennan (1986) for the average REE concentration of unaltered FP (open red circles), sodic altered FP (red triangles), mineralized zone FP (red circles), unaltered CP (open blue circles), mineralized zone CP (blue circles), and mafic-rich CP (blue squares). The average REE concentration for each group displays the same profile, with the only difference being a concentration increase in the REE.

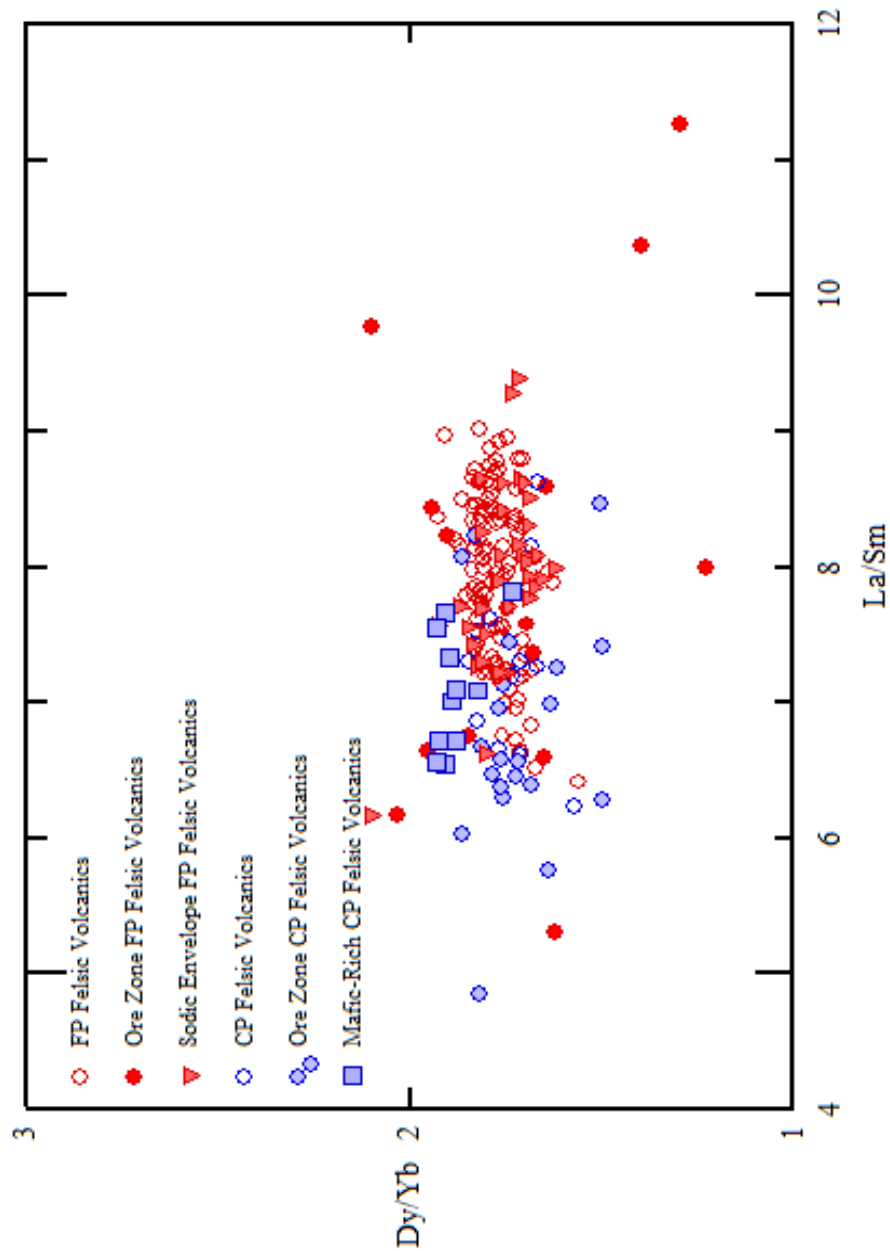


**Figure 4.10:** REE ratio-ratio plot of La/Sm vs. Dy/Yb (in terms of ppm) for the unaltered FP (open red circles), sodic altered FP (red triangles), mineralized zone FP (red circles), unaltered CP (open blue circles), mineralized zone CP (blue circles), and mafic-rich CP (blue squares). All samples roughly plot together with a Dy/Yb ratio of  $\sim 0.8$  and a La/Sm ratio of  $\sim 7$ . The samples show a linear trend with the La/Sm ratio.

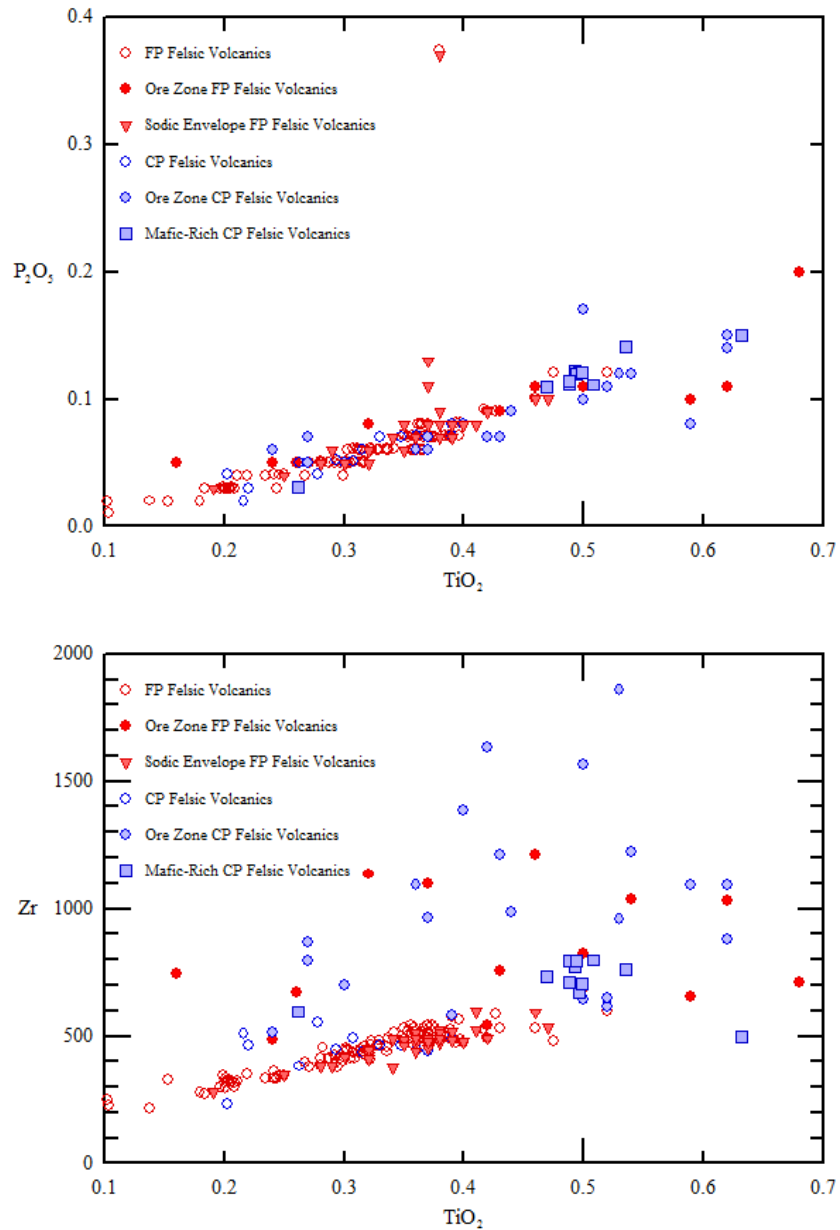


**Figure 4.11:** Immobile-immobile bivariate element plots of  $\text{TiO}_2$  vs.  $\text{P}_2\text{O}_5$  (in terms of oxide wt.%) and  $\text{TiO}_2$  vs. Zr (in terms of oxide wt.% and ppm respectively) for the unaltered FP (open red circles), sodic altered FP (red triangles), mineralized zone FP (red circles), unaltered CP (open blue circles), mineralized zone CP (blue circles), and mafic-rich CP (blue squares). With the exception of samples from the mineralized zone, all samples plot in a linear trend that projects through the origin.





**Plate 4.1:** Approximate surface expression of the Michelin deposit outlined in red, view is towards the south. Deposit strikes SW-NE at 070 and dips to the SE approximately 40-60° underneath Ranjan Lake.

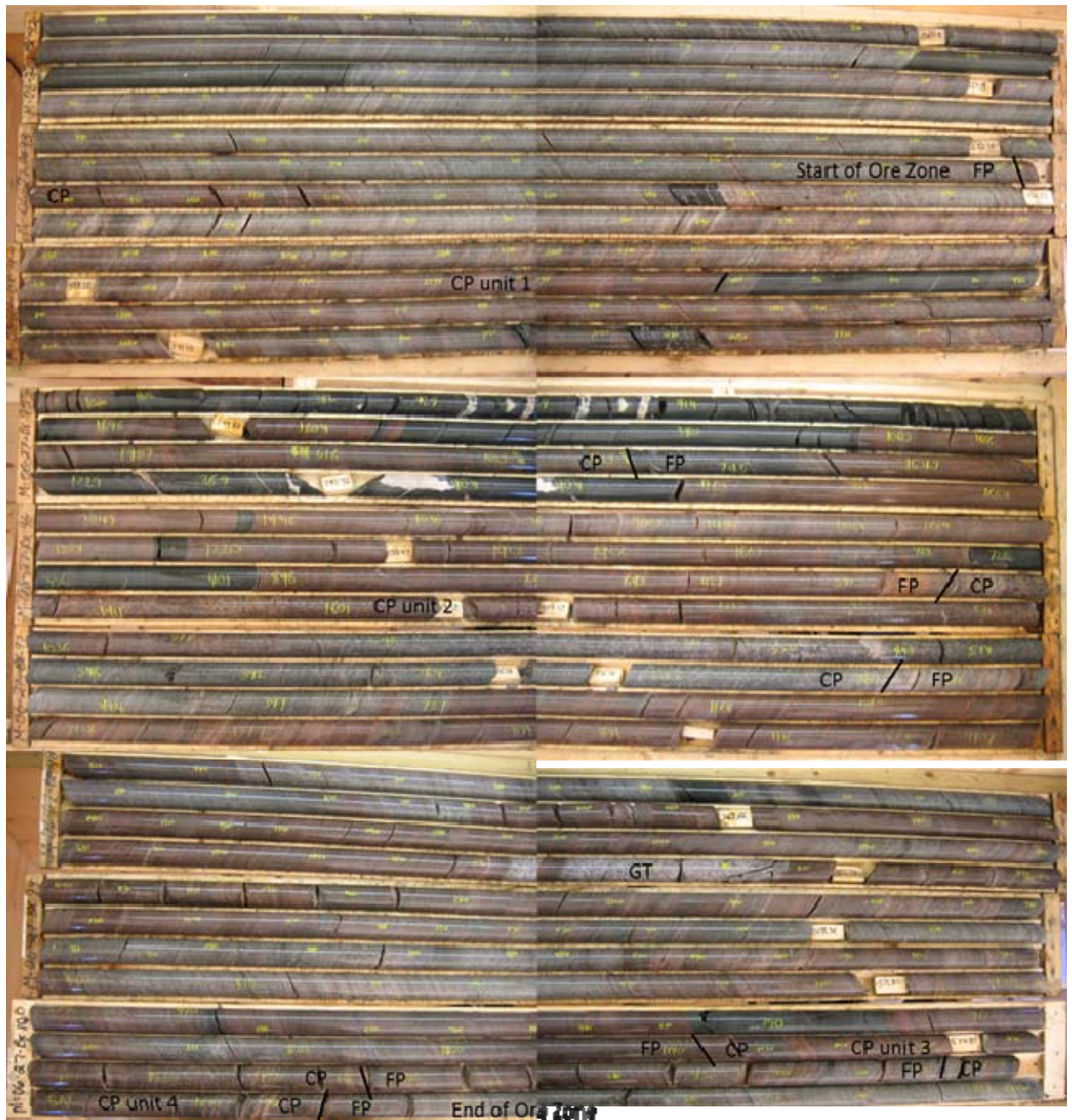


**Plate 4.2:** Complete drill section (core diameter 4.2 cm) through the Ore Zone in drill hole M06-027, zone is approximately 31 m thick. Ore zone starts with the start of the upper most CP unit (A Group) which is ~12.5 m thick, within the middle of the zone is the second CP unit ~5 m thick (one of either A or B or C Groups), the ore zone ends with two small (~1 m and 0.5 m) thick CP units (either C and F Group) (groupings are difficult to extrapolate to this depth, ~500 m below surface).



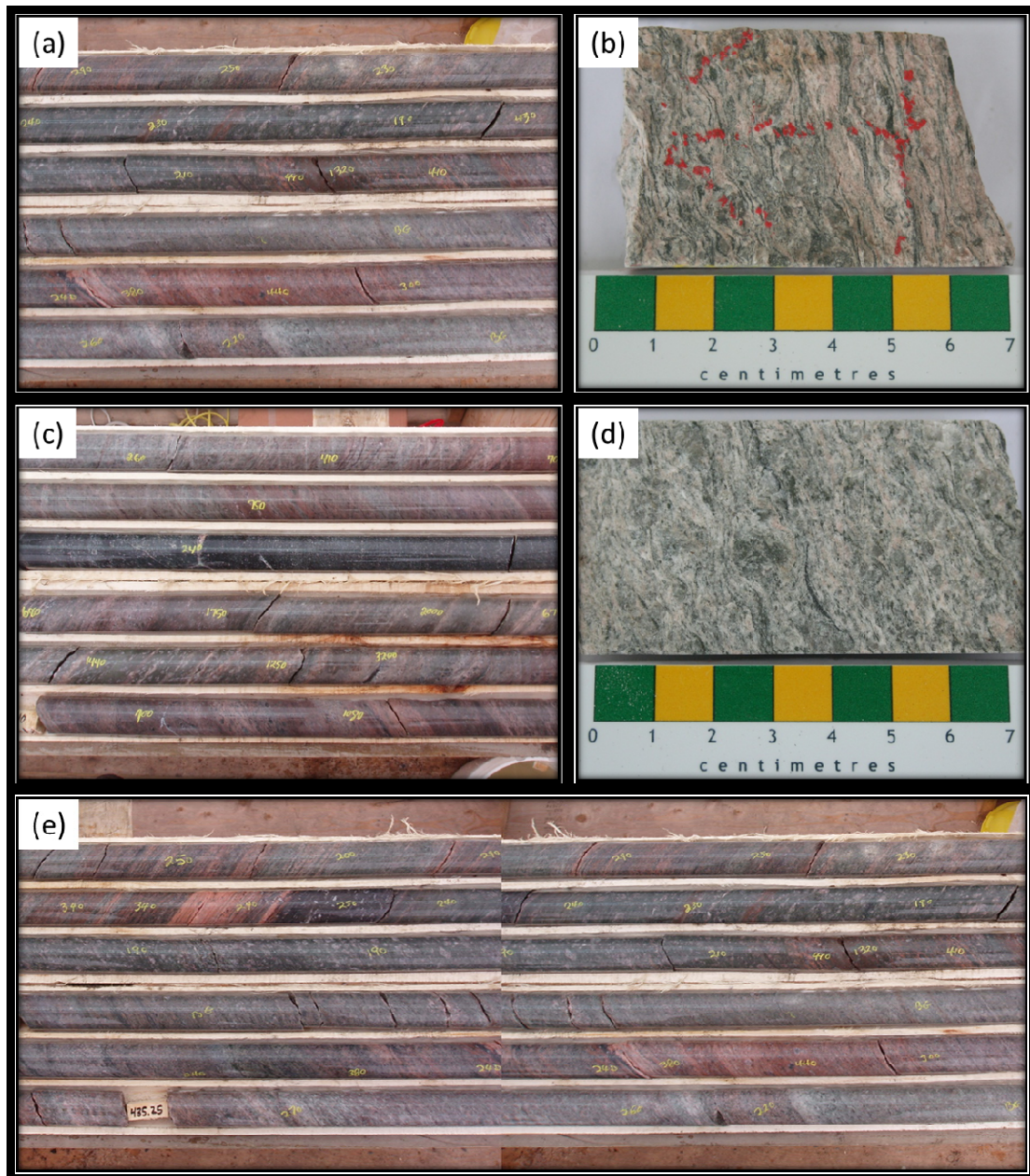


**Plate 4.3:** Drill core segments of CP felsic volcanic rocks from throughout the mineralized ore zone (core diameter is 4.2 cm), (a) typical hematitized CP rocks, (b) split-sample of altered CP with large phenocrysts and abundant mafic material, (c) strongly altered CP, (d) split-sample showing large feldspar phenocrysts augened by the foliation, (e) elongated-joined section of drill core showing a CP unit, alteration and mineralization vary down hole.



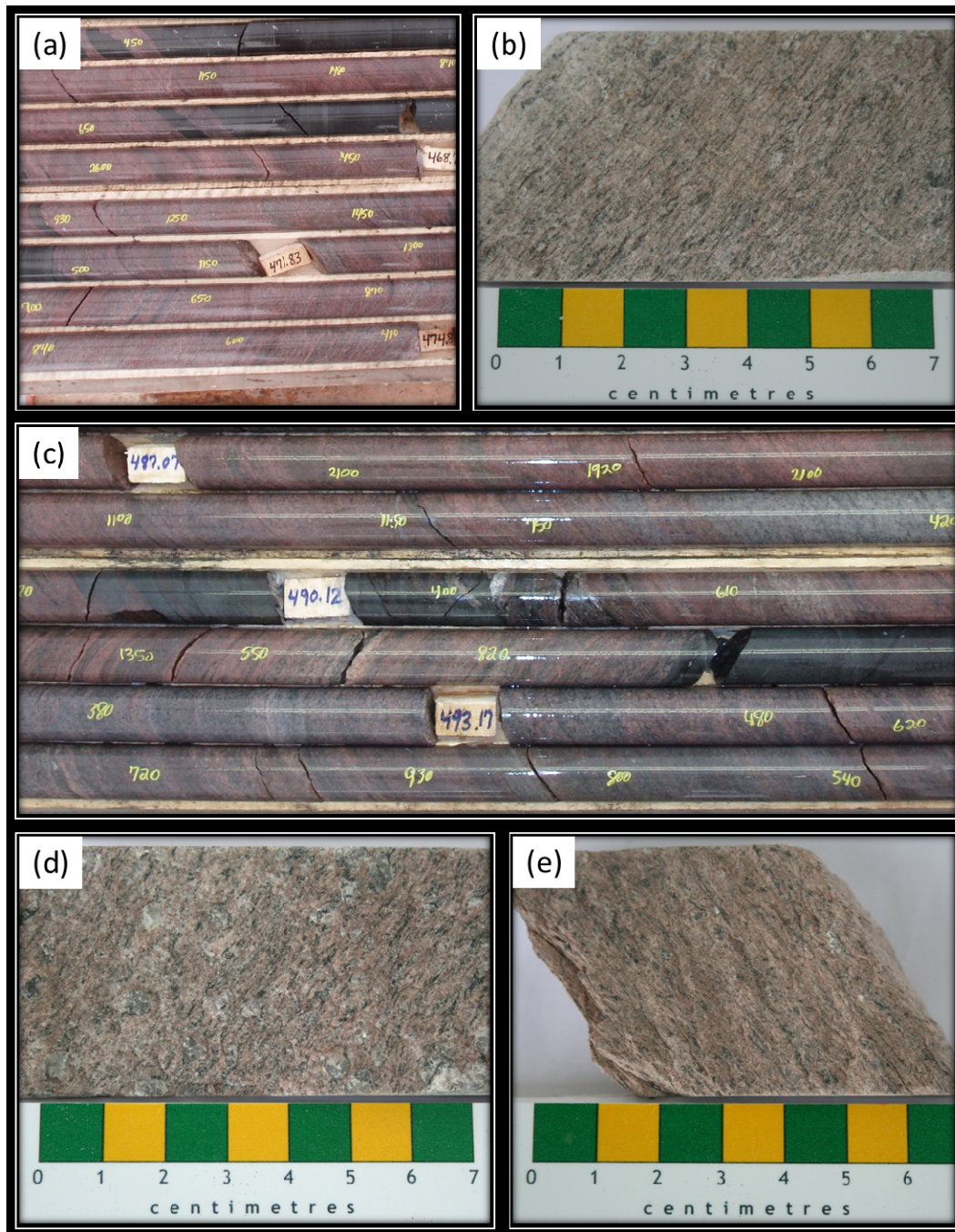


**Plate 4.4:** Drill core segments of FP felsic volcanic rocks from throughout the mineralized ore zone (core diameter is 4.2 cm), (a) typical hematitized FP rocks, (b) split-sample of altered FP, with foliation defined by mm-thin mafic streaks, (c) elongated section showing a FP unit and the variation change in color, alteration, mineralization (cps) down hole, and concordant contacts with pre-kinematic strongly foliated dikes, (d) split-sample of strongly altered FP rock, (e) split-section showing individual fine-grained phenocrysts.



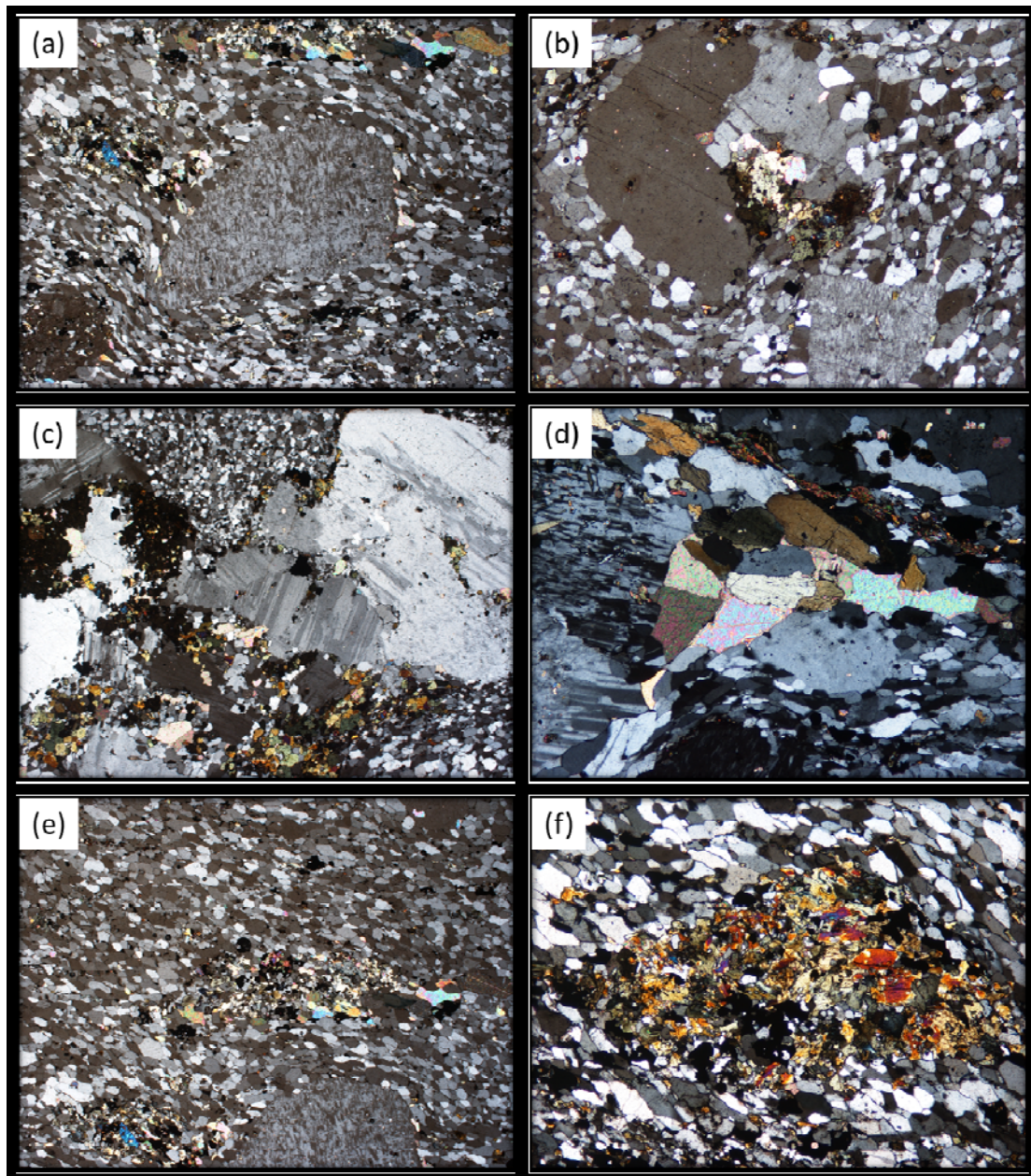


**Plate 4.5:** Petrographic sections of the CP and FP felsic volcanic rocks from throughout the mineralized ore zone, (a) sodic-altered potassium feldspar (kf) phenocrysts consisting of a single grain showing chessboard-style twinning (mag. = 2.5x, cpl), (b) potassium feldspar phenocryst consisting of 2-3 grains, part of grain has been replaced by mafic minerals (mag. = 2.5x, cpl), (c) large, recrystallized primary albite phenocryst with abundant mafic material (mag. = 2.5x, cpl), (d) secondary albite phenocryst with chessboard twinning, with a pressure shadow filled with multiple calcite grains (mag. = 2.5x, cpl), (e) possible dissolved quartz phenol with cavity space filled with secondary alteration minerals (mag. = 2.5x, cpl), and (f) same as (e) (mag. = 5x, cpl).



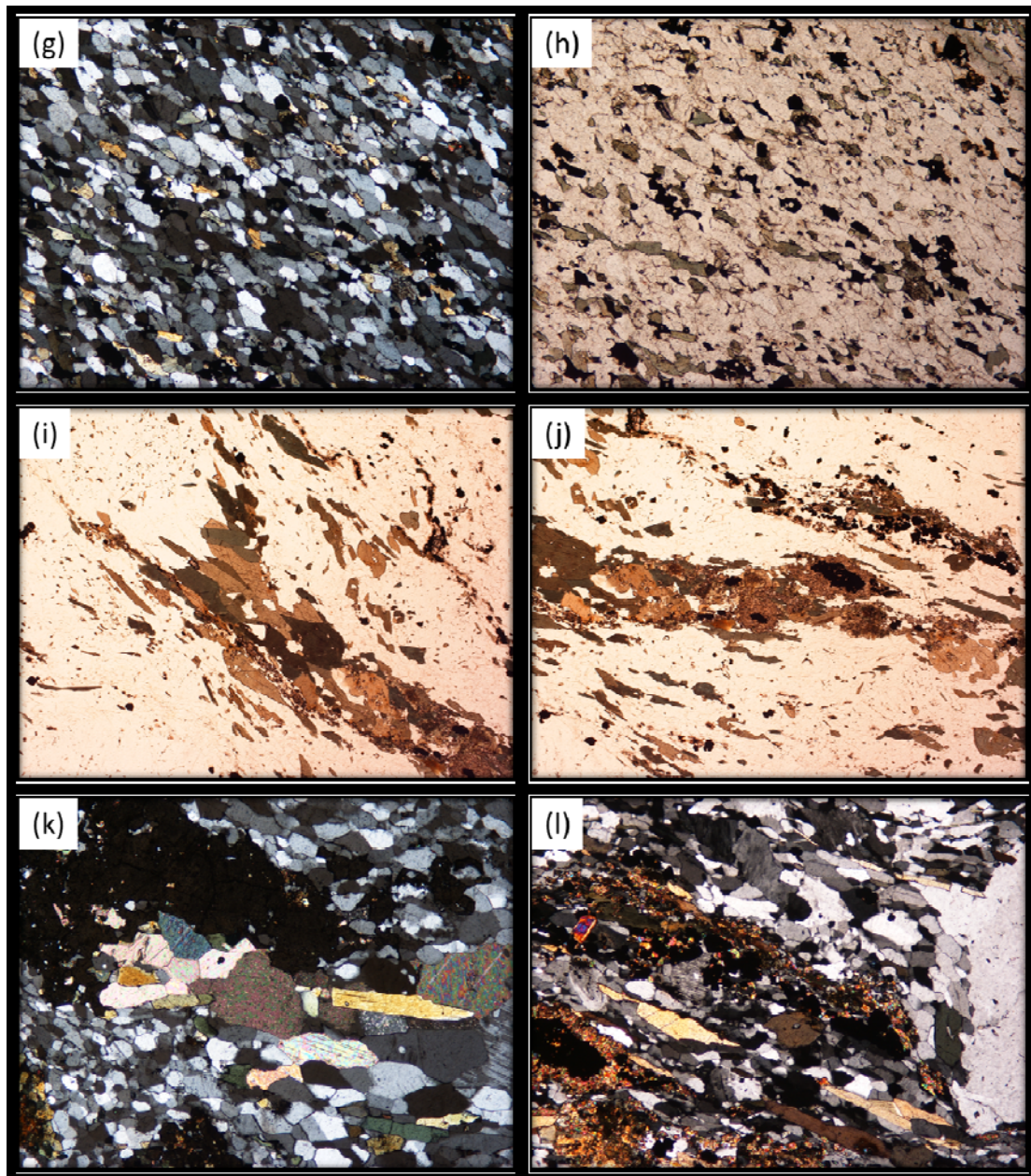


**Plate 4.5:** Continuation of Plate 4.5, (g) fine-grained quartz-feldspar matrix, individual grains are equant, polygonal and slightly elongated parallel to foliation (mag. = 5x, cpl), (h) same view but in ppl showing the increased mafic content of the matrix within the mineralized zone (mag. = 5x, ppl), (i) elongated sodic amphibole with 120/60 cleavage, defining the foliation, possibly pseudomorph of original biotite (mag. = 2.5x, ppl), (j) mafic mineral clot consisting of sodic amphibole and pyroxene, opaque grains (mag. = 2.5x, ppl), (k) abundant, euhedral calcite grains in pressure shadow of larger phenocryst (mag. = 5x, cpl), and (l) mafic minerals (mag. = 5x, cpl).

## **Chapter 5     Uranium Mineralization**

### **5.1     Introduction**

Uranium mineralization within the Michelin ore zone is not consistent throughout. The extent and concentration of uranium mineralization is dependent on a number of factors including, lithology, intensity of deformation, alteration style and alteration mineral assemblages. Uranium mineralization appears to be more strongly associated with certain lithological units within the ore zone sequence. Mineralization is also more intense in deformed sections of the rock and appears to be associated with certain alteration styles.

This chapter will focus on uranium mineralization, identifying the main areas where uranium ore is concentrated. The uranium-bearing mineral phases will be identified and characterized, and their spatial and mineral associations within the ore zone will be discussed. In addition, an attempt will be made to characterize the alteration mineral phases that are associated with mineralization.

. Drill core will be utilized to identify areas where uranium mineralization is concentrated. This will be done through visual observation, scintillometer measurements of core and assay results. Uranium bearing phases will be identified through SEM-MLA analysis of petrographic thin sections, thereby allowing these phases to be characterized based on size, shape, spatial location and mineral association. Petrographic thin section and SEM-MLA analysis will also be utilized to identify and characterize accessory minerals located within the mineralized zone. Most of the accessory minerals may be the

result of, or enriched by alteration, since they are often directly associated with uranium mineralization.

## **5.2 Uranium Mineralization**

Uranium concentrations typically increase anywhere from 20-100 m before the start of the main mineralized zone. As a general observation, in areas where the mineralized zone is the thickest, the trace mineralization envelope is also thicker. Trace mineralization begins and ends the same, manifested by sporadic spots of anomalous uranium within small patches of weak hematite alteration. These hematite patches may be 5-25 cm long and locally contain, spotty, anomalous uranium mineralization, averaging 300-500 counts per second (cps) and occasionally up to 1,000 cps (Plates 5.1a-b). Cps measurement however does not directly translate to  $U_3O_8$  concentration, as the measured value of radiation in cps depends on the sample size and the distance the measurement is taken from the sample. However, there is a loose correlation that is observed from cps measurements to geochemical assay results, where 1,000 cps generally equates to approximately 0.1 %  $U_3O_8$ .

Towards the mineralized ore zone, the anomalous, uranium-enriched, hematite patches become larger and more frequent, eventually leading to 100 % covering of the core. Uranium cps remains spotty until the beginning of the mineralized zone, which is marked by mineralization readings that are consistently above 500 cps. This is generally coincident with the appearance of the first CP felsic volcanic unit of the Mine Series within the mineralized zone (Plate 5.1c). The mineralized zone in the foot wall ends the



same way as it began, with uranium readings no longer consistently above 500 cps. Mineralization then follows the same pattern as within the hanging wall where hematite alteration and uranium mineralization gradually decrease and eventually grade into sporadic, 5-25 cm thick, hematitized zones which contain spotty, anomalous mineralization. These zones or patches gradually die out anywhere from 20-80 m beyond the end of the mineralized ore zone.

Within the mineralized ore zone uranium values are not consistent, typically there are zones of strong mineralization between zones with weaker mineralization, and locally there are small zones with intense mineralization. The changes in mineralization intensity are related to a number of factors, such as lithology, deformation and alteration intensity.

Throughout the mineralized ore zone uranium mineralization is strongly associated with the CP felsic volcanic units (Plate 5.1i). These units are always moderately to strongly mineralized. Uranium mineralization is also associated with the FP felsic volcanic units but to a lesser extent, as they are generally only poorly to moderately mineralized; typically they contain sections that are only very weakly mineralized. It appears that mineralization was focused along the CP units, but does transgress contacts into the FP units, it is possible that mineralization was focused along the contacts between the two units. Within the FP units, mineralization is strongest near the contacts, decreasing towards the center and then increasing again towards the lower contact with another CP unit. Typically in thicker units of the FP volcanics, the center of the unit, furthest away from the surrounding CP units are only weakly mineralized and altered.

Uranium mineralization is intensified throughout the mineralized zone in several small zones that are associated with deformation or intrusions. These often occur as small ~0.5 m mylonitic zones within the CP units (Plate 5.1e), or as along the contact between CP and FP felsic volcanic units (Plate 5.1d). These zones are strongly foliated, appear intensely hematitized and have associated intense uranium mineralization. Within one of the CP units in the mineralized zone there is evidence of greater deformation and shearing (Plate 5.1h). Larger feldspar phenocrysts have been augened and rotated by thin wisps of secondary alteration minerals, creating pressure shadows, often filled by calcite (Plate 5.1j). This zone is marked by extreme, deep red hematite alteration and very intense uranium mineralization.

Uranium mineralization is also intensified at contact zones with syn-kinematic gabbroic dikes. Although the dikes themselves are not mineralized the areas immediately adjacent to the contacts, within both the CP and FP volcanic rocks are extremely mineralized and hematite altered. This increase in mineralization and alteration extends for ~1 m from the contact, gradually grading back to normal background mineralization (Plate 5.1f-g). It appears that the emplacement of the syn-kinematic dikes remobilized uranium mineralization through some mechanism, possibly related to a temperature increase which increased the oxidation of hematite or it caused an influx of oxidized fluids which strongly oxidized magnetite to hematite and then reduced uranium out of solution. No similar enrichment effect is seen at the contacts with the pre-kinematic biotite-hornblende schists.

As a general observation, cps readings from within the mineralized zone generally range between 300-1,000 cps for the poorly mineralized material; 1,000-3,000 cps for the moderately mineralized material; and greater than 3,000 cps for the strongly mineralized material. The areas that contain the more intense uranium mineralization have been more strongly hematitized and where hematite alteration weakens, generally within the finely porphyritic units, so does the uranium mineralization. Despite the different zones of uranium mineralization intensity within the mineralized zone, the average uranium grade remains fairly consistent throughout the entire deposit. Areas within the heart of the mineralized zone have nearly the same average grade over depth as the areas near the edge of the mineralized zone, the only difference being the thickness of the mineralized zone. The uranium grade throughout the mineralized zone averages approximately 0.18 %  $U_3O_8$ , ranging from 0.1-0.3 % (Wilton and Giroux, 2007).

### **5.3 Uranium-Bearing Phases**

Geochemical analyses indicate that the economically exploitable mineralization at the Michelin deposit is entirely uraniferous. Within the mineralized zone uranium is concentrated to a level 180x background; based on the average for unmineralized FP and CP volcanics of approximately 10 ppm and an average ore zone grade of about 1,800 ppm or 0.18 %  $U_3O_8$ . Other elements such as Zr are concentrated within the ore zone, but not at a high enough level to be economically viable or exploitable. Metallurgical testing also indicates that the uranium mineralization has an approximate 88.0 % recovery rate, indicating that it is indeed economically exploitable (Wilton and Giroux, 2007).

Uranium mineralization within the Michelin ore zone is extremely fine grained, and in hand sample is not identifiable to the naked eye. In rare areas, fractures are infilled or contain agglomerates of black minerals. These often assay very high, and elicit extremely high cps readings from a hand held scintillometer. The dark material could be uraninite or a mixture of uraninite and other dark colored minerals, however individual uraninite grains cannot be distinguished. In petrographic thin section, uranium-bearing phases are generally only a few microns in size and are barely visible under high powered magnification.

The only way to accurately examine uranium phases is through SEM-MLA analysis. A total of 10 polished thin sections were made from both the FP and CP units throughout the mineralized zone and examined with the SEM-MLA method. The purpose was to identify the uranium bearing phases within each thin section, to classify each phase based on its mineral spectra, to map out their locations and mineral relationships within the mineralized zone, and to determine the size and shapes of the uraniferous grains.

SEM-MLA analyses identified four different uranium minerals within the Michelin ore zone. The predominant phase, accounting for over 90 % of the uranium mineralization is uraninite ( $\text{UO}_2$ ). However, none of the uraninite mineral grains are pure  $\text{UO}_2$ . EDX analyses indicate that there are several other elements within the crystal structure of the uraninite grains. These elements include Pb, Si, Ca, Zr, Ti, and Fe. It seems that uraninite grains are always associated with at least one of these elements, and sometimes include up to three or four different element substitutions.

The most common uraninite grains are those which contain Si and Ca as elemental substitutions. These equate for well over half of the uranium minerals and generally contain at least one other element substitution of Zr, Ti, Fe, Pb or the LREE Ce. There appear to be two distinct subtypes based on elemental concentrations. The first subtype contains a large U peak on the spectral image, followed by moderate Si and O peaks and a lower Ca peak. These can contain other elemental concentrations where the concentrations of the other elemental constituents are always lower than calcium and consist of either Pb by itself (Figure 5.1b), Pb with Ce (Figure 5.1a), or Pb with Zr (Figure 5.1c). The second subtype contains a large Si peak, followed by moderate U and O peaks and a lower Ca peak. These often contain low elemental concentrations of Zr, Ti, and Fe, in combinations of just Zr (Figure 5.2b), Zr with Fe (Figure 5.2a), Zr with Ti (Figure 5.2c), or just Fe. In back scatter electron (BSE) images there is no real distinction between the two subtypes. They occur as irregular, anhedral grains which range from a few microns to tens of microns in diameter and typically enclose smaller lead-uraninite grains suggesting that they formed later than these grains or from the alteration of these grains. In most instances, these grains occur within the large mineral aggregates, associated with sodic pyroxenes and amphiboles, zircon, hematite, titanite, albite and calcite. Seldom have they been observed within the albite-rich matrix.

The second most common uraninite grains (30-40 %) are those which contain only Pb as the elemental substitution. The spectral image for these grains (Figure 5.3) shows a large peak with U and moderate peaks with both O and Pb. In back scatter electron (BSE) images these grains always appear lighter in color than every other

uranium-bearing phase. The lead-enriched grains are equant, subhedral and generally no more than a few microns in diameter. These grains appear to be the earliest uranium phase to crystalize as they are often included or surrounded by several other mineral phases. The grains typically occur in large mineral aggregates and are generally surrounded by other uraninite grains, or included within zircon and titanite grains (Figure 5.4). This uraninite phase also occurs by itself within the albite-rich matrix as extremely small grains along crystal boundaries within the groundmass. Since  $\text{Pb}^{2+}$  has a larger ionic radius than  $\text{U}^{4+}$  it is incompatible with the crystal structure and will not substitute therefore the Pb that is present in these grains is radiogenic Pb created through the decay of  $^{238}\text{U}$  and  $^{235}\text{U}$  to  $^{206}\text{Pb}$  and  $^{207}\text{Pb}$  respectively (Alexandre and Kyser, 2005). The other uraninite grains contain little to no Pb in their mineral spectrums suggesting that the Pb in these phases may have been mobilized out and possibly substituted for the other elements observed.

The remaining three uraniferous mineral species identified during SEM-MLA analysis occur in trace quantities and were only identified in a couple of thin sections. These consist of Brannerite  $(\text{U,Ca,Ce})(\text{Ti,Fe})_2\text{O}_6$ , Coffinite  $\text{U}(\text{SiO}_4)_{1-x}(\text{OH})_{4x}$ , and Uranophane  $\text{Ca}(\text{UO}_2)_2\text{SiO}_3(\text{OH})_2 \cdot 5(\text{H}_2\text{O})$ . Brannerite grains are the most abundant of the three and are generally associated with titanite grains. They are only a few microns in size, subhedral in shape, and the SEM analyses suggest that they have a strong niobium component, as most grains analyzed were rich in the HFSE. Coffinite was only recognized in a couple of thin sections. In BSE images the mineral appears very similar to uraninite with Si and Ca as elemental substitutions; it is possible that the two grains are

related as they share common elements. These grains are subhedral in shape, up to ten microns across. And typically form around lead-uraninite grains, associated with the mineral aggregates. Uranophane is generally present within fractures in the rock and are only a few microns in diameter and are anhedral in shape. They are interpreted to be supergene mineralization of uraninite grains; the result of oxidation of the primary uraninite grains.

It is possible that due to the extremely small grain size of some uranium phases, the EDX spectrum produced picks up interference from surrounding grains such as titanite, calcite, zircon etc., which could account for the large variation of elemental substitutions included within the uraninite grains. All of the elements that substitute within the uraninite grains are major constituents of accessory minerals within the mineral aggregates where the majority of uranium mineralization occurs. Hematite, zircon, titanite, and calcite, which are commonly found in the mineral aggregates, could all supply the elemental constituents identified during SEM-MLA analysis. Alternately, it could just indicate that these elements were present when the uraninite grains crystallized because of the presence of these mineral grains and they substituted within the uraninite crystal structure. Since EDX analysis display relatively consistent mineral spectra for each uraninite variety, the later situation is most likely as these elements were all available and somewhat mobile within the mineralized zone during alteration.

Reports by Minatidis (1976), Gandhi, (1978), Booth *et al.* (1979), Evans (1980), Ross (2006), and Wilton and Giroux (2007) have reported a number of different uranium-bearing minerals from within the Michelin ore zone. Most name uraninite or pitchblende

as the main uranium mineral constituent with a variety of other elements present. Panterra Geoservices Inc. (Ross, 2006) examined several polished thin section samples from the mineralized zone, and identified uraninite as the primary uranium bearing phase but with variable Pb, Y, Al and Ca components. Ross could not explain the Al component within the uraninite grains and noted that other uranium species have not been reported anywhere that contained a major Al component. The aluminum could be due to contamination from adjacent albite grains, but the report identified consistent mineral spectra for uraninite grains which suggested that it is not a result of contamination. Ross (2006) also identified uranophane as fracture-fill inside micro fractures.

Based on energy dispersive spectra and silicate analysis from uranium-lead bearing grains within sphene, andradite and Fe, Ti, Al and Si-rich clots, Evans (1980) concluded that the dominant ore mineral was pitchblende. The microprobe analysis did not show any enrichment except for Pb and U, however analysis of hydrated alteration patches containing Pb and U averaged 10.6 % FeO, 19.4 % TiO<sub>2</sub>, 12.6 % SiO<sub>2</sub>, and 2.5 % Al<sub>2</sub>O<sub>3</sub>. Evans suggested that the uranium was partly associated with secondary Fe-Ti oxides and/or oxyhydroxides. Gandhi (1978) also reported the mineralization as pitchblende, associated with sphene. The report noted that the host mineral has the optical properties of sphene and that its energy dispersive spectrum reveals the presence of only Ca, Ti, and Si. The X-ray diffraction pattern of the intergrowth minerals contains only the spectral lines characteristic of pitchblende or uraninite. Gandhi concluded that the host sphene was metamict, indicating the sphene lost its crystalline structure as a result of radioactivity from the uranium.



BRINEX reports also state that uranium mineralization occurs almost entirely as finely disseminated specks of pitchblende, and possibly uraninite (Booth *et al.*, 1979). They also indicate the presence of soddyite which they state is a sodium-uranium silicate, but contains no sodium within its chemical formula  $(\text{UO}_2)_2\text{SiO}_4 \cdot 2(\text{H}_2\text{O})$ . Yellow stains due to uranium hydroxides were also observed.

Minatidis (1976) noted that the main radioactive mineral appeared to be davidite rimmed by sphene. The mineral was described within the feldspar porphyroblasts and is also associated with amphiboles. Davidite,  $(\text{Ce},\text{La})(\text{Y},\text{U})(\text{Ti},\text{Fe})_{20}\text{O}_{38}$  is an ill-defined mineral that contains oxides of titanium and iron plus variable amounts of rare earth minerals, uranium, vanadium and chromium. Microprobe analysis performed by Evans (1980), however, indicated that uranium minerals lack any of the trace element characteristics of davidite such as rare earths, thorium, vanadium or chromium.

Metallurgical testing on Michelin ore samples by SGS Lakefield indicated that most of the uranium is present as a uranium-lead-calcium mineral, possibly Wolsendorfitite  $[(\text{Pb},\text{Ba},\text{Ca})\text{U}_2\text{O}_7 \cdot 2\text{H}_2\text{O}]$  or Fourmarierite  $[\text{Pb}(\text{UO}_2)_4\text{O}_3(\text{OH})_4 \cdot 4\text{H}_2\text{O}]$ . The mineralogical work also showed that the Michelin composite contained 9 % of the uranium in titanite grains and 3 % in zircon grains (Wilton and Giroux, 2007).

#### **5.4 Location of Uranium-Bearing Phases in the Mineralized Zone**

SEM-MLA analysis of polished thin sections from within the mineralized zone indicates that the uranium-bearing phases occur in several distinct areas. The bulk of the uranium phases are associated with accessory minerals which are discussed in section 5.5

(Figures 5.5, 5.6, 5.7, 5.8 and 5.9). Most of these accessory minerals formed as a result of alteration within the mineralized zone and occur as aggregates of several different minerals, such as sodic pyroxene and amphibole, hematite, magnetite, zircon, titanite, albite and calcite. These mineral aggregates contain micron-sized uraninite grains distributed throughout. Brannerite grains sometimes occur within the aggregates but are generally associated with titanite grains. These aggregates appear to have formed in small cavities within both the CP and FP felsic volcanics where both quartz phenocrysts and quartz within the groundmass had been dissolved. The dissolution of quartz created open spaces for the alteration minerals and uranium-bearing phases to precipitate.

Micron-sized uraninite grains are also sparsely distributed throughout the albite-rich groundmass. These grains typically occur without accessory minerals in small spaces created from the dissolution of quartz within the groundmass, or in triple point intersections between albite and quartz grains within the groundmass (Figure 5.10). One common spot for the precipitation of uraninite is along the grain boundaries of large albite phenocrysts. In general, the phenocrysts edges have been damaged, and appear to be chewed up and irregular, due to the alteration processes. It is in this space that uraninite grains precipitate. In places, uraninite grains are enclosed in zircon, titanite, sodic pyroxene, and/or other uraninite grains. Some of these inclusions result from the host mineral forming after the uraninite phase, surrounding the grain; as in Si-Ca-rich uraninite grains. Others result from uraninite precipitating along small fractures and cracks within the mineral grain, like zircon and possibly titanite grains. Finally, uranium mineralization can occur along small fractures within the rock and in larger albite

phenocrysts. These generally consist of uranophane and are thought to represent later stages of weathering where uranium has become oxidized, forming supergene uranium minerals in the open micro-fractures.

## **5.5 Accessory Minerals to Mineralization**

Within the mineralized zone are a number of mineral phases that are not present in unaltered felsic volcanic rocks or their concentrations are increased in the mineralized zone. In both the CP and FP volcanic rocks which make up the mineralized zone, these mineral phases typically comprise 15-25 % of the rock. This is an overall increase over unaltered FP and CP rocks in which mafic minerals, opaques and other accessory mineral phases average only 10-15 % of the rock. The mineral phases within the mineralized zone appear to result from the alteration of primary mafic and accessory mineral phases and the formation of further secondary alteration minerals in spaces created from the dissolution of quartz phenocrysts and groundmass quartz. They occur either as individual grains within the groundmass, as larger aggregates comprised of several mineral phases, or as thin, wispy streaks, that enclose albite phenocrysts and help define foliation.

Some of these mineral phases are closely associated with uranium mineralization and commonly occur with uranium-bearing phases in small clusters. Petrographic thin section and SEM-MLA analysis indicate that there are almost a dozen of these mineral phases including: 1) sodic alteration minerals such as sodic pyroxenes, sodic amphiboles and albite, 2) opaque minerals hematite, magnetite, ilmenite, and sulfide minerals, 3)

silicate minerals zircon, titanite, allanite, andradite, and thorite, 4) phosphate minerals monazite and apatite, and 5) calcite as well as barite.

### **5.5.1 Sodic Minerals**

Sodic alteration is a very pervasive and characteristic feature of the Michelin deposit and is described in considerable detail in Chapter 6, section 6.2. As such, only the associated sodic alteration minerals observed within the mineralized zone will be discussed albeit briefly in this section. Sodic alteration is responsible for the alteration of primary minerals such as potassium feldspar, biotite and hornblende into albite as well as sodic amphiboles and pyroxenes. In addition, sodic alteration leads to the formation of new secondary sodic minerals such as sodic amphiboles and pyroxenes, and albite. Sodic amphibole and pyroxene comprise the majority of the associated minerals discussed in this section, equaling approximately 10-20 % of the rock. It should be noted that although albite is an alteration mineral and is associated with the mineral aggregates that contain most of the uranium mineralization, it is not included as part of the 15-25 % of the mineral phases even though secondary albite is the predominant alteration mineral within the mineralized zone.

### **5.5.2 Opaque Minerals**

Magnetite content within the strongly altered mineralized zone is low; as is supported by magnetic susceptibility readings which are consistently lower within the mineralized zone than in unaltered rocks. As observed in reflected light microscopy, the

magnetite grains are grey with lighter grey alteration rims. These rims result from oxidation of magnetite to hematite, a very characteristic alteration feature of the Michelin deposit. This alteration process is described in detail in Chapter 6, section 6.3 and will only be discussed briefly in this section. Within the mineralized zone the degree to which magnetite has been oxidized corresponds with the intensity of hematite alteration. In areas where hematite alteration is weak to moderate, magnetite grains generally display a thin oxidation rim. In areas of intense alteration, hematite oxidation rims are thick or oxidation has completely altered the magnetite grain. Tiny magnetite grains within the groundmass appear to be completely oxidized, most likely due to their fine grain size, while complete replacement of larger magnetite grains requires more intense alteration. Magnetite and hematite grains are the most abundant opaque mineral phases within the mineralized zone. Large opaque grains predominantly occur as part of larger mineral aggregates, commonly comprised of sodic pyroxene, uraninite, zircon, titanite, albite and calcite. Sodic pyroxene grains can completely surround the opaque grains; this most likely reflects the primary assemblage of the rock where biotite and hornblende commonly surround magnetite grains in unaltered volcanics.

Ilmenite is a minor opaque mineral phase within the unaltered and altered felsic volcanic rocks. According to Ross (2006), magnetite grains analyzed with SEM indicate that these grains have a Ti and to a lesser extent Mn component to them. Evans (1980) reported ilmeno-magnetite as the dominant opaque mineral species and constituting part of the gangue mineralogy associated with uranium mineralization. Ilmenite is the predominant opaque mineral phase in some of the syn-kinematic mafic dikes.

There is very little sulfide mineralization associated with the felsic volcanic rocks of the Michelin deposit, especially within the mineralized zone. The main sulfide phase present is galena, which predominantly occurs within the FP rocks. This is followed by pyrite as well as trace amounts of disseminated chalcopyrite and sphalerite. In general, sulfide contents within the mineralized zone are the same as in unaltered felsic volcanics, whereby sulfide mineralization occurs as tiny disseminated grains in the groundmass. There is no petrographic or SEM-MLA evidence indicating that sulfide mineralization is associated with uranium mineralization.

### **5.5.3 Silicate Minerals**

There are a number of silicate minerals, namely zircon and titanite, observed within CP and FP rocks within the mineralized zone that appear to result from the alteration directly associated with uranium mineralization. Both silicate minerals have a close affinity with larger mineral aggregates which tend to host most of the uranium mineralization, in fact, the silicate grains appear to be closely associated with uranium mineralization, often enclosing uraninite grains. Allanite, andradite and thorite are also present, but they seem to be more sporadically distributed throughout the mineralized zone and are not directly associated with uranium mineralization. It is uncertain if the allanite, andradite and thorite are related to alteration or are just rare mineral phases within the felsic volcanic host rocks.

Zircon grains occur within the unaltered FP and CP host rocks to the Michelin deposit. They are typically associated with mafic mineral assemblages. Generally, zircon

grains are < 0.1 mm in size, occurring as subhedral to euhedral prismatic to subprismatic grains; sometimes grains are rhombic to equant in shape (Plate 5.2 a and b). They often display growth zonation patterns typically the result of a compositional variation of trace elements during crystal growth, most likely reflecting a compositional change in the melt as the crystal grew (Corfu *et al.*, 2003). In rare locations, zircon grains contain xenocrystic cores with new magmatic zircon growth surrounding them. These cores are most likely inherited zircons. They are very irregular in shape, mottled in appearance and contain tiny uraninite grains. Mottled grains which are very common in the pre-kinematic mafic dikes, also display new magmatic growth surrounding their xenocrystic core.

Zircon grains within the sodic alteration envelope appear the same as those in unaltered rocks, but there is a distinct difference for grains within the mineralized zone. Zirconium content appears to increase; mass balance calculations indicate that there is a large mass gain for Zr in both the FP and CP rocks within the mineralized zone. According to Evans (1980), both U and Zr have a positive correlation. SEM-MLA analyses indicate that zircon grains in the mineralized zone occur both within the groundmass and as part of larger mineral aggregates; a similar association as in the unaltered volcanics. There appears to be two varieties of zircon within the mineralized zone. The first consists of large zircons, 20-100  $\mu\text{m}$  in diameter. These grains are subhedral to euhedral and rhombic to subprismatic. They typically display growth zonation patterns and are similar to zircon grains in the unaltered volcanics.

The main difference in this first group of zircons between the mineralized zone and equivalent zircon grains in unaltered hanging wall and foot wall is that the zircon

grains within the mineralized zone display a distinct outer rim of new growth (Plate 5.2 c and d). This growth rim formed through hydrothermal alteration. Alkali-rich solutions either transported or remobilized Zr ions, most likely from the sodic envelope where samples show a consistent mass loss in Zr.  $\text{SiO}_2$ , made available from the dissolution of quartz within the mineralized zone combined with the transported zirconium ions to form secondary zircon growth along the outer edge of primary zircon grains. The secondary zircon growth is closely associated with uraninite and typically contains tiny uraninite inclusions. Uraninite also occurs within fractures and open spaces inside the primary zircon grains, it is absent in grains that are not fractured or cracked (Plate 5.2e).

The second type of zircon within the mineralized zone consists of small, less than 20  $\mu\text{m}$ , anhedral to subhedral grains. These grains have an overall mottled appearance and contain numerous tiny uraninite inclusions (Plate 5.2f). It is unknown whether these grains are secondary, formed through hydrothermal alteration or are inherited zircons similar to the xenocrystic cores found in the unaltered rock, as they have a similar style to the xenocrystic cores found in zircon grains in unaltered rocks. The grains contain little to no magmatic growth as seen in similar zircons in the unaltered rock, but it is possible that this rim was removed during early sodic alteration. This would explain the mass loss in the sodic envelope and then possibly be the source of the remobilized zircon in the mineralized zone. It could also indicate that it is easier for secondary zircon to form on magmatic grains, than mottled xenocrystic cores.

Metallurgical testing of mineralized rock from the mineralized zone indicates that 3 % of the uranium mineralization is contained within zircon grains, whereas 9 % is



contained within titanite grains (Wilton and Giroux, 2007). Titanite has a strong affinity with uranium mineralization and is often closely associated with uraninite and especially, brannerite grains. Minatidis (1976) interpreted that the main uranium bearing mineral, davidite, was closely associated with titanite and that titanite commonly rimmed the uranium bearing mineral. It does not appear that titanite is a secondary mineral grain formed during alteration. Mass balance calculations indicate that out of all the immobile elements,  $\text{TiO}_2$  remains the most conserved, experiencing little mass change between unaltered samples and altered samples from the mineralized zone. According to Ross (2006) titanite is present in most samples and is not confined to, or more abundant in any particular mineral assemblage or rock type. Titanite grains occur as anhedral to subhedral shaped grains, associated with magnetite grains within mafic mineral aggregates; micron sized grains also occur within the groundmass. These grains are a common occurrence in the alteration mineral aggregates within the mineralized zone. These aggregates also contain sodic pyroxene, zircon, magnetite and hematite, albite, calcite and the uranium bearing phases. The exact relationship with titanite and the uranium bearing phases is poorly understood but often titanite grains possess tiny uraninite and brannerite inclusions that seem to have formed in micro fractures within the grain, or form as a result of the alteration of titanite grains, creating a spotted texture within the titanite grain. It is possible that the titanite grains provide a source of  $\text{TiO}_2$  for the brannerite grains as these two minerals are often associated with each other.

The mineral phases, allanite, andradite and thorite occur sporadically throughout the mineralized zone and were only detected through SEM-MLA analysis in a select

number of samples. Their relationships to uranium mineralization are not well understood but it does not seem that they are related. It is not certain whether these grains form through alteration or are just primary minerals within the rock. Allanite and thorite grains occur as tiny subhedral grains, less than 0.1 mm in size, disseminated within the groundmass but more commonly occur within the alteration mineral aggregates. They do not appear to be related to uranium mineralization. It is possible that allanite grains are the result of alteration as the FP and CP rocks within the mineralized zone experienced a mass gain in the light REE, which are a major constituent in allanite. Mass balance calculations indicate that there is no mass change for thorium, suggesting it remained relatively immobile during alteration. This would suggest that the trace amounts of thorite identified in SEM-MLA analysis are most likely a primary mineral constituent of the felsic volcanic rocks throughout the Aillik Group. Andradite grains occur as large, 0.5-1.5 mm subhedral equant grains in select samples throughout the mineralized zone. Garnet alteration is discussed further in Chapter 6, section 6.6.2, but it does not appear that garnet formation is related to alteration or uranium mineralization. In all likelihood, its formation can be attributed to metamorphism of the felsic volcanic rocks.

#### **4.5.4 Phosphate Minerals**

Phosphate minerals in the form of apatite and monazite occur in both the FP and CP felsic volcanic rocks. Mass balance calculations indicate that  $P_2O_5$  was generally conserved during alteration within the ore zone, indicating that secondary phosphate minerals were not created within the mineralized zone during alteration. However,

monazite grains are present in sporadic samples from the mineralized zone, occurring as very fine-grained, subhedral to euhedral, sub-prismatic grains intergrown with alteration mineral aggregates. The presence of monazite in the mineralized zone could help explain the mass gain experienced by the light REE which are a major constituent in monazite grains. It does not appear that monazite grains are associated with uranium mineralization, but it is possible that monazite grains are formed from the alteration of apatite. Apatite grains occur in trace amounts in the unaltered felsic volcanics rocks as subhedral to euhedral, sub-prismatic grains. Although apatite grains occur within the mineralized zone their concentration does not seem to be as high as within the unaltered rocks. It is possible that apatite grains were altered to monazite grains in the presence of an altering fluid rich in LREE and yttrium (Fullerton, 2014), however, further study is required to confirm this assumption.

#### **4.5.5 Other Mineral Phases**

There are other minerals found within the mineralized zone that may be associated with alteration. These include calcite, barite and fluorite. The three will be discussed in more detail in Chapter 6, section 6.6. Of the three minerals, calcite is the only phase that appears to increase within the mineralized zone as a result of alteration. Calcite increases in samples that have undergone intense alteration within the ore zone, occurring as micron-sized grains within the groundmass; larger grains approximately 1.0 mm in size form in pressure shadows created from increased deformation and as 0.5-1 mm sized grains associated with alteration mineral aggregates. Although calcite is

associated with these mineral aggregates, it does not appear to be directly related to uranium mineralization, but rather, it appears to form later in the alteration history of the rock. SEM-MLA analysis indicates that barite has a strong strontium component, and is commonly associated with calcite grains. It does not appear to be an alteration mineral though, as barium displays strong mass losses within the mineralized zone for some samples. It is most likely that the occurrence of barite throughout the deposit is very sporadic and occurs naturally within the felsic volcanic rocks of the Michelin deposit. It is possible that barite grains that were already present within the mineralized zone were enriched due to alteration, possibly explaining some of the mass gain found in some samples.

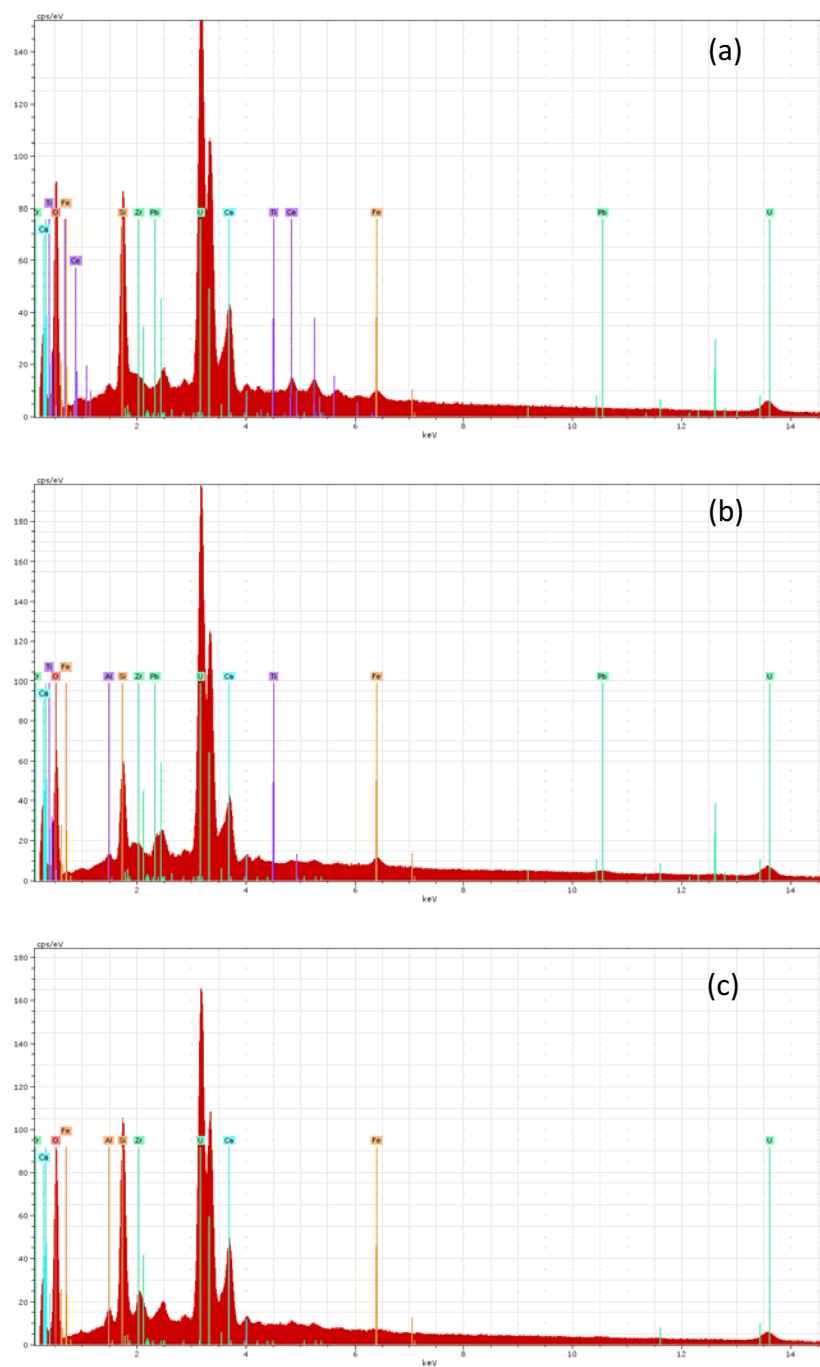


**Figure 5.1:** EDX analysis of uraninite grains showing a large U peak with cationic substitutions of (a) Si, Ca, Pb and Ce, (b) Si, Ca, Pb, and (c) Si, Ca, Pb and Zr.

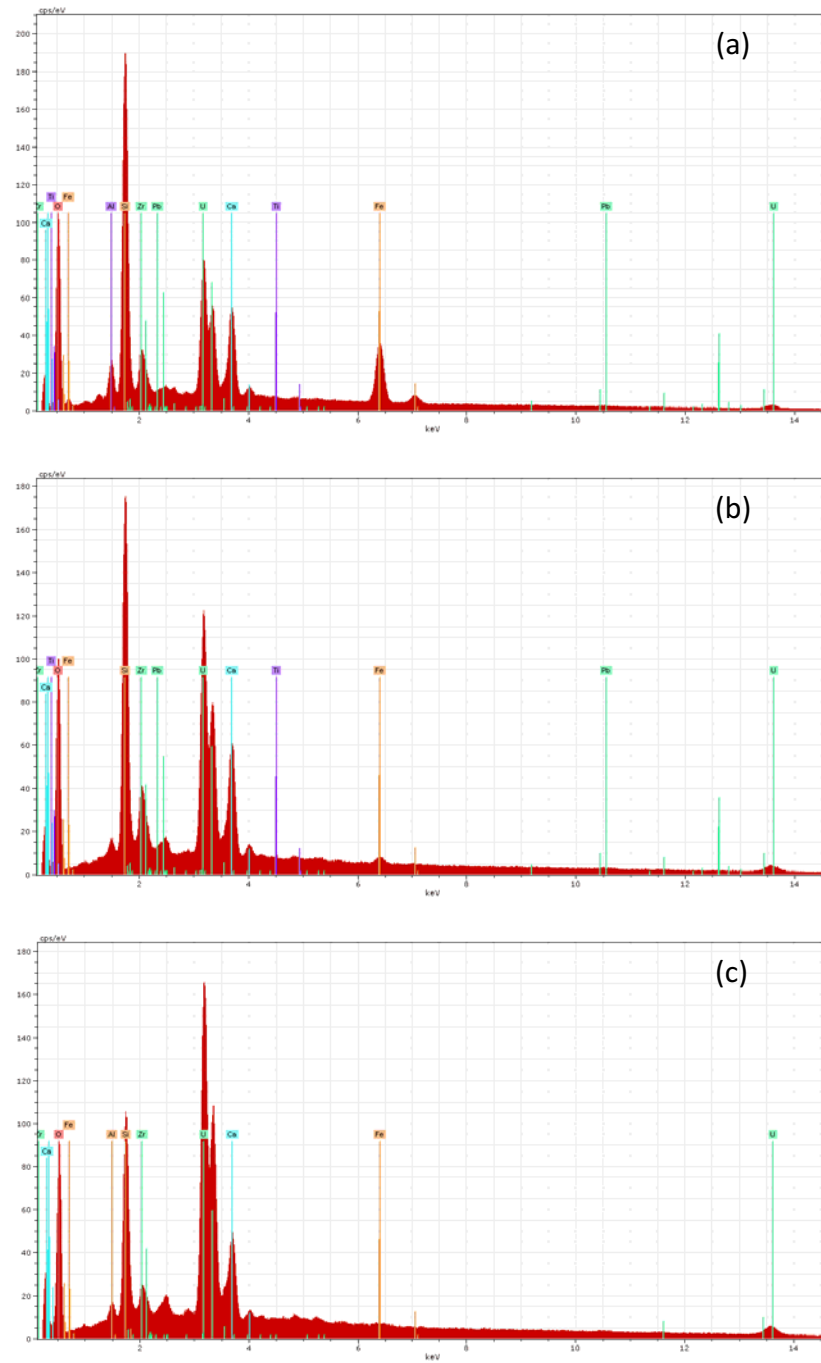


**Figure 5.2:** EDX analysis of uraninite grains showing a large Si peak with smaller U peak and cationic substitutions of (a) Ca, Zr and Fe, (b) C and Zr, and (c) Ca, Zr and Ti.

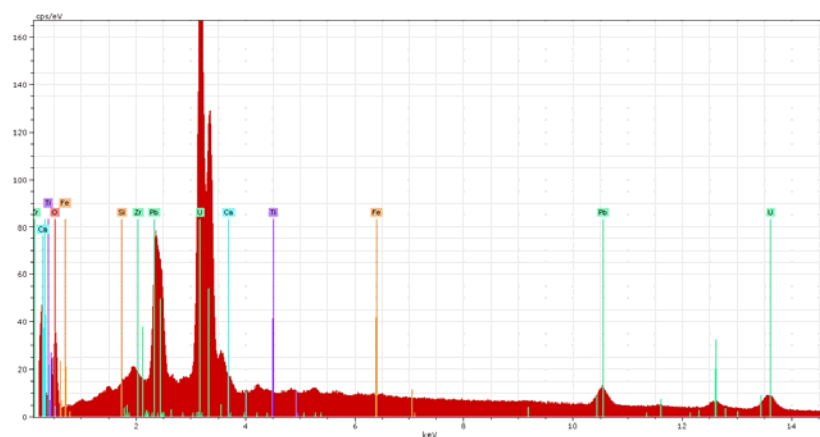


**Figure 5.3:** EDX analysis of uraninite showing a large U peak with a smaller Pb peak.

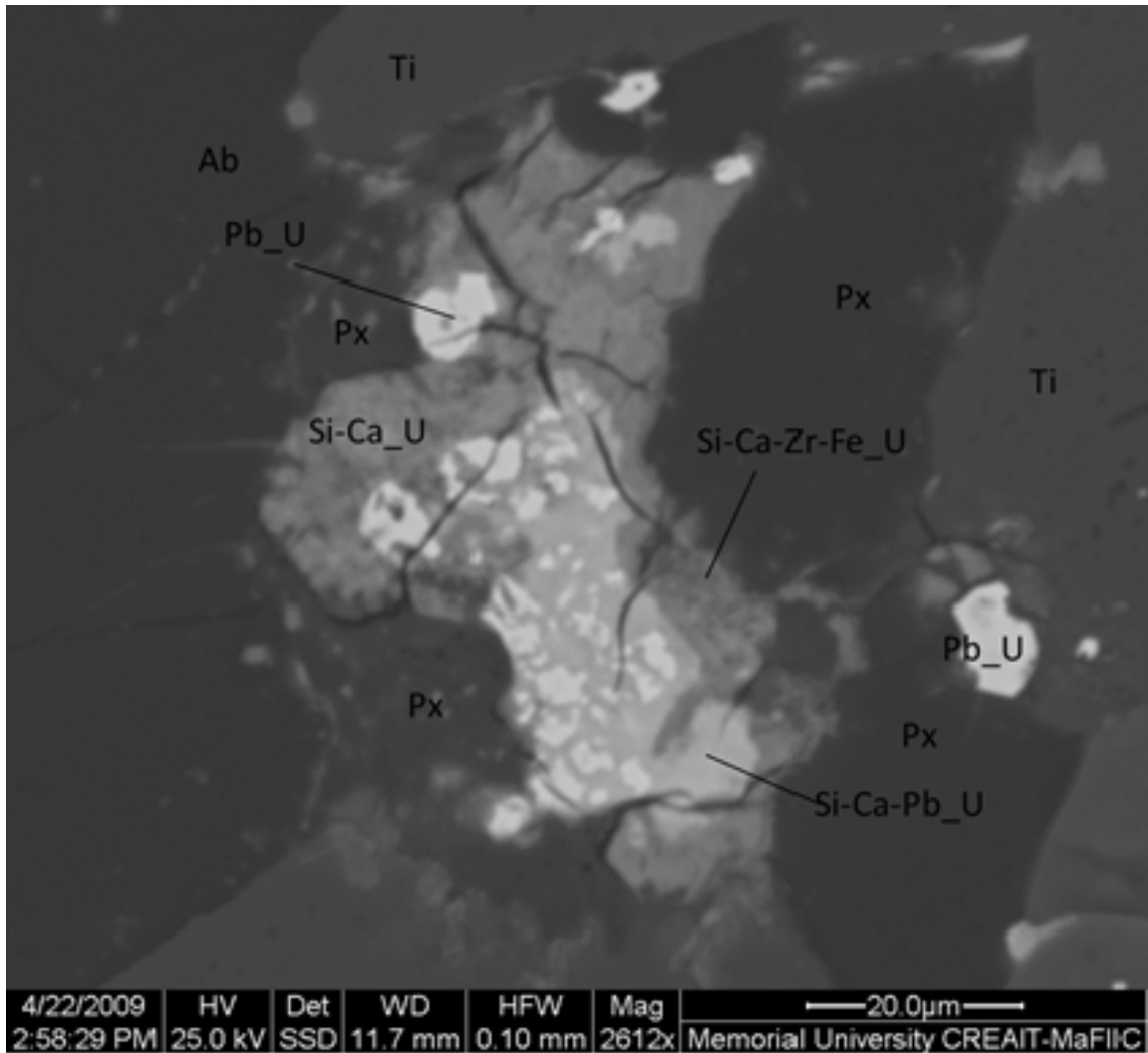


**Figure 5.4:** Back scatter electron (BSE) image of uraninite showing uraninite with Pb (Pb\_U) occurring as subhedral grains (lightest grey) surrounded by uraninite with Si-Ca-Pb (Si-Ca-Pb\_U) (slightly darker grey), which are then surrounded by uraninite with Si-Ca (Si-Ca\_U) and uraninite with Si-Ca-Zr-Fe (Si-Ca-Zr-Fe\_U) which are both slightly darker grey still.



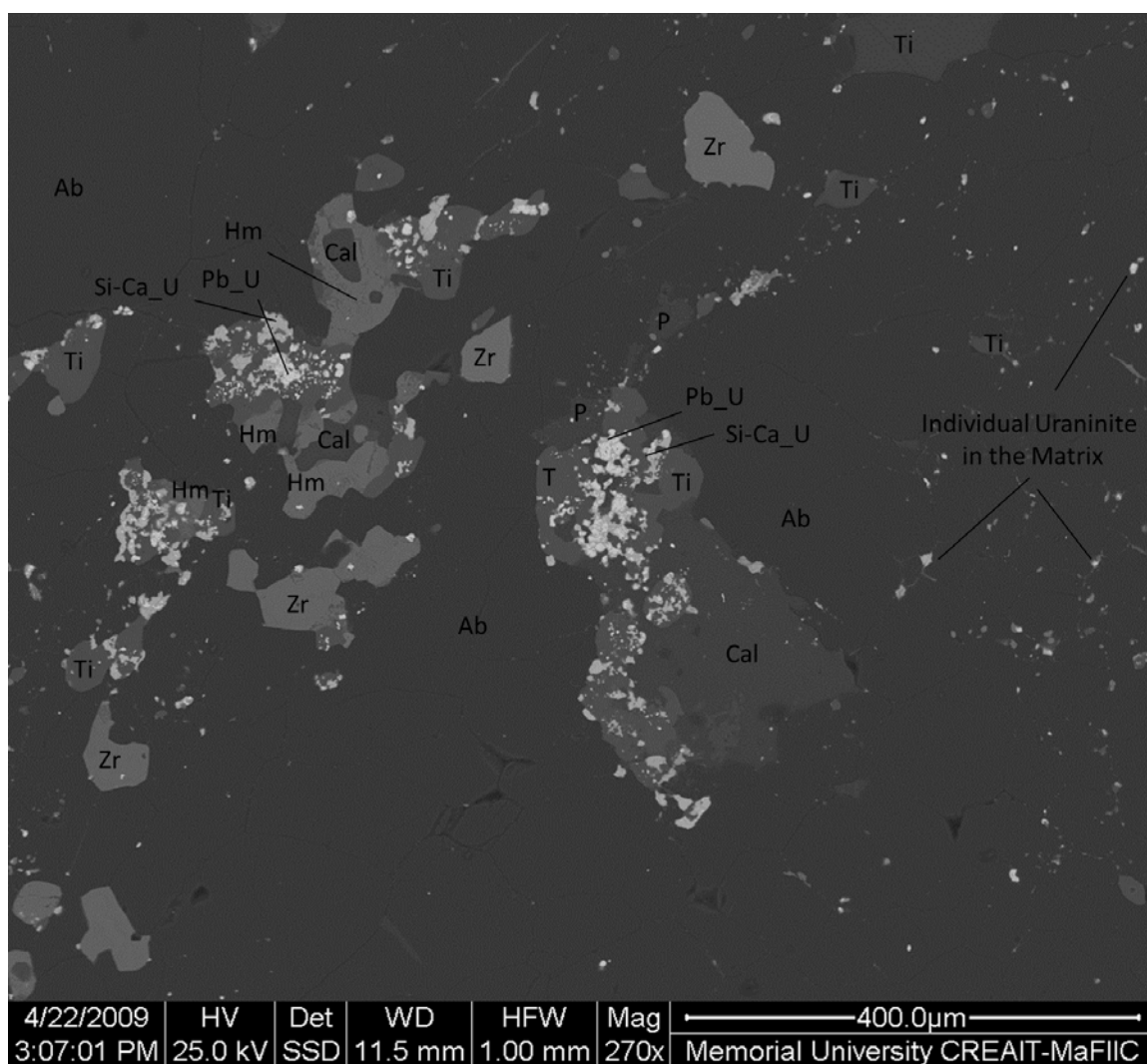


**Figure 5.5:** BSE of mineral aggregate consisting of titanite (Ti), Hematite (Hm), Zircon (Zr), sodic pyroxene (Px), Calcite (Cal) in an albite (Ab) matrix. Uraninite grains are hosted throughout but are mostly associated with Ti grains, they occur as uraninite with Pb (Pb\_U) which are the lightest grey and uraninite with Si-Ca (Si-Ca\_U) which are slightly darker grey. Individual uraninite grains occur within the matrix.

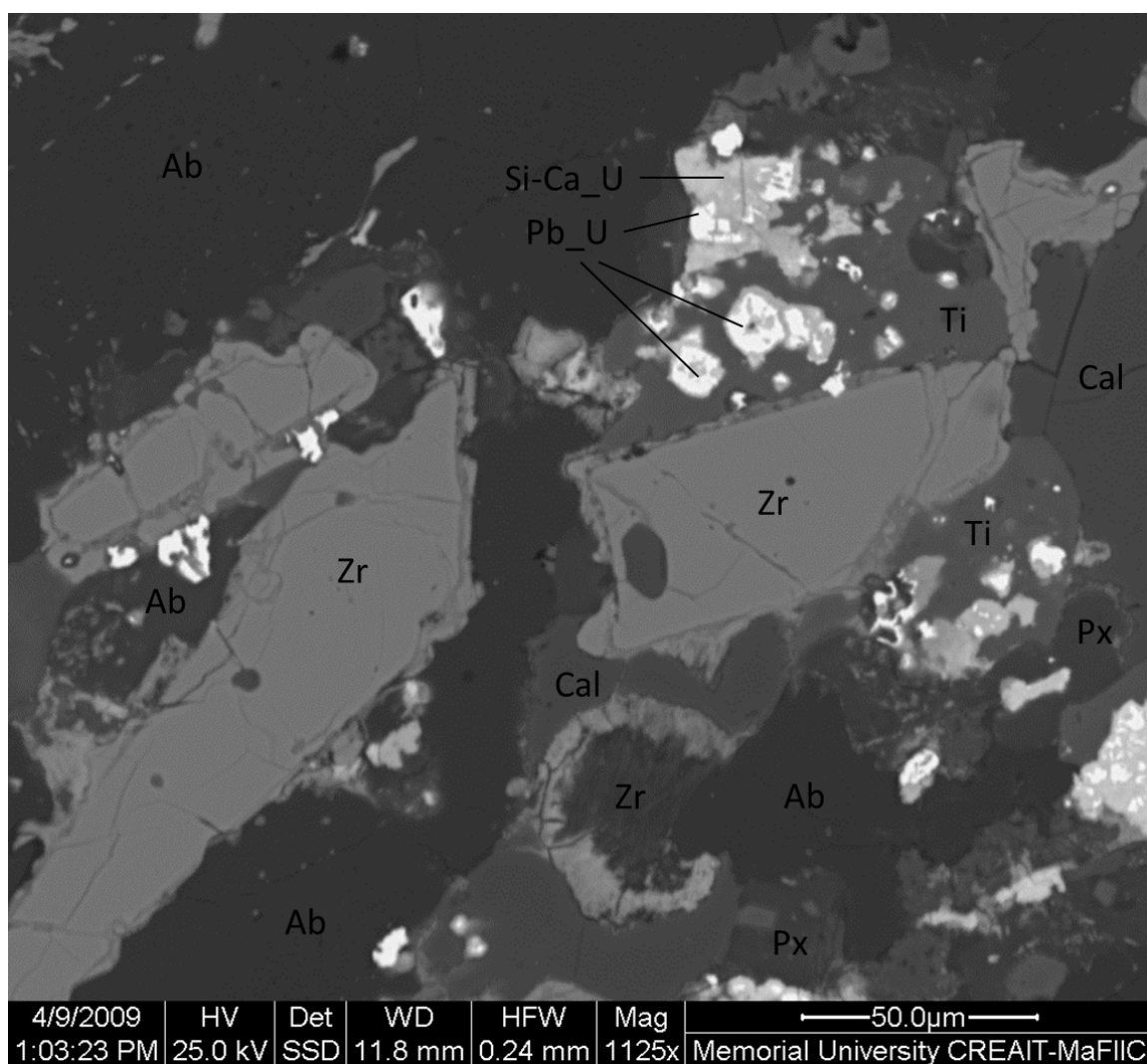


**Figure 5.6:** BSE image of mineral aggregate consisting of zircon (Zr), titanite (Ti), sodic pyroxene (Px), albite (Ab), calcite (Cal) in an albite matrix. Uraninite grains occur throughout but are predominantly associated with titanite grains and occur a euhedral uraninite with Pb (Pb\_U) that is surrounded by uraninite with Si-Ca (Si-Ca\_U). Two distinct varieties of zircon are present, euhedral grains with secondary growth rims, and a rounded grain with a different color core, most likely an inherited grain.

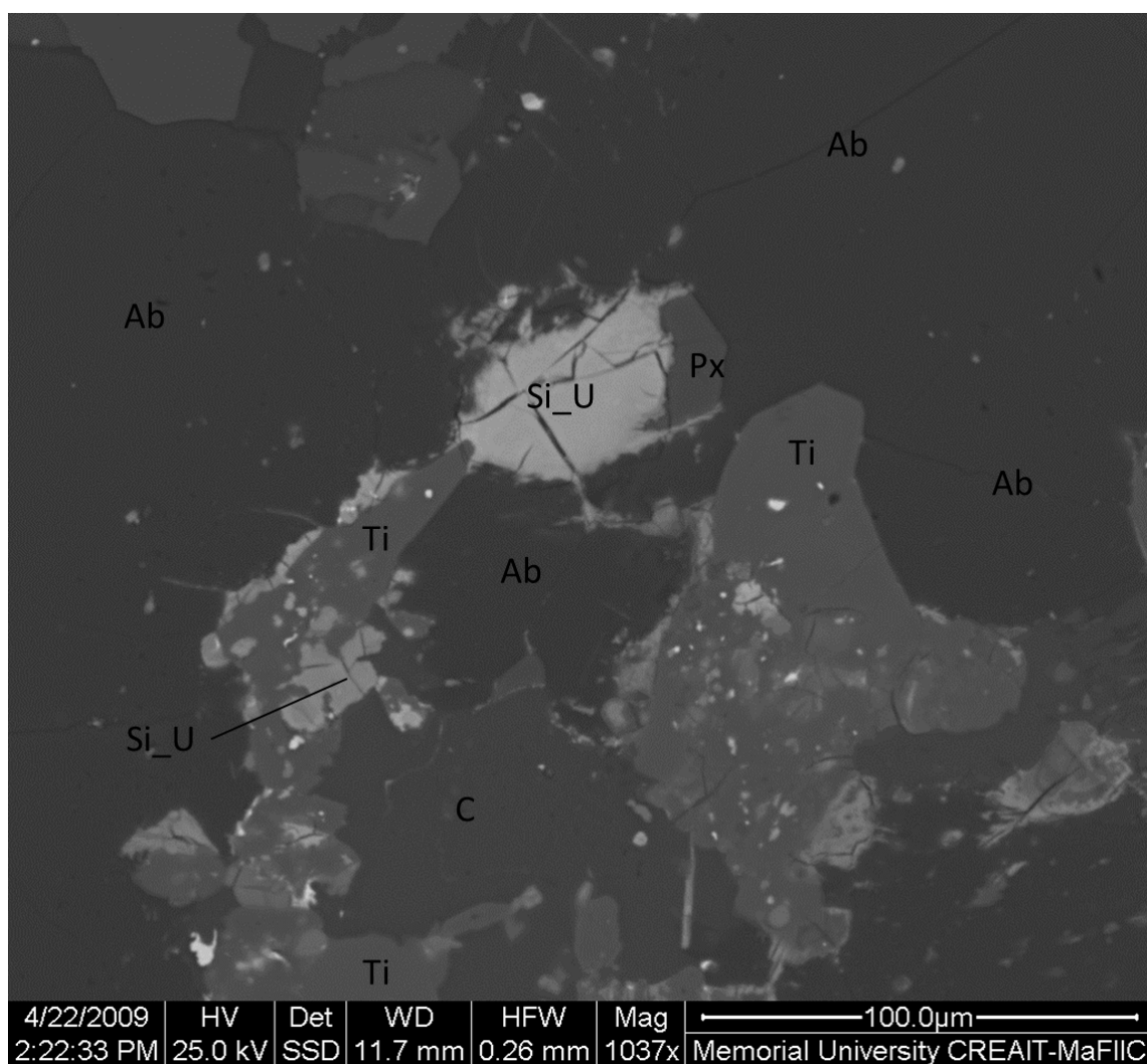


**Figure 5.7:** BSE of a mineral aggregate of titanite (Ti), calcite (cal), albite (ab), and sodic pyroxene (Px) in an albite matrix. Hosts large grains of uraninite with silica (Si\_U), possibly coffinite.

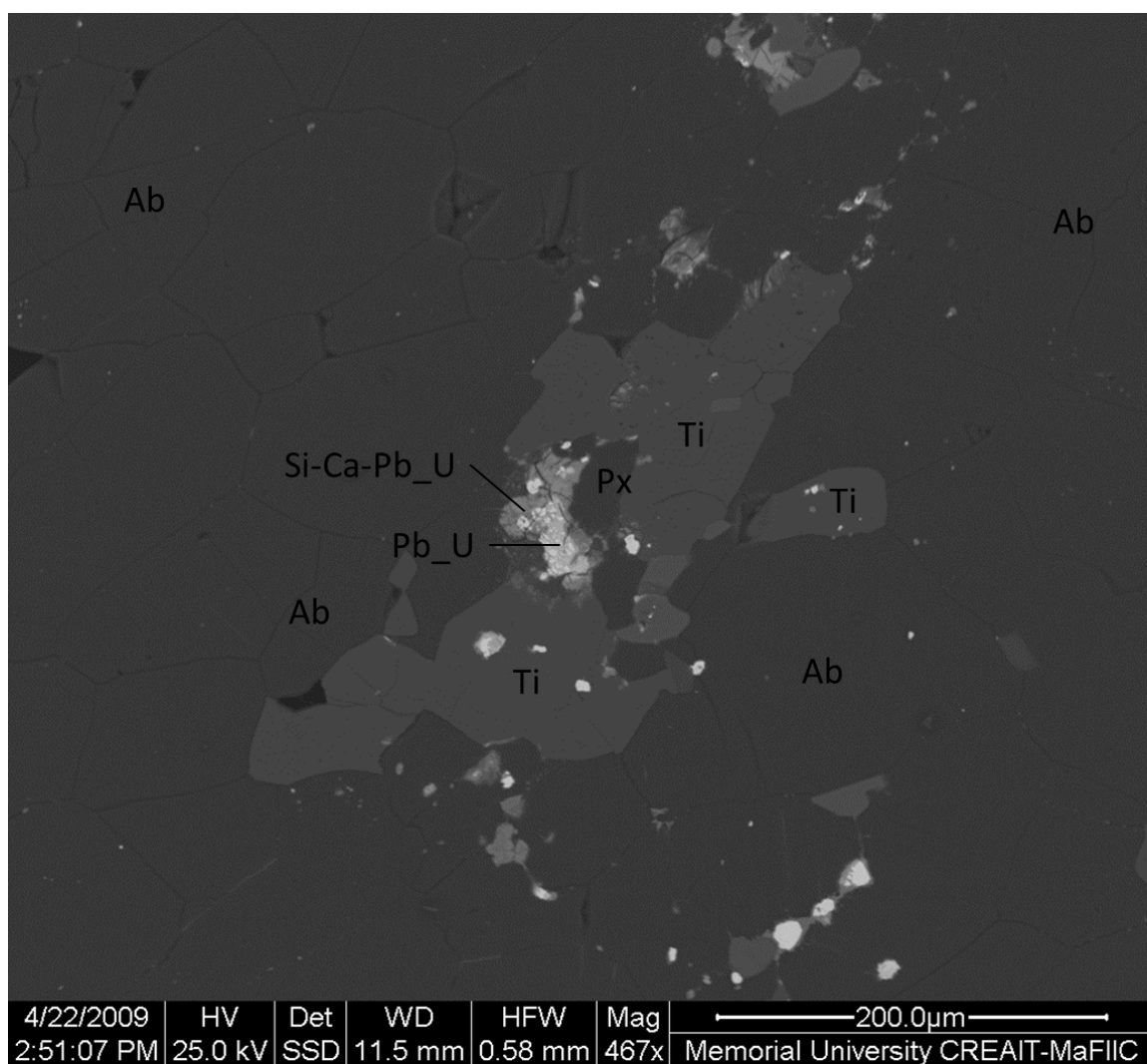


**Figure 5.8:** BSE image of a small aggregate of titanite (Ti) and sodic pyroxene (Px) within an albite (Ab) rich matrix. Uraninite grains are associated with the sodic pyroxenes and consist of uraninite with Pb (Pb\_U) which is surrounded by uraninite with Si-Ca-Pb (Si-Ca-Pb\_U).

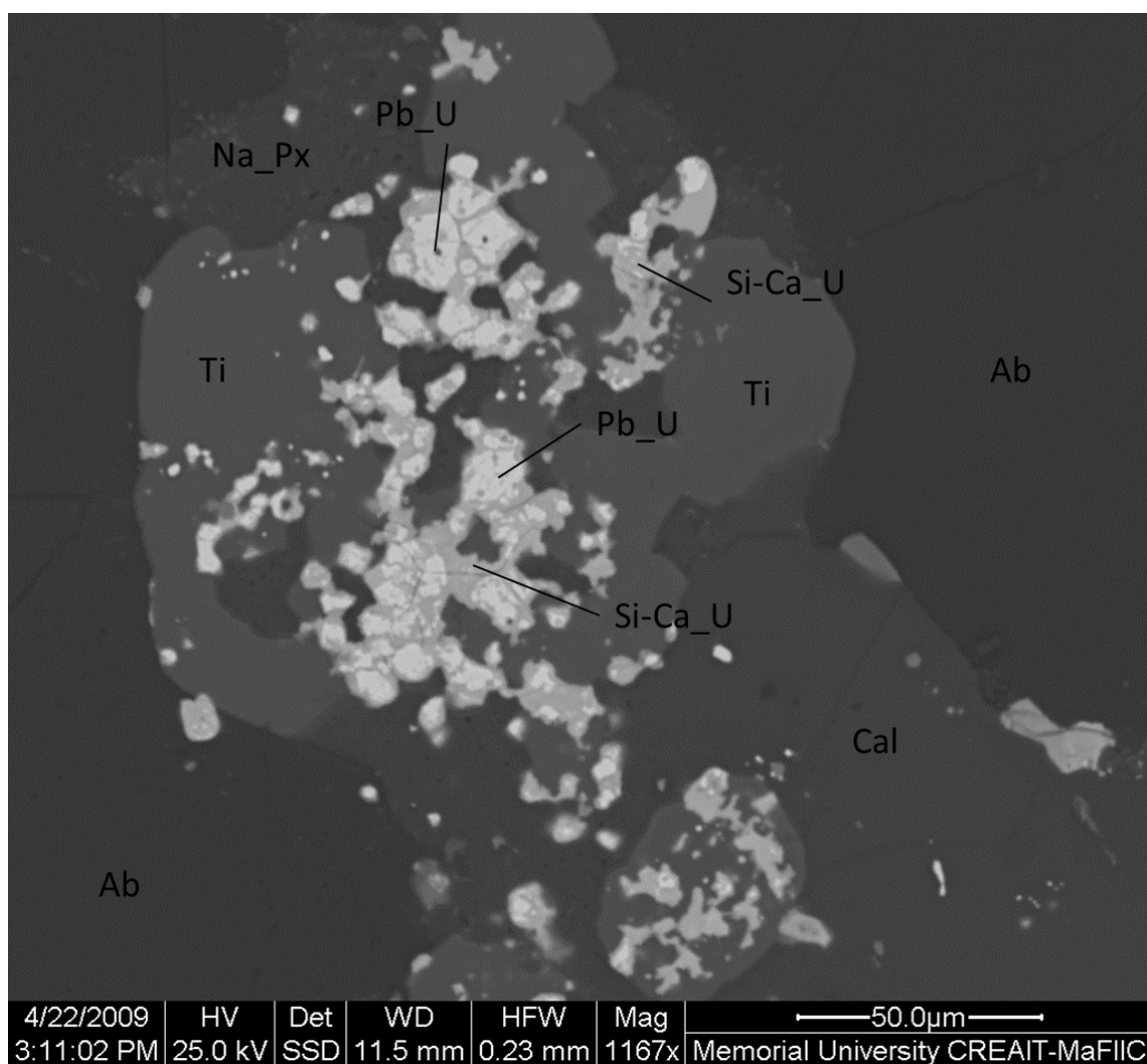


**Figure 5.9:** BSE image of a mineral aggregate consisting of titanite (Ti), sodic pyroxene (Na\_Px) and calcite (Cal) in an albite (Ab) matrix. The aggregate is strongly mineralized with grains of uraninite with Pb (Pb\_U) being almost completely surrounded by uraninite with Si-Ca (Si-Ca\_U).

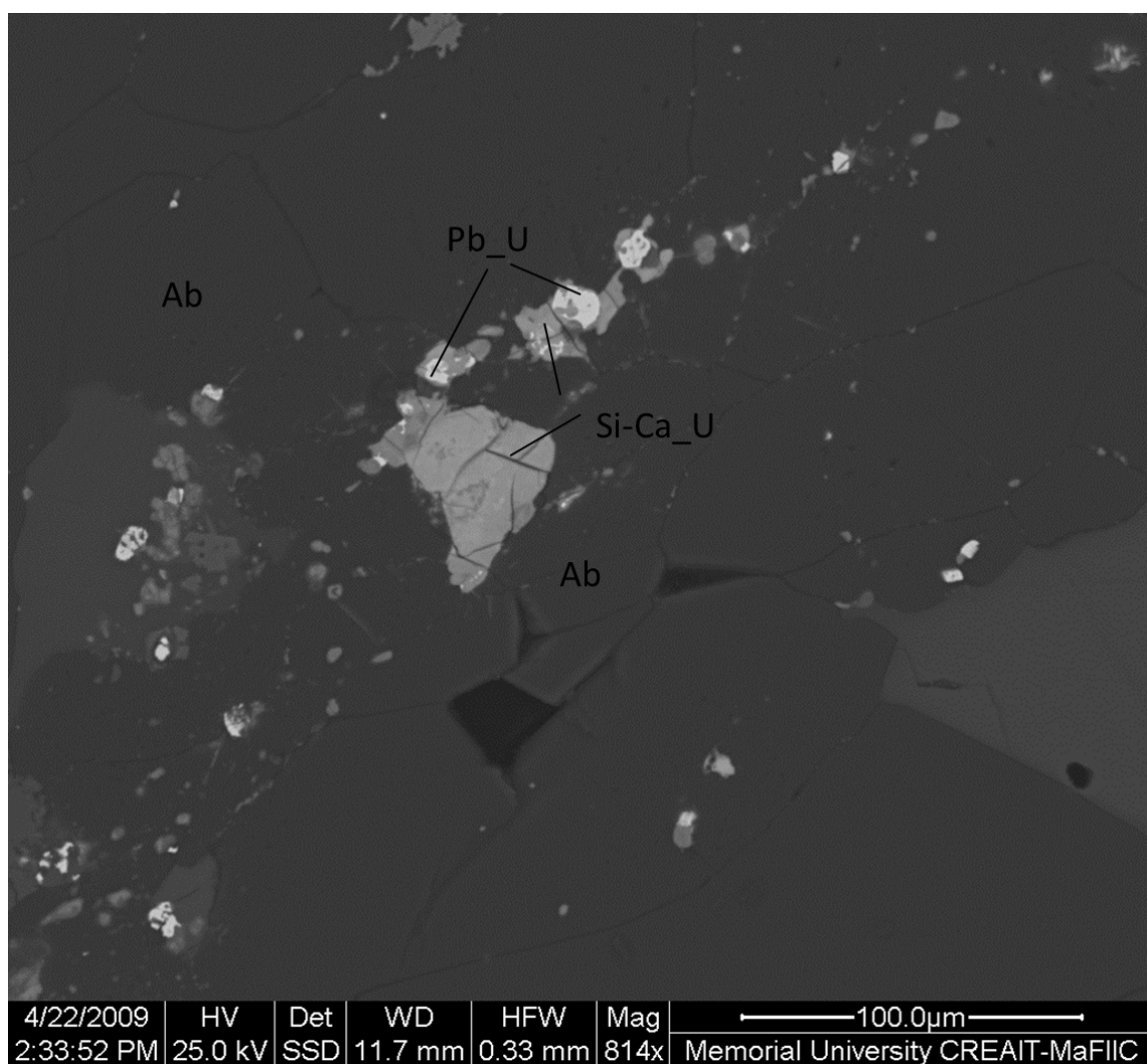


**Figure 5.10:** BSE image of the albite (Ab) rich matrix hosting individual uraninite grains at the triple-point junctions between grains. Uraninite grains consist of uraninite with Pb (Pb\_U), and uraninite with Si-Ca (Si-Ca\_U).











**Plate 4.6:** Location of uranium mineralization throughout the Michelin deposit (core diameter 4.2 cm), (a-b) spots of anomalous mineralization associated with small concordant, patches of weak hematite alteration, cps values between 250-650cps, (c) sporadic hematite patches become more frequent approaching the start of the main ore zone, with is marked by the start of the first CP unit within the Mine Series (lowest row of core), (d) CP unit (second row of core) within FP units, mineralization is concentrated within this unit and the adjacent contacts of the FP units, gradually decreasing to the centers of the FP units, (e) small, intensely foliated, non-porphyritic mylonite zone with strong hematite alteration and mineralization, (f-h) zones adjacent to the syn-kinematic mafic dikes display a strong increase in both hematite alteration and mineralization, which gradually returns to background away from the dike contact, (h) zone of intense shearing and abundant calcite, marked by increase hematite alteration and mineralization (within the 5<sup>th</sup> row of core), (i) Showing the CP unit (bottom 2 rows of core) being strongly mineralized and altered, the FP units above it are not as strongly mineralized or altered, (j) small zone of strong mineralization associated with strong hematite and calcite alteration, pre-kinematic dike above this zone has no mineralizing-upgrade effect on the adjacent core.

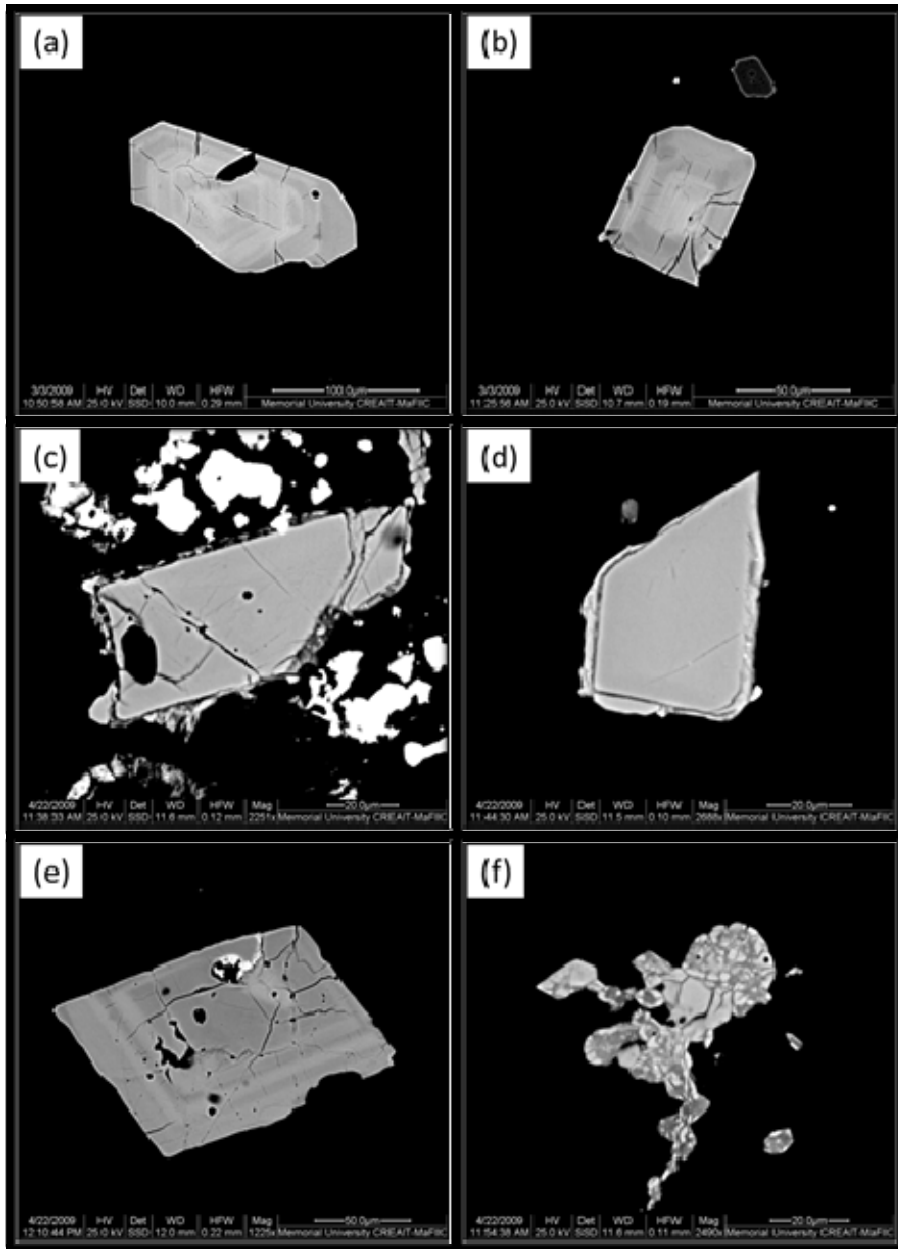


**Plate 4.7:** BSE images of zircon grains from the unaltered felsic volcanics (a-b) and mineralized zone (c-f), (a and b) euhedral, prismatic, zoned zircon grains from FP felsic volcanic units, (c) un-zoned equant zircon grain showing secondary growth along the outside rim that includes several small uraninite grains, zircon grain is a part of a mineral aggregate that contains abundant uranium mineralization, (d) equant, un-zoned zircon grain with secondary growth along its outside rim which contains a couple of tiny uraninite grains, (e) zoned, euhedral grain with uraninite grains developing along fractures within the grain, and (f) anhedral zircon grain with strongly mottled appearance.

## **Chapter 6     Alteration**

### **6.1     Introduction**

At first glance it is evident that the FP and CP felsic volcanic host rocks of the Michelin deposit have undergone varying degrees of alteration. Alteration effects are visible in surface trenches and in a rock face adjacent to an old BRINEX adit tunneled into the deposit. These showings have limitations because they do not allow for direct comparison between altered and unaltered rock. This is best achieved through the use of drill core. Thousands of meters of diamond drill core were extracted and logged during earlier exploration programs and this core provides a valuable record into the different alteration styles affecting the deposit.

This chapter is an attempt to characterize and define the different alteration styles and their respective intensities which affect the Michelin deposit. Through detailed observation it appears that alteration at Michelin occurs as two distinct styles: 1) a widespread alteration where its effects are intensified, or centralized within the mineralized zone and extend into the hanging wall and foot wall of the deposit, thereby creating an envelope around the deposit, and 2) a more localized alteration that seems to be directly associated with the mineralized zone. Both styles appear to be a result of hydrothermal alteration and not regional metamorphism. Each alteration style is related to or intensified within the mineralized zone and can be followed into fresh, unaltered rocks. If alteration was the effect of regional metamorphism then unaltered rocks should exhibit similar changes as seen in altered zones.

The two most noticeable alteration styles that affect the deposit are 1) a pervasive sodic alteration which envelopes the mineralized zone, intensifying towards and becoming most intense within the mineralized zone, and 2) a sporadic hematite alteration, that is the result of the oxidation of magnetite. This hematitic alteration style becomes very intense within the mineralized zone and appears to be closely related to uranium mineralization. A closer examination of drill core reveals several other styles of alteration throughout the deposit. Some of these appear to be closely related and are associated with uranium mineralization. These include the dissolution of quartz within the mineralized zone and the formation or enrichment of several mineral species such as zircon, titanite, ilmenite, allanite, calcite, barite, pyroxene, amphibole and garnet within the mineralized zone. Other alteration styles appear to create mineral halos that envelope the mineralized zone, gaining intensity within the mineralized zone. These are more poorly understood and they may or may not be directly associated with uranium mineralization. These include the presence of garnet, calcite, and possibly barite, fluorite, and gypsum that are newly formed or enriched around the mineralized zone.

Alteration throughout the deposit takes on numerous forms including chemical metasomatism of one element for another, mineral replacement, oxidation, mineral destruction, and the formation of new minerals and mineral assemblages. To accurately characterize and define the different alteration styles drill core observations will be used to measure visual and textural changes in the rock. This will be combined with petrographic thin section examination, geophysical analysis and SEM-MLA analysis to identify alteration mineral assemblages and the mineralogical changes that occur as

alteration intensity increases. Major, trace and rare earth element geochemistry will also be used to measure and characterize the geochemical changes that occur with each alteration style. It will also be used to identify any trace-elemental halos that cannot be measured through drill core or mineralogical changes. Mass balance calculations will be completed for samples within the ore zone to identify actual elemental changes that are a result of alteration and not the result of apparent elemental change due to the effects of closure and mass and/or volume change of the altered rock. Average, low and high values for the major oxides, trace elements, REE, and normative mineral percentages for the felsic volcanic rocks within the sodic envelope are in Table 4.1.

## **6.2 Sodic Alteration**

Sodic alteration is one of the more obvious alteration styles and a distinctive characteristic of the Michelin deposit, as well as other deposits and showings hosted in felsic volcanic rocks throughout the Aillik Group. This alteration is easily recognizable in drill core as well as in outcrop surrounding the mineralized zone, and is marked by a distinct color, textural and mineralogical change in the rock.

It is an integral part to the mineralizing system at Michelin; however, its exact relationship to uranium mineralization is poorly understood. The effect of the hydrothermal altering fluids create a large foot print which envelopes the mineralized zone, extending well into the unmineralized hanging wall and foot wall. As traced down-hole, the initial onset of sodic alteration marks the beginning of the alteration system. The

width and intensity of this alteration generally reflects the size and grade of the mineralized ore zone.

The sodic alteration footprint has an approximate thickness between 80-150 m. At the center of the deposit where the mineralized zone is thickest, the sodic envelope is also thickest, being approximately 130-150 m thick. Outwards from the center of the mineralized zone the sodic envelope thins and near the outer edges of the deposit it is about 80-100 m thick. It appears that the thickness of the sodic alteration envelope quickly thins and eventually pinches out, moving away from the deposit. Further drilling will be required to determine the full extent of the sodic alteration zone.

The effects of sodic alteration can be observed between 10-100 m before the beginning of the mineralized zone, and ends anywhere between 10-50 m beyond the end of the mineralized zone. However, within the sodic alteration envelope, the mineralized zone is not spatially consistent and does not appear to be centered within the sodic envelope. At the center of the deposit where the thickest intercepts of mineralization occur, sodic alteration begins approximately 75-100 m before the start of the mineralized zone and ends almost abruptly, approximately 10-20 m after the end of the mineralized zone. Moving outwards in all directions, particularly with depth, away from the center of the system, sodic alteration begins approximately 10-25 m before the beginning of the mineralized zone and extends for 40-50 m beyond the end of the mineralized zone.

Sodic alteration presents itself gradually within the hanging wall; fresh, pinkish-grey felsic volcanic rocks which are hard, smooth to the touch, and polished in appearance gradually transition into altered, whitish-grey volcanics (Plate 6.1c). These

volcanics are soft, friable and somewhat granular in appearance. This pervasive change occurs over a 15-25 m distance and affects both the FP and CP felsic volcanic rocks evenly; however the FP volcanic rocks alter before the CP equivalents (Plate 6.1a-b).

Alteration begins as a metasomatic or chemical change of sodium for potassium, whereby potassium feldspar is being altered to albite. The intensity of alteration then gradually increases towards the mineralized zone and includes both the continuation of the metasomatic change of potassium feldspar to albite and the alteration of mafic minerals to sodic amphiboles, where all altered grains become pseudomorphs of the original grain. Sodic alteration reaches its peak intensity within the mineralized zone and new sodic rich minerals are formed. This includes first of all, the formation of sodic amphiboles, followed by the alteration-to or formation-of sodic pyroxenes and the formation of secondary albite. From the mineralized zone into the footwall the process is almost a complete reversal of that seen for the hanging wall. The mineralogical changes and intensity of alteration steadily decrease until the host rocks reach their fresh, unaltered state.

### **6.2.1 Mineralogical Changes**

There are several mineralogical changes which take place as a result of the sodic alteration. Petrographic thin section and SEM-MLA analysis enables these changes to be tracked as alteration intensity increases, thereby providing a means to identify any new minerals created as a result of the alteration.

Initially, alteration begins with an almost one for one replacement of potassium feldspar for albite. During this metasomatic process no new minerals are created, only alteration of the already present potassium feldspar grains to sodium feldspar (albite). All microcline feldspar grains, both within the matrix and phenocrysts alike are affected. In unaltered, felsic volcanic host rock the matrix contains equal percentages in the 30-35 % range for potassium feldspar, albite and quartz, as well as minor amounts of mafic and opaque minerals.

Due to the very fine grained nature of the matrix, alteration effects within potassium feldspar grains is difficult to qualify, but based on observation, alteration of all potassium feldspar grains within the matrix to albite takes place early and within the first 10-20 m of the sodic alteration halo. Therefore, it appears logical that this is the first step in the overall alteration process. The matrix after initial alteration now consists of about 60-70 % albite, 30-35 percent quartz and a minor amount of mafic and opaque minerals. For larger potassium feldspar phenocrysts, it is apparent that hydrothermal fluids attack outer grain edges and slowly alter the phenocryst inward towards its center until the entire phenocryst is altered to albite. The degree of intensity that is required to fully alter these grains is dependent on the size of the phenocrysts, but in general most have been entirely altered leading up to the mineralized zone. Completely altered potassium feldspar phenocrysts display a chessboard twinning, which is a common occurrence when potassium feldspar is completely replaced by albite (Kaur *et al.*, 2012) (Plate 6.2a-f).

As alteration intensity increases mafic minerals begin to alter. Mafic minerals, predominantly in the form of biotite, minor hornblende and chlorite are present in fresh



felsic volcanics and comprise on average approximately 5-10 % of the rock (Plate 6.3a). During this stage no new minerals are created, only mafic grains already present are being altered. The altered grains become pseudomorphs, still maintaining their original size, shape and texture. Biotite grains maintain their original lath shape but they have been altered to a sodic amphibole. These grains now exhibit a bluish-green color in plain polarized light instead of the light brown color of the original biotite (Plate 6.3b). Amphibole grains also change from greenish-brown when fresh to green to greenish-blue. None of these altered grains were analyzed with the SEM-MLA, so exact mineral compositions are unknown, but based on the bluish color they are interpreted to be sodic amphiboles.

Inside the mineralized zone, the intensity of sodic alteration continues to increase and eventually reaches its peak. The end result is the creation of new sodic bearing amphiboles, sodic pyroxenes and secondary albite. Sodic amphiboles form first and these grains are very fine grained, ranging in size from less than 0.1-2 mm, but can get as large as 5-10 mm. Within the matrix individual grains do occur but frequently they appear as aggregates of several amphibole grains bound together. Usually they are associated with unidentified opaque minerals as well as zircon and titanite. Grains are typically subhedral to euhedral, subprismatic to equant in shape and range in color from green to bluish-green to yellowish-green in plain polarized light (Plate 6.3d-e). Due to their small grain size only one cleavage plane is visible but larger grains do sometimes exhibit the distinctive 120/60 amphibole cleavage (Plate 6.3c).

Sodic amphibole grains are generally aligned parallel to the foliation, and often comprise a percentage of the thin mafic wisps which define the foliation throughout the felsic volcanic rocks of the deposit. In areas of increased deformation, these wisps wrap around the larger albite phenocrysts thereby creating an augened appearance. Often, several small sodic amphibole grains will form larger aggregates and infill vugs or spaces created through the dissolution of quartz phenocrysts. Smaller grains situated within the matrix may have been created in void space from the dissolution of quartz within the matrix.

The range in color displayed by sodic amphibole grains most likely indicates that there is more than one distinct mineral phase. In this study SEM-MLA work was not completed on the amphibole grains, but in a separate petrographic report by Ross (2006), it is suggested that the blue grain color may be indicative of a sodic amphibole. This assumption was later verified by SEM analysis. The report also postulates that the sodic amphiboles either lie in the arfvedsonite – eckermanite  $[\text{Na}, \text{Na}_2\text{Fe}^{2+}_4\text{Fe}^{3+}\text{Si}_8\text{O}_{22}(\text{OH})_2]$  –  $[\text{Na}, \text{Na}_2\text{Mg}_4\text{AlSi}_8\text{O}_{22}(\text{OH})_2]$  solid solution series or the riebeckite – glaucophane  $[\text{Na}_2\text{Fe}^{2+}_3\text{Fe}^{3+}_2\text{Si}_8\text{O}_{22}(\text{OH})_2]$  –  $[\text{Na}_2\text{Mg}_3\text{Al}_2\text{Si}_8\text{O}_{22}(\text{OH})_2]$  series. Microprobe work will be necessary to determine the exact stoichiometry for accurate mineral identification.

Inside the mineralized zone, areas which are strongly mineralized also seem to show a higher intensity of sodic alteration. It is primarily within these areas that sodic pyroxenes and secondary albite form. Sodic pyroxene grains either form as new mineral constituents within the ore zone or as a result of alteration of sodic amphibole grains to sodic pyroxenes. Although sodic amphiboles and sodic pyroxenes occur together within

the mineralized zone usually one or the other will predominate. As a generalization, weakly mineralized samples tend to contain a higher abundance of sodic amphibole, whereas strongly mineralized samples possess a higher percentage of sodic pyroxene.

Pyroxene grains like amphiboles are generally aligned parallel to foliation and often form a percentage of the thin mafic wisps that define foliation and warp around larger albite phenocrysts. Typically pyroxene grains are closely associated with opaque minerals, where they often form clusters surrounding the opaque grains (Plate 6.3f). A number of minerals, including zircon, titanite, albite, calcite, hematite, and uraninite are associated with these clusters. Pyroxene grains range in size from less than 0.1-5 mm but longer prismatic grains can grow up to 10 mm in length. The grains are typically subhedral to euhedral, subprismatic in shape and display a pale to strong grass green color in plain polarized light.

SEM-MLA analyses of mineralized thin sections indicate that the pyroxenes fall within the aegirine – augite compositional range, defining it as a sodium bearing clinopyroxene. According to a petrographical report by Ross (2006), the variation in grain color indicates a range in mineral composition and in addition, the pyroxene crystals which SEM analysis confirmed had a sodic component may lie in the aegirine-augite  $[(\text{Na,Ca})\text{Fe}^{3+}\text{Fe}^{2+}\text{Mg,Al Si}_2\text{O}_6]$  or omphacite  $[(\text{Ca,Na})(\text{Mg,Fe}^{2+}\text{Fe}^{3+},\text{Al})\text{Si}_2\text{O}_6]$  compositional field.

Secondary albite is found in samples having the highest concentration of sodic alteration and typically this corresponds as well to higher concentrations of uranium mineralization. These grains are often associated with the larger mineral clusters of sodic

pyroxenes, zircon, titanite, calcite, hematite, uraninite and sodic amphibole. They most likely form in void spaces created from dissolution of quartz phenocrysts and groundmass. Secondary albite grains range in size from 2-10 mm, appear subhedral to euhedral and are prismatic to lath-shaped. They display a distinct Carlsbad twinning and show very little signs of alteration or deformation. These secondary albites appear very fresh, unlike primary albite which appears mottled and deformed and microcline grains which are altered to albite and display a chessboard twinning. SEM-MLA analysis of samples within the mineralized zone show that most of the rock within the mineralized zone is comprised of albite, and that it forms most of the groundmass (Figure 6.3). These grains are too small to accurately describe but most seem to retain the original equant shape of the original quartz grains that were dissolved during alteration.

### **6.2.2 Geochemical Changes**

Drill hole M06-019, which is situated within the centre of the mineralized zone and intersects the thickest portion of the alteration envelope was sampled systematically from top to bottom at a sample interval of approximately every 10-30 m. This tight sampling profile allows the geochemical changes caused by alteration to be tracked and measured.

The unaltered FP felsic volcanic host rocks have on average 3.7 wt. %  $\text{Na}_2\text{O}$  and 5.0 wt. %  $\text{K}_2\text{O}$ , while the equivalent CP felsic volcanics display similar concentrations in both oxides averaging 3.5 wt. %  $\text{Na}_2\text{O}$  and 5.6 wt. %  $\text{K}_2\text{O}$ . Based on geochemical results and drill core observations the dividing line between unaltered and altered rock is 5.0 wt.

% Na<sub>2</sub>O. Samples that assay above this value typically display visible signs of weak to moderate, pervasive sodic alteration, most noticeably a change in color and texture. Examining whole rock geochemical data for M06-019, the onset of sodic alteration is very abrupt and occurs in the span of ~10 m. Within these 10 m there is a strong change in the concentrations of both sodium and potassium with Na<sub>2</sub>O and K<sub>2</sub>O values at 329.19 m measuring 3.4 wt. % and 5.7 wt. %, respectively. At 338.13 m, oxide values measure 7.4 wt. % Na<sub>2</sub>O and 0.14 wt. % K<sub>2</sub>O. The sodium content more than doubles and the potassium content decreases to near zero. This corresponds with the start of the sodic alteration envelope where potassium feldspar within the matrix is altered to sodium feldspar. The extremely low value of K<sub>2</sub>O would suggest that the alteration of potassium feldspar within the matrix is very pervasive. Within the foot wall, the end of sodic alteration is also very abrupt and occurs within the span of 10 m. At a depth of 479.42 m the Na<sub>2</sub>O and K<sub>2</sub>O values are 10.1 wt. % and 0.08 wt. %, respectively, 10 m further down hole at 488.37 m the Na<sub>2</sub>O and K<sub>2</sub>O values measure 4.2 wt. % and 4.4 wt. %, respectively. Figure 6.1 shows a plot of Na<sub>2</sub>O versus K<sub>2</sub>O, this clearly shows the alteration of potassium to sodium and then the further increase in sodic alteration.

The early stages of sodic alteration appear to be an almost one for one alkali ion exchange between a hot hydrothermal fluid that is alkaline rich, with a high Na<sup>+</sup>/K<sup>+</sup> ratio, and potassium-bearing minerals in the host rock. During this exchange K<sup>+</sup> ions are replaced by Na<sup>+</sup> ions leaving the rock completely depleted in K<sub>2</sub>O and enriched in Na<sub>2</sub>O (White and Martin, 1980). CIPW weight normative calculations, after Irvine and Baragar (1971), of unaltered samples of FP rocks and equivalent rocks within the sodic envelope

supports the metasomatic change of potassium feldspar to albite. Unaltered rocks give normative mineralogy of approximately 30-35 % quartz, orthoclase and albite. Within the sodic envelope the normative mineralogy is approximately 30-35 % quartz, 0.5-2 % orthoclase, and 60- 70 % albite.

Towards the mineralized zone the intensity of sodic alteration gradually increases, and Na<sub>2</sub>O content slowly increases as the remainder of the larger potassium feldspar phenocrysts completely alter to albite, completing the exchange of K<sup>+</sup> for Na<sup>+</sup> in potassium feldspars. When the Na<sub>2</sub>O content of the rock reaches approximately 8.5 wt. %, alteration of mafic minerals to sodium-rich minerals begins. At this point nearly all K<sub>2</sub>O has been removed from the system.

Inside the mineralized zone the formation of sodic amphiboles, sodic pyroxenes, and secondary albite leads to a further increase to approximately 9-10 wt. % in the Na<sub>2</sub>O content of the altered rock. CIPW normative calculations of both CP and FP felsic volcanic rocks within the mineralized zone indicate the normative mineralogy consists of approximately 0-5 % quartz, 0-1 % orthoclase, and 90-95 % albite (Table 4.1). Therefore, based on these calculations, secondary albite accounts for approximately 30 % of the rock within the mineralized zone, and that over 90 % of the rock is comprised of albite. These percentages do not reflect overall rock chemistry as some of the Na<sub>2</sub>O is contained within the sodic amphiboles and pyroxenes. It must also be noted that CIPW calculations may not be the best method to use when dealing with altered rock. The calculations do however prove useful for some generalities, for instance, quartz is depleted within the mineralized zone and most of it has been replaced by secondary albite.

### **6.3 Hematite Alteration**

Hematite alteration is the most visibly obvious alteration style that affects the Michelin deposit and it appears to be a very distinctive characteristic related to uranium mineralization throughout the felsic volcanic rocks of the Aillik Group. This alteration is easily recognizable in drill core and outcrop and is marked by a moderate to strong, sometimes intense color change in the rock.

Hematitization is an integral part to the mineralizing system at Michelin and appears to be directly related to uranium mineralization, as uranium mineralization always occurs with hematite alteration. Although the more intense hematite alteration is restricted to the mineralized zone, weak to moderate hematite alteration does extend into both the hanging wall and foot wall of the deposit, thereby outlining a poorly defined deposit envelope.

It is important to note that hematite alteration occurs throughout the Michelin area and not all of it appears to be associated with the mineralized deposit. Some of the hematite alteration appears to be post-mineralization and occurs along small faults and micro-fractures, particularly within fracture zones, sporadically along contacts between the felsic volcanic rocks and intruding granite and/or mafic dikes, and in small shear or mylonitic zones.

The effect of hematite alteration related to the mineralized zone generally begins around the same depth as the start of the sodic alteration envelope,  $\pm 30$  m. At the heart of the mineralized zone where mineralization and the sodic envelope is thickest, hematite alteration generally begins just before the start of sodic alteration. Moving outwards

towards where the mineralized zone narrows, hematite alteration generally begins after the start of sodic alteration. There are rare occasions where hematite alteration will begin well before the sodic alteration envelope. Due to the variability or uncertainty in trying to define the limits of hematite alteration, predicting thickness and grade of the mineralized zone based on the extent of hematite alteration in the hanging wall is almost impossible.

Hematite alteration follows the same pattern within the foot wall of the deposit. In general, hematite alteration eventually dies out around the same depth that sodic alteration dies out,  $\pm 30$  m. More often than not, in areas where the mineralized zone is thickest, hematite alteration generally extends beyond the sodic alteration zone while towards the edges of the deposit, and at depth where the mineralized zone thins; hematite alteration generally ends before the end of the sodic alteration envelope.

Hematite alteration produces a pinkish-red to red discoloration of the host rock. This is in stark contrast to the whitish-grey color of the sodic altered felsic volcanic rocks. Unlike sodic alteration, which is pervasive in nature, hematite alteration within the hanging wall and foot wall is very sporadic. It typically begins as small millimeter to centimeter thick bands concordant with the foliation of the host volcanics. These bands generally occur in small clusters and manifest as 10-25 cm patches or zones of hematite alteration (Plate 4.3a and c). These zones are usually weakly mineralized, producing scintillometer readings in the range of 300-500 counts per second and locally as high as 1,000 counts per second. Rarely, these patches will be highly mineralized, possibly due to a thin, uraninite rich stringer.



Moving towards the mineralized zone, hematite alteration gradually intensifies and the small, patchy hematite zones gradually thicken with depth and become more frequent. At the beginning of the mineralized zone, hematite alteration becomes consistent and covers 100 % of the host rock (Plate 5.1c). In addition to the increase in thickness and frequency of the patchy hematite zones near the ore zone, alteration intensity also increases. This produces a gradational color change within the host rock, transitioning from pinkish-red to light red along outer boundaries, then to red and locally deep red inside the ore zone.

Within the mineralized zone, rocks have been entirely hematite altered, but alteration intensity varies due to rock type, contact relationships and deformation. Hematite alteration is for the most part strongest within the CP felsic volcanics as opposed to their FP equivalents (Plate 5.1d). Generally, the CP units have a deep red color as opposed to the more pinkish-red to red color displayed by the FP volcanics. Usually the intensity of hematite alteration will increase along the contacts between both units and gradually decrease in intensity moving into the FP units. The syn-kinematic mafic dikes have strong altering effect on the surrounding volcanics. Immediately adjacent to dike contacts hematite alteration is extremely intense and a very deep red color (Plate 5.1f-h). This quickly decreases over a 50-100 cm width returning back to normal levels for the mineralized zone. Deformation areas within the mineralized zone also tend to be more intensely altered. Mylonitic zones, which generally range in size from 15-25 cm are intensely foliated and are strongly hematitized (Plate 5.1h). One CP unit within the ore zone displays evidence of shearing where albite phenocrysts have

been augmented by wisps of sodic amphiboles, sodic pyroxenes and other accessory minerals. This unit is extremely hematitized, thus imparting a deep red color to the host rock (Plate 5.1j).

Similar to sodic alteration, the hematite alteration envelope follows the same pattern, moving from the mineralized zone into the foot wall. Alteration intensity gradually decreases outwards into non-mineralized rock. This manifests itself as a gradual color change from red to light pink towards the end of continuous alteration into sporadic zones which get thinner and spaced further apart with depth. Eventually the hematite alteration becomes less frequent, appearing as small concordant bands, coinciding approximately with the sodic envelope boundary. Since this is where most of the exploration drilling ended, it is unknown if hematite alteration extends further with depth. One hole, M-06-027 was drilled approximately 300 m deeper, beyond the end of the mineralized zone. Hematite alteration was encountered further at depth. The alteration style however was similar to that observed in the hanging wall in association with fractures, contacts and deformed zones. No uranium mineralization was noted.

### **6.3.1 Mineralogical Changes**

Hematite alteration appears to be the result of the oxidation of magnetite to hematite. This process is a change in the oxidation state of iron where the ferric  $\text{Fe}^{2+}$  in magnetite loses an electron to become ferrous  $\text{Fe}^{3+}$  in hematite (McSween *et al.*, 2003). Magnetite grains occur throughout the felsic volcanics host rocks, often occurring as 2-6 mm sized grains associated with mafic minerals or as very fine grains disseminated

amongst the quartz-feldspar groundmass (Plate 6.4a-b). Reflected light petrography indicates that magnetite is the most common opaque grain found throughout the felsic volcanic host rocks, followed by pyrite, ilmenite and other sulfide species. In reflected light magnetite grains are light grey in color and show no signs of alteration. The oxidation of magnetite begins within the hematite alteration envelope. Alteration of magnetite begins at grain edges and slowly moves inward toward the center of the grain. Extremely small matrix magnetite grains seem to be completely oxidized first. Depending on the intensity of oxidation, magnetite grains are either slightly altered around the edges or completely oxidized to hematite.

Reflected light images from within the ore zone display grey magnetite grains which have lighter-grey discoloration along the edges. The lighter grey mineral is hematite that is forming from the oxidation of magnetite (Plate 6.4c). Areas within the ore zone having intense hematite alteration have magnetite grains that are completely altered to hematite (Plate 6.4d). Reflected light images for these areas show no alteration rims within the opaque grains, instead they all appear as light-grey in color indicating that they have been completely altered to hematite.

#### **6.3.1.1 Magnetite Destruction**

Down hole measurements of magnetic susceptibility, a dimensionless parameter that measures the degree of magnetization of the rock, were taken for all drill holes at Michelin. This tool is a good measurement for the relative amount of magnetite in the rock and can track magnetite changes down hole. The unaltered felsic volcanics rocks in

both the hanging wall and foot wall are moderately magnetic and generally give magnetic susceptibility values ranging 20-30, with the CP rocks generally measuring slightly higher than the CP rocks. The felsic volcanic rocks remain moderately magnetic, with consistent magnetic susceptibility readings throughout the sodic alteration envelope until the mineralized zone is reached. The sporadic hematite alteration present within the sodic envelope only creates a small local decrease in magnetic susceptibility; the alteration is not strong enough to have pervasive effect on magnetite content.

Within the mineralized zone magnetic susceptibility readings are variable, depending on rock type and hematite intensity. CP rocks within the mineralized zone give readings ranging from  $< 1$ -5. These units are generally very weakly to non-magnetic, strongly hematite altered and well mineralized. Magnetic susceptibility readings for the FP rocks range from  $< 1$  to as much as 20. The rocks are variable magnetic, ranging from very weak to moderate in value. Areas that are strongly hematitized are very weakly magnetic, and give readings of 1-5. Areas that are only moderately hematitized are more magnetic and give readings of 10-20. Within the mineralized zone the magnetic susceptibility measurements correlate very well with the intensity of hematite alteration, suggesting that the two are connected.

### **6.3.2 Geochemical Changes**

It is difficult to track the geochemical changes related to the oxidation of magnetite to hematite. This reaction is generally conservative and iron is neither added nor removed from the system. Mass balance calculations for the CP and FP felsic

volcanic rocks within the mineralized zone show that there is a slight mass gain for iron. This means that the oxide was not conserved and was added to the system during alteration. It is difficult to determine whether this iron is used to create hematite or in the creation of secondary sodic amphibole and pyroxene grains.

Without knowing the exact stoichiometry of the sodic amphibole and pyroxene grains, it is impossible to determine if iron is a major component, and whether these grains could have formed from the alteration of minerals in the protolith, or with elements such as  $\text{Al}_2\text{O}_3$ ,  $\text{FeO}$  and  $\text{CaO}$  that were added during alteration. It does appear that hematite intensity and magnetite destruction, as measured by magnetite susceptibility correlate very well within the mineralized zone. Areas that have been intensely hematitized are almost absent of magnetite. While areas only moderately hematitized appear weakly to moderately magnetic but not as magnetic as the non-hematitized volcanic rocks. This strong correlation leads to the assumption that most, if not all of the hematite alteration is a direct result of the oxidation of magnetite.

#### **6.4 Silica Alteration**

Silica alteration is not as obvious as the other major alteration styles but it is a distinctive characteristic of the Michelin deposit. It is difficult to identify in drill core and seems to be absent in Aillik Group felsic volcanic rocks situated outside of the deposit. The alteration has only been observed within the actual mineralized zone, being only noticeable in drill core by the absence of quartz phenocrysts.

The loss of quartz seems to play an integral part to the mineralizing system at Michelin; however its exact relationship to uranium mineralization is not well understood. It appears that the dissolution of quartz, often referred to as episyenization creates space within the rock, analogous to a sponge, where alteration minerals and uranium-bearing phases form. Generally, most samples observed within the mineralized zone that are mineralized are also depleted in silica. There are however some samples depleted in silica that are not well mineralized and some samples that are not depleted in silica; these are also generally unmineralized (Figure 6.2)

The loss of silica is only limited to the main mineralized zone but this loss is not consistent throughout the entire mineralized zone. There are sections where there has been little to no silica loss. These sections are generally weakly mineralized and occur predominantly in the FP rocks of the mineralized zone, although they can also be found in the CP rocks. In the unaltered and sodic altered felsic volcanic rocks of the hanging wall and foot wall, visible quartz occurs in the form of tiny, 1-3 mm sized phenocrysts. These are easily identifiable in drill core due to their clear to white color and preferential, elongated alignment parallel with foliation. The equivalent FP and CP felsic volcanic rocks within the mineralized zone show a consistent absence of these quartz phenocrysts.

Stronger alteration intensity within the mineralized zone has caused the rock to become very friable and discolored, thereby making it difficult to identify specific minerals. This makes it difficult to identify the transition between rocks with quartz phenocrysts and those without. It is also difficult to judge whether this transition is gradual over some distance or abrupt. Absence of quartz phenocrysts seems to coincide

with the appearance of the first CP unit within the mineralized zone. Occasionally, quartz phenocrysts can be seen in some of the less-intensely altered sections of FP volcanics within the zone; however even these are difficult to identify due to the intense sodic alteration of the drill core.

#### **6.4.1 Mineralogical Changes**

Silica alteration appears to be the result of quartz dissolution within both the CP and FP felsic volcanic rocks of the mineralized zone. This involves the loss of quartz phenocrysts, as evidenced from drill core as well as loss of quartz from the groundmass. Petrographic thin section and SEM-MLA analysis indicate that quartz phenocrysts no longer exist within the CP and FP rocks of the mineralized zone.

In the mineralized zone, less altered FP rocks contain agglomerates of mafic and opaque minerals about the same shape and size as that seen for quartz phenocrysts within unaltered volcanic rocks. These agglomerates of secondary minerals appear to have formed in the space created from the dissolution of quartz phenocrysts (Plate 6.4f). The same phenomenon occurs in strongly altered CP rocks within the mineralized zone. Within these rocks, agglomerates of mafic minerals, uranium bearing phases, opaques, albite, zircon, calcite and several other mineral species as described in Chapter 5 can be found. The secondary minerals occupy space created primarily through dissolution of quartz phenocrysts as well as the finer grained, groundmass quartz.

The dissolution of quartz in the groundmass is difficult to identify in petrographic thin section (Plate 6.4e). Grains within the matrix are predominantly less than 0.1 mm in

size and appear very similar to feldspar both in plain polarized light and crossed polars. SEM-MLA analysis of thin section samples from within the mineralized zone show that most of the matrix is comprised of albite and only minor quartz (Figure 6.3). The quartz grains that made up the matrix were dissolved during alteration leaving the rock like a sponge, filled with microscopic spaces. These secondary voids within the groundmass have subsequently been filled by secondary albite, uraninite, opaque grains, sodic amphiboles and pyroxenes, and other alteration minerals.

#### **6.4.2 Geochemical Changes**

Although silica destruction is very difficult to determine from drill core, it is possible to do so with geochemistry. Both the CP and FP felsic volcanic rocks within the mineralized zone that have undergone silica dissolution show about a 10 wt. % decrease in  $\text{SiO}_2$ . This decrease is caused by the complete dissolution of quartz phenocrysts and the near complete dissolution of quartz within the groundmass.

Mass balance calculations indicate that there has been a strong mass loss for both the CP and FP felsic volcanic rocks within the mineralized zone. Both rock types give an average loss of over 15 wt. % and this mass loss can be attributed to silica dissolution.  $\text{SiO}_2$  was not conserved during alteration and most of it was removed from the system. The decrease in  $\text{SiO}_2$  would have been much greater but some of the silica was reused in the formation of secondary albite and other secondary silicate minerals, such as sodic amphiboles and pyroxenes.



SEM-MLA images show that most of the quartz has been removed from the rock (Figure 6.3). CIPW normative calculations done for samples within the mineralized zone support what is seen in the SEM-MLA images (Table 4.1); there is very little quartz remaining in the rock. Within unaltered and sodic altered felsic volcanic rocks, the CIPW norm for quartz is between 30-35 %. Inside the mineralized ore zone this percentage drops, averaging between 1-8 %.

## **6.5 Mass Balance Calculations**

Examination of the major, trace and rare earth element geochemistry for samples within the mineralized zone compared to those in unaltered host rock show that there are concentration differences for almost every element analyzed. Some of these elemental gains and losses are attributed to hydrothermal alteration but some are apparent changes attributed to closure, and changes in the mass and/or volume of the rocks during the alteration process. According to Piercey (2009) during alteration two processes occur: 1) there is a change in the size of the system, i.e. volume and/or mass; and 2) there are elemental fluxes in and out of the system during this process. This causes apparent gains or losses in concentration for elements that are conserved during alteration. This is due to the change in mass and/or volume of the system coupled with closure, as geochemical data for a sample has to sum up to 100 %. Therefore a direct comparison between altered and unaltered data is not possible. In order to accurately quantify the absolute elemental gains and losses caused by alteration a correction must be made for the mass and/or volume change of the system. The aim of the calculation is to eliminate the apparent

change in an elements concentration due to the change in mass and/or volume of the system. Once this is completed the comparison between unaltered and altered rocks can be made, and the geochemical effects of alteration can be determined.

There are several methods for calculating the mass transfer of elements in altered rocks including Gresens (1967), Grant (1986), MacLean and Barrett (1993), and Stanley and Madeisky (1996) which are all described in Appendix 3. These methods depend on the recognition of conserved, immobile elements within the system. For this study, the methods introduced by MacLean and Barrett (1993) will be utilized for mass balance calculations. The reason for this is based on its relative ease of use and the fact that it will provide the total mass change and the mass change for each element, represented as grams per 100 grams (g/100g). The single precursor method will be used in order to compare the FP felsic volcanic rocks of the mineralized zone with the unaltered FP felsic volcanic rocks. Likewise, CP felsic volcanics of the mineralized zone will be matched to their unaltered CP equivalents.

The single precursor mass transfer technique as outline by Gifkins *et al.* (2005), and Piercey (2009) first requires all geochemical data to be recalculated to volatile free. Since the LOI for each sample is relatively low, usually less than 2 %, it will not be included as part of the mass transfer calculations. Its omission is not likely to distort the data. The next step is to determine a conserved, immobile element that will be used to calculate the enrichment factor. This is achieved by constructing immobile-immobile bivariate plots for both the FP and CP felsic volcanic rocks, these plots can be found in Figure 6.4. The element that generally has the highest correlation out of all the immobile

elements is titanium, which will be used to calculate the enrichment factor (EF). Even though there is titanite present within the unaltered host rock and mineralized zone,  $\text{TiO}_2$  still correlates rather well and seems to have remained mostly conserved during alteration.

The next step is to determine the precursor sample, which is the least altered sample. The precursor sample for the FP felsic volcanic rocks is sample CMB 20164 which is from the foot wall of drill hole M06-039 and CMB 20019 for the CP felsic volcanic rocks, which is taken from the hanging wall of drill hole M06-019. Next, an enrichment factor is calculated by dividing each sample by the conserved immobile element of the precursor sample. The EF is then used to correct the altered data to remove the effects of mass and/or volume change that occurred during alteration. This is achieved by multiplying all of the elements of an altered sample, by that samples enrichment factor, equating to the reconstituted composition of the sample. Once the reconstituted composition is known the mass change for each individual element can be calculated by subtracting the original precursor sample from the reconstituted composition sample. A more comprehensive explanation of the single precursor mass transfer technique as well as the volatile free geochemical data, enrichment factor, reconstituted composition, and mass change for every sample can be found in Appendix 3.

#### **6.5.1 Mass Changes within the Mineralized Zone**

The mineralized zone is comprised primarily of two distinct but similar rock types: the CP and FP felsic volcanic rocks. Through examination the CP units seem to

have undergone a higher intensity of alteration and are generally more mineralized in comparison to the FP rocks. However, when utilizing the mass balance techniques described above it appears that for the most part both rock types experience similar elemental and mineralogical changes due to alteration. There are minor differences noted between the two units. For the elements that are not conserved during alteration, the mass loss or gain is generally greater in the CP rocks; mostly due to the fact that they have undergone a greater intensity of alteration. Also, there are elemental differences between the two units, particularly so with the volatile elements, whereby an element in one rock type is conserved while in the other it is mobile.

It should be noted that there are a few samples, mostly within the CP rocks that have higher than average mass gains in nearly every element. This is because initial  $\text{TiO}_2$  values for those samples are initially low, well below the precursor samples. Therefore the enrichment factor for these samples is over one. This will lead to some samples showing a mass gain when they actually experience a mass loss during alteration. False values resulting from mass balance calculations must be taken into consideration at all times and data must be examined with caution in order to account for erroneous interpretations, as they will change the overall mass change average of an element.

#### **6.5.1.1 Major Oxides**

The total mass change for both the CP and FP rocks is near identical, with both being strongly negative, giving totals of -14.7 and -15.7, respectively. The high negative total indicates that both rocks types experienced a high percentage of mass loss during

alteration within the mineralized zone. Most of this mass loss for both rock types can be attributed to  $\text{SiO}_2$ . Bar graphs displaying the total mass change and the mass change for each major oxide can be found in Figure 6.5, and mass change values can be found in Table 6.1. The mass change for  $\text{SiO}_2$  is greatest out of all the oxides and is strongly negative, suggesting that  $\text{SiO}_2$  was removed from the mineralized zone during alteration. The CP and FP rocks average -16.1 and -18.2, respectively. This large mass loss is attributed to the dissolution of quartz within the mineralized zone. The majority of samples within the mineralized zone exhibited a large mass loss for  $\text{SiO}_2$ ; these samples correspond to samples which assay  $\text{SiO}_2$  percentages in the mid 60's. There are some samples from the mineralized zone that either had a very small mass loss or a slight mass gain. These samples correspond to parts of the mineralized zone that have not been intensely altered, where quartz has not been dissolved. These samples assay  $\text{SiO}_2$  with a percentage in the low 70's, close to the average value for unaltered felsic volcanic rocks. There are a couple of samples that showed very high mass gains in  $\text{SiO}_2$ . This can be attributed to a low amount of  $\text{TiO}_2$  in the sample and therefore a high enrichment factor. These samples in fact should have had a mass loss as they returned assay values for  $\text{SiO}_2$  in the mid 60's.

The major oxides  $\text{Al}_2\text{O}_3$ ,  $\text{FeO}$ , and  $\text{CaO}$  all give a slight mass gain during alteration of the mineralized zone for both the CP and FP felsic volcanic rocks.  $\text{Al}_2\text{O}_3$  experiences a mass gain of 0.74 and 1.7 respectively for the CP and FP rocks. The change for  $\text{FeO}$  and  $\text{CaO}$  are both less than 1, giving values of 0.43 and 0.58 respectively for the CP rocks and 0.34 and 0.49 respectively for the FP rocks. The mass gain for each oxide

attributed to alteration is mostly a factor of the secondary minerals like albite, calcite, sodic pyroxene and amphibole which formed during alteration.

There is zero mass change in both the CP and FP rock types for the major oxides MgO, MnO, and P<sub>2</sub>O<sub>5</sub>. All three of these oxides were conserved during alteration, with all samples returning mass change values close to zero. The loss on ignition value was also very close to zero, particularly within the FP rocks. The CP rocks experienced a slight mass gain, giving an average of 0.91. This is most likely attributed to the higher alteration intensity affecting the CP rocks.

Finally, the remaining two major oxides, Na<sub>2</sub>O and K<sub>2</sub>O have relatively consistent mass change values for each sample in both the CP and FP felsic volcanics. This is especially true for K<sub>2</sub>O which respectively has an average mass loss of -5.2 and -5.0 in the CP and FP volcanics. This consistent mass loss is not surprising and is attributed to the complete removal of potassium from both rock types during sodic metasomatism. Na<sub>2</sub>O is the exact opposite and experiences a mass gain, averaging 4.8 and 4.8, respectively, for the CP and FP volcanics within the mineralized zone. All samples for Na<sub>2</sub>O experienced mass gains, with some samples having a very high mass gain. The mass gain for sodium is attributed to the sodic alteration of the rocks at Michelin.

#### **6.5.1.2 Trace Elements**

For both the CP and FP felsic volcanics, trace elements display almost the exact same mass change for each element. The only difference between the two is with Sr and Pb. Bar plots displaying the mass change for both the LFSE and HFSE can be found in

Figure 6.6, and the mass change values for each element can be found in Table 6.1. For the LFSE, Ba has a large mass loss in both the CP and FP rocks, averaging -894.1 and -679.6, respectively. The large mass loss for Ba indicates that it was not conserved during alteration and that a lot of barium, most likely in the form of barite was removed from the mineralized zone. Not all of the Ba was removed however, as SEM-MLA analysis of some samples from the mineralized zone contained Sr-rich Ba. These analyses are from the FP rocks and can be used to explain why the mass loss for Ba was much less than that seen in the CP rocks, as no CP rocks analyzed with the SEM-MLA contained barite. This could also explain the mass gain of 30 for strontium within the FP rocks; while the CP samples had almost no mass change in strontium, averaging 1.52.

The other trace element besides Sr that has a different mass change between the two rock types is Pb. FP rocks have a weak Pb mass gain with an average of 4.3. The CP volcanics have a moderate mass loss, averaging -76.2. Samples analyzed with the SEM-MLA indicate that FP samples from the mineralized zone contain galena, while most of the CP samples analyzed contain little to no galena.

Rb has a consistent strong mass loss for all samples, averaging -145.0 and -134.1, respectively, for the CP and FP volcanics. This strong mass loss is attributed to the fact that  $\text{Rb}^+$  commonly substitutes for  $\text{K}^+$  in potassium feldspar, and therefore was removed along with potassium during sodic metasomatism of the rocks. U experiences a very large mass gain for both rock types within the mineralized zone. Both rock types have a mass gain of over 1,200 and this is attributed to uranium mineralization. Individual samples are mixed within the mineralized zone as most samples have a very large mass gain while

some have a low mass gain. There seems to be a strong correlation with samples that experience a mass loss in  $\text{SiO}_2$ , most of these samples have a strong mass gain in U. Finally, Cs, Ga and Th are relatively conserved during alteration of the mineralized zone. For each element, both rock types show almost no mass change.

For the most part, HFSE display a mass gain during alteration of the mineralized zone. This gain is attributed to the formation of new, secondary minerals such as zircon, allanite, monazite, uraninite and brannerite within the mineralized zone. Of all the HFSE, Zr experiences the greatest mass gain, averaging 372.7 and 228.9, respectively, for the CP and FP volcanics. This mass gain is attributed to the abundance of zircon found in the mineralized zone, especially within the CP rocks. Y also experiences a mass gain during alteration, indicating that it too was not conserved during alteration. The element was added to the system, most likely during the formation of allanite grains, or possibly garnets within the mineralized zone. The CP volcanics have an average mass gain of 57.6 while the FP volcanics have a smaller mass gain, averaging only 30.6. Nb also has a relatively small mass gain of 14.2 and 11.1, respectively, for the CP and FP volcanics within the mineralized zone. SEM-MLA analysis indicates that Nb is associated with brannerite grains, as these have a high Nb content. The final two HFSE, Hf and Ta, both experience almost no mass change and appear to be conserved in both rock types during alteration.



### 6.5.1.3 Rare Earth Elements

The rare earth elements display almost identical mass change patterns for both the CP and FP felsic volcanic rocks within the mineralized zone. Most of the REE exhibit mass gains or are conserved during alteration, none display a mass loss. It is interesting to note that every second REE, when examining from lightest to heaviest in atomic weight has an increase in mass change. These same elements have an overall higher concentration within the rock. This is mostly likely due to the Oddo-Harkins effect where elements with even atomic numbers are more abundant than elements with odd atomic numbers (Faure, 1998). The higher concentration may explain the higher mass gain for these elements. Bar plots displaying the mass change for each element can be found in Figure 6.7 and mass change values can be found in Table 6.1.

The Light REE display the greatest amount of mass change of all the REE. Each LREE has a moderate to strong mass gain, indicating that these elements were not conserved during alteration, and were added to the system. These LREE elements occur in secondary minerals like allanite and monazite which formed during alteration. The mass gain for each LREE, except for Nd, is generally the same in both the CP and FP felsic volcanics. CP rocks have a greater mass gain for Nd averaging 47.8, in comparison to 31.7 for the FP rocks. It is possible that this increase in Nd is caused by an Nd-rich monazite found mostly within the CP rocks. Further microprobe work would be needed to test this idea. Both the Middle REE and Heavy REE were very similar and had very little mass change during alteration. The slight mass change could be attributed to the extremely sporadic presence of garnets within the ore zone.

#### 6.5.1.4 Volatile Elements

The volatile elements display the biggest differences between CP and FP felsic rocks. There are several similarities between the two rock types but there are a few elements that behaved differently during alteration. Bar plots displaying the mass change for each volatile element can be found in Figure 6.8 and the mass change for each element can be found in Table 6.1. Several of the volatile elements, for instance, Ag, Ge, In, Mo and W remain relatively conserved during alteration.

Both As and Be experience mass gains within the mineralized zone. These gains are consistent for both rock types and would suggest that these elements were added during alteration. It is uncertain if these elements are associated with one of the secondary minerals that formed during alteration or are part of their own alteration halo. Tl is also consistent between the two rock types but experiences a mass loss during alteration. The mass loss is almost exactly the same for each sample and seems to suggest that almost all of the Tl was removed from the host rocks during alteration. Thallium in the form of  $Tl^+$  is rather mobile during alteration and will substitute for  $K^+$  in potassium feldspar (Gomez-Gonzalez, 2015). This would explain why almost all of the Tl, likewise Rb and  $K_2O$  were removed from the rock during sodic metasomatism.

The main differences between the CP and FP rocks are with the elements Bi, Sn, and Sb. During alteration these elements are generally conserved in one rock type but are either added or removed from the other rock type. Bi is relatively conserved during alteration within the FP volcanics. For the CP rocks however, Bi is not conserved and experiences a high mass loss, indicating the element was stripped from the rock during

alteration. The mass loss for the element averages -10.7 and all samples have a consistent value for mass loss. Why bismuth is stripped from the CP rocks while remaining in the FP rocks is unknown. It could be that the CP rocks are generally more intensely altered. Sb has the exact opposite effect, it is generally conserved during alteration within the CP rocks but is removed from the FP rocks during alteration. FP rocks average a mass loss of -5.7 for Sb and all samples have a consistent mass loss. It seems that the element was completely stripped from the FP rocks, but it is uncertain why this did not happen with the CP rocks during alteration. Finally, Sn is the only element that has a mixed effect where it was added to one rock type but removed from the other rock type during alteration. The FP rocks are generally stripped of Sn during alteration, with most samples having a mass loss. There are a few samples that experience a mass gain, raising the average to near zero but these are attributed to a high enrichment factor. However, within the CP rocks, Sn appears to be added to the system during alteration.

### **6.5.2 Mass Changes within the Sodic Alteration Envelope**

The sodic alteration envelope, as described in section 6.2 appears to be the extent of the altering fluids within the Michelin system. Alteration inside of this envelope is not as intense as the alteration within the mineralized zone but there are still geochemical and mineralogical changes that take place. For the most part, geochemical analyses of samples from within the sodic envelope appear to be consistent with that of the unaltered host rocks, with the notable exception of a few elements. In order to accurately determine the geochemical effects of alteration within the sodic envelope a mass balance calculation

was completed on samples inside the sodic envelope, but excluding samples from within the mineralized zone. FP felsic volcanic rocks make up most of the host rock within the sodic envelope so only samples from that unit were used for the mass balance calculations. Examining the mass balance data for these rocks reveals the obvious elemental changes that are observed from the sodic metasomatism but there are also a few other elemental changes that are the result of alteration. Due to the lower intensity of alteration within the sodic envelope more of the elements remain conserved during alteration, and the elements that are mobile have generally not experienced a mass loss or gain as great as within the mineralized zone.

#### **6.5.2.1 Major Oxides**

The total mass change for the FP felsic volcanic rocks within the sodic envelope is moderately negative having an average mass loss of -9.6. This indicates that the rocks lost mass during alteration; however the total mass change is not representative of alteration of the rocks within the sodic alteration envelope. Most of the mass loss of the rocks is attributed to  $\text{SiO}_2$ , which has an average mass loss of -7.2. However, the mass change for  $\text{SiO}_2$  and to a lesser extent  $\text{Al}_2\text{O}_3$  which has an average mass loss of -0.91 are a misrepresentation of the actual mass change within the rock. They are actually a product of the initial amount of quartz and feldspar within the host rock. Unaltered FP rocks have a range in  $\text{SiO}_2$  content from 71.4 to 77.6 wt. % and a range in  $\text{Al}_2\text{O}_3$  of 11.5 to 12.9 wt. %. The least altered sample chosen for the mass balance calculations had an average value for both oxides near the middle of the range in wt. %. Therefore there are a

number of samples below and above the average value. This generates a lot of mass gains and mass losses for samples even though there was actually no change at all due to alteration. It is possible that there may be a slight mass loss of  $\text{SiO}_2$  due to alteration but the change in mass loss is most likely due to the original  $\text{SiO}_2$  content of each sample being lower than the precursor.

A bar graph displaying the total mass change and the mass change for each major oxide can be found in Figure 6.9, and the value of each mass change can be found in Table 6.1. For most of the other major oxides,  $\text{FeO}$ ,  $\text{MgO}$ ,  $\text{MnO}$ ,  $\text{CaO}$ , and  $\text{P}_2\text{O}_5$  there is little to no mass change during alteration. All of the oxides appear to be conserved during the alteration within the sodic envelope. The same can be said for loss of ignition which also remains conserved and has little to no mass change.

$\text{K}_2\text{O}$  and  $\text{Na}_2\text{O}$  are the only two major oxides that experience a mass change during sodic alteration and it is directly attributed to sodic metasomatism where potassium feldspar is converted to albite.  $\text{K}_2\text{O}$  has a mass loss of -4.6 and appears to have been completely removed from the rocks during alteration. This mass change is very similar to mass loss experienced by the rocks within the mineralized zone indicating that potassium is nearly completely removed during the early stages of sodic alteration. Within the sodic envelope  $\text{Na}_2\text{O}$  has an average mass gain of 3.0, attributed to a  $\text{Na}^+$  rich solution. The average mass change within the sodic envelope is lower than that within the mineralized zone indicating the sodic alteration intensifies in the mineralized zone with the formation of sodic amphiboles, pyroxenes and secondary albite.

#### 6.5.2.2 Trace Elements

The majority of the trace elements remain conserved during alteration within the sodic envelope. The mass change for each trace element can be found in Table 6.1 and a bar graph displaying the mass change can be found in Figure 6.10. For the most part the LFSE have similar mass changes, which are caused by alteration, as within the mineralized zone. The elements Cs, Ga, and Th all display little to no mass change, remaining relatively conserved during the alteration within the sodic envelope. Likewise, Rb has a consistent mass loss, averaging -124.5. This loss is consistent with each sample and suggests the complete removal of the element during alteration. Like in the mineralized zone the mass loss is attributed to  $\text{Rb}^+$  substituting for  $\text{K}^+$  in potassium feldspar grains and when  $\text{K}_2\text{O}$  was removed from the system during sodic metasomatism so was Rb.

Within the sodic envelope Ba has an average mass gain of 53.9. This average is not consistent between individual samples, as some samples experience mass gains while others experience a mass loss during alteration. Barite occurs sporadically throughout the deposit therefore some samples will have more barite and thus an apparent mass gain and vice versa. Sr has an average mass gain of 23.6, and nearly all samples experience a mass gain in the element, whether it be small or large. It appears that Sr was added to the system during the alteration of FP rocks within the sodic envelope. Sr was also a mass gain in FP rocks of the mineralized zone, averaging a mass gain close to 30. It is possible that the mass gain in both the sodic envelope and mineralized zone is attributed to a low

Sr concentration in the original precursor sample and that the element was actually conserved during alteration, or from Sr substituting for Na<sub>2</sub>O within albite.

Within the sodic envelope U has a strong mass gain, averaging 176.1. This is caused by the mineralization of some samples; and one strongly mineralized sample. Most unmineralized samples show little to no mass change in U. Finally, Pb is a mixture of samples that experienced a mass loss and ones that experienced a mass gain. It appears that these gains and losses are more to do with the original amount of galena in each sample and not alteration, indicating that galena was most likely conserved during the alteration of the sodic envelope.

For the HFES, Hf, Nb, Ta, and Y display relatively no mass change at all within the sodic envelope. These elements appear to be conserved during sodic alteration indicating that the secondary minerals formed in the mineralized zone, brannerite and allanite did not form during the lower intensity alteration within the sodic envelope. Zr however displays a moderate mass loss, averaging -27.1. All samples express a mass loss for the element, some strongly negative and others only slightly. Zirconium appears to have been removed from the FP rocks within the sodic envelope, a contrast to the mass gains within the mineralized zone due to the formation of secondary zircon grains. It is possible that the Zr removed from the felsic volcanic rocks within the sodic envelope was the source of Zr for the formation of secondary zircons within the mineralized zone.

### **6.5.2.3 Rare Earth Elements**

The REE are mostly conserved within the sodic envelope, in particular the MREE and the HREE. The LREE do exhibit a slight mass change, in particular La and Ce. These two LREE display a modest mass gain, similar to the mass change of the felsic volcanic rocks of the mineralized zone. However, the LREE Pr and Nd display a modest mass loss, which is the opposite of the mass change exhibited by the felsic volcanic rocks of the mineralized zone. This is most likely due to the presence of an alteration mineral present in both the sodic envelope and mineralized zone that contains the elements La and Ce and another element that contains Pr and Nd only being present within the ore zone, and these elements were stripped from the rocks in a similar fashion as zirconium.

The MREE and HREE display almost no mass change, remaining generally conserved during alteration within the sodic envelope. The Otto-Harkins effect is apparent again with these elements as the even atomic numbered elements have a slightly higher mass change than the odd numbered elements. This is attributed to the even numbered elements having a higher concentration in the original FP rock. The mass change for each rare earth element can be found in Table 6.1 and a bar graph displaying the mass change can be found in Figure 6.11.

### **6.5.2.4 Volatile Elements**

The mass changes observed of the volatile elements within the FP rocks of the sodic envelope are not as severe as the mass changes within equivalent rocks within the mineralized zone. The mass change for each volatile element can be found in Table 6.1



and a bar graph displaying the mass change can be found in Figure 6.12. The elements As, Be, Bi, Ge, In, Mo and W all appear to have been conserved during alteration and exhibit little to no mass change.

The elements Ag, Sb, Sn, and Tl all display nearly consistent mass losses for all samples for each element. None of these elements appear to be conserved during alteration, being removed from the FP rocks during alteration within the sodic envelope. Sb and Tl show consistency with the altered FP rocks of the mineralized zone, which also had complete removal of these elements. Tl was most likely removed during sodic metasomatism as  $\text{Tl}^+$  substitutes for  $\text{K}^+$  in potassium feldspar. It is unknown why Sb has been completely removed from the system; it could be the result of its own elemental halo caused by the altering fluids. Ag and Sn display similar results as most samples display mass losses and appear to have been completely removed from the rocks. However, there are some samples that have large mass gains, indicating that these samples have minor amounts of either Ag or Sn mineralization.

## **6.6 Other Alteration Styles**

### **6.6.1 Calcite Alteration**

Calcite commonly occurs throughout the felsic volcanic rocks of the Michelin deposit, most often occurring in the form of tiny disseminations within the groundmass or as thin, millimeter wide concordant veinlets. There does not seem to be an increase in the amount of calcite within the sodic alteration envelope compared to unaltered rocks

outside of the envelope. There may be a slight increase observed in drill core but this increase is unidentifiably in geochemistry.

Within the mineralized zone the content of calcite does increase, significantly in some places. The addition of the mineral appears to be a result of alteration of the mineralized zone. It is commonly associated with uranium mineralization but does not appear to be directly related to uranium mineralization. There are plenty of mineralized samples within the ore zone that contain little to no calcite. The mineral occurs within both the FP and CP rock types but is more commonly associated with the CP felsic volcanics, in particular one unit that is strongly deformed (Plate 5.1h).

This particular unit of CP felsic volcanic appears to be more intensely altered than the other units within the mineralized zone. It contains intense hematite alteration, strong mineralization and is highly deformed. Large albite phenocrysts within the unit have been strongly augened by thin wisps of secondary alteration minerals, mostly in the form of sodic pyroxenes and to a lesser extend sodic amphiboles. This unit contains an abundance of calcite, generally occurring within the pressure shadows of the augened phenocrysts. Calcite also occurs within the matrix, and is associated with the larger aggregates of sodic minerals, opaque grains, zircon, titanite, and uranium mineralization.

Mass balance calculations from the mineralized zone indicate that there is a slight mass gain of CaO. This could be attributed through the formation of calcite, along with possibly some of the other alteration minerals. There are a few individual samples that have a larger mass gain of CaO than the others, some are attributed to a high enrichment factor but some are caused by the increase in calcite in the sample.

The fact that calcite fills the pressure shadows created from the augened albite phenocrysts would suggest that the influx of calcite is a later stage of alteration. This is supported by the fact that calcite alteration is focused within the mineralized zone, and does not seem to extend to the sodic envelope and secondary calcite forms in the groundmass and with other secondary alteration minerals in space created from the dissolution of quartz. All of this evidence would suggest that calcite alteration occurred late during the alteration history of the Michelin deposit.

#### **6.6.2 Garnet Alteration**

Garnets occur throughout the felsic volcanic rocks of the Michelin deposit, both within the hanging wall and foot wall as well as the ore zone of the deposit. Their occurrence seems to increase in all directions moving towards the mineralized zone but it is unknown whether they occur as an alteration style or are just part of the rock, most likely an effect of metamorphism.

Outside of the mineralized zone garnets generally occur in stringers, or veinlets that are concordant with the foliation. They commonly occur with epidote, which usually completely coats the garnets, leaving them greenish in color and moderately soft, in drill core. There is also commonly actinolite, chlorite, biotite and minor calcite associated with these stringers. These garnet stringers are commonly concentrated in groups but their frequency is sporadic throughout the hanging wall and foot wall. The majority of these stringers are located outside the extent of the sodic alteration envelope, but they do occur within the sodic envelope and mineralized zone.

SEM-MLA analysis of samples from within the mineralized zone indicates the presence of andradite, a calcium-iron garnet. Andradite garnets were also identified by Ross (2006) from the SEM-MLA analysis of two samples from within the mineralized zone. The study indicated that the garnets did not contain significant amounts of uraninite inclusions despite the fact that both samples were highly mineralized. The relationship between uranium mineralization and the garnets is unknown but they do not appear to be associated with each other, outside of the fact that they both occur within the mineralized zone. The frequency of garnet within the mineralized zone is no greater than that within the unaltered hanging wall or foot wall, and most of the samples analyzed by SEM-MLA contained no garnets at all.

This evidence would suggest that the formation of garnet is not related to mineralization or the altering fluids. They occur well outside the sodic alteration envelope in both the hanging wall and foot wall. All evidence seems to suggest that the sodic envelope is the extent of the altering fluids. This would suggest that the formation of garnets is a metamorphic effect, and the epidote coating is most likely a retrograde alteration along the rims of the mineral. According to the Ross (2006) report the garnets appear to be later in timing, and a retrograde overprint on the peak metamorphic assemblage of pyroxene and amphibole, possibly reflecting a second metamorphic pulse.

### **6.6.3 Other Possible Alteration Halos**

Throughout the deposit the occurrence of barite, fluorite, and gypsum are common to the felsic volcanic rocks of the hanging wall, foot wall and to a lesser extent

mineralized zone. It is uncertain if these minerals are the result of alteration or are just part of the original composition of the volcanic rocks. None of these minerals appear to create or form alteration halos around the deposit, and their occurrence does not appear to increase or decrease moving towards the mineralized zone. For the most part these minerals occur in the form of thin, millimeter wide veinlets that are concordant with the foliation. Although these minerals most likely formed as secondary minerals they do not seem to have formed as a result of the alteration associated with the mineralizing system at Michelin. Their occurrence is most likely a result of metamorphism of the Aillik Group rocks, or from the intrusion of a granitoid body.

Out of the three minerals barite is the only one known for certain to occur within the mineralized zone. Sr-rich barite has been identified in several samples from the mineralized zone, particularly in the FP volcanics. However, its concentration changes from sample to sample, indicating that the barite in the mineralized zone is most likely not a factor of alteration but just a part of the original composition of the rock. The same pattern occurs in unaltered samples where some are rich in Ba and some samples, even though they are only 10-15 m apart are Ba poor.

## **6.7 Alteration of the Mafic Dikes**

Mafic dikes are a common occurrence throughout the Michelin deposit, with several different varieties intruding throughout the hanging wall, foot wall and ore zone. Despite the fact that numerous dikes intrude through the sodic alteration envelope and mineralized zone these dikes do not display visible effects of alteration, as the felsic

volcanic rocks display. Therefore it is difficult to determine whether these dikes have been affected by the altering fluids, or if the lack of visible alteration is due to the mineralogical differences between the mafic dikes and felsic volcanic rocks, or if the dikes intruded after alteration occurred.

In order to accurately determine whether the mafic dikes have been affected by the altering fluids the geochemistry of the dikes must be used to identify any elemental differences that are common to the several different alteration styles at Michelin. There are difficulties with this however as there is a very small sample size of mafic dikes from within the sodic envelope and mineralized zone. Only five samples from within the sodic envelope were collected for this thesis study, and no samples were collected from inside the mineralized zone. All of the mafic dikes within the mineralized zone have been sampled over during the initial exploration program. Most dikes are very small and were not broken out during sampling; however some were large enough to be broken out as single samples. The pulps of these samples were reanalyzed for trace element analysis, but it appears that most contain contamination from the mineralized felsic volcanic host rocks. Several of the dike samples contained an elevated uranium concentration. However, mafic dikes within the ore zone appear to be unmineralized and consistently give very low scintilometer readings. The samples that appear to be affected by contamination were discarded as best possible.

The geochemical evidence from the dikes within the sodic envelope and mineralized zone suggest that at least some of the dikes have been affected by the altering fluids, showing similar, but not as drastic, elemental changes as experienced by the felsic

volcanic host rocks; this mostly consists of sodic enrichment. For the mafic dike samples within the mineralized zone no petrographic thin sections were collected, therefore petrographic and SEM-MLA analysis could not be performed. To precisely characterize the alteration of the mafic dikes future work, including detailed, precise sampling and SEM-MLA analysis would be needed to determine if and to what intensity the mafic dikes have been altered.

#### **6.7.1 Alteration of Mafic Dikes within the Sodic Envelope**

A total of five mafic dikes from within the sodic envelope were sampled; including one sample of the pre-kinematic biotite-hornblende schists dike; two samples of the syn-kinematic gabbroic dikes; and two samples of post-kinematic intermediate dikes. Obviously this is a very small sample size to use for a concrete interpretation but the samples do show interesting results, most likely relating to alteration.

The one sample of pre-kinematic dike does appear to have been affected by sodic alteration. For this sample there is an approximate 1 % increase in Na<sub>2</sub>O content and an approximate 1 % decrease in K<sub>2</sub>O content, in comparison to the average composition of the pre-kinematic biotite-hornblende schists. This sample also has the highest concentration of Na<sub>2</sub>O, approximately 0.75 % greater than any other samples, and has the lowest concentration of K<sub>2</sub>O, approximately 0.25 % less than any other sample. The samples also had apparent depletion in the concentration of Rb and Tl, as their respective concentrations were lower than every other sample. As seen in the felsic volcanic rocks these two elements are closely associated with K<sub>2</sub>O as they commonly substitute for the

oxide. There are no other apparent changes in concentration for the other major oxides or trace elements.

These dikes contain an abundance of biotite and it is possible that there was a transfer of  $K^+$  ion in biotite for  $Na^+$  ions from the altering fluids, or altered them to sodic amphiboles. This would be similar to the alteration of the mafic minerals within the felsic volcanics. These dikes do not contain the same mineralogy as the host volcanics and contain no potassium feldspar therefore alteration is not as severe. It is obvious that the dikes were not as strongly affected by alteration as not all of the  $K_2O$  was removed from the dike like in the volcanic rocks. No SEM-MLA analysis was completed on this sample so the mineralogical changes due to alteration cannot be identified. Examination of the petrographic thin section gives no difference between this altered dike and the unaltered dikes. The only difference, which is most likely a result of alteration, is in the geochemistry.

The two syn-kinematic dike samples display almost no difference in the major oxide and trace element concentration when compared to unaltered samples outside of the sodic envelope. These two samples are only slightly elevated in  $Na_2O$  content, when compared to the average composition for these dikes. However, the sample with the highest concentration of  $Na_2O$  is only 0.20 % greater than samples located outside of the sodic envelope. Therefore it is possible that elevated sodium content is a factor of the dikes original composition and not due to alteration. These two samples display almost no difference in  $K_2O$  content, the same for the trace elements Rb and Tl. These elements are within the average compositional range for unaltered syn-kinematic dikes; it appears



that these elements have not been removed during alteration. All other major oxides and trace elements are within average compositional range for the dike variety.

Finally, the two post-kinematic dikes display no effects related to alteration. The major oxide and trace element composition for these two samples are within the average compositional range for dikes located outside of the sodic envelope.

### **6.7.2 Alteration of Mafic Dikes within the Mineralized Zone**

Pre-kinematic biotite-hornblende schists are common within the mineralized zone, and there are several samples of the dike where the geochemistry display signs of alteration, but not as intense as the alteration affecting the felsic volcanic host rocks within the mineralized zone. When compared to the average composition of pre-kinematic dikes outside of the alteration zone the pre-kinematic dikes within the mineralized zone have a much greater  $\text{Na}_2\text{O}$  content, averaging 4.9 % and ranges between 4-6 %. This is an almost half a percent increase in the  $\text{Na}_2\text{O}$  content of the pre-kinematic dike located within the sodic envelope. Indicating that sodic alteration is more intense within the mineralized zone, the felsic volcanic rocks were also more intensely sodic altered within the mineralized zone.

The sodic alteration appears to not be a result of the replacement of  $\text{K}^+$  for  $\text{Na}^+$ . The average  $\text{K}_2\text{O}$  content for the pre-kinematic dikes within the mineralized zone is approximately 1.4 %, and ranges between 1-2 %. This is only approximately half a percent lower than the unaltered average; most samples are actually higher in  $\text{K}_2\text{O}$  than the pre-kinematic dike sample from the sodic envelope. The trace elements Rb and Tl,

which have been completely removed from the felsic volcanic rocks as a result of alteration, also fall within the average compositional range as unaltered samples.

It appears that some of the other major oxides have also been affected by alteration, as these dikes average an approximate 1 % decrease in CaO, a 1.5 % decrease in MgO, and a 2 % decrease in FeO, they also have an approximate 1 % increase in Al<sub>2</sub>O<sub>3</sub>. For the most part the trace elements remain unchanged during alteration, with the only exceptions being Th and Pb. Both of these elements have an increased concentration within the dikes, but this could be result of contamination from felsic volcanic material.

The syn-kinematic dikes are also common throughout the mineralized zone and appear to only have minor effects related to alteration. Similar to the samples located within the sodic envelope, samples within the mineralized zone exhibit a sodic enrichment, but much more pronounced. These dikes average 4.25 % Na<sub>2</sub>O, ranging from 3.5-5.5 %. This is an almost 1.3 % increase in Na<sub>2</sub>O concentration over the average composition of unaltered samples. There is however no decrease in the potassium content. K<sub>2</sub>O averages 1.3 % for samples within the mineralized zone. This value is slightly higher than the compositional average for the unaltered syn-kinematic dikes. There is a slight, 0.5 % decrease in CaO, but the remaining major oxides remain unchanged and their values are consistent with the compositional average of these dikes outside of the alteration zone. With the exception of Zr and Pb, which have slightly elevated concentrations within the mineralized zone, all other trace element concentrations remain unchanged and unaffected by alteration.

### 6.7.3 Interpretation of Mafic Dike Alteration

Geochemical evidence suggests that the pre-kinematic biotite-hornblende schists have undergone similar, but not as intense, alteration as the felsic volcanic host rocks. If these dikes were emplaced before the onset of sodic alteration it would make sense that the dikes would also be affected by the pervasive, altering fluid. These dikes have been affected by less intense sodic alteration within the sodic envelope and a more intense sodic alteration within the mineralized zone. This would explain the increase of  $\text{Na}_2\text{O}$  within the mineralized zone without the further deletion of  $\text{K}_2\text{O}$ . Secondary, sodium bearing minerals are forming within the mineralized zone similar to the felsic volcanic host rocks. It is also likely that within the mineralized zone calcium rich plagioclase is altering to albite. This would explain the decrease in  $\text{CaO}$  content. The feldspar grains are most likely easier to alter, explaining why most of the  $\text{K}_2\text{O}$ , which is in the biotite grains remains in the dike.

The formation of secondary albite could explain the increase in both  $\text{Na}_2\text{O}$  and  $\text{Al}_2\text{O}_3$ . The loss of  $\text{CaO}$ ,  $\text{MgO}$  and  $\text{FeO}$  could have transferred to the felsic volcanic rocks, used in the formation of secondary alteration minerals such as sodic amphiboles, sodic pyroxenes, calcite etc. The dikes have not been affected by the other alteration styles simply as a result of the dikes mineralogy. These dikes contain little to no free quartz. Therefore there would be little to no open space created within these dikes for secondary alteration minerals to form like within the felsic volcanic rocks. These dikes are also almost absent in magnetite content. Hematite is formed by the oxidation of magnetite, therefore there would be no hematite alteration associated with these mafic

dikes. Hematite alteration is also related to uranium mineralization, so if the dikes contained no hematitic alteration and no open space for secondary minerals to form they would stay unmineralized.

Geochemical evidence also suggests that the syn-kinematic dikes have been altered, but not to the intensity as the pre-kinematic dikes. These dikes have undergone a sodic enrichment, particularly within the mineralized zone. This is on par with the felsic volcanic rocks and pre-kinematic dikes which have a greater intensity of sodic alteration within the mineralized zone. The enrichment of  $\text{Na}_2\text{O}$  is not at the replacement of  $\text{K}_2\text{O}$ , more than likely it is at the replacement of  $\text{CaO}$ .  $\text{Ca}^{2+}$  has been removed from calcium rich plagioclase and replaced with  $\text{Na}^+$  to form albite. Secondary albite most likely also formed as well as the formation of sodic amphiboles.

The emplacement of these dikes creates a unique effect in the adjacent felsic volcanics, creating strong hematization and mineralization within the volcanics, but not within the syn-kinematic dikes. This effect, combined with the fact that  $\text{K}_2\text{O}$  has not been removed from the system would suggest that the syn-kinematic dikes intruded into the system during the latter stages of alteration. At this stage most of the mineralization has formed, some of it was remobilized during the emplacement of the dikes. There was still ongoing sodic alteration which affected these dikes. This would explain why they are sodic altered in the mineralized zone but not in the sodic envelope and why they are not as strongly sodic altered as the pre-kinematic dikes.

These dikes also contain little to no quartz and magnetite indicating that they would not become hematitized and there would be no open space created for the

formation of secondary alteration minerals and uranium bearing minerals like in the felsic volcanic rocks. This would explain why these dikes remain unmineralized.

## **6.8 Elemental Alteration Halos**

The alteration finger print of the Michelin deposit is quite extensive, reaching just over 150 m thick in places. This extensive reach would provide an excellent exploration tool to identify other “Michelin style” deposits throughout the Aillik Group felsic volcanic rocks. Elemental halos, which have an extensive reach would be the best for this, especially if they could easily be identified in geochemical analysis or portable XRF analysis of rocks that might not show the visible signs of alteration. Therefore it is important to identify elemental alteration halos that envelope the deposit. The further this alteration envelope is away from the deposit the better for alteration.

Down hole geochemical analysis indicates that the altering fluids that affect the Michelin deposit only extend as far as the sodic alteration envelope. There are several elemental halos that are easily identifiable to this position but none in the unaltered felsic volcanic host rock. There are some elemental changes beyond the sodic alteration envelope but none of these are consistent between samples to be real elemental halos related to alteration. The elemental halos that exist within the sodic envelope are sodium and potassium. The replacement of  $\text{Na}^+$  for  $\text{K}^+$  in rocks is rather abrupt and at the very start of the onset of sodic alteration the  $\text{K}_2\text{O}$  content has decreased to near zero. This would be the best alteration precursor to a Michelin like deposit within the vicinity. Potassium is also a fairly heavy oxide and is easily detected with a handheld portable

XRF analyzer making alteration exploration relatively easy and extremely quick. The increase in  $\text{Na}_2\text{O}$  is not as extensive as the decrease in  $\text{K}_2\text{O}$  and sodium is a lighter oxide and some portable XRF analyzers are not capable of identifying it.

There is also the change with a few trace elements, and similar to the change in sodium and potassium the change for these elements occurs almost instantly at the onset of sodic alteration. Most of these are directly related to the loss of  $\text{K}_2\text{O}$  but for some there is no direct association and their concentration change most likely represents a separate elemental alteration halo. The trace element with the most noticeable change is Rb. The concentration of Rb drops drastically corresponding to the beginning of sodic alteration. Its concentration goes from approximately 150 ppm in unaltered rocks to approximately 1-3 ppm as sodic alteration begins. The decrease in Rb correlates very well with the decrease in  $\text{K}_2\text{O}$  and is attributed to the fact that  $\text{Rb}^+$  commonly substitutes for  $\text{K}^+$  in potassium feldspar.

Similar to the effect seen by potassium and Rb, Tl also decreases in concentration at the onset of sodic alteration. In unaltered rocks Tl averages approximately 0.8 ppm. It decreases to under 0.1 ppm throughout the sodic alteration envelope and mineralized zone. The abrupt change is evident as Tl goes from 1 ppm to below trace levels within the 10 m that alteration begins and from 0.025 to 0.71 ppm within the 10 m that the alteration envelope ends. Similar Rb the decrease in Tl is attributed to  $\text{Tl}^+$  substituting for  $\text{K}^+$  in potassium feldspar.

The other elemental change which corresponds with the onset of sodic alteration is the volatile element Be. Be increases at the onset of sodic alteration. In unaltered rocks

the Be concentration averages approximately 3 ppm, it doubles in concentration to 6 ppm within the 10 m that sodic alteration begins, and decreases in concentration from 16 ppm to 3 ppm within the 10 m that sodic alteration ends. Be concentration is elevated throughout the sodic envelope and mineralized zone but is most likely not related to the metasomatism of  $K^+$  for  $Na^+$ . Instead it most likely represents its own elemental halo as a result of the altering fluids. The beginning and end of Be alteration coincides with the sodic envelope because that most likely represents the extent of the altering fluid system.

**Table 6.1:** Average mass changes for the major oxides, trace elements, rare earth elements and volatile elements during mass balance calculations for CP and FP felsic volcanic rocks within the mineralized zone and the FP felsic volcanic rocks within the sodic alteration envelope.

	CP rocks from the mineralized zone	FP rocks from the mineralized zone	FP rocks from the sodic alteration envelope
Major Oxides			
SiO <sub>2</sub>	-16.1	-18.2	-7.2
Al <sub>2</sub> O <sub>3</sub>	0.74	1.7	-0.9
Fe <sub>2</sub> O <sub>3</sub> (T)	0.43	0.3	0.1
MnO	0.0	0.01	0.01
MgO	0.04	0.01	0.0
CaO	0.58	0.5	0.1
Na <sub>2</sub> O	4.81	4.8	3.0
K <sub>2</sub> O	-5.21	-5.0	-4.6
TiO <sub>2</sub>	0.0	0.0	0.0
P <sub>2</sub> O <sub>5</sub>	0.0	0.01	0.01
LOI	0.92	0.05	-0.05
Total	-14.7	-15.7	-9.4
Trace Elements			
Ba	-894.1	-679.6	53.9
Cs	-1.5	-0.73	-0.7
Ga	7.8	8.8	-2.2
Rb	-145.0	-134.1	-124.5
Sr	1.5	30.0	23.6
Pb	-76.2	4.3	5.6



Th	7.6	6.3	-1.5
U	1237.4	1308.2	176.1
Hf	3.3	1.8	-1.6
Nb	14.2	11.1	-0.2
Ta	0.67	1.1	-0.2
Y	57.6	30.6	-1.5
Zr	372.7	228.9	-27.1

Rare Earth Elements

La	41.9	45.1	4.3
Ce	87.7	89.2	3.6
Pr	11.1	10.2	-0.5
Nd	47.8	31.7	-3.8
Sm	9.0	5.8	-0.4
Eu	0.7	0.3	0.2
Gd	8.0	5.4	0.02
Tb	1.6	1.0	0.1
Dy	10.0	5.6	-0.1
Ho	1.9	1.1	-0.05
Er	5.9	3.4	-0.2
Tm	0.9	0.6	-0.03
Yb	5.7	3.7	-0.2
Lu	0.8	0.5	-0.05

Volatile Elements

Ag	0.4	0.3	-0.3
As	4.3	2.5	2.3
Be	3.2	3.2	0.7
Bi	-10.7	0.6	0.5
Ge	0.08	0.0	-0.3
In	0.1	0.07	0.02
Mo	-0.01	1.1	3.9
Sb	0.04	-5.7	-5.3
Sn	2.4	-0.03	-2.3
Tl	-0.7	-0.9	-0.8
W	0.6	-0.2	0.1

Transition Elements

Co	-0.3	17.4	-0.3
Cr	37.1	90.6	32.1
Cu	-77.7	-0.4	9.0
Ni	8.2	8.4	6.5
Sc	-0.4	1.1	0.1
V	73.3	33.6	36.8
Zn	-31.6	-0.4	14.7

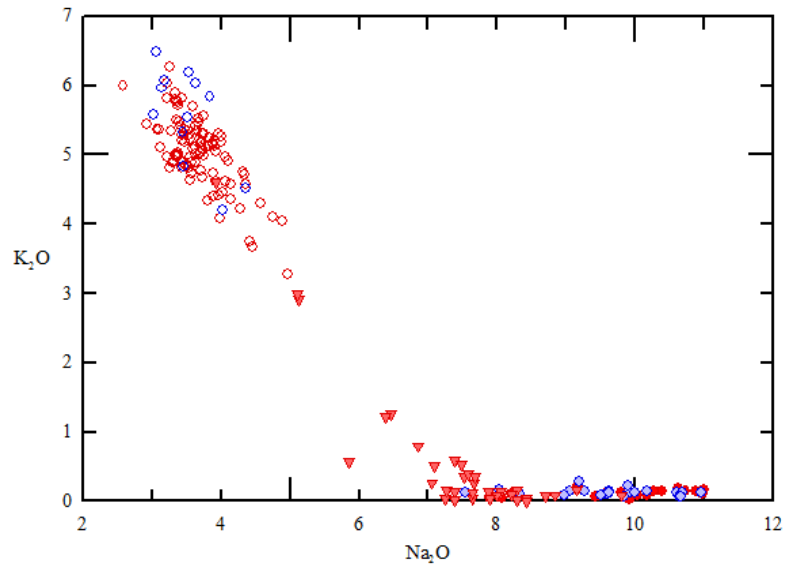


**Figure 6.1:** Bivariate plot of  $\text{Na}_2\text{O}$  vs.  $\text{K}_2\text{O}$  (in terms of oxide wt.%) for all felsic volcanic samples within the Michelin deposit. Unaltered FP (open red circles) and CP (open blue circles) plot together at ~5.5 wt.%  $\text{K}_2\text{O}$  and 3.5 wt.%  $\text{Na}_2\text{O}$ , samples trend towards samples within the sodic envelope (red triangles) which show an increase in  $\text{Na}_2\text{O}$  and decrease in  $\text{K}_2\text{O}$ , mineralized FP (red circles) and CP (blue circles) show a further increase in  $\text{Na}_2\text{O}$ .

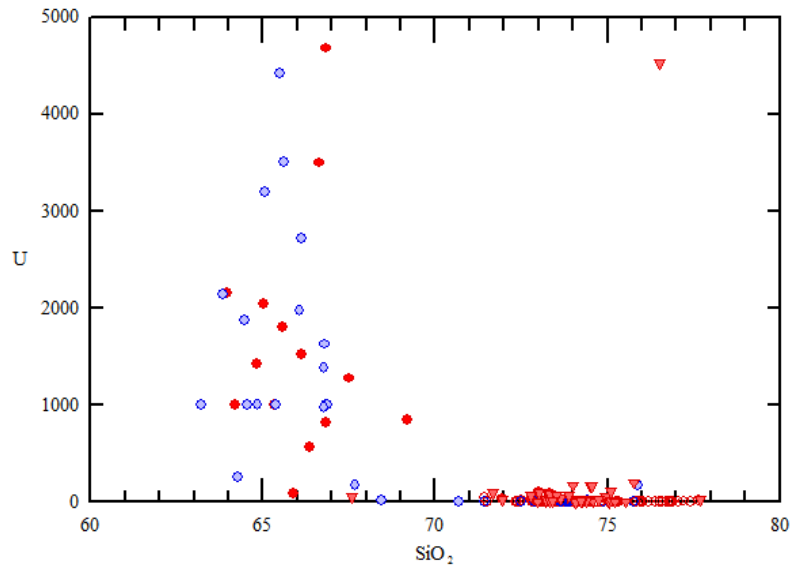


**Figure 6.2:** Bivariate plot of  $\text{SiO}_2$  (oxide wt.%) vs. U (ppm), the plot shows that nearly all of the mineralized samples have a decrease in  $\text{SiO}_2$ .

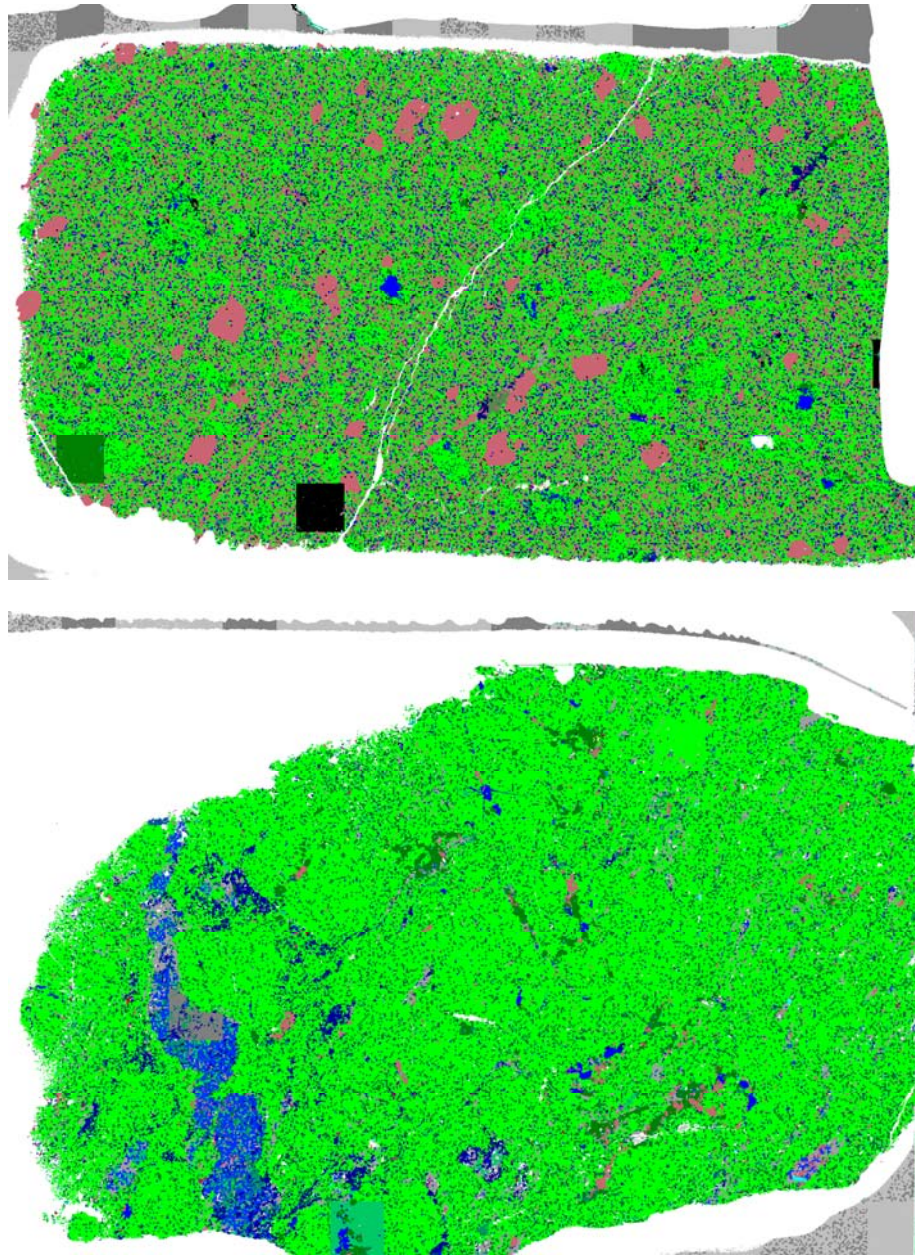


**Figure 6.3:** SEM-MLA mineral map from within the sodic envelope (top) and mineralized zone (bottom), (top) the light green color is albite which occurs as phenocrysts and constitutes most of the matrix, the pink color is quartz which occurs as phenocrysts and about 30 % of the matrix, the remaining colors are various amounts of magnetite, biotite, hornblende and calcite, and (bottom) the light green color is albite which constitutes most of the rock, equating to about 80 %, the blue color(s) are sodic amphibole and pyroxene which is located throughout the rock, and forms a large mafic clot with calcite (grey), the red and green are a combination of other alteration minerals including titanite, zircon, and hematite.

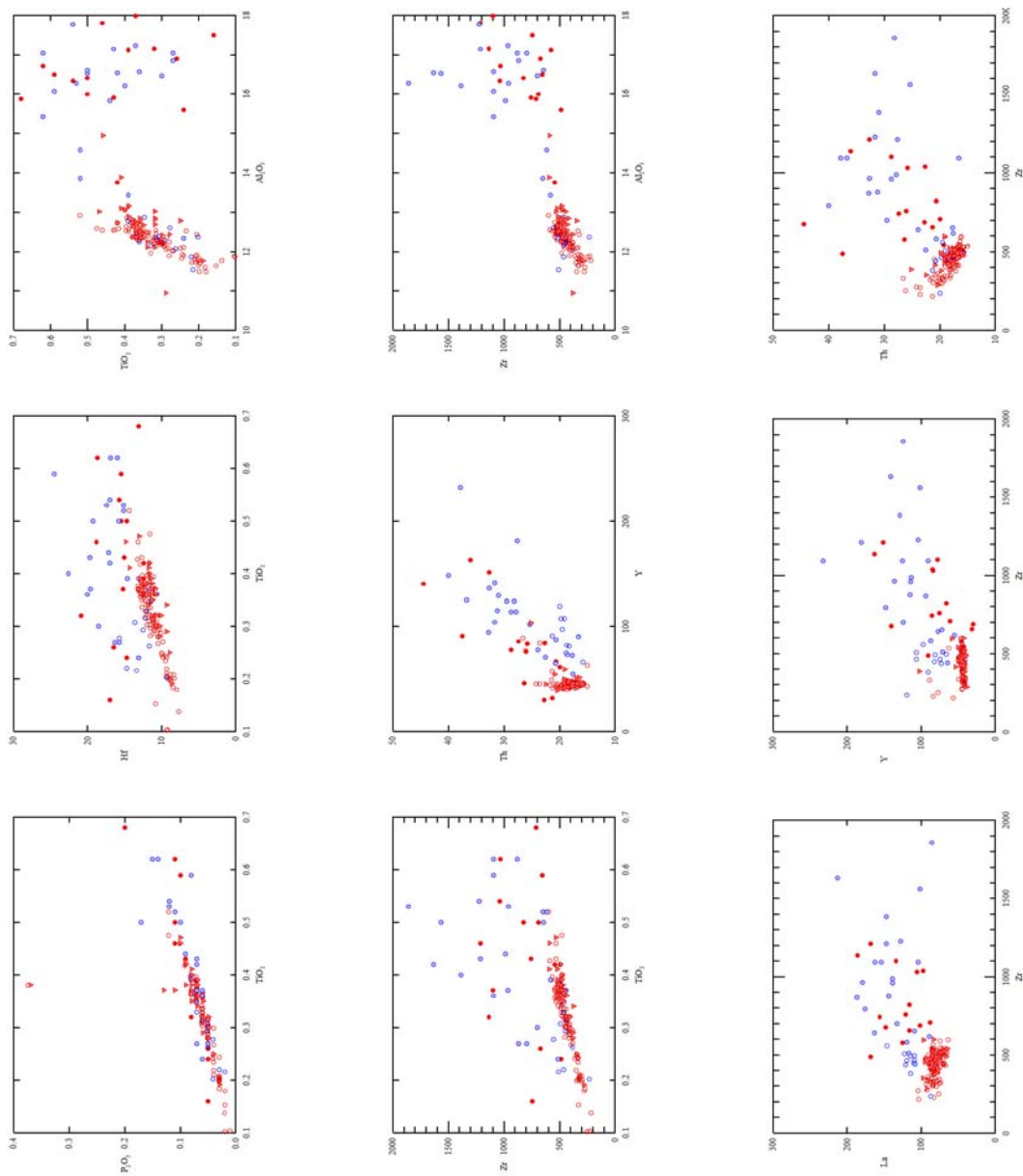


**Figure 6.4:** Immobile-immobile element bivariate plots of unaltered and altered felsic volcanic rocks from the Michelin deposit.  $TiO_2$  appears to be the most conserved element during alteration and generally forms the more linear trends.

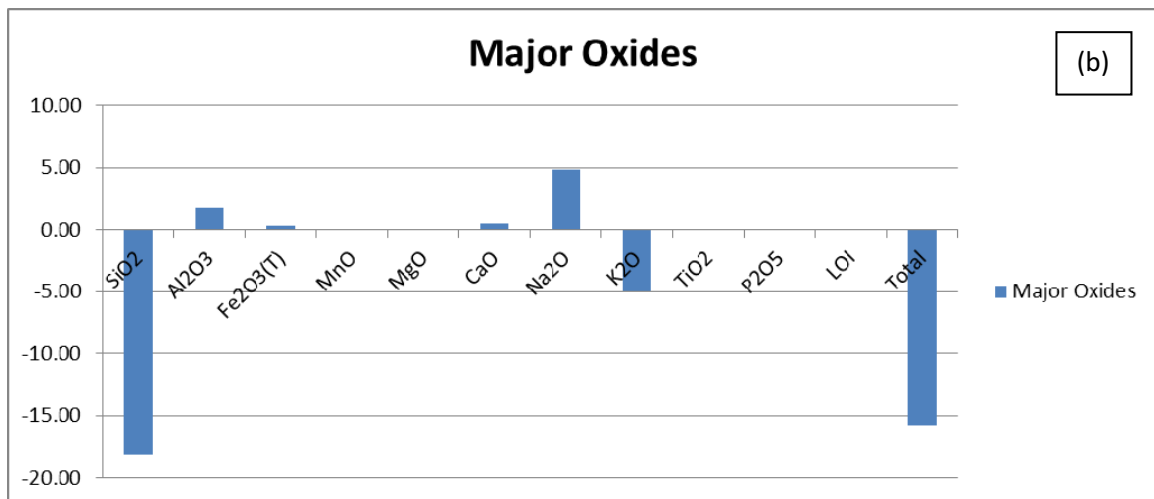
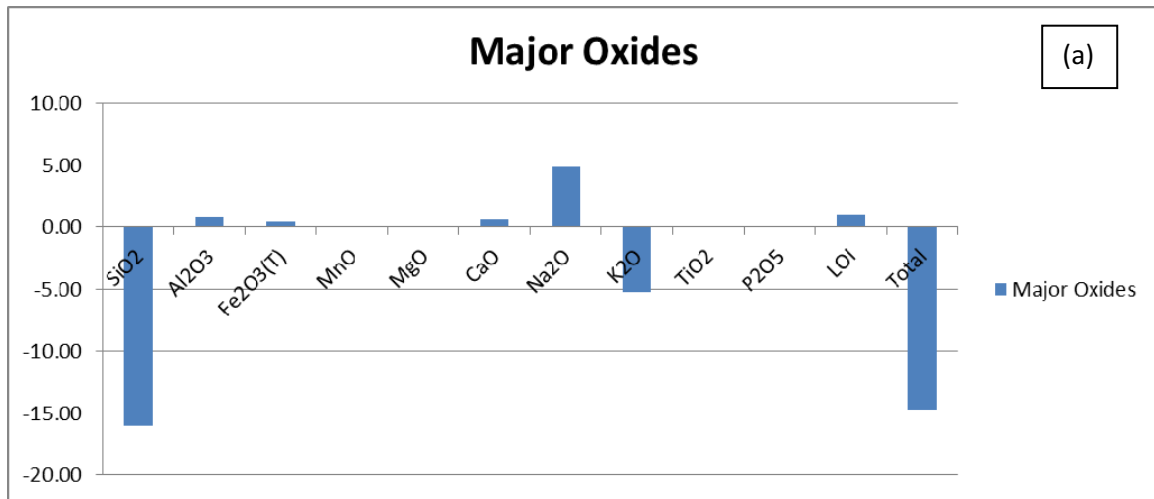


**Figure 6.5:** Mass change for the major oxides for the (a) CP and (b) FP felsic volcanic rocks from the mineralized zone. Both rock types display an overall large total mass loss, attributed to a large mass loss in SiO<sub>2</sub>, there are slight mass gains in Al<sub>2</sub>O<sub>3</sub>, Fe<sub>2</sub>O<sub>3</sub> (total iron) and CaO, Na<sub>2</sub>O shows a strong mass gain while K<sub>2</sub>O displays a strong mass loss.

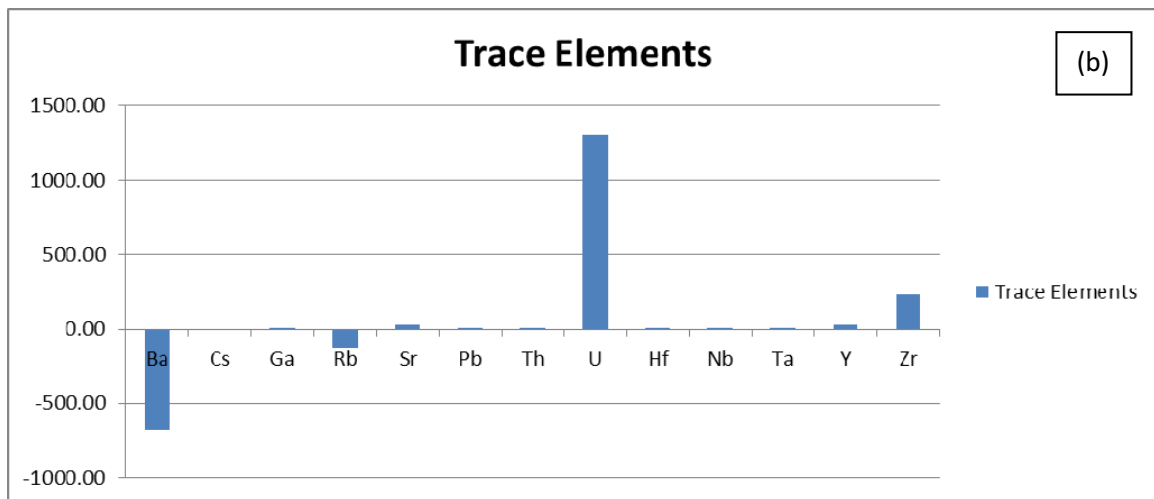
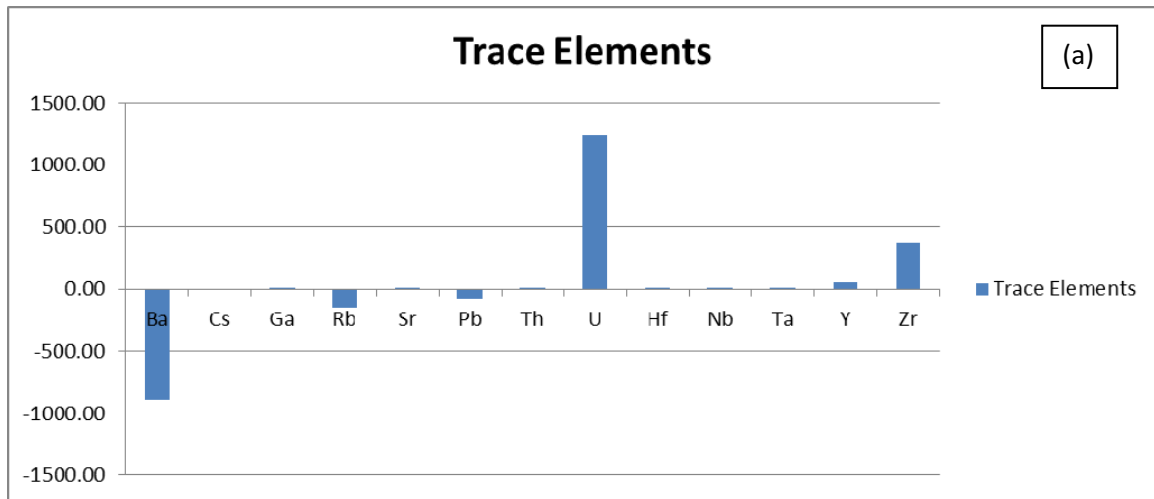


**Figure 6.6:** Mass change for the trace elements for the (a) CP and (b) FP felsic volcanic rocks from the mineralized zone. The trace elements for each rock type display a similar mass change, with U experiencing a strong mass gain, Zr having a moderate mass gain, and Y and Sr having a weak mass gain, and Ba having a strong mass loss, and Rb having a weak mass loss.

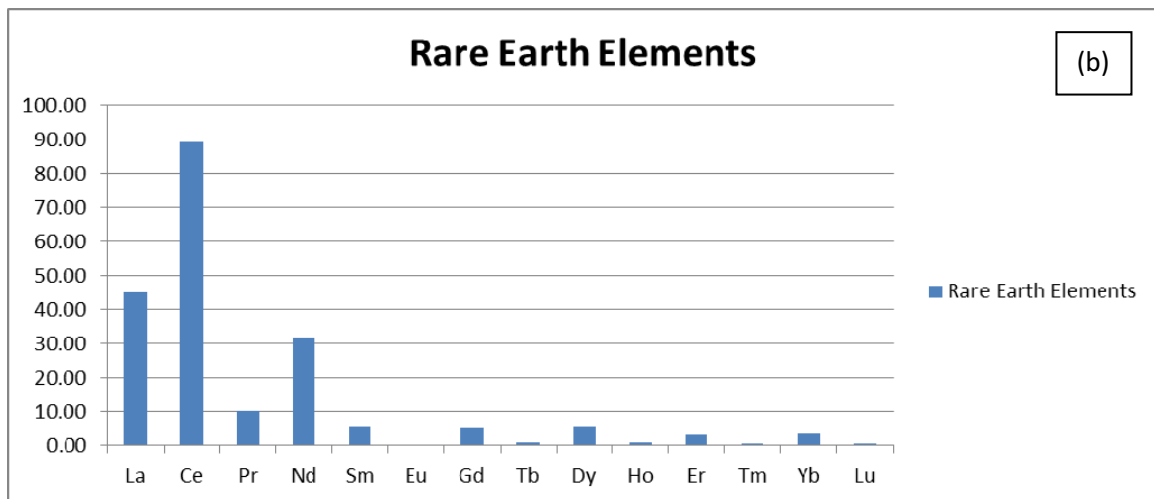
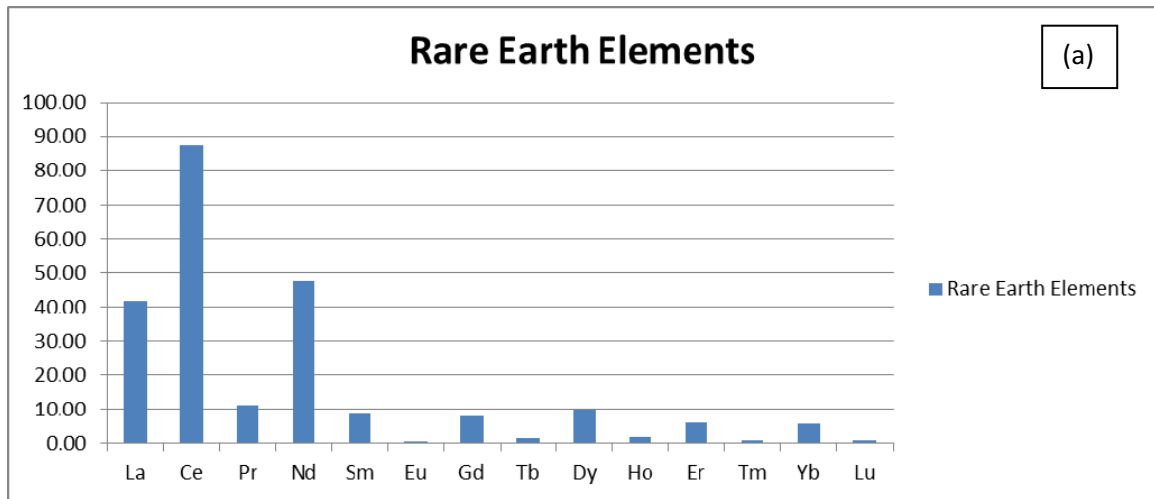


**Figure 6.7:** Mass change for the rare earth elements for the (a) CP and (b) FP felsic volcanic rocks from the mineralized zone. The rare earth elements for each rock type display a similar mass change, with the LREE displaying a strong mass gain, and the MREE and HREE displaying slight mass gains.



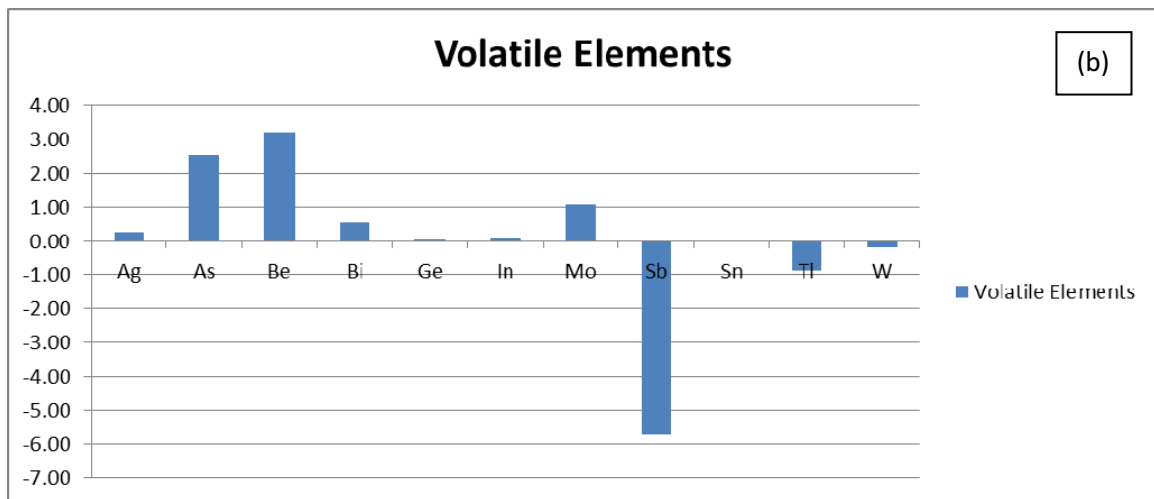
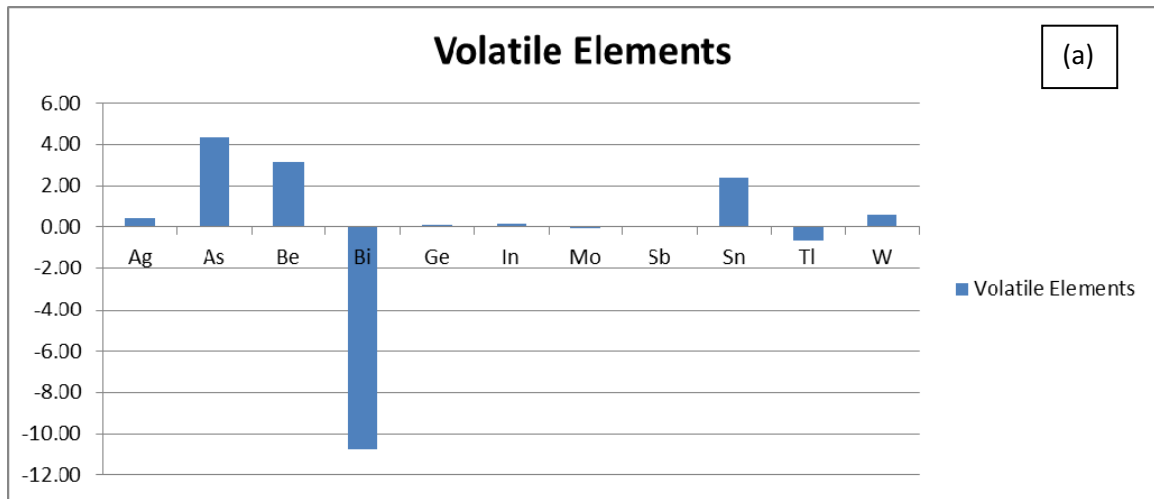


**Figure 6.8:** Mass change for the volatile elements for the (a) CP and (b) FP felsic volcanic rocks from the mineralized zone. The volatile elements display different mass changes between the FP and CP units with the (a) CP units displaying a mass gain in As, Be and Sn, and a mass loss in Bi and Tl, while the (b) FP units display a mass gain in As, Be, Bi and Mo, and a mass loss in Sb and Tl.

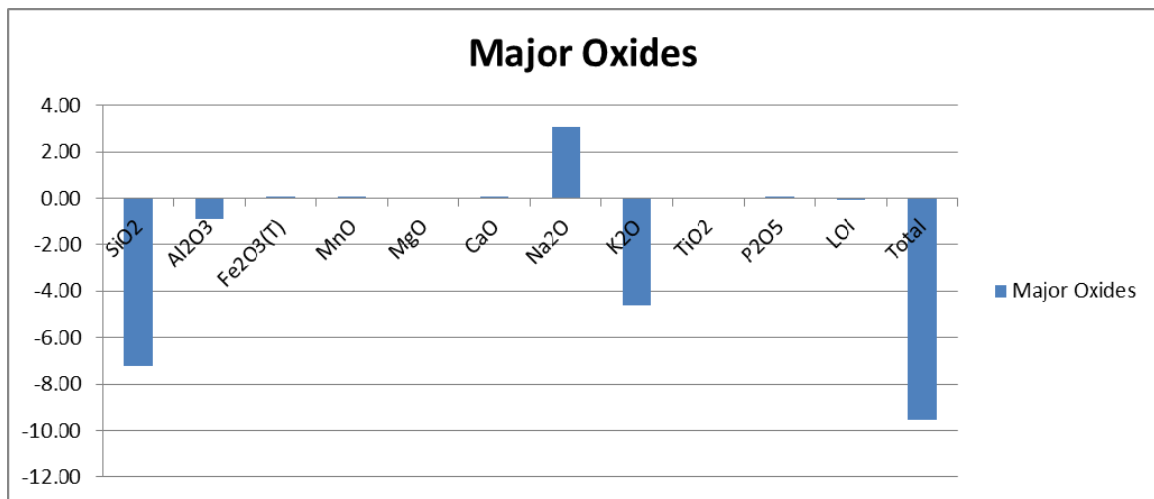


**Figure 6.9:** Mass change for the major oxides for the FP felsic volcanic rocks from the sodic alteration envelope. These rocks show an overall total mass loss, attributed to a mass loss in SiO<sub>2</sub> and, Al<sub>2</sub>O<sub>3</sub> and K<sub>2</sub>O, Na<sub>2</sub>O displays a strong mass gain, attributed to sodic metasomatism.

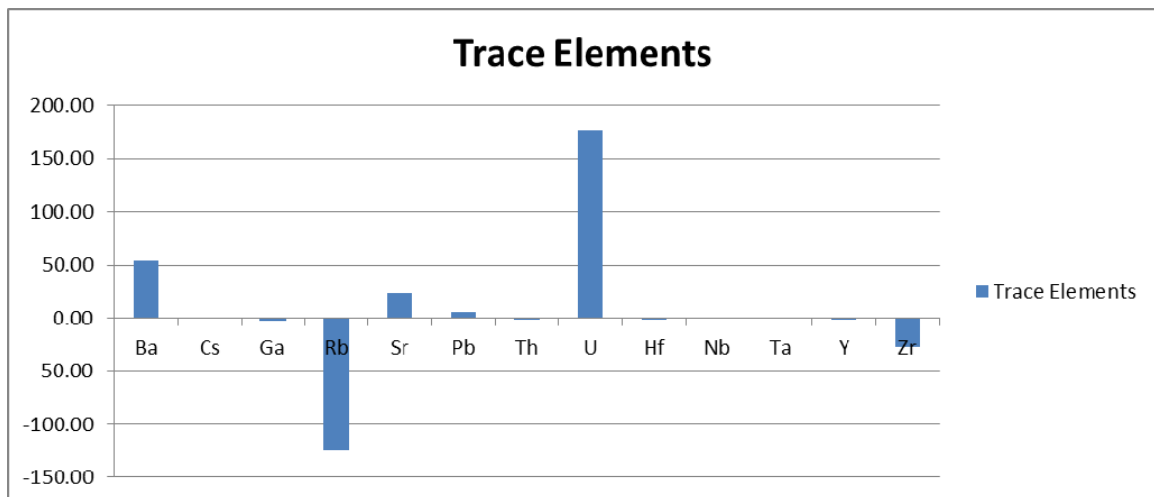


**Figure 6.10:** Mass change for the trace elements for the FP felsic volcanic rocks from the sodic alteration envelope. These rocks show a strong mass loss in Rb, and a weak mass loss in Zr. They also display a strong mass gain in U, and weak mass gains in Ba and Sr.

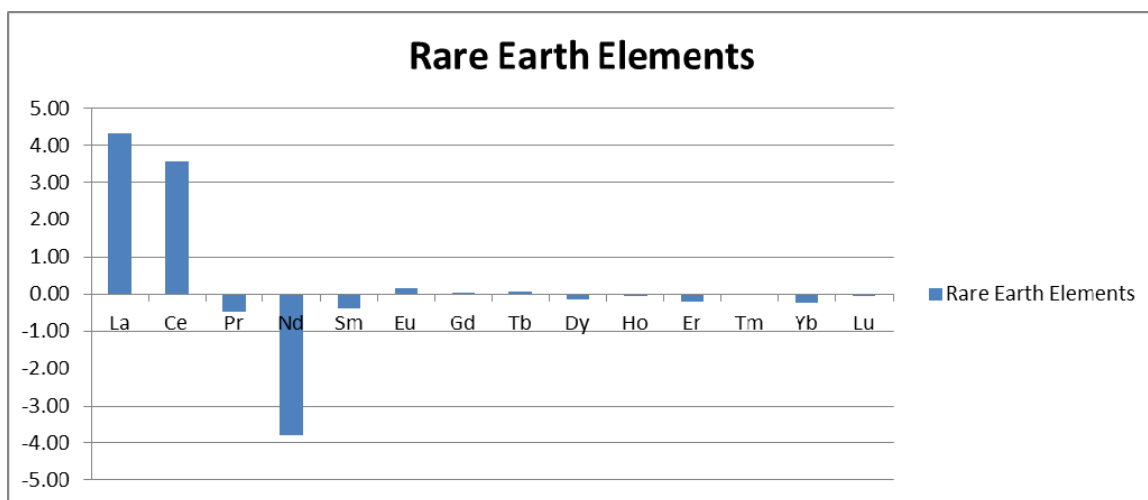


**Figure 6.11:** Mass change for the rare earth elements for the FP felsic volcanic rocks from the sodic alteration envelope. These rocks show a strong mass gain in La and Ce, but a mass loss in Pr and Nd of the LREE, the MREE and HREE for the most part show no change, with the exception of very weak mass loss in some elements.

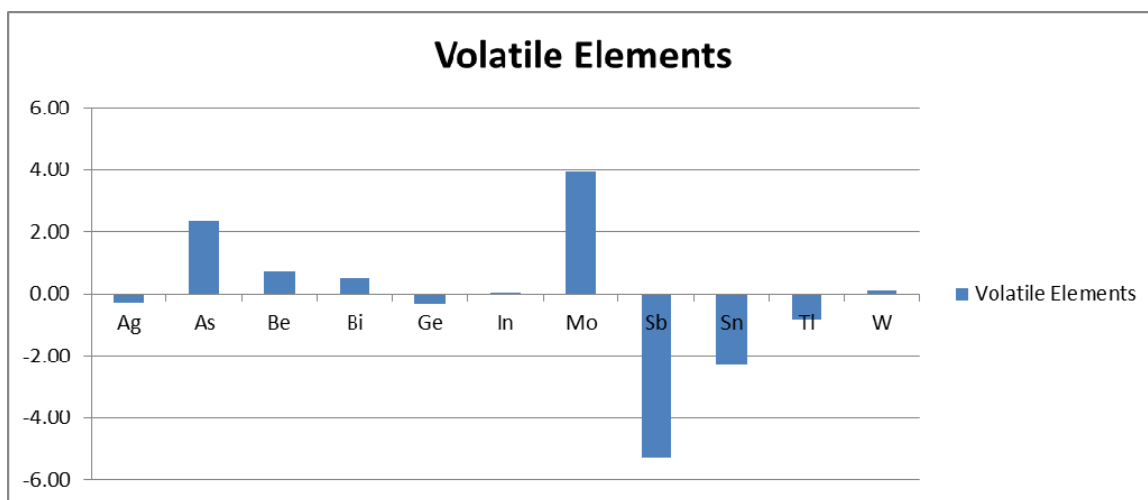


**Figure 6.12:** Mass change for the trace elements for the FP felsic volcanic rocks from the sodic alteration envelope. These rocks show a strong mass gain in As and Mo with weak mass gains in Be and Bi, they show a strong mass loss in Sb, Sn and Tl.





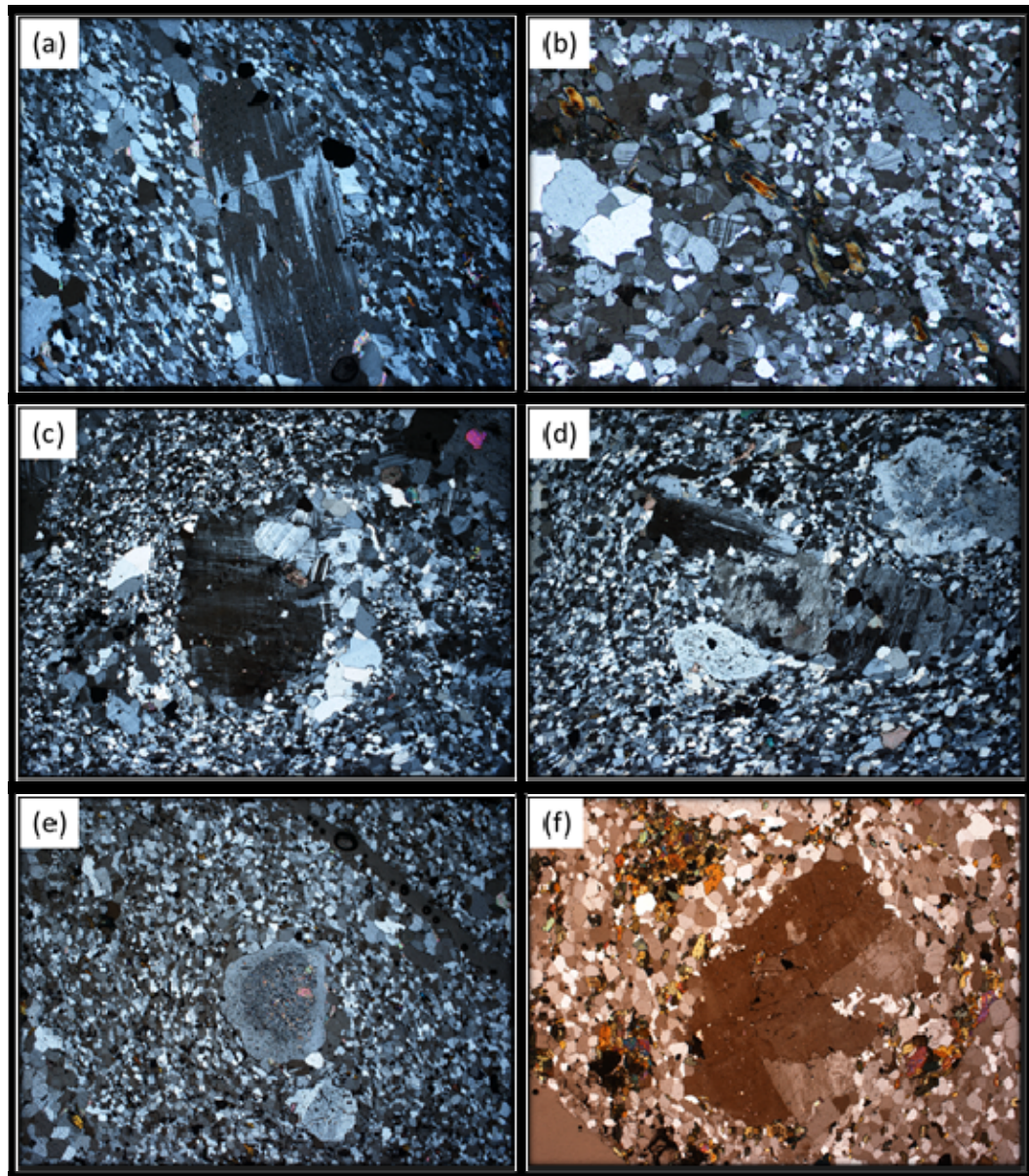


**Plate 6.2:** Petrographic sections of FP felsic volcanic rocks from throughout the sodic alteration envelope, (a) potassium feldspar phenocryst in the process of being altered to albite showing early stages of chessboard-style twinning (mag. = 2.5x, cpl), (b) recrystallized phenocryst with individual grains showing chessboard-style twinning suggesting they are altered potassium feldspar grains (mag. = 5x, cpl), (c) large, recrystallized potassium feldspar phenocryst altered to albite, showing chessboard-style twinning (mag. = 2.5x, cpl), (d) chessboard-style twinning in altered albite grain (mag. = 2.5x, cpl), (e) primary albite phenocryst that has an inner core strongly altered to sericite (mag. = 2.5x, cpl), and (f) large recrystallized phenocryst showing chessboard-style twinning indicating it has been altered to albite (mag. = 2.5x, cpl).



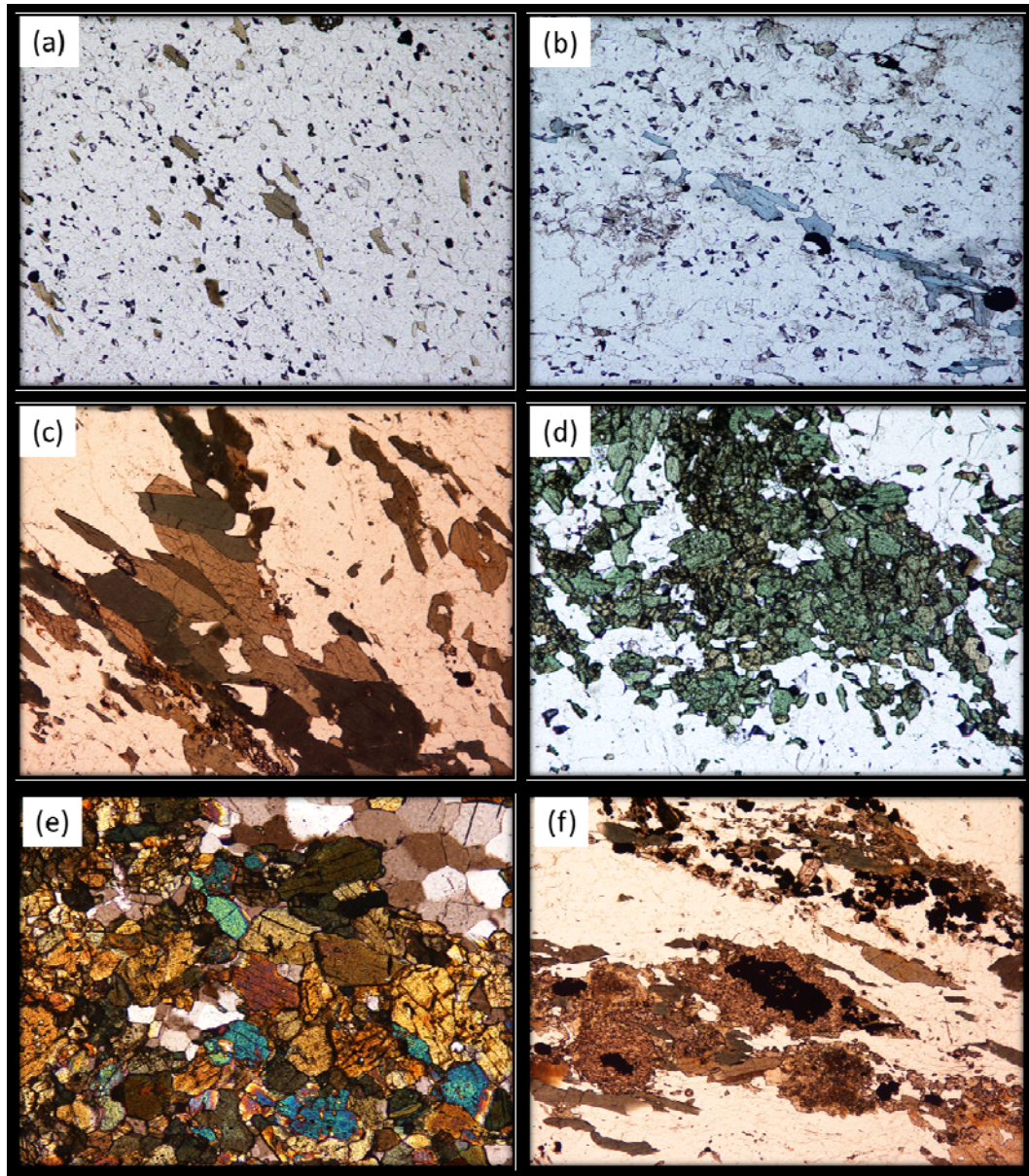


**Plate 6.3:** Petrographic sections of FP felsic volcanic rocks from throughout the sodic alteration envelope and mineralized zone, (a) primary brown biotite within unaltered FP rock (mag. = 5x, ppl), (b) blue sodic amphibole as a pseudomorph of primary biotite within the sodic envelope (mag. = 5x, ppl), (c) large, grass-green sodic amphibole grain with distinct cleavage as a pseudomorph of original elongated mafic grain (mag. = 5x, ppl), (d) secondary, fine-grained grass-green sodic amphibole grains (mag. = 5x, ppl), (e) secondary, equant, fine-grained sodic amphibole grains (mag. = 5x, cpl), and (f) opaque grains surrounded by fine-grained aggregates of sodic pyroxene, individual grains are not elongated but the mineral agglomerate is elongated suggesting that these grains altered from a primary mafic mineral (mag. = 5x, cpl).



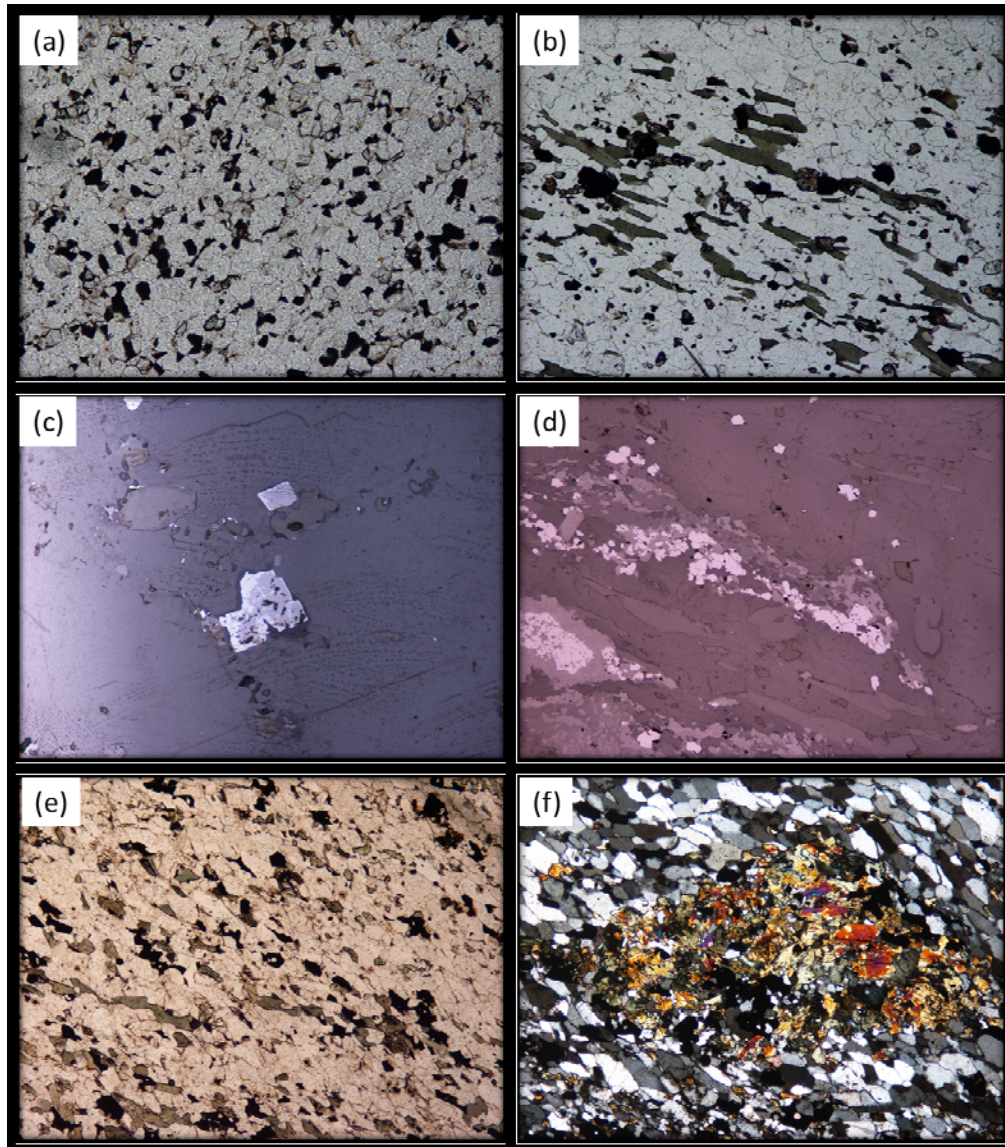


**Plate 6.4:** Petrographic sections of FP felsic volcanic rocks, (a) very fine-grained magnetite within the quartz-feldspar matrix of an unaltered FP unit (mag. = 10x, ppl), (b) larger grain of magnetite in unaltered FP associated with biotite and hornblende (mag. = 5x, ppl), (c) magnetite (darker grey) grain oxidizing to hematite (lighter grain) within the mineralized zone (mag. = 10x, rfl), (d) mineral aggregate within the mineralized zone containing abundant hematite (light grey) (mag. = 5x, rfl), (e) multiple sodic amphibole grains within the matrix in the mineralized zone, dissolution of individual quartz grains within the matrix left the rock like a sponge creating open space for alteration minerals to form (mag. = 5x, ppl), and (f) agglomerate of secondary alteration minerals taking the shape of a quartz phenocryst, space most likely created from the dissolution the quartz phenocrysts and then filled with alteration minerals (mag. = 5x, cpl).

## **Chapter 7    Age Dating and Relative Timing of Events**

### **7.1    Introduction**

The Michelin deposit is comprised of multiple units of FP felsic volcanic rocks intercalated with several units of CP felsic volcanic rocks. Although these units appear to be geochemically related it is unknown what the age relationship is between both rock types. Also unknown is the timing relationship between these lithological units and the various intrusive events, deformation and metamorphism, and alteration and mineralization.

The focus of this chapter will be on the relative timing of events of the Michelin deposit. This will include uranium-lead, zircon geochronology of select lithological units throughout the deposit, and a review of other notable age dates. These will be utilized, along with relative dating techniques to determine an approximate time line for the formation of the lithological units, and deformational events. Finally, the timing relationships between the various alteration events, mineralization and deformation will be reviewed.

Age dating will be attempted using in-situ zircons from polished thin sections. Select units from throughout the deposit will be analyzed using LA-ICP-MS to determine isotope values for uranium-lead geochronology. Drill core, polished thin sections, and SEM-MLA images will be utilized to examine textures and mineral grain relationships with other grains.



## 7.2 Age Dating of the Felsic Volcanic Units

The age of the felsic volcanic host rocks at Michelin have been U-Pb zircon dated at  $1856 \pm 2$  Ma by Scharer *et al.* (1988) from a weakly cleaved ash-flow tuff at Michelin Ridge, and by Sparkes and Dunning (2015) at  $1858 \pm 2$  Ma from a unit of FP felsic volcanic rock in the foot wall of the deposit. Michelin Ridge lies to the north of the deposit and is interpreted to lie stratigraphically below the mineralized zone, based on a stratigraphic younging direction towards the south. The error limits overlap suggesting that the ages correlate and thus, that the age of the host volcanic rocks are ca. 1857 Ma.

LA-ICP-MS U-Pb age dating of in-situ zircon grains was attempted on several samples from different lithological units and stratigraphical sections through the Michelin deposit. All of the zircon grains analyzed were similar in size and appearance. Only zircon grains greater than 50 microns that did not exhibit evidence of inherited cores or contamination were analyzed. The results were not favorable as the in-situ process proved unreliable for these rocks as they often did not contain enough large zircon grains to accurately ablate with the laser in order to produce an accurate age date. Many of the zircon grains experienced Pb-loss, creating large error limits. A number of samples also contained, older inherited cores that affected the data.

Another problem was that Zr was not conserved during alteration, resulting in the formation of new zircon grains or alteration rims on existing zircon grains. In addition, most of the zircon grains from the mineralized zone contain uraninite mineralization. All of these factors affected the accuracy of the age dating for each sample, and therefore

accurate age dating for the most part was not possible. Outlined below is a breakdown of the age dating undertaken and the results obtained for each sample.

Two samples of the FP felsic volcanics were age dated. One sample was from the foot wall of the deposit, approximately 150 m below the mineralized zone in drill hole M06-027, and the other sample was obtained from the hanging wall of the deposit, approximately 300 m above the mineralized zone in drill hole M06-010. The purpose for age dating these samples is to identify an age for the FP volcanics at the Michelin deposit; to determine if the FP rocks in the foot wall are older than equivalent rocks in the hanging wall; and to evaluate whether there were age differences between the foot wall and hanging wall.

In both samples only large zircons, greater than 50  $\mu\text{m}$  in diameter and without older cores, were analyzed. The zircon grains produced very noisy data, exhibiting considerable Pb-loss. The samples from the foot wall yielded an approximate age of ca. 1900 Ma, and the sample from the hanging wall produced a very large spread in age dates with an approximate age of ca. 1950 Ma; with one zircon dating as old 2020 Ma. These dates do not generally correlate with ages produced for Aillik Group felsic volcanic rocks from throughout the Makkovik Province, and instead they yield ages that are much older. U-Pb age dating of zircon grains within felsic volcanic rocks throughout the Aillik Group produce consistent ages from ca. 1883 to 1856 Ma (Scharer *et al.*, 1988; Hinchey and Rayner, 2008; Sparkes and Dunning, 2015).

Although care was taken to analyze the most pristine zircon grains, the erroneous ages produced during in-situ LA-ICP-MS most likely resulted from a combination of

inherited zircons, Pb-loss experienced during deformation and metamorphism, and interference from micron sized uraninite grains within the zircon. In Chapter 5 it was noted that many of the zircon grains exhibit inner cores that have a digested appearance. These cores often contain tiny uraninite grains and secondary growth patterns. These cores are interpreted to be inherited zircons. Similar zircon grains were described from the rhyolite tuff at Michelin Ridge by Scharer *et al.* (1988) who noted that some zircons contained microscopically distinguishable cores, and that at least two populations contain older components, containing traces of older material and partially resorbed cores that would cause difficulties for precise dating.

The inherited zircon cores are most likely related to the juvenile crust onto which the felsic volcanic rocks were deposited and are not associated with the Archean Nain craton upon which these rocks were accreted. Age dates for rocks from the Nain craton range from 3115 to 2800 Ma (Scharer *et al.*, 1988). These ages are much older than the oldest zircon ages produced from the inherited zircon grains at Michelin. Sparkes and Dunning (2015) dated the Kitts metagabbro unit of the Post Hill Group to  $2018 \pm 15/-8$  Ma. This age is more in-line with the ages produced from the inherited zircons, suggesting that the source could be from Post Hill and Moran Lake group aged rocks or equivalents, on which the Aillik Group stratigraphically overlie. The foot wall sample which yielded an age of ca. 1900 Ma is much older than the  $1858 \pm 2$  Ma age obtained from FP rocks that are stratigraphically above it in the foot wall, and much older than the  $1856 \pm 2$  Ma age produced from underlying felsic tuffs at Michelin Ridge. The only way

this age is accurate would be if the FP unit that produced the ca. 1900 Ma age was emplaced onto younger strata.

A sample from a CP unit from the hanging wall, approximately 280 m above the mineralized zone in drill hole M06-019 was dated to determine if the age matched that of the FP felsic volcanic rocks, thus indicating that the two rock types were deposited in sequence; or if the unit is younger, thus indicating that it intruded as a dike or sill. U-Pb age dating of in-situ zircons, although experiencing minor Pb-loss, produced a concordia age of  $1855 \pm 16$  Ma. This age is within age error limits defined by Scharer *et al.*, (1988) and Sparkes and Dunning (2015), suggesting that despite the Pb-loss it is most likely a reliable age for the unit. The correlation in age would suggest that this unit is a separate ash-flow layer deposited in sequence with the other ash-flow units. Lack of thermal alteration footprint, absence of xenoliths, and textural evidence also suggest that it is an ash-flow layer.

A sample of CP material from the mineralized zone was dated to determine if it correlated with the ages of the other FP and CP units within the deposit, or if the mineralized zone units were younger, suggesting that they are volcanic sills intruding the FP volcanics. Age dating analysis of this sample produced very messy data with the zircon grains experiencing a large amount of Pb-loss. However, dating did produce a concordia age of  $1893 \pm 16$  Ma. This age is much older than ages yielded elsewhere in the Aillik Group, particularly in the area of the Michelin deposit. The zircon grains are most likely affected by uranium mineralization within the mineralized zone, and consist of inherited grains, suggesting that the age produced is not reliable. However, the lower

error limit of this age does correlate with ages produced by Hinchey and Rayner (2008) of  $1883 \pm 7$  Ma. Therefore it is possible that this age is reliable and that this unit is older than surrounding strata and was thrust or folded into place between younger felsic volcanic strata.

A sample from the distinctly mafic-rich CP unit was age dated to determine if this unit is a separate ash-flow event with a similar age to the other felsic volcanic rocks, or whether this unit is a younger volcanic dike or sill. The U-Pb data from the zircon grains was very messy producing ages older than 1900 Ma, with the oldest being 2050 Ma. These appear to be inherited zircons, similar to zircon grains from the FP felsic volcanic unit from the hanging wall. This age does not reflect the depositional age, or emplacement age of this distinct marker unit.

Finally, a sample collected from the granitoid intrusive located within the hanging wall of the deposit was dated to determine its emplacement age, in order to correlate this age with other intrusive events that occurred throughout the Makkovik Province. Zircon grains for this unit were generally larger but they still exhibited Pb-loss. The granitoid produced an age of  $1840 \pm 120$  Ma. This is an extremely large error limit; the best estimation from the analysis is that the unit is ca. 1800 Ma. This age correlates with other granitoid intrusives representing an intrusive event at ca. 1800 Ma, associated with the Makkovikian Orogeny. These intrusive rocks that emplaced during this event are described as being variably foliated feldspar-porphyritic, potassic-rich granite to monzonite which contains biotite, hornblende, and magnetite that define foliation (Kerr, 1994; Hinchey and LaFlamme, 2009). This description closely matches that of the

granitoid intrusive within the hanging wall of the Michelin deposit suggesting that this unit is associated with the intrusive event at ca. 1800 Ma.

Age dating was attempted on the four varieties of mafic dike in order to define an age of emplacement. In-situ zircons were mapped from petrographic thin sections of each generation of dike using the SEM-MLA. Zircon grains were identified in each generation of dike but are too small to analyze using LA-ICP-MS age dating techniques so an age could not be determined. Determining the ages of each dike variety is important as it could identify if dike emplacement was related to other intrusive events that affected the Makkovik Province, and could help in narrowing down an age limit to the timing of mineralization and alteration. Interestingly, each mafic dike variety contained characteristically different zircon grains, potentially creating another method for differentiating between dike varieties.

Zircon grains in the biotite-hornblende schists dikes are subprismatic to equant and euhedral ranging in size from 10-100 microns. Grains exhibit distinct zoning with an inner, xenocrystic core that has a mottled appearance and contains tiny grains that appear to be uraninite. Surrounding these cores is new magmatic growth which contains no visible grains of uraninite. These grains are similar to some of the zircon grains found within the FP felsic volcanic host rocks, suggesting that the cores are most likely inherited. The syn-kinematic dikes contain zircons that are anhedral in shape and range in size from 5-microns. They display no zonation patterns and do not contain xenocrystic cores or inclusions. Zircons of the post-kinematic strongly magnetic gabbroic dikes are subprismatic to equant and subhedral in shape, ranging in size from 10-20 microns.

Grains display faint growth zonation patterns, with some grains containing inner cores of baddeleyite. The final post-kinematic, intermediate dikes contain subprismatic anhedral to subhedral grains, ranging in size from 5-10 microns. Grains exhibit very faint zoning and often have a mottled appearance, but do not contain xenocrystic or baddeleyite cores.

Dating of in-situ zircons in the felsic volcanic rocks at the Michelin deposit via LA-ICP-MS did not produce the desired results, as zircons were not large enough to compensate for noisy data related to inherited zircons, Pb-loss, and uranium mineralization. The age dating attempt, however, did show that both the FP and CP units from throughout the Michelin area contained abundant inherited zircons that are much older than the felsic volcanic sequences. These inherited zircons produce ages of 1900 to 2050 Ma suggesting that they are too young to be derived from the Archean Nain craton but match ages from rocks within the Post Hill and Moran Lake groups which unconformably overlie the Nain craton and structurally underlie the Aillik Group. The age dating produced one semi-reliable result from a CP unit within the hanging wall of the deposit. The age of this sample matches those derived by Scharer *et al.* (1988) and Sparks and Dunning (2015). If regional deformation of the felsic volcanic rocks at Michelin occurred then it is possible that some of older age dates are reliable and therefore reflect older units that formed early in the volcanic and depositional history of the Aillik Group felsic volcanics that were emplaced between younger strata through folding or faulting.

### 7.3 Relative Timing of the Felsic Volcanic Units and Deformation

Age constraints on the FP and CP felsic volcanics throughout the Michelin deposit remain unclear. Age dating at two separate locations in the area produced an age of ca. 1857 Ma for the FP felsic volcanics, and a CP unit from the area gave an age of  $1855 \pm 16$  Ma. These ages correlate with each other suggesting that ca. 1857 Ma is an accurate depositional age for both the FP and CP felsic volcanic units at Michelin. Evidence suggests, but is not conclusive, that regional deformation in the form of faulting or folding occurred, potentially increasing the thickness of the volcanic sequence by emplacing older strata amongst younger strata. However age dating attempts for the felsic volcanic rocks at Michelin produce ages that are older than ca. 1855 Ma, suggesting this as a minimum depositional age for the felsic volcanic rocks at Michelin.

It is evident that the FP, CP and mafic-rich CP felsic volcanic units throughout the deposit have been strongly deformed. Deformation is consistent throughout all of the felsic volcanic units of the deposit and consists of a prominent, regionally penetrative foliation that strikes to the northeast ( $\sim 70^\circ$ ) and dips moderately to the southeast (Evans, 1980; Otto *et al.*, 2013). These units have also been metamorphosed to lower amphibolite facies, resulting in identical textures and mineralogies between the units. The regional penetrative foliation and metamorphism resulted from the Makkovikian Orogeny, during which supracrustal rocks of the Makkovik Province were accreted onto the Archean Nain craton. The orogeny occurred from ca. 1810 to 1790 Ma, but evidence from geology and similarities with the Ketilidian Orogen of Southern Greenland suggests that it may of ranged from as early as ca. 1850 Ma to as late as ca. 1750 Ma (Gower and Ryan, 1986;



Wilton 1996). There is also evidence suggesting a minimum age of  $1798 \pm 2$  Ma which correlates to the crystallization age of an undeformed granodiorite to quartz monzonite intrusive unit that truncates the foliation in the foot wall of the Jacques Lake deposit (Sparkes and Dunning, 2015). The Makkovikian Orogeny produced the characteristic structures, textures, and mineralogy of the felsic volcanics. These include an interlocking matrix of quartz and feldspar that hosts recrystallized feldspar and quartz phenocrysts as well as thin wisps of mafic minerals, which define the penetrative foliation. These mafic wisps are composed predominantly of biotite and hornblende and represent peak metamorphic conditions suggesting that peak metamorphism correlates with regional deformation.

Since deformation and metamorphism are consistent between all felsic volcanic units, all of them are interpreted to have been deposited before the Makkovikian Orogeny. Also, if faulting or folding occurred this is also interpreted to have occurred prior to the deformation that caused the regional penetrative foliation. If the units were thrust into place after the formation of the penetrative foliation then the foliation would not exhibit a consistent strike and dip between all felsic volcanic units. The same reasoning may be applied to the folded sequences, if the penetrative foliation occurred prior to folding then the rocks of one limb in an isoclinal fold would have a foliation with a different orientation than the foliation exhibited by the other limb. Also, the contacts between all of the felsic volcanic units are concordant with foliation suggesting they were emplaced prior to the formation of the penetrative foliation. Finally, metamorphic grade is consistent between units, suggesting that the units were in their current stratigraphic

position prior to metamorphism. However, the more intense deformation evident in the mineralized zone and marked by an increase in small, 0.5 m mylonite zones and moderate to intense shearing in some of the CP units is interpreted to have occurred during deformation or in the late stages of deformation. Evidence for this may be seen in the highly deformed zones. They still maintain a consistent foliation with respect to the other units throughout the deposit, with the exception that the foliation is more exaggerated, containing stretched quartz and feldspar phenocrysts in the mylonite zones and rotated, augened phenocrysts in the intensely sheared units. This would suggest that deformation was mostly focused through the mineralized zone, being possibly related to a regional shear zone that extends throughout the Aillik Group felsic volcanics of the Michelin Zone and potentially encompassing the Michelin, Jacques Lake, and Rainbow deposits as well as other numerous occurrences including White Bear, Aurora West, and Mustang Lake (Sparkes and Kerr, 2008).

The felsic volcanic rocks of the Michelin deposit have also been affected by the ca. 1650 Ma Labradorian Orogeny and the ca. 1000 Ma Grenvillian Orogeny (Ross, 2006). These orogenic events resulted in 1) the emplacement of post-kinematic mafic dikes throughout the deposit, 2) brittle deformation resulting in the formation of fracture sets and hematitized breccia zones that post-date the penetrative foliation (Evans, 1980), and 3) remobilization of uranium mineralization into fractures and veins. Sparkes and Dunning (2015) noted that there are several generations of titanite growth within the mineralized zone most likely related to separate metamorphic events. One growth event is associated with the Labradorian Orogeny and the other being Grenvillian in age.

The granitoid intrusive within the hanging wall of the deposit is interpreted via textures and age dating to have been emplaced ca. 1800 Ma during the Makkovikian Orogeny. This unit has been variably deformed and contains the same mineral assemblages as the felsic volcanics but does not appear to be as strongly metamorphosed. This could be related to emplacement age, indicating that it was emplaced after the period of strong metamorphism, indicating that deformation continued after metamorphism which is also evident in elongated recrystallized quartz-feldspar grains with the matrix of felsic volcanic rocks. It is also possible that the coarse-grained nature of the unit, in particular the almost porphyritic feldspar grains enabled the intrusive to withstand deformation more than the felsic volcanic host rocks, as mafic-poor areas of the rock appear to be not as strongly foliated as mafic-rich areas, and at the margins. The granitoid intrusive is host to all phases of mafic dike, with exception of strongly deformed biotite-hornblende schist dikes; varieties of this dike intrude the granitoid but are not as strongly deformed as within the felsic volcanics. This would suggest that the granitoid intrusive was emplaced during the Makkovikian Orogeny after the main metamorphic event but before deformation had ended, and due to its coarse grain nature was able to withstand deformation, particularly within the center of the unit more than the other units. Supporting evidence for this can be found at the margins of the granitoid which are finer grained and more strongly deformed than within the center of the intrusion.

Four distinct variations of mafic intrusives have been identified throughout the Michelin deposit. Variations have been differentiated from each other based on their deformation history, texture, mineralogy, and geochemistry. Variation in the intensity of

deformation exhibited by each dike indicates they were emplaced at different times in relation to regional deformation and metamorphism associated with the Makkovikian Orogeny.

The earliest phase of mafic dike, the biotite-hornblende schists display a consistent metamorphic grade and foliation similar to the felsic volcanic host rocks. These dikes have been metamorphosed to lower amphibolite facies, consisting of biotite, hornblende, plagioclase, and chlorite and exhibit a consistent penetrative foliation. The contacts of these dikes with the felsic volcanics are also concordant to the foliation. Based on this evidence it is interpreted that these dikes intruded into the felsic volcanic units prior to the regional deformation and metamorphism associated with the Makkovikian Orogeny. Observed differences in foliation and deformation, and geochemistry within these dikes suggest that there may be several different variations that were emplaced at different times. Some of these dikes are pre-kinematic and intruded prior to metamorphism and deformation while others appear to be early-syn-kinematic and are not as strongly deformed. Hinchey (2007) noted that there are at least two suites of metamorphosed amphibolite dikes that intrude the Aillik Group, suggesting multiple intrusive events and Evans (1980) noted two distinct varieties, including a weakly porphyritic variety of pre-kinematic dike intruding the mineralized zone. It appears that only the weakly deformed, early-syn-kinematic variety intrude the granitoid unit which is only variably foliated and interpreted to have intruded during the Makkovikian Orogeny at ca. 1800 Ma.

There is also evidence that suggests that some dikes were emplaced prior to regional faulting or folding. Some dikes contain small, chlorite-rich fault gouge material at the contact with the felsic volcanic host rock. This suggests that movement occurred along these dikes during faulting. It is possible that movement occurred along early dikes as they would most likely represent a plane of weakness within the felsic volcanic sequence. Other dikes display kink or chevron style folding of the foliation, possibly due to shearing caused by adjacent felsic volcanic units moving along the dike, or shortening of the mafic dike in response to stress produced during regional folding. There is also no evidence of these dikes being cut off by felsic volcanic units, or having contacts that are discordant to the foliation, indicating that some dikes possibly intruded after regional faulting or folding. More mapping would be required to determine when these dikes intruded into the felsic volcanic rocks.

A second phase of mafic dike, the gabbroic dikes are moderately deformed and weakly metamorphosed. Deformation for the most part is consistent with the felsic volcanic host rocks, with the exception that some contacts are not concordant to the foliation. The emplacement of these dikes is interpreted to have occurred during the later stages of deformation during the Makkovikian Orogeny when peak deformation and metamorphism had already taken place.

The final two phases of dike, the strongly magnetic gabbroic dikes and the diorite dikes exhibit no signs of deformation suggesting that both dike varieties were emplaced after the main kinematic event affecting the deposit and are not associated with the Makkovikian Orogeny. Age dating could not be completed for these dikes but they are

most likely associated with the ca. 1650 Ma Labradorian Orogeny or the ca. 1425 Ma Michael Gabbro (Scharer *et al.*, 1986). According to Kerr (1994) the rocks of the Aillik Group were intruded by a number of felsic and mafic intrusives related to the Labradorian Orogeny.

A summary of relative timing for the formation of the lithological units and deformational events at Michelin is as follows:

- 1) 1900 to 1855 Ma, eruption, deposition and emplacement of the FP, CP and mafic-rich CP units.
- 2) 1855 to 1800 Ma, intrusion of the pre to early syn-kinematic biotite-hornblende schist dikes. This most likely consists of several sub-groups of mafic dike that possibly intruded at various times prior to the peak deformation caused by the Makkovikian Orogeny.
- 3) 1855 to 1810 Ma, possible thrust faulting or folding of Aillik Group felsic volcanic sequences.
- 4) 1810 to 1798 Ma, main regional deformation and metamorphism event of the Makkovikian Orogeny.
- 5) ca. 1800 Ma, emplacement of the granitoid intrusive and latest phases of the biotite-hornblende schists.
- 6) 1800 to 1798 Ma, emplacement of the late syn-kinematic gabbroic dikes during the later stages of the Makkovikian Orogeny, after peak deformation and metamorphism but prior to its conclusion.

- 7) 1798 to 1425 Ma, emplacement of the two phases of post-kinematic mafic dike, occurring after deformation and metamorphism related to the Makkovikian Orogeny.
- 8) ca. 1650 Ma, brittle deformation, remobilization of uranium mineralization, and weak metamorphism resulting in new titanite growth during the Labradorian Orogeny.
- 9) ca. 1000 Ma, weak metamorphism resulting in new titanite growth, and possible brittle deformation and/or remobilization of uranium mineralization during the Grenvillian Orogeny.

#### **7.4 Relative Timing of the Various Alteration Styles**

There are several alteration styles present at the Michelin deposit, each one is unique and appear to be related to the mineralizing event. In this section the timing of each alteration style will be discussed, identifying the relationship between the individual alteration styles and mineralization with deformation and the mafic dikes.

##### **7.4.1 Widespread Sodic Metasomatism**

First stage mineral alteration at the Michelin deposit corresponds to widespread sodic metasomatism of the FP and CP felsic volcanic rocks which envelope the mineralized zone. This involves the alteration of potassic-rich minerals to sodic-rich equivalents. Sodic metasomatism is the process of alkali ion exchange between a hot hydrothermal fluid that is alkaline rich, with a high  $\text{Na}^+/\text{K}^+$  ratio, and potassium-bearing

minerals in the host rock. During this exchange  $K^+$  ions are replaced by  $Na^+$  ions leaving the rock completely depleted in  $K_2O$  and enriched in  $Na_2O$  (White and Martin, 1980).

Sodic metasomatism affecting the potassic-rich minerals is non-destructive, meaning that the altered grains still maintain the original size, shape, and texture, becoming pseudomorphs of the original grain. This makes it difficult to determine whether sodic metasomatism occurred before, during, or after metamorphism and deformation. Biotite and hornblende grains that have been metasomatized to sodic amphiboles occur as elongated grains, parallel to the foliation, defining the foliation in altered felsic volcanic rock. The fact that these grains look identical to unaltered grains outside of the sodic envelope suggests that they were metamorphosed and deformed first and then sodic altered. Finally, potassic phenocrysts display chessboard style twinning as a result of sodic alteration. It is most likely that this texture would be destroyed during metamorphism and deformation. The evidence suggests that sodic metasomatism occurred after regional metamorphism and after the early stages of deformation. It most likely occurred during ductile deformation where alkaline fluid was transported along regionally deformed zones, and not through brittle deformation such as faults or fractures.

Two possible scenarios exist for the formation of widespread sodic metasomatism. The first, and most likely scenario, is that sodic metasomatism occurred around the same time as alteration within the mineralized zone. In this scenario the mineralized zone is the focal point for a hot, oxidized, alkaline solution. Host rock interaction within the mineralized zone caused the fluid to weaken away from the mineralized zone, where it only had the ability to metasomatize the host rock, and create



weak, sporadic hematite alteration, until it eventually died out. In the second scenario sodic metasomatism occurs prior-to, and independently of the other alteration styles, occurring as a separate altering event. This fluid was not hot or alkaline enough to cause quartz dissolution, or oxidized enough to cause strong hematitization.

Sodic metasomatism appears to be independent of the uranium mineralization as most of the sodic envelope is unmineralized. Areas that are mineralized correspond to hematite alteration, suggesting that uranium mineralization is associated with that and not sodic metasomatism.

#### **7.4.2 Hematitization**

Hematitization of the felsic volcanic rocks is widespread, creating a large halo around the mineralized zone, similar to Na-metasomatism. However, hematitization is not as pervasive as sodic metasomatism, and is more sporadic outside of the mineralized zone. Inside the mineralized zone the intensity changes, with higher intensity areas corresponding to the contacts between CP and FP units, strongly deformed zones, and within CP units. Hematite alteration leaves the rock a pinkish-red color, with more intensely altered areas being deep red in color and results from the oxidation of magnetite to hematite through the interaction with oxidized hydrothermal fluids.

Due to the sporadic nature of hematitization within the sodic envelope, oxidation most likely occurred with strongly alkaline, oxidized fluids that caused quartz dissolution and increased sodic alteration within the mineralized zone. The sporadic nature of hematitization that gradually decreases away from the mineralized zone is most likely

results from the fluid becoming less and less oxidized as a result of host rock interaction. The formation of hematite into mm-cm bands that align with the foliation suggests that magnetite grains were aligned during the early stages of deformation, and were later oxidized.

Hematite alteration is closely related to uranium mineralization and either occurs prior-to or concurrently with mineralization. The reason being is that hematite alteration can occur independently of uranium mineralization, but uranium mineralization always occurs with hematite alteration, and in general, the greater the intensity of hematite alteration, the more strongly mineralized is the rock. The oxidation of magnetite directly leads to the reduction of uranyl species in solution causing uranium to precipitate.

#### **7.4.3 Quartz Dissolution**

The dissolution of quartz, often referred to as episyenization occurs as a result of hydrothermal leaching of the original quartz of the felsic volcanic rock and only affects the CP and FP rocks within the mineralized zone, typically throughout the CP units and along adjacent to the contacts within the FP units, decreasing towards the centers of the FP units. In thicker units, the centers are not affected by quartz dissolution.

The dissolution of quartz occurs through the interaction with hot, strongly alkaline hydrothermal fluids where alkaline species leach quartz from the rock at a rate dependent on grain size, and alkalinity and temperature of the fluid (El-Kammar *et al.*, 2001). The leaching of quartz from the rock within the mineralized zone occurs in zones, which begin and end rather abruptly. Within these zones quartz phenocrysts and quartz grains in

the groundmass have been leached, whereas outside of these zones, quartz remains. Zonation is mostly a result of fluid flow concentrated in specific areas within the mineralized zones, most likely along the contacts between the CP and FP units, or within zones that are more deformed. This alteration affect preserves the original texture of the quartz grains, creating cavities, vugs and pore space whose volume coincides with those of the dissolved grains. The open spaces that are created are then filled with secondary alteration minerals such as albite, sodic amphiboles, sodic pyroxenes, calcite, and uranium mineralization.

The dissolution of quartz at Michelin appears to have occurred after metamorphism and peak deformation, as cavities, vugs and pore space created from quartz loss maintain the original shape of the quartz grain created during deformation. During metamorphism the groundmass was recrystallized creating a granoblastic texture, these grains were then slightly elongated during deformation. Also, during deformation quartz phenocrysts was elongated creating an almost football-shaped grain with the long axis being two to three times the length of the short axis. The cavities created from dissolved quartz grains, although filled with secondary alteration minerals, maintain these textures created during metamorphism and deformation, indicating that the dissolution of quartz occurred after these events.

It is difficult to determine if quartz dissolution occurred along with sodic metasomatism or if it occurred afterwards. It would not occur prior to sodic metasomatism as the dissolution of quartz is caused by strongly alkaline fluids which would also cause metasomatism within the rock. Based on the widespread, pervasive

nature of sodic metasomatism it is most likely that it occurs before quartz dissolution. However the dissolution of quartz occurs prior to the formation of secondary alteration minerals that fill the empty space created from dissolution. This includes secondary albite, not created during ion-exchange during sodic metasomatism, newly formed sodic amphiboles and sodic pyroxenes, calcite, and possibly some uranium mineralization.

The dissolution of quartz is interpreted to have occurred prior to the precipitation of some of the uranium minerals as mineralization occurs in the open spaces created from the leaching of quartz. Also, in general highly mineralized samples contain SiO<sub>2</sub> values between 64-68 wt. %. However, some highly mineralized samples contain SiO<sub>2</sub> values of 72-74 wt. % suggesting no quartz dissolution has taken place, indicating that the mineralizing event and hematitization may have been independent of quartz dissolution, but most likely are a result of the same fluid.

#### **7.4.4 Increased Sodic Alteration**

Following the dissolution of quartz the felsic volcanic rocks of the mineralized zone were affected by an increase in sodic alteration. This involves the creation of new sodic rich minerals, mainly albite, sodic amphibole and sodic pyroxene. The formation of these grains only occurred within the mineralized zone, in the empty spaces created from the dissolution of quartz.

This increased sodic alteration resulted from hot, strongly alkaline fluids interacting with both the CP and FP rocks within the mineralized zone. The same fluid which caused quartz dissolution via reaction with an alkaline species led to the creation

of secondary albite through a chemical reaction wherein  $\text{Na}_2\text{O}$  and  $\text{SiO}_2$  combined to precipitate albite in available pore spaces (eg., El-Kammar *et al.*, 2001; Cuney *et al.*, 2012). Most of this secondary albite formed tiny equant, to elongated grains that fill in pore space within the matrix created from the removal of quartz.

When the quartz phenocrysts dissolved they left behind large cavities that maintained the ellipsoidal shape of the elongated phenocrysts. These cavities were then filled with multiple, small grains of sodic amphibole and sodic pyroxene. Larger secondary albite grains as well as sodic amphiboles and pyroxenes formed adjacent to existing mafic mineral grains, including sodic amphibole and pyroxene which are pseudomorphs of previously elongated biotite and hornblende grains, hematitized magnetite, titanite, zircon, and uranium bearing minerals. All of these minerals formed large mafic mineral aggregates that host most of the uranium mineralization at the Michelin deposit. These aggregates formed in spaces created from dissolved phenocrysts and adjacent groundmass, creating large, irregular shaped cavities. The formation of secondary sodic minerals occurs concurrently with silica dissolution, filling the available pore space.

The formation of these secondary sodic-rich minerals appears to have occurred after deformation ended, as all of the grains appear to be undeformed. None of the grains are elongated, most are equant in shape. All of the larger albite grains exhibit perfect Carlsbad twinning, with no indication of stress. These grains formed after the dissolution of silica, and most likely after the precipitation of uranium mineralization as they often enclose small uraninite grains.

#### **7.4.5 Formation of Secondary Zircon and Other Minerals**

Secondary zircon most likely formed concurrently with quartz dissolution and increased sodic alteration. Mass balance calculations indicate that there is a strong enrichment of zircon within the mineralized zone. Average Zr concentrations within the FP rocks increase from about 440 ppm in unaltered rock to 750 ppm within the mineralized zone. The increase is even greater in the CP rocks going from an average of 450 ppm in unaltered rock to 990 ppm within the mineralized zone.

SEM-MLA backscatter images of zircon grains indicate that secondary zircon formed as new growths on pre-existing zircon grains. This new growth is only observed on zircon grains from within the mineralized zone and it typically contains micron-sized uraninite grains, indicating growth concurrently with the precipitation of uraninite. The existing zircon grains do not contain uraninite grains except along small fractures. It is interpreted that fluid infiltrated along these fractures, precipitating uraninite. Outside of the mineralized zone none of the zircon grains contain uraninite, except for mottled, inherited cores. The inclusion of uraninite within zircon is a feature of zircon growth within the mineralized zone.

The source of zircon is interpreted to be from the host felsic volcanics, which have a high concentration of Zr. Zr, was removed from these rocks either within the sodic envelope or through broad scale stripping of the felsic volcanic rocks during devitrification. Mass balance calculations indicate that small amounts of Zr were removed within the sodic envelope during metasomatism. Kaur *et al.* (2012) notes that in general the metasomatic process involving highly-alkaline fluids can cause severe

leaching of Zr, Y, the REE as well as other trace elements, and that precipitation could have occurred through a number of mechanisms including oxidation-reduction, changing pH, or decreasing alkalinity of the solution. Hf remains unaffected by alkaline solutions so its concentration will remain the same in unaltered and altered rock. Zr/Hf ratios in unaltered FP and CP rocks average about 40 and 35 respectively. Within the mineralized zone the FP rocks have an average Zr/Hf ratio of 50 and the CP rocks 57. This suggests that the increase in zirconium is caused by hydrothermal fluids.

Mass balance calculations indicate that there is slight enrichment in Y, LREE, As, Be, Sn and V within both the FP and CP units in the mineralized zone. The increase in these elements is most likely associated with the same process that was involved with the increase in Zr. SEM-MLA analyses do not indicate the presence of any minerals in which these elements form, and it is most likely that they are incorporated into other minerals such as monazite, allanite, apatite, andradite etc. that occur sporadically through the mineralized zone.

Titanite which has a strong affinity with uranium mineralization and is typically associated with uranium-bearing grains appear to have been affected by alteration. Bivariate immobile element plots suggest that Ti was conserved during the alteration processes that affected the mineralized zone. When Hf was used as the conserved element during mass balance calculations there was no change in Ti, suggesting it also was conserved during alteration. However, evidence from Sparkes and Dunning (2015) suggests that Ti was remobilized during different deformational events relating to the Labradorean and Grenvillian orogenies. Studies by Minatidis (1976), Evans (1980), and Ross (2006)

indicate that titanite is strongly associated with uranium mineralization, and that titanite grains commonly host micron-sized grains of uranium-bearing minerals, suggesting that the two minerals formed concurrently. Unlike zircon, there does not appear to be new growths on preexisting titanite grains that host uranium mineralization, and that mineralization is located throughout these grains. Uranium-bearing grains could form along fractures within the titanite grains but they generally display no alignment patterns. Cuney *et al.* (2012) indicate that brannerite forms from the replacement of previously deposited Ti- and Fe-bearing minerals. SEM-MLA analysis suggests that brannerite is closely associated with titanite, and could form from the replacement of titanite during interaction with uranium-bearing hydrothermal fluid, explaining the poikilitic texture of uranium mineralization within titanite grains. It is also possible that titanium was liberated from biotite and hornblende grains during metasomatism and forming new titanite growths, which then incorporated uranium bearing grains.

#### **7.4.6 Calcite Alteration**

The final stage of alteration affecting the felsic volcanic rocks in the mineralized zone was the formation of calcite. Newly formed calcite is present within open spaces created by quartz dissolution as well as within pressure shadows around augened and rotated feldspar phenocrysts that formed during the final stages of deformation. Calcite grains are non-deformed and anhedral, filling the available space. Locally calcite includes small uraninite, or other, grains, but generally it formed around larger albite, sodic amphibole and pyroxene, titanite, zircon and magnetite/hematite grains within the large



mafic mineral agglomerates. This suggests that calcite formed during the final alteration stage at Michelin.

Andradite occurs very sporadically within the mineralized zone, but a link between their occurrence and the alteration has yet to be established as andradite also occurs outside of the sodic envelope and could just be a result of metamorphism. It is possible that the presence of these minerals indicate a very late stage of calcic metasomatism, which is a common late stage feature in other uranium deposits that have been affected by sodic metasomatism and quartz dissolution (Cuney and Kyser, 2008; Cuney et al., 2012).

#### **7.4.7 Uranium Mineralization**

Uranium mineralization at the Michelin deposit is closely associated with hematite alteration but appears to have also occurred concurrently with quartz dissolution, increased sodic alteration, and zircon and titanite formation and remobilization. The mechanism of uranium leaching, transport and precipitation will be discussed in Chapter 8 which describes a genetic model for metallogenesis for the Michelin deposit; this section will discuss the chemical composition of uranium mineralization and its relationship with the alteration.

The predominant uranium-bearing mineral at the Michelin deposit is uraninite, which seemingly precipitated out of solution due to the oxidation of magnetite to hematite. None of the other alteration styles observed provide mechanisms for the precipitation of uranium that is as closely associated as hematitization is with

mineralization. Uraninite grains forming in the space created from dissolved quartz indicate that quartz dissolution occurred prior-to uraninite precipitation. The inclusion of uraninite grains in zircon, titanite, albite, sodic amphibole and pyroxene indicate that these alteration styles occurred concurrently as the precipitation of uraninite. Uraninite grains occur throughout the FP and CP felsic volcanic rocks and are not exclusively associated to one particular mineral phase. The sporadic occurrence of uraninite suggest that precipitation occurred wherever there was available space, but uraninite grains are commonly associated with titanite, Figures 5.5-5.10, suggesting that the precipitation of uraninite and remobilization of titanite occurred together.

SEM-MLA analyses indicate that individual uraninite grains contain variable cationic substitutions consisting of Pb, Si, Ca, Zr, Ti, Fe, and LREE, in particular Ce. Three distinct groups can be identified based on the type and concentration of cationic substitution. The first group consists of uraninite grains which contain only Pb. Alexandre and Kyser (2005) suggest that this is radiogenic Pb in the structure of the uraninite grain, created from the radioactive decay of uranium.  $\text{Pb}^{2+}$  has a larger radius and different valence state than  $\text{U}^{4+}$  and therefore it is not compatible with the crystal structure of uraninite so it is most likely not a cationic substitution. These grains most likely precipitated out of solution first as they are often complexly surrounded by the other groupings of uraninite grains.

The second group consists of cationic substitutions of Si and Ca with variable amounts of Pb, Zr, or LREE. Generally these have lower concentrations of Si and Ca in comparison to U. According to Alexandre and Kyser (2005),  $\text{Ca}^{2+}$  will replace  $\text{U}^{4+}$  in the

structure of uraninite because they have a similar ionic radius, and  $\text{Pb}^{2+}$  is attributed to radiogenic Pb. They also suggest that uraninite is a chemically active mineral and readily exchanges elements or recrystallizes during fluid-circulation events after the initial formation of uraninite. This causes Pb and other elements to be displaced from the uraninite crystal and substituted by Ca, Si, Zr, and REE. The final group which contains greater amounts of Si followed by U and Ca, with variable amounts of Zr, Ti, and Fe was most likely more strongly affected by fluid-circulation events than the previous group. Alexandre and Kyser (2005) report that uraninite with little to no Pb has most likely been converted to coffinite or other uranium silicates such as soddyite.

It appears that after the initial precipitation of uraninite grains, wall rock interaction with the alkaline hydrothermal fluid continued, causing the grains to alter or to precipitate with variable amounts of cationic substitutions. With the exception of Na, the elements that substitute within the uraninite grains are the main elements mobilized during alteration, including Si (quartz dissolution), Ca (carbonate formation), Fe (Magnetite oxidation), Zr (Zircon formation), Ti (titanium remobilization), and the LREE (enrichment in alteration minerals). All of these elements were available within the hydrothermal solution for substitution. Sparkes and Dunning (2015) note that titanite grains were affected later deformational events. Individual grains were remobilized yielding age dates correlating with the Labradorian and Grenvillian orogenies. During these events localized oxidation could have occurred leading to the remobilization of uraninite into fracture-seams and formation of uranophane.

#### 7.4.8 Mafic Dikes

Sample size is very limited but the biotite-hornblende schist dikes appear to have undergone sodic metasomatism, similar to the host felsic volcanics. Samples of these dikes from within the sodic envelope display an approximate 1 % increase in  $\text{Na}_2\text{O}$  and a 1 % decrease in  $\text{K}_2\text{O}$  in comparison to equivalent dikes outside of the sodic envelope. These samples also exhibit an apparent depletion in Rb and Tl, similar to the felsic volcanic rocks affected by sodic metasomatism. Dike samples from within the mineralized zone show further enrichment of approximately 0.5 %  $\text{Na}_2\text{O}$  over samples from the sodic envelope, but no further decrease in  $\text{K}_2\text{O}$ , Rb, or Tl. This correlates very closely with the alteration of the felsic volcanic rocks which have an almost 1:1 replacement of  $\text{Na}_2\text{O}$  for  $\text{K}_2\text{O}$  within the sodic envelope during metasomatism, and then a continued increase in  $\text{Na}_2\text{O}$  inside the mineralized attributed to further sodic alteration.

The geochemical data suggest that the biotite-hornblende schists were emplaced prior, or during the sodic metasomatic event that pervasively altered the felsic volcanic rocks. It should be noted that not all of the  $\text{K}_2\text{O}$  was removed from the dikes, and that the loss of  $\text{K}_2\text{O}$  within the dikes most likely came from biotite grains. These dikes do not contain potassium feldspar which in the felsic volcanics was readily altered to albite. The biotite and hornblende grains within the felsic volcanic rocks did not completely alter to sodic minerals until the intensity of sodic metasomatism increased. Therefore it is possible that due to mineralogy these dikes will not experience as strong an affect as the felsic volcanics, or that these dikes were emplaced during metasomatism, when most of the removal of  $\text{K}_2\text{O}$  had already occurred.

Within the mineralized zone these dikes show increased sodic alteration, with no more potassic loss, suggesting that they were emplaced prior to the increased sodic alteration that affected the felsic volcanic rocks of the mineralized zone. These dikes also do not have a remobilization effect on uranium mineralization relating to their emplacement, suggesting that these dikes were emplaced prior to mineralization. These dikes are not mineralized though, some dikes do show a slight enrichment in uranium and zirconium suggesting that they were affected by the mineralizing fluids, but mineralization is not as high as what it should be if these dikes were affected by the mineralizing fluid. Several authors, Gandhi (1978), Evans (180), Ross (2006), and Sparkes and Kerr (2008) suggest that because these dikes are not mineralized and contain titanite and Fe-oxides which are associated with uranium mineralization than they were emplaced post mineralization, or that most were emplaced post-mineralization and the dikes that contain small amounts of mineralization were emplaced either pre-mineralization or during mineralization.

It is more likely that these dikes did not have the right mineralogies and characteristics to facilitate uraninite precipitation. Uranium mineralization precipitated from the oxidation of magnetite to hematite and concentrated in open spaces within the felsic volcanic rocks formed through the dissolution of quartz. These dikes contain no quartz, so therefore no spaces could be created within the dikes. Also, and most importantly, these dikes contain little to no magnetite, having magnetic susceptibility readings of only 1 to 2. The oxidation of magnetite to hematite is the key component for the precipitation of uraninite. Uraninite grains precipitated very closely to the

hematitization and therefore would not precipitate within the mafic dikes if they contain no magnetite. Finally, these units may not have been as permeable to fluid flow as the felsic volcanic rocks, therefore there would not be as much interaction with the altering and mineralizing fluid as with the felsic volcanic rocks, possibly explaining why alteration is not as intense and the lack of mineralization.

Syn-kinematic gabbroic mafic dikes within the sodic envelope show no increase in  $\text{Na}_2\text{O}$  and no decrease in  $\text{K}_2\text{O}$ , Rb, or Tl indicating that these dikes were not affected by sodic metasomatism. However, within the mineralized zone these dikes show an enrichment of approximately 1.25 % in  $\text{Na}_2\text{O}$  concentrations but do not show a decrease in  $\text{K}_2\text{O}$ . This suggests that these dikes were affected by the increased sodic alteration within the mineralized zone. These dikes produce a strong remobilization effect on uranium mineralization within the felsic volcanic host rocks adjacent to the dike contacts. Hematite alteration and uranium mineralization is intensified immediately adjacent to the dike contact and gradually decreases away from the contact into normal hematitization and mineralization.

These dikes are unmineralized, and this remobilization effect does not produce any uranium mineralization within the dike. This would suggest that these dikes were emplaced after the mineralizing event, remobilizing it during emplacement, but before the end of alteration as these dikes seem to be affected by sodic alteration. These dikes are similar to the biotite-hornblende schists in that they also contain no quartz and very little magnetite, suggesting that the reason they contain no uranium mineralization is that

they do not provide a suitable host rock to cause the precipitation and allow for the concentration of uranium mineralization.

#### **7.4.9 Relative Timing of Deformation, Mineralization and Alteration Events**

Based on the observations made during this study and the relationships between deformation, mineralization, alteration, and the mafic dikes, the following is a summary of the relative timing for the formation of the Michelin deposit. This will be a separate component from the relative time line presented in section 7.3 which gave an approximate age to the formation of lithological units, metamorphism and deformation. An age will not be given for these alteration events as they most likely formed concurrently or very close together.

Metamorphism appears to have occurred before alteration. The pre-kinematic, biotite-hornblende schists were probably emplaced prior to sodic metasomatism. Deformation was ongoing and started during metamorphism and extended until nearly the end of alteration, only the very final stages of alteration occurred after deformation ended.

Sodic metasomatism was the first stage of alteration to affect the rocks at Michelin, occurring after metamorphism, emplacement of the biotite-hornblende schists, and primary deformation which elongated biotite and hornblende grains. The next stage of alteration appears to be quartz dissolution, which predated increased sodic alteration, calcite formation, and some hematitization and uranium mineralization. It is most likely that quartz dissolution, hematitization, uranium mineralization and increased sodic

alteration occurred together, most likely the result of the same oxidized, alkaline fluid. Increased sodic alteration along with hematitization and uranium precipitation continued after quartz dissolution had ended. Since quartz dissolution occurred in smaller zones, it is most likely that fluid flow was focused through these areas and due to wall rock interactions, the fluid lost the ability to dissolve quartz but was still able to oxidize magnetite, precipitate uranium, and form sodic minerals. The formation of secondary zircon and remobilization of titanite most likely occurred during this stage as zircon grains contain tiny uraninite crystals and titanite is strongly associated with uraninite mineralization.

Emplacement of the syn-kinematic, gabbroic dikes occurred during this period of alteration and mineralization, as it remobilized already existent uranium mineralization. The dike is foliated but not metamorphosed suggesting that deformation was still ongoing. The dike also shows evidence of being sodic altered suggesting that increased sodic alteration was still ongoing.

During the later stages of alteration, the deformation stopped, as newly formed grains of albite, sodic amphibole and pyroxene and calcite show no indications of being deformed. Some of these grains also do not contain abundant uranium mineralization indicating the precipitation of uranium had mostly ceased by this point. This is most likely due to the fact that there was no more magnetite left to oxidize to facilitate the precipitation of uraninite. The final stages of alteration appear to be some albite formation but mostly the formation of calcite, which occurred last and after deformation, filling the remaining open space in the rock.



Finally, during the Labradorian and Grenvillian orogenies brittle deformation occurred where uranium was remobilized and concentrated into these fractures. Also, titanite grains and uranium minerals, were affected and subsequently remobilized forming new titanite grains, possibly forming or adding to the strong poikilitic texture that titanite grains display, containing several micron sized uranium crystals.

## **Chapter 8      Discussion and Conclusion**

### **8.1      Introduction**

The Michelin deposit is hosted in a broad series of metamorphosed felsic volcanics, comprising part of the Aillik Group. This group consists of both FP and CP felsic volcanic units which have been intruded by several generations of mafic and granitoid intrusives. Approximately 1810 to 1790 Ma, the felsic volcanics were regionally deformed and metamorphosed during the Makkovikian Orogeny, leading to destruction of almost all primary depositional textures and original mineral content. Macro- and micro-structures, overall textures and mineralogy observed today is a reflection of this orogenic event. Within the Michelin deposit, uranium mineralization occurs as micron-sized grains concentrated within a tight sequence of alternating units of CP and FP volcanic rock, termed the Mine Series. These units which range in thickness between 2-40 m and average between 5-10 m are strongly deformed and pervasively altered. Alteration appears to have occurred in stages, with one or more of these stages responsible for the concentration and precipitation of uranium mineralization.

Through the detailed investigation of lithology, mineralization, and alteration at the Michelin deposit conducted in this study the following information has been derived: 1) the overall geological setting of the deposit; 2) the style and extent of alteration; 3) the timing of mineralization and alteration in relation to each other, to deformation and deposition. This data provides great insight into the metallogensis of the deposit, including the source of uranium, transportation, and precipitation. When all of this data is

evaluated it provides a depositional model for the Michelin deposit and potentially aid further exploration throughout the Aillik Group and possibly the rest of the Central Mineral Belt.

## **8.2 Genetic Model for Metallogenesis**

The uranium mineralization at Michelin is thought to have developed as a result of widespread uranium stripping from Aillik Group felsic volcanic rocks, which was then transported via hydrothermal fluid to specific sites. The specific mechanisms involved during this process remain poorly understood. The relationship between uranium and thorium is a very useful tool in defining genetic models for uranium mineralization. The Th/U ratio can provide insight into both the source and timing of uranium mineralization, and determine if uranium was transported in solution, and the nature of that solution.

The Th/U ratio is an important indicator of uranium mobility because unlike uranium, thorium has no oxidized state and is therefore immobile due to oxidation caused by weathering, diagenesis, alteration, and/or metamorphism. Rocks that have very high ratios will be depleted in uranium and rocks that have very low ratios will be enriched in uranium. Rocks that have extremely low Th/U ratios involve hydrothermal processes as fractional crystallization could not account for a strong enrichment in U with no enrichment in Th (Misra, 2000; Cuney, 2010).

Both the FP and CP rocks from the mineralized zone at Michelin have extremely low Th/U ratios, averaging 0.10. These rocks have Th values that average approximately 28 ppm, and exhibit almost no increases during alteration in mass balance calculations.

The extremely low Th/U ratios indicate that uranium mineralization at Michelin resulted from hydrothermal fluid processes and textural evidence indicates that mineralization took place after metamorphism; therefore uranium mineralization at Michelin is epigenetic.

### **8.2.1 Source of Uranium**

The source of uranium in most global deposits is highly evolved felsic plutonic and volcanic rocks, consisting predominantly of granitic plutons, rhyolites, and glassy volcanic ash or ash-rich sediments. The reason for this is that uranium is fractionated into felsic rocks. Typical granites and rhyolites contain about 5 ppm U, but highly evolved and differentiated felsic rocks generally average 10 ppm to as much as 15 ppm U (Misra, 2000). This high concentration of U combined with the fact that U is easily leached from these rocks makes them the primary source rocks. The uranium in the Michelin deposit, and other deposits and occurrences in the vicinity, was most likely sourced from the felsic volcanic rocks which host the deposit.

The FP and CP rocks which host the Michelin deposit are interpreted to be felsic volcanic ash-flows that are the products of highly evolved felsic melts. These rocks constitute part of a larger assemblage of intermediate to felsic rhyolitic flows, ash flows, volcanoclastic, and associated sedimentary rocks of the Aillik Group. Upon deposition, the ash-flow tuffs were interpreted to be mostly glassy, based on evidence from less deformed and metamorphosed equivalent rocks within the Aillik Group and most likely

enriched in alkalis, uranium, thorium, zirconium and a host of other incompatible elements (White and Martin, 1980).

Samples of unaltered FP felsic volcanics at Michelin average 9.26 ppm U, ranging from 5.1-79.3 ppm. Most of these rocks are not interpreted to be mineralized as 93 out of 103 samples unaltered samples analyzed U concentrations below 10 ppm. The samples above 10 ppm appear to be weakly mineralized. The average Th concentration for these rocks is 18.03 ppm, ranging from 15.0 to 26.6 ppm. The average Th/U ratio is 2.3 which is much lower than most evolved felsic rocks (Sighinolfi and Sakai, 1974), indicating uranium enrichment compared to Th. The low Th/U ratios of the rocks and high average Th and U contents suggests that the felsic volcanic rocks which host the Michelin deposit are highly evolved and enriched in uranium making them excellent source rocks.

### **8.2.2 Leaching and Transport of Uranium**

Th/U ratios of mineralized felsic volcanic rock are extremely low indicating that uranium mineralization most likely resulted from circulating hydrothermal fluids and not magmatic differentiation. In order for a fluid to be enriched in uranium, U has to be leached from the initial source rock into the hydrothermal fluid to be transported to the site of deposition. Uranium is very easily leached and transported under oxidizing conditions (Rich *et al.*, 1977; Misra, 2000).

Cuney (2010) notes that several global deposits that share similar alteration styles are the result of thermal events that are able to circulate large volumes of hydrothermal fluid at high temperatures to produce sodic metasomatism along crustal scale structures

either during or after major orogenic or other tectonic events. The circulating fluid would form discontinuous occurrences of sodic metasomatism along regional ductile structures, most often consisting of fairly narrow but regionally extensive shear zones. The hydrothermal fluid would have temperatures ranging from 350 to 550 °C and be very alkaline rich and oxidizing. The oxidizing solution would leach uranium from the host rock as it circulated through the regional structure.

Within the mineralized zone at Michelin there is strong evidence of shearing in one of the CP units. This unit contains rotated feldspar phenocrysts which have been strongly augened by thin wisps of mafic alteration minerals. The formation of aegirine and the occurrence of small mylonite zones within the mineralized zone provide evidence of high temperature deformation. Evidence from regional mapping suggests that the Michelin deposit is situated within one of several large regional shear zones within the Aillik Group that host most of the uranium occurrences in the area, including Michelin, Rainbow, Jacques Lake, Mustang Lake, White Bear (formally Burnt Lake) to name a few (Sparkes and Kerr, 2008). There is also evidence of Zr leaching from within the sodic envelope suggesting that the hydrothermal fluids which caused the sodic metasomatism may have also leached Zr and possibly other trace elements from the rock along this regional deformation zone to be deposited in favorable horizons. The geochemical evidence did not indicate that U was leached from the sodic envelope but most of the samples collected contained weak mineralization which would mask the effect of leaching. The thermal energy required to heat the hydrothermal fluid was either a result of metamorphism which based on the granoblastic texture of the matrix is interpreted to

have taken place at high temperatures, 400 to 500 °C, or from a deep seeded plutonic intrusive. There are several granitoid plugs which intrude the Aillik Group volcanics at ca. 1800 Ma.

When uranium is oxidized and leached from the host rock, the highly soluble uranyl ion ( $\text{U}^{6+}\text{O}_2$ )<sup>2+</sup> will form stable complexes with a number of ionic species. These species depend on the characteristics of the hydrothermal fluid, including temperature, alkalinity, pH, and the host rocks. Generally under alkaline conditions, with a pH > 8 the ionic species is carbonate (Misra, 2000). Due to the sodic metasomatism and increased sodic alteration, the hydrothermal fluid which carried the uranyl ions is interpreted to be strongly alkaline, with a relatively high pH, of about 8 to 10. This would suggest that the ionic species would either be carbonate or hydroxyl as both are favored in solutions with a high pH. The presence of calcite as a late stage alteration mineral in the mineralized zone suggests that the hydrothermal fluid was rich in carbonate. Therefore uranium was most likely transported through solution as uranyl carbonate complexes. According to Rich *et al.* (1977), the predominant uranium complexes in alkaline solutions are  $[\text{UO}_2(\text{CO}_3)_2]^{2-}$  and  $[\text{UO}_2(\text{CO}_3)_3]^{4-}$  and that the amount of uranium that can be carried by these complexes in oxidizing solutions is more than sufficient to account for the formation of economic deposits. Due to the high concentration of alkalies and the high ratio of  $\text{Na}^+/\text{K}^+$  in solution these uranyl carbonate complexes may have been sodium-bearing as well. Studies done by White and Martin (1980) suggest that fluorine was probably also involved in U transport at Michelin, indicated by the presence of fluorite sporadically throughout the deposit. Fluorite is found sporadically throughout the

Michelin deposit but in very minimal amounts, not enough to account for the amount of uranium mineralization at Michelin.

The strong sodic alteration that affects the mineralized zone suggests that the hydrothermal fluid was strongly alkaline-rich, and had a high  $\text{Na}^+/\text{K}^+$  ratio. This would explain the ion exchange of  $\text{K}^+$  for  $\text{Na}^+$  and the formation of sodic-rich alteration minerals. The fluid also passed through the volcanic rocks of the Aillik Group which are strongly alkaline with a combined total alkalies of about 9 wt. %. Based on the strong hematite alteration, combined with magnetite destruction, the fluid was oxidized. This would also explain the leaching of uranium from the host rock into solution. An oxidizing and alkaline-rich solution would also explain the crystallization of the  $\text{Fe}^{3+}$  bearing sodic amphiboles and sodic pyroxenes.

The different alteration styles at Michelin would indicate that the hydrothermal fluid interacted with the felsic volcanic host rocks at a variety of temperatures. Sodic metasomatism outside of the mineralized zone which involves the ion exchange of  $\text{K}^+$  for  $\text{Na}^+$  favors a lower temperature fluid, in the range of 200 to 300 °C (White and Martin, 1980). However, the specific alteration styles within the mineralized zone indicate a hotter hydrothermal fluid in the range of 350 to 550 °C, as evidenced by quartz dissolution. According to White and Martin (1980), the solubility of quartz increases with increasing temperature and the efficient quartz dissolution in the mineralized zone at Michelin is consistent with a relatively hot hydrothermal fluid. A hot hydrothermal fluid could have penetrated the rocks of the Michelin deposit along favorable horizons, either within the CP rocks or along the contacts. This would explain why the dissolution of



quartz occurs in zones quartz still remains in the middle of thicker units. During wall rock interaction as the fluid circulated throughout the rock away from its point of ingress, the temperature of the fluid decreased to a point where it could no longer dissolve quartz. Oxidation would most likely also decrease through wall rock interactions, becoming weaker thus explaining why hematitization, magnetite destruction and mineralization are not as strong near the centers of thicker units, in particular the FP units. As the hydrothermal fluid moved away from the center of infiltration, further and further into the hanging wall and foot wall, ion exchange, metasomatism, sporadic hematitization and mineralization eventually dyed out.

### **8.2.3 Precipitation and Concentration**

SEM-MLA analyses of samples from the Michelin mineralized zone indicate that the uranium mineralization consists predominantly of uraninite, with minor amounts of brannerite and coffinite. According to Misra (2000) there are several mechanisms which reduce uranyl complexes, including carbon either as organic matter or graphite, reduced sulfur species ( $\text{H}_2\text{S}$  or  $\text{HS}^-$ ), and  $\text{Fe}^{2+}$ , reduction by  $\text{Fe}^{2+}$  involves the oxidation of  $\text{Fe}^{2+}$  to  $\text{Fe}^{3+}$ .

There is no organic matter or graphite at Michelin deposit so this would eliminate these two mechanisms for reduction. Also, there is little to no sulfide mineralization associated with the Michelin deposit so the reduction of uranyl complexes due to a reduced sulfur species is also extremely unlikely. As described in Chapter 6, section 6.3 hematite alteration at Michelin is attributed to the oxidation of magnetite. Hematite

alteration at Michelin is also closely associated with uranium mineralization suggesting that the two are genetically linked. Uranium mineralization is always accompanied by hematite alteration, and the two correlate very well as more intensely mineralized areas are also strongly hematitized, suggesting a strong paragenetic association between the two. The high temperature of the hydrothermal fluid also suggests that  $\text{Fe}^{2+}$  is an effective reductant as uranous minerals in global deposits are seldom found in paragenetic association with ferric oxides in low-temperature deposits, but such an association is common in high-temperature deposits (Misra, 2000).

During the process of oxidation of magnetite to hematite there is a change in the oxidation state of ferric  $\text{Fe}^{2+}$  in magnetite which reduces the soluble uranyl species to insoluble an insoluble one, precipitating uraninite (El-Kammar *et al.*, 2001). The reduction of the uranyl species occurs almost instantaneously once the redox potential changes, explaining why uranium mineralization is so strongly associated with hematite alteration

The concentration of uranium at Michelin is due to a number of factors. At the Michelin deposit fluid flow appears to be focused through the CP units transgressing the contacts with the adjacent FP units. One CP unit in particular appears to be strongly sheared and mineralized suggesting that mineralizing fluids were focused through the area of deformation. It seems that deformation of the CP units channeled the hydrothermal fluid through the deposit and the individual CP units were more permeable for the fluid explaining why they are more strongly altered and mineralized compared to the FP units. The hotter and more alkaline fluid that was focused through these permeable

horizons dissolved quartz which created room for alteration minerals and uranium to precipitate.

### **8.3 Deposit Classification**

Since its discovery, the Michelin deposit has been classified as several different uranium deposit types, including: volcanic-hosted, Na-metasomatic, fenitization, metamorphic, hydrothermal, IOCG, and vein type (Minatidis, 1976; Rich *et al.*, 1977; Gandhi, 1978; Evans, 1980; Gandhi and Bell, 1996; Smith *et al.*, 2005; Sparkes and Kerr, 2008; Cuney *et al.*, 2012).

Based on the alteration and mineralization styles the Michelin deposit is interpreted to be a Na-metasomatic uranium deposit as described in Chapter 2. The Michelin deposit contains numerous similarities with these deposits in relation to alteration, and metallogenesis. The host rocks of the Michelin deposit consist of metamorphosed felsic volcanics that are alkali and uranium rich, containing approximately 9 wt. % total alkalies and 9 ppm U. It is thought that these rocks, or equivalent rocks within the Aillik Group may have provided uranium and sodium for the altering fluid. The felsic volcanic host rocks of the Michelin deposit have undergone intense, pervasive sodic alteration consisting of sodic metasomatism of potassium feldspar along with the formation of secondary sodium rich minerals such as albite, aegerine-augite and sodic amphiboles. These rocks have also undergone quartz dissolution resulting in the removal of quartz phenocrysts and groundmass quartz, and hematitization from the oxidation of magnetite. Mass balance calculations indicate a

strong enrichment in  $\text{Na}_2\text{O}$  and U, moderate enrichment in Zr, V, and As, and a slight enrichment in the LREE, Y and Sr within the mineralized zone. These calculations also indicate near total depletions in  $\text{K}_2\text{O}$ , Rb, Tl, and Sb, and moderate depletions in  $\text{SiO}_2$ . Finally, late stage carbonatization occurs within the mineralized zone along with the possible formation of andradite and allanite. The formation of these minerals could correspond to a late stage calcium-magnesium alteration. Uranium occurs as micron sized uraninite grains with minor brannerite and the deposit has an average grade of 0.18 %  $\text{U}_3\text{O}_8$ .

The Michelin deposit is interpreted to have formed in a regional shear zone that stretches from Michelin to Jacques Lake and includes several uranium occurrences that have been sodic altered, including White Bear, formally Burnt Brook. Sodium, uranium, zirconium and other elements are interpreted to have been leached from the felsic volcanic host rock by an alkaline rich, oxidizing hydrothermal solution. This fluid was then transported through the shear zone, creating sodic alteration within the rock. The shear zone was focused through the Mine Series of CP and FP felsic volcanics and particularly within the CP units, where the oxidizing solution oxidized the magnetite grains to hematite, leading to the reduction of  $\text{U}^{6+}$  out of solution and precipitation as uraninite. Precipitation of uraninite was concentrated into open space created through the dissolution of quartz.

At the Michelin deposit there appear to be several late stage events that post-date the main stage of mineralization, where remobilized uranium is concentrated in veins, mylonitic zones, and fractures. Evans (1980) reports that several drill holes intersected a

massive pitchblende seam about 3 cm wide which the author interpreted to be fracture-controlled mineralization. Rare fractures at the Michelin deposit are filled with agglomerates of black colored minerals that assay very high in uranium. The dark material is interpreted to be uraninite grains or a mixture of both uraninite and mafic minerals. Uranium mineralization appears to have been remobilized into these fractures, concentrating as fracture-controlled veins, most likely during the Labradorian and Grenvillian orogenies.

The mineralizing event at Michelin corresponds with other Na-metasomatized deposits which formed between 1.9 to 1.7 Ga. This time period is host to a number of Na-metasomatic deposits, including the highly mineralized Krivoy-Rog district in the Ukraine, and the Skuppesavon and Bjorkramyran deposits in northern Sweden (Cuney and Kyser, 2008).

#### **8.4 Conclusion**

The Michelin deposit is hosted in a tight sequence of alternating units of CP and FP felsic volcanics termed the Mine Series. The Mine series is hosted in a broader stratigraphic sequence of FP felsic volcanics intermixed with sporadic units of CP felsic volcanics, which have both been intruded by several generations of mafic and granitoid intrusives. Individual units generally maintain their thickness over the approximate 1,200 m strike length of the deposit, striking towards the northeast (~070) and dipping to the southeast at 40-60 degrees. The felsic volcanic rocks have been regionally metamorphosed to lower amphibole facies and deformed during the Makkovikian

Orogeny. Deformation has created a prominent, regionally penetrative foliation, defined by thin wisps of biotite and hornblende, which have a similar orientation to the stratigraphic units.

The FP and CP felsic volcanics are identical with the only difference between the two rock types being the size and abundance of the feldspar phenocrysts. Geochemically the two rock types are equivalent and are classified as being metaluminous, high-K, subalkaline, calc-alkaline rhyolites. Four distinct varieties of mafic dikes, distinguished by deformation and geochemistry, intrude these volcanic rocks, including pre-kinematic biotite-hornblende schist, syn-kinematic gabbroic dike, post-kinematic strongly magnetic gabbroic dike, and a post-kinematic diorite dike.

The mineralized zone is comprised of a series of tightly layered FP and CP felsic volcanics which have been intensely altered and strongly mineralized. These units are geochemically related and texturally equivalent to unaltered units outside the mineralized zone but they have a drastically different mineralogy and geochemistry. These units are comprised predominantly of albite, which can reach up to 85 % in intensely altered rock. The matrix is 80-90 % albite with minor amounts of calcite and sodic amphiboles. Mafic minerals have been altered to sodic amphiboles and sodic pyroxenes forming small agglomerates with zircon, titanite, magnetite/hematite, albite, calcite, and uranium bearing minerals. Geochemically these rocks are classified as metaluminous to peralkaline, low-K, alkaline, calc-alkaline rhyolites, but now with average  $\text{SiO}_2$  contents of 67.5 wt. % and  $\text{Na}_2\text{O}$  and  $\text{K}_2\text{O}$  contents averaging 9.5 and 0.10 wt. %, respectively.

Uranium mineralization is concentrated along the contacts between the CP and FP units, within the CP units, adjacent to the contacts with syn-kinematic mafic dikes, and in strongly deformed shear and mylonite zones. Uranium mineralization consists of micron-sized grains of uraninite that are closely associated with hematite alteration and titanite. Uraninite grains contain cation substitutions within the crystal structure consisting of Pb, Si, Ca, Fe, Zr, Ti, and LREE. Based on the different cation substitutions there are three distinct uraninite groups recognized. The first consists of only Pb, the second consists of Si, Ca, Pb, Zr, or Ce, and the third consists of Si, Ca, Fe, Zr, and Ti. The latter two groups will often enclose the first group, indicating that the first group was most likely the first to precipitate. Minor amounts of brannerite, coffinite and uranophane also occur within the mineralized zone. Uraninite grains are often associated with several minerals which are either primary, or as a result of alteration. These minerals include: albite, sodic amphibole, sodic pyroxene, magnetite, hematite, zircon, titanite, calcite plus possibly allanite, andradite, apatite, monazite and barite.

There are two styles of alteration that affect the felsic volcanic rocks of the Michelin deposit. The first is a widespread pervasive sodic metasomatism that envelopes the deposit, extending into the hanging wall and foot wall. Sodic metasomatism is marked by an ion exchange of  $K^+$  for  $Na^+$  in potassium feldspar, altering them to albite. This pervasively affects all of the potassium feldspar grains in the matrix and the large potassium feldspar phenocrysts. This process completely removes  $K_2O$ , Rb, and Tl from the rock and increases the  $Na_2O$  content by as much as 3-5 wt. %.

The second style of alteration is focused towards the mineralized zone. This alteration is very intense and several different styles of alteration are observed. The first quartz dissolution, during which quartz is nearly completely removed from the rock, is marked by  $\text{SiO}_2$  decreases of about 8 wt. %. The space created from the dissolution of quartz within the groundmass and phenocrysts is filled with alteration minerals including sodic amphibole, sodic pyroxene, albite, calcite, and uraninite. During quartz dissolution there is a further increase in sodic alteration, which is marked by the alteration of pre-existing biotite and hornblende into sodic amphiboles and pyroxenes and the formation of new sodic amphiboles, sodic pyroxenes, and albite, increasing the  $\text{Na}_2\text{O}$  content of the rock to 9-11 wt. %. Oxidation of magnetite to hematite occurs throughout the mineralized zone, occurring at different intensities, which seems to be a function of fluid flow. The oxidation of magnetite causes the reduction of uranyl species in the hydrothermal fluid leading to the precipitation of uraninite in available space. Titanite appears to have remained conserved during alteration but is closely associated with uraninite grains, suggesting that it was remobilized during alteration and reformed with uraninite. Zirconium is also mobilized during alteration, forming as new secondary growth around pre-existing grains, the zirconium content within the mineralized zone doubles going from an average of 450 ppm in unaltered rock to 950 ppm in mineralized rock. Mass balance calculations indicate slight enrichments of  $\text{Al}_2\text{O}_3$ ,  $\text{CaO}$ ,  $\text{FeO}$ ,  $\text{Sr}$ ,  $\text{V}$ ,  $\text{Y}$ , LREE,  $\text{As}$ , and  $\text{Be}$  during alteration, and slight depletions in  $\text{Ba}$  and  $\text{Sb}$ . Finally, calcite forms near the later stages of alteration filling in the remaining available pore space within the rock.



## **8.5 Recommended Work**

The following is a list of recommendations that would complement and expand upon the results of this study. Further understanding of the geological, deformational, alteration and mineralization processes of the Michelin deposit will be beneficial for understanding other uranium deposits and occurrences in the Aillik Group, helping with future uranium exploration throughout the CMB.

Microprobe analysis of the altered and non-altered mineral assemblages found in the felsic volcanic rocks of the Michelin deposit is recommended. Microprobe work would allow for the determination of the mineral constituents and their exact stoichiometry of the mineral grains. This would be beneficial in determining the exact alteration changes that took place. Uranium-bearing grains need to be analyzed with the microprobe to determine which cations have substituted within the uraninite structure, and the amount of cation exchange that occurred.

More controlled sampling of the mafic dikes within both the sodic envelope and mineralized would be beneficial to build a better database of the mafic dikes, and to determine if the dikes have been affected, and to what intensity, by alteration and mineralization. Limited sampling during this study suggests that the pre-kinematic dikes have undergone some degree of sodic-metasomatism and weak mineralization, suggesting they were emplaced prior to both events. While the syn-kinematic dikes contain only weak sodic alteration, suggesting they were emplaced after mineralization but before alteration and deformation had ceased. More dikes need to be sampled to determine if they have been affected by alteration and better control measures during

sampling is needed to make sure the samples are not contaminated by adjacent felsic volcanic rocks, which many of the mafic dikes sampled in the ore zone have been.

Age dating of the mafic dikes would also be beneficial to determine their age of emplacement. This could allow several of the dike varieties to be correlated with other intrusive and deformational events that affect the felsic volcanic rocks of the Makkovik Province. Age dating would also narrow the timing of mineralization and alteration as the syn-kinematic dikes appear to have been emplaced during the final stages of mineralization and alteration and the pre-kinematic dikes appear to have been emplaced prior to both events. Age dating of the mafic dikes was attempted during this thesis but the availability of large, quality in-situ zircons from thin sections was too low and of poor quality. A new method would be needed to age date these units, a greater sample amount and a technique that will enable smaller zircons to be analyzed as some of the units only contain zircons that are 5-20 microns in diameter.

More, detailed age dating of the individual units within the felsic volcanic sequence at Michelin is needed. Several attempts were made during this thesis to age date several felsic volcanic units throughout the Michelin deposit but getting an accurate age date was not possible. A larger sample would be required to provide enough large, quality zircons for age dating. Extensive age dating of the felsic volcanic units would determine if the units were deposited in succession, or if they were folded or faulted into place, putting older strata adjacent to younger strata.

Finally, more detailed regional mapping is required to understand the deformational history of the rocks. Evidence suggests that the volcanic sequences at

Michelin have been deformed and possibly thrust faulted or folded into their current position. Outcrop exposure is very limited throughout this portion of the CMB but correlations could be made from drilling combined with outcrop. Also, if the Michelin deposit is hosted in a regional shear zone, that possibly hosts other uranium deposits/showings then better constraints on this shear zone is needed as it would be the most prospective place to host more undiscovered, significant uranium mineralization.

## References

- Alexandre, P. and Kyser, T. K. (2005):** Effects of Cationic Substitutions and Alteration in Uraninite, and Implications for the Dating of Uranium Deposits. *The Canadian Mineralogist*, volume 43, pages 1005-1017.
- Bailey, D. G. (1978):** The Geology of the Walker Lake – Maclean Lake Area (13K/9, 13J/12), Central Mineral Belt, Labrador. Report of Activities for 1977, R.V. Gibbons (Editor), Mineral Development Division, Department of Mines and Energy, Government of Newfoundland and Labrador, St. John's, Newfoundland, 8 pages.
- Bailey, D. G. (1979):** Geology of the Walker – Maclean Lake Area, 13K/9E, 13J/12, Central Mineral Belt, Labrador. Mineral Development Division, Department of Mines and Energy, Government of Newfoundland and Labrador. Report 78-3, St. John's, Newfoundland, 22 pages.
- Barker, F. (1979):** Trondhjemite; definition, environment and hypotheses of origin. *In* Barker, F. (Editor), Trondhjemites, dacites, and related rocks, pages 1-12.
- Barrett, S., Barbour, D. and Glover, J. (2008):** 2007/2008 Assessment Report on Diamond Drilling Programs on the Michelin Property of the CMB Project, Labrador, Canada on licence 9412M, NTS Sheets: 13K/09E & 13J/12. Aurora Energy Resources, Assessment Report, 556 pages.
- Barrett, S. and Ash, S. (2009):** 6<sup>th</sup> Year Supplemental Report on Diamond Drilling On The Michelin Property Of The CMB Project, Labrador, Canada for licence 9412M, NTS Sheets: 13K/09E & 13J/12. Aurora Energy Resources, Assessment Report, 441 pages.
- Batterson, M. and Liverman, D. (2000):** Contrasting Styles of Glacial Dispersal in Newfoundland and Labrador: Methods and Case Studies. Government of Newfoundland and Labrador, Department of Mines and Energy, Geological Survey, 31 pages.
- Beaven, A. P. (1958):** The Labrador Uranium Area. Geological Association of Canada Proceedings, volume 10, pages 137-145.
- Beaven, A. P. and Gandhi, S. S. (1976):** Uranium Joint Venture Areas, Labrador, 1976. BRINEX Limited, Internal Report, 33 pages.
- Best, M. G. and Christiansen, E. H. (2001):** Igneous Petrology. Blackwell Science Inc., Malden, Massachusetts, 458 pages.

- Booth, J. K. B., Leigh, O. E. and Archer, D. J. (1979):** Michelin/Kitts Project, Volume 1, Report on the Geology and Reserves. BRINEX Ltd., In-house technical report, 227 pages.
- Bouman, C., Schwieters, J., Cocherie, A., Robert, M. and Wieser, M. (2014):** In Situ U-Pb Zircon Dating Using Laser Ablation – Multi Ion Counting – ICP-MS (LA-MIC-ICP-MS). Thermo Scientific, Application Note 30021, 6 pages.
- BRINEX (1976):** Kitts-Michelin Geological Evaluation, Base Data Report. BRINCO Projects Group, BRINEX Limited, Internal Report, 62 pages.
- BRINEX (1977):** Technical Review of Kilborn Feasibility Study for Kitts/Michelin Project, March 1977. BRINEX Limited, Internal Report, 380 pages.
- BRINEX (1979a):** Kitts-Michelin Project, Project Report. BRINEX Limited, Internal Project Report, volume 1, 29 pages.
- BRINEX (1979b):** Kitts-Michelin Project Information Summary. BRINEX Limited, Internal Report, 35 pages.
- BRINEX (1980):** Labrador Uranium Joint Venture Including the Kitts-Michelin Project, Progress Report for the Third Quarter, 1980. BRINEX Limited, Internal Report, 66 pages.
- Burns, P. C. (1999):** The Crystal Chemistry of Uranium. *In* P. C. Burns and R. Finch (Editors) Uranium: Mineralogy, Geochemistry and the Environment. Mineralogical Society of America, Reviews in Mineralogy volume 38, pages 23-90.
- Corfu, F., Hanchar, J. M., Hoskin, P. W. O. and Kinny, P. (2003):** Atlas of Zircon Textures. Reviews in Mineralogy and Geochemistry, January 2003, volume 53, pages 469-500.
- Cornelius, K. D. (1976):** Preliminary Rock Type and Genetic Classification of Uranium Deposits. Scientific Communications, Economic Geology, volume 71, pages 941-948.
- Cuney, M. and Kyser, K. (2008):** Recent and Not-So-Recent Developments in Uranium Deposits and Implications for Exploration. Mineralogical Association of Canada, Short Course volume 39, Quebec City, Canada, 257 pages.
- Cuney, M. (2010):** Evolution of Uranium Fractionation Processes Through Time: Driving the Secular Variation of Uranium Deposit Types. Economic Geology, volume 105, pages 553-569.

- Cuney, M., Emetz, A., Mercadier, J., Mykchaylov, V., Shunko, V. and Yuslenko, A. (2012):** Uranium Deposits Associated with Na-Metasomatism From Central Ukraine: A Review of Some of the Major Deposits and Genetic Constraints. *Ore Geology Reviews*, volume 44, pages 82-106.
- Cunningham-Dunlop, I. and Lee, C. (2008):** An Update on the Exploration Activities of Aurora Energy Resources Inc. on the CMB Uranium Property, Labrador, Canada, During the Period January 1, 2007 to December 31, 2007, Part II – CMB Mineral Resources. Located on NTS Sheets: 13J/11, 13J/12, 13J/13, 13J/14, 13K/03, 13K/06, 13K/09. 43-101F1 Technical Report, 215 pages.
- Doak, R. S., Gandhi, S. S. and Kataki, T. (1969):** Exploration in the Kaipokok Bay – Big River Area, Labrador, Surface Exploration of Michelin Prospect, Labrador. Annual Report, 1969. BRINEX/Metall. A.G. Joint Venture, 12 pages.
- El-Kammar, A. M., Salman, A. E., Shalaby, M. H. and Mahdy, A. I. (2001):** Geochemical and Genetical Constraints on Rare Metals Mineralization at the Central Eastern Desert of Egypt. *Geochemical Journal*, volume 33, pages 117-135.
- Evans, D. F. (1980):** Geology and Petrochemistry of the Kitts and Michelin Uranium Deposits and Related Prospects, Central Mineral Belt, Labrador. Ph.D. Thesis; Queen's University, Kingston, Ontario, 350 pages.
- Ewing, R. C. (1999):** Radioactivity and the 20<sup>th</sup> Century. *In* P. C. Burns and R. Finch (Editors) *Uranium: Mineralogy, Geochemistry and the Environment*, Mineralogical Society of America, *Reviews in Mineralogy*, volume 38, pages 1-22.
- Faure, G. (1977):** Principles of Isotope Geology. Smith-Wyllie Intermediate Geology Series. John Wiley and Sons Inc., Canada, 464 pages.
- Faure, G. (1998):** Principles and Applications of Geochemistry. Prentice Hall, Second Edition, 625 pages.
- Ferguson, J. (1988):** The Uranium Cycle. Recognition of Uranium Provinces of a Technical Committee Meeting, International Atomic Energy Agency, pages 3-16.
- Fullerton, W. (2014):** REE Mineralisation and Metasomatic Alteration in the Olserum Metasediments. Dissertations in Geology at Lund University, Master's Thesis, number 411. Department of Geology, Lund University, 110 pages.

- Gandhi, S. S. (1978):** Geological Setting and Genetic Aspects of Uranium Occurrences in the Kaipokok Bay – Big River Area, Labrador. *Economic Geology*, volume 73, 31 pages.
- Gandhi, S. S. and Bell, R. T. (1996):** Volcanic-associated Uranium. *Geology of Canadian Mineral Types*, Geological Survey of Canada, *Geology of Canada*, number 8, pages 269-276.
- Garsed, I. (2005):** Confidential Memo on the Results of Michelin East Mapping. Frontier Development Group Internal Report, 17 pages.
- Gifkins, C., Large, R. R. and Herrmann, W. (2005):** Altered Volcanic Rocks, A Guide to Description and Interpretation. University of Tasmania, 275 pages.
- Gomez-Gonzalez, M. A., Garcia-Guinea, J., Garrido, F., Townsend, P. D. and Marco, J-F. (2015):** Thallium and Manganese Complexes Involved in the Luminescence Emission of Potassium-Bearing Aluminosilicates. *Journal of Luminescence*, volume 159, pages 197-206.
- Gower, C. F., Flanagan, M. J., Kerr, A. and Bailey, D. G. (1982):** Geology of the Kaipokok Bay – Big River Area, Central Mineral Belt, Labrador. Mineral Development Division, Department of Mines and Energy, Government of Newfoundland and Labrador. Report 82-7, St. John's, Newfoundland, 81 pages.
- Gower, C. F. and Ryan, B. (1986):** Proterozoic Evolution of the Grenville Province and Adjacent Makkovik Province in East-Central Labrador. *In* J. M. Moore, A. Davidson and A. J. Baer (Editors) *The Grenville Province*. Geological Association of Canada, Special Paper 31, pages 281-295.
- Gower, C. F. and Ryan, B. (1987):** Two Stage Felsic Volcanism in the Lower Proterozoic Upper Aillik Group, Labrador, Canada: Its Relationship to Syn- and Post- kinematic Plutonism. *In* Pharaoh, T. C., Beckinsale, R. D. and Rickard, D. (Editors), *Geochemistry and Mineralization of Proterozoic Volcanic Suites*, Geological Society Special Publication number 33, pages 201-210.
- Grant, J. A. (1986):** The Isocon Diagram – A Simple Solution to Gresens' Equation for Metasomatic Alteration. *Economic Geology*, volume 81, pages 1976-1982.
- Gregory, M. J., Wilde, A. R. and Jones, P. A. (2005):** Uranium Deposits of the Mount Isa Region and Their Relationship to Deformation, Metamorphism, and Copper Deposition. *Economic Geology*, volume 100, pages 537-546.

- Gresens, R. L. (1967):** Composition – Volume Relationships of Metasomatism. Chemical Geology, volume 2, pages 47-55.
- Guilbert, J. M. and Park, C. F. jr. (1986):** The Geology of Ore Deposits. W. H. Freeman and Company, New York, 985 pages.
- Hertel, M., Podhorski-Thomas, M., Durston, K., Edwards, C. and Allard, S. (2009):** Michelin Uranium Project, Labrador, Canada. NI 43-101 Technical Report on Preliminary Assessment, 221 pages.
- Hinchey, A. M. (2007):** The Paleoproterozoic Metavolcanic, Metasedimentary and Igneous Rocks of the Aillik Domain, Makkovik Province, Labrador (NTS Map Area 13O/03). Current Research, Newfoundland and Labrador Department of Natural Resources Geological Survey, Report 07-1, pages 25-44.
- Hinchey, A. M. and Rayner, N. (2008):** Timing Constraints on the Paleoproterozoic, Bimodal Metavolcanic Rocks of the Aillik Group, Aillik Domain, Makkovik Province, Labrador. In GAC-MAC 2008, Abstract volume 33.
- Hinchey, A. M. and LaFlamme, C. (2009):** The Paleoproterozoic Volcano-Sedimentary Rocks of the Aillik Group and Associated Plutonic Suites of the Aillik Domain, Makkovik Province, Labrador (NTS Map Area 13J/14). Current Research, Newfoundland and Labrador Department of Natural Resources Geological Survey, Report 09-1, pages 159-182.
- Hitzman, M. W. and Valenta, R. H. (2005):** Uranium in Iron Oxide-Copper-Gold (IOCG) Systems. Society of Economic Geology, Economic Geology, volume 100, pages 1657-1661.
- Hoffman, E. L. (1992):** Instrumental Neutron Activation in Geoanalysis. Journal of Geochemical Exploration, volume 44, 23 pages.
- Irvine, T.N., and Baragar, W.R.A. (1971):** A Guide to the Chemical Classification of the Common Volcanic Rocks. Canadian Journal of Earth Science, issue 8: pages 23-548.
- Kaur, P., Chaudhri, N., Hofmann, A. W., Raczek, I, Okrusch, M., Skora, S. and Baumgartner, L. P. (2012):** Two-Stage, Extreme Albitization of A-type Granites from Rajasthan, NW India. Journal of Petrology, volume 53, number 5, pages 919-948.



- Kerr, A. (1994):** Early Proterozoic Magmatic Suites of the Eastern Central Mineral Belt (Makkovik Province), Labrador: Geology, Geochemistry and Mineral Potential. Government of Newfoundland and Labrador Department of Natural Resources Geological Survey, Report 94-3, 303 pages.
- Kerr, A., Ryan, B., Gower, C., Wardle, R. and Hall, J. (1994):** The Makkovik Province: Geological Overview, Unanswered Questions and Unexplained Reflections. Compiled by Wardle, R. J. and Hall, J.: Eastern Canadian Shield Onshore-Offshore Transect (ECSOOT), Transect Meeting (December 10-11, 1993), The University of Quebec and Montreal, number 34, pages 35-52.
- Ketchum, J. W. F., Culshaw, N. G. and Dunning, G. R. (1997):** U-Pb Geochronological Constraints on Paleoproterozoic Orogenesis in the Northwestern Makkovik Province, Labrador, Canada. Canadian Journal of Earth Science, issue 34, pages 1072-1088.
- LaFlamme, C., Hinchey, A. M. and Sylvester, P. J. (2009):** Preliminary Report on the Lithology of Volcano-Sedimentary Rocks of the Aillik Group, Aillik Domain, Makkovik Province. Current Research, Newfoundland and Labrador Department of Natural Resources Geological Survey, Report 09-1, pages 203-223.
- LeBas, M.J., LeMaitre, R.W., Streckeisen, A., and Zanettin, B. (1986):** A Chemical Classification of Volcanic Rocks Based on the Total Alkali Silica Diagram. Journal of Petrology, volume 27, pages 745-750.
- MacDougall, C. S. (1988):** A Metallogenic Study of Polymetallic, Granoplite Mineralization Within the Early Proterozoic Upper Aillik Group, Round Pond Area, Central Mineral Belt, Labrador. M.Sc. Thesis, Department of Earth Sciences, Memorial University of Newfoundland, St. John's, Newfoundland, 245 pages.
- MacKenzie, L. M. (1991):** Geology, Geochemistry and Metallogeny of the Burnt Lake Area, Central Mineral Belt Labrador, Canada. M.Sc. Thesis, Department of Earth Sciences, Memorial University of Newfoundland, St. John's, Newfoundland, 381 pages.
- MacLean, W. H. and Barrett, T. J. (1993):** Lithogeochemical Techniques Using Immobile Elements. Journal of Geochemical Exploration, volume 48, Pages 109-133.
- Maniar, P.D. and Piccoli, P.M. (1989):** Tectonic discrimination of granitoids. Geological Society of America, Bulletin 101, pages 635-643.

- Marmont, S. (1987):** Ore Deposit Models # 13. Unconformity-Type Uranium Deposits. Geoscience Canada, volume 14, pages 219-229.
- McConnell, J.W. and Ricketts, M.J. (2008):** A high-density lake-sediment and water survey in eastern Labrador (NTS map areas 13J/11, 13J/12, 13J/13, 13K/9, 13K/16, 13N/1 and 13O/4). Government of Newfoundland and Labrador, Department of Natural Resources, Geological Survey, Open File LAB/1427, 53 pages.
- McDonough, W.F. and Sun, S. (1995):** The Composition of the Earth. Chemical Geology, volume 120, number 3-4, pages 223-253.
- McSween, JR., H. Y., Richardson, S. M. and Uhle, M. E. (2003):** Geochemistry Pathways and Processes, Second Addition. Columbia University Press, New York, USA, 363 pages.
- Minatidis, D. S. (1976):** A Comparative Study of Trace Element Geochemistry and Mineralogy of Some Uranium Deposits of Labrador, and Evaluation of Some Uranium Exploration Techniques in a Glacial Terrain. M.Sc. Thesis, Department of Earth Sciences, Memorial University of Newfoundland, St. John's, Newfoundland, 216 pages.
- Misra, K. C. (2000):** Understanding Mineral Deposits, Chapter 14 Uranium Deposits. Kluwer Academic Publishers, Dordrecht, The Netherlands, pages 613-659.
- Neuendorf, K.K.E., Mehl Jr., J.P. & Jackson, J.A., (2005):** Glossary of Geology. American Geological Institute, Alexandria: 779 pp.
- Otto, A., Thomas, W., Barrett, S., Walsh, M. and Jory, J. (2013):** The Geology of the Michelin Rainbow Trend in the Central Mineral Belt, Labrador. Aurora Energy Internal Report, 30 pages.
- Peccerillo, A. and Taylor, S.R. (1976):** Geochemistry of Eocene Calc-Alkaline Volcanic Rocks from the Kastamonu Area, Northern Turkey. Contributions to Mineral Petrology, volume 58, pages 63-81.
- Piercey, S. J. (2004):** Calculating Analytical Precision and Accuracy with Geochemical Analysis. Mineral Exploration Research Centre and Department of Earth Sciences, Laurentian University, Sudbury, ON, 8 pages.
- Piercey, S. J. (2009):** Preliminary Evaluation of Drill Core Geochemical Data from the Jacques Lake Uranium Deposit, Central Mineral Belt, Labrador. Technical Report Prepared for Aurora Energy Resources, 24 pages.

- Piloski, M. J. (1976):** Annual Report on Exploration at Michelin Prospect, Part 1, BRINEX/Urangesellschaft Joint Venture, Labrador. British Newfoundland Exploration Limited Annual Report, 68 pages.
- Polito, P. A., Kyser, T. K. and Stanley, C. (2009):** The Proterozoic, Albitite-Hosted, Valhalla Uranium Deposit, Queensland, Australia: A Description of the Alteration Assemblage Associated With Uranium Mineralization in Diamond Drill Hole V39. Mineral Deosita, volume 44, pages 11-40.
- Rene, M. (2005):** Geochemical Constraints of Hydrothermal Alterations of Two-Mica Granites of the Moldanubian Batholith at the Okrouhla Radoun Uranium Deposit. Acta Geodynamica et Geomaterialia, volume 2, number 4 (140), pages 63-79.
- Rich, R. A., Holland, H. D. and Peterson, U. (1977):** Hydrothermal Uranium Deposits. Developments in Economic Geology 6. Elsevier Scientific Publishing Company, Amsterdam, The Netherlands, 274 pages.
- Robb, L. (2005):** Introduction to Ore-Forming Processes. Blackwell Publishing, Oxford, United Kingdom, 373 pages.
- Roberts, D. E. (1988):** The Olympic Dam Copper-Uranium-Gold Deposits. Recognition of Uranium Provinces of a Technical Committee Meeting, International Atomic Energy Agency, pages 263-272.
- Rollinson, H. (1993):** Using Geochemical Data: Evolution, Presentation, Interpretation. Pearson Education Limited, Essex, England, 352 pages.
- Romer, R. L., Scharer, U, Wardle, R. J. and Wilton, D. H. C. (1995):** U-Pb Age of the Seal Lake Group, Labrador: Relationship to Mesoproterozoic Extension-Related Magmatism of Laurasia. Canadian Journal of Earth Sciences, volume 32, number 9, pages 1401-1410.
- Ross, K. (2006):** Petrographical Study of the Michelin Uranium Deposit, Labrador. Prepared for Aurora Energy Resources Inc. by Panterra Geoservices Inc., 55 pages.
- Ruzicka, V. (1971):** Geological Comparision Between East European and Canadian Uranium Deposits. Canada Geology Survey Paper 70-40, pages 111-112.
- Ruzicka, V. (1996):** Unconformity-Associated Uranium. Geology of Canadian Mineral Deposit Types, Geological Survey of Canada, Geology of Canada, number 8, pages 197-210.

- Ryan, B. (1989):** Revolution in Distant Ages – the Precambrian Geology of Labrador. Newfoundland Section of the Geological Association of Canada, volume 10, pages 77-84.
- Ryan, B. (2000):** The Nain-Churchill Boundary and the Nain Plutonic Suite: A Regional Perspective on the Geologic Setting of the Voisey's Bay Ni-Cu-Co Deposit. Economic Geology, volume 95, number 4, pages 703-724.
- Scharer, U., Krogh, T. E. and Gower, C. F. (1986):** Age and Evolution of the Grenville Province in Eastern Labrador from U-Pb Systematics in Accessory Minerals. Contributions to Mineralogy and Petrology, 94, pages 438-451.
- Scharer, U., Kroug, T. E., Wardle, R. J., Ryan, B. and Gandhi, S. S. (1988):** U-Pb Ages of Early and Middle Proterozoic Volcanism and Metamorphism in the Makkovik Orogen, Labrador, Canadian Journal of Earth Science, issues 25, pages 1098-1107.
- Sharpley, f. J. (1980):** Michelin Deposit, Report on the Geology and Reserves. BRINEX Limited, in-house technical report, 84 pages.
- Sighinolfi, G. and Sakai, T. (1974):** Uranium and Thorium in Potash-Rich Rhyolites From Western Bahia (Brazil). Elsevier Scientific Publishing Company, Amsterdam, The Netherlands, Chemical Geology, volume 14, pages 23-30.
- Sinclair, S. M., Barr, S. M., Culshaw, N. G. and Ketchum, J. W. F. (2002):** Geochemistry and Age of the Aillik Group and Associated Plutonic Rocks, Makkovik Bay Area, Labrador: Implications for Tectonic Development of the Makkovik Province. Canadian Journal of Earth Science, issue 39, pages 731-748.
- Smith, R. L., Valenta, R., Butler, R., Hall, R. and Wilton, D. H. C. (2005):** First and Second Year Assessment Report Covering Geological, Geophysical, and Geochemical Investigations Pertaining to Map-Staked Licences: 9410M, 9411M, 9412M, 9413M, 9414M, 9482M, 9718M, 9719M, 9720M, 9721M, 9722M, 9723M, 10022M, 10046M, 10047M, 10048M, 10049M, 10050M, 10051M, 10052M, 10053M, 10054M, 10055M, 10056M, 10057M, 10058M, 10059M, 10343M, and 10344M. Located in the Central Mineral Belt of Labrador, Eastern Canada NTS Sheets: 13J/11, 13J/12, 13J/13, 13J/14, 13K/09. Altius Resources Inc. and Fronteer Development Group Inc., Assessment Report, 100 pages.
- Sparkes, G. W. and Kerr, A. (2008):** Diverse Styles of Uranium Mineralization in the Central Mineral Belt of Labrador: An Overview and Preliminary Discussion. Current Research (2008), Newfoundland and Labrador Department of Natural Resources, Geological Survey, Report 08-1, pages 193-227.

- Sparkes, G. W. and Dunning, G. R. (2009):** Preliminary Investigations into the Style, Setting and Timing of Uranium Mineralization, Jacques Lake Deposit, Central Mineral Belt, Labrador. Current Research (2009) Newfoundland and Labrador Department of Natural Resources Geological Survey, Report 09-1, pages 81-93.
- Sparkes, G. W. and Dunning, G. R. (2015):** New U-Pb Age Constraints on the Development of Uranium Mineralization Within the Central Mineral Belt of Labrador. Current Research (2015) Newfoundland and Labrador Department of Natural Resources Geological Survey, Report 15-1, pages 105-123.
- Stanley, C. R. and Madeisky, H. E. (1996):** Lithogeochemical Exploration for Metasomatic Zones Associated with Hydrothermal Mineral Deposits using Pearce Element Ratio Analysis. In: Short Course Notes on Pearce Element Ratio Analysis. Mineral Deposit Research Unit, University of British Columbia, Canada.
- Streckeisen, A. and Le Maitre, R.W. 1979.** A Chemical Approach to the Modal (QAPF) Classification of the Igneous Rocks. N. Jb. Miner.Abh. v. 136 volume 2, pages 169-206.
- Sun, S. S. and McDonough, W. F. (1989):** Chemical and Isotopic Systematics of Oceanic Basalts: Implications for Mantle Composition and Processes. Geological Society, London, Special Publications, volume 42, pages 313-345.
- Taylor, S.R., and McLennan, S.M. (1985):** The continental crust: its composition and evolution: Blackwell, Oxford, 312 pages.
- Wardle, R.J., Gower, C.F., James, D.T., Kerr, A., Miller, R.R., Nunn, G.A.G., Ryan, B., Swinden, S. and Wilton, D.H.C. (1995):** The Geology and Mineral Deposits of Labrador: A Guide for the Exploration Geologist. (Compiled by Wardle, R.J.) Geological Survey, Department of Natural Resources, Government of Newfoundland and Labrador, 134 pages.
- Wardle, R. J., Wilton, D. H. C. and Kerr, A. (1995):** The Makkovik Province. The Geology and Mineral Deposits of Labrador: A Guide for the Exploration Geologist, A Handout to Accompany a Workshop on the Geology and Mineral Deposits of Labrador, St. John's, Newfoundland, October 25, 1995, (Compiled by Wardle, R. J.), Government of Newfoundland and Labrador, Department of Natural Resources Geological Survey, pages 42-49.
- Wardle, R. J. (2005):** Uranium in Labrador, Preliminary Version, Government of Newfoundland and Labrador, Department of Natural Resources, 8 pages.

- Whalen, J.B., Currie, K.L., and Chappell, B.W. (1987):** A-Type Granites: Geochemical Characteristics, Discrimination and Petrogenesis. Contributions to Mineral Petrology, volume 95, pages 407-419.
- White, M. V. W. and Martin, R. F. (1980):** The Metasomatic Changes That Accompany Uranium Mineralization in the Nonorogenic Rhyolites of the Upper Aillik Group, Labrador. Canadian Mineralogist, volume 18, pages 459-479.
- Wilton, D. H. C. (1994):** The Mugford Group, Northern Labrador, Revisited: Notes From a Continuing Study. Current Research 1994, Government of Newfoundland and Labrador, Department of Mines and Energy, Geological Survey Branch, Report 94-01, pages 409-414.
- Wilton, D. H. C. (1996):** Metallogeny of the Central Mineral Belt and Adjacent Archean Basement, Labrador. Mineral Resources Report 8, Government of Newfoundland and Labrador, Department of Mines and Energy, Geological Survey, 178 pages.
- Wilton, D.H.C. and Cunningham-Dunlop, I. (2006):** The Exploration Activities of Aurora Energy Resources Inc. on the CMB Uranium Property, Labrador, Canada, During the Period June 2005 to December 2005. 43-101F1 Technical Report, 137 pages.
- Wilton, D. H. C. and Giroux, G. H. (2007):** The Exploration Activities of Aurora Energy Resources Inc. on the CMB Uranium Property, Labrador, Canada During the Period January 2006 to January 2007. Located on NTS Sheets: 13J/11, 13J/12, 13J/13, 13J/14, 13K/03, 13K/06, 13K/09. 43-101F1 Technical Report, 228 pages.
- Wilton, D. H. C., Giroux, G. H., Cunningham-Dunlop, I., Lee, C., Lincoln, J. and O'Dea, M. (2007):** An Update on the Exploration Activities of Aurora Energy Resources Inc. on the CMB Property, Labrador, Canada During the Period January 1, 2007 to October 31, 2007. Located on NTS Sheets: 13J/11, 13J/12, 13J/13, 13J/14, 13K/03, 13K/06, 13K/09. 43-101F1 Technical Report, 198 pages.
- Wilton, D. H. C. and Winter, L. (2012):** SEM-MLA (Scanning Electron Microprobe – Mineral Liberation Analyser) Research on Indicator Minerals in Till and Stream Sediments – An Example from the Exploration for Awaruite in Newfoundland and Labrador. Mineralogical Association of Canada Short Course 42, St. John's, NL, 18 pages.
- Winter, J. D. (2001):** An Introduction to Igneous and Metamorphic Petrology. Prentice-Hall Inc. Upper Saddle River, New Jersey, USA, 697 pages.

- Winter, L., Churchill, R. and Seymour, C. (2009):** Second and Third Year Assessment Report on Reconnaissance Radiometric Prospecting, Manual Trenching, Geological Mapping, and Rock Sampling for Map staked Licenses 015710M, 015746M and 015747M, Notakwanon River Property, Northern Labrador, NTS 13M09 and 13M16. Altius Resources Inc. Unpublished Report, 111 pages.
- Winchester, J. A., Floyd, P. A. (1977):** Geochemical Discrimination of Different Magma Series and their Differentiation Products Using Immobile Elements, Chemical Geology, volume 20 (4), pages 325-343.

# APPENDIX 1

**Sample Information for the 208 Geochemical Samples and 238 Thin Sections  
Collected for this Thesis, and the Additional 57 Geochemical Samples and Thin  
Sections Provided by Dr. Derek Wilton.**

## Legend

FP FV	Fine Grained Porphyritic Felsic Volcanic Rocks
CP FV	Coarse Grained Porphyritic Felsic Volcanic Rocks
MCP FV	Mafic-Rich Coarse Grained Porphyritic Felsic Volcanic Rocks
NP FV	Non Porphyritic Felsic Volcanic Rocks
Granite	Granite to Granodiorite
PRE MD	Pre-Kinematic, Biotite Hornblende Schist Dikes
SYN MD	Syn-Kinematic Gabbroic Dikes
PST1 MD	Magnetite-Rich Post-Kinematic Gabbroic Dikes
PST2 MD	Post-Kinematic Andesite Dikes
HW	Hanging Wall
FW	Foot Wall
SE	Sodic Envelope
OZ	Ore Zone



Sample Information for the 208 Geochemical Samples Collected for this Thesis, and the Additional 30 Thin Sections, 238 in Total.

Geochemical					Corresponding	
Sample #	Drill Hole	From (m)	To (m)	Rock Type	Thin Section #	Location
20001	M06-019	29.59	30.13	SYN MD	20255	HW
20003	M06-019	38.21	38.71	FP FV	20256	HW
20004	M06-019	40	40.5	PRE MD	20257	HW
20005	M06-019	42.34	42.84	CP FV	20258	HW
20006	M06-019	43.78	44.28	PRE MD	20259	HW
20008	M06-019	51.69	52.19	FP FV	20260	HW
20012	M06-019	74.16	74.66	FP FV	20261	HW
20014	M06-019	84.73	85.23	SYN MD	20262	HW
20015	M06-019	87.94	88.44	PST2 MD	20263	HW
20017	M06-019	94.41	94.91	FP FV	20264	HW
20018	M06-019	98.92	99.42	Granite	20265	HW
20019	M06-019	104	104.5	CP FV	20266	HW
20022	M06-019	117.3	117.8	PRE MD	20267	HW
20023	M06-019	123.86	124.36	FP FV	20268	HW
20025	M06-019	137.7	138.21	FP FV	20269	HW
20028	M06-019	154.98	155.48	FP FV	20270	HW
20029	M06-019	156.61	157.11	CP FV	20271	HW
20031	M06-019	164.38	164.88	FP FV	20272	HW
20032	M06-019	168.34	168.84	CP FV	20273	HW
20033	M06-019	171.5	172	FP FV	20274	HW
20034	M06-019	173.94	174.44	PRE MD	20275	HW
20035	M06-019	184.03	184.53	FP FV	20276	HW
20036	M06-019	188.48	188.98	PST1 MD	20277	HW
20038	M06-019	198.47	198.97	FP FV	20278	HW
20041	M06-019	220.37	220.87	CP FV	20279	HW
20044	M06-019	237.4	237.9	FP FV	20280	HW
20046	M06-019	248.44	248.94	PST2 MD	20281	HW
20048	M06-019	255.76	256.26	FP FV	20282	HW
20051	M06-019	272.14	272.64	FP FV	20283	HW
20052	M06-019	274.71	275.21	SYN MD	20285	HW
20053	M06-019	278.56	279.06	MCP FV	20286	HW
20054	M06-019	280.64	281.14	MCP FV	20287	HW
20056	M06-019	291.07	291.58	FP FV	20288	HW
20060	M06-019	317.15	317.65	FP FV	20289	HW

20062	M06-019	326.55	327.05	PRE MD	20290	HW
20063	M06-019	329.19	329.69	FP FV	20291	HW
20064	M06-019	332.6	333.1	PRE MD	20292	HW
20065	M06-019	338.13	338.63	FP FV	20293	SE
20066	M06-019	342.29	342.79	CP FV	20294	SE
20067	M06-019	347.6	348.1	SYN MD	20295	SE
20068	M06-019	350.22	350.72	CP FV	20296	SE
20071	M06-019	370.14	370.64	FP FV	20297	SE
20074	M06-019	387.44	387.94	FP FV	20298	SE
20077	M06-019	403.81	404.31	SYN MD	20299	SE
20079	M06-019	416.47	416.97	FP FV	20300	SE
20081	M06-019	422.54	423.02	PRE MD	20301	SE
20085	M06-019	495.01	495.51	FP FV	20302	FW
20086	M06-019	499.43	499.93	PRE MD	20303	FW
20088	M06-019	512.86	513.36	FP FV	20304	FW
20090	M06-019	531	531.5	FP FV	20305	FW
20091	M06-019	533.91	534.41	PST2 MD	20306	FW
20092	M06-019	536.12	536.62	Granite	20307	FW
20095	M06-019	549.53	550.03	FP FV	20308	FW
20098	M06-019	561.68	562.18	FP FV	20309	FW
20099	M06-019	564.19	564.69	PST2 MD	20310	FW
20101	M06-016	34.7	35.2	Granite	20311	HW
20102	M06-016	58	58.5	FP FV	20312	HW
20103	M06-016	87.85	88.35	SYN MD	20313	HW
20104	M06-016	94	94.5	FP FV	20314	HW
20105	M06-016	126.35	126.85	PST1 MD	20315	HW
20106	M06-016	153.25	153.75	FP FV	20316	HW
20107	M06-016	170.5	171	CP FV	20317	HW
20108	M06-016	180.5	181	PRE MD	20318	HW
20109	M06-016	207.5	208	FP FV	20319	HW
20110	M06-016	220	220.5	PST2 MD	20320	HW
20111	M06-016	228.8	229.3	PST2 MD	20321	HW
20112	M06-016	240.4	240.9	PRE MD	20322	HW
20113	M06-016	256.7	257.2	FP FV	20323	HW
20114	M06-016	263.7	264.15	MCP FV	20324	HW
20115	M06-016	269	269.5	MCP FV	20325	HW
20116	M06-016	303.5	304	FP FV	20326	HW
20117	M06-016	320.2	320.7	CP FV	20327	HW
20118	M06-016	333.2	333.7	PRE MD	20328	HW
20119	M06-016	334	334.5	PST1 MD	20329	HW

20120	M06-016	360	360.5	SYN MD	20330	HW
20121	M06-016	375	375.5	FP FV	20331	HW
20122	M06-016	403.5	404	FP FV	20332	SE
20123	M06-016	419.8	420.3	FP FV	20333	SE
20124	M06-016	432.5	433	FP FV	20334	SE
20125	M06-016	509.5	510	FP FV	20335	SE
20126	M06-016	522	522.5	CP FV	20336	SE
20127	M06-016	532.5	533	PRE MD	20337	FW
20128	M06-016	541	541.5	FP FV	20338	FW
20129	M06-010	26.6	27.1	Granite	20339	HW
20130	M06-010	56.5	57	FP FV	20340	HW
20131	M06-010	65	65.5	PST2 MD	20341	HW
20132	M06-010	71	71.5	PRE MD	20342	HW
20133	M06-010	100	100.5	PST1 MD	20343	HW
20134	M06-010	106.7	107.2	FP FV	20344	HW
20135	M06-010	158.2	158.7	FP FV	20345	HW
20136	M06-010	171.55	172.05	PRE MD	20346	HW
20137	M06-010	177.5	178	PRE MD	20347	HW
20138	M06-010	198.2	198.7	FP FV	20348	HW
20139	M06-010	199.85	200.35	PST2 MD	20349	HW
20140	M06-010	253	253.5	FP FV	20350	HW
20141	M06-010	255.25	255.75	PST2 MD	20351	HW
20142	M06-010	273.5	274	PST1 MD	20352	HW
20143	M06-010	301.5	302	FP FV	20353	HW
20144	M06-010	315.3	315.8	SYN MD	20354	HW
20146	M06-010	444.5	445	FP FV	20355	FW
20147	M06-039	15	15.5	FP FV	20356	HW
20148	M06-039	52	52.5	FP FV	20357	HW
20149	M06-039	99.8	100.3	FP FV	20358	HW
20150	M06-039	105.2	105.7	PRE MD	20359	HW
20151	M06-039	146.5	147	FP FV	20360	HW
20152	M06-039	179	179.5	Granite	20361	HW
20153	M06-039	200	200.5	PRE MD	20362	HW
20154	M06-039	260	260.5	FP FV	20363	HW
20155	M06-039	303	303.5	PRE MD	20364	HW
20156	M06-039	308	308.5	FP FV	20365	HW
20157	M06-039	351	351.5	FP FV	20366	HW
20158	M06-039	402	402.5	FP FV	20367	HW
20159	M06-039	419	419.5	MCP FV	20368	HW
20160	M06-039	421.7	422.2	MCP FV	20369	HW

20161	M06-039	435.6	436.1	PST2 MD	20370	HW
20162	M06-039	455	455.5	FP FV	20371	HW
20163	M06-039	491.8	492.3	PRE MD	20372	HW
20164	M06-039	501	501.5	FP FV	20373	HW
20165	M06-039	542	542.5	PST1 MD	20374	HW
20166	M06-039	552.5	553	FP FV	20375	HW
20167	M06-039	558	558.5	SYN MD	20376	HW
20168	M06-039	600	600.5	FP FV	20377	HW
20169	M06-039	686	686.5	PST1 MD	20378	SE
20170	M06-039	691.5	692	FP FV	20379	SE
20171	M06-039	704.5	705	FP FV	20380	FW
20172	M06-039	717.5	718	FP FV	20381	FW
20173	M06-027	76	76.5	Granite	20382	HW
20174	M06-027	156	156.5	FP FV	20383	HW
20175	M06-027	222	222.5	FP FV	20384	HW
20176	M06-027	254.31	254.81	PRE MD	20385	HW
20177	M06-027	304	304.5	FP FV	20386	HW
20178	M06-027	344.2	344.7	MCP FV	20387	HW
20179	M06-027	358.5	359	FP FV	20388	HW
20180	M06-027	389	389.5	PRE MD	20389	HW
20181	M06-027	408.7	409.2	FP FV	20390	HW
20182	M06-027	442	442.5	PST1 MD	20391	SE
20183	M06-027	591.4	591.9	PST1 MD	20392	SE
20184	M06-027	600	600.5	FP FV	20393	FW
20185	M06-027	627	627.5	FP FV	20394	FW
20186	M06-027	650	650.5	FP FV	20395	FW
20187	M06-027	701	701.5	FP FV	20396	FW
20188	M06-027	719	719.5	PRE MD	20397	FW
20189	M06-027	752.5	753	FP FV	20398	FW
20190	M06-027	802.8	803.3	PRE MD	20399	FW
20191	M06-027	838	838.5	FP FV	20400	FW
20192	M06-026	43	43.5	FP FV	20401	HW
20193	M06-026	153	153.5	FP FV	20402	HW
20194	M06-026	239	239.5	FP FV	20403	HW
20195	M06-026	245	245.5	SYN MD	20404	HW
20196	M06-026	311.5	312	SYN MD	20405	HW
20197	M06-026	355.5	356	FP FV	20406	HW
20198	M06-026	450.5	451	FP FV	20407	HW
20199	M06-026	552.5	553	FP FV	20408	HW
20200	M06-026	601.5	602	MCP FV	20409	HW

20201	M06-026	655	655.5	FP FV	20410	HW
20202	M06-026	702.5	703	FP FV	20411	HW
20203	M06-026	708.5	709	PST1 MD	20412	HW
20204	M06-026	801.5	802	CP FV	20413	HW
20205	M06-026	832	832.5	FP FV	20414	SE
20206	M06-026	878	878.5	FP FV	20415	FW
20207	M06-025	30	30.5	FP FV	20416	HW
20208	M06-025	125	125.5	FP FV	20417	HW
20209	M06-025	196	196.5	FP FV	20418	HW
20210	M06-025	264.5	265	NP FV	20419	HW
20211	M06-025	313.5	314	FP FV	20420	HW
20212	M06-025	405	405.5	FP FV	20421	HW
20213	M06-025	497.5	498	FP FV	20422	HW
20214	M06-025	565.5	566	PRE MD	20423	HW
20215	M06-025	568.5	569	MCP FV	20424	HW
20216	M06-025	602	602.5	FP FV	20425	HW
20217	M06-025	649.5	650	FP FV	20426	HW
20218	M06-025	705.5	706	FP FV	20427	HW
20219	M06-025	797	797.5	FP FV	20428	SE
20220	M06-025	826	826.5	FP FV	20429	SE
20221	M06-024	41	41.5	FP FV	20430	HW
20222	M06-024	153	153.5	FP FV	20431	HW
20223	M06-024	201	201.5	FP FV	20432	HW
20224	M06-024	217.5	218	MCP FV	20433	HW
20225	M06-024	246	246.5	FP FV	20434	HW
20226	M06-024	305.5	306	FP FV	20435	HW
20227	M06-024	358	358.5	FP FV	20436	HW
20228	M06-024	381	381.5	FP FV	20437	SE
20229	M06-024	448	448.5	FP FV	20438	SE
20230	M06-024	474	474.5	FP FV	20439	SE
20231	M06-024	498	498.5	FP FV	20440	FW
20232	M06-020A	39.5	40	Granite	20441	HW
20233	M06-020A	92	92.5	FP FV	20442	HW
20234	M06-020A	127.8	128.3	PRE MD	20443	HW
20235	M06-020A	155	155.5	FP FV	20444	HW
20236	M06-020A	210	210.5	FP FV	20445	HW
20237	M06-020A	218.5	219	MCP FV	20446	HW
20238	M06-020A	248.5	249	CP FV	20447	HW
20239	M06-020A	302	302.5	FP FV	20448	HW
20240	M06-020A	352	352.5	FP FV	20449	HW

20241	M06-020A	428.5	429	FP FV	20450	SE
20242	M06-020A	447.5	448	FP FV	20451	SE
20243	M06-021	17	17.5	Granite	20452	HW
20244	M06-021	28.5	29	SYN MD	20453	HW
20245	M06-021	51	51.5	FP FV	20454	HW
20246	M06-021	96.5	97	SYN MD	20455	HW
20247	M06-021	126.5	127	PST1 MD	20456	HW
20248	M06-021	165.5	166	FP FV	20457	HW
20249	M06-021	218.5	219	FP FV	20458	HW
20250	M06-021	254.5	255	FP FV	20459	HW
20251	M06-021	302	302.5	FP FV	20460	HW
20252	M06-021	362.5	363	FP FV	20461	HW
20253	M06-021	384.5	385	MCP FV	20462	HW
20254	M06-021	403.5	404	FP FV	20463	SE
	M06-024	405.63	405.83	CP FV	20464	OZ
	M06-024	400.39	400.55	FP FV	20465	OZ
	M06-024	411.85	412.05	CP FV	20466	OZ
	M06-024	417.41	417.39	FP FV	20467	OZ
	M06-024	424.4	424.58	PRE MD	20468	OZ
	M06-024	430.23	430.4	FP FV	20469	OZ
	M06-024	436.63	436.8	FP FV	20470	SE
	M06-020A	376.77	376.92	FP FV	20471	SE
	M06-020A	378.85	379	CP FV	20472	OZ
	M06-020A	387.81	387.98	FP FV	20473	SE
	M06-020A	404	404.15	CP FV	20474	SE
	M06-020A	418.66	418.82	FP FV	20475	SE
	M06-025	774.76	774.92	CP FV	20476	SE
	M06-025	785.3	785.52	FP FV	20477	SE
	M06-025	727.63	727.82	FP FV	20478	OZ
	M06-025	734.65	734.8	FP FV	20479	OZ
	M06-025	739.55	739.7	PRE MD	20480	OZ
	M06-025	753.58	753.75	CP FV	20481	OZ
	M06-025	763.37	763.55	FP FV	20482	OZ
	M06-025	770.74	770.92	CP FV	20483	OZ
	M06-039	624.27	624.45	CP FV	20484	OZ
	M06-039	625.51	625.69	PRE MD	20485	OZ
	M06-039	620.2	620.39	FP FV	20486	OZ
	M06-039	637.95	638.14	FP FV	20487	OZ
	M06-039	643.68	643.66	CP FV	20488	OZ
	M06-039	646.34	646.52	SYN MD	20489	OZ

M06-039	649.53	649.7	FP FV	20490	OZ
M06-039	659.7	659.85	FP FV	20491	SE
M06-039	669.01	669.19	FP FV	20492	SE
M06-039	682.6	682.78	FP FV	20493	SE

Sample Information for the 57 Geochemical Samples and Thin Sections Provided by Dr. Derek Wilton, Collected in 2006 for a Separate Study.

Geochemical						
Sample #	Drill Hole	From (m)	To (m)	Rock Type	Corresponding Thin Section #	Location
CMB 5205	M06-019	430.55	430.6	CP FV	7884	SE
CMB 5207	M06-019	432.4	432.45	CP FV	7885	SE
CMB 5211	M06-019	436.05	436.1	CP FV	7886	SE
CMB 5214	M06-019	439.65	439.7	CP FV	7887	OZ
CMB 5221	M06-019	446.72	446.77	FP FV	7889	OZ
CMB 5232	M06-019	454.54	454.59	CP FV	7890	OZ
CMB 5301	M06-019	454.8	454.85	CP FV	7891	OZ
CMB 5316	M06-019	473.9	473.95	FP FV	7892	OZ
CMB 5318	M06-019	476.2	476.25	FP FV	7893	OZ
CMB 5321	M06-019	479.42	479.47	FP FV	7895	OZ
CMB 5330	M06-019	488.37	488.42	FP FV	7896	FW
CMB 5332	M06-019	506.32	506.37	FP FV	7897	FW
CMB 6002	M06-026	766	766.05	FP FV	7927	SE
CMB 6015	M06-026	778	778.05	FP FV	7928	OZ
CMB 6018	M06-026	780.98	781.03	CP FV	7929	OZ
CMB 6028	M06-026	787.3	787.35	CP FV	7930	SE
CMB 6038	M06-026	797.32	797.37	FP FV	7931	SE
CMB 6551	M06-027	452.33	452.38	FP FV	7932	SE
CMB 6552	M06-027	453.37	453.42	FP FV	7933	SE
CMB 6555	M06-027	525.73	525.78	FP FV	7934	SE
CMB 6562	M06-027	531.34	531.39	FP FV	7936	SE
CMB 6567	M06-027	537.02	537.07	CP FV	7937	OZ
CMB 6573	M06-027	542.1	542.15	CP FV	7950	OZ
CMB 6585	M06-027	549.72	549.77	FP FV	6953	OZ
CMB 6590	M06-027	553.52	553.57	FP FV	6954	OZ
CMB 6592	M06-027	554.72	554.77	CP FV	6955	OZ
CMB 6596	M06-027	559.56	559.61	FP FV	6956	OZ
CMB 6611	M06-027	571.4	571.45	FP FV	6957	SE

CMB 6620	M06-027	577.2	577.25	FP FV	6958	SE
CMB 6624	M06-027	581.95	582	FP FV	6959	SE
CMB 7017	M06-016	440.48	440.53	FP FV	7819	SE
CMB 7020	M06-016	443.08	443.13	CP FV	7820	OZ
CMB 7027	M06-016	447.55	447.6	FP FV	7821	OZ
CMB 7031	M06-016	451.34	451.39	CP FV	7822	OZ
CMB 7038	M06-016	457.49	457.54	CP FV	7823	OZ
CMB 7045	M06-016	463.19	463.24	CP FV	7825	OZ
CMB 7057	M06-016	473.41	473.46	FP FV	7827	OZ
CMB 7064	M06-016	478.64	478.69	FP FV	7828	OZ
CMB 7067	M06-016	484.14	484.19	FP FV	7829	OZ
CMB 7087	M06-016	500.14	500.19	FP FV	7831	OZ
CMB 7091	M06-016	505.3	505.35	FP FV	7833	SE
CMB 7109	M06-021	446.86	446.91	FP FV	7898	SE
CMB 7114	M06-021	496.04	496.09	FP FV	7899	OZ
CMB 7116	M06-021	498.39	498.44	CP FV	7902	OZ
CMB 7126	M06-021	505.52	505.57	CP FV	7903	SE
CMB 7132	M06-021	511.64	511.69	CP FV	7904	SE
CMB 7142	M06-021	521.5	521.55	FP FV	7905	SE
CMB 7145	M06-021	541.15	541.2	FP FV	7906	SE
CMB 7148	M06-021	555.64	555.69	FP FV	7908	FW
CMB 8052	M06-010	363.79	363.84	FP FV	7909	SE
CMB 8059	M06-010	384.98	385.03	FP FV	7910	SE
CMB 8073	M06-010	395.35	395.4	CP FV	7911	OZ
CMB 8082	M06-010	404.42	404.47	CP FV	7916	OZ
CMB 8084	M06-010	406.65	406.7	CP FV	7917	OZ
CMB 8089	M06-010	411.58	411.63	CP FV	7919	OZ
CMB 8104	M06-010	424.05	424.1	FP FV	7921	SE
CMB 8114	M06-010	437.6	437.65	FP FV	7922	FW



## **APPENDIX 2**

**Description of Actlabs 4lithores Fusion ICP and ICP-MS package; Analysis of the QA/QC measures on the samples, including the accuracy and precision of the geochemical data; the raw geochemical data collected for this study.**

**Raw Geochemical Data for Actlabs can be found in Associated Excel Files**

**and**

**Modified Geochemical Data Used for This Thesis can be Found in Associated Excel Files**

#### **4lithores Fusion ICP and ICP-MS Package**

All samples collected and used for this study were analyzed using Actlabs 4lithores Fusion ICP and ICP-MS analysis. This analysis package is research grade and has a very low detection limit. It uses a Lithium Metaborate / Tetraborate Fusion ICP for whole rock analysis and ICP-MS for trace element analysis. For this process a 1.0 g sample is digested with aqua regia and diluted to 250 ml volumetrically. Samples are then analyzed on a Thermo Jarrell Ash ENVIRO II simultaneous and sequential ICP or a Perkin Elmer Optima 3000 ICP (Hoffman, 1992).

#### **QA/QC of the Geochemical Data**

Actlabs also completed their own quality assurance and quality control (QA/QC) measures on the samples throughout the analysis procedure. Certified reference material (CRM), which has a known elemental value were analyzed to determine the overall accuracy of the analysis. The accuracy is determined by subtracting the actual value of the CRM from the measured value for the CRM and then dividing this by the actual value of the CRM (Piercey, 2004). Overall the accuracy results produced from the CRM appeared satisfactory with most of the CRM having an excellent to good accuracy. There were some elements that measured a poor accuracy in some of the CRM tests but were excellent in others. In order to test for precision during the analysis, Actlabs reanalyzed the pulps of several of the samples that were submitted. The values obtained for these duplicate samples are averaged together to find the mean value. The standard deviation of these values is then divided by the mean value and multiplied by 100 to get the percent

relative standard deviation. This is a measure of overall precision, with a value closer to zero being the best and any value under ten considered to be of good precision (Piercey, 2004). As with the accuracy measurements, a better measure of the precision would benefit from several duplicate samples to achieve a more accurate mean value. Overall precision was very good for most of the samples, and there were only a handful of elements with a precision that is considered to be poor.

### **Raw Geochemical Data**

The raw geochemical data provided by Actlabs for the 208 samples collected in 2007 for this study can be found in two associated excel files, while the geochemistry of the 265 samples used for this study, organized to the specifics listed in Section 1.6, can be found in its associated excel file.

## **APPENDIX 3**

### **Mass Balance Calculations, a Continuation of Section 6.5**

**Mass Balance Calculations for the Fine and Coarse Grained Porphyritic Felsic Volcanics can be found in their respective excel files.**

## **Mass Balance Calculations**

Examination of the major, trace and rare earth element geochemistry for samples within the mineralized zone compared to those in unaltered host rock show that there are concentration differences for almost every element analyzed. Some of these elemental gains and losses are attributed to hydrothermal alteration but some are apparent changes attributed to closure, and changes in the mass and/or volume of the rocks during the alteration process. According to Piercey (2009) during alteration two processes occur: 1) there is a change in the size of the system, i.e. volume and/or mass; and 2) there are elemental fluxes in and out of the system during this process. This causes apparent gains or losses in concentration for elements that are conserved during alteration. This is due to the change in mass and/or volume of the system coupled with closure, as geochemical data for a sample has to sum up to 100 %. Therefore a direct comparison between altered and unaltered data is not possible. In order to accurately quantify the absolute elemental gains and losses caused by alteration a correction must be made for the mass and/or volume change of the system. The aim of the calculation is to eliminate the apparent change in an elements concentration due to the change in mass and/or volume of the system. Once this is completed the comparison between unaltered and altered rocks can be made, and the geochemical effects of alteration can be determined.

There are several methods for calculating the mass transfer of elements in altered rocks Gresens (1967), Grant (1986), MacLean and Barrett (1993), and Stanley and

Madeisky (1996). These methods depend on the recognition of conserved, immobile elements within the system.

The first method for this was published by Gresens (1967) and it utilizes a volume factor of the unaltered rock to the altered rock. This, along with the density of each rock and the weight fraction of each element are put into an equation to determine the absolute change of the element caused by alteration. By assuming a hypothetical volume factor the absolute change for each element can be calculated. This information then creates a linear equation for each element and these lines are plotted on a graph of absolute change versus volume factor. Immobile elements will intersect in a group near an absolute change of zero. The real volume factor can then be read graphically and entered back into the original equation to determine the absolute change for the other, mobile elements.

Another method is using the Grant (1986) method which simplified the Gresens method and utilizes isocon diagrams to determine elemental mass loss or gain. The diagram involves plotting the elements of the unaltered rock along the x-axis versus elements of the altered rock along the y-axis. Immobile elements will plot along a straight line of equal concentration that intersects with the origin. Elements that plot above this line represent mass gains and elements that plot below the line represent mass losses. The slope of the line can then be used to calculate the mass changes for the mobile elements.

MacLean and Barrett (1993) method involves using an enrichment factor to calculate mass changes, and can be applied to both single and multiple precursor scenarios. In order to calculate the enrichment factor the most immobile element that is

conserved during alteration must be chosen. The enrichment factor is the ratio of the immobile element of the least altered sample over the immobile element of the altered sample. The reconstituted composition of the rock is then determined by multiplying the enrichment factor by the weight percent or ppm of the elements in the altered samples. The mass change for each element is then calculated by subtracting the precursor value from the reconstituted composition.

One final method is by Stanley and Madeisky (1996) which utilizes Pearce element ratios (PER) to eliminate the effects of closure and the constant sum of geochemical analysis to 100 %. This method uses a common conserved element which is an element that has not been affected by alteration or fractional crystallization. The ratios of the individual elements against the conserved element are measured and these ratios are plotted on graphs. Plotted along the x and y-axis are element ratios that are common to a similar mineral. If the points plot together then the element was conserved in the system, if the points lie upon a straight line it indicates that they formed as a result of fractional crystallization. If points plot off the line then they have been affected by alteration.

For this thesis, the methods introduced by MacLean and Barrett (1993) will be utilized for mass balance calculations. The reason for this is based on its relative ease of use and the fact that it will provide the total mass change and the mass change for each element, represented as grams per 100 grams (g/100g). The single precursor method will be used in order to compare the FP felsic volcanic rocks of the mineralized zone with the

unaltered FP felsic volcanic rocks. Likewise, CP felsic volcanics of the mineralized zone will be matched to their unaltered CP equivalents.

The single precursor mass transfer technique as outline by Gifkins *et al.* (2005), and Piercey (2009) first requires all geochemical data to be recalculated to volatile free (volatile free Geochem data is included in the Appendix). Since the LOI for each sample is relatively low, usually less than 2 %, it will not be included as part of the mass transfer calculations. Its omission is not likely to distort the data. The next step is to determine a conserved, immobile element that will be used to calculate the enrichment factor. This is achieved by constructing x-y bivariate plots where immobile elements are plotted against each other. If an immobile element is conserved during alteration then all samples will plot on a straight line that intersects the origin. The immobile element that consistently occurs in highly correlated trends is the most conserved element and best element to use for the mass change calculations.

Immobile-immobile element plots for both the FP and CP felsic volcanics can be found in Figure 6.4. The data shows that most of the immobile elements have not been conserved during alteration. Aluminum, thorium, niobium, yttrium, zirconium and the rare earth elements do not correlate very well on bivariate plots, particularly with samples from the mineralized zone due to the increase in albite, zircon, allanite, garnets and other mineral species. The element that generally has the highest correlation out of all the immobile elements is titanium, which will be used to calculate the enrichment factor (EF). Even though there is titanite present within the unaltered host rock and mineralized



zone,  $\text{TiO}_2$  still correlates rather well and seems to have remained mostly conserved during alteration.

The next step is to determine the precursor sample, which is the least altered sample. The least altered or precursor sample for the FP felsic volcanic rocks is sample CMB 20164 which is from the foot wall of drill hole M06-039 (Highlighted Red). This sample was chosen based on its major oxide geochemistry which best matches that of the average, unaltered major oxide geochemistry of the FP felsic volcanics, which is found in Table 3.1. The least altered of the precursor sample for the CP felsic volcanic rocks is sample CMB 20019 (Highlighted Red) which is taken from the hanging wall of drill hole M06-019. Again it was chosen as the precursor because its major oxide geochemistry best matches that of the unaltered average for CP rocks, as seen in Table 3.1.

The enrichment factor (EF) is the mass correction factor and it corrects for the changes in the size of the system during alteration. The EF for each sample is calculated by taking the chosen, conserved immobile element of the precursor and dividing it by the same immobile element for each sample. The equation is as follows:

$$\text{EF} = Z_{\text{precursor}} / Z_{\text{altered}} \quad \text{i.e. } \text{EF} = \text{TiO}_2_{\text{precursor}} / \text{TiO}_2_{\text{altered samples}}$$

For this study  $\text{TiO}_2$  was chosen as the precursor, and the EF for each sample can be found in this Appendix, highlighted blue. The EF is then used to correct the altered data to remove the effects of mass and/or volume change that occurred during alteration. This is achieved by multiplying all of the elements of an altered sample, by that samples enrichment factor, where:

$$RC = EF \times C_a$$

The reconstituted composition (RC) is the composition of what the altered sample should be if the change in mass and/or volume is removed. In the above equation  $C_a$  represents the individual elements of an altered sample expressed in either weight percent or ppm. The reconstituted composition for all samples can be found in this Appendix. Once the RC is known the mass change (MC) for each individual element can be calculated. This is achieved by subtracting the original precursor sample,  $C_{\text{precursor}}$  from the reconstituted composition sample, where:

$$MC = RC - C_{\text{precursor}}$$

This is completed for every element within an altered sample revealing the mass change for that element during alteration. To determine the total mass change of the system all of the individual mass changes for the major oxides must be added together. The mass change for each altered sample can be found in this Appendix. The entire process can be simplified into the following equation:

$$MC = [(Z_{\text{precursor}} / Z_{\text{altered}}) \times C_{\text{altered}}] - C_{\text{precursor}}$$

The mass balance calculations for the Coarse Grained Porphyritic Felsic Volcanic rocks are presented in an accompanying excel file. All Coarse Grain samples are included. Data includes the volatile free geochemistry, enrichment factor (highlighted blue), reconstituted composition, and the mass change. The precursor sample is also included (highlighted red). Samples from the Mineralized Zone are highlighted light blue, and samples from the sodic envelope are highlighted pink.

The mass balance calculations for the Fine Grained Porphyritic Felsic Volcanic rocks are presented in an accompanying excel file. All Fine Grain samples are included. Data includes the volatile free geochemistry, enrichment factor (highlighted blue), reconstituted composition, and the mass change. The precursor sample is also included (highlighted red). Samples from the Mineralized Zone are highlighted light blue, and samples from the sodic envelope are highlighted pink.

## **APPENDIX 4**

**Aurora Energy Drill Logs for Diamond Drill Holes M06-010, M06-016, M06-019,  
M06-020A, M06-021, M06-024, M06-025, M06-026, M06-027 and M06-039**











Hole No. M06-019										Page 1 of 1																																																																																																																																																																																																																																																																																																																																																																																																																																																																																																																																																																																																																																																																																																																																																																																																																																																																																																																																																																																																																																							
PROPERTY:		EASTING: 307049		GRID E: 9 + 40W		COMMENCED:		JUNE 12 / 06		AZIMUTH:		330		CORE SIZE:		BTW		SURVEYS:																																																																																																																																																																																																																																																																																																																																																																																																																																																																																																																																																																																																																																																																																																																																																																																																																																																																																																																																																																																																																															
License:		9412M		NORTHING: 6062118		GRID N: 4 + 38S		JUNE 17 / 06		DIP:		-77		OBJECTIVE:		Delineation																																																																																																																																																																																																																																																																																																																																																																																																																																																																																																																																																																																																																																																																																																																																																																																																																																																																																																																																																																																																																																	
Grid Line:		9 + 40W		ELEVATION: 340.4		NAD 83 zone: 21		% RECOVERY:		NOTES:		W. Lepore logged from 458 m																																																																																																																																																																																																																																																																																																																																																																																																																																																																																																																																																																																																																																																																																																																																																																																																																																																																																																																																																																																																																																					
GEOLOGY NOTES																																																																																																																																																																																																																																																																																																																																																																																																																																																																																																																																																																																																																																																																																																																																																																																																																																																																																																																																																																																																																																																	
DEPTH		GRAPHIC		LITHOLOGY		%pheno		MIn-1		%Porph		Bleach		Hm		Int-1		Mt		Int-2		Am		Cb		Kf		Ab		Vn		L-1		SF		M-9		M-10		M-11		DEPT		TYPE		CA																																																																																																																																																																																																																																																																																																																																																																																																																																																																																																																																																																																																																																																																																																																																																																																																																																																																																																																																																																																																			
RX COMP		NOTES		FORM																																																																																																																																																																																																																																																																																																																																																																																																																																																																																																																																																																																																																																																																																																																																																																																																																																																																																																																																																																																																																																													














3a
2a
3a
2a
4a
2a
4b
3a
2a
5
2a
5
2a
9

484.73	491.19	Coarsely porphyritic felsic meta- volc...as above... 18 cm pink mylonite @ lower contact	
491.19	493.14	Finely porphyritic felsic meta-volc..... Weakly mineralized @ 180- 240 cps...str. Altered	
		Coarsely porphyritic felsic meta-volc... starts with 36 cm of chlorite- biotite rich dike with 4- 5 % calcite... some internal thin mylonite zones... str. Altered, with 200- 240 cps to 494.3 m, then increasing to 470 by 495m ... part of the unit is finer gr. internally.. 494.3 - 497.3 m ..... 470- 900 cps, average 700 cps..... 497 3- 500.0 m 970-2600 cps... average 1650 cps... 500.0- 502.6 m ..... 510-1430 cps, average 800 cps.... 502 6- 503.7 m .... 750-2250 cps, average 1700 cps... 503.7- 506.5 m .... 280- 520 cps, average 350 cps... 506.5- 513.62 m ... 550- 2700 cps, average 1100 cps... 513.62- 514.13m .... pre- kinematic chloritic mafic dike..... 514.13- 516.4 m .... 310- 2400 cps, average 1100 cps..... - 35 cm of pink mylonite @ bottom of zone.	
493.14	516.4		
516.4	517.56	Finely porphyritic felsic meta- volc.. 440- 1400 cps, average 850 cps	
517.56	520.15	Coarsely porphyritic felsic meta-volc...upper contact fairly sharp, lower contact on a mafic dike .... 310- 1880 cps, average 1000 cps... 519.66-520.15m.. 1/2 chloritic dike , 1/2 mylonitic contact zone..... 300 cps	
520.15	522.67	Finely porphyritic felsic meta- volc..weakly mineralized at 250-700 cps, average. 350 cps	
522.67	524.36	F.gr. str. Chloritic & foliated, mafic dike with ... 3- 4 % up to 6mm long anhedral / subhedral plagioclase phenos	
524.36	533.54	Finely porphyritic felsic meta- volc... str. Altered (soft & porous) , decreasing down hole ... 20 % then chloritized mafic dikes, some with the plagioclase phenos.... Sporadic weak mineralization to 350 cps.	
533.54	534.79	F.gr., str. Chloritic & foliated mafic dike	
		Coarsely porphyritic felsic meta- volc..... Cut by a couple of mafic dikes to 539.15m, eg. 536.26- 537.08m, and only weak alteration & traces of mineralization (to 250 cps) ... 539.15- 540.39m ... stronge hematization with 200- 700 cps, average 350 cps .... lower contact sharp & sheared.	
534.79	540.39	Finely porphyritic meta-volcanics...mod HM. late epidote vts...mineralization weak averaging 230 cps increasing with depth...last metre of interval 250-588 cps avg 300 cps.	
540.39	543.05		
543.05	544.84	Well foliated, moderately chloritic late-syn kinematic mafic dyke, sharp contacts...biotite rich, defining foliation	
544.84	553.56	Finely porphyritic meta-volcanics...weakly HM .increasing late px-ep veinlets with depth....very weakly mineralized over interval avg 200 cps up to 248 cps	
553.56	555.34	Mafic dyke as above, 1% dsm 1mm py grains throughout.	
		Finely porphyritic meta-volcanics... mafic dyke as above from 557.64-558.52... weakly mineralized above dyke, 210-270 cps. Weakly mineralized below dyke as well...236-404 cps for 0.5 m below dyke.....Veins of ep-ac-gt+/-ca sporadically throughout interval.	
555.34	580.92	Grey, medium-grained granite to granodiorite, locally weakly foliated, contact sharp and sub-parallel to foliation	
580.92	581.86		

	484.73	491.19	Coarsely porphyritic felsic meta- volc...as above.... 18 cm pink mylonite @ lower contact	MT.FV.por.cgr	1 15}1	fp/qz				4 dsm	2 dsm	1		dsm/vlt 2}1					
	491.19	493.14	Finely porphyritic felsic meta-volc..... Weakly mineralized @ 180- 240 cps...str. Altered	MT.FV.por.fgr	1 5}1	fp/qz				4 dsm	2 dsm	1		dsm	2				
			Coarsely porphyritic felsic meta-volc... starts with 36 cm of chlorite- biotite rich dyke with 4- 5 % calcite... some internal thin mylonite zones... str. Altered, with 200- 240 cps to 494.3 m, then increasing to 470 by 495m .... part of the unit is finer gr. internally.. 494.3 - 497.3 m ..... 470- 900 cps, average 700 cps..... 497 3- 500.0 m 970-2600 cps... average 1650 cps... 500.0- 502.6 m ..... 510-1430 cps, average 800 cps.... 502 6- 503.7 m .... 750-2250 cps, average 1700 cps... 503.7- 506.5 m .... 280- 520 cps, average 350 cps... 506.5- 513.62 m ... 550- 2700 cps, average 1100 cps... 513.62- 514.13m .... pre- kinematic chloritic mafic dyke..... 514.13- 516.4 m ..... 310- 2400 cps, average 1100 cps..... - 35 cm of pink mylonite @ bottom of zone.	MT.FV.por.cgr	1 15}1	fp/qz			4 dsm	3 dsm	1		dsm/vlt 2}1						
3a	493.14	516.4		MT.FV.por.fgr	1 15}1	fp/qz			4 dsm	3 dsm	1		px	2					
	516.4	517.56	Finely porphyritic felsic meta- volc.. 440- 1400 cps, average 850 cps	MT.FV.por.fgr	1 4}1	fp/qz			4 dsm	3 dsm	1			ct	2				517 fol
2a		517.56	Coarsely porphyritic felsic meta-volc...upper contact fairly sharp, lower contact on a mafic dike .... 310- 1880 cps, average 1000 cps... 519.66-520.15m.. 1/2 chloritic dike , 1/2 mylonitic contact zone..... 300 cps																
3a	517.56	520.15	Coarsely porphyritic felsic meta-volc...upper contact fairly sharp, lower contact on a mafic dike .... 310- 1880 cps, average 1000 cps... 519.66-520.15m.. 1/2 chloritic dike , 1/2 mylonitic contact zone..... 300 cps	MT.FV.por.cgr	1 10}1	fp/qz			4 dsm	3 dsm	1			ct	2				
2a	520.15	522.67	Finely porphyritic felsic meta- volc..weakly mineralized at 250-700 cps, average. 350 cps	MT.FV.por.fgr	1 5}1	fp/qz			4 dsm	2 dsm	1			1 ct	2				521 fol
4a	522.67	524.36	F.gr. str. Chloritic & foliated, mafic dike with ... 3- 4 % up to 6mm long anhedral / subhedral plagioclase phenos	MI.dk.ct.pk	1 4 pg		4							ct	5				
	524.36	533.54	Finely porphyritic felsic meta- volc... str. Altered (soft & porous) , decreasing down hole ... 20 % then chloritized mafic dikes, some with the plagioclase phenos.... Sporadic weak mineralization to 350 cps.	MT.FV.por.cgr	1 6}1	fp/qz			4 dsm	2 dsm	1			1 ct	2 ep	1			526 fol
	533.54	534.79	F.gr., str. Chloritic & foliated mafic dike	MI.dk.ct.bt.pk			4							ct	4 bt	4			
4b			Coarsely porphyritic felsic meta- volc..... Cut by a couple of mafic dikes to 539.15m, eg. 536.26- 537.08m, and only weak alteration & traces of mineralization (to 250 cps) ... 539.15- 540.39m ... stronge hematization with 200- 700 cps, average 350 cps .... lower contact sharp & sheared.	MT.FV.por.cgr	1 15}1		4 dsm	2 dsm	1										
3a	534.79	540.39	Finely porphyritic meta-volcanics...mod HM.late epidole vts...mineralization weak averaging 230 cps increasing with depth...last metre of interval 250-588 cps avg 300 cps.	MT-FV.por.fgr	1 5}1	fp/qz			4 dsm	2 dsm	2								
2a	540.39	543.05	Well foliated, moderately chloritic late-syn kinematic mafic dyke. sharp contacts...biotite rich, defining foliation	MT-FV.por.fgr	1 5}1	fp/qz		4 dsm	2 dsm	2			ep	1 ct	1 px	2			542 fol
5	543.05	544.84	Finely porphyritic meta-volcanics...weakly HM .increasing late px-ep veinlets with depth....very weakly mineralized over interval avg 200 cps up to 248 cps	MI.dk.isk	1		3							ct	2 bt	2			543.5 fol
2a	544.84	553.56	Finely porphyritic meta-volcanics...weakly HM .increasing late px-ep veinlets with depth....very weakly mineralized over interval avg 200 cps up to 248 cps	MT-FV.por.fgr	1 5}1	fp/qz		3 dsm	1 dsm	2			ep	2 ac	1 gt	1			551 fol
5	553.56	555.34	Mafic dyke as above, 1% dsm 1mm py grains throughout.	MI.dk.isk	1		3						py	2 ct	2 bt	2			555 fol
			Finely porphyritic meta-volcanics..... mafic dyke as above from 557.64-558.52.....weakly mineralized above dyke, 210-270 cps. Weakly mineralized below dyke as well...236-404 cps for 0.5 m below dyke.....Veins of ep-ac-gt+/-ca sporadically throughout interval.																
2a	555.34	580.92	Grey, medium-grained granite to granodiorite, locally weakly foliated, contact sharp and sub-parallel to foliation	MT-FV.por.fgr	1 10}2	fp/qz		3 dsm	1 dsm	2			ep	1 ac	1 gt	1			572.5 fol
	580.92	581.86		FI.gr.mgr.fol	1		1	dsm	1										

	45
	44





[illegible]























## **APPENDIX 5**

**Comprehensive Work History of the Michelin deposit,**

**an add on to Section 1.4.1**

## **Industry Work History**

In response to the global demand for uranium, the British Newfoundland Exploration Limited (BRINEX) entered into a joint venture exploration agreement in 1966 with Metallgesellschaft A. G. Prior to this, BRINEX had made uranium discoveries in the Postville - Makkovik area, including the Kitts deposit, in the 1950s. The aim of the contract was to explore for uranium in two adjacent locations; Area A and Area B situated to the south, southeast and southwest of the Kitts deposit and encompassing a combined area of about 750 sq. mi. The sole operator throughout the agreement would be BRINEX (Beavan and Gandhi, 1976).

In 1967 Barringer Research Ltd. were commissioned to carry out a low level, airborne survey over Area A. This survey involved the collection of magnetic, electromagnetic and gamma-ray spectrometer data over a total of 3,000 line mi. (Beavan and Gandhi, 1976; Booth *et al.*, 1979). The results revealed numerous radiometric anomalies throughout Area A. In 1968, during ground follow up investigations, prospector Leslie Michelin identified the bedrock source for one of these anomalies; this would become known as the Michelin showing and later the Michelin deposit (Booth *et al.*, 1979).

Subsequent work throughout the rest of 1968 and 1969 included; a) a detailed ground radiometric survey, conducted using a handheld scintillometer, along lines spaced 400 ft apart; b) a geochemical soil and stream sediment survey, in which 453 soil samples were collected at 100 ft intervals along lines located 400 ft apart, and 55 stream sediment

samples were collected; c) geological mapping at a 1" to 400' scale over the Michelin area; as well as d) trenching and boulder tracing (Doak *et al.*, 1969). Based on encouraging results, a surface drill program was initiated on the prospect in 1969 and by 1970 a total of 92 holes, designated M-69-1 to M-70-92, was drilled on the property (Booth *et al.*, 1979). This represented 39,794 ft of subsurface information and enabled BRINEX to delineate the deposit over a strike length of 3,900 ft and to a depth of approximately 850 ft (BRINEX, 1979a). Overall, a total of 1,909 core samples were assayed for  $U_3O_8$ . Ore reserve calculations indicated a resource totaling 2.6 million tons having an average grade of 0.182 %  $U_3O_8$ . This was based on a 450 ft subsurface depth and cut-off grade of 0.100 %  $U_3O_8$  (BRINEX, 1976).

According to Piloski (1976), an underground program was proposed in 1975 with the following objectives; a) expose the mineralization in underground workings to permit a geological assessment of its nature and distribution; b) provide openings in order to sample the mineralization thoroughly and systematically; c) obtain a bulk sample for metallurgical testing; and d) provide openings from which closely spaced diamond drilling could be carried out to delimit the boundaries of the mineralization. In mid-April of that year an 8 by 12 ft decline portal was collared at the prospect. The decline was driven northward into the hanging wall at an inclination of -12 degrees and then turned about 80 degrees to the west and driven -9 degrees for a total length of 640 ft, down to the 100 ft sub-surface level. From this point it was continued a further 1,332 ft at the 100 ft level (Booth *et al.*, 1979). A series of 56 underground drill holes, MU-75-1 to MU-75-56, totaling 5,820 ft of AXT core were drilled between late August and early December.

Most of the holes were horizontal, spaced at 50 ft centers and drilled to the south to outline and sample the main mineralized zone (Booth *et al.*, 1979). Along with underground drilling, a total of 412 face samples were taken from the adit as well as 261 muck samples (Booth *et al.*, 1979). A bulk sampling program involving the collection of 86 samples from across the entire adit was also undertaken. Samples were obtained from muck loads and stored within individual 45 gallon drums (Booth *et al.*, 1979). A 25 ton bulk sample was shipped to Lakefield Research of Canada Limited in Lakefield, Ontario for metallurgical testing and for pilot plant scale testing (BRINEX, 1976).

Also in 1975, a surface in-fill diamond drill program, comprising holes M-75-93 to M-76-183 was started and completed by 1976. This represented 90 AQ drill holes with a combined footage of 52,922 ft. Over 5,180 drill core samples were assayed by radiometric methods at the Michelin site. Approximately 10 % of these samples were sent to commercial laboratories for check assays (BRINEX, 1976). In 1976, the adit was dewatered and a second bulk sample totaling 48 tons was collected from four separate locations and sent for further metallurgical testing (Booth *et al.*, 1979). In late 1976 three NQ holes, GM-1, 2 and 3 were drilled by Golder Drilling in order to obtain rock mechanic information on the deposit (Booth *et al.*, 1979). In April 1976, a geostatistical study was carried out by the Mineral Exploration Research Institute utilizing assay information available prior to the 1976 drill program. This study which applied a 0.05 % cut-off grade estimated reserves at 7.8 million tons containing 0.105 %  $U_3O_8$ , equating to 16.5 million pounds of  $U_3O_8$  (BRINEX, 1976).



BRINEX also retained Kilborn Limited in early 1976 to produce a preliminary engineering, capital cost and operating report for their Kitts-Michelin project. The report was completed in July, 1976, and considered two separate concepts for mine development: a) mill and docking facility to be located at Three Rapids and all ore trucked to the mill from the two mine sites or b) the mill located at Michelin adjacent to the main deposit and ore trucked from Kitts (BRINEX, 1979b). In August 1976, BRINEX again retained Kilborn Limited to produce a detailed feasibility study for the Kitts-Michelin project based on what appeared to be the most attractive concept as defined in the preliminary report. This report, which was completed in 1977, also gave permission for Kilborn to proceed with engineering, procurement and construction of certain minimum facilities on site. Kilborn formed a project task force and retained companies with expertise in ore reserve calculations, mine planning, surveying, geotechnical engineering, metallurgical testing, environmental investigations and dock design. Study results showed that projected costs for the project would be too high to warrant a production decision (BRINEX, 1979b). These results were supported by Bechtel, a second company commissioned by BRINEX to undertake a similar study (BRINEX, 1979b). Environmental baseline studies by Dames and Moore were commenced in the summer of 1976 and completed by summer 1978 (BRINEX, 1979b).

A surface in-fill drill program, totaling 13,145 ft of AQ diameter core was completed in 1979 (Sharpley, 1980). Of the 65 holes collared, 28 were placed strategically down dip and along strike to infill gaps remaining from a previous drill program. The other 37 holes were drilled to test the near surface continuity of the deposit

and for exploration and/or geotechnical purposes around the plant site area and within the tailings disposal area. (Sharpley, 1980). Also in 1979, BRINEX contracted Kilborn once again to prepare a comprehensive feasibility study based on a more economical development plan (BRINEX, 1979a). The results of this study which included: a) compression of the development schedule, b) maximization of use for existing facilities in Goose Bay, c) utilization of hydro power from Churchill Falls, d) maximum utilization from open pit mining and e) underground mining during more favorable conditions, all suggest the project would be economically viable (BRINEX, 1979a). As part of the study, work was completed on: a) road studies between the Michelin site and Goose Bay, b) geotechnical and hydrogeological field studies of the proposed tailings storage area and tailings dam design, c. ore reserve studies, d) metallurgical studies and e) engineering studies (BRINEX, 1979a). Based on the 1979 feasibility study, final ore reserve numbers for the Michelin deposit based on indicated and inferred ore, totaled 7,458,800 tons grading 2.6 lbs./ton of  $U_3O_8$  (BRINEX, 1979a).

In 1980, the Urangesellschaft Canada Limited interest was purchased by Edison Development Canada Inc. who then announced a delay in their desire to proceed with the project (BRINEX, 1980). This delay was attributed to a number of factors. First and foremost the company failed to obtain environmental approval for the project. In addition to this, the company wished to continue their research programs geared towards disposal of uranium mill tailings, dam stability, seepage, monitoring arrangements and contingency planning (BRINEX, 1980).

Kilborn Limited completed their Kitts-Michelin feasibility study and afterwards, technical activity on the project remained minimal, pending a decision by the company to advance the project (BRINEX, 1980). During this slowdown, only minor field mapping and prospecting activity took place in an area surrounding the deposit. Meanwhile, the company continued with their public relations efforts and maintained talks with government and other interested officials (BRINEX, 1980). In the early 1980's with BRINEX now focused on other uranium targets outside the Michelin deposit, the demand and price for uranium collapsed. Subsequently, the Michelin deposit was not worked again except for sporadic site cleanup attempts until the early 2000's.

In 2003, Altius Resources Inc. formed a strategic alliance with Fronteer Development Group Inc. to search for IOCG systems within Labrador's Central Mineral Belt (CMB). A large area of the CMB was staked, including the Michelin deposit (Smith *et al.*, 2005). This was followed by field prospecting and examination of mineral occurrences previously identified by BRINEX. In July and August of 2004, FUGRO Airborne Surveys Corp. flew a 13,092 line km high resolution magnetic and gamma-ray radiometric survey over the region (Smith *et al.*, 2005). This led to further prospecting and geological reconnaissance over the Michelin area. In late 2004, digital compilation of Michelin drill data was completed and plotted values indicated the deposit appeared open at depth, thereby presenting a good exploration target. Work conducted during the 2004 field season included outcrop sampling for whole rock chemistry and petrography (Smith *et al.*, 2005).

A wholly owned company called Aurora Energy Inc. was formed in June 2005 with ownership split between Altius and Fronteer. Also in 2005, FUGRO Airborne Surveys Corp. flew a detailed magnetometer and gamma-ray spectrometer survey over the Michelin property as part of a 5,783.2 line km survey (Wilton and Cunningham-Dunlop, 2006). An IKONOS Photographic Survey was also completed over the project area in 2005 using a high resolution satellite system. Environmental baseline studies were also commenced in 2005. These included a literature review, an environmental and surface water quality assessment, regional water quality baseline program, historical site assessment and a scintillometer survey of waste rock piles (Wilton and Cunningham-Dunlop, 2006). Field work initiated in 2005 consisted of locating old BRINEX drill collars and line grids, re-cutting approximately 11.65 km of old line grids, detailed geological and structural mapping, prospecting, humus sampling and conducting a scintillometer survey over the area (Wilton and Cunningham-Dunlop, 2006). From August to November in 2005, a diamond drill program was carried out on the Michelin property. Ten holes were collared with nine completed to their intended target depth. A total of 4,547.19 m was obtained and based on core logging and geochemical sampling the company was able to confirm the presence of uranium mineralization as documented by past BRINEX programs. In addition to duplicating archival BRINEX data, Aurora hoped to extend the known zones of mineralization below the previously tested vertical depth of 250 m. Results of the drilling proved positive as the BRINEX data was successfully duplicated and the zone of mineralization was extended from 250 to 750 m. (Wilton and Cunningham-Dunlop, 2006).

Aurora conducted further drilling on the Michelin deposit in 2006. From May to November, the company drilled 41 holes totaling 24,999.83 m. The program goal was to extend the known zones of mineralization below the previously tested vertical depth of 750 m and to conduct infill drilling in an effort to verify the inferred resource defined in their 2005 drill program (Wilton and Giroux, 2007). With respect to the 41 holes, 18 were drilled on the extension of the A-zone in order to obtain infill data for the zone between 250 and 700 m vertical depth, 21 holes were drilled to determine the extent of mineralization down plunge and 2 holes drilled for additional mineralized shoots to the east of the A-zone mineralization (Wilton and Giroux, 2007). According to Wilton and Giroux (2007), the 2006 program was successful in extending the main zone of mineralization an additional 250 m down plunge beyond the limit of the 2005 program. In addition, the in-fill holes allowed the company to verify the mineralized grade and thickness calculated from results obtained during the 2005 drill program. Metallurgical testing was also completed on the Michelin core by SGS Lakefield. They tested the following parameters: a) process mineralogy, b) comminution, c) physical concentration, d) acid leaching, e) liquid-solid separation, f) uranium extraction, g) neutralization and effluent control and h) ore, waste rock and tailings environmental stability (Wilton and Giroux, 2007).

In January 2006, Roscoe Postle Associates undertook a 43-101 compliant resource calculation for the deposit. They based their assessment on historic BRINEX drilling and assay samples as well as data obtained from 2005 drilling (Wilton and Giroux, 2007). Resource estimates for the deposit were pegged at a combined 22,225,000

lbs.  $\text{U}_3\text{O}_8$  measured and indicated and 13,360,000 lbs.  $\text{U}_3\text{O}_8$  inferred. In January 2007, the resource estimate was updated by Gary Giroux to include the drilling completed in 2006, and divided the ore into open pit and underground reserves. Updated values indicate the deposit has an open pit reserve of a measured resource of 3,410,000 tons grading 0.07 %  $\text{U}_3\text{O}_8$  for a net total of 5,340,000 lbs.  $\text{U}_3\text{O}_8$ ; an indicated resource of 7,930,000 tons grading 0.06%  $\text{U}_3\text{O}_8$  for a net total of 10,840,000 lbs.  $\text{U}_3\text{O}_8$  open pit and an inferred resource of 460,000 tons grading 0.04 %  $\text{U}_3\text{O}_8$  for a net total of 440,000 lbs.  $\text{U}_3\text{O}_8$ . It has an underground reserve of 14,310,000 tons grading 0.12 %  $\text{U}_3\text{O}_8$  for a net total of 36,290,000 lbs. indicated and 13,950,000 tons grading 0.11 %  $\text{U}_3\text{O}_8$  for a net total of 32,610,000 lbs.  $\text{U}_3\text{O}_8$  inferred (Wilton and Giroux, 2007).

Further baseline environmental studies were also continued at the Michelin site during the 2006 calendar year. They would be used to compile an environmental baseline report sufficient to support a pre-feasibility study for uranium mine development at the Michelin and satellite exploration sites (Wilton *et al.*, 2007). Baseline hydrological and wildlife studies were conducted in 2007. Also in 2007, a new drill program was completed between June and November totaling 50 drill holes and 21,611.49 m drilled. The drill program included five phases: a) a shallow exploration program to test the eastern extension of the deposit, b) down-plunge extension of the main zone, c) down-plunge extension of the eastern shoot, d) confirmation drilling of the defined upper BRINEX zone and e) the western shoot program (Wilton *et al.*, 2007; Cunningham-Dunlop and Lee, 2008). Results indicate that although rocks are still strongly altered towards the east, mineralization does not continue in that direction. Drilling also

confirmed that the main zone could be extended down-plunge an extra 185 m westward of previous drilling. The eastern-shoot could also be expanded a further 300 m horizontally and to a vertical depth of 600 m. Furthermore, the confirmation drilling was successful in correlating with known BRINEX values obtained from drill programs undertaken in the late 60's and 70's. In a similar fashion to the eastern extension, the western extension also proved unfavorable for significant mineralization (Wilton *et al.*, 2007; Cunningham-Dunlop and Lee, 2008). Metallurgical testing continued throughout 2007. An updated 43-101 compliant resource estimate for the Michelin deposit based on 2007 drill results indicates a measured and indicated resource of 17,459,000 tonnes grading at 0.12 %  $U_3O_8$  for a net total of 47,892,000 lbs.  $U_3O_8$  underground and 12,941,000 tonnes grading 0.07 %  $U_3O_8$  for a net total of 19,542,000 lbs.  $U_3O_8$  open pit and an inferred resource of 12,577,000 tonnes grading 0.12 %  $U_3O_8$  for a net total of 33,647,000 lbs.  $U_3O_8$  underground and 1,564,000 tonnes grading 0.05 %  $U_3O_8$  for a net total of 1,818,000 lbs. open pit (Cunningham-Dunlop and Lee, 2008).

In early 2008, Aurora drilled an additional 23 holes, totaling 9,001.78 m (Barrett *et al.*, 2008). This drilling was a continuation of 2007 efforts undertaken to extend mineralization towards the east, to further delineate the main zone and to confirm the extent of the eastern and western shoots. In combination with this, another 631.8 m was drilled for geotechnical work (Barrett *et al.*, 2008). Aurora drilled an additional 29 holes totaling 9,056.0 m during the summer of 2008. There were four phases of drilling: a) main zone infill, b) Michelin East exploration, c) geotechnical, and d) metallurgical (Barrett and Ash, 2009). The infill program consisted of 17 drill holes totaling 7,053.6 m.

Its goal was to further define the main zone, so that inferred resources could be verified and placed in the indicated and measured resource categories. The Michelin East drilling consisted of three holes totaling 511.5 m. Drilling was designed to target small surface radiometric anomalies located to the east of the deposit (Barrett and Ash, 2009). A total of 6 holes totaling 1,228.4 m were drilled for the geotechnical program. The geotechnical program was designed to provide detailed data on rock quality within the hanging wall, ore zone and footwall as well as determine the rate of underground water flow and water geochemistry (Barrett and Ash, 2009). Three holes totaling 262.5 m were also drilled for metallurgical testing to determine a supply of non-ore grade material for mill design and beneficiation studies.

In 2008, a three year moratorium for uranium mining was put in place by the local Nunatsiavut government on all Labrador Inuit Lands (LILs). This halted exploration until the moratorium was lifted in March of 2012 (Barrett and Ash, 2009). Since that time, Aurora Energy has been purchased by Fronteer Development Group which has been subsequently purchased by Paladin Resources. They began drilling on the Michelin deposit in mid-2012. According to Hertel *et al.* (2009), the deposit as of 2009 has a measured resource of 34,080,000 lbs. of  $U_3O_8$ , and an indicated and inferred resource of 72,910,000 lbs.  $U_3O_8$ .